CANADIAN THESES ON MICROFICHE

THÈSES CANADIENNES SUR MICROFICHE

National Library of Canada
Collections Development Branch

Canadian Theses on
Microfiche Service

Ottawa, Canada
K1A 0N4

Bibliothèque nationale du Canada
Direction du développement des collections

Service des thèses canadiennes
sur microfiche

NOTICE

The quality of this microfiche is heavily dependent upon the quality of the original thesis submitted for microfilming. Every effort has been made to ensure the highest quality of reproduction possible.

If pages are missing, contact the university which granted the degree.

Some pages may have indistinct print especially if the original pages were typed with a poor typewriter ribbon or if the university sent us an inferior photocopy.

Previously copyrighted materials (journal articles, published tests, etc.) are not filmed.

Reproduction in full or in part of this film is governed by the Canadian Copyright Act, R.S.C. 1970, c. C-30. Please read the authorization forms which accompany this thesis.

AVIS

La qualité de cette microfiche dépend grandement de la qualité de la thèse soumise au microfilmage. Nous avons tout fait pour assurer une qualité supérieure de reproduction.

S'il manque des pages, veuillez communiquer avec l'université qui a conféré le grade.

La qualité d'impression de certaines pages peut laisser à désirer, surtout si les pages originales ont été dactylographiées à l'aide d'un ruban usé ou si l'université nous a fait parvenir une photocopie de qualité inférieure.

Les documents qui font déjà l'objet d'un droit d'auteur (articles de revue, examens publiés, etc.) ne sont pas microfilmés.

La reproduction, même partielle, de ce microfilm est soumise à la Loi canadienne sur le droit d'auteur, SRC 1970, c. C-30. Veuillez prendre connaissance des formules d'autorisation qui accompagnent cette thèse.

THIS DISSERTATION
HAS BEEN MICROFILMED
EXACTLY AS RECEIVED

LA THÈSE A ÉTÉ
MICROFILMÉE TELLE QUE
NOUS L'AVONS REÇUE

Canada

NL 339 (r. 86/09)

National Library of Canada
Bibliothèque nationale du Canada

Canadian Theses Division
Division des thèses canadiennes

Ottawa, Canada
K1A 0N4

67469

PERMISSION TO MICROFILM — AUTORISATION DE MICROFILMER

• Please print or type — Écrire en lettres moulées ou dactylographier

Full Name of Author — Nom complet de l'auteur

Stephen Patrick Goff

Date of Birth — Date de naissance	Country of Birth — Lieu de naissance
17th March 1949	U.K.

Permanent Address — Résidence fixe

Dept. of Geology, University of Alberta

Title of Thesis — Titre de la thèse

The Magmatic and Metamorphic History of the East Arm of the Great Slave Lake, N.W.T.

University — Université

Alberta

Degree for which thesis was presented — Grade pour lequel cette thèse fut présentée

Ph.D.

Year this degree conferred — Année d'obtention de ce grade	Name of Supervisor — Nom du directeur de thèse
1984	C.M. Scarfe

Permission is hereby granted to the NATIONAL LIBRARY OF CANADA to microfilm this thesis and to lend or sell copies of the film.

The author reserves other publication rights, and neither the thesis nor extensive extracts from it may be printed or otherwise reproduced without the author's written permission.

L'autorisation est, par la présente, accordée à la BIBLIOTHÈQUE NATIONALE DU CANADA de microfilmer cette thèse et de prêter ou de vendre des exemplaires du film.

L'auteur se réserve les autres droits de publication; ni la thèse ni de longs extraits de celle-ci ne doivent être imprimés ou autrement reproduits sans l'autorisation écrite de l'auteur.

Date	Signature
24th April 1984	S.P. Goff

THE UNIVERSITY OF ALBERTA

The Magmatic and Metamorphic History of the East Arm, Great Slave Lake, N.W.T.

by

S.P.Goff

A THESIS

SUBMITTED TO THE FACULTY OF GRADUATE STUDIES AND RESEARCH

IN PARTIAL FULFILMENT OF THE REQUIREMENTS FOR THE DEGREE

OF Doctor of Philosophy

Department of Geology

EDMONTON, ALBERTA

Spring 1984

THE UNIVERSITY OF ALBERTA

RELEASE FORM

NAME OF AUTHOR S.P.Goff

TITLE OF THESIS The Magmatic and Metamorphic History of the East Arm, Great Slave Lake, N.W.T.

DEGREE FOR WHICH THESIS WAS PRESENTED Doctor of Philosophy

YEAR THIS DEGREE GRANTED Spring 1984

Permission is hereby granted to THE UNIVERSITY OF ALBERTA LIBRARY to reproduce single copies of this thesis and to lend or sell such copies for private, scholarly or scientific research purposes only.

The author reserves other publication rights, and neither the thesis nor extensive extracts from it may be printed or otherwise reproduced without the author's written permission.

(SIGNED) S.P. Goff

PERMANENT ADDRESS:

Dept. Geology
University of Alberta
Edmonton

DATED 24th April 1984

THE UNIVERSITY OF ALBERTA

FACULTY OF GRADUATE STUDIES AND RESEARCH

The undersigned certify that they have read, and recommend to the Faculty of Graduate Studies and Research, for acceptance, a thesis entitled The Magmatic and Metamorphic History of the East Arm, Great Slave Lake, N.W.T. submitted by S.P.Goff in partial fulfilment of the requirements for the degree of Doctor of Philosophy.

.....
Supervisor

.....

.....

.....

.....
External Examiner

Date 28 March 1984

ABSTRACT

An extensive field mapping, petrographic and geochemical study was made of the major volcanic and intrusive suites associated with the Aphebian and Helikian strata of the East Arm graben, Great Slave Lake. In an attempt to relate magmatism in the graben to possible tectonic controls in the Wopmay orogen (Coronation fold belt), a new tectonic model was proposed for the development of the orogen involving the growth and closure of a back arc basin. This model is based on that of Hoffman (1980a) who sees the East Arm as an aulacogen which was genetically connected to the Wopmay orogen.

Element mobility caused during metamorphism of the volcanics precluded normal petrochemical classification techniques and therefore an extensive review of element mobilities under these conditions was made. A critique and subsequent synthesis of available statistical magmatic and tectonic classification techniques was developed, based on the use of high field strength elements and supplemented by analyses of remnant clinopyroxenes. Variations in trace elements were used to determine the amount and type of low pressure crystal fractionation within each suite and to deduce that almost every suite was produced from a different magma batch. Magmatic $^{87}Sr/^{86}Sr$ ratios and $\delta^{18}O$ compositions were obtained from remnant igneous clinopyroxene and, in conjunction with $^{87}Sr/^{86}Sr$ ratios from Rb/Sr isochrons, indicate a mantle derivation for most magmas.

The relationship between the geochemistry of the volcanics, tectonism, and the metamorphic history is summarized below.

A preliminary cycle of graben development was associated with potassic continental tholeiite (Wilson Island Group). After initial major [illegible] of the Slave craton and alkalic plutonism at about 2200 Ma, a period of crustal extension was associated with several separate pulses of mantle-derived transitional basaltic volcanism (Union Island Group). Contemporaneously, on the western edge of the Slave Craton, a marginal basin was developed, which is now represented by the Akaitcho Group.

Subsequent east-west compression and flexing of the craton produced mantle-derived potassic alkaline mafic volcanism. These magmas produced oversaturated and mildly undersaturated sequences in close association (Sosan Group) and some appear to have been produced from heterogeneous mantle segments (Kahochella Group).

Later subduction, associated with the growth of the Hepburn mass coincided with subalkaline basaltic andesites in the East Arm which have chemical affinities to both arc tholeiites and continental tholeiites that underwent marked crustal contamination (Pearson Formation).

A subsequent period of calc-alkaline plutonism (Compston laccoliths) coincided with the growth of the Great Bear massif and a phase of regional metamorphism which reset Rb/Sr isochrons in the volcanics (1809±30 and 1810±19 Ma).

Metamorphic facies ranged from pumpellyite-actinolite to epidote-amphibolite with increasing depth of burial and characteristic "low-grade" assemblages may have been produced under very-low-grade conditions by metamorphic fluids with Xco_2 values of up to 0.2.

During the Helikian, localized continental tholeiites were produced (Et-Then Group) during major dextral movement on the Macdonald fault system.

ACKNOWLEDGMENTS

Acknowledgements are owed to the following people who, and institutions which have all had a hand in the production of this work: C. M. Scarfe, my supervisor, R. D. Morton, R. St.J Lambert and D. G. W. Smith, my committee, H. Baadsgaard and W. Day, for much help with isotopic analysis, K. Mueulenbachs, for oxygen isotope analyses, J. G. Holland and R. McNutt for XRF analyses, K. Koke and C. Banks for field assistance, P. F. Hoffman, W. Padgham and R. Olson for useful logistic field information, K. Montgomery for much help with computing and typing, the Department of Indian and Northern Affairs (grants OTT 75 - 015 and OSU 76 - 00043), NRC (grant A8394) and the Boreal Institute of the University of Alberta for finance, and finally my fellow graduate students, notably T. Hamilton who persuaded me that the whole thing was worthwhile.

Table of Contents

LIST OF TABLES

LIST OF FIGURES

I. INTRODUCTION

The East Arm of the Great Slave Lake is a 290km long, WSW-ENE trending graben of Proterozoic age, located on the boundary of the Churchill and Slave structural provinces of the Canadian Shield. The basin contains a 16 km thick section of Aphebian and Helikian sediments, the sedimentary succession being similar to that of the Goulburn Basin, which is on the northern margin of the Slave province (Fig. 1-1). Both basins appear to be genetically related to the Coronation fold-belt of the Bear province (Hoffman, 1973; Hoffman *et al.*, 1974).

These three basins are of considerable importance because Hoffman has argued that the whole system represents an example of plate tectonics in the Proterozoic. The East Arm and Goulburn basins are considered to be aulacogens - intracratonic grabens abutting at a high angle into the Coronation Fold belt (Wopmay Orogen) and genetically related to its development. The Wopmay Orogen represents at least one orogenic event and was interpreted more recently by Hoffman (1980a) as having undergone at least one period of spreading and subsequent continental collision. If this model is correct, this structural system represents the oldest example of plate tectonics yet described and was thought worthy of a comprehensive igneous and metamorphic study in addition to the published stratigraphical studies (Hoffman, 1968 and 1969). Unlike the Goulburn Basin, the East Arm contains several interlayered volcanic and

subvolcanic formations which occur throughout the Aphebian and Helikian sequences, sometimes at several contemporaneous volcanic centres.

The main purpose of the present research was to study the variation in chemistry and eruptive style of the volcanics throughout the active life of the East Arm graben and to attempt to relate this to tectonism. Because of the stratigraphical correlation between the East Arm basin and the Wopmay orogen, it appeared to be possible to relate the timing of each volcanic pulse to separate tectonic events within the orogen. These events, in turn, might have acted as triggering mechanisms for the volcanism.

Each of the volcanic centres were mapped on a scale of 1:50,000 to elucidate variations in eruptive style throughout space and time and to add to palaeogeographical reconstructions based on previous sedimentological studies (Hoffman, 1968 and 1969). Because all igneous rocks were metamorphosed, their classification and petrogenesis could not be based primarily on major element compositions which might vary drastically as a result of metamorphism. A literature review of element mobility under various conditions of subsolidus alteration was made to identify the most stable, petrogenetically-useful elements under the observed conditions of metamorphism. These elements were used to determine the original alkalinity of the metamorphosed volcanic rocks (Winchester and Floyd, 1977) and, in as far as their relative concentrations can indicate

the chemistry of the mantle segment from which a mafic magma is derived, they were used to evaluate the tectonic environment of volcanism (Pearce, 1975 and 1980; Pearce and Norry, 1979). An extensive review was made of the various published magmatic and chemical classification schemes for altered volcanic rocks and a "flow-chart" classification scheme was made from the most petrologically valid techniques, in order to make the best available use of the published information. In the present case, field evidence clearly indicated that all igneous activity in the East Arm was ensialic, therefore tectonic classfication diagrams were only used to check each diagram for consistency, and as variation diagrams to compare the stable-element contents of each suite. The main thrust of the petrogenetic study was, therefore, to use variations in high field strength elements (HFSE), firstly, to determine the relative alkalinity of each suite and compare these to modern analogues and, secondly, to look for possible consanguinous relationships between suites and to study their fractional crystallization and/or partial melting history.

Because clinopyroxene is often the only remnant igneous phase in metabasites, several electron microprobe analyses were made of this phase in order to classify, indirectly, the chemical composition of the host magma (Nisbet and Pearce, 1977). This phase was also analyzed isotopically to provide estimates of the initial $^{87}Sr/^{86}Sr$ and $\delta^{18}O$ of the magma.

Because the metamorphic mineral assemblages of the altered volcanics are often complex, a detailed petrographic and chemographic study was made of all suites to determine the extent to which variations in the composition of the metamorphic fluid could cause this complexity.

Finally, an attempt was made to produce Rb/Sr isochrons for the oldest and one of the youngest volcanic formations in the East Arm in order to assess the time period needed for sedimentary accumulation in the graben. Both dates, however, recorded the same metamorphic event of Hudsonian age.

II. GEOLOGICAL HISTORY OF THE EAST ARM AND ITS RELATIONSHIP TO THE WOPMAY OROGEN

A. REGIONAL GEOLOGY AND STRATIGRAPHY OF THE EAST ARM

The regional geology and stratigraphy of the East Arm have been described by Stockwell (1933) and Hoffman (1968, 1969 and 1972) with later detailed 1:50,000 mapping by Hoffman (1977). The Great Slave Supergroup and associated Wilson Island, Union Island and Et-Then groups form a Proterozoic clastic wedge more than 16 km thick in the East Arm of the Great Slave Lake. These sediments and interlayered volcanic rocks have been preserved in a 290 km long tectonic basin on the south margin of the Archean Slave structural province (Fig. 2-1). The Great Slave tectonic basin is assymetrical: the gentle flexure of the north limb forms a sedimentary platform, whereas to the south, a fault-controlled trough occurs which is bounded on the south side by the MacDonald Fault System. These are transcurrent faults forming arcuate splays with sigmoidal connecting faults. Vertical movement on these faults has exposed the Slave basement as small horsts in the southwest of the East Arm (Fig. 2-2). The supracrustal sequence on the platform is thin and dips gently towards the south, but in the basin it thickens considerably and becomes tightly folded along northeast-trending axes within the MacDonald fault system.

Three major supracrustal sequences occur in the East Arm, each separated by an unconformity. These are, in order

of decreasing age, the Wilson Island Group, the Union Island Group plus the Great Slave Supergroup, and the Et-then Group (Fig. 2-2). The Union Island Group and Great Slave supergroup are possibly separated by an unconformity but in recent publications have both been included under the name Great Slave Supergroup (Badham, 1978a; Hoffman, 1981). The supergroup consists of a succession of dolomite and black shale (Union Island Group); fluvial arenites and minor dolomite (Sosan Group); concretionary mudstones (Kahochella Group); stromatolitic limestones and greywackes (Pethei Group) and dolomite breccias and mudstones (Christie Bay Group). The underlying Wilson Island Group comprises fluvial arenites and the overlying Et-Then Group is composed of alluvial fan conglomerate. All groups contain volcanic formations. A brief description of the stratigraphy is given in Fig. 2-3.

These sedimentary rocks were deposited predominantly in fluviatile, coastal and shallow marine environments between approximately 2300 and 1800 Ma. Changes in sedimentary facies and thickness across the basin were controlled by protracted subsidence in the trough: the braided fault splays in the southwest separated the thicker, often distal sediments from the shallower water facies of the platform.

B. DEPOSITIONAL, VOLCANOLOGICAL AND STRUCTURAL HISTORY OF THE EAST ARM AND ITS RELATIONSHIP TO THE GOULBURN AND EPWORTH BASINS

In order to relate volcanism in the East Arm to possible structural controls, a review was made of sedimentological, structural and volcanological data for the East Arm and two other closely-related Proterozoic basins. An attempt was then made to synthesize the data so that each stage in the development of the East Arm could be compared with contemporaneous events in the related basins. This compilation was then used as a framework to assess different and controversial theories on the origin of the East Arm and the related Wopmay orogen and to advance a new structural model for the latter.

The stratigraphy of the East Arm graben shows a marked similarity to that of two other structural basins at the margin of the Slave Province, both containing Aphebian supracrustal sequences. These structures are the Epworth basin (Wopmay orogen, zones 1 and 2) and the Goulburn basin (Kilohigok aulacogen). (See Fig. 2-1). This stratigraphic similarity suggests a genetic relationship between the three structures (Hoffman *et al.*, 1970; Hoffman, 1973) which has led to a plate tectonic interpretation (Hoffman, 1973).

The Great Bear plutonic volcanic belt, the Hepburn plutonic-metamorphic belt and the Epworth thrust belt (Wopmay orogen, zones 4, 3 and 2, Fig. 2-1) are interpreted as an orogen whereas the East-Arm basin is a fault-bounded

trough extending at high angles from this orogen into the adjacent foreland platform (i.e. an aulacogen) (Hoffman *et al.*, 1974; Hoffman, 1980a). The Goulburn basin shows a very similar stratigraphic succession to the East Arm but with very scarce volcanics. The Goulburn basin is interpreted as a branch of a now submerged aulacogen (the Taktu) which was also connected to the Wopmay orogen (Campbell and Cecile, 1981).

Because the volcanology of the East Arm is clearly connected to the structural history of the trough, which is in turn controlled by the development of the Wopmay orogen, a correlation of depositional, volcanological and structural events between the three basins, and the Great Bear belt is outlined below. This compilation was made using the work of Campbell (1980) and Campbell and Cecile (1981) for Goulburn basin stratigraphy; Hoffman (1969) for East Arm sedimentology and paleocurrent data; Hoffman (1973; 1980) for the stratigraphy of the Hepburn and Epworth thrust belts and Hoffman (1981) for the stratigraphical correlation. The correlation between the three sedimentary basins and the Bear Province is dependent upon recent U/Pb isotopic dates from zircons (Van Schmus and Bowring, 1980). These events are outlined below, each lettered stage referring to a diagram in Fig. 2-4. Some correlations are ambiguous, however, and this compilation must be considered as partly interpretive. The zones referred to in this figure are the structural zones of Hoffman (1980a) as shown in Fig. 2-1.

Age dating and the sequence of events in the East Arm will be discussed in Ch. 6

a) Early crustal thinning and trough formation

Within the East Arm, a bimodal basalt-rhyolite sequence gave way to fluvial arkose, distal turbidite and pelite (Wilson Island Group). Paleocurrent studies by Yeo (1976) suggested that a WSW-ENE rift system had already developed in the East Arm, probably following the Hearne Channel to La Loche River faults.

Although the Wilson Island Group is considered to have no equivalent in the other basins (Hoffman, 1981), the lower 4 km of the Akaitcho Group in Zone 3 (Easton, 1980, 1981) consists of continental tholeiites (Ipiutak Formation) overlain by arkosic turbidites. In both areas, no unequivocal basement has been seen. The lack of rhyolites and trough-bedded arkose suggest that a more thinned-crust had evolved in the western Slave. However, a period of intense folding affected the Wilson Island Group, whereas no unconformity has been reported for the Akaitcho Group. If the groups are equivalent, an early period of intense deformation in the West Slave either did not occur or has not been detected (the entire Akaitcho Group is intensely deformed and has now been metamorphosed to amphibolite facies.

b) Crustal extension, alkali plutonism and uplift

Localized alkaline intrusions were intruded on the south and west margins of the Slave craton: alkali gabbros in the East Arm, alkali gabbros and peralkaline granite in Blachford Lake, and nepheline syenite and carbonatite at Big Spruce Lake. These were cut by a regional swarm of mid-Aphebian (Dogrib) diabase dykes (~2100 Ma) and were thought to mark an initial period of rifting caused by hot spot activity (Hoffman, 1980a).

c) Crustal stretching with an incipient ocean basin on the western margin of the Slave craton

Both the western Slave and the East Arm underwent crustal thinning giving a restricted-shallow sea or lacustrine environment (black shale and dolomite). The upper 4 km of the Akaitcho Group in the western Slave margin contains subaqueous basalt-rhyolite complexes: these are continental tholeiites which became oceanic (or marginal-basin) tholeiites with time. Subaqueous basaltic volcanism occurred in the East Arm (Union Island Group). Hoffman (1973) suggested that the walls of the East Arm graben would have been uplifted during this stage. However, the notable lack of silicic detritus in the basin suggests that crustal extension was more likely, with severe rifting in the Western Slave. Lacustrine conditions probably extended across the whole craton.

d) Emergence following rifting

Sediments ranging from craton-derived, fluvio-deltaic sandstones to submarine turbidites were deposited in the western Slave. Fluvial west-flowing braided streams occurred in the basins. Fault movement took place both before and during deposition of the Sosan Group-Hornby Channel Formation in the East Arm (Hoffman *et al.*, 1977; Walker, 1977) at the same time as minor tuff bands were laid down. This stage marked the cessation of rifting with slight uplift of the craton accompanied by vertical movement on the MacDonald fault system.

e) Downwarping of the west margin of the Slave craton

Clastic sedimentation continued in the Goulbourn basin (Campbell and Cecile, 1981) while the West Slave and East Arm subsided producing dolomitic inter-deltaic tidal flats (Sosan Group-Duhamel Formation in the East Arm). The tidal flats passed westward into the black shales of zone 3. These facies are interpreted by Hoffman (1980a) as the shelf and rise, respectively, of a mature continental margin. However, the black shales suggest that a more restricted marginal basin was developed.

Minor basalts and tuff occur in the Jackson Island of the East Arm (Hoffman *et al.*, 1977). These lie on a major transcurrent fault, indicating that fault movement took place in the East Arm during downwarping.

f) Continued downwarping of the west margin and continued flexure of the craton

Black shale extended eastward into zone 2, indicating a further subsidence of the western margin. However, craton-derived, fluvial orthoquartzites which fill all basins indicate the emergence of most of the craton at this time, suggesting an upward flexure as a response to east-west compression. Despite the onset of fluvial sedimentation, the East Arm paradoxically underwent its most profound subsidence to date, with fluvial sedimentation on a submerged platform (Sosan Group-Kluziai Formation) giving way to deltaic and shallow marine siltstones in the trough (Sosan Group-Akaitcho Formation). This indicates spreading of the splayed fault system, some faults of which served as conduits to the several localized volcanic centers.

g) Growth of the Hepburn massif

Peraluminous, hornblende-poor quartz monzonites intruded zone 3 (Hoffman, 1980b). These gave U/Pb zircon ages of 1910 to 1890 Ma (Hoffman, pers. comm., 1981; Van Schmus and Bowring, 1980) and were coeval with the granodiorites which intrude the basement south of zone 3 (~1900 Ma Rb/Sr isochrons, Frith *et al.*, 1977). The Hepburn plutons migrate to the east, becoming smaller, more basic and less deformed with time (Hoffman, 1980 a and b; Hoffman *et al.*, 1980). The Hepburn plutons clearly postdate an important phase of compressive deformation marked by two

regionally kinked, thrust faults in zone 3 (the Okrark and Marceau thrusts). The rising massif shed a thick flysch wedge eastward into a shallow sea, or lake, which is now represented by concretionary mudstones (Kahochella Group in the East Arm). Eastward-migrating plutons cut this flysch wedge and gabbro sills, as much as 200m in thickness, cut the flysch on the boundary of zones 2 and 3. Localized volcanism continued in the East Arm.

h) Mature Hepburn massif

On the basin margins, thin limestones with gypsum casts (possibly sabkhas: Badham and Stanworth, 1977) were overlain by a shallow-marine to supratidal, stromatolitic carbonate platform. Flysch was shed along the axes of the two basins reaching its furthest extent eastwards (Pethei Group in the East Arm). The listric thrust belt in zone 2 was probably initiated at this time because paleocurrent directions in the flysch are precisely axial to tectonic folds (Hoffman, 1980a).

i) Molasse phase

Intertidal red mudstones in the East Arm (Christie Bay Group-Stark Formation), and evaporites and solution breccias in all three basins were overridden by easterly-directed post-tectonic prograding alluvial fans of molasse (Christie Bay Group-Tochatwi and Portage Inlet Formation in the East Arm). As molasse deposition waned, basalt flows were

extruded in the East Arm (Christie Bay Group-Pearson Formation) with very minor, thin flows in the Goulburn basin.

In zone 4, the basement was overlain by fluvial arkose interlayered with basalt and rhyolite ignimbrites. The minimum date of this sequence (1875 Ma), is comparable to the youngest dates for post-tectonic Hepburn plutons (Van Schmus and Bowring, 1980) and therefore it may have been contemporaneous with the volcanism in the basins. This sequence gave way to a K-rich calc-alkali volcanic-plutonic complex (Hildebrand, 1981).

j) Growth of the Great Bear massif

Compression in the East Arm produced at least two N.W.-directed nappes (Hoffman *et al.*, 1977). These were cut by hornblende-quartz diorite laccoliths of calc-alkaline type (Badham, 1981). In the Bear province, "I-type" plutons of a similiar composition to those of the East Arm occurred with ignimbrite sheets, as resurgent calderas. The latter plutons became larger and more silicic with time (Hoffman and McGlynn, 1977; Hoffman, 1980b). These two suites are contemporaneous: the dates are both 1860 ±10 Ma (Hoffman, pers. comm., 1981).

After dextral wrench faulting on the Wopmay fault, this zone was invaded by K-rich leucogranites (~1845 Ma: Hoffman, pers. comm, 1981). Rb/Sr dates in the orogen appear to be reset from 1700-1850 Ma (Hoffman 1981, pers. comm; Easton,

1980) and similiar data for the East Arm laccoliths show a very wide scatter (1750 to 1910 Ma).

k) Transcurrent faulting

The final event in the orogen was the development of hexagonal thrust plates joined by conjugate sets of transcurrent faults.

Dextral transcurrent movement of 60-80 km on the Wilson Island fault plus uplift of the Churchill province shed thick alluvial-fan conglomerates into the East Arm (Et-Then Group). Downfaulting at this time was probably responsible for the present increase in crustal thickness below the East Arm, from 34 to 38 km (Barr, 1971). The MacDonald fault system again acted as the locus for basalt volcanism. Basement horsts were uplifted at this time, exposing the old mylonite belt, and the older strata in the basin.

C. THE DEVELOPMENT OF THE WOPMAY OROGEN

Because the Wopmay orogen appears to be genetically linked to the structural history of the East Arm, a knowledge of the tectonic development of the orogen is essential to understanding the tectonic development of the graben. The model of Hoffman (1980a) will be considered first, and then an alternative model will be proposed for the development of the orogen.

a) The Model of Hoffman

The most comprehensive model so far available for the development of the Wopmay orogen is that of Hoffman (1980a). Two aspects of the model will be considered separately: the nature of initial rifting and the development of the Hepburn and Great Bear arc massifs.

(i) Initial rifting

The East Arm and Goulburn basins are considered to be the failed arms of connected triple-rift systems. These systems developed as successful spreading ridges on their remaining arms with subsequent ocean basin formation and continental collision (Wopmay orogen). The rifts were thought to be generated by mantle plumes. This theory is supported by the alkaline intrusions and the extensive Dogrib diabase injection, but especially by the development of basalts similiar to ocean floor tholeiites in the western margin of the Slave craton (Easton, 1981). However, such compositions can also characterize extensively thinned continental crust which has probably undergone massive sheeted-dyke injection but has not yet generated ocean ridges, (e.g. Afar, Mohr, 1978). Hoffman considers the earliest deposits in the East Arm, the penetratively deformed Wilson Island Group, to be a remmnant of a previous cycle of rifting. However, Badham (1978a, 1979a) considers this to be the initial step in a single cycle. By stressing the incompatibility of early mylonitization of the basement

with the tensional environment of a classic graben, he proposed that the deflection of compression between the Taltson and Slave cratons during stabilization of the Churchill Province produced continuous transcurrent faulting during the deposition of the Great Slave Supergroup. However, the MacDonald fault system clearly postdates the mylonite belt (Hoffman *et al.*, 1977), and there is no evidence of alluvial-fan conglomerate deposition in the pre-Et-Then Group sequences, as one would expect if transcurrent movement were dominant. The marked similarity between the Wilson Island Group and the lower Akaitcho Group suggests that a graben system may have bounded the west and south flanks of the Slave craton before injection of "plume-generated" alkaline intrusions.

(ii) The development of the arc massifs - two collision model

Hoffman's (1980a) model for the development of the Wopmay orogen (see Figs. 2-5 and 2-6) involves two continental collisions and is an elaboration of the single-collision model of Hoffman (1979). The deep water facies on the west margin of the Slave craton (Stage e, Fig. 2-4) is seen as continental rise sedimentation on a mature continental margin and the Great Bear province is considered to have been, at this time, a separate micro-continent further west. The foundering of this

margin was caused by a westerly-dipping oceanic subduction below the Great Bear microcontinent. Collision with this micro-continent resulted in thrusting in zones 3 and 2 (see Fig. 2-1), involving continental rise sediments, and the subsequent intrusion of the Hepburn batholiths (Fig. 2-5).

A period of easterly-dipping subduction then began producing the Great Bear massif and the calc-alkaline laccoliths of the East Arm. This was terminated by a second collision with a second microplate to the west of the Great Bear which caused deformation of the Hepburn plutons, leucogranite intrusion, and finally regional transcurrent fault movement (Fig. 2-6).

There are a number of problems with this model. First, the Hepburn batholiths occur on the underthrust plate. Hoffman explains this by partial delamination of the lithosphere from the underthrust plate (Fig. 2-5) and by two other mechanisms. However, on all post-Eocene continental collisions, calc-alkali volcanics (eg. Turkey-Iran and Zagros) and plutons (eg. Alps) occur on the overriding plate ~150 km from the suture (Sengor and Kidd, 1979; Haynes and McQuillan, 1974; Hsu, 1979). Furthermore, syntectonic magmatism in the underthrust plate is normally sparse and leucogranitic, for example, in the high Himalayas (Hamet and Allegre, 1976) and in the central tin belt of Malaysia (Mitchell, 1981). Clearly, the Hepburn massif was not produced by such

magmatism.

Secondly, it is difficult to explain the lack of proximal flysch which should have been deposited in the Hepburn massif area by a contemporary arc massif, which ought to have been developed on the overriding plate. On the contrary, the Hepburn massif is itself the source of the easterly-directed thick flysch wedge.

Thirdly, the difference in the style of deformation between the Great Bear and the Hepburn massifs is not easily understood, if Hoffman's model is adopted. Finally, it is not easy to explain the lack of a continental suture zone, containing amphibolites and fore-arc sediments between the two massifs.

b) An alternative model

Whereas Hoffman's model for initial rifting explains the data well, his model for the development of the arc-massifs needs to be revised. An alternative model is outlined below.

(i) The development of the arc massifs - marginal basin model

The model proposed here postulates a marginal basin of extensively thinned continental crust or incipient ocean floor development on the western margin of the Slave. This is analogous to the southern Andes where an early Cretaceous back-arc basin appeared (Bruhn *et al.*, 1978). Subsequent orogeny deformed the earliest plutons

and created a back-arc thrust belt while syntectonic plutonism became younger to the east (Dalziel and Elliot, 1973). In the southern Andes, the early arc appears on the outer micro-continent; however, because rifted continental margins are likely to have an irregular outline (Dewey and Burke, 1974), a subsequently-formed marginal basin may be irregularly shaped, causing a linear belt of plutons to intrude part of the marginal basin. On the westerly margin of the Slave craton, a notable re-entrant is seen between zones 3 and 4 and the Hepburn plutons occur in both the rifted zone and the craton. The model is illustrated in Fig. 2-7 and is outlined below. Each numbered paragraph refers to a particular stage in the tectonic development of the orogen, which is depicted in Fig. 2-7. Each corresponding stage in the stratigraphical development is noted by an index letter, in brackets, which refers to a relevent illustration in Fig. 2-4.

1. Continental extension and rifting.

An irregular marginal basin was formed with the development of ocean-floor tholeiitic volcanism. More evolved basalts are developed in the East Arm (Stage c).

This stage of volcanism was followed by a period of east-west compression which was associated with the initiation of easterly-directed subduction. The back-arc shelf first flexed (Stage e) and then

buckled and uplifted (Stage f) causing the keystone-like fault blocks in the East Arm to spread apart, deepening the basin and producing progressively more volcanism.

2. Oceanic subduction and the growth of the Hepburn arc massif.

The thinned marginal basin was an unstable platform for erecting an arc massif and the massif was deformed as the basin closed. Contemporaneous thrusting, thrust-kinking, pluton injection and uplift took place (Stage g). The overall lateral shrinkage caused plutons to migrate to the east and become less deformed with time. The onset of subduction and the deformation of the marginal basin transformed the east-west compressive strain from the craton interior to it's margin. This caused the craton to subside from it's upwarped state and caused the splayed faults in the East Arm to close, leading to the cessation of volcanism. Thus, back-arc folding in zone 2 was associated with less abundant, deeper water volcanism in the East Arm (Stage g). Back-arc thrusting was not associated with volcanism (Stage h).

3. Closure of the marginal basin.

The plastic deformation in zone 3 was completed and molasse was shed eastward. The closure of the

basin effectively isolated the MacDonald fault system from transferring stress from the subduction trench to the lithosphere beneath the East Arm. Magmatism was now related to subduction rather than to directly tapping the asthenosphere. Subalkaline basalts appear in the Arm and for the first time in the Kilohigok basin (Stage i). The deformation style changed in the East Arm: high-angle faulting gave way to N.E.-directed gravity slides, each separated by low-angle thrust faults.

4. The growth of the Great Bear Arc Massif.

Continued easterly subduction produced a calc-alkali volcanic massif (Stage j). Thermal uplift of the Great Bear massif, while the Hepburn massif cooled, may have exploited an old fault boundary of the marginal basin and produced the Wopmay fault.

The change in focus of the arc volcanism may have been produced by a sudden increase in the angle of subduction as a response to the final closure of the marginal basin. The steepening of a subduction zone during the life of a single orogen has been advanced as a model for the Miocene of the western U.S.A. (Davis, 1980).

5. Continental collision and shear melting.

Collision of the Great Bear massif with the continent to the west produced shear melting along the Wopmay fault. This Hudsonian thermal event reset Rb/Sr isotopes, was terminated by transcurrent faulting, and appears to have predated the fanglomerate deposition by ~50 Ma. The suture zone is now covered by Phanerozoic sediments.

This model answers the problems of Hoffman's theory but has some drawbacks. First, the initial rifting to form the marginal basin showed no thick outpouring of felsic ignimbrite, as was the case in the southern Andes. This lack of felsic volcanism may have been caused by the much thinner crust in the Slave province. Secondly, the initial flysch from the Hepburn shows only plutonic and metamorphic fragments and no evidence of an eroded volcanic carapace, which should have developed. However, the overall composition of the flysch wedge is even less adequately explained by Hoffman's model (see above). The present model gives a more reasonable explanation of the more important elements in the Wopmay orogen, notably the composition and nature of deformation of the Hepburn batholith, and the absence of a continental suture zone. It also calls for only one phase of crustal subduction.

D. CONCLUSION

The sediments of the Goulburn basin, East Arm and Epworth basin all indicate a similiar connected history but show progressively deeper water conditions and more rifting.

The western edge of the Great Slave craton was thinned to form a marginal basin and areas of the craton, already weakened by Archean shearing, fractured in response. Only limited rifting took place before east-west compression buckled the craton causing splayed faults in the East Arm to tap the asthenosphere by pressure-release melting.

The onset of subduction produced an arc massif along with contemporaneous deformation in the marginal basin, but very little compressive stress was transferred to the East Arm transcurrent faults. This resulted in limited movement of these faults and, therefore, in less volcanism. With closure of the basin, movement of these faults ceased. Volcanism in the East Arm now became subduction-related and volcanism also appeared in the Goulburn basin. Further calc-alkali plutonism was followed by continental collision and over 70 km of displacement on the transcurrent faults.

Unlike the Goulburn basin, the East Arm was more favorably oriented and closer to the orogen to react to compressive stress. East-west compression from the orogen would have caused dilation of the splayed fault system of the East Arm, whereas the faults of the Goulburn basin, which has a N-S orientation, would have closed. This may explain the lack of volcanism in the Goulburn basin. The

foundered, E-W oriented coastal margin which connects the Goulburn basin to the orogen (the "Taktu aulacogen" of Campbell and Cecile, 1981) may have had a similar history to the East Arm.

The volcanism in the East Arm can therefore be related to the tectonic controls in the Wopmay orogen. A new model for the development of this orogen has been advanced which, by invoking the occurrence of a marginal basin, explains the structural history of the Hepburn batholith without invoking a second phase of crustal subduction.

III. FIELD RELATIONSHIPS OF VOLCANIC AND INTRUSIVE ROCKS

A total of 18 weeks of field work were spent mapping and measuring sections in almost all volcanic localities in the East Arm. The scales used ranged from 1:67,000 up to 1:35,000 for detailed work. The objectives were to detail the facies variations within the main volcanic sequences in order to elucidate the environment and style of eruption.

The six major volcanic sequences are described below in stratigraphical order. Fig. 3-1 shows the location and approximate outcrop pattern and Fig. 3-2 shows the relative stratigraphical position of the volcanic suites.

A. WILSON ISLAND GROUP VOLCANISM (WIGM, WIGF, and UWIGM)

The basal part of the Wilson Island Group contains the oldest sequence of volcanic rocks in the East Arm (Fig. 3-3). A bimodal basal unit of over 1400 m of amygdaloidal basalt (WIGM) and red to purple rhyolite (WIGF) forms an individual massive flow unit, (3 to 30 m thick) interbedded with chlorite-muscovite schists, fluvial trough-cross-bedded quartzites and conglomerates. The quartzites display scour structures, ripple marks and basalt intraclasts and are similiar to the following thick fluvial sequence. Local flows of amygdaloidal and plagioclase porphyritic basalt (UWIGM) occur in the Pekanatui Point area (Fig. 3-23). The volcanics have been metamorphosed to epidote-amphibolite facies (the highest grade observed in the East Arm) and are

cut by a penetrative cleavage. Neither of these phenomena have been seen in the later sequences.

B. ALKALI GABBRO INTRUSIONS

An important suite of differentiated alkaline intrusions, which were not included in the present study, occur within the area (Fig. 2-4b). The Blachford Lake alkaline to peralkaline complex, on the north shore of the East Arm, northwest of Seton Island, consists of olivine gabbro-norite to leucodiorite plutons, with later plugs of syenite and of predominantly riebeckite granite (Davidson, 1978; Badham, 1979b). In addition, on North Simpson Island, and associated islands is an east-west trending alkali diorite to monzodiorite dyke (see Fig. 3-4) (Burwash and Cavell, 1978). The petrology of this dyke has also been described by Badham (1979b) who reported a greater number of alkali-rich syenite analyses.

C. MID APHEBIAN (DOGRIB) DIABASE DYKES (MADM)

These dykes commonly show trends of 035° to 070°, thicknesses of 10-30 m, and traceable lengths of only 300 m. Notable exceptions exist, and most samples were taken from a vertically dipping dyke on North Simpson Island, which was 100 to 225 m in thickness (Fig. 3-4). These dykes cut both the Archean basement and the alkali-gabbro intrusions and

are unconformably overlain by the Union Island Group (Hoffman *et al.*, 1977) and by Sosan Group sediments (Fig. 3-4). They may be commonly sheared, displaying marginal carbonate veins. Variation in alteration and trend has caused Badham (1979a) to suggest two periods of early diabase injection. However, the freshest dykes observed invariably show a 130° trend which was included by Reinhardt (1972) in the later, Mackenzie diabase swarm. The latter is a Helikian phase of intrusion of regional extent.

D. UNION ISLAND GROUP VOLCANICS AND INTRUSIONS

Volcanics are observed in three closely related localities on the south side of the East Arm (Fig. 3-5). Two distinct ages of volcanism are seen. The early massive dolomite and black slate is overlain by a subaqueous basaltic sequence on the mainland. A change in depositional conditions, from an anaerobic to an aerobic environment, is indicated by an upper banded, possibly stromatolitic dolomite and red shale. This later dolomite clearly underlies a thicker basaltic flow package, 10 km west of the mainland flows.

The sketched stratigraphical section of Hoffman *et al.* (Fig. 2, 1977)(see Fig. 3-6) implies a similiar age for the two flow packages. However, the mainland section is clearly overlain by the banded dolomite (not shown in this sketch) and is itself interlayered with black slate and thin

greywacke beds (Fig. 3-7). This indicates a change to a less restricted shallow sea before before extrusion of the thicker volcanic flows. Furthermore, the latter 1000 m section of basalts, northeast of Union Island, disappears 2 km south (Fig. 3-5) leaving Sosan Group sediments resting directly on the banded dolomite. Clearly, pre-Sosan Group block faulting is evident but local 40 m thick quartz-pebble conglomerates and black-slate intraclasts in the banded dolomite, plus the very thick, localized wedge of volcanics, suggests that faulting may have been contemporaneous with volcanism and probably controlled the sedimentological changes.

a) Early Mainland Basalts (UIG1M)

A 300 m thick massive to pillowed basalt sequence divides into two distal flow-units which thin towards the southwest but produce overlying pillow-talus deposits. The lava-flows have massive bases but the upper halves of the flows are pillowed. These pass upwards into broken pillow breccias with angular pillow fragments, as much as 10 cm across. The groundmass consists of coarse lobate ash particles of chilled, amygdaloidal basalt set in finer, chloritized vitroclastic ash. A finer, chloritic ash matrix may be largely replaced by carbonate.

These breccias grade upwards into massive lapilli tuffs. A related group of basalts occurs on an island 12 km southwest (Fig. 3-5), where a 200 m thick pillowed sequence

overlies pillow breccias.

b) Late Union Island area Basalts (UIG2M)

This sequence is approximately 1000 m thick. It is composed entirely of pillows 0.3 to 1 m across, with concentric rings of amygdales and 3 cm chloritized chilled selvages. Some are elongated into 10 m long lava tubes, a few of which were drained and now display a geopetal infilling of dolomite, ankerite and quartz. A matrix of a similiar composition fills interpillow spaces. Only minor pillow-breccia is seen.

c) Union Island Group Diabase (UIGDM)

At least two plagioclase-phyric, glomeroporphyritic diabase sills, up to 200 m thick, intrude the mainland sequence below UIG1M. They have chilled margins and columnar jointing. Their age relationship to the lava suites is unknown, but chemical similarity with UIG1M suggests that they may represent a related sub-volcanic magma-pulse.

d) Summary of Union Island Group Volcanism

The early volcanic suite produced a typical pillow breccia sequence from at least two southerly directed flows, possibly formed by wave action in shallow-water (see Kahochella Group discussion). The bedded sequence may represent ash fall or shallow water reworking. The later, thicker sequence was deposited in a fault-guided trough,

which was rapidly subsiding in deeper water and did not produce pillow breccias.

E. SOSAN GROUP AND KAHOCHELLA GROUP VOLCANISM

These groups contain the most widespread and texturally varied volcanics. The volcanic suites were originally included in the Kahochella "Formation" (Stockwell, 1936) then referred to as the Seton Formation (Hoffman, 1968).

Volcanism was most abundant in three main localities, each of which was studied in detail (Taltheilei Narrows, Seton Island and Pekanatui Point). Each area represents a slightly different paleogeography and style of volcanism, indicating an increase in depth of water to the south and west. Taltheilei Narrows was tectonically active during deposition of both groups. These centers are described below according to stratigraphical sequence. The composite stratigraphy is illustrated in Fig. 3-8.

a) Sosan Group Volcanism (SOGTNM, SOGTNF, SOGSI1M, SOGSI2M, SOGSI3I and SOGSIF)

(i) Taltheilei Narrows: description

This area marks a fault line on the northern platform of the graben which first underwent subsidence and volcanism during this period. A gently-dipping southeasterly directed sequence, now largely covered by water, occurs southeast of the narrows (Fig. 3-9) and a

felsic volcanic center occurs further west (Fig. 3-10).

In both areas, massive amygdaloidal flow packages 70 to 130 m thick (SOGTNM) occur, and in one place pass laterally into pillow basalt and pillow breccia. Deepening water is evidenced by localized, bedded lapilli-tuffs to agglomerates (pyroclastic flows).

This sequence is overstepped by a felsic volcanic center (SOGTNF) which lies directly on the basement (Fig. 3-10). Rhyolitic domes 0.5 to 2 km across are draped by over 200m of unbedded, white to purple, felsic ash tuff composed of crystal and lithic fragments. At the margins of the domes, a mantle of agglomerate occurs with well rounded rhyolite fragments 20 to 30 cm in size, set in a felsic matrix. Dips from 0° to 30° are seen in bedded tuffs, and slump structures and cross beds occur locally.

In thin section (Fig. 3-11) these tuffs display angular to sub-rounded lithic fragments in a hematite-stained matrix of crushed crystals and ash. Angular shards of (now chloritized) basalt scoria are a minor component but may be dominant in thin beds near the base of the sequence. Welding was observed in the groundmass of one ash tuff which was strongly banded: discontinuous shards were observed moulded around quartz and feldspar megacrysts (Fig. 3-12).

(ii) Taltheilei Narrows: interpretation

The distinct bedding, cross-bedding, slumping and lack of welding indicates shallow subaqueous deposition, probably of an ash flow around a growing rhyolitic dome. Several examples of the subaqueous welding of felsic tuffs has been described (see Lowman and Bloxham, 1981), welding being possible at temperatures as low as 700 to 350 °C (Maury and Szeky-Fux, 1975). The exact mechanism of eruption is speculative because modern examples of submarine felsic flows are unknown. Pichler (1965) presented a model for the development of such flows, based on Ponza, Italy. The model involves the in-situ formation of a talus deposit by the subaqueous spallation of a rhyolite dome, producing proximal breccias and distal, unwelded ash tuffs. This model has been criticized by Lajoie (1979) who pointed out that one would expect only a small volume of clasts to be produced by the subaqueous extrusion of rhyolite, owing to the thick chilled margin that would be developed. This mechanism would also not explain the rounded nature of the clasts in the conglomerate blanket. The volcanic complex at Taltheilei Narrows was more likely produced by a shallow, subaqueous, phreatomagmatic eruption. The eruption produced an ash flow containing large blocks which were abraded and rounded in a gas-solid fluidized system within the vent. Almost certainly, some of the ash was erupted subaerially, but deposited subaqueously.

After a period of tuff accumulation, the proximal agglomerates were intruded by rhyolite domes.

(iii) Seton and West Keith Islands: description

Forty km southwest of Taltheilei Narrows an easterly dipping, dextrally-faulted sequence occurs of massive flows and volcaniclastics occurs. Stratigraphical columns were produced for part of the section (on the north shore of Seton Island) by Olade and Morton (1972) and Hoffman (1972). In the present study, the whole area was mapped in detail in order to document the style of eruption more fully (Fig. 3-13). Volcaniclastics and lava-flows form 40% of a 2500 m section of shallow marine siltstone to sandstone which is equivalent to the upper Kluziai and the Akaitcho Formations. Each major lithology is described below and illustrated in Fig. 3-8.

1. Flows and high level intrusions (SOGSI1M, SOGSI2M, SOGSI3I and SOGSIF)

Despite the metamorphism of these lavas, the original textures are preserved well enough to estimate the original plagioclase content and roughly classify them into mafic or intermediate types. As a result, two phases of volcanism were recognised which indicated a notable change in the

petrology and style of eruption: an early bimodal suite was followed by the intermittent extrusion of mafic to more intermediate lavas.

The early mafic flows (SOGSI1M) are massive, grey-green to grey-blue in color, with amygdaloidal flow tops, and form flow-packages 20 and 100 m thick. A later group of thin basalt flows (SOGSI2M), occurs just below a suite of more siliceous volcanics (SOGSI3I), which reaches 200 m in thickness. SOGSI3I is composed of grey-purple to grey-brown intermediate lavas with lenticular, pink amygdaloidal trachyte domes. The latter reach 700 m by 120 m in thickness in the final flow package on Keith Island. The later flows show flow-top and flow-foot breccias.

High-level felsic volcanism is represented by a series of quartz-feldspar porphyritic laccolithic plugs (SOGSIF). These are granular-textured, have chilled margins and are emplaced 100 m above the lower level basalts. They range from 1 to 3 km in length and have length to thickness ratios of 10:1. One laccolith is seen intruding the Akaitcho River Formation 10 km north of Seton Island (SE117). These intrusions are correlated with the felsic dome at Taltheilei Narrows (Hoffman *et al.*, 1977) although their depth of intrusion is clearly greater.

2. Heterogeneous breccia to agglomerate

A prominent wedge-shaped pyroclastic unit, reaching 200 m in thickness, was mapped in detail. It's thickness is greatest in the southwest of Seton Island, where it is intruded by the felsic plugs which are veined and brecciated and which clearly shed detritus into the unit. The wedge thins northward where it is clearly mappable as three lenticular units (Fig. 3-8 and 3-13).

a. Massive agglomerate to lapilli tuff.

This is a discontinuous wedge-shaped unit, 35 m thick, just above the rhyolite domes. Sub-angular blocks and rounded lapilli of basalt are set in a groundmass of flattened unwelded amygdaloidal scoria and a silt matrix. Distal parts of the wedge show an increase of felsic and red sandstone fragments with slumps and ripples in the silty matrix.

b. Bedded agglomerate to lapilli tuff.

The bed is over 30 m thick, poorly sorted and with 5-20 cm bands of alternating fine to coarse lapilli tuff. It is characterized by 1 to 4 cm angular and rounded rhyolite lapilli, with albite and microcline phenocrysts and an equal volume of rounded lapilli of plagioclase-phyric

basalt and intermediate rocks. Only the bedded nature and the higher mafic content distinguishes the unit from the overlying breccia.

c. Heterogenous breccia to agglomerate.

This is the dominant lithology. The unit thins to a thickness of 40 m on the north shore and shows discontinuous internal stratigraphy. Lenticular units of unsorted and unbedded breccia (Fig. 3-14) may each be over 5 m thick, but thin rapidly to 20 cm thick beds which alternate with banded lapilli tuff of a similiar composition.

Rounded to angular blocks of plagioclase-porphyritic rhyolite occur, as much as 20 cm across. They are lithologically similiar to the felsic plugs but may show fractured, chilled margins. Basalt fragments are minor. Smaller lapilli are siltstone, sandstone and fractured and deformed chloritized scoria. The fine lapilli and ash fraction indicates a heterolithic source : basalt, intermediate lavas, rhyolite and siltstone plus fractured albite and quartz crystals (Fig. 3-15). No welding is seen. The matrix is commonly sericite and quartz, but with varying

amounts of carbonate and with more chlorite, albite and K feldspar in the lower part of the sequence. Other, thinner, wedge-shaped units occur above the main phase.

d. Heterogeneous, bedded ash to lapilli tuffs.

These are well-bedded, well-sorted, beds, as much as 2 m in thickness. They are composed of dominantly felsic volcanic detritus with a siltstone matrix and occur interleaved with the siltstone above the agglomerates. A somewhat similar agglomerate to lapilli sequence occurs at the base of the succession on Seton Island, indicating an earlier phase of felsic volcanism.

3. Homogeneous agglomerate to lapilli tuff

This unit is a lateral extension of the intermediate lavas on Keith Island. It is unwelded, poorly-graded and composed of the same intermediate chilled lava fragments with a chlorite-plagioclase matrix.

(iv) Seton and West Keith Islands: interpretation

The felsic tuffs show a heterogenous composition, lack of welding, rounded grains and are interlayered with deltaic to marine siltstones. The tuffs are clearly subaqueous and reworked and probably largely epiclastic (Fisher, 1966). However, the variable "igneous" matrix

and the chilling and rounding of large blocks in the agglomerate suggest fluidization in a phreatomagmatic eruption. Therefore, as the water level deepened after initial mafic volcanism, felsic lava injection led to updoming, the production of a proximal subaqueous agglomerate edifice in the south of the island, with reworking of subaqueous flows on the (northern) flank. Explosive disaggregation of previous lithologies led to a progressive increase in the degree of felsic detritus. Later intermediate volcanism was more quiescent, followed a progressive coarsening of the clastic detritus, and probably represented the subaqueous flanks of a localized subaerial to shallow-subaqueous volcanic cone.

b) Kahochella Group Volcanism (KAGPPM, KAGPPF and KAGTNM)

Deeper water, marine conditions occurred throughout the arm during the deposition of this group. The Seton Island center became inactive and breccia pipes became active in the Maclean Bay area, where they cut the highest Kahochella Group formations. Volcanism continued on the platform in the Taltheilei narrows area.

(i) Taltheilei Narrows: description

Volcanism is exclusively basaltic in type and is centered on a linear array of volcanic necks, now marked

by breccia pipes (Fig. 3-9). The main lithologies are described below.

1. Vent breccias

At least eight cylindrical pipes from 15 m to 500 m in diameter cut all lithologies up to the McLeod Bay Formation.

This is a massive, unsorted, coarse lapilli tuff to breccia composed of 40% pale green, ovoid basalt lapilli (2-15 cm in diameter) and 10% of angular to sub-rounded blocks of porphyritic rhyolite with chilled margins. The size of resistant, angular blocks of porphyritic basalt, disrupted reworked tuffs and Sosan to Kahochella Group sediments may reach 30 cm. Minor rounded inclusions of Archean basement granodiorite and muscovite-pegmatite also occur. 50% of the breccia is fine grained volcanic ash and ash-sized vitroclastic scoria. The latter is angular to subrounded and has an amygdaloidal texture (Fig. 3-16). No distortion or welding is seen. The matrix is fine-grained quartz and feldspar with varying amounts of carbonate.

2. Massive lapilli tuffs to agglomerates

On the flanks of the four central breccia pipes are remnants of massive, wedge-shaped units, 10-50 m

thick, similiar to those that occur near the close of Akaitcho Group sedimentation. These show an identical petrography and range of inclusions to the breccia pipes, but with fewer angular fragments. Fine lapilli show varying ratios of lithic to vitric fragments with lithic being dominant (> 70%) possibly indicating a greater degree of reworking than the breccias.

Near the tuff pipes, the agglomerates show a similiar massive texture (Fig. 3-17) and display a partly erosive base: the bed rests on mudstones showing soft-sediment slumping and containing partially rotated and disrupted ironstone intraclasts. The basal few meters also show a higher concentration of large breccia fragments.

In some more distal units a persistent bedding occurs and the wedge is divided into 2 m thick bands of alternating beds of coarse and fine lapilli tuff. Both types of bed show poor sorting and no grading (Fig. 3-18).

3. Thin-bedded lapilli to ash tuff

A massive agglomerate forms the basal unit of a 140 m bedded volcanic sequence which mantles two prominent breccia pipes. This sequence is dominated by thin, parallel-bedded, well-sorted lapilli to ash-tuffs. These form alternating coarse and fine

bands and normally well-graded units, 1 to 5 m in thickness (Fig. 3-19). The tuff sequences are interlayered with an equal thickness of rippled siltstones.

On the flanks of the bedded sequence, thicker lapilli tuffs may show low-angle, unidirectional cross-bedding (Fig. 3-20). These tuffs contain only small basalt lapilli (< 1 cm) with interstitial ash forming a grain supported network. The coarse ash is composed of sub-angular to rounded, fine-grained mafic and felsic lithic fragments. The remainder is chloritized, vitroclastic, angular granules. The matrix forms 50% of the rock and may be chloritic or largely winnowed and replaced by carbonate and quartz. There is a rough correlation between the increase of lithic fragments, the greater rounding of fragments and the increased replacement of groundmass. There is a wide variation in the ratio of lithic to vitric fragments (Figs. 3-21 and 3-22).

4. Lava flows (KAGTNM)

Massive, amygdaloidal, wedge-shaped flows occur in the upper part of the bedded sequence (KAGTNM). These flow packages thicken rapidly and coalesce just south of a prominent tuff cone. Three km from this center, the flows become pillowed (Fig. 3-9) with individual pillows reaching 1 m, in size. Two km further south, the upper surface becomes a broken

pillow breccia. Sub-angular pale-green pillow fragments of varying vesicularity are set in a dark green, lapilli tuff matrix. The pillow fragments locally form as much as 50 % of the rock, with the groundmass composed of a dark green to purple unstratified, unsorted mass of chloritized, unwelded glass shards and granules.

(ii) Taltheilei Narrows: interpretation

These lithologies suggest a subaqueous mode of deposition for the entire pyroclastic sequence. This is indicated by the notable lack of welding, and the common presence of undeformed vitroclastic ash and of interlayered siltstones. A lithological gradation occurs between the vent breccias, the proximal poorly sorted massive agglomerates and the distal, crudely bedded agglomerates, and all three units contain abraded, preexisting lithologies and much vesicular scoria. This sequence fits a model of an explosive phreatomagmatic eruption producing a subaqueous pyroclastic flow which developed a laminar flow regime. This is a feasible model because modern, laharic flows are often seen passing downslope into bedded varieties (McBirney and Williams, 1979). Within thicker lapilli tuffs, bed-load transport is also indicated by cross-bedding. Such textures may indicate low-density base-surge deposits which can occur on the distal edges of submarine flows (Wright *et al.*, 1980) although extensive dune bedding

is not seen. Alternatively, this feature may represent wave action on an emergent volcanic edifice.

The equant, subangular ash fragments are well-sorted and the thin bedded-nature of the ash to lapilli tuffs are typical of subaqueous ash falls (Walker and Croasdale, 1971). The notable lack of accretionary lapilli and the presence of rounding and winnowing was probably caused by subaqueous reworking.

The emergent volcanic centre was capped by very shallow subaqueous or possibly subaerial, lava-flows, which flowed into the sea and were disaggregated by wave action. This produced every stage in the characteristic autoclastic sequence of massive lavas to pillow-talus deposits (Carlisle, 1963). Production of pillow breccias in this way has been observed by Moore *et al.* (1973), although these breccias are normally formed from highly channelized or pahoehoe flows. Subaqueous pyroclastic tuff rings are commonly abraded and reworked, unless they are preserved by a lava capping (Ayres, 1977).

(ii) Pekanatui Point: description

This section occurs 30 km south of Talthei Narrows (Fig. 3-23). Because it is included in two northerly directed thrust slices, the sequence probably originated 10 km farther southeast, where the tuff pipes of McLean Bay would have acted as lava conduits.

Two 500 m thick sequences of pillow talus deposits (KAGPPM) occur. The youngest displays separate flow units 25 to 100 m thick, which show all or part of a standard, fining-upward, autoclastic pillow-talus sequence (pillow lava, circular whole-pillow breccia, broken-pillow breccia, see Fig. 3-24). Each of these stages may be as much as 30 km thick, with repeated injection suggested by lava-flows overlying sparse lapilli tuff.

The matrix of the pillow talus deposits is a grain-supported network of two different fragment types. Quenched-basalt lapilli to ash occur with a vitric suite of cuspate shards and vesicular granules of scoria which is now chloritized (Fig. 3-25). Although welding is not seen in the vitric fragments, some flattening of the vesicules occurs. The lower sequence shows thinner flows with less well-defined units which display rapid lateral facies changes. During deposition of the McLeod Bay Formation, muscovite-bearing rhyolite domes, over 2 km in length, intruded the volcanics at sufficient depth to preclude any extrusive equivalent.

(iv) Pekanatui Point: interpretation

This thick sequence was entirely extruded as a fissure eruption under deep-water conditions. Thus, vitroclastic talus deposits were formed as a result of thermal shock during the rapid quenching of basalt in water (Carlisle, 1963) rather than by wave action.

c) Jackson Gabbro (JAGPPM and JAGTNM)

This is a suite of diabase dykes (up to 1 km in length) and rarer plug-like intrusions (up to 3 km across) which cut both the Sosan and Kahochella group strata (Figs. 3-10 and 3-23). These were sampled in both the Pekanatui Point and the Taltheilei Narrows area (JAGPPM and JAGTNM, respectively).

Within the Taltheilei Narrows felsic center (Fig. 3-10) a differentiated gabbro to diorite plug indicates a much deeper level of intrusion than the Sosan Group lavas which it cuts. This indicates that the Jackson Gabbro intrusions are probably all of Kahochella Group age.

d) Summary of Sosan and Kahochella Group Volcanism

The field relationships and lithologies are outlined in Fig. 3-26. As the basin subsided and fluvial gave way to marine conditions, bimodal volcanism took place in shallow water, causing the suppression of subaerial (but water-lain) ash in favor of a more violent phreatomagmatic eruption in deeper water. Volcanic cones were built in both areas.

As the basin subsided, subaqueous basaltic tuff rings were produced and eroded on the platform. The tuff rings were preserved from erosion only where wedge-shaped flows were present. Some of these rings were over 6 km across. Thicker basalt flows were produced from fissure eruptions in the deep water of the basin. The volcanic stratigraphy is therefore remarkably sensitive to the tectonic picture

produced from sedimentary isopachs.

F. PEARSON FORMATION (PEM)

This formation (PEM) consists of 200 m of subaerial basalt flows each commonly 2 to 4 m in thickness, but extending up to 20 m in some cases (Fig. 3-27). The flows which exhibit sporadic hematite staining, are uniformly amygdaloidal, have weathered flow-tops and chilled flow-bases, and display flow-top and flow-foot breccias. Locally, they are columnar jointed. They are interlayered with red shales and brown siltstones which display ripple marks, dessication cracks and scour structures. In places, there are very thin lithic ash layers. The Pearson Formation has a comparatively large outcrop area and may have spread south of the Macdonald fault system to an unknown extent.

G. QUARTZ DIORITE LACCOLITHS

A group of hornblende to biotite quartz diorite laccoliths, each up to 20 km long, outcrop over a distance of 220 km along the graben. These are calcalkaline and chemically resemble the plutons of the Great Bear batholith; however no obvious chemical trends are seen along the graben (Badham, 1978c; 1981) giving no evidence as to the polarity of the subduction zone which probably caused them.

H. ET-THEN GROUP BASALTS (ETGM)

On a peninsula next to the Macdonald fault system, as much as 1100 m of massive, amygdaloidal basalts are interdigitated with wedges of cross-bedded, alluvial fan conglomerate of the Preble Formation (Fig. 3-28). The conglomerate wedges are thickest in the lowest part of the unit and rapidly thin to the northwest. Some of the sandstones are baked by the overlying lava flows.

Flows are from 2 to 40 m in thickness, but average 4 m, and display an irregular hematite stain. Pipe and sheet amygdales (now filled with calcite, chlorite and microcline), each up to 20 cm long, occur respectively in flow-foot and flow-top clusters. The oldest flows are glomeroporphyritic with plagioclase phenocrysts up to 1 cm in size. The youngest flows locally display flow-top brecciation and contain mudstone and sandstone fragments up to 30 cm across. The environment is clearly subaerial: the baking, hematite staining and, particularly, the pipe and sheet amygdales being notable characteristic (Ayres, 1977).

The Preble Formation was deposited next to an active fault system. Volcanism took place during active subsidence on the Macdonald fault system as indicated by the great stratigraphical thickness of the lavas, the arcuate nature of their bedding and the rapid thinning of the sequence to the northwest. The lava thus became ponded and limited in outcrop.

A similiar, localized basalt sequence occurs in the Murky Formation on the the south side of Preble Island (Hoffman, 1977).

IV. PETROGRAPHY OF THE LAVAS AND INTRUSIVE ROCKS

The volcanic suites of the East Arm are subdivided according to stratigraphic position, location, and composition. They have also undergone differing grades and degrees of metamorphism. To avoid excessive repetition, the detailed petrography is presented in Table 4-1. This table includes only the original igneous mineralogy. Optical data are given for the remnant phases and percentages are estimated where the original texture has survived metamorphism. Details of the alteration mineralogy are given in Tables 4-2, 4-3 and 4-4.

A. THE WILSON ISLAND GROUP

The sequence on Wilson Island has been metamorphosed to epidote-amphibolite facies and represents the highest grade of metamorphism seen in the East Arm. The rocks also preserve a unique penetrative deformation: flattening and shearing is indicated by granulated blastophenocrysts with quartz-filled pressure shadows (Fig. 4-5); deformed amygdules, and flattened, sinuous groundmass quartz veins.

a) Basalts (WIGM)

The mafic lavas are dominantly blasto-porphyritic but contain rarer medium-grained blasto-ophitic bands. The former display recrystallized plagioclase with Carlsbad twins and embayed, recrystallized margins. These are now completely albitized but may retain zones of hornblende and

biotite inclusions (Fig. 4-1) and contain granular clinozoisite (Fig. 4-2).

The completely recrystallized schistose groundmass contains aggregates of blue-green actinolitic hornblende, dark brown biotite and accessory epidote, representing altered clinopyroxene (Fig. 4-3). The best schistosity is displayed in the finest groundmass; the mafic minerals being interlayed with clear, granoblastic albite. The groundmass also contains clusters of granular sphene. The coarser grained blasto-ophitic rocks probably represent diabase and may preserve a lower-temperature, partial greenschist-facies metamorphism (remnant labradorite plus chlorite and carbonate). Some samples with a colour index of 70-90 may represent tuffs. The limited mobility of Fe during metamorphism is suggested by the occurrence of clinozoisite in plagioclase and epidote in the mafic aggregates.

Rare intermediate lavas occur which show a colour index of less than 35 and as much as 35% biotite with minor K-feldspar (Fig. 4-4). The hornblende to biotite ratios show extreme variation in the few intermediate samples found.

b) Rhyolites (WIGF)

These are blastoporphyritic and display up to three euhedral and subhedral blastophenocrysts. Orthoclase occasionally displays a granophyric margin and perthitic replacement, plagioclase is pseudomorphed by albite with minor clinozoisite inclusions and quartz, which is rare, is

normally corroded. The granoblastic, hematite-stained groundmass is composed of K-feldspar (or sericite), untwinned albite and quartz, and accessory epidote (Fig. 4-5).

c) **Upper-Wilson Island Group basalts (UWIGM)**

The mafic flows from the Upper Wilson Island Group shales of Basile Bay are pilotaxitic to intersertal, and are composed of 55% albite with a matrix of intergrown chlorite, epidote and tan biotite, the biotite ranging from 5 to 35% in one outcrop. Titanomagnetite pseudomorphs are composed of sphene.

B. MID-APHEBIAN (DOGRIB) DIABASE (MADM)

These are ophitic to intergranular and display the crystallization order olivine-labradorite-titanomagnetite-augite. Olivine is pseudomorphed by chlorite and dolomite but also shows the typical greenschist alteration assemblage of epidote-actinolite and chlorite (Fig. 4-6).

The plagioclase shows a narrow range of composition: An_{55} to An_{57} in chilled margins and phenocryst cores, but displays zones as sodic as An_{47}. It is 50-70% altered to albite and sericite. The oxide phase is composed of ulvospinel with exsolved blades of ilmenite. The augite is pleochroic, pink to lilac-brown, and shows various degrees of alteration to fibrous chlorite, actinolite and colourless

to pleochroic epidote (Fig. 4-7). Eighty percent of the samples show traces of brown amphibole and biotite in the chlorite.

C. UNION ISLAND GROUP

a) Union Island Group Lavas (UIG1M and UIG2M)

Intergranular, massive to variolitic pillow basalts occur, with metamorphic recrystallization more extensive in the glassy textures. Olivine pseudomorphs contain a diagnostic greenschist assemblage (Fig. 4-8), while skeletal plagioclase may be entirely altered to albite (An_0 to An_5) or sericite (Fig. 4-9), with rare patches of K-feldspar.

Clinopyroxene shows a quench, herringbone texture in the pillows and is over 50% altered to fibrous chlorite and dolomite. Intersertal mats of lower-refractive-index chlorite form up to 45% of the mode and replace the original glass. The equant oxide phase is altered to sphene or leucoxene and crystallizes after the augite.

b) Union Island Group Diabase (UIGDM)

These olivine diabase sills are texturally similiar to MADM but show a greater compositional range in mineralogy. Fine grained margins display labradorite (An_{63} to An_{56}), but the very coarse plagioclases have margins as sodic as An_{34}. The plagioclase is 60% altered to albite (An_0 to An_8) and

clinozoisite, mainly at the cores. Yellow to pink augite is over half altered to actinolite-chlorite but minor idioblastic brown amphiboles occur with a green actinolite overgrowth as an alteration of the clinopyroxene. Resorbed titanomagnetite is now altered to sphene with remnant ilmenite exsolution lamellae along [111]. A remnant chloritized glass or granophyric matrix occurs containing fresh apatite needles.

D. SOSAN GROUP LAVAS

a) Seton and W. Keith Islands (SOGSI1M, SOGSI2M, SOGSI3I and SOGSIF)

This sequence of intergranular to pilotaxitic massive lavas was subdivided according to modal colour index, revealing a basalt to trachyte succession (Table 4-5). Names for the intermediate lavas are based on chemical data.

(i) Basalts (SOGSI1M and SOGSI2M)

Olivine pseudomorphs are found in a few of the most Mg-rich lavas (Fig. 4-10). Plagioclase microlites are completely altered to albite but patchy replacement by K-feldspar may locally reach 15 modal% (this reflects K-mobility during metamorphism, rather than an original trachybasalt composition, because these rocks have an anomalously high alkali composition). Pink augite is very rare, but some of the fibrous chlorite-dolomite

pseudomorphs represent pre-plagioclase nucleation. Titanomagnetite is over 50% replaced by sphene. Within the chloritized groundmass, a high content of accessory epidote occurs only with a low dolomite content, and vice-versa.

(ii) Trachybasalt to Tristanite (SOGSI3I)

The intermediate flows (colour index <35) display the same mineralogy as the mafic flows but with no olivine pseudomorphs. The matrix is dominantly albite with minor apatite. Extensive replacement by K-feldspar again indicates non-igneous compositions.

(iii) Trachytes (SOGSI3I)

These have a colour index of ~10 and <5% groundmass quartz (Fig 11), and are pink in hand specimen. Euhedral feldspar is set in an aphanitic feldspar matrix with minor sphene and apatite. Both feldspar phases are dominantly albite with 10-15% patchy replacement by K-feldspar. Equant chlorite-actinolite patches may be clinopyroxene pseudomorphs.

(iv) Trachy-rhyolite porphyries (SOGSIF)

These plugs are porphyritic with phenocrysts of checkerboard albite with minor sericite or K-feldspar alteration (Fig. 4-12). Quartz forms corroded phenocrysts. The groundmass shows albite microlites followed, in crystallizational sequence, by anhedral K-feldspar and over 10% quartz with minor granophyic

intergrowths. K-feldspar forms as much as half of the total feldspar. Its association with albite and the absence of a calcic alteration phase suggests that anorthoclase may have been the dominant phase in the trachytes and trachy-rhyolites.

b) Taltheilei Narrows (SOGTNM and SOGTNF)

(i) Basalts (SOGTNM)

Intersertal basalts occur with rare olivine pseudomorphs. Plagioclase may be partly xenocrystal, being strongly zoned and resorbed and showing a wide range in composition (An_{72} to An_{34}). It is ~60% altered to albite and dolomite. Remnant augite cores occur in chlorite pseudomorphs. Epidote varies inversely with dolomite content and is not present when the latter reaches 15 modal%. A few intermediate compositions occur, containing 65% plagioclase and 5% K-feldspar.

(ii) Rhyolites (SOGTNF)

Rhyolites are amygdaloidal and sparsely porphyritic with resorbed quartz and sericitized orthoclase phenocrysts. Rare albite phenocrysts occur with patchy K-feldspar replacement. The groundmass feldspar is half albite, half K-feldspar. This rock is more fine grained and potassic than SOGSIF.

E. KAHOCHELLA GROUP LAVAS

a) Pekanatui Point (KAGPPM and KAGPPF)

(i) Basalts (KAGPPM)

The basalts show a similiar range of textures and alteration to the Union Island Group. Originally glassy pillow basalts with minor olivine pseudomorphs, they contain plastically deformed plagioclase (Fig. 4-13) now altered to albite and/or sericite, and minor K-feldspar. Glass and pale brown clinopyroxene is almost completely altered to chlorite and epidote and/or dolomite (Fig. 4-14). Epidote does not occur if dolomite is present in amounts greater than 5%, and dolomite can form 20% of the mode. The groundmass may be very quartz-rich and amygdales show chlorite compositional zoning.

(ii) Rhyolite (KAGPPF)

Fine-grained non-amygdaloidal rhyolite domes contain phenocrysts of resorbed quartz, plagioclase and orthoclase (the latter have albite and sericite replacement). Rare muscovite phenocrysts occur and the matrix is dominantly K-feldspar (Fig. 4-15).

b) Taltheilei Narrows (KAGTNM)

(i) Basalts (KAGTNM)

These olivine basalts show a similiar alteration mineralogy to SOGTNM. Pillows are more extensively

altered. Labradorite (An_{72} to An_{50}) is at least 80% altered to albite and dolomite. The mafic component may contain epidote or clinozoisite plus chlorite.

Amygdales are zoned with calcite-quartz and varied chlorite compositions. Carbonate appears to represent a late-stage infilling, occurring in veinlets as well as the largest amygdales.

F. JACKSON GABBRO (JAGPPM and JAGTNM)

The dykes are texturally similiar to the olivine diabase UIGDM. Plagioclase (An_{70} to An_{40}) is ~75% altered to albite and carbonate. Altered, colourless clinopyroxene displays characteristic greenschist facies assemblages but also traces of a deep blue-green amphibole and biotite.

The circular pluton at Taltheilei Narrows is mineralogically similar to the dykes but contains a lilac to brown augite. Notably, the pluton displays a porphyritic dioritic northern margin containing up to 70% sericitized plagioclase, with minor K-feldspar replacement. One sample has twinned, euhedral, salitic ($2V = 60°$) augite (Fig. 4-16).

G. PEARSON FORMATION BASALTS (PEM)

Intergranular to hyalopilitic massive basalts display the crystalline order plagioclase, clinopyroxene, titanomagnetite. Labradorite (An_{61} to An_{56}) may show margins of sodic andesine, but may have cores partially altered to

albite, blue-green pumpellyite and clinozoisite or strongly-pleochroic, white to yellow epidote. Colourless clinopyroxene is over 30% altered to hematite-stained chlorite with granular pumpellyite and sphene (Fig. 4-17). Traces of a rare olive-brown amphibole are seen, but no K-feldspar is present. In coarser textured rocks, the oxide phase is preserved as equant magnetite pseudomorphs (now replaced by sphene) and with ilmenite intergrowths. The originally glassy groundmass is now chlorite plus granular sphene and hematite. An alteration assemblage of pumpellyite-chlorite and late calcite-quartz fills veinlets and amygdales. Pumpellyite is not observed in thin sections with >0.5% calcite. The chlorite is invariably first-order grey to yellow in thin section, in contrast to the more magnesian anomalous chlorites, showing anomalous blue interference colours, the lavas lower in the sequence.

H. ET-THEN GROUP BASALTS (ETGM)

These massive basalts contain rare olivine pseudomorphs and labradorite (An_{71} to An_{56}) almost entirely altered to albite and sericite. Some intermediate compositions are suggested by 75% plagioclase. Colourless clinopyroxene and groundmass glass are altered to chlorite, epidote and sphene. Large sheet amygdales (> 5 cm) contain concentric zones of calcite, quartz-magnetite and microcline. Like the Pearson Formation, the groundmass contains no K-feldspar or dolomite.

I. SUMMARY OF PETROGRAPHY

The original mineralogy of the predominantly mafic rocks appears to have been titaniferous augite, labradorite, Fe-Ti oxide and varying amounts of glass in the lavas. Olivine occurred in all except the Wilson Island Group and Pearson Formation, and no evidence of orthopyroxene crystallization was observed. Typical igneous textures are preserved although the mineralogy is partially or wholly replaced by metamorphic assemblages.

At the base of the succession, the Wilson Island Group textures indicate total replacement of clinopyroxene by actinolite, hornblende, biotite and epidote and plagioclase by albite and clinozoisite. The stratigraphically higher Union Island, Sosan and Kahochella Groups contain diabase suites which display better preservation of primary mineralogy than the associated lavas. In the diabases, augite alters to chlorite, epidote and actinolite and labradorite-andesine is partially replaced by albite and sericite or clinozoisite. In the lavas augite is almost completely replaced by chlorite, dolomite and epidote and Fe-Ti oxides by sphene. Near the top of the sequence the Pearson Formation contains albitized plagioclase and displays a chlorite-pumpellyite-epidote alteration of non-pleochroic augite.

The Sosan Group contains metamorphosed trachybasalts to trachytes which have a colour index of less than 35 and a high content of K-feldspar in the matrix. Trachy-rhyolite

contains albite-Potassium feldspar intergrowths in both megacrysts and groundmass which may represent original anorthoclase. Rhyolites from the the Wilson Island and Kahochella Groups have remnant orthoclase and calcic plagioclase phenocrysts.

V. METAMORPHISM AND METAMORPHIC MINERALOGY

A. METAMORPHIC FACIES AND MINERAL CHEMISTRY

A summary of the metamorphic mineralogy of the East Arm suites is illustrated in Table 4-3. Briefly, three distinct facies characteristic of very-low to low-grade metamorphism (Winkler, 1979) are observed, the grade becoming higher with increasing stratigraphic age. The mafic and intermediate suites are plotted on ACF diagrams along with analyses of facies-diagnostic minerals, where these are available (Fig. 5-1). All suites show some chemical compositions outside the the normal range expected for basalts, and invariably contain samples with low CaO values.

Figures 5-1a and b illustrate the extremes of metamorphism, from the albite-epidote-actinolite facies to the pumpellyite-actinolite facies. These facies are described below.

a) Albite-Epidote-Amphibolite Facies

Only the Wilson Island Group has been metamorphosed to this facies. The whole-rock compositions are not well defined by the analyzed epidote and hornblende assemblages on an ACF plot because biotite cannot strictly be represented (Fig. 5-1a). However, a whole-rock compositional trend extends toward $A_{10}F_{90}$, which is the biotite piercing-point on this diagram.

The amphiboles are actinolitic hornblende and ferro-pargasitic hornblende (Leake, 1978) and appear to show a compositional gap (Figs.5-1a and 5-2a). Despite the limited data the gap may be real because the two compositions can be observed in one thin section (e.g. in WI 8b). A compositional gap in actinolite to ferropargasite, with a minimum of data points at an Al(IV) content per formula unit of 1, is commonly seen in the transition from low grade to medium grade metamorphism. Because the gap varies in size and composition, Grapes and Graham (1978) ascribed it to disequilibrium and kinetic factors involved in hornblende forming reactions. However, Oba (1980) has found a solvus in the system tremolite-pargasite at 1 kb.

Estimates of the pressures of equilibration of amphiboles have been estimated by the degree of substitution of the glaucophane molecule (Brown, 1977), i.e.

$$Na(M_4)Al(IV) = CaMg$$

This value, however, is dependent upon the Fe^{3+} content since as this value increases, the total number of cations per formula unit will decrease leading to lower $Fe(M_4)$ and higher $Na(M_4)$ and Al(IV). Fig. 5-2 shows data points for a range of possible Fe^{3+}/Fe^{2+} ratios, the most relevant ratios being those obtained from a linear equation relating Fe_2O_3 to total Fe for a series of epidote-amphibolites and amphibolite-bearing, Fe-Ti oxides and sphene (Grapes *et al.* 1977).

Fig. 5-2b is an empirical plot (after Fleet and Barnett, 1978) that displays the moderate Al-contents of amphiboles, characteristic of kyanite-free zone amphibolites. Fig. 5-2c shows a semiquantitative estimate of equilibration pressure (after Brown, 1977) based on the $Na(M_4)$ content of the amphiboles, which suggests a pressure of formation of 2 to 3 kb.

Fig. 5-3 summarizes the experimentally-determined relationships linking low-grade to medium-grade metamorphism. Chlorite-free, hornblende-bearing assemblages are restricted by the chlorite-out curve determined for a natural basalt (Liou *et al.*, 1974; curve 2, Fig. 5-3). Minimum temperatures of 550°C at reasonable pressures are also supported by the presence of staurolite in Wilson Island Group pelites at Isles du Large (Hoffman *et al.*, 1977). Staurolite (Mg/Fe = 0.66) has been produced from chlorite and muscovite above 540 and 565 °C at 4 and 7 kb respectively (Hoschek, 1969). Further constraints on pressure and temperature can be made by analyzing the pistacite content of epidote, because the stability field for epidote is partly dependent upon oxygen fugacity (Liou 1973). An analyzed epidote has a composition of Ps_{27} and contains some remnant pyrite and titanomagnetite; hematite is absent. Therefore, the oxygen fugacity during metamorphism was probably higher than that of the QFM buffer, which stabilizes an epidote of composition Ps_{25}, but lower than that of the HM buffer, which produces a Ps_{33}

epidote (Fig. 5-3).

If NNO is taken as an approximate oxygen buffer during metamorphism, 2 kb is the minimum pressure needed to produce an albite-epidote-hornblende assemblage. If burial metamorphism only was significant, and the complete Union Island Group - Great Slave Supergroup section were present above the Wilson Island Group, the minimum metamorphic pressure would have been 3.2 kb. The possible stability field of the Wilson Island Group is indicated in Fig. 5-3.

b) Pumpellyite-Actinolite-Chlorite Facies

The Pearson Formation (Fig. 5-1b) shows the very-low grade pumpellyite-actinolite-chlorite assemblage but actinolite is only sporadically developed. The commonest assemblage is epidote-pumpellyite-chlorite. This assemblage, which has a high Al_2O_3 content, is common because it largely occurs as an alteration product of plagioclase. The host basalts are not unusually rich in Al_2O_3.

Both the epidotes and the pumpellyites are iron-rich. The negative correlation between total Fe and Al in pumpellyites suggests that most of the Fe is ferric (Liou, 1979). These samples contain over 50% of the ferric julgoldite molecule and are similiar in composition to those from the Quebec Appalachians and the Taiwan ophiolite where pumpellyite also replaces plagioclase (Trzcienski and Birkett, 1982). The high Fe-content in pumpellyite does not necessarily correlate with rock composition (Offler *et al.*,

1981), but does show a trend of inverse correlation with depth of burial (Coombs *et al.*, 1976; Liou, 1979).

The chlorite observed is Al-poor diabantite (Fig. 5-4), the Fe/Mg ratio of which depends upon the Fe/Mg ratio of the whole-rock, with Fe being preferentially concentrated in the chlorite. No minerals diagnostic of metamorphic facies are seen in the Et-then Group. However, as in the Pearson Formation, calcite is the only carbonate, and the Group's stratigraphic position above the Pearson Formation suggests metamorphism at a similar or even lower temperature.

The pressure of metamorphism of the Pearson Formation is difficult to determine. A minimum pressure for the occurrence of pumpellyite-actinolite in an iron-free system is defined by an invariant point which occurs between 1 and 3 kb (Winkler, 1974). The minimum pressure caused by burial due to the strata exposed in the gravity slides would have been 0.6 kb. Because pumpellyite-prehnite assemblages are not observed, either Fe may be effective in increasing the stability field of pumpellyite or compressive stress was more important than burial during metamorphism.

c) Epidote-Actinolite-Chlorite Facies

The Union Island Group (Fig. 5-1c) commonly contains the typical low-grade assemblage epidote-actinolite-chlorite but shows an alteration trend, towards chlorite-rich or calcite-dolomite-rich samples. The chlorites are pycnochlorites showing lower refractive indices than those

of the Pearson Formation and notably more Al (Fig. 5-4). The amphibole is typical actinolite (Leake, 1978; Fig. 5-2) and epidote is Ps_{28}. The trace occurrence of brown hornblende and biotite in the intrusions suggest that the epidote-amphibolite facies may have been briefly achieved.

The Sosan and Kahochella Groups (Figs. 1d and 1e) show epidote-actinolite-chlorite assemblages in a few cases, notably in coarser grained intrusions, but are extensively replaced by chlorite, dolomite and Fe-dolomite. Chemical alteration is greatest in the glassy-textured samples, a complete range of dolomite-chlorite mixtures being indicated in the Kahochella Group. One Al-rich point in the latter group is a plagioclase-rich pillow fragment.

B. THE EFFECT OF THE VARIATION IN THE COMPOSITION OF THE METAMORPHIC FLUID ON ALTERATION ASSEMBLAGES

a) Field Evidence and Relevant Theoretical and Experimental Work

Assemblages diagnostic of metamorphic facies are often poorly developed in these rocks, whereas chlorite and carbonate-bearing assemblages are commonly observed. The latter assemblages tend to obscure conditions of metamorphism because they can be stabilized under conditions of temperature and pressure characteristic of several different facies. Carbonate-chlorite assemblages are found

elsewhere as small domains throughout laumontite, pumpellyite-prehnite, pumpellyite-actinolite and epidote-actinolite facies metabasalts and meta-andesites, e.g. Taveyenne, France (Vuagnat, 1974), Kii peninsula, Japan (Seki *et al.*, 1970), N. Maine, U.S.A. (Richter and Roy, 1974) and Woodsville, Vermont, U.S.A. (Harte and Graham, 1975), respectively. Antipathetic relationships between pumpellyite and calcite, and between epidote and dolomite, have also been observed elsewhere i.e. Karmutsen tuffs, B.C. (Surdam, 1973) and Fortesque river, W. Australia (Vallance, 1969). Vallance explained these phenomena by postulating a high activity of CO_2 in the metamorphic fluid. High CO_2 would stabilize Ca and Al in carbonates and chlorites rather than in facies-diagnostic hydrous silicates.

Thermodynamic calculations relevant to assemblages typical of metabasalt at very-low grade and low to moderate pressures (2 kb) indicate that pumpellyite and prehnite bearing assemblages would be suppressed by a fluid with X_{CO_2} < 0.2 (Glassley, 1974), and that prehnite and laumontite would be restricted to equilibrium with a fluid of X_{CO_2} < 0.01 (Zen and Thompson, 1974).

From fluid inclusion studies, the composition of metamorphic fluids appear to be grade dependent. The CO_2 content increases with grade into upper amphibolite facies in both Alpine and Himalayan metapelites and fluids with X_{CO_2} of 0.1 to 0.6 are found in the amphibolite facies (Crawford, 1981). This increase may be caused by the

oxidation of reduced species such as CH_4, which is present in solution below the pyrophyllite isograd, or by progressive decarbonation reactions. It is therefore evident that even small increases in the activity of CO_2 in a fluid, possibly caused by the solution of nearby sedimentary carbonates, could have a profound effect on the metamorphic mineralogy of a basalt.

b) Chemography

The observations above suggest that variations in the equilibrium assemblage may occur at a fixed pressure and temperature, giving rise to the assemblages observed in Table 4-2. Relevant reactions were inferred from observed combinations of the six ACF-sensitive minerals among these assemblages.

Assuming fixed temperature and pressure and mobile CO_2 and H_2O, a multisystem of six, five-phase invariant points is theoretically possible (Fig. 5-5). The reactions were derived and placed using Shreinemaker's analysis (Korzhinsky, 1959). The observed incompatibility of pumpellyite and dolomite defined the first two stable invariant points which, in turn, define a stable actinolite-absent invariant point. The three other invariant points are metastable. The eleven reactions used to construct the chemical-potential diagram are given in Table 5-1. The suites are identified according to area rather than stratigraphic horizon in order to emphasize possible

differences in local metamorphic conditions.

The topology derived in Fig. 5-5 is presented on an isobaric plot of temperature versus Xco_2 (Fig. 5-6). The phases referred to in Fig. 5-6 and in the text below are identified in Table 5-1. A few comments on the construction of this diagram are necessary.

The estimated depth of burial for the epidote-actinolite-bearing suites range from 1.5 to 2.5 kb (Kahochella to Union Island Groups) and so a pressure of 2 kb was chosen for illustration, assuming P(fluid) = P(total). Where possible, 2 kb experimental data in iron-free systems was used to construct this diagram. The reaction (Dl,Ch) was investigated by Pluysnina and Ivanova (1981) with Xco_2 ranging from 0.005 to 0.1. Reaction (Pu,Ch) was extrapolated to high H_2O values from an e[redacted]ental bracket at 480°C and Xco_2 = 0.85 by Kerrick (1974). Kerrick's corrections for non-ideal mixing in the fluid render his long extrapolation valid. The (Dl,Pu) was calculated using the thermodynamic data of Richardson and Powell (1976). The intersection of these three curves define two invariant points, but because (Dl,Pu) was not corrected for non-ideal mixing of the fluid, depicted temperatures are uniformly too low and the invariant points too close together. Furthermore, the small angle of intersection and the long extrapolation means that the position of the Pu-absent invariant point is only poorly known. Other reaction curves were drawn using an integrated form of the

equation of Greenwood (1967):

$$\frac{dT}{dxCO_2} = \frac{RT^2}{Hr}\left[\frac{nCO_2}{xCO_2} - \frac{nH_2O}{xH_2O}\right]$$

where Hr is the enthalpy of reaction, and $nCO_2+nH_2O=1$ and are stoichiometric coefficients for the reaction. The integration constant is evaluated at each invariant point. The equation assumes ideal mixing in the fluid and a constant Hr over the reaction interval. The latter is a valid assumption over a few hundred degrees for many mixed-volatile reactions (Kerrick, 1974). Thermodynamic data for zoisite is from Zen (1972) and for Dumpellyite from Glassley (1974). Other data are from Richardson and Powell (1976). There is considerable variation in the published enthalpies of formation for these minerals. Those for clinozoisite and chlorite (Glassley, 1974) appear to be too high when used with the other data because they give curves with incorrect slopes (e.g. Pu-Ac). The slopes can be qualitatively determined from the Greenwood formula.

The extrapolated reaction (Dl,Ct) takes place at 350 °C, but short extrapolations of reversals for this reaction in iron-free systems, with $X_{CO_2} = 0$ give 325 °C at 2 kb (Nitsch, 1971; Schiffman and Liou, 1980), strongly suggesting that the Dl-absent invariant point is placed at too high a temperature. Because the (Dl,Ct) and (Dl,Ch) reactions are probably degenerate, owing to the wide

variation in the composition of pumpellyite, this may indicate a discrepancy in the experimental data for the two curves. Finally, the inclusion of iron in the system will significantly reduce the temperature of the reaction curves, e.g. 30 to 50 °C for the (Dl,Ct) reaction (Pluysnina and Ivanova, 1981).

c) Discussion

Even considering the limitations of Fig. 5-6, a few general observations can be made about the effect of CO_2 on facies-diagnostic assemblages. Firstly, the common, low-grade assemblage of Ep-Ac-Ch is relatively insensitive to wide variations in Xco_2. Secondly, very-low-grade pumpellyite-bearing assemblages are suppressed by a very a small Xco_2 and can produce instead the Ep-Ac-Ch assemblage at the same temperature. Thirdly, Xco_2 values greater than 0.2 produce an Ep-Dl-Ch assemblage, in pumpellyite-bearing rocks, which probably extends to low-grade assemblages at higher Xco_2 values.

Both the very-low-grade and low-grade assemblages of the East Arm volcanics can be explained by a narrow range in temperature (300 to 400 °C) and metamorphic fluids with Xco_2 ranging from 0.0 to 0.2. Because the Pearson Formation was probably metamorphosed at less than 2kb, Xco_2 could have been higher than indicated because both reactions (Dl,Ac) and (Dl,Pu) move to higher Xco_2 values with a reduction in pressure (Glassley, 1974; Pluysnina and Ivanova, 1981).

The apparent low-grade assemblages in the middle of the stratigraphic succession appear to be very-low-grade. These display an ideal sequence characterized, respectively, by Ep-Ac-Ch, Ct-Ac-Ch, Ct-Dl-Ch and [illegible]-Dl-Ch with increasing Xco_2. Since at least two reaction curves have been crossed in each suite, evidence of buffering of the fluid composition (i.e. that the assemblages are constrained to one reaction curve) is not present, at least not on a scale as large as an outcrop.

Because carbonate-bearing assemblages are associated with late stage veins, large amygdales and the most porous lithologies, it appears likely that some fluid compositions were externally controlled and became more CO_2-rich with time. If this were accompanied by a decline in temperature, the same paragenetic sequence could be produced from initial low-grade as well as very-low-grade conditions.

Fig. 5-7 displays the metamorphic parageneses from each locality in the East Arm in order of increasing Xco_2. Within the "low-grade" sequences there is a striking correlation between composition and texture. The Mid-Aphebian diabase dykes in the basement of Simpson Island indicate a low Xco_2, whereas progressively higher values are indicated in the Union Island area, Pekanatui Point, Taltheilei Narrows and Seton Island. This is a trend of an increasing percentage of pyroclastics and, to some extent, decreasing depth of burial. There is no correlation, however, with bedded carbonates in the sequence.

The initial metamorphic fluid was probably connate water and therefore may have involved locally-buffered reactions. Subsequent dissolution of the interlayered dolomites would have increased the X_{CO_2} of the metamorphic fluid but this fluid will only be widely dispersed where the porosity is high. Alternatively, a contemporaneous variation in fluid composition could have occurred with a diffusion gradient existing between two extremes: on the one hand an externally controlled, CO_2-rich fluid in the porous zones, and on the other a locally buffered, H_2O-rich fluid in the massive zones.

VI. RB-SR ISOCHRON AGES, MAGMATIC $^{87}Sr/^{86}Sr$ INITIAL RATIOS AND OXYGEN ISOTOPE GEOCHEMISTRY

A. INTRODUCTION

The present study attempts to record the timing and duration of sedimentation in the East Arm by dating the oldest and one of the youngest volcanic units using the Rb-Sr method. This in effect dates both the time of initial rifting in the East Arm and the end of molasse sedimentation derived from the Coronation geosyncline. Comparison with other, mainly K-Ar, dates available from the East Arm provides a dating framework for each magmatic and tectonic event.

Because these rocks have undergone metamorphism, Sr and O isotopic studies were made of remnant igneous mineral phases in order to determine magmatic, rather than metamorphic, $^{87}Sr/^{86}Sr$ initial ratios. This approach also provides petrogenetic constraints for a sequence of altered lavas from a major Proterozoic sedimentary sequence: an approach not previously presented.

A brief description of the volcanics is given below along with their measured dates and probable ages. Controversial points concerning the stratigraphy of the East Arm are discussed and finally the isotope systematics are described.

B. THE DATED VOLCANIC ROCKS

The areal extent and location of the volcanic units are outlined in Fig. 3-1. These units, presented in stratigraphic order in Table 6-1, are based on the sequence of Hoffman *et al.* (1977); the style of intrusion and chemical classification of each magma type is also included. The ages given in this sequence, and in the following discussion were based on K-Ar and Rb-Sr isotopic dates and were published by Goff *et al.* (1982). Since then, U-Pb zircon data (Hoffman, pers. comm., 1981) has allowed a correlation with the tectonic events of the Wopmay Orogen. This correlation was used for developing the model for the tectonic history of the East Arm, given above. If the U-Pb ages are valid, 50 Ma should be added to the ages for the Union Island Group and Great Slave Supergroup, given in Table 6-1. Secondly, this would indicate that the Rb-Sr isochrons of the Sosan Group and Pearson Formation were produced by metamorphism.

The lavas from which dates were obtained were the oldest and one of the youngest volcanic units in the Proterozoic sequence of the East Arm (Table 6-1). The oldest is the Wilson Island Group, a 1500 m thick basalt-rhyolite suite intercalated with continental fluvial sandstones, whereas the younger Pearson Formation is a 180 m thick partly columnar basalt sequence above a succession of non-marine sedimentary rocks. This unit caps the Great Slave Supergroup.

A range in metamorphic facies is seen from pumpellyite-prehnite or pumpellyite-actinolite in the Pearson Formation to albite epidote amphibolite in the Wilson Island Group. Intermediate volcanic sequences are epidote actinolite facies.

C. RESULTS OF DATING

A Rb-Sr whole rock isochron was produced for each of the Wilson Island Group and the Pearson Formation. The data are shown in Tables 6-2 and 6-3. Analytical techniques and errors are discussed in Appendix I.

The Wilson Island Group gives a date of 1810 ± 19 Ma (Fig. 6-1). A mean square weighted deviation (MSWD) of 6.03 suggests some Rb-SR mobility after an isotopically closed system was achieved (McIntyre *et al.* 1966). A moderately high initial ratio of 0.7051 ± 0.0008 was obtained. This is a very similar date and initial ratio to a 12-point isochron/produced for the same suite by Frith (1980; 1846 ± 24 Ma, 0.7048 ± 0.0008).

The Pearson Formation shows a virtually identical date of 1809 ± 30 Ma. The isochron (Fig. 6-2) shows a high degree of colinearity: the MSWD of 1.51 suggests only a slight variation beyond analytical error. The initial ratio of 0.7089 ± 0.0004 is very high.

D. DISCUSSION OF DATES

In order to evaluate the importance of the present work, the above dates are discussed both in the context of other dates available from the East Arm and in the light of controversy concerning the sequence of events in the area. Published isotopic ages are given in Table 6-1 along with approximate ages based on Phanerozoic sedimentation rates.

a) Age of Basement Mylonitization

The East Arm graben is floored by an Archean basement of granulite grade paragneiss and quartz-monzonite plutons (Reinhardt 1972) which is exposed in small horsts. K-Ar ages range from 2370 to 2575 Ma (Table 6-1); thus the basement is a southerly continuation of the Slave Province.

The basement is transected by a N.E. trending belt of mylonitization of controversial age, which is well developed on the south shore of the Arm (Reinhardt, 1969a). The Wilson Island Group is recognized as the oldest stratigraphic sequence in the area because of its high angle folding and penetrative deformation which does not affect the Union Island Group or the Great Slave Supergroup. This deformation is considered by Hoffman *et al.* (1977, Table 25.1) to be contemporaneous with mylonitization. Alternatively, Badham (1978a) has noted that the intensity of the penetrative deformation of the Wilson Island Group is less marked than in some basement migmatites and has postulated a period of transcurrent faulting and mylonitization prior to deposition

of the Wilson Island Group. Much of the basement (eg. the paragneisses of the Simpson Islands), however, has an equivalent deformation to that of the Wilson Island Group with intense shearing and mylonitization restricted to narrow belts of migmatite (Reinhardt, 1969b, Fig. 1). Badham (1978a) has also pointed out that at Basile Point, a Wilson Island Group succession overlies a sheared and weathered basement gneiss. This outcrop was also identified as gneiss by the mapping of Wright (1951; Stockwell *et al.* 1968), but Stockwell (1936) and Hoffman (1977) show this outcrop to be Wilson Island Group arkose.

The age of the mylonitization is still enigmatic but definitely occurred before deposition of the Union Island Group and Great Slave Supergroup, which do not show the penetrative deformation characteristic of the Wilson Island Group.

b) The Age of the Wilson Island Group

A minimum age for the Wilson Island Group is obtained from the dates of the N. Simpson Island dyke and Blachford alkaline complexes. Both plutons lack the folding and penetrative deformation which, within the Proterozoic sequence, is restricted to the Wilson Island Group. They must therefore post-date it.

The N. Simpson Island dyke has a K-Ar date of 2200 Ma and the final granitic phases of the Blachford Lake complex a K-Ar date of 2057 Ma (Table 6-1). These alkaline

intrusions are thus thought to be contemporaneous by Badham (1979b) and may be grouped with the alkali syenite to carbonatite complex of Big Spruce Lake further north on the west margin of the Slave craton. An Rb-Sr isochron for the Big Spruce Lake complex gives an age of [illegible]39 Ma (Martineau and Lambert, 1974). In [illegible] the Isles du Large (Fig. 3-1), a biotite quartz monzonite ("Butte Granite") intruded the Wilson Island Group (Hoffman *et al.* 1977) and gives a Pb-Pb zircon age of 2050 Ma which is comparable to the Blachford Lake complex (oral presentation by Hoffman, 1980; and see Table 6-1).

The Wilson Island Group therefore appears to have a minimum age of about 2200 Ma and thus the Rb-Sr isochron age of 1810 ± 19 Ma must represent a later metamorphic event rather than the age of extrusion.

c) The Stratigraphic Position of the N. Simpson Island and Blachford Lake Differentiated Alkaline Intrusions

Although these intrusions post-date the Wilson Island Group, some controversy exists about their relationship to the beginning of Great Slave Supergroup sedimentation.

The N. Simpson Island alkali-diorite dyke is apparently in fault contact with the Hornby Channel Formation of the Sosan Group but Badham (1979b) has recognized an albite trachyte border phase which, in one locality, appears to be gradational between the main part of the dyke and a marginal breccia zone which cuts the Hornby Channel Formation (Fig.

3-4). The breccias contain calcareous blocks which Badham correlated with the Sosan Group and he also identified xenoliths of Sosan Group sandstone in the dyke.

This evidence can be seriously questioned, but this issue has been confused by Badham's attempt (1978c, 1979b) to draw a genetic connection between the albite-trachyte matrix of the breccias and a chill zone of a similar composition at the margin of the dyke. He postulates that the volatile-rich magma of the main dyke initiated [redacted] brecciation of the sandstone. However, trachyte bearing breccias are found along narrow fault zones parallel to, but in most cases separate from the margin of the dyke and as much as 10 km distant from it (Reinhardt, 1972). Furthermore, detailed mapping in Badham's crucial locality has shown the breccias to be centred on a 200 m. syenite plug 500 m. south of the dyke margin. The sandstone becomes progressively less brecciated towards this margin where it is largely only sericitized (Walker 1977, Map 9). Badham's crucial breccia has a matrix similar to the adjacent dyke margin but is separated from it by a faulted trough. A discontinuous line of breccias can be traced from this outcrop to the trachyte plug further east.

This pattern of brecciation is clearly the opposite of what one would expect if the diorite were its source, and yet the dyke margins are unfractured. In addition, the dyke clearly represents a deeper level of intrusion than the trachyte plugs: the chilled margin of the former is only a

few cms. thick while the latter intrusions are entirely fine-grained. Because these two rock types appear unconnected one must conclude that there is no clear evidence of the diorite dyke cutting the Sosan Group. Secondly; sandstones are abundant in the Wilson Island Group, thus the xenoliths in the Simpson Island dyke are not necessarily from the Sosan Group.

More importantly, Reinhardt (1972) pointed out that many diabase dykes (i.e. Mid-Aphebian Diabase) cut both the Simpson Island dyke and the Archean basement. Even if there are two ages of diabase as claimed by Badham (1979b), no dykes are seen to cut the very large outcrop of Hornby Channel Formation on S. Simpson Island. In fact, excellent examples can be seen of these dykes overlain by the Hornby Channel Formation (Reinhardt, 1972, p. 6 and 7). It thus seems more likely that the differentiated alkaline intrusions predate the Sosan Group sediments.

d) The Albite Trachyte Plugs

The later, shallower level, trachyte veined breccias contain blocks of limestone from the Stark Formation of the Christie Bay Group (Hoffman, 1978). Because the Stark Formation is not present in this area, this suggests a time of intrusion after the post Aphebian fault movements (which would have brought the Hornby Channel Formation to a subvolcanic level) and before the removal of the overlying Christie Bay Group which occurred before early Et-then

deposition. These plugs may therefore be almost contemporaneous with the Et-then volcanism.

e) The Age of the Mid-Aphebian Diabase dykes

These dykes, which were named by Hoffman *et al.* (1977), have not been dated but, because they intrude a basement which shows the typical Kenoran dates of the Slave craton (Table 6-1) they can be correlated with dated swarms within that province. These dykes have 030° and 070° trends comparable to dykes in the Slave Province which Burwash *et al.* (1963) named Mackenzie I to IV according to their respective regional trends. Table 6-4 shows relevant Rb-Sr ages for different trends in the Slave Province and diabase swarms of comparable age from other Archean cratons. These data indicate two widespread events of tholeiitic diabase intrusion at approximately 2600 Ma and 2100 Ma. Furthermore the low initial $^{87}Sr/^{86}Sr$ of most of these swarms is comparable with that obtained for the Mid-Aphebian diabase (see below).

The 2635 ± 78 Ma Rb-Sr date for a dyke of the Mackenzie I trend ("Dogrib" trend of McGlynn and Irving, 1975) was considered to represent the time of dyke emplacement by Gates and Hurley (1973) but the date is very old compared to the Rb-Sr age of the Slave Province (2460 to 2660 Ma, see Fig. 6-3). Because these dykes are only mildly metamorphosed the majority must have ages younger than 2635 Ma. Dykes of different ages may have the same structural trend because

K-Ar dates for Mackenzie I range from 2200-2400 Ma (Burwash *et al.* 1963; Leech, 1966) and Leech considers a second possible period of emplacement of 2100 to 1900 Ma along the same trend. Reported Rb-Sr dates for the Mackenzie II and IV trends also record this event (approximately 2100 Ma, Table 6-4) and are a reasonable age for emplacement of the Mid Aphebian diabase given that the earlier differentiated alkaline intrusions are 2057-2200 Ma.

f) The Age of the Union Island Group Igneous Rocks

No published dates are available for the Union Island Group flows or diabase sills but Hoffman *et al.* (1977) reported that this group unconformably overlies the Mid-Aphebian Diabase. Using the approximate age based on sedimentation rates (Table 6-1) these lavas are 1930 Ma, assuming no unconformity at the top of the Union Island Group.

g) The Age of the Sosan Group Volcanism

Voluminous, localized volcanism occurs in the Sosan Group, expecially in the Seton Island area and to a lesser extent in the Taltheilei Narrows area (Fig. 3-1). An estimated date from Phanerozoic sedimentation rates is approximately 1880 Ma (Table 6-1); however, a similar age was obtained from a whole-rock Pb-Pb isochron from a mineralized Sosan breccia pipe in Taltheilei Narrows (1870 ± 15 Ma; Blackadar, 1981). A Rb-Sr isochron produced for the

Seton Island volcanics gives a significantly younger age (1832 ± 10) and will be discussed below.

h) The Age of the Pearson Formation

The youngest widespread basalt flow-package in the Great Slave Supergroup, the Pearson Formation, was erupted before a period of nappe formation and subsequent quartz-diorite intrusions. An unpublished Rb-Sr isochron date for these intrusions (R.K. Wanless, pers. comm., 1977) shows a date of 1811±81 Ma, similar to that of the Pearson Formation, which is corroborated by the oldest K-Ar dates on these intrusions (Table 6-1). The high linearity of the Pearson Formation isochron and preservation of the magmatic initial ratio (see below) suggests that the date is little affected by metamorphism or that metamorphism was contemporaneous with extrusion. The 1809 Ma. date therefore appears to be a reasonable age for the extrusion of the Pearson Formation and restricts the whole of the Great Slave Supergroup to the Aphebian, i.e. older than 1800 Ma (Donaldson *et al.* 1976).

i) Evidence for a Hudsonian Metamorphic Event

Although the date obtained from the Pearson Formation is probably close to that of extrusion, other evidence suggests that this date also represents a metamorphic event which may have reset both Rb-Sr and Pb isotopic systems.

A six-point Rb-Sr isochron giving 1832 ± 10 Ma was produced for the Sosan volcanics of Seton Island (Baadsgaard, *et al.* 1973) although a similar seven-point study gave a date statistically similar to that of the Pearson Formation 1805 ± 16 Ma (Loveridge, in Cumming, 1980). Furthermore the Pb-Pb whole rock age of the same samples as used by Baadsgaard, *et al.*, (1973) also matches that of the Pearson Formation (1804 ± 23 Ma, Cumming, 1980).

More striking is the obvious similarity of the Rb-Sr dates of the Pearson Formation and Wilson Island Group suggesting a possible contemporaneous metamorphism of the Proterozoic sediments ranging from pumpellyite-prehnite to epidote-amphibolite facies. The Wilson Island Group is nowhere exposed in unfaulted contact with the Great Slave Supergroup. This led Hoffman *et al.* (1977) to speculate that the Wilson Island Group originally had lain further south and may have been juxtaposed with the relatively unmetamorphosed Great Slave Supergroup by nappe tectonics. This would explain a post-Great-Slave -Supergroup age for the metamorphism of the Wilson Island Group, however, no evidence for such a nappe is known. Alternatively, if the Wilson Island Group overlies basement (Badham, 1978a) and is therefore autochthonous, this suggests that different depths of burial were involved during the metamorphism. Such an explanation is more consistent with the vertical tetonics expected in a graben. Individual fault blocks in the East Arm have thus undergone considerable vertical movement since

the ~1810 Ma metamorphic event. Petrographic evidence of alkali mobility is difficult to find owing to the partially recrystallized fabric of the epidote amphibolites. However, the albite contains biotite and hornblende inclusions as well as marginal replacement by biotite, hornblende and K-felspar.

Although all Wilson Island Group, Sosan Group and Pearson Formation Rb-Sr and Pb-Pb dates are within acceptable error (2 standard deviations) of each other, the remarkable linearity of the Sosan Group isochrons has been interpreted as representing the dates of extrusion (Baadsgaard, *et al.* 1973; Cumming, 1980). If these dates, and that of the Pearson Formation, are extrusion dates then the error in their precision is greater than the time needed to deposit the intervening sediments. The slowest rate of subsidence acceptable (3.8 km in 60 Ma) would be comparable to the fastest rates calculated using Phanerozoic sedimentation rates (Table 6-1). However, faster and more realistic rates of subsidence have been noted in some modern troughs such as Suez which has subsided 5 km. in 25 Ma (Burke, 1977). Furthermore, acceptance of 1832 Ma as the age of extrusion of the Sosan Group volcanics would fail to explain the significantly older (1870 Ma), extremely linear and geologically feasible Pb-Pb isochron of Blackadar (1981). Alternatively, Olade (1975) noted the high correlation between K_2O, Rb and $^{87}Rb/^{86}Sr$ in the Sosan Group volcanics and the obviously secondary K-felspar and biotite

in some samples. He considers isotopic homogeneity to have resulted from metasomatic "splitization". The explanation of the Sosan Group dates is thus equivocal, but suggests either rapid although acceptable rates of subsidence before the extrusion of the Pearson Formation, or reequilibration of both Sr and Pb isotopes. There is no question however that the Wilson Island Group date is metamorphic since later plutons show K-Ar and Pb-Pb dates greater than 2000 Ma. Even if affected by metamorphism, these would be minimum ages.

It should be pointed out that Rb-Sr isochrons are normally resistant to low grade metamorphic events, the limited diffusion of Rb and Sr allowing mineral isochrons to be reset but not the whole rock isochrons (e.g. Baadsgaard, *et al.* 1976). However, the Churchill Province underwent extensive alkali metasomatism during the Hudsonian orogeny (Burwash, *et al.* 1973), with Rb and Sr being mobile under greenschist facies conditions (Burwash and Krupicka, 1970). Other evidence for resetting of Rb-Sr isochrons under greenschist facies conditions has been documented by Bell and Blenkinsop (1978). The East Arm, positioned on the north edge of this alkali enrichment zone, may have been partly affected by a Rb-bearing metamorphic fluid. The composition of the metamorphic fluid is probably a more important factor than grade when Rb/Sr whole-rock isochrons are reset.

A metamorphic and tectonic event thus took place involving alkali metasomatism of the Archean basement to the south, nappe formation, laccolith injection and continued

folding.

j) The Age of the Et-Then Group Volcanism

The age of the Et Group volcanics has not been determined isotopically. However, a consideration of the palaeomagnetic polar wandering curve for various formations in the East Arm and dated Helikian units, specifically the Sparrow dykes of the Nonacho Group (McGlynn and Irving, 1978, Fig. 10), suggests an approximate age for the Et-Then group of 1750 Ma. This thermal event may be connected with two "young" dates from five and six-point Rb/Sr isochrons by Wanless (pers. comm., 1977), ie. 1750±52 Ma and 1759±30 Ma.

k) The Age of the Helikian Gabbro

Thick gabbro cone sheets form a body 125 km in diameter centred on the eastern section of the East Arm. (Hoffman, *et al.* 1977). The minimum age for these intrusions is given by a 1315 Ma date for the cross-cutting, N.E.-trending Mackenzie III diabase swarms (Fahrig and Wanless, 1963).

E. SR-ISOTOPIC RATIOS OF THE MAGMATISM

Because of the metamorphism, clinopyroxene is commonly the only remnant igneous phase. Pure clinopyroxene concentrates were therefore extracted from selected samples in order to determine their Sr-isotopic compositions. These measured values will be close to, but higher than, the $^{87}Sr/^{86}Sr$ initial ratio of the magma because of the low but

finite Rb content in clinopyroxenes. Measured and suitably corrected values are given in Table 6-5.

a) The Provenance of the East Arm Magmas

The high initial ratio for the Pearson Formation Rb-Sr isochron (0.7089) is confirmed as a magmatic rather than a metamorphic value by the higher initial ratio shown by the separated pyroxenes (0.7102). The difference in the two values can be explained if one assumes a higher than normal Rb-Sr value for the clinopyroxene of 0.019. Because augite from modern alkali basalt has an Rb/Sr of 0.016 (Griffin and Murthy, 1969), this is a reasonable value for augites from a tholeiite contaminated with crustal material. Upper crustal contamination of the primary magma is strongly suggested by comparing the high value of the isochron initial ratio to the simple single stage growth curve for Sr^{87}/Sr^{86} in the mantle and to that estimated for the Slave Province (Fig. 6-3).

Further evidence of contamination is given by plots of initial $^{87}Sr/^{86}Sr$ vs. Sr and Rb contents and Rb/Sr ratio (Fig. 6-4a and b). The Sr content is low compared to those for modern continental basalts and would therefore have been susceptible to a marked change in initial ratio had upper crustal contamination occurred (Faure and Powell, 1972). Rubidium contents are high and variable for continental basalts, whereas Rb/Sr (Fig. 6-4c) shows extreme variation and a range that extends beyond that for modern continental

basalts. Such extreme variations in one basaltic flow package of limited overall compositional variation is likely evidence of contamination. These diagrams also emphasize the high initial ratio of the Pearson Formation even when compared to modern basalts.

As well as Rb, the Zr/Ti ratio of this formation is very high. This is a common feature of continental tholeiites which have been contaminated with crustal material (see Ch.8).

The provenance of the various magmas can be estimated by plotting corrected $^{87}Sr/^{86}Sr$ initial ratios, from both augites and whole rock isochrons, against time (Fig. 6-5). Unlike the unequivocal evidence for the Pearson Formation, the confirmation of upper crustal contamination for most Proterozoic rocks, using this diagram, is complicated by various models used for the evolution of Sr isotopes in the mantle. Two extreme models are illustrated; one assumes the beginning of mantle heterogeneity at ~1500 Ma (Hart and Brooks, 1977), whereas the other is based on Rb-Sr ratios for South African mafic rocks, which suggest very high mantle $^{87}Sr/^{86}Sr$ ratios during the Aphebian (Davies and Allsopp, 1976).

Regardless of the model adopted, certain conclusions (see Table 6-5) can be drawn concerning the origin of the East Arm magmas. Early mafic magmas are probably derived directly from the mantle, but later ones indicate some upper crustal contamination. Because these conclusions, with the

exception of the Sosan Group volcanics, are based on Sr isotopic initial ratios from relict igneous minerals, metamorphic alteration can be ruled out as a cause of high values. In the case of the Sosan Group volcanics, for which no pyroxeme data are available, the low initial ratio indicates a mantle provenance regardless of whether the measured age is metamorphic or extrusive. No fresh augite could be separated from the Union Island Group basalts; but two unpublished isochrons (R.K. Wanless, pers. comm., 1977) alghough giving widely divergent ages, have similar, mantle initial ratios (0.7028±0.0003 and 0.7032±0.0001) to those obtained in this study for the crosscutting diabases (0.7021 to 0.7030).

The unpublished nine-point isochron obtained for the quartz-diorite laccoliths (R.K. Wanless, pers. comm., 1977) gives an initial ratio of 0.7043±0.0014. These are high, but possible values for the Aphebian mantle and probably reflect partial melting of a mafic lower crust.

The Wilson Island Group volcanics pose a problem in terms of their provenance. If 2200 Ma marks the age of extrusion of these lavas from a mantle source, then Sr isotope homogenization caused by a metamorphic event 400 Ma later would produce an observed "initial ratio" as low as 0.7051 if the source material had an Rb/Sr raio of no more than 0.21. However, the Rb/Sr of the most mafic rock sampled was 0.39. Even allowing for a possible 30% increase in Rb/Sr compared to source material for low-percentage partial melts

(Duncan and Compston, 1976), the initial ratio would have to be a very low 0.7003 at 2200 Ma (Fig. 6-5). Furthermore, uncontaminated mafic rocks derived from the mantle normally have an Rb/Sr of less than 0.1 (Green and Ringwood, 1967). Thus, if the high Rb/Sr of the mafic flows is original, this would suggest crustal contamination, but because the initial ratio is unreasonably low for this Rb/Sr only two interpretations are possible. Firstly, the Wilson Island Group date may be magmatic, suggesting some crustal contamination. This would explain both the high Rb/Sr ratios and the voluminous associated rhyolites, but would not be compatible with the geological evidence which restricts this suite to an age greater than 2100 Ma. Alternatively and more realistically, the high Rb and K contents must have been introduced during a metamorphic event which reset the isochron at 1810 Ma.

F. OXYGEN ISOTOPIC RATIOS OF THE MAGMATISM

Measurements were made of the $\delta^{18}O$ of the clinopyroxenes extracted for the Sr isotopic study. These range from 5.43 to 6.48% and are listed in Table 6-5 along with $\delta^{18}O$ values for the host rock. Since fresh basalts commonly have a $\delta^{18}O$ value which is 0.5 °/₀₀ greater than their contained clinopyroxenes, Table 6-5 suggests that the epidote actinolite facies metamorphism of the early diabases produced varying degrees of alteration on a small scale. The whole rock $\delta^{18}O$ for the Mid Aphebian dykes is only 0.5 to

0.8°/$_{oo}$greater than that expected for the magma but the Union Island Group sills indicate increases of 0.4 to 2.0 °/$_{oo}$.

The pyroxenes from the early, mantle - derived continental tholeiitic diabase of the East Arm (Mid - Aphebian and Union Island Group) indicate magmas with original $\delta^{18}O$ values of 5.9 to 6.7°/$_{oo}$. The late Jackson Gabbro and Pearson Formation, whose Sr-isotopic compositions indicate some crustal contamination, suggest magmas with a $\delta^{18}O$ of 6.6 to 7.0°/$_{oo}$.

These values are all in the range expected for fresh, Phanerozoic continental tholeiites (eg. Yakima, Washington, J. Cocker, pers. comm. 1981). In a study of basalts from ocean basins, ie. those uninfluenced by crustal chemistry, Kyser and O'Neil (1978) showed a range in $\delta^{18}O$ from 5.0 to 6.7 °/$_{oo}$, but 5.8 °/$_{oo}$ separated the lower model value for tholeiites from that for alkali basalts.

The oxygen isotopic compositions of Mid Aphebian and Union Island Group magmas can therefore be derived from a mantle source. However, the few data available for the Jackson Gabbro and Pearson Formation support evidence from the Sr-isotopic compositions of crustal contamination.

G. CONCLUSIONS

Rb-Sr isochrons for two volcanic units from the East Arm give similar dates despite an obvious separation in time of several hundred million years and contrasting grades of

metamorphism. This suggests that the Rb-Sr isotopes of the older Wilson Island Group were reset during a Hudsonian thermal event at 1810 Ma. This event may have also reset the Rb-Sr and Pb of the Sosan Group volcanics. The intensity of Hudsonian metamorphism was probably a function of burial depth with later vertical fault movements juxtaposing fault blocks of differing metamorphic grade. Surprisingly, the reequilibrated "initial" $^{87}Sr/^{86}Sr$ of the Wilson Island Group lavas is unexpectedly low if one considers their high Rb/Sr ratios. It is also difficult to reequilibrate Sr isotopes under epidote-amphibolite facies conditions, as explained above. However, the penetrative deformation and high - angle folding within the Wilson Island Group restricts its age stratigraphically and evidence of reequilibration from other areas of comparable metamorphic grade supports reequilibration of Sr isotopes. The "low" initial ratio of the Wilson Island Group lavas can then be explained by requilibration of a mantle-derived magma with the high Rb/Sr ratios resulting from an influx of Rb and K_2O during metamorphism.

The estimated initial $^{87}Sr/^{86}Sr$ ratios of the magmas obtained from both isochrons and remnant igneous clinopyroxenes indicate a mantle origin for early tholeiitic diabases and imply that all pre-Kahochella Group magmas were derived from the mantle. The late Jackson diabase and especially the Pearson Formation tholeiite show notable crustal contamination. The extrusion of the last

mantle-derived magmas of the East Arm, the alkali-basaltic suite of the Sosan Group, coincides with a period of subsidence in the graben (Hoffman, 1973). This may indicate the end of a period of mantle-upwelling.

The clinopyroxene-separates exhibit $\delta^{18}O$ values typical of the clinopyroxenes from Phanerozoic continental tholeiites. A study of the whole rocks indicates that during epidote-actinolite facies metamorphism, variable increases in $\delta^{18}O$ took place, ranging from 0.4 to 2.0 ‰ even within a single outcrop.

VII. ELEMENTS USEFUL IN THE STUDY OF ALTERED OR METAMORPHOSED VOLCANIC ROCKS

A. INTRODUCTION

Over the past few years there has been a growing awareness of the problems of the characterization of altered volcanic rocks (see for example Irvine and Baragar, 1971). This problem has been accentuated by the increasing interest in volcanic rocks in the Precambrian and their relationship to the development of the early crust. As one goes further back in geological time the chances of encountering volcanics which have undergone some degree of alteration, weathering or metamorphism multiplies. The classification of altered volcanics, whether from a purely descriptive or from a genetic, tectonic standpoint, becomes an important problem.

Most chemical classification schemes established for volcanic rocks depend upon major elements such as Na, K, Mg, Ca and Si that can be shown to be mobile during alteration or metamorphism. A number of classification schemes that have been derived to overcome this problem are based on the use of elements which are stable during alteration. These schemes have mainly fallen into two groups: those which follow descriptive, non-genetic classifications and those which discriminate between possible tectonic environments.

There is a voluminous literature on this topic; however, there has been no real attempt to integrate all

aspects of this problem and to provide a working scheme for the classification of altered volcanic rocks.

In this chapter the evidence for element mobility during different types of alteration and metamorphism is reviewed. Elements which are stable to alteration effects are identified and are used, in the following chapter, to construct a scheme or flowchart for the classification of altered volcanics, both in a classical descriptive sense and in the more recently identified tectonic sense.

B. THE MOBILITY OF MAJOR AND TRACE ELEMENTS IN ALTERED VOLCANICS

An element must be acceptable into the lattice of a stable mineral in order to show limited mobility, but mineral parageneses vary according to the conditions of metamorphism. Therefore, the type of alteration or metamorphism affecting volcanic rocks can influence the pattern of element mobility. Since retrogressive effects and weathering may have been involved prior to or subsequent to metamorphism, it is necessary to review element mobility under several different conditions of alteration in order to establish which elements are most stable. Such studies have concentrated on mafic and intermediate rather than felsic rocks since the former give more information as to the tectonic environment and, when altered, metamorphic grade.

A compilation of element mobility studies is given in Table 7-1. Attention is focused on elements which can be

analyzed by routine AA and XRF techniques. Elements normally analyzed by NAA (REE) are listed separately. Each major type of weathering will be discussed briefly below.

a) Sea-Floor Weathering

(i) Mineralogy

Sea floor weathering takes place at <50°C and is the result of the interaction of seawater with basalts of the ocean crust. The main mineral formed is a smectite group clay, which commonly replaces matrix glass. This is usually an Fe-saponite which can form at 25°C (Seyfried *et al.*, 1978), although nontronite has also been observed (Scheidegger and Stakes, 1977). Calcite, hydrous ferric oxides and hematite might be additional phases (Baragar *et al.*, 1978; Scarfe and Smith, 1977; Humphris, 1978). With progressively more intense alteration there is an increase in K_2O content in the smectite and the appearance of K-feldspar and celadonite. Stakes and Scheidegger (1978) and Scarfe and Muehlenbachs (1977) noted the appearance of celadonite in seafloor lavas over 50 m.y. old.

Zeolites such as phillipsite (Scarfe and Smith, 1977; Stonecipher, 1977), clinoptilite (Lawrence *et al.*, 1979) and chabazite (Mariner and Surdam, 1970) can also occur during sea-floor weathering. However, because these may occur at higher temperatures during zeolite facies metamorphism, all studies of zeolite-bearing

rocks are grouped separately.

(ii) Element Mobility

From Table 7-1 it is clearly seen that Li, K, Rb and Cs are all very mobile and increase with sea-floor weathering. Fe shows a smaller increase and Ca, Si and S decrease. Amongst the trace elements, Sr, Y, Zr, Nb and Hf appear stable, but Sc, V, Cr, Co and Ni are stable or show a slight depletion.

These studies have largely been carried out by comparing various element concentrations from fresh and altered portions of pillowed basalt. The problem with this approach is that non-systematic chemical variations can occur between rim and core in unaltered samples (Scott and Hajash, 1976). Where this involves a change in Fe and Mg (e.g. Shido *et al.*, 1974), a logarithmic change can occur in Cr and Ni (Miyashiro and Shido, 1975). This factor may explain the small variations in otherwise stable transition elements. Thompson (1973) has also demonstrated that glass undergoes a more extreme alteration than crystalline basalt.

Similar alteration patterns are seen where chemical indices of weathering are used, such as the consistent increase in H_2O^+ and Fe^{+3}/Fe^{+2} and decrease in Ca (Baragar *et al.*, 1977; Nicholls and Islam, 1971). Because density and volume changes will occur during hydration, variations in element concentration may be corrected by normalizing to constant volume (Thompson

and Humphris, 1977; Matthews, 1971) or constant Al (Hart, 1970). The latter authors both noticed small variations in Ti. Alternatively, Cann (1970) demonstrated that inter-element ratios amongst the group Ti, Y, Zr, Nb show high coherence, despite variations in measured concentrations which are apparently caused by density changes. The small inconsistent variations in Ti (and P) may thus be an artifact of the technique of measurement, while the moderate variation in Al appears to be real.

The heavy rare earths show small but varied changes in concentration, whereas the light rare earths undergo inconsistent and much larger changes, in some cases displaying a fourfold increase (Ludden and Thompson, 1979). La can also decrease (Frey *et al.*, 1974), whereas Ca may show an inconsistent behavior, sometimes showing the extreme relative depletion characteristic of seawater itself (Robertson and Fleet, 1976). This will depend upon the length of the exposure time to weathering, therefore patterns from dredge and drill samples will vary (Ludden and Thompson, 1979). Wood *et al.*, (1979) point out that extensive alteration of a glass-rich lava will increase La and Th, the latter being otherwise very stable. Menzies *et al.*, (1979) have pointed out that LREE are more affected by weathering than by low-grade metamorphism.

b) Very Low Grade Metamorphism (zeolite facies)

(i) Mineralogy

Hydrothermal activity in the oceanic crust is thought to proceed at temperatures >100°C. Zeolites and carbonates are the major products of this alteration. Because calcite and siderite commonly occur, carbonate geothermometers may be used to estimate alteration temperatures. Muehlenbachs (1977) noted that seawater weathering causes an increase in $\delta^{18}O$, whereas alteration above 200°C causes depletion (Friedrichsen and Hoernes, 1978). In continental rocks, the appearance of laumontite is normally taken to mark the onset of metamorphism, but it can coexist with zeolites which are characteristic of weathering (e.g., Wood *et al.*, 1976).

(ii) Element Mobility

For sea-floor basalts, no consistent major-element trends are seen apart from a depletion in Si and K. V, Cr, Co, Y, Zr and Ba appear to be stable. Wood *et al.* (1976) showed that the Ti, Y, Zr and Nb variation in zeolitized basalts from Mull and Iceland was within the limits of variation for fresh flows. Menzies *et al.*, (1977) found that the upper part of an ophiolite which had seen limited sea-floor weathering and zeolite formation showed Ce-depletion, but all HREE were stable.

(iii) Experimental Work

A series of experiments on the basalt-seawater system have been carried out at 0.5 to 1 kb and 200° to >300°C (i.e. zeolite and pumpellyite-prehnite facies conditions) and therefore allow an independent confirmation of the above results.

All experiments confirm a severe depletion in Ca and an increase in Mg. In a study of andesite, Liou and Dixon (1978) reported that these elements show the greatest solubility variation with temperature and solution type. Si, Fe and Mn show smaller depletions, but the latter two elements show an initial increase according to Bischoff and Dixon (1975). Ti shows a small increase in one study while varied concentrations are seen for Na and K. A problem with some studies is the appearance of anhydrite which suggests metastability at the temperature of the experiment.

c) Very Low and Low Grade Metamorphism (pumpellyite-prehnite to epidote-actinolite facies)

(i) Mineralogy

Under conditions of very low and low grade metamorphism of mafic and intermediate rocks, the assemblages formed are rich in albite and chlorite with accessory sphene and minor amounts of Ca-Al silicates, which act as indicators of grade. With increasing grade the common assemblages are pumpellyite - prehnite

pumpellyite - actinolite and epidote - actinolite. The first two are commonly associated (e.g. N. Maine, Richter and Roy, 1974), while occasionally all three occur in one area (Central Chile, Levi, 1969; Kii Peninsula, Japan, Seki *et al.*, 1970). In addition, epidote can occur in abundance in all three zones (Winkler, 1979). Because of the overall similarity in their mineralogy, these assemblages are considered here collectively.

The common mineralogical heterogeneity in mafic rocks provides some information on compositional variation. In particular, massive flows undergoing very low grade metamorphism display two rock types formed as separate domains within a single outcrop. The first is a zone containing abundant chlorite and albite, the latter tending to pseudomorph primary plagioclase and thereby preserve the microlitic texture of unaltered basalts; and the second is a subordinate zone of epidote and quartz (with or without smaller zones of pumpellyite and quartz) which has a remnant primary texture identical to the surrounding rock. These zones form irregular patches which vary in size from a few centimetres (Donnelly, 1966) to several metres (Reed and Morgan, 1971). In a study of the Keweenawan basalts of the U.S.A. (Jolly and Smith, 1972) and Canada (Smith, 1974) both domain types were seen to occur in flow tops and brecciated zones in an otherwise little-altered volcanic pile. The second

domain type appears to coincide with infilled fluid conduits (fractures) and reactive glass zones on a small scale (Smith, 1974) but remnant textures indicate total rock replacement in large domains.

Mineralogical variation is particularly noticable in pillowed zones. Glassy selvedge zones contain no remnant plagioclase laths which would provide nucleation sites for the growth of albite; thus they tend instead to form a chlorite-rich rim with sporadic growth of epidote, prehnite or pumpellyite (Vallance, 1965).

(ii) Element Mobility

The mineralogical variation and domain structure formed by metamorphism creates problems of representative sampling and therefore also of comparison with unaltered material. Alternatively, chemical comparisons between domains will give an indication of relative chemical mobility. Results from both approaches are given below and are tabulated in Table 7-1.

In a detailed study of the Catoctin greenstones in Virginia, Reed and Morgan (1971) showed that Ca and Fe^{3+}/Fe^{2+} increase in epidote rich zones, Na, Mg and H_2O are concentrated in the albite-chlorite domains, whereas Al, Si, P, Ti, Fe and Mn remain relatively immobile A study by Smith (1968) of a single Ordovician domain-structured outcrop at Cliefden, N.S.W., confirmed these results except for the greater mobility of Si and Fe. The antipathetic nature of Fe^{3+}/Fe^{2+} and H_2O^+ and

their respective correlation with epidote and chlorite growth has been demonstrated also for diabases from S.W. England (Floyd, 1976). Reed and Morgan (1971) calculated an average composition for their altered outcrop, noting that it compared closely with that of some unaltered feeder dykes. Mg and Ca showed some variation, whereas K suffered a marked depletion. Smith (1968) noted that Reed and Morgan's average composition was comparable to a basaltic andesite except for Na. A similar technique was used by Vallance (1969), who used frequency histograms to compare 2000 basalts with three selected groups of basalts which had undergone low-grade metamorphism. He showed that there was a strong variation in Na, Mg and Ca with the development of albite and chlorite-rich domains, but that little overall change occurred in Al, P, Ti and Mn.

Other studies, comparing rocks of varying degrees of alteration from the same outcrop or formation but without the extreme development of zones, indicate similar large variations in Mg and depletions in Ca. In addition Na, K and Si tend to show high and inconsistent variations. For example, Davies *et al.* (1979) found that Na was as mobile as Ca, whereas Si was comparable in stability with Al. Cann (1979) noted an overall conservation of Na if the compositions of different textural types were integrated, but Si was more mobile than Ca. K normally undergoes depletion, but increases

have been noted (Humphris and Thompson, 1978) and this may be locally important where albite has been sericitized (Lidak, 1965; Hekinian, 1971). The tendency of K to be depleted under low grade has been confirmed experimentally by Bischoff and Dixon (1975) who noted a loss of K from basalt reacted with seawater at temperatures above 200°C. In that study, other major elements displayed small and inconsistent variations.

Unfortunately, where no fresh material is available, initial chemical changes cannot be determined. Furthermore, if complete alteration has taken place, different mineralogical domains are in effect being compared. Thus one cannot consider relative gains or losses if the whole outcrop remains isochemical. For example, Strong *et al.* (1979) compared an "altered" and "unaltered" population on the basis of increased Si content, but this increase was accompanied by an average decrease in H_2O^+. Therefore, both sequences must be considered altered and the magnitude of element variations are important rather than the direction of change in concentration.

A solution to this problem was suggested by Davies *et al.* (1979). They modified a complicated routine of Beswick and Soucie (1978) which showed that binary plots of the molecular ratios of major element oxides are confined to a narrow compositional range regardless of composition. These plots were seen to be linear over a

restricted (i.e. mafic) range of composition and the coherence between major element pairs (e.g. SiO_2 vs. TiO_2) was tested by comparing both to a highly mobile element (i.e. SiO_2/K_2O vs. TiO_2/K_2O). If the two test elements are immobile, such a plot should produce a straight line through the origin. This has an advantage over direct correlations in that a wide spread in data points may be obtained with only a limited variation in the concentrations of immobile elements. However, an erroneous mobility will be suggested if significant chemical variation exists in the original material (e.g. Fe/Mg variation in a continental tholeiite).

Other more direct approaches to the study of mass balance have involved the direct comparison of fresh and altered material from the same outcrop or sample. Ocean-ridge basalts are important in this respect since they have a restricted range in composition compared to continental magmas, and a range of fresh to medium-grade rocks are juxtaposed in ridge fracture systems. Dredge samples of different grade can therefore be directly compared (Cann, 1969, 1970; Melson and Van Andel, 1966). Ocean ridge basalts have thus been considered important for the study of element mobility and are listed separately in Table 7-1. However, since small scale, primary compositional variation can still occur (Bryan and Thompson, 1977), the results are discussed along with those from studies of subaerial volcanics. These

include comparisons from partly altered Archean tholeiites (Condie *et al.*, 1977), ophiolites (Coish, 1977) and Phanerozoic pillowed sequences (Vallance, 1974). Humphris and Thompson (1978) took care to select fresh and altered samples from adjacent zones in ocean floor basalts.

Among the major elements, Ti and P show the greatest stability regardless of study technique. These include using H_2O^+ as an alteration index (Hattori *et al.*, 1972; Coish, 1977), stability of correlations with Zr (Cann, 1970; Coish, 1977; Hellman *et al.*, 1979; Winchester and Floyd, 1976, data from their Fig. 1), and no increase in variance using both raw data (Melson and Van Andel, 1966) and normalizing to constant Al (Humphris and Thompson, 1978a; Strong *et al.*, 1979) or to constant volume (Cann, 1969). However, the data of Humphris and Thompson indicate a variation in Ti/P that suggests a decrease in P with alteration. Moderate Ti and P mobility was also recorded by Condie *et al.* (1977), but they chose samples which included extreme (60%) epidotization and (10%) calcite content. In the latter case, the use of raw concentration data, uncorrected for density may not be strictly correct. Furthermore, this is the only study showing an increase in Ca with alteration.

Al displays only a limited mobility. Cann (1969) using linear combinations of the three adjacent textural

types of greenstone pillows and comparing these to nearby fresh material calculated a maximum loss of 4% of the original Al. Data from Condie *et al.* (1977) suggest a loss of 6%. The stability of Al, P and Ti between domain types has already been mentioned.

Total Fe tends to show an increase with alteration. This will vary with domain structure and any subsequent precipitation of sulphides (Humphris and Thompson, 1978a). Cann (1969) determined that Fe was more stable than Al, whereas Davies *et al.* (1979) found it to be slightly more mobile.

In fresh versus altered adjacent samples the trace elements V, Cr, Co and Ni display good stability regardless of the technique of study, e.g. direct comparison (Humphris and Thompson, 1978b), H_2O^+ as an alteration index (Floyd, 1976), and stable correlation coefficients (Coish, 1977). In a totally altered sequence, coherence between Co and Cr is high (Davies *et al.*, 1979). Notable exceptions are the slight depletions in raw concentrations of these three elements caused by extreme epidote and calcite development (Condie *et al.*, 1979) and a depletion in Cr in mid-ocean ridge basalts (Melson *et al.*, 1968). In the second case, this is probably caused by original variation in the samples, since Ni and V are stable and Cr shows the greatest sensitivity to slight changes in Fe/Mg in basaltic rocks. Similarly Strong *et al.* (1979)

noted that Cr, Ni and V varied inversely with Zr content in an altered pillow suite considered to be calc-alkali basalt or andesite. However, such initial variations would be expected, especially in Zr and V amongst intermediate compositions (Nockolds and Allen, 1956). The sparce data available for Sc suggest that it behaves in a similar fashion. Humphris and Thompson (1978b) conclude that Sc, V, Cr and Ni may be only locally mobile, but again basaltic pillows were used and part of the variation may be real. Bischoff and Dixon (1975) noted however that Ni depletion occurred in a basalt reacted with seawater at 0.5 kb and 200°C. Despite evidence of slight mobility, Sc, V, Cr and Ni can be considered relatively stable.

Zr and Y appear to be stable either when plotted against H_2O^+ for a large suite of ocean floor basalts (Humphris and Thompson, 1978b) or by retaining stable ratios with Ti (Cann, 1970; Coish, 1977). Smith and Smith (1976) demonstrated a very strong coherence between these three elements amongst the domains of the Cliefden outcrop. The weight concentrations show considerable variation, but rather than being indicative of mobility (Hellman *et al.*, 1979) they may reflect density changes caused by extreme chemical redistribution. The data of Condie *et al.* (1977) show a similar pattern. Nb shows coherent ratios with Zr (Cann, 1970) but some variation in an altered andesite (Strong

et al., 1979). Sr tends to alter in the same sense as Ca (normally depletion), while Rb and Cs are depleted along with K.

Heavy rare earths all show stability. Hellman and Henderson (1977) suggested that some LREE were mobile by comparing the altered base of the Bhoiwada volcanics with the overlying fresh tholeiites. Floyd (1977), however, argued that the marked differences in La/Yb ratios amongst the least altered samples indicated an original compositional variation in the sequence. This may also explain the marked difference in P content within the formation, Hellman *et al.* (1979) observed a greater variation in LREE than in HREE in the Cliefden outcrop, but noted that the variations are small.

Other studies on ocean ridge basalts (Herrmann *et al.*, 1974) and on an ophiolite (Menzies *et al.*, 1977) indicate immobile LREE. Menzies *et al.* (1979) noted no changes in LREE or HREE during basalt-seawater reaction at 0.5 kb and 150-350°C. This stability remained even when the charge was totally altered to chlorite-smectite. They concluded that retrogressive effects may cause instability at low temperatures.

Hf appears to be stable under extreme alteration (Condie *et al.*, 1977), whereas no significant variation was noted by Wood *et al.* (1979). One study of Ga (Melson *et al.*, 1968) suggests its stability.

In conclusion, the most stable elements appear to be Ti, Y, Zr, Nb, Ga and the HREE. Slight, but uncommon variations occur in Al, P, Sc, Cr, V, Co, Ni and LREE while Fe can show a moderate variation, especially if sulphides are formed. Na, Si, Ca, K, Rb and Sr are highly mobile.

d) Medium Grade Metamorphism

Very few studies have been carried out on the mobility of major and trace elements under medium grade metamorphism. Field and Elliot (1974) studied binary plots, each of a single element in adjacent gabbro-amphibolite pairs. Small variations were seen in P, Ti and Cr; however, Sc, V, Co, Ni, Y, Zr, Nb, Ga showed little significant variation. A drawback with their method is that concentrations in altered rocks were not corrected for changes in density.

A comparison of correlation coefficients for relatively stable element pairs between fresh and altered rocks may eliminate some of the variation in V, Co and Zr. Cann (1970) used this technique to illustrate stable Ti/Zr. However, Saunders and Tarney (1977) indicated stable Ti, Zr and Y by directly comparing the element concentrations in fresh and altered parts of an ophiolite. Part of the problem with Field and Elliot's data may be the expected small scale variation in Fe/Mg in coarse textured gabbros and its effect on Cr variation more than on the other trace elements.

C. FACTORS AFFECTING ELEMENT MOBILITY

Important factors affecting the mobility of an element are the stability of the host mineral during alteration, the availability of stable lattice sites and the intrinsic properties of the element itself, notably charge density. The pH of the alteration fluid and the water/rock ratio are also extremely important.

The elements which show the least mobility are transition series elements with incomplete d-shells (Sc to Ni, Y to Nb and La to Ta) and f-shells (Ce to Lu, Th). The high charge densities of these ions inhibit the formation of soluble complexes in aqueous solutions of moderate pH. Within the Sc to Ni group, Mn shows a minimum charge density which may explain its higher relative mobility. Al, Ga and P similarly show high charge densities. As a group these elements contrast strongly with the alkalies and alkali-earths.

Fig. 7-1 displays the likely host mineral sites for immobile minor and trace elements in a mafic rock and their most likely repositories during sea-floor weathering and low-grade metamorphism.

The breakdown of plagioclase largely explains the mobility of Ca, which has been noted under all forms of alteration, and of Sr and Ba, because plagioclase is the main repository for these elements. The stability of Sr noted by Hart *et al.* (1974), may reflect limited smectite formation. At low grade, Ba would be lost while Sr is fixed

in epidote. The evidence for this is the proportional increase of Sr with modal epidote (Melson and Thompson, 1968; Smith and Smith, 1976). Condie *et al.* (1977) noted a similar but smaller effect with Ga. Y, Zr and La have only a negligible concentration in plagioclase and therefore, will not be significantly affected by the alteration of this mineral.

Within continental tholeiites and alkali basalts with little or no K-feldspar, K is concentrated predominantly in interstitial glass along with Cs and Rb. The increase in these alkalies during sea-floor weathering indicates fixation in the interlayer sites of clay minerals. Under low grade conditions, such large ions can find available lattice sites within muscovite, but they are usually lost. Sodium is the only alkali ion small enough to be retained within the original feldspar structure (now albite) and thus can sometimes show limited mobility (Cann, 1969; Reed and Morgan, 1971). At medium grade, alkalis can be accomodated in the amphibole or biotite lattice causing a more limited variation in their concentration (Cann, 1970). Residual glass will also preferentially concentrate the LREEs. Because glass is very susceptible to alteration, its presence or absence may account for the varied stability of LREE (Humphris *et al.*, 1978). At low grade, REEs may be accomodated by chlorite (Copeland *et al.*, 1971; Menzies *et al.*, 1979) or within the structure of sphene or epidote. P may be similarly altered in a glassy rock with no apatite.

Apatite is the main repository for P as well as LREE and Y, both of which concentrate in the magma with fractionation. The stability of apatite even at medium grade metamorphism ensures the immobility of these elements.

The refractory nature of zircon under varying grades of metamorphism accounts for the immobility of Zr and Hf and, to some extent, of Y, P and Th. Zr in pyroxenes decreases with the fractionation of a basaltic magma (Wager and Mitchell, 1951) but concentrates in the residual melt in zircon. Zircon thus becomes an increasingly important phase as silica content rises.

The Fe-Ti oxides may contain 80% of the Ti and over half of the V in a basaltic rock, as well as much Zr, Cr and Sc. All of these elements can be accomodated within the structure of sphene which commonly occurs as a partial-replacement rim on the oxide phase, at both low and medium grades. This suggests a high stability for Ti.

Clinopyroxene contains significant amounts of almost all the stable trace elements in mafic rocks. It concentrates most of the Sc and Cr and much of the Co, Ni and V. Therefore, different alteration patterns observed amongst these elements may reflect the relative stability of clinopyroxene versus Fe-Ti oxides. Orthopyroxene and olivine have a minor effect on all these elements except Ni. At low grade, the data of Condie *et al.* (1977) indicates stability of Sc and Cr with increasing epidotization and slight depletion of Co and Ni. An opposite effect was noted with

chlorite-carbonate alteration. This suggests that divalent Co and Ni are accomodated in actinolite and chlorite, while trivalent Sc and Cr are preferentially contained in epidote. Epidote can also contain considerable Ti.

Actinolite-chlorite-epidote alteration of clinopyroxene could therefore retain all of the stable elements (see Fig. 7-1). The small scale variation of Ni and Co (Humphris and Thompson, 1978b) may reflect partial solution during the growth of new hydrous phases, whereas variability in Mn, which is mainly (~70%) contained in clinopyroxene, indicates a greater degree of solution. Under conditions of sea-floor weathering, limited mobility of these elements will occur owing to the formation of hydroxides, their adherence to clay particles, and the incorporation (of Ni) within expandable clays. Clinopyroxene may contain about one third of Y in a mafic rock, but this element does not appear to be easily dispersed.

D. CONCLUSIONS

From a review of the response of volcanic rocks to different types of alteration, the most stable elements are seen to be P, Ti, Y, Zr, Nb, Ga, HREE, Hf and Th, i.e. those elements associated with refractory accessory minerals. For petrogenetic modelling and magmatic classification, auxiliary use can be made of LREE, Sc, V, Cr, Co and Ni.

VIII. THE CLASSIFICATION OF ALTERED VOLCANIC ROCKS

A. INTRODUCTION

In chapter 7, a review was made of the relative stability of major and trace elements under varying conditions of metamorphism. This is considered important data in the study of metamorphosed volcanic rocks because commonly-used, chemical classification schemes depend upon elements which are mobile during metamorphism and which are, therefore, of limited use. As a result, a number of classification schemes have been derived which are based on the use of relatively stable elements. Alternatively, some schemes rely on mobile elements but attempt to screen out heavily-altered samples from a population before a classification is attempted. This is achieved by eliminating those samples which have major-element concentrations uncharacteristic of unaltered volcanic rocks. The ab[redacted] schemes include both non-genetic classifications and those which discriminate between different tectonic environments.

In this chapter, the classification schemes in current use are reviewed and some new ones are proposed. The most efficient of these have been incorporated into a flowchart, the use of which should avoid many of the misleading deductions which are possible with this work.

B. NON-TECTONIC CLASSIFICATIONS

Common schemes divide rock types into alkaline and subalkaline groups (e.g. Kennedy 1933, Wilkinson 1968), the former containing the alkali-olivine basalt series which contains both sodic and potassic-rich differentiates (MacDonald, 1968; Baker et al., 1964). The schemes below all group the shoshonite series (Joplin, 1965 and 1968) with the potassic basalts. The subalkaline group is composed of the tholeiitic series and calc-alkaline association (Tilley, 1950). In recent years komatiites have been added as an additional group.

These series have been chosen by many authors because they appear to be natural divisions, without necessarily having genetic implications. However, because the subdivision of subalkaline magmas can be suggestive of tectonic environment, it will be dealt with in a later section. The division of volcanic suites into alkaline and subalkaline types is important because the mafic differentiation trends of these groups are effectively separated by a low-temperature thermal divide and could thus have a genetic significance. These types of classification are outlined below.

a) Major Element Classifications

A number of schemes exist for classifying a limited number of volcanic rock types in terms of major-element-oxide combinations (Church, 1975) or normative

plots (Arculus & Johnson, 1978). Le Maitre (1976) used a data file of over 8000 analyses to identify volcanic and plutonic rocks using major-element-oxide plots and discriminant function analysis, but because each rock name was taken from the literature and therefore erected on a wide variety of criteria, large overlaps were seen and methods of subdivision attempted.

The most comprehensive and widely used scheme is that of Irvine and Baragar (1971). These authors suggested its use for altered rocks. It classifies 21 rock types and is based on a series of integrated cation-normative plots. Leucite-bearing and peralkaline (acmite-normative) rocks are excluded.

(i) Ol-Ne-Q, Cpx-Ol-Opx and Alkalies-Silica Diagrams:

Yoder and Tilley (1962), working in the clinopyroxene olivine-nepheline-quartz system, found a thermal divide coincident with the clinopyroxene-olivine-albite plane. Based on this, Irvine and Baragar used a cation normative ol-ne-Q plot as their main separation diagram. The tendency for an alkaline series to cross this plane from the nepheline to hypersthene normative side has necessitated an empirical shift in the boundary curve. Poldervaart (1964) suggested that this reflected the true position of the thermal divide, but because the boundary is absent at the higher pressures (approximately 10kb) more suitable to the production of alkali olivine basalt

(Green and Ringwood, 1968; O'Hara, 1968; Kushiro, 1969), a real overlap should exist on all variation diagrams. The olivine-tholeiite compositional range thus represents a transitional basalt zone. Basalts from alkali suites may cover half of this area (Fig. 8-1). Because a single dividing line has no real meaning in separating these magma types, the dividing lines added by Poldervaart to Irvine and Baragar's plot should be viewed only as marking empirical limits for the compositional extent of alkaline suites into the olivine tholeiite field.

This problem occurs again if one uses Chayes (1966) plot of cpx-ol-opx, specifically designed for olivine tholeiites. Chayes used a hyperbolic dividing line which gives a good statistical separation between the two magma types. Irvine and Baragar (1971) pointed out that many ocean-floor basalts plot in the alkaline field of this diagram. However, because such rocks are products of low pressure partial melting (of aluminous peridotite) one should expect such compositions to plot throughout the cpx-ol-opx field and, therefore to overlap with ol-hy normative compositions which are grouped within the alkaline field. Chayes' boundaries again mark the observed extent of moderate-pressure partial melting.

A simpler plot to use, not requiring a norm calculation, is the alkalies - SiO_2 diagram. Irvine and

Baragar (1971) found only a moderate overlap across a single dividing line, but when compared to the much more detailed plot of Cox *et al.* (1979) this line is seen to occur within the hy-normative field. Detailed boundaries cannot be constructed within this field because the simple dividing lines of MacDonald and Katsura (1964) and Irvine and Baragar (1971) simply represent the compositional variation in plagioclase (McBirney and Williams, 1969), therefore a whole series of parallel dividing lines could be generated depending upon colour index. This is illustrated by Schwarzer and Rogers (1974, Fig.1). On their diagram the boundary of Irvine and Baragar (1971) appears to classify many subalkaline compositions as alkaline. This plot therefore is imprecise but again shows overlap between the two magma types.

The low pressure thermal divide therefore represents, in theory, the maximum compositional extent of subalkaline magmas towards the alkaline field and is the only meaningful boundary on alkaline versus tholeiitic variation diagrams. This "subalkaline limit" has largely been ignored in the construction of variation diagrams.

The problem with all of the above systems is their limitation to only mildly altered rocks. Before using these diagrams the analyses must be recalculated volatile-free and assigned a value for the oxidation

ratio of iron. This value, which will change to some extent during metamorphism has a marked effect on the calculated norm and can strongly affect the assignment of subalkaline or alkaline character (Chayes 1966). Irvine and Baragar suggest calculating a maximum oxidation ratio by using $Fe_2O_3 = TiO_2 + 1.5$; however Johnson *et al.* (1978) found no basis for this in their data. It is probably better therefore to use the oxidation ratio of the least altered material available.

(ii) The Igneous Spectrum:

The discriminating power of Irvine and Baragar's approach is offset by its reliance upon cation-normative feldspar calculations at several stages of the classification. These depend in turn upon the stability of Na and K which are normally highly mobile under low-grade metamorphism. The efficiency of the classification could be improved by a simple test for the limited mobility of alkalies.

Hughes (1973) produced a binary plot of two separate functions of Na_2O and K_2O. This plot defined an area ("igneous spectrum") including all unaltered volcanic rock types which was subdivided into zones characteristic of each main type. Stauffer *et al.* (1975) extended the field to include the low-K tholeiities of island arcs. Komatiites have not been included in this plot but these are normally detectable by other means (see below). Miyashiro (1975) devised a similar

discrimination plot.

Hughes's "igneous spectrum" is suggested for use as a preliminary screen to eliminate most non-igneous compositions. A subsequent Irvine and Baragar routine can then be used for a more detailed classification. It is important to realise that this screen will not check the stability of Na and K but will select rocks which show only a limited mobility of these elements.

(iii) CaO/Al_2O_3-$MgO/10$-$SiO_2/100$ plot:

Because the igneous spectrum plot essentially tests only for unaltered felspar, it was found, in practice, to give an unaltered classification to rocks with an igneous alkali composition but with widely varying Ca contents. A further test for Ca mobility was made using the CaO/Al_2O_3-$MgO/10$-$SiO_2/100$ plot of P.A. Davis (pers.comm. 1979). The logarithmic variation of CaO normalized to the relatively stable oxide Al_2O_3 is compensated for by the similar variation in MgO. Unaltered continental lavas are restricted to a narrow zone of increasing SiO_2. Further testing by the author established that this zone was valid for oceanic island and calc-alkaline suites. This diagram was used in conjunction with the igneous spectrum on a test suite of 24 mafic samples from the Kahochella Group, Great Slave Lake, on which norms had been calculated. There were only four samples which had acceptable igneous norms (i.e. no corundum or wollastonite), and which also could

be classified as unaltered by both of the alteration screens above (see Ch.10).

(iv) Correlation Matrix:

An alternative technique which may involve the use of more data would be to modify the correlative technique of Davies *et al.* (1979) (see above). Assuming K_2O to be the most mobile oxide, molecular ratios of each oxide to K_2O could be compared for a suite of samples using a simple correlation matrix.

For a limited range in composition, high correlation coefficients should be expected for stable element pairs. These could subsequently be checked for a near-zero intercept. The elements showing high correlations could then be used to define the magma type. A problem would occur however, in a differentiated suite where the correlation coefficients between unaltered element pairs may not be high. Even amongst a limited compositional range, correlations between "stable" elements may be low in unaltered rocks e.g. Cann (1970) noted the stability of Nb and Y concentrations between fresh and altered basalts even though the correlation coefficients were both very low (-0.23, -0.34). More importantly, binary plots of ratios which use the same variable as a denominator will develop spurious positive correlations, particularly if the variance of this variable is comparatively large (Chayes, 1971).

Most major element studies should therefore be treated with caution because many samples may not be usable. A better approach is to use stable elements.

b) Stable Element Classifications for Mafic Rocks

Most stable element classifications have again been primarily concerned with mafic rocks.

(i) Nb/Y:

Pearce and Cann (1973) separated alkaline from tholeiitic basalts by the consistently higher Nb/Y ratio of the former. Although they grouped their data on a tectonic basis, a range of overlap and transitional compositions occurs between Nb/Y values of 0.5 to 1.0.

Floyd and Winchester's (1975) data indicate an overlap of alkaline and tholeiitic fields from 0.67 to 1.2, while Winchester and Floyd's (1977) scheme shows the transitional Easter Island suite plotting in this overlap region. Because these compositions should be included with alkaline suites they suggest a dividing line of 0.67 between tholeiitic and alkaline compositions. While other transitional suites (e.g. Zubair; Gass *et al.*, 1973) also plot in this range, inclusion of others (e.g. Mid Atlantic Ridge, 45°N; Cann, 1970; Pearce and Cann, 1973) reduces this divide to 0.5, and Hebridean Plateau basalts (Morrison, 1978) further reduce it to 0.4. The latter group is dominantly ol-hy normative (Thompson *et al.*, 1972) and displays

Nb/Y ratios as low as those from ocean floor basalts (<0.5, Pearce and Cann, 1973).

Nb/Y therefore appears insensitive to the separation of quartz and hy-normative compositions although only a small number of tholeiites have Nb/Y > 0.67. Compositions with Nb/Y >1 are unequivocally ne-normative.

(ii) Nb/Y and TiO_2 vs. Zr/P_2O_5:

Floyd and Winchester (1975) produced binary discrimination diagrams for alkaline vs. subalkaline basalts (i.e. 45-52% SiO_2) based on immobile elements which tend to be more highly concentrated in alkaline rocks.

The best discrimination was obtained from a Nb/Y vs. Zr/P_2O_5 diagram (Fig. 8-2); their only plot which uses element ratios on both axes. No meaningful tectonic discrimination was claimed by the authors with any plot. However, although these authors group ocean-floor and oceanic-island basalts together, they take note of the consistently higher Ti and Zr contents of the latter. The authors classified a number of altered rock suites with these diagrams (Winchester and Floyd, 1976) but did no detailed check of the consistency in classification of each plot.

The commonly used TiO_2 vs. Zr/P_2O_5 plot (e.g. Graham, 1976b; Morrison, 1979; Strong *et al.*, 1979) sometimes suggests a more alkaline composition than the

Nb/Y vs. Zr/P_2O_5 plot. de Albuquerque (1979) noted that the ne to hy- normative basalts of the Red Sea (Zubair Island) and Mauritus were respectively classified as alkaline and transitional with these plots, while Morrison (1978) noted that the Hebridean Plateau layas were likewise classified as transitional and subalkaline.

This tendency for the former plot to emphasise alkalinity can also be seen by its alkaline classification of the spilites of N.W. Germany (Winchester and Floyd, 1976) although this suite displays a tholeiitic REE patte[illegible] and a clinopyroxene composition suggestive of mild[illegible]kaline conditions (Floyd and Winchester, 1978). [illegible] difference cannot be caused by the inclusion of intermediate compositions because these will tend to plot towards the subalkaline field boundary in the TiO_2 vs. Zr/P_2O_5 diagram and further into the alkaline field on the Nb/Y vs. Zr/P_2O_5 plot i.e. in the opposite sense of the anomaly. Nb/Y therefore appears to be a more sensitive indicator of alkalinity than TiO_2, the latter being unable to discriminate between alkaline and transitional basalts.

Because these diagrams must both contain a finite area of overlap analagous to part of an ol-hy normative field we may expect transitional compositions to range into the subalkaline field. The Nb/Y vs. Zr/P_2O_5 plot therefore usefully restricts re-normative compositions

to its alkaline field, but like the Nb/Y ratio allows a large overlap between transitional and primitive (i.e. low - pressure, MgO rich) melts. TiO_2 vs. Zr/P_2O_5 legitimately classes transitional compositions with alkalic suites but usefully restricts transitional Hebridean basalts to >1.4% TiO_2 (Fig. 8-3) and separates them from the primitive Preshall Mhor type.

The Preshall Mhor dykes deserve special mention here. These have major and trace element patterns very similar to ocean floor basalts (Mattey *et al.*, 1977) but show slightly lower TiO_2 (~1%) and SiO_2 (~47%) and higher CaO (11-13%) they would therefore appear to be the product of extensive low-pressure partial melting except for the occasional appearance of ne in the norm. This may be caused, however, by the low (1.5%) Fe_2O_3 content which was assumed by Mattey *et al.*, (1977). Other primitive continental basalts (e.g. the olivine-poor tertiary Baffin Bay lavas, Clark, 1970, Table 1, col. 5) have a very similar chemistry to the Preshall Mhor dykes but show no ne-normative compositions. A ne-normative analysis which is closely comparable, except for higher K_2O, occurs at Girnar, W. Deccan (Bose, 1972, Table 1, col. 16) but this is an isolated gabbro intrusion, apparently unrelated to the main Deccan volcanism. Although the Preshall Mhor dykes are probably all hy-normative, one should consider the possibility of assigning a transitional character to

altered basalts which have the stable element composition of a primitive tholeiite but occur in a continental environment.

In addition, the high overlap between transitional and subalkaline compositions on these diagrams by a continental suite is a rarity and could be explained by a high Zr content caused by crustal contamination. The high Th content (Wood *et al.*, 1979) and low $^{143}Nd/^{144}Nd$ (Carter *et al.*, 1978) of the Hebridean suite is considered to be strong evidence of crustal contamination.

These two plots are therefore best used in sequence to separate ne-normative compositions (Nb/Y vs. Zr/P_2O_5) and then transitional types (TiO_2 vs. Zr/P_2O_5), both a result of medium pressure melting, from some primitive subalkaline compositions which may include quartz-normative types.

A final point is that these plots do not apply to lavas from compressive environments. de Albuquerque (1979) showed that island arc tholeiites plot close to the transitional boundary but still within the subalkaline field on the TiO_2 vs. Zi/P_2O_5 plot. Similarly the Chitaldrug amphibolites (Floyd and Winchester, 1978) which show the low Ga and high Zr/TrO_2 of andesites plot as transitional on this diagram. Intermediate compositions should be screened before these plots are used.

c) Stable Element Classifications using Mafic to Felsic Compositions

Problems can arise with basaltic rock classifications if altered intermediate compositions are confused with mafic rocks. Under low-grade metamorphism, the common Ca depletion and Na increase of altered basalts may lead to a superficial chemical similarity with andesites but the common preservation of igneous textures allows intermediate rocks to be separated by low colour index, the threshold value being variably defined between 30 and 40. Alternatively, under medium-grade metamorphism, igneous textures and modal colour indices are not preserved. The normative color index may be of use here although this is often modified somewhat by alteration.

Identification of intermediate alkaline compositions has been hindered by varied chemical divisions using major elements; e.g. hawaiite is varyingly defined as including a range in differentiation index of 30-45 (Thompson *et al.*, 1972), 35-56 (Nockolds *et al.*, 1978) and 38-51 (Tilley and Muir, 1964; Floyd, 1976). The latter classification forms the basis of Irvine & Baragar's (1971) subdivisions.

Floyd (1976) produced a plot for discriminating rock-types of the sodic alkaline series using major elements (SiO_2 vs. TiO_2/P_2O_5). The high overlap of the basalt and hawaiite fields is notable but mugearites are restricted to TiO_2/P_2O_5 values of <3.5.

(i) Zr/TiO_2 vs. Nb/Y:

Winchester and Floyd (1977) attempted to classify rock suites by the use of differentiation indices based on immobile elements. Zr/TiO_2 was shown to increase markedly with SiO_2 content while Nb/Y stayed relatively constant or showed a slight increase for subalkaline suites. Both indices displayed a characteristic range of values depending upon the alkalinity of each suite.

The combination of these indices in a Zr/TiO_2 vs. Nb/Y diagram produces a plot analogous to a SiO_2 vs. alkalies diagram (Fig. 8-4). It allows classification of 10 mafic to felsic rock types, but because the complete range of volcanic rocks is included, each subdivision represents an agglomeration of similar groups. This is especially the case with the alkaline suites. Both the sodic and potassic suites are indistinguishable on the diagram. Furthermore, the Zr/TiO_2 ratio, like TiO_2/P_2O_5, is relatively insensitive to intermediate differentiates, thus alkali basalts are grouped with hawaiite and mugearite (and trachybasalt) but separated from benmorite (and tristanite).

Although they show a large overlap, mugearites may be distinguished from basalts by their higher average Zr/TiO_2 ratio (0.017 compared to 0.008). However, Floyd's (1976) data set considered mugearites to have a minimum Zr/TiO_2 of 0.017. Futhermore, the limitations of the alkaline/subalkaline dividing line of Nb/Y = 0.67

used on this diagram has already been commented upon (see above). No precise names therefore can be given to alkaline intermediate rocks using this diagram but it is petrogenetically useful for distinguishing intermediate from mafic rock types as a group. types.

Subalkaline compositions on this diagram show a small overlap between andesites and basalts. The Zr/TiO_2 ratio is plotted in other diagrams against Ce and Ga, both of which increase with the alkalinity of the suite. These diagrams are, however, based on smaller data sets and display a higher overlap between basalts and andesites and between different basalt types.

The above diagrams can be used in conjunction with colour index to identify felsic and intermediate compositions before checking the mafics on a more suitable diagram.

(ii) REE:

As pointed out above, LREE are mobile under conditions of sea floor weathering, especially La and Ce. Under medium grade metamorphism, LREE may show moderate mobility. HREE appear to be stable under all conditions.

The usefulness of REE in magma classification is apparent when the REE contents of samples from different tectonic environments are normalized to a chondritic composition (e.g. see Garcia, 1978). High SiO_2 and alkalies are typified by enhanced LREE contents although

considerable overlap exists between fields.

K-poor tholeiites from both island arcs and ocean ridges have identical horizontal profiles with most REE yielding chondrite-normalized concentrations of between 8 and 35. A characteristic, relative depletion of La, Ce and Yb occurs giving a La (& Yb) range in concentration of 5 to 25 times chondritic values. Ocean island and calc-alkaline basalts can largely be included in this envelope but show a negative chondrite-normalized slope from La (20 to 40) through Gd (10 to 20) to Lu (6 to 12), (Condie, 1976, Fig.1).

Alkali basalts show an even steeper negative slope than ocean island basalts. HREE are similar but with Gd > 20 and a strong La and Ce enrichment (La from 60 to >100). Nephelinites have similar slopes but with a higher range in concentrations (e.g. La >400). K-rich basalts will show even steeper profiles (Kay and Gast, 1973, Sullivan and Keen, 1977). Floyd suggested that alkali basalts could be characterized by La/Yb ratios of 11 to 40 compared with the range of 2 to 7 for continental tholeiite.

Andesites show a range of concentration profiles which overlap the fields of calc-alkali to alkali basalts. They also display a negative Eu anomaly which distinguishes them from silicified basalts (Kay and Senechal, 1976).

Therefore, if intermediate compositions are excluded, concentration profiles of HREE from chondrite normalized plots will allow the identification of three groups of basalts: alkali, ocean island tholeiite/calcalkali and ocean floor basalt/arc tholeiite. Owing to the wide range in REE concentration for each suite, ranges in ratios such as Gd/Yb may be useful discriminants under all conditions of alteration.

C. TECTONIC CLASSIFICATIONS

Several attempts have been made in recent years to characterise volcanic rocks from different structural settings using plate tectonic models. Because this presupposes the existence of rigid sialic plates, such models cannot be used for the study of Archean environments.

Such studies commonly compare the basaltic components from each environment using an identification scheme such as the one below (after Pearce, 1976).

1. Within-plate basalts (WPB) include both alkaline (WPA) and tholeiitic (WPT) types erupted through continental crust (CON) and as ocean islands and seamounts (OIB).
2. Ocean floor basalts (OFB) are erupted at divergent plate margins.
3. Volcanic arc basalts (VAB) are erupted at convergent plate margins and include island arc tholeiites (IAT) which are generally low in K (LKT), from near deep ocean trenches; calc-alkali basalts (CAB) erupted behind the

trench or on a continental margin; and shoshonites (SHO) discussed below.

The major element chemistry of each of the above groups is illustrated in Fig. 8-5, although considerable overlap exists between these mean values.

OFB and MgO and CaO-rich tholeiites which connect two chemical trends, one of increasing TiO_2 and FeO characterizing WPB (Hubbard, 1969) and a second showing the high SiO_2 and Al_2O_3 of VAB. IAT and CAB are not clearly separable in terms of their tectonic environment (Arculus and Johnson 1978) but both tend to show higher K, Rb, Cs, Sr, Ba and Pb and lower MgO, Ni and Cr than OFB (Jakes and Gill, 1970).

The SHO series is distinguished from the potassic basalts by a notable lack of FeO and Na_2O enrichment, a high Al_2O_3 content (16-20% for SHO), the appearance of modal orthopyroxene and a common field occurrence as ignimbrites. Joplin (1968) considers the series to be representative of newly stabilized continental margins while a recent review of arc-trench systems (Arculus and Johnson, 1978) states that they are most common in regions with a long history of plate interactions. Joplin (1968) however, notes the association of shoshonites with leucite-bearing rocks and continental rifts (E. Africa and River Rhine) thus they are, in isolation, non-diagnostic of tectonic environment.

Although OFB show little variation in their major element chemistry, some unusual compositions do occur. In

the Indian ocean, granitic to peridotitic complexes are found (Engel and Fisher 1975) while transitional to alkaline compositions are found in the Mid-Atlantic Ridge (Bonatti *et al.*, 1971; Aumento *et al.*, 1971) and the East Pacific Rise (Johnson, 1979). These, however, are rare and localized and should not affect the overall tectonic classification.

a) Major Element Classifications for Mafic Rocks

(i) Discriminant function analysis:

Pearce (1976) used factor analysis of eight major elements determined on 358 basalts to identify the above mentioned tectonic groups. To avoid compositional overlap from intermediate differentiates, samples were restricted to a CaO + MgO contents of 12 to 20%.

Three discriminant functions allowed visual separation of five magma types with F_1 effectively separating WPB form VAB, F_2 subdividing VAB and identifying OFB, and F_3 identifying LKT. Because F_2 is strongly dependent upon K_2O and MgO, low grade metamorphism could cause the misclassification of many magma types as OFB. Sea-floor weathering, with its associated increase in K_2O would cause the opposite effect.

F_1 being strongly dependent upon TiO_2 content appears to be alteration resistant and a value of <0.34 is therefore useful for identifying WPB. OFB cannot be identified by F_1 alone, however MgO-rich WPB from Baffin

Bay (Clarke, 1970) and Scoresby Sund (Fawcett *et al.*, 1973) which were not included by Pearce (1976) in his data set, plot within the OFB field in F_1, F_2 space.

Where extensive alteration has taken place, discriminant function analysis may be no more of a tectonic guide than TiO_2 content.

(iii) TiO_2 - K_2O - P_2O_5:

T.H. Pearce *et al.* (1975) plotted the incompatible elements Ti, K and P for subalkaline basalts indicating the low TiO_2/K_2O ratios of OFB compared to most WPB.

They also showed that a number of WPB had a primitive character similar to OFB. This included the shield-stage basalts from Hawaii as well as continental basalts such as those from Greenland, Deccan and some Karroo lavas from South Africa and Lesotho. These basalts occur on continental margins and can be related to a tensional feature approximately parallel to an adjacent mid-oceanic ridge (Gibson, 1966). This may be related to the initial rifting of a continent and the first stage of ocean formation (e.g. Brooks, 1973).

This diagram does not include VAB and therefore only demonstrates the overlap between OFB and WPB. It can be useful for identifying the more evolved WPB, or if an ensialic environment is certain, for suspecting an advanced stage of continental rifting.

As with factor analysis, the identification of OFB relies greatly upon stable K_2O, therefore this diagram,

although widely used (e.g. Graham, 1976a; Strong *et al.*, 1978; Strong, *et al.*, 1979), is of limited use with altered material.

(iii) P_2O_5 vs. TiO_2:

A simple diagram which assumes that the suite contains no VAB is a binary plot of P_2O_5 vs. TiO_2 (Ridley *et al.*, 1974). This discriminates OFB from OIT and WPA. Although designed for use in ocean basins, continental lavas can be plotted and an OFB character assumed if the samples contain less than 2.3% TiO_2 and 0.3% P_2O_5. The accuracy of this diagram is likely to be higher because it avoids the use of K_2O.

(iv) MgO - FeO* - Al_2O_3:

Both Pearce's (1976) F_1, F_2 plot and Fig. 8-5 display two overlapping but divergent trends amongst basalts; that of WPB and of VAB. By using the least mobile minor element components of Fig. 8-5, it should be possible to construct a triangular plot which preserves this trend.

Pearce *et al.* (1977) constructed such a diagram for subalkaline compositions using MgO, Al_2O_3 and total Fe as FeO (i.e. FeO*) (Fig. 8-6). They found that basaltic andesites gave a better separation of tectonic environment than basalts, each group forming isolated clusters. These authors therefore claim that the effects of crystal fractionation are of a smaller magnitude than

any effects caused by the environment of eruption. However, the best discrimination is between the continental and orogenic fields, and an increasing divergence in Fe-enrichment between tholeiitic/alkaline and calc-alkaline magmas would be expected amongst intermediate rather than mafic compositions. The discrete clustering of OFB and OIB fields may be also related to the much smaller sample sizes used to establish these groups. Few OFB occur with over 51% SiO_2 and so an observed Fe-enrichment will be limited, causing a separation between OFB and OIB fields. Furthermore only 6% of the OIB sample - set qualified for plotting on this diagram and would probably enhance the effect of a single locality. Therefore, tectonic discrimination does appear to be enhanced by fractionation provided that it is of limited extent. However, the study made use of 8400 analyses and showed a usable difference in Fe-enrichment between basalts from ocean floors/rifted continents and unrifted continents.

Although orogenic and continental environments can be readily distinguished using this plot and their identification will be little affected by MgO mobility, other groups will not be readily determined owing to the large number of samples needed. A test should also be made for limited SiO_2 mobility before this plot is used.

b) Stable Trace Element Classifications for Mafic Rocks

(i) Ti-Zr-Y:

The Ti-Zr-Y diagram of Pearce and Cann (1973) has been widely used for plotting mafic compositions (e.g. Wilkinson and Cann, 1974; Aleinikoff, 1977; Furnes *et al.*, 1978; Tull and Stow, 1980). It makes use of three elements which retain the most stable inter-element ratios during alteration, and indicates four tectonic environments.

The arrangement of these fields is comparable to those of Pearce (1976) who used a similar data set. WPB are separated from VAB/OFB by higher Zr/Y ratios, whereas within each group an increase in K_2O is proxied by a Zr/TiO_2 increase. A limited data set was used to define the WPB field, magnesian continental basalts being omitted. Where data for the latter are available they are seen to plot in the OFB field e.g. Baffin Bay (Clarke, 1977) and the Lesotho Karroo (Fig. 8-7).

Some tholeiitic WPB are seen to plot in the CAB field. These include the Deccan traps (Vallance, 1974a); some N. Wales diabase (Floyd *et al.*, 1976) and Hebridean non-porphyritic central basalts (Morrison, 1978). The latter two suites have TiO_2 contents too high (>1.7%) for CAB, while all three are too FeO rich. The moderate FeO enrichment of the latter two suites is comparable with that of the Ferrar diabase (Gunn, 1966), an extreme continental tholeiite showing Zr enrichment

close to that of a calc-alkaline magma.

Floyd *et al.* (1976) argue that the N. Wales diabases represent a continental margin environment but where high level sills are studied, a high Zr/TiO_2 and apparent CAB affinity may be caused by the accidental sampling of basaltic-andesitic compositions. The least altered Deccan and Hebridean samples, however, all have basaltic compositions. An alternative explanation could be crustal contamination causing increased Zr. This has been shown to occur for the Hebridean suite (see above).

Owing to the nature of Zr/TiO_2 as a fractionation index, cumulate rocks must not be plotted on this diagram. Graham (1976a) found that WPB greenstones of a transitional composition plotted in the CAB field because of cumulate ilmenite. Some undifferentiated transitional compositions (OFB from Mozambique basin - Fleet *et al.*, 1976) also plot in this field. This diagram therefore separates unequivocal WPB from others which may be associated with continental rifting. In the Hebridean suite, this corresponds to a comparison of alkalic and transitional compositions versus ol-hy normative types (see Morrison, 1978, Fig. 6). Calc-alkaline compositions are not well differentiated on this diagram because their compositional trend is superimposed upon the OFB field; basaltic-andesites and andesites may plot in the CAB field (Pearce and Cann 1971), and a considerable overlap occurs between IAT and

CAB. The plot should be used only as a partial test for WPB, as Pearce and Cann (1973) originally intended; the VAB fields should be ignored. Because biaxial plots may be more easily generated by computer, and because the important WPB field is identified by critical ratios of Ti and Zr to Y, this plot may be replaced by the binary Z/Y vs. Ti/Y diagram of Pearce and Gale (1977).

(ii) REE:

A strong suggestion of tectonic environment is given by the slopes of chondrite normalized REE profiles. Thorpe (1972) used a triangular plot of weight concentrations of Ce, Y and La to delineate fields of OFT, WPT and alkali-basalt, forming a consecutive series of increasing Ce/Y ratios. An andesite field showed higher La than this series. Keppie *et al.* (1979) demonstrated consistent results with Ti, and Zr and Y for medium grade metamorphism. In view of the noted depletion of Ce and La during weathering, chondrite normalized REE profiles would probably be more useful.

(iii) Th-Hf-Ta plot:.

In order to devise a tectonically sensitive diagram in which silicic magmas would plot close to their mafic associates, Wood *et al.* (1979) devised a triangular plot of Th-Hf/3-Ta. Owing to the lack of Hf and Ta analyses in the literature and the geochemical coherence of these elements with Zr and Nb, the diagram could be similarly

constructed using Th-117Zr-16Nb.

Two compositionally divergent series are again indicated; OFB to WPB showing an increase in Ta/Hf whereas a VAB field shows a comparative enrichment in Th/Hf. No compositional overlap is seen between the VAB and OFB fields, although this may be caused by the lack of data for IAT.

A large OFB field characterises this plot. Between the OFB and WPB fields these authors delineate an area characteristic of anomalous segments of mid-oceanic ridges which are enriched in incompatible elements. Erlank and Kable (1976) noted such zones, defining them in terms of Nb/Zr, a ratio comparable to but more stable than Ba/K. This compositional range corresponds to Nb/Zr values of 0.06 to 0.26 and would include WPB such as the Lesotho Karroo. The Hebridean basalts would plot in the normal OFB field. The main use of this diagram is in demonstrating the importance of Th in distinguishing intermediate and silicic lavas from VAB, WPB and OFB. However, routine neutron activation analysis, rather than the more common XRF, is necessary to determine Th concentrations.

D. COMBINED NON-TECTONIC AND TECTONIC CLASSIFICATIONS

a) The Subdivision of Subalkaline Compositions

In addition to identification of alkali basalts, which are usually WPB, the above tectonic plots can identify Fe and TiO_2 rich tholeiites characteristic of oceanic islands and continental rifts. A different series of plots are needed for the detailed subdivision of subalkaline compositions. Techniques designed to do this from either a compostional or tectonic viewpoint essentially serve the same purpose, that is, the separation of calc-alkaline from tholeiitic trends, the former being characteristic of an island arc or continental margin environment. Several schemes can be devised which separate OFB from CAB but, by referring to Fig. 8-5, two classification difficulties can be seen:

a. IAT are tectonically associated with CAB but have a lower K_2O content (Pearce, 1976), and therefore a lower Zr/TiO_2 ratio. A group so defined includes both a common Fe enrichment trend (e.g. Hokone, Japan, Nockolds and Allen 1956) but also a rare suite of basalts e.g. from Guam (Stark, 1963) which show high Cr comparable to OFB, no Fe enrichment and a gradation into CAB compositions; this suite is best grouped with CAB.

b. MgO-rich WPB are chemically indistinguishable from OFB. To resolve the latter point, field evidence is essential. Garcia (1978) pointed out the use of paired metamorphic belts, dominant pyroclastic

textures and thick interlayered sequences of greywackes and mudstones in identifying island arcs. Continental deposits are characterized by associated fluviatile or lacustrine sediments and commonly, underlying basement is seen.

Recognition of continental environments, particularly close to continental margins can be difficult. For instance:

1. The Late Proterozoic Harbour Main Group of Newfoundland consisting of lavas, pyroclastics, volcanic sediments and associated quartz monzonite plutons is interpreted both as an island arc sequence (Hughes, 1970; Hughes and Bruckner, 1971) and as a Basin and Range Sequence (Papezik, 1970; Strong and Minatidis, 1975).
2. The Proterozoic Cape Smith - Wakeham bay Belt of N. Quebec has basalts and komatiites bedded with dolomite, quartzite and shale but also andesitic compositions (Baragar, 1974). The field relationships of the northern part of the belt are obscured by medium-grade metamorphism (Moore, 1977).

Other WPB environments can also be equivocal, e.g. the Ordovician Roberts Arm Group of Newfoundland shows a bimodal basalt-dacite suite interleaved with siltstone and greywacke and has been compared to both an island arc and oceanic island (Strong, 1973).

Despite the equivocal field evidence of the above examples, the alternatives of arc versus within-plate volcanism would likely be solved if tholeiitic (TH) as

opposed to calc-alkaline (CA) trends could be distinguished.

b) The Subdivision of Mafic to Felsic Compositions using Major Elements

(i) AFM:

The division of subalkaline volcanics has commonly involved use of the AFM plot, the TH suites being distinguished from CA by their notable trend of Fe enrichment. However, a complete gradation in FeO enrichment trends appears to exist for the subalkaline suites (Ernst, 1976, Fig. 4.50).

This gradation may be caused by the interplay of a number of different mechanisms advanced to explain the suppression of an Fe-enrichment trend. These include a high magmatic fO_2 (Osborn, 1959), separation of amphibole (Cawthorn and O'Hara, 1976) and a high alkali content (Irvine, 1976). It would thus appear that no sharp chemical distinction exists between TH and CA suites. Using Papua as an example of this gradation in Fe-enrichment, Johnson *et al.* (1978) showed that compositionally coherent and separate groups overlapped the normal TH/CA dividing lines on the AFM plot. They suggested the identification of circumoceanic rocks on a regional basis and rejected divisions into artificial world-wide standard associations. However, some of their overlap is caused by the inclusion of alkaline compositions. One suite (Papua, Rabaul and Bougainville)

is entirely CA and their suggested plot of normative ne or quartz + hy vs. a differentiation index, still indicates considerable overlap amongst these suites.

This example suggests that LKT/CAB separation in island arcs is artificial. However, because only compressional environments can eliminate FeO-enrichment entirely, and because the terms tholeiitic and calcalkaline are in general use in the literature, an arbitrary boundary is suggested which is defined by the minimum Fe-enrichment trend seen in other-than compressional environments. This trend is demonstrated by the nonporphyritic central basalts of the Herbrides (Nockolds and Allen, 1956) and the Ferrar diabase of Antarctica (Gunn, 1966). When plotted on a AFM diagram these trends correspond very closely to the TH/CA division of Irvine and Baragar (1971). A CA trend so defined should therefore eliminate the inclusion of any within-plate volcanism.

Because all basaltic compositions plot close together on an AFM diagram, the TH/CA distinction is largely defined by a compositional trend rather than the position of a localised concentration of data points. Comagmatic intermediate compositions should therefore always be plotted where available. By the same token, the use of this diagram may be misleading in the study of altered rocks, where varying trends may be caused by a variation in alkalies. In addition, Gibson and

Watkinson (1979) showed that the silicification of basalts could cause a false CA trend, whereas Garcia (1978) demonstrated that variation in MgO amongst intermediate CA compositions could cause a TH trend.

(ii) FeO*/MgO:

Miyashiro (1973) demonstrated CA versus TH trends simply by plotting SiO_2 or FeO* (i.e. total Fe as FeO) against a differentiation index (FeO*/MgO). The limitations of both these plots are shown by a very wide scatter of both the Karroo and Hebridean tholeiites on both plots (Miyashiro and Shido, 1975, Fig. 3). This caused these authors to reclassify subsets from the above two suites as CA. Because this classification serves no useful petrogenetic purpose and because silicification can cause an erroneous CA trend on both of these plots (Gibson and Watkinson, 1979; Pearce, 1975), the use of these diagrams is not recommended.

c) The Subdivision of Mafic Rocks using Stable Elements

Several diagrams using mainly transition elements as indicators of Fe-enrichment and Zr and Y as indicative of increasing K_2O and SiO_2 have been developed for the subdivision of subalkaline rocks.

Miyashiro and Shido (1975) and Miyashiro (1975) showed that both Cr and Ni will decrease logarithmically with an increase in FeO*/MgO for basaltic rocks, a similar profile being observed regardless of tectonic environment.

Therefore, although Ni and Cr concentrations alone may not be characteristic of a tectonic environment, they will tend to show very high values in OFB and may be a useful differentiation index.

(i) Ti vs. Cr:

This diagram has been used by Bloxham and Lewis (1972), Pearce (1975), and developed further by Garcia (1978). For a given Cr content, OFB show consistently higher TiO_2 values that VAB. VAB with over 200 ppm Cr cannot be distinguished from OFB. This includes the IAT/CAB from Guam.

(ii) Ti/Cr vs. Ni:

An essentially similar plot to the Ti vs. Cr diagram was produced by Beccaluva *et al.* (1979). By normalizing the Ti content to Cr, the discriminating power is increased among low Ti basalts. The empirical field boundary correctly classifies 93% and 97% of the respective VAB and OFB test populations. A rare group of Ca-rich OFB occurs within the VAB field but coincides with minimum concentration of the latter.

Because this diagram was designed for lavas with SiO_2 contents of 40-58%, differentiation effects introduced by plotting altered basaltic andesitic compositions will be insignificant.

(iii) Ti vs. Zr:

This plot was used by Pearce and Cann (1973) to subdivide subalkaline compositions separated by their Ti-Zr-Y diagram. Garcia's (1978) version gives essentially the same result and separates a trend of TiO_2 enrichment (OFB) from that of Zr enrichment (CAB). The diagram is therefore analagous to the FeO*/MgO vs. SiO_2 plot of Miyashiro (1973). The convergence of the two trends is defined by an area containing both LKT and OFB. The use of Zr therefore allows subdivision of the VAB field. If OFB are eliminated from a sample suite using one of the above plots, LKT of both types could be identified by restricting this diagram to the study of VAB.

A limitation of all three of these diagrams is illustrated by Fig. 8-8 which displays mafic compositions from a number of continental tholeiitic suites, using the Ti-Zr diagram as an example. The weak Fe-enrichment trend of the Ferrar, Deccan and Hebridean suites makes them appear to be CA. Because these primitive compositions are restricted to a within-plate environment, (a) field evidence which proscribes a continental environment or (b) an independent check precluding Fe enrichment is necessary before assigning a CA classification to a suite. Identification of such continental suites can be petrogenetically important. The high Zr of the Ferrar coincides with high Rb, U, Th and $^{87}Sr/^{86}Sr$, which has been interpreted to represent mantle

heterogeneiity (Compston *et al.* 1969) probably occurring on a massive scale at 1600 m.y. (Brooks and Hart, 1978). Nd and Sm isotopic data for the Hebridean suite suggest that this "mantle isochron" is an artifact of crustal contamination (Carter *et al.* , 1978). The TiO_2 - Zr diagram has been extended by Pearce (1980) to accomodate intermediate and felsic compositions.

d) The Subdivision of Mafic to Intermediate Compostions using Stable Elements

V shows a common tendency to display a near constancy or increase in concentration as FeO*/MgO increases in a TH suite (Nockolds and Allen, 1956). This is in contrast to the depletion noted for CA suites. (Nockolds and Allen, 1953).

(i) V vs. Cr and Ni:

Miyashiro and Shido (1975) developed a plot of V vs. Cr for separating TH and CA trends, both of which diverge from a field of OFB compositions . Owing to the meagre evidence available (Field and Elliot, 1974) that Ni may show greater stability than Cr under medium grade metamorphism, a similar plot was produced using V vs. Ni.

Both diagrams show high V and high Cr or Ni areas to be characteristic of tholeiitic compositions exclusively but a high overlap area occurs between the two trends. This is because moderate to low FeO enrichment trends display a V depletion, and because

basaltic-andesitic compositions >56% SiO_2 will in general undergo V depletion. In addition on both plots, IAT showed both the strongest V enrichment (Hakone) and the greatest V depletion (Gaum). Therefore, rather than a primary means of distinction between TH and CA, these plots could be used to confirm a TH trend suggested by another technique.

e) The Subdivision of Mafic to Felsic Compositions using Stable Elements

(i) "YTC" diagram:

An ingenious plot was derived by Davies *et al.* (1979) to classify mafic to felsic composition. Y + Zr, Ti and Cr are used as stable trace-element proxies for alkalies, Fe and MgO; major elements with which they respectively show a strong coherence. The diagram is therefore analagous to an AFM plot. Davies *et al.* displayed two separate subalkaline trends but based these upon analyses of Archean metavolcanics. Because these are almost certainly altered and of doubtful tectonic environment, the diagram was redrawn using Phanerozoic compostions (Fig. 8-9).

The logarithmic change of Cr with MgO stongly controls the subparallel trend of both the CA and TH fields. A high overlap exists for basaltic compositions and divergence of the two trends occurs only for intermediate compostions. IAT show a wide scatter. This

plot should therefore be used for a suite showing a wide range in composition.

(ii) FeO* vs. Zr/TiO_2:

Because a tholeiitic trend is essentially determined by Fe enrichment, a less ambiguous classification diagram could be developed by the inclusion of this element. Because Fe/Mg could be seriously affected by Mg mobility and Fe/Cr was found to be too sensitive to Fe enrichment, total Fe as FeO (i.e. FeO*) for an anhydrous compostion, was plotted against Zr/TiO_2 for Phanerozoic subalkaline suites (Figs. 8-10 and 8-11).

A range of Fe-enrichment trends is seen from high (Skaergaard) to low (Ferrar) but all have a marked positive slope. CA trends, on the other hand, invariably display negative slopes and are confined to an FeO*-poor field which excludes WPB. Although derived for mafic to intermediate compositions, the same trends can be observed just for mafic rocks. Mg rich LKT are confined to a small Zr and Fe-poor field. Most LKT show an enrichment in Fe and cross from the Fe-poor to Fe-rich fields.

This diagram will therefore distinguish all WPT but not all OFB from CAB. However, trends as well as location are important on this plot. Although Fe may undergo a mild enrichment during alteration, it is unlikely that a magmatic Fe variation trend would be

totally obliterated.

(iii) TiO_2 vs. Zr and Cr vs. Y diagrams

Pearce (1980) produced two binary plots based on more than 3000 analyses which show the clearest discrimination yet available between within plate and arc suites, including mafic to felsic compositions. yet available. Very little overlap is seen between the two suites on the TiO_2 vs Zr diagram which shows consistently lower values of both elements in the arc suite for any given SiO_2 content. Using the data of Garcia (1978), the field for arc lavas can be subdivided into a low Zr region, characteristic of IAT, and a field for CAB and intermediate to felsic rocks. The diagram was used in this modified form.

A second diagram, used to test the same subdivision, is Cr vs Y, in effect a fractionation index versus a measure of depleted mantle. Y, like HREE, tends to concentrate in clinopyroxene and garnet and shows consistently low values in arc lavas.

f) The Discrimination of Volcanic Rocks using Relict Clinopyroxenes

In metamorphosed and weathered basalts, fresh clinopyroxene often occurs as the only remnant phase of the original rock. They therefore represent a useful petrogenetic indicator, if their chemistry can be related to the original rock type. Such information helps to

substantiate petrogenetic models based on immobile elements.

(i) Division into Alkaline and Subalkaline Groups:

Coombs (1963) suggested that normative cpx compositions would reflect the original rock chemistry, ne-normative cpx being representative of an alkaline magma. Although this approach has proved popular (Vallance, 1974b; Barron, 1976), ne-normative augites have been found in LKT (Nisbet and Pearce, 1977).

Clinopyroxene from alkaline magmas show high proportions of non-quadrilateral components. In a study of over 800 cpx, Schweitzer *et al.* (1978) showed that TiO_2, Na_2O and Al_2O_3 were enriched in alkaline cpx, and Cr_2O_3 was enriched in cpx from tholeiites. CaO and SiO_2 showed no systematic difference; however, this may be because of restriction of the samples to OFB.

Nisbet and Pearce(1977) produced a discriminant analysis of 8 major element oxides for groundmass pyroxenes from basaltic rocks. Using mainly the difference in these components, WPA were easily separated from subalkaline basalts by their higher Ti, Na and Ca and lower Si. VAB, which were not subdivided, were separated in turn from WPT by lower Ti, Si and Al. OFB form a zone of overlap. Essentially the same results were obtained from phenocryst cpx. The WPT field was based on a small sample size and some primitive CON plot in the VAB/OFB overlap field (Scoresby Sund data from Fawcett, *et al.*, 1973). The most important use of the

diagram therefore is the separation of WPA from other magma types. This can be achieved with 88% accuracy, and mainly depends on a function F_1 of less than -0.9.

Combinations of SiO_2, Al_2O_3, and TiO_2 have been used in binary plots for separating cpx from alkaline and subalkaline magmas (e.g. LeBas, 1962; Garcia, 1979) but they do not subdivide the subalkaline field. Intermediate compositions must be avoided when using non quadrilateral components because their depletion causes alkaline differentiates to plot in subalkaline fields (Barron, 1976; Nisbet and Pearce, 1977). Quench textures must also be shown experimentally to favour the entry of Ca, Fe, Al and Ti into the pyroxene lattice (Donaldson *et al.*, 1975).

Such disequilibrium crystallization has been observed in chilled zones in basalt flows (Vallance, 1974b; Coish and Taylor, 1978) and noticeably where cpx crystallizes before plagioclase (Rowbotham and Bevins, 1978).

(ii) The Subdivison of Subalkaline Magmas:

The compositional trend of cpx plotted as coordinates within the pyroxene quadrilateral has long been known to reflect the alkalinity of the magma (e.g. Deer *et al.*, 1963). Trends established for cpx from tholeiitic magmas show a strong fe-enrichment which at low temperatures appears to coincide with a cotectic curve, while those from alkaline magmas show a greater

increase in CaO. This CaO enrichment, however, is observed in cpx from olivine tholeiites which is interlayered with quartz tholeiites showing a normal Fe-enrichment in their cpx (Fawcett *et al.*, 1973). The pyroxene quadrilateral is therefore of limited use in determining alkalinity in volcanic rocks.

Garcia (1975 and 1978) used the pyroxene quadrilateral to show that cpx phenocrysts from differentiates within a CA series have only 20% Ferrosilite compared with up to 40% for TH differentiates. Because cpx from CA and TH basalts can show identical compostional ranges, the intermediate nature of altered volcanics showing such a limited range should be checked using, for example, the Zr/TiO_2 index before they are considered CA.

In conclusion, clinopyoxene from basalts showing no quench textures may be used to determine the alkalinity of a suite. Clinopyroxene from differentiates may be used on the pyroxene quadrilateral to subdivide the subalkaline compostions.

E. A SUGGESTED CLASSIFICATION SCHEME FOR ALTERED VOLCANICS

From the above discussion, it can be seen that a given classification should be checked to ensure consistency and can be refined by the use of diagrams in sequence.

Fig. 8-12 illustrates a suggested integrated classification scheme. Other steps can be added and

refinement or verification made by the additional use of REE, Th and cpx studies.

a) Major Elements

The Irvine and Baragar (1971) scheme is valid as a primary classification tool if limited Na and K mobility is indicated by the Igneous Spectrum diagram (Hughes 1973; Stauffer *et al.*, 1975). Ca stability is then tested by the CaO/Al_2O_3 - $MgO/10$ - $SiO_2/100$ diagram of P.A. Davis (see above). Unlike stable element schemes, this routine distinguishes between Na and K rich series among alkaline rocks (Fig. 8-12a). Among basaltic compositions, OFB and primitive WPB may be distinguished by using the TiO_2-K_2O-P_2O_5 diagram of Pearce *et al.* (1975) or, if CaO and SiO_2 are also stable, a subdivision of VAB may be gained by using the discriminant functions of Pearce (1976).

To select intermediate samples for the MgO-FeO^*-Al_2O_3 tectonic plot of Pearce *et al.*, (1977), SiO_2 must be relatively stable. A rapid check may be made by comparing the consistency of classification between the SiO_2 vs. Zr/TiO_2 and Zr/TiO_2 vs. Nb/Y diagrams (Winchester and Floyd, 1977). A smooth curve would be expected on the former plot if SiO_2 mobility has been limited. For the purposes of this classification, this method is preferred to using the more time-consuming molecular-ratio plots of Strong *et al.*, (1979).

b) Stable Elements

Major element studies of altered rocks should always be checked using stable element schemes. An illustrated routine (Fig. 8-12b) uses nine commonly analysed elements (Al, P, Ti, Cr, Fe, Ni, Y, Zr, Nb).

The Zr/TiO_2 vs. Nb/Y diagram is used as the basis for this classification and allows most alkalic differentiates to be separated from basalts. Detailed subdivision of these differentiates is not possible but by using a threshold of $Zr/TiO_2 > 0.017$, mugearites to trachytes can be separated using nomenclature consistent with Irvine and Baragar (1971) (see above).

If original textures are still remnant in the rocks, those with an estimated colour index of >35 would be hawaiite rather than basalt. For subalkaline suites, a threshold value of 30 would better separate basaltic-andesites from basalts. This would again achieve an approximate consistency with the terminology of Irvine and Baragar (1971).

Basaltic rocks separated by the above routine can be checked for consistency using the Nb/Y vs. Zr/P_2O_5 plot (Floyd and Winchester, 1975). This will also allow definite ne-normative compositions to be separated. Usage of the Ti-Zr-Y plot (Pearce and Cann, 1973) will confirm the separation of definite WPB from those which are similar to OFB.

Subdivision of subalkaline basalts uses Ti/Cr vs. Ni (Beccaluva *et al.*, 1979). Ti vs. Zr (Garcia, 1978) and FeO* vs. Zr/TiO_2 to separate respectively OFB, most IAT, CAB and WPT with crustal contamination.

FeO* vs. Zr/TiO_2 is also used to confirm Mg-rich IAT and, along with the YTC diagram to separate differentiated subalkaline suites into TH or CA types.

F. CONCLUSIONS

A review of classification diagrams for altered volcanics using stable elements suggests that the alkalic, tholeiitic and calc-alkaline classifications can be made with some confidence. In addition, preservation of enrichment trends of certain stable elements, and high contents of the somewhat less-stable elements Fe and Al, can be indicative of tholeiitic and calc-alkaline suites respectively. The three major magmatic groups can be subdivided further to give tectonically useful information.

Any division of basalts into tholeiitic and alkalic must include a finite area of overlap caused by ol-hy normative melts caused at low and intermediate pressure. A comprehensive integrated scheme based on nine relatively stable elements (Al, P, Ti, Cr, Fe, Ni, Y, Zr, Nb) can be used to identify definite ne-normative basalts, definite WPB, basaltic komatiite, MgO-rich IAT, normal CAB and WPT contaminated with continental crust. MgO-rich magmas formed during the profound rifting of a continental crust are

indistinguishable for OFB, thus field evidence of ensialic environment producing such a magma may represent an initial stage of ocean development.

Intermediate alkalic compostions cannot be subdivided with the same success, partly owing to the imprecise definitions existing in the literature.

An FeO* discrimination vs. Zr/TiO_2 diagram has been developed which shows a clearer separation between tholeiitic and calc-alkaline suites than in existing plots. It is also used in the above scheme to recognise contaminated WPT. This is important in environments [illegible] old continental margins where basin and range and compressive-margin environments ha[illegible] confused. This diagram can be supplemented by the [illegible] vs. Zr and Cr vs. Y plots of Pearce (1980).

Fi[illegible]ly any division of basalts into tholeiitic and alkalic must include a finite area of overlap caused by ol-hy normative melts produced at low and int[illegible]ediate pressures. The low pressure thermal divide is therefore the only meaningful boundary on such diagrams.

IX. IGNEOUS MINERALOGY

Compositional ranges of remnant plagioclases were included in the petrographic descriptions (Ch. 4) and are not included here. Ilmenite-magnetite intergrowths, in the lavas, are largely altered and therefore could give no information on geothermometry. Where fresh, these intergrowths appear in the diabases and therefore yield sub-solidus reequilibration temperatures. Oxides were therefore not analyzed. The only remnant igneous mineral of petrogenetic significance is clinopyroxene (see Ch. 8). The clinopyroxenes from each suite are described below; the fifty seven electron microprobe analyses are listed in Appendix M.

A. CLINOPYROXENES

Two groups of pyroxenes are described which show contrasting compositions: those from the transitional basalt and diabase suites (MADM, UIG1M, UIG2M and UIGDM, see Ch. 10) and from the Pearson Formation (PEM).

a) Major Elements

In terms of "quadrilateral" components, all clinopyroxenes are augitic rather than salitic (Fig. 9-1). Within the first group, an increase in Wo component appears to be related to the temperature of crystallization: the diabase sills (UIGDM) plot close to the tholeiitic solvus intersection, dykes and flows show somewhat higher Wo, and

quench-textured pyroxenes from all units yield high Wo contents, typical of clinopyroxenes from alkali basalts. The Wo contents are high for tholeiitic pyroxenes, UIGDM shows an Fe-enrichment trend and only a weak alkalic trend (i.e. of constant Wo) is developed in UIGDM. This is in keeping with augites from transitional magmas. On the other hand, the PEM unit displays a contrasting subalkaline quench trend with hypersthene solid-solution (Fig. 9-1d).

b) Minor Elements

The apparent high Wo in the transitional pyroxenes is caused by the substitution of non-quadrilateral components for Mg and Fe in the M1 site, and it has been observed elsewhere that these components can be enhanced by chilling (Ch. 8). However, the order of crystallization also has a notable effect on the concentration of non-quadrilateral components, particularly with regard to Ti and this may, in turn, depend upon cooling rate. The pyroxenes from the transitional magmas are all distinctly titaniferous (0.7 to 2.9% TiO_2), but in the diabases Ti markedly declines as Fe increases, whereas in the lavas Ti is positively correlated with Fe. This latter trend also characterizes the Ti-poor (<0.6% TiO_2) pyroxenes (Fig. 9-2). Furthermore, despite the low contents of high field-strength elements (HFSE) in the UIG2M magma, its pyroxenes have higher Wo and Ti contents than those of UIG1M. UIG2M is an entirely pillowed sequence and its vertical trend shown on Fig. 9-2b suggests Ti

enrichment caused by rapid cooling. The lavas all display crystallization of clinopyroxene before the oxide phase. In the diabases, crystallization of Fe-Ti oxides, during continuous growth of clinopyroxene, reduced the local supply of Ti cations.

The structural formulae were calculated with total Fe as ferrous, but plots of charge deficiency (Na+Al(IV)) vs. charge excess (Al(VI)+2Ti+Cr) give a positive deviation from linearity in the case of the transitional suites. This indicates that a maximum of only 5 to 10% of Fe can be ferric. The commonest coupled substitution observed in pyroxenes from continental basalts and MORBs are Fe^{3+}-Al(IV) and Ti(IV) + 2Al(IV) (Papike, 1980). The Al(IV)/Ti ratio of 3 for the Union Island Group suggests that both of these exchanges occurred simultaneously. The PEM suite has Al(IV)/Ti = 6 and a negligible ferric iron content, therefore the above exchanges are not significant. More relevant is Al(VI)-Al(IV) which is also the commonest coupled exchange in arc pyroxenes (Papike, 1980). Thus the pyroxenes of the PEM suite reflect the arc-like chemistry of the whole rocks (see Ch. 10).

c) Tectonic Environment

The tectonic environment in which the pyroxenes have crystallized largely controls their relative contents of Ti, Ca, Al and Na (Nisbet and Pearce, 1977). Because the order of crystallization can have an effect on the

non-quadrilateral components, Leterrier *et al.* (1982) suggested the use of phenocrysts rather than the groundmass phases. However, their data (Leterrier *et al.*, 1982, Figs 1 and 2) indicate no significant difference between the two groups. The Nisbet and Pearce diagram is most efficient in discriminating alkalic from subalkalic environments and WPT from VAB.

The transitional suites plot in the within plate field, close to the boundary with alkalic basalts (Fig. 9-3). This is an acceptable location for transitional basalt, but in isolation the data suggest several tectonic possibilities. The trace elements of the PEM lavas indicate a magma type similar to both WPT and IAT (see Ch. 10), but the pyroxenes clearly suggest a volcanic arc environment. Some overlap between the two fields does occur in this plot (Fig. 9-3) and the WPT field was based on a small population of twenty six samples. However, the Ti+Cr vs. Ca plot of Leterrier *et al.* (1982) also favors an orogenic environment, although the discrimination is less clear.

X. GEOCHEMISTRY AND PETROGENESIS

Each of the igneous formations are classified accoording to the major and trace element scheme described above (Ch. 8). The petrogenesis of each formation is then discussed.

A. BASIS FOR THE MAJOR ELEMENT CLASSIFICATION

Because metasomatic alteration, notably of alkalies and CaO will strongly affect the major element classification, all rocks were tested using the alteration screens of Hughes (1973) and P.A. Davis (pers. comm., 1979). Fine-grained and originally glassy-textured rocks showed the greatest compositional variation. The pillowed suites with sericitized plagioclase displayed extensive equimolal replacement of Na by K on Hughes's "igneous spectrum" variation ranges from normal igneous ratios to complete replacement within one outcrop. CaO is invariably low (Fig. 10-1), no doubt having contributed to the predominant carbonate veining and matrices of the tuffs. Twenty five percent of all samples were classified as "unaltered" (10 to 50% of each suite). Norms were calculated and based on an oxidation ratio of 24, i.e.

$$(100\ Fe_2O_3)/(Fe_2O_3+FeO) = 24$$

This is a mean value for a suite of transitional basalts from the Red Sea (Gass *et al.*, 1973) which lies near to the observed median value of the mean oxidation ratio for most

transitional basalt suites. This value is also close to the mean for olivine diabase (i.e. 22; Manson, 1967) which is not likely to be affected by surface oxidation. Transitional basalts are common in continental rifts and were chosen as the standard because both alkaline and tholeiitic lavas occur in the East Arm. The norms calculated on this basis agree well with the normative classification obtained from Cox *et al.* 's (1979) subdivision of the alkalies vs. SiO_2 diagram (Fig. 10-2). The average composition of each of the rock types are given in Table 10-1.

B. BASIS FOR THE TRACE ELEMENT CLASSIFICATION

Magmatic and tectonic classifications were based on the previously described routine (Ch. 8) using some transitional elements but mainly the incompatible minor and trace elements or high field strength elements (HFSE): specifically Nb, P, Zr, Ti and Y. The large ion lithophile elements (LILE) are of secondary importance because, unlike the HFSE, they are mobilized in most geologically-important aqueous fluids. The classification results are printed in Table 10-2.

The partition coefficients of the HFSE in petrologically-relevant minerals are all less than one, but show real differences, and display a variation from very low (e.g. Nb) to relatively high (e.g. Y). This behavior approximately follows an order of increasing charge density (Saunders *et al.* , 1980). Ratios such as Nb/Zr and Nb/Y are

therefore analogous to ratios reflecting LREE compared to MREE (e.g. La/Sm) and to HREE (e.g. Ce/Yb) which both increase with increasing alkalinity of basalt. As with REE, discrete differences in small partition coefficients between HFSE will be reflected in the relative fractionation of these elements when the melt to crystal ratio is low. Therefore in alkalic melts, the HFSE element with the lowest partition coefficient will be relative strongly concentrated in the melt. In general, there is an increase in the ratio of relatively high to relatively low field strength HFSE as one passes through the sequence of basalts: VAB, MORB, WPT and alkaline.

C. MEASUREMENT OF THE EXTENT OF LOW-PRESSURE FRACTIONATION

Semi-quantitative measurements were made of the amount of low-pressure fractional crystallization needed to explain the observed elemental variations. Variations in the quasi-incompatible HFSE were used to estimate overall fractionation, whereas key compatible elements were used to calculate the contribution of a particular phase, i.e. olivine has a high partition coefficient (Kd) for Ni; clinopyroxene has high Kd's for Sc and Cr, and magnetite-ilmenite has high Kd's for V.

Partition coefficients for the HFSE were taken from Pearce and Norry (1979) and for the transition elements from Irving (1978). However, these are largely from experimental studies and compositional differences between experimental

melts and natural systems can impose limits on the suitability of the measured Kd's. Also, partition coefficients may vary according to pressure, temperature and kinetic disequilibrium (Allegre *et al.*, 1977). The Kd's of some elements may vary considerably because of these factors and some assumptions had to be made. A Kd of 10 for Ni in olivine was used. This is valid for a mafic melt with 10% MgO (comparable to the most primitive lavas sampled) and is the best value at about 10kb pressure (Elthon and Ridley, 1979). A pressure of 10Kb is a reasonable estimate for the minimum pressure at which olivine fractionation begins below a 30 km thick crust. A Kd value of 10 may therefore overestimate olivine fractionation when used for less magnesian lavas having higher Kd's for Ni in olivine.

Published values of Kd for Cr in clinopyroxene vary widely from 1.7 (Irvine, 1978) to 15 (Allegre *et al.*, 1977) and values of Kd for Cr in magnetite are even more extreme: a value of >100 (Irving, 1978) allowed for no clinopyroxene fractionation. The values chosen are from natural basalts: Kd for Cr in cpx=10 (Sun *et al.*, 1979) and a Kd for Cr in ilmenite/magnetite=10 (Allegre *et al.*, 1977). Furthermore, very high recorded values of Kd for V in ilmenite are dependent upon high fo_2 and at QFM the Kd is as low as 0.11 (Shervais, 1982). This latter value was used for modelling oxide fractionation.

The above choice of Kd's allowed Rayleigh fractionation vectors to be modelled on binary plots, each plot depicting

two elements, where each element has a significantly high Kd for only one phase of petrological interest. The Al_2O_3/TiO_2 vs. Ti plot of Pearce and Flower (1977) was used to estimate plagioclase fractionation, Ni vs. Cr for olivine and clinopyroxene fractionation, and V vs. Sc for ilmenite-magnetite and clinopyroxene fractionation. Confidence in the choice of Kd's was established by agreement between these plots, along with confirmation of the total fractionation using HFSE plots (see Figs. 10-3 to 10-13). Visual estimates of the degree of fractionation can be obtained from relevant Rayleigh fractionation vectors which are given on each of these plots. Values for the calculated amounts of low-pressure fractionation in each suite are given in Table 10-3.

Binary logarithmic plots of the HFSE, e.g. Nb vs. Y or Nb vs. Zr, will show straight-line, sub-parallel trends between basaltic suites which have undergone low-pressure fractionation, but which are unconnected by it. Therefore, suites with notably different Nb/Y or Nb/Zr indicate partial-melting of different source materials, or progressive partial melting of the same source. In the second case, the basaltic products would show a systematic decrease in HFSE concentrations.

Using this logic, the flow packages at any volcanic centre could be subdivided into separate, consanguinous suites. Also, the degree and type of fractional crystallization could be calculated, using HFSE and

compatible elements, as outlined above. Although curved, batch-partial melting vectors for relevant mantle materials are not shown on Figs. 10-3 to 10-13, qualitative estimates were made of the types of mantle materials needed to explain the differences in HFSE contents between the various basaltic suites.

D. WILSON ISLAND GROUP

a) WIGM and WIGF

The remnant, unaltered mafic to intermediate samples from WIGM are q-hy normative and fall close to the one atmosphere equilibrium cotectic for olivine, clinopyroxene and plagioclase in the natural tholeiite system of Cox and Bell (1972). One ol-hy normative, possibly cumulate, sample falls in the olivine field. On an alkalies vs. SiO_2 plot (Fig. 10-2), the mafic and felsic (WIGF) suites show a bimodal distribution with two intermediate tholeiitic andesites. Bimodality and limited SiO_2 mobility is confirmed by bimodal Zr/TiO_2 values and a small variance in SiO_2 (Fig. 10-3a and b). The trend in Fig. 10-2 suggests alkali rich tholeiites, because they straddle the boundary with transitional basalts ("Coombs trend" of Miyashiro, 1978). The least-altered WIGM samples average 2.2% K_2O which closely compares with 2.1% for the whole group, thus the high K_2O value is close to the original.

The Nb/Y ratio (Fig. 10-3a and b) establishes the suite as alkalic, as does the high Zr/Nb value (~15). The classification plots involving Zr/P_2O_5 (Fig. 10-3c and d) do not strictly apply to intermediate rocks but the fractionation trend of increasing Zr/P_2O_5 does not affect their subalkaline and transitional classification. The possible transitional classification on TiO_2 vs. Zr/P_2O_5 (Fig. 10-3d) is artifically enhanced by cumulate oxides in some of the coarser-textured samples (indicated by high TiO_2 in Fig. 10-4).

Using HFSE, the tectonic classification is clearly within plate (Fig. 10-3f and g) but the TiO_2 contents are lower than average for WPT. The resulting low Ti/Y ratios cause an incongruous "plate margin" basalt classification on the Zr/Y vs. Ti/Y plot (Fig. 10-3e). However, this diagram (from Pearce and Gale, 1977) is based on a more limited data set for WPB which omits the more primitive (i.e. TiO_2 poor) continental tholeiites. Owing to this deficiency, the diagram has not been used.[1] Despite problems concerning enrichment of LREE during metamorphism, (La/Ce) shows only a limited variation of 1 to 1.4 and the mean LREE concentrations (La =160, Ce =131) are characteristic of WPT. The few major-element analyses available support a continental environment. The least altered compositions form a tightly clustered field on the K_2O-TiO_2-P_2O_5 plot (Pearce

---

[1] If WIGM was considered of plate margin type, they would subsequently classify as borderline IAT to MORB or primitive WPT using TiO_2 vs. Cr and Ti/Cr vs. Ni.

et al., 1975), indicating a continental environment. Two basaltic andesites plot on the continental/oceanic island boundary on the MgO-FeO-Al_2O_3 diagram (Pearce *et al.*, 1977).

Variation in WIGM of HFSE (Fig. 10-3f,h,i and j) and transition elements plus Al_2O_3 (Fig. 10-3k,l,m) can be explained by pl-cpx-oxide fractionation of 30:30:3. The mafic and felsic suites (WIGM and WIGF) form continuous trends on the HFSE binary plots and display constant Zr/Nb (Fig. 10-3h). This strongly suggests that the Wilson Island Group is derived from a single batch of magma despite the bimodal SiO_2 and TiO_2 distributions. The complete range of HFSE variation can be explained by 80% fractionation. The bimodality in SiO_2 probably occurs because the SiO_2 content of the tholeiitic melt was buffered by cotectic pl-cpx crystallization in the absence of fractionating olivine. SiO_2 would have rapidly increased when oxides began to crystallize (cf. Thingmuli, Carmichael, 1964) which would likewise cause a rapid depletion in TiO_2 (Fig. 10-3f). Such rapid changes are indicated in tholeiitic andesite compositions at a mafic index greater than 77, although there are few sample points (Fig. 10-4). Non-igneous compositions, possibly cumulates, are illustrated by the high TiO_2 and CaO at M.I. = 70.

b) UWIGM

The Upper Wilson Island (UWIGM) suite consists of only four samples, none of which show "unaltered" major element compositions; the SiO_2 content (48.6±0.8%) is possibly original (Fig. 10-3a and b). They classify as alkaline on all diagrams and have the very high Nb and low Y characteristic of alkali basalt to basanite. The Zr/Nb indicates a clearly different origin from WIGM and WIGF (Fig. 10-3h) and rapid Ni depletion indicates limited olivine fractionation (Fig. 10-3k).

c) Comparison and Petrogenesis

Continental bimodal suites which contain a rhyolite, rather than a trachyte unit have a mafic or mafic to intermediate component which is transitional in composition, (e.g. Hebrides, Beckinsale *et al.*, 1978; Miocene of Rio Grande, Elston and Bornhorst, 1979) or transitional to alkaline, (e.g. Lebombo, Burke and Dewey, 1973) during periods of flexure. If major rift development took place, the associated felsic volcanics can be over 25% of the sequence and the mafic component is dominantly high- or low-K_2O olivine tholeiite to transitional basalt with a minor tholeiitic andesite component, (e.g. Keweenawan, Green, 1977 and Wallace, 1981; and the post-rift lavas of the Rio Grande, Elston and Bornhorst, 1979). A high degree of partial melting can produce rhyolites which are clearly unrelated to the basalts and are probably the result of

crustal melting (Wallace, 1981). Because the Wilson Island Group contains post-rift, continental, high-K tholeiites to tholeiitic andesites with a third of the sequence composed of rhyolite, it is similar to the bimodal sequences related to major rifts. However, the mafic and felsic units appear to be comagmatic, and, because over 80% fractionation would be needed to produce the rhyolite component, a thicker more mafic component of the group is postulated to exist unexposed.

WIGM has far higher HFSE and LILE than the possibly contemporaneous, bimodal Ipiutak suite of the Wopmay orogen (see Ch. 2); however, both suites show similar La and Ce enrichment. The Ipiutak Formation is otherwise similar to MORB and reflects extensive crustal rifting (Easton, 1981).

The original extent of the Wilson Island Group is not known, but its thickness, tholeiitic composition, abundant rhyolite rift environment, probable mantle provenance (see Ch. 6) and comparison with the above suites all suggest mantle derivation with high degrees (> 20%) of partial melting of the source. However, limited crustal extension, as indicated by the contemporaneous fluvial sedimentation, may have produced extensive fractionation in crustal magma chambers and extrusion of only the fractionated intermediate and felsic components.

At a given mafic index, WIGM has similar HFSE to, but higher K_2O and SiO_2 than, Icelandic tholeiites (Wood, 1978) and is even more enriched in HFSE than the transitional

basalts of the Hebrides (Morrison *et al.*, 1980) and the Quaternary lavas of the Gregory Rift (Norry *et al.*, 1980). The latter two suites are thought to be derived from a depleted mantle source. Although these two suites are transitional in composition, they contain lower HFSE contents than the tholeiitic WIGM, probably was produced by a greater degree of partial melting. These comparisons, plus the chondritic Zr/Nb ratio of 14 (similar to C3 of Pearce and Norry, 1979) indicate an undepleted mantle source for WIGM.

The highly alkaline UWIGM basalts have strikingly different Zr/Nb values from those of the WIGM suite (Fig. 10-3h) and are clearly unrelated by fractional crystallization. They belong to a later event of high-pressure, limited partial melting close to the peridotite solidus.

E. ALKALI GABBRO INTRUSIONS

The Blachford Lake complex has been described by Davidson (1978) and Badham (1979b) and consists of olivine gabbro and norite to leucodiorite cut by late syenite and dominant riebeckite granite. The north Simpson Island dyke consists of differentiated diorite to syenite (Burwash and Cavell, 1978; Badham, 1979b). The analyses given by these authors indicate an average potassic alkali basalt to trachybasalt composition for the dyke (Irvine and Baragar, 1971 classification) and the average Nb and Y concentrations

(140±41 and 98±23) are by far the highest observed in the East Arm.

In the development of continental rifts on thick crust, where no profound crustal thinning or crustal separation takes place, minor alkali basalt and abundant, consanguinous peralkaline to alkaline trachyte and rhyolite magmatism follows updoming and precedes graben development e.g. Oslo (Segalstad, 1978), N. Kenya (Baker *et al.*, 1978) and Ethiopia (Meyer *et al.*, 1975).

F. MID APHEBIAN DIABASE (MADM) AND THE UNION ISLAND GROUP (UIG1M, UIG2M AND UIGDM)

These appear to be a group of transitional, mainly ol-hy normative magmas of mafic composition. The intrusive units show limited Na-K exchange and SiO_2 mobility (Fig. 10-5b) and erratic high TiO_2 values on mafic index plots (Fig. 10-6). The high TiO_2 values are caused by cumulate oxides and produce a false alkaline rather than transitional classification on a TiO_2 vs. Zr/P_2O_5 plot (Fig. 10-5d). Tectonic classifications are all of within-plate type (Fig. 10-5e,f and g).

a) MADM

The least altered samples are ol-hy normative basalts (K_2O=1.15±0.38%) which classify as transitional (alkalies vs. SiO_2; Fig. 10-2) and plot on the normative ol-plag one atmosphere natural cotectic of Cox and Bell (1972). Stable

trace element classifications are transitional (Fig. 10-5a,c and d). Y and Zr variation gives a calculated total of 30% low pressure fractionation of ol+pl+cpx.

b) UIG1M

The ol-hy to q-hy normative compositions of the least-altered lavas are no doubt affected by mobile SiO_2 and are of limited use because only one sample is diopside normative. Although Nb/Y indicates an alkaline classification, the high Zr content gives transitional to subalkaline values of Zr/P_2O_5 (Fig. 10-5a,c and d). Remnant pyroxenes indicate a transitional to alkaline nature (see above), therefore the suite is best viewed as transitional.

Mafic index plots show that UIG1M has higher Y, Zr and Nb, at all M.I. values, than any of the other suites in this group of transitional magmas (Fig. 10-6). This argues against a genetic connection between the suites. The slight decrease of Cr with increasing mafic index suggests that the M.I. values may be original and thus the most Fe-rich lavas are hawaiites.

Trace elements indicate ol-pl to cpx-pl cotectic crystallization of 60%. This is closely comparable to the degree of low pressure fractionation needed to produce hawaiite compositions from Afar transitional basalts (Boina and Erta Ale; Bizouard *et al.*, 1980).

c) UIG2M

The least altered samples are ne to q normative, subalkaline on an alkalies vs. SiO_2 plot, and have the lowest K_2O of the Union Island Group (0.85±0.24%). HFSE values are notably lower than for other groups, and classifications range from subalkaline to transitional. The subalkaline classifications are the result of low Nb. Because the Nb varies rapidly at constant Zr (Fig. 10-5c), a detection-limit problem in the XRF analysis may have been involved. A break in the curve occurs at Nb=4 ppm. If this is used as a minimum detection limit, the subalkaline classifications become transitional, which accords with the clinopyroxene classification. Tectonically, UIG2M is a within-plate basalt but shows notably low Y for such an environment (Fig. 10-5g). Thus HFSE ratios suggest that the unit is transitional but HFSE concentrations are unusually low.

According to the variation in the stable elements, only 15% crystal fractionation (mainly of ol-pl) has taken place, although high and constant values of Cr and Ni occur over a very large variation in mafic index (Fig. 10-6). This can only be explained by Mg-loss or Fe-gain (total Fe as FeO exceeds 19%). The limited fractionation, high Cr and Ni, and low HFSE indicate a more primitive magma than the others in this group of transitional magmas, but the distinct Ti, Zr and Nb intercorrelations (Fig. 10-5f,i and j) imply partial melting of a separate mantle source; the varied Zr/Nb ratios

indicating heterogeneity. This problem is referred to later in this chapter. Slopes of the UIG2M trends on these plots suggest that Zr had a higher partition coefficient than other HFSE during partial melting; this is not readily explained by any combination of reasonable mantle materials.

d) UIGDM

These diabase sills range in composition from ol-hy basalt to minor q-hy tholeiitic andesite in the coarse upper levels. Alkalies vs. SiO_2 and HFSE indicate a transitional composition. The average K_2O of the least altered samples (1.02±0.36%) is similar to that for UIG1M. In addition, UIGDM covers the same range in mafic index and its HFSE variation is also explained by 60% crystal fractionation. The consistently lower HFSE values for UIGDM could be explained by a mixture of average UIG1M plus plagioclase, except that P concentrations are higher in UIGDM and apatite is not a cumulus phase. The source magmas are therefore similar but not cogenetic.

e) Comparison and Petrogenesis

Compared to the other transitional mafic magmas at a similar mafic index, MADM has similar HFSE concentrations to flows from east Greenland (TRANS-1) and the axial ranges of Afar (Erta Ale) (Nielsen, 1978; Bizouard *et al.*, 1980). Both these suites are extruded onto thin crust after major rifting. UIG1M is richer in HFSE, but still poorer than

lavas extruded on a rifted, thick crust e.g. the Kenya Rift (Barker, 1977). The HFSE-poor UIG2M is similar to the Mg-rich continental tholeiites of Svartenhuk, west Greenland (Brooks, 1973) and, except for its high Rb and K, to the Hebridean Skye Main Lava series, a suite thought to be derived by partial melting of a previously depleted mantle (Morrison *et. al.*, 1980). Apart from SiO_2, K_2O and CaO differences, the mean UIG2M composition is similar to SK971 of Skye, which is in equilibrium with a four phase spinel-peridotite at 1230°C and 10kb (Thompson, 1974). At this pressure (close to the base of the crust), anhydrous partial melting of over 20% would be needed to generate an ol-hy normative magma (Green and Ringwood, 1967). Stratigraphically equivalent lavas in the Wopmay orogen have a primitive (MORB-like) geochemistry (Easton, 1981) and reflect more extensive crustal rifting. These are the lower Kaapvik, Tuertok and Belleau Formations of the Akaitcho Group as well as the associated Stanbridge and Vaillant Formations.

The Mid Aphebian Diabase and Union Island Group are therefore transitional, mainly ol-hy normative, mafic magmas, comparable to those from Tertiary continental rifts which have been produced by crustal thinning. Each suite was derived from a discrete batch of magma by partial melting at pressures at which the ol-cpx-plag thermal divide in the basalt system was inoperative, i.e. at greater than 8 to 10 kb. It is tentatively inferred that partial melting took

place close to the base of the crust. UIG1M and UIGDM underwent 60% crystal fractionation, largely in crustal magma chambers and produced tholeiitic andesitic compositions. UIG2M was produced by melting of a more depleted, heterogeneous mantle and, because of little evidence of fractionation, was rapidly emplaced from depth.

G. SOSAN GROUP

Two areas were studied, both having potassic alkali basalts: Seton Island has both a bimodal and a continuously differentiated sequence, whereas Taltheilei Narrows has a bimodal sequence.

a) Seton and West Keith Islands (SOGSI1M, SOGSI2M, SOGSI3I and SOGSIF)

The lower part of the sequence is classified as K-alkaline olivine basalt (SOGSI1M) and potassic trachy-rhyolite (SOGSIF). The upper part is K-alkali basalt (SOGSI2M) differentiated to tristanite (SOGSI3I). The last rock type ranges from trachybasalt to trachyte.

The high HFSE concentrations, notably of Nb and P, classify these suites as alkaline (Fig. 7a,c,d), but sodic and potassic suites cannot be distinguished by this criterion alone (Winchester and Floyd, 1977). One least-altered sample of SOGSI1M and two samples of SOGSI3I established the above classification, using Irvine and Baragar (1971); however, none of these samples have

normative diopside. The potassic nature of the sequence is shown by the presence of a primary K-feldspar. Its primary nature is established by the coherent decrease of Ba with the mafic index. The normative classification of these samples is hy-normative, thus the assumed oxidation ratio is too high. The highly potassic rocks found in the upper sequence do not have igneous compositions (Fig.10-1) and appear to have gained their K_2O from interlayered trachytes during metamorphism.

The correspondence of the SiO_2 and Zr/TiO_2 classifications (Fig. 10-7a and b) indicates that SiO_2 is fairly stable. SOGSI3I, which has a colour index less than 35, has SiO_2 over 50%. Except for a single composition, the tightly clustered SiO_2 values of SOGSIF are probably original and therefore classify these rocks as trachyrhyolite rather than alkali rhyolite. The three least-altered samples are highly potassic and suggest a trend to pantelleritic rather than comenditic compositions. The sequences all classify as within-plate (Fig. 10-7e,f and g), although Y contents vary widely and show values as low as 17 ppm.

The upper and lower sequences are divided because each displays a separate but continuous path of Nb, Y and Ti enrichment (Fig. 10-7f,h,i and j) which precludes their derivation from the same magma. The mafics of the bimodal suite, SOGSI1M, contain higher Nb and P_2O_5 than those of the late differentiated suite, SOGSI2M, (65±18 ppm and

0.89±0.54% compared to 35±7 ppm and 0.54±0.20% respectively and thus appear to be more alkaline. K_2O, for all samples from each suite, shows the opposite trend (1.81±1.55 to 2.80±2.37%), although these values may be the result of alteration. Only one "least-altered" sample was obtained from both suites and therefore no comparison of K_2O could be made using this technique.

This difference is noted on the mafic index plots (Fig. 10-8) and differences in the crystal fractionation paths are revealed. The mafic index attains a maximum value in the tristanites, owing to the subsequent rapid reduction in Fe content.

At low M.I. values, the rapid reduction of Cr and Ni in SOGSI1M indicates clinopyroxene and olivine fractionation. In SOGSI2M, starting at an M.I. of 71, the rapid reduction of V and Fe suggests Fe-Ti oxide crystallization, but TiO_2 increases up to an M.I. of 80. The linear depletion of Ba in the tristanites (SOGSI3I) indicates K-feldspar crystallization, which was probably represented modally as anorthoclase before subsequent metamorphism (see Ch. 4).

The variation in stable elements in the basalts is explained by at least 40% crystal fractionation, dominantly of plagioclase. HFSE variation in the bimodal group suggests trachy-rhyolite would be produced by 85-90% fractionation of the basalts, very similar figures to those calculated for the transitional to alkaline bimodal suites of Afar (Boina and Erta Ale; Bizouard *et al.*, 1980). The observed

elemental range in basalt-tristanite to trachyte sequence can be explained by 75-80% fractionation (approximately $ol_5pl_{45}cpx_{25}mt_3$). This degree of fractionation is close to that calculated to explain a similar suite produced from transitional basalts of the Gregory Rift (Ol Tepesi, $ol_8pl_{40}cpx_{27}mt_3$; Baker *et al.*, 1977).

No definite petrographic evidence was seen to support olivine fractionation, but the Ni reduction is clearly apparent. The break in slope on the Cr-Ni fractionation plot (Fig. 10-7k) indicates clinopyroxene crystallization before olivine. This evidence of clinopyroxene as a liquidus phase suggests minor fractionation at moderate pressure (>8 kb).

b) Taltheilei Narrows (SOGTNM and SOGTNF)

(i) SOGTNM

The mafic component of this bimodal suite (SOGTNM) clearly classifies as alkaline and within plate on all the HFSE diagrams. Chemical alteration is much more extensive, leaving only one least altered sample which is a potassic alkali olivine basalt (using Irvine and Baragar, 1971). HFSE concentrations are comparable with those of SOGSI2M, and also clinopyroxene phenocrysts are found in some samples. However, unlike SOGSI2M, no tristanites are found. Starting at an M.I. value of 71, a rapid decrease in both V and TiO_2 suggests the crystallization of an Fe-Ti oxide phase.

(ii) SOGTNF

The associated rhyolites (SOGTNF) are clearly alkaline (Fig. 10-7a) but they contain negligible Na_2O and have non-igneous alkali compositions. If, however, the total alkali compositions have been preserved, these rocks are peraluminous and therefore unrelated to the basalts. The HFSE trends for the basalts and rhyolites show separate groups with no clear evidence of consanguinity (Fig. 10-7f,h,i and j).

) Comparison and Petrogenesis

The most alkalic mafic flows (SOGSI 1M) are comparable to the "low-K" ALK2 basalts of East Greenland (Nielsen, 1978). These were extruded after major crustal flexure and rifting and form a bimodal association with undersaturated trachytes. However, the SOGSIF plugs are oversaturated trachytes and have similar HFSE contents to those in bimodal associations with transitional, rather than alkali basalts (Erta Ale, Bizouard *et al.*, 1980; TRANS-1, Nielsen, 1978).

It is difficult to see how these oversaturated rocks could fractionate from a nepheline normative magma when there is no evidence of kaersutite fractionation. If this basalt suite is a consanguinous bimodal association, SOGSI 1M may represent a transitional basalt from a mantle segment rich in HFSE elements. However, these concentrations are far higher than are found in any transitional basalt so far described.

The high alkalinity of the magmas, their association with a period of flexure and faulting (see Ch. 2) and the evidence for medium pressure fractionation suggests a lower degree of mantle melting at a higher pressure and in a lower geothermal gradient than was involved in the production of the older transitional magmas (i.e. of the Union Island Group). This is best explained as pressure-release melting along deep fractures of the braided, transcurrent fault system. These fractures were dilated by a phase of E-W compression and doming of the Slave craton which preceded the onset of subduction. That these major faults tap the mantle today is shown by a seismic refraction profile (Barr, 1971). Transitional to alkaline central eruptions are observed after graben development on both thick crust (Ethiopia, Meyer *et al.*, 1975) and thinned crust (Afar, Civetta *et al.*, 1975).

The close association of alkali basalt - tristanite - trachyte with alkali (or transitional) basalt and trachy- rhyolite suggests varied degrees of partial melting at high pressure to form mafic melts. These were later fractionated at pressures below the onset of the thermal divide to form an oversaturated and an undersaturated trend. A similar association has been explained by this mechanism in the Hebridean suites of Skye (Thompson *et al.*, 1972). However, this mechanism can only be accepted if uncharacteristically high HFSE values are assumed for a transitional basalt, and if two distinct mantle sources are posed. The data presently

available are not sufficient to resolve this problem.

H. KAHOCHELLA GROUP AND JACKSON GABBRO

These transitional to alkaline volcanic and intrusive suites are grouped together because each suite occurs at two separate centres and each centre yields volcanic products with a characteristic trace element signature.

a) Taltheilei Narrows (KAGTNM and JAGTNM)

Two of the least-altered samples of the KAGTNM flows classify as ol-ne normative trachybasalts (using Irvine and Baragar, 1971 and Fig. 10-2). This probably represents their original compositions because the suite yields high concentrations of HFS elements, characteristic of alkali basalts (Fig. 10-9a,c and d) and similar to those for the Sosan Group mafics. The other two remnant samples appear to have suffered some K_2O loss (Fig. 10-2) and their major elements yield an incongruous K-tholeiite classification.

The HFSE ratios, notably the parallel trends on the Nb-Zr plot (Fig. 10-9i), suggest that two magma sources may be present. The stable trace element variation can be explained by 30% low pressure crystal fractionation of each suite, with plagioclase forming over half of the fractionated mineral assemblage (Table 10-3).

The two least-altered major-element compositions of the differentiated Jackson gabbro plug (JAGTNM) are ol-hy normative basalts (although one is q-hy normative in Fig.

10-2). The HFSE classify the mafic part of the plug as transitional to alkaline (Fig. 10-9a,c and d); whereas the unanalyzed marginal phase is undersaturated syenite, showing no modal quartz. When plotted versus mafic index, the HFSE have trends similar to the associated KAGTNM lavas, except in yielding higher Zr contents (700±70 ppm vs. 113±20 ppm). The bimodal TiO_2 distribution indicates the presence of cumulate oxides.

Both lavas and intrusives appear to be closely related and may represent varied degrees of partial melting of the mantle (10 to 20%) to produce ol-ne to ol-hy normative melts. Differing Nb/Zr ratios suggest some mantle heterogeneity.

b) Pekanatui Point (KAGPPM, KAGPPF and JAGPPM)

(i) KAGPPM

The largely pillowed basalt suite (KAGPPM) is more strongly altered than the massive KAGTNM flows and yields SiO_2 contents of over 58%, but the original mafic composition is confirmed by the low and restricted range in Zr/TiO_2 ratios (Fig. 10-9a and b). The mafic index plots (Fig. 10-10) show considerable scatter for alkalies, CaO, Ba and Sr; however, the Mg/Fe ratios have been subject to metamorphic alteration because with increasing mafic index, Ni increases and Nb, Zr and Y decrease. This cannot be achieved by any realistic origin by partial melting or crystal fractionation, and

an origin by contamination would have to involve an unlikely, Mg-poor, Fe-Ni-rich contaminant.

Two of the four least-altered samples of KAGPPM are ol-ne normative potassic alkali basalts with over 2% K_2O (Fig. 10-2). The remaining two compositions classify as q-hy normative and plot in the subalkaline field of Fig. 10-2. This is inconsistent with the trace element classification, and is probably caused by SiO_2 addition. The HFSE yield an alkali-basalt classification (Fig. 10-9a and b) but high Zr/P_2O_5 indicates possible transitional compositions (Fig. 10-9c and d). The HFSE show lower concentrations than those of the KAGTNM or Sosan Group basalts. Y and P_2O_5, in particular, display wide ranges in concentration and reach extremely low values (7 to 28 ppm and 0.01 to 0.77% respectively). Tectonically, the suites classify as within-plate (Fig. 10-9e and f) but Y is unusually low for basalts of this environment (Fig. 10-9g).

The wide ranges in trace element concentrations in KAGPPM for a limited variation in fractionation index (i.e. Zr/TiO_2) cannot be explained by low pressure crystal fractionation because an impossibly high percentage of crystallization would be needed, i.e. over 85% within a formation which shows no evidence of differentiates of intermediate composition (Table 10-3 and Fig. 10-9i to m). In addition, distinct trends occur on HFSE plots (Fig. 10-9i to j) and a wide range (2 to

8) occurs in the Zr/Nb ratio (Fig. 10-9h). Clearly, a multiple source origin is involved, either by progressive melting of a mantle source and magma-removal in discrete pulses, or by melting of a mantle which has small-scale chemical heterogeneities.

KAGPPM displays asymptotic trends to the Zr axis on logarithmic plots of Ti and Y vs. Zr (Fig. 10-9f and j) and to the Nb axis on a plot of Nb vs. Zr (Fig. 10-9i). On logarithmic plots this indicates an intercept on the opposite axis of the binary plot. An intercept on the axis of a particular element suggests a relatively-higher partition coefficient for that element during melting. Comparison of the intercepts of HFSE, on these binary plots suggests a relative incompatibility during melting of Ti=Y>Zr>Nb, i.e. Ti shows an unexpectedly high compatibility for normal mantle materials. Variation in the contribution of key mantle-phases, which host these elements, to the primary melt would be a mechanism to explain the observed variation in interelement ratios. Using the partition-coefficients for mafic phases in Pearce and Norry (1979), the only phases which could explain such a variation in the four elements is a mixture of hornblende and clinopyroxene, and even this does not quite explain the rapid increase of Nb with Zr (Fig. 10-9i). However, the hornblende/basalt partition coefficients of Zr and Nb are fairly similar (0.5 and

0.8 respectively) and, within error, could probably give the observed trend. The sharp increase in Nb cannot be caused by residual garnet because no corresponding depletion in Y is observed. Phlogopite cannot be involved in melting because it will not fractionate Nb or Ti in a mafic melt.

Geochemical studies of Tertiary to Recent potassic alkali-basalt complexes suggest that these rocks originate by 7 to 20% partial melting of garnet peridotite (Sun and Hanson, 1975; White *et al.*, 1979; Fernandez, 1980). It is difficult to see how an amphibole could survive as a residual mantle phase with this degree of partial melting. It therefore seems most likely that KAGPPM lavas were formed by similar degrees of partial melting of a heterogeneous mantle source which contained different amounts of amphibole and clinopyroxene. A recent survey found that the commonest amphibole in upper mantle nodules is pargasite (Dawson and Smith, 1982). The range in concentrations of the HFSE, notably of the most compatible element in the group, Y, suggests that mantle heterogeneity may be related to a previous thermal event. Small scale partial melting and subsequent recrystallization would lead to a redistribution of LILE and HFSE in localized amphibole and clinopyroxene veins, owing to inefficient extraction of the melt, i.e. continuous or dynamic partial melting giving contiguous zones of enrichment and depletion

(Langmuir *et al.*, 1977; Wood, 1979). Such continuous, rather than batch, partial melting for this mantle sample is indicated by straight-line trends, rather than concave-upward curves on a Zr/Y vs. Zr plot (Pearce and Norry, 1979). Furthermore, elemental redistribution about mean values typical of mantle concentrations, is indicated by the slopes and positions of the curves for KAGPPM on binary HFSE plots. The mid-sections of the KAGPPM trends transect the "mafic" ends of the curves for all other suites (Fig. 10-13). The sub-parallel fractionation trends of these other suites indicate that they have all evolved from discrete magma batches which cannot be connected by any model of low pressure crystal fractionation. This may have involved partial melting of different mantle segments, different degrees of melting of the same segment, or a combination of both mechanisms. Because KAGPPM includes and cuts across these trends, it appears to represent within one suite the entire observed range of relative enrichment and depletion in Nb and Zr for the mantle below the East Arm.

(ii) KAGPPF

The associated rhyolite domes (KAGPPF) display a limited SiO_2-variation and have lower HFSE contents than SOGTNF. Remnant quartz phenocrysts and the high SiO_2 content indicate that these were originally oversaturated. This, plus the high Nb/Y ratio,

classifies these rocks as high-alkali rhyolites. However, if the total alkali content is original and only equimolal Na-K exchange has occurred during metamorphism, the suite is peraluminous rather than peralkaline. This is in keeping with the muscovite phenocrysts observed in one sample. However, this suggests that either the muscovite is a pseudomorph of another phase, or that peralkaline rhyolites might contain high Nb. The sparce and anomalous nature of the petrographic evidence suggests that the former explanation is the more likely one. Unfortunately, only few data are available; however, the markedly different Zr/Nb ratios indicate no consanguinity with the KAGPPM flows (Fig. 10-9h and i).

(iii) JAGPPM

Only two samples were collected from the Jackson Gabbro sills and dykes which had igneous major-element compositions. Both of these were q-hy normative tholeiitic andesites (using Irvine and Baragar, 1971). The Zr/TiO_2 ratios confirm the intermediate classification (Fig. 10-9a and b) but HFSE classifications indicate a transitional to alkali-gabbro suite (Fig. 10-9a to d). Low HFSE concentrations are similar to those of KAGPPM and, according to Fig. 10-9e and f, could indicate a possible plate margin environment, as does the lack of Fe-enrichment. On the hand, other data do not support this classification,

notably the high Cr and Ni contents which are more characteristic of a primitive within-plate basalt. In addition, volcanic arc basalts have high contents of LILE, but not of HFSE with very low partition coefficients, e.g. Nb (Saunders *et al.*, 1980). JAGPPM, however, has Nb and Nb/Y values far too high for arc basalts. Furthermore, data are sparse and the classification diagrams were not designed for intrusive rocks. The similarity in the trace-element signature between the intrusions (JAGPPM) and the associated lavas (KAGPPM) indicates that they were derived from the same heterogeneous mantle segment.

c) Comparison and Petrogenesis

The Kahochella Group in the two areas is thus characterized by different magma products. Taltheilei Narrows has trachybasalt flows (KAGTNM) cut by a transitional to alkali gabbro plug with a syenite margin (JAGTNM). Pekanatui Point also displays potassic alkali basalts (KAGPPM) cut by transitional to alkaline dykes and sills (JAGPPM), but they have much lower HFSE contents and were produced by partial melting of a markedly heterogeneous mantle segment showing small-scale variations in amphibole and possibly clinopyroxene.

Lateral chemical heterogeneity in the mantle has been deduced from the study of mantle xenoliths, sea-floor basalts and also Phanerozoic mafic suites from continents

and oceanic islands. This was observed in continental transitional basalts from the Hebridean Province (Beckinsale *et al.*, 1978; Morrison *et al.*, 1980) and the Midland Valley of Scotland (Macdonald, 1980). The former group, represented by the Skye basalts, is thought to have been formed from a mantle depleted in HFSE by a previous phase of melting. Alkali basalts from the Azores (Flower *et al.*, 1976) and from Kenya (Norry *et al.*, 1980) show the same feature. The latter case is thought to have involved partial melting, at depths less than 20kb, of a mantle locally enriched in LILE and HREE which were mobilized in a CO_2-rich fluid. Such mobilization has been produced experimentally at high pressures (Wendlandt and Harrison, 1979).

The Kahochella Group represents renewed pressure-release melting along splayed transcurrent faults during E-W compression of the Slave craton. In the Taltheilei Narrows area, the fault system which fed the Sosan Group volcanoes acted as a renewed conduit and produced alkali basalts similar to those of the Sosan Group. Further south, dilation of a new fault system tapped a more heterogeneous mantle segment.

I. PEARSON FORMATION (PEM)

a) Classification

The two least-altered samples are q-hy normative tholeiitic basalts and tholeiitic andesites, but both have high Al_2O_3, indicating a borderline calc-alkaline composition (using Irvine and Baragar, 1971). Their K_2O content is 2.12±0.78%. The alkalies vs. SiO_2 distribution of the whole suite suggests that it is subalkaline (Fig. 10-2); while the Zr/TiO_2 vs. SiO_2 coherence and limited SiO_2 variability (55.34±1.30%) indicates that the suite is dominantly basaltic andesite.

The low HFSE contents, notably of Nb and P_2O_5, clearly classify these rocks as subalkaline (Fig. 10-11a and b). Plots which use Zr/P_2O_5 classify these suites as subalkaline (Fig. 10-11c and d). It should be remembered that this type of plot applies strictly to mafic rather than intermediate rocks, because of the effect of fractionation on Zr/P_2O_5. However, the data plot well into the subalkaline field, indicating that even the most mafic samples would not classify as alkaline. Subalkalinity is also clearly indicated in the compositions of the remnant pyroxenes (see Ch. 9).

The classification of the tectonic regime is more complex. The HFSE indicate a volcanic arc environment and the low Cr (9±8 ppm) supports this (TiO_2 vs. Cr plot, Garcia, 1978). However, the high Ni contents (92±18 ppm) are more characteristic of non-arc (WPT and MORB) sequences (Ti/Cr vs. Ni plot, Beccaluva *et al.*, 1979). On the Ti-Y-Cr

diagram (Fig. 10-11n), PEM does not show the relative TiO_2 enrichment that would be expected in intermediate fractionation products of a continental tholeiite. The Ti/V ratio is dependent upon the oxidation state of V (i.e. upon fH_2O of the melt) and has been used by Shervais (1982) to distinguish IAT, with low Ti/V ratios, from WPT and MORB, which have Ti/V>20. PEM has a Ti/V of 27±3 which does not suggest an arc environment. Therefore the PEM lavas show chemical affinities with both continental and arc tholeiites.

Using the major elements MgO-FeO $-Al_2O_3$, the tectonic definition is less equivocal (Fig. 10-11o). The two least-altered compositions plot on the boundaries of the continental and orogenic fields, whereas the suite as a whole indicates a linear trend towards MgO, which is the least-stable element in the diagram. However, this trend might not be the result of alteration because MgO shows a good correlation with Ni and Cr. Taking field evidence into consideration, PEM is best classified as continental from this diagram, although altered samples, richer in Mg, do overlap into the field for ocean floor basalts.

Regardless of the environment, a coherent iron enrichment trend is indicated on the FeO vs. Zr/TiO_2 plot (Fig. 10-11p) but at a very high Zr/TiO_2 ratio. This trend is similar to that shown by the Ferrar diabase, a continental suite thought to be derived either from a mantle segment rich in HFSE and LILE or by crustal contamination.

Crustal contamination in the PEM flows is indicated by the extremly high $^{87}Sr/^{86}Sr$ initial ratio. This mechanism may also explain the variation in Zr/Nb ratios by one order of magnitude (Fig. 10-11h), but the vertical slope on the Nb-Zr diagram (Fig. 10-11i) and the low values of Nb in these rocks indicate that a detection limit problem for Nb is involved.

Trace element variation, apart from Nb, can be explained by moderate plagioclase-clinopyroxene cotectic crystallization, specifically $pl_{1.0}cpx_{1.5}oxides_1$ (Fig. 10-11j,k,l and m). Apart from the Fe enrichment trend, the lack of magnetite fractionation is illustrated in the constancy of SiO_2 content with increasing mafic index (Fig. 10-12). Crystallization of magnetite causes an inflexion on the trend and a rapid increase in SiO_2 content. In tholeiitic andesites from WPT magmas, magnetite precipitates at higher mafic index values than are reached in the PEM lavas (e.g. 75 in the case of Thingmuli, Carmichael, 1964). The high SiO_2 values even at very low mafic indices are noteworthy and may also be an effect of crustal contamination.

b) Comparison and Petrogenesis

The Pearson Formation therefore shows the high Fe and Ni characteristic of continental tholeiitic andesites, but with the low Cr and HFS element contents and the high Zr/TiO_2 of an arc tholeiite magma. Clearly, the field and

isotopic evidence (Ch.3 and Ch. 6) indicate a continental tholeiite whose composition has been modified by crustal contamination. Approximately 5% assimilation of a typical Slave granodiorite by a WPT would explain the alkali and Al_2O_3 contents but would produce high SiO_2values. Rather than bulk assimilation, a selective transfer of elements may have taken place. Alternatively, the tectonic model outlined in Ch. 2 indicates that the PEM flows were extruded after the development of a subduction zone on the western margin of the Slave craton, and before the intrusion of calc-alkaline laccoliths in the East Arm. The laccoliths suggest that the subduction zone influenced the magmatism of the East Arm, and it may therefore have partly influenced the chemistry of the PEM lavas. The high K_2O/Na_2O of the two least altered samples (>0.6), if original, indicates a borderline shoshonite classification (Mackenzie and Chappell, 1972): a rock series which normally marks recently stabilized convergent crustal margins.

The isotopic evidence of contamination (Ch. 6) makes the first hypothesis for the origin of the Pearson Formation the most likely, i.e. that it was formed by the upper-crustal contamination of a continental tholeiite. The flows compare most closely with the "high-Ti" member of the two Triassic diabase magma types of the Appalachians (de Boer and Snider, 1979; Smith *et al.*, 1975; Papezik and Hodych, 1980). The term "high-Ti", only refers to the relative TiO_2 content in these Triassic diabases. Both

suites have notably low TiO_2. At the same mafic index, the "high-Ti" diabase shows the same Al_2O_3, TiO_2, P_2O_5, Ni and Nb as PEM but with lower Na_2O, K_2O, Rb, Ba, SiO_2 and Zr and with higher Ca and Cr. Different theories have been put forward for the petrogenesis of this group, one of which is crustal contamination of an olivine-tholeiite magma (Smith *et al.*, 1975). Because subduction did not occur in the area at that time, no crustal subduction-related origin was involved, and the group is not as enriched in elements of high crustal abundance as is the Pearson Formation.

Despite these comparisons, it is difficult to envisage a crustal contaminant which would increase the Zr content in a WPT without adding considerably to the Nb and P contents, which would already be quite high. However, Nb and P have very low concentrations in PEM, suggesting that the uncontaminated magma was even more depleted in these elements (Fig. 10-14). The only magma which would show such an HFSE pattern would be an arc tholeiite.

The evidence is therefore equivocal and highly dependent on models for the nature of selective contamination. However, on continental margins one would expect to find a zone of transition between VAB and WPT. For example, high alumina basalts with <1 to >2% TiO_2 from the Ordovician of N. Wales have been interpreted as representing such a transition (Floyd *et al.*, 1976). The Pearson Formation may also represent such a transition.

J. QUARTZ DIORITE LACCOLITHS

These intrude late-stage gravity slides (Hoffman *et al.* 1977) and are composed of hornblende diorite with sporadic K-feldspar overgrowths on the plagioclase. Chemical data, given by Badham (1978c and 1981), indicate no systematic change from monzonite to diorite in these laccoliths along the length of the East Arm, as claimed by Hoffman *et al.* (1977).

Major elements indicate a calc-alkaline trend (AFM and Peacock index plots), but the suite contains less CaO, FeO and K_2O than the contemporaneous plutons of the Great Bear Province. K/Rb shows no trend with SiO_2 and this has been taken as evidence that the plutons did not differentiate from a single source (Badham, 1978c, 1981). However, it is not essential for a comagmatic suite to show this feature.

Using the Nb vs. SiO_2 tectonic discrimination plot for felsic intrusions (Pearce and Gale, 1977) this suite plots in the overlap of arc and within-plate plutons, but such low values of Nb (~15 ppm) are rare for within-plate plutons with more than 55% SiO_2. On the other hand, the Rb data is more characteristic of silicic plutons from a within-plate rather than a continental-arc environment. The Rb contents are all less than 100 ppm which is lower than Pearce and Gales' range for plutons from a continental arc (i.e. >200 ppm). In addition, evidence of crustal influence on the chemistry of the plutons is equivocal. The $^{87}Sr/^{86}Sr$ ratio, although high, could still indicate a mantle or lower crust

origin (see Ch. 6). Using the data of Pearce and Gale (1977) this suite is most closely comparable to the felsic plutons of Bolivia which occur in a tensional environment behind an arc on a continental margin.

K. ET-THEN GROUP (ETGM)

The least altered samples are q-hy normative tholeiites to tholeiitic andesites with 1.45±0.74% K_2O. One ol-hy normative sample is so classified, both by norm and by the alkalies-SiO_2 plot (Fig. 10-2). The SiO_2 content appears to be primary and Zr/TiO_2 indicates compositions ranging from tholeiite to tholeiitic andesite (Fig. 10-11a and b).

The HFSE indicate subalkalinity (Fig. 11a to d) and, tectonically, indicate a within plate environment with a possible transition to one of plate margin type (Fig. 10-11e,f and g). Additional use of the TiO_2 vs. Cr and Ti/Cr vs Ni discriminant plots preclude an arc-type setting and indicate a trace element pattern characteristic of a primitive (i.e. "MORB"-like) WPT. The MgO-FeO -Al_2O_3 diagram yields an unequivocal continental setting (Fig. 10-11o) and a tholeiitic iron enrichment trend at Zr/TiO_2 ratios lower than those for PEM is also observed (Fig. 10-11o). The sudden break in slope on the Nb vs. Zr plot at low concentrations of Nb (Fig. 10-11i) indicates a detection limit problem during analysis. The variation of the other stable elements is explained by 20% low pressure fractionation including 5% olivine (Fig. 10-11j to m).

The ETGM lavas are therefore continental tholeiitic andesites, but with low HFSE element contents (notably of Nb, P and Zr) more characteristic of a primitive WPT. This indicates that the mafic parent was even more depleted in all HFSE elements. Such depletion would be expected in IAT rather than WPT, but the inter-element ratios are not characteristic of arc lavas. This suggests an origin by the melting of a mantle depleted in these constituents, or by moderate, but selective crustal contamination of WPT. Unfortunately, no Sr isotopic data are available for this suite.

L. SUMMARY OF TRACE ELEMENT VARIATIONS IN THE VOLCANIC AND INTRUSIVE SUITES

The most important HFSE elements are plotted for each suite in Fig. 10-13 using Zr as a differentiation index. The parallelism of the trends indicates a separate magma source for each suite, unconnected by low pressure, crystal fractionation. Notably WIGM (1) and SOGSI1M (4) show continuous fractionation trends into their associated felsic units. In addition, the radically different slopes of KAGPPM (5) and UIG2M (3a) clearly indicate heterogeneous sources for these suites. The sudden breaks in slope below Nb values of 4 to 10 ppm cannot be explained by crystal fractionation and indicate an analytical detection limit problem.

Regarding only the changes in the mafic source compositions with time, the changes from transitional to

alkaline suites involved an overall increase in Nb and a slight decrease in Zr for all suites. The Sosan Group shows an increase in TiO_2 and similar or notably-lower values of Y, whereas the Kahochella Group shows a marked decrease in TiO_2 and Y. This pattern cannot be explained by varied degrees of partial melting of the same type of source. Variation of garnet in the mantle source is the only mechanism which can explain these changes, notably the rapid decrease in Y/Zr for source basalts of similar mafic index. Using the partition coefficient of Pearce and Norry (1979), clinopyroxene cannot give the same depletion. The alkaline Sosan and Kahochella Group lavas have thus tapped source regions depleted in garnet when compared to the sources for the earlier transitional MADM and Union Island Group.

Furthermore, the cycle of rift development which contains all the above suites, with the exception of the Wilson Island Group, begins with the Simpson Island alkali gabbro (not illustrated) which has higher concentrations of Nb, Ti and Y than any other suite (Burwash and Cavell, 1978; Badham, 1979b). Therefore the trend in Y (and probably garnet) depletion lasts throughout the whole cycle of rifting and compression, regardless of magma type.

The change in concentration of several elements through time can be seen more clearly in Fig. 10-14 which plots the least fractionated, non-cumulate sample from each suite. Concentrations are shown for a group of HFSE and transition elements which are listed in order of increasing overall

partition coefficients in petrologically relevant minerals. The concentrations are normalized to an average MORB (Pearce, 1980). This diagram is thus analogous to a Masuda REE plot and illustrates relative enrichments in elements of low partition coefficient (Nb and P) for alkali basalts and WPT (Fig. 10-14a and b respectively). Note that there is very little variation in Y, which tends to concentrate in garnet and clinopyroxene. The Simpson Island dyke is not plotted because no unequivocal chilled-margin composition is available from the data of Badham (1979a) and Burwash and Cavell (1978). However, the average analysis of this dyke is higher in all these elements than any later alkaline rocks of the Sosan or Kahochella Groups.

The transitional basalt profiles clearly show a separate origin for UIG1M and UIG2M, the latter yielding a primitive (MORB-type) WPT profile. Despite the detection limit problem for Nb, P concentrations are correspondingly low and the more fractionated samples (Nb>4 ppm) display a similarly shaped profile. Therefore the "flat" pattern seen is probably genuine.

The alkali basalts display a progressive depletion in all HFSE in both time and space: from the Sosan Group to the Kahochella Group, and from Seton Island to Taltheilei Narrows to Pekanatui Point. The Pekanatui Point magmas show different profiles with notable depletions (relative to MORB) in all elements except Nb and Ti. Because mafic indices do not vary greatly, and because the compatible

element Cr behaves in a similar fashion to the HFSE, this pattern suggests relative HFSE depletion of at least two different mantle segments with time. The Pekanatui Point data appear to show that mantle segments strongly depleted in Y, have been enriched in secondary amphibole, causing the addition of Nb and Ti.

The later ETGM and PEM suites have notably different element patterns. ETGM is similar to a primitive WPT but has a tendency toward the convex-upward pattern (Fig. 10-14) of an arc basalt (Pearce, 1980). This trend is more clearly developed in PEM, which in addition shows unusually high Zr contents, indicative of crustal contamination.

M. THE RELATIONSHIP OF MAGMATISM TO TECTONICS

Each stage of the magmatic development of the East Arm is clearly associated with its tectonic history which, in turn, is related to the structural development of the Wopmay orogen. This orogen has undergone at least one complete Wilson cycle of rifting, crustal separation, subduction and continental collision, which has been complicated by the development of a backarc basin and late stage gravity slides in the East Arm itself (see Ch. 2).

Because the structural controls on the development of continental rifts vary and because they may be observed in different stages of development, no single pattern is observed in the magmatic history of continental grabens. In the present case, the particular order of tectonism within

the Wopmay orogen has controlled the order of magmatism within the East Arm graben and the two are described together below:

(I). An early phase of potassic continental tholeiite in the Wilson Island Group (WIGM) followed the development of a graben and underwent low-pressure fractionation to tholeiitic andesite and rhyolite (WIGF). This sequence ends with the extrusion of highly alkaline basalts/nephelinites in the Upper Wilson Island Group (UWIGM) and, from the nature of its subsequent deformation, appears to represent an earlier cycle of rifting and graben development.

(II). A new cycle of updoming and graben development was accompanied by the intrusion of potassic alkaline gabbro to syenite and peralkaline granite (N. Simpson Island and Blachford Lake) and even carbonatites on the W. margin of the Slave Craton (Big Spruce Lake).

(III). A subsequent period of extensive crustal separation in the orogen produced a back arc basin and concomitant MORB-type magmatism (Akaitcho Group, Stanbridge and Vaillant Formations). In the East Arm, a period of erosion and limited crustal extension was accompanied by extrusion and high-level intrusion of within-plate transitional basalts, each unit of which represented a separate phase of shallow-level partial melting of the mantle. These units

include the Mid Aphebian (Hogrib) diabase (MADM) and the mafic rocks of the Union Island Group (UIG1M and UIGDM). A later, thicker mafic unit in the Union Island Group represented partial melting of a mantle segment of different composition (UIG2M).

(IV). Renewed fault movement caused by E-W compression and flexure of the Slave craton (associated with the preliminary stages of crustal subduction in the orogen) produced several, discrete potassic alkali basalt magmas, during Sosan Group times, by localized pressure release along transcurrent faults. These magmas are represented by two mafic units at Seton Island (SOGSI1M and SOGSI2M) and one at Taltheilei Narrows (SOGTNM). At Seton Island these magmas underwent low-pressure fractional crystallization to produce two separate differentiated series. The first produced a "bimodal" sequence with trachy-rhyolite plugs (SOGSIF) and the second produced a trachybasalt, tristanite, undersaturated trachyte series (SOGSI3I). The third alkali basalt flow-package, at Taltheilei Narrows (SOGTNM), is associated with alkali-rhyolite (SOGTNF) to which it shows no clear genetic connection.

(V). During Kahochella Group times, the commencement of easterly crustal subduction, which caused the growth of the Hepburn massif, temporarily relieved E-W stress in the graben. As a result there was a deepening of the graben and

continued pressure-release melting, sometimes along the same fault channelways which fed the volcanic centres of the Sosan Group, as at Taltheilei Narrows (KAGTNM).

In the Pekanatui Point area, potassic alkali basalts to trachybasalts (KAGPPM) were produced by melting of a heterogeneous mantle segment which may have had variable contents of amphibole and clinopyroxene. Other flows (KAGTNM) were produced from a distinctly different mantle segment which was richer in HFSE. Subsequent (Jackson Gabbro) intrusions of transitional to alkaline gabbro (to syenite) retained the characteristic HFSE pattern of each mantle segment (JAGPPM, JAGTNM). Problematic rhyolite domes in the Pekanatui Point area (KAGPPF) are associated with the mafic flows but were not consanguinous. They yield alkaline HFSE ratios but contain remnant muscovite phenocrysts.

The alkali basalt suites of the Kahochella Group and some from the Sosan Group, yield lower Y values than the transitional basalt suites and indicate a relative depletion of the mantle source in garnet.

(VI). As subduction and Hepburn plutonism continued, closure of the back-arc basin in the orogen restricted further dilation of the transcurrent faults in the East Arm. Magmatism of the Pearson Formation (PEM) was then similar to an arc tholeiite but with high Ni and Fe. Residence time in upper crustal magma chambers produced extremly high initial $^{87}Sr/^{86}Sr$.

Unlike all of the other mafic suites, except WIGM, this flow-package shows no evidence of olivine fractionation. The dominant rock type is tholeiitic andesite produced by low pressure fractionation of, mainly, clinopyroxene and plagioclase.

(VII). After closure of the marginal basin in the Wopmay Orogen, renewed compression produced gravity slides in the East Arm. A possible change in the angle of subduction triggered the development of a new calc-alkaline continental arc (Great Bear massif) with contemporaneous hornblende quartz diorites in the East Arm.

(VIII). After a period of continental collision, low grade metamorphism and shear melting in the orogen, a Helikian stage of E-W compression caused 70 km dextral strike-slip movement on the Macdonald-Wilson Island fault in the East Arm. This caused contemporaneous, localized continental tholeiite extrusion within the Et-Then Group (ETGM). The HFSE concentrations in this final stage are similar to those for a primitive WPT or even an arc tholeiite.

XI. CONCLUSIONS

An extensive field-mapping, petrographic and geochemical study was made of each of the fifteen major volcanic and intrusive suites of the East Arm of Great Slave Lake.

Because these units are interlayered with a 16 km thick clastic wedge, each formation of which can be related to a similar lithology and to specific tectonic events in the Wopmay Orogen (Hoffman, 1980a), an attempt was made to relate magmatism in the East Arm with tectonism in the orogen.

Hoffman (1980a) sees the East Arm as an aulacogen, or graben which abuts into the Wopmay orogen at a high angle, and whose tectonics have been controlled by the development of at least one Wilson cycle (of continental rifting and subsequent collision) in the orogen. After a compilation of published sedimentological and tectonic data was made, a new model for the Wopmay orogen was proposed in order to help explain magmatic development in the East Arm. This model was based on that of Hoffman, and invokes crustal rifting, development of a back-arc basin, subduction and subsequent closure of the basin by continental collision.

Major and trace element analyses were obtained for at least ten samples from each major igneous formation giving a total of over 200 analyses. Element mobility caused during metamorphism of the lavas and intrusions precluded the use of normal petrochemical classification techniques. This led to a review of element-mobility studies to ascertain the

most stable elements under various conditions of alteration and metamorphism. A critique and synthesis of available statistical classification techniques was made, based mainly on the relatively stable elements Al, P, Ti, Y, Zr Nb and the less stable transition elements Fe, Cr and Ni. The classification attempts to divide rock suites into alkaline and subalkaline types and then to classify subalkaline suites further, on a tectonic basis. Separation of intermediate from mafic compositions in each suite was supplemented by estimating the original colour index where igneous textures were preserved. In addition, a series of plots was used as geochemical "screens" to determine the least altered major element compositions. Norms of the latter compositions gave magmatic classifications consistent with those derived from trace elements.

These magmatic and tectonic classifications were supplemented by major element analyses of remnant igneous clinopyroxenes which again gave classifications consistent with the above. Clinopyroxene chemistry is closely related to the composition of the host magama. Variations in trace elements were used to determine the amount of low pressure crystal fractionation that had taken place in each suite using Rayleigh fractionation calculations, and to deduce that most suites were produced from a different magma batch. Magmatic $^{87}Sr/^{86}Sr$ ratios and $\delta^{18}O$ compositions were obtained from remnant igneous clinopyroxene. In conjunction with initial $^{87}Sr/^{86}Sr$ ratios from isochrons, they indicate

a mantle derivation for most magmas.

Dates obtained from the oldest and youngest Aphebian suites (Wilson Island Group, 1810±19 Ma and Pearson Formation, 1809±30 Ma) suggested that a metamorphic event of Hudsonian age reset the Rb/Sr clocks in the East Arm. The rocks show a progressive increase in metamorphic facies from pumpellyite - actinolite to epidote - amphibolite with age and thus with depth of burial. Metamorphism mobilized many major elements, particularly in fine-grained samples. Relevant thermodynamic and experimental data were used to construct a petrogenetic grid in terms of pressure, temperature and fluid composition. In all but the highest grade epidote - amphibolite facies, externally buffered metamorphic fluids, with Xco_2 values of up to 0.2, stabilized carbonate-bearing metamorphic mineral assemblages and appear to have produced the common "low-grade" epidote - actinolite - chlorite assemblage at temperatures characteristic of very low-grade (i.e. 300 to 400 °C). The CO_2 was supplied by limestone dissolution.

The relationship between the geochemistry of the volcanics and the tectonic history can be summarized as follows. After initial major rifting of the Slave craton and alkaline plutonism at about 2200 Ma, a period of crustal extension was associated with mantle-derived transitional basaltic volcanism. On the western edge of the Slave Craton, a marginal basin was developed. Subsequent east-west compression and buckling of the craton produced

mantle-derived mafic alkaline volcanism. Later, subduction, associated with the growth of the Hepburn massif, coincided with subalkaline basaltic andesite flows in the East Arm which have chemical affinities to both continental and arc tholeiites and which underwent marked crustal contamination. A following period of calc-alkaline plutonism coincided with the growth of the Great Bear massif and a phase of regional metamorphism at about 1810 Ma. During the Helikian, localized continental tholeiites were produced during major dextral movement on the Macdonald fault system. A more detailed outine of these events is set out below.

(1). An early phase of potassic continental tholeiite in the Wilson Island Group (WIGM) followed the development of a graben and underwent low-pressure fractionation to tholeiitic andesite and rhyolite (WIGF). This sequence ended with the extrusion of highly alkaline basalts/nephelinites (UWIGM) and, from the nature of its subsequent deformation, probably represented an earlier cycle of rifting and graben development.

(2). A new cycle of updoming and graben development was accompanied by the intrusion of potassic alkaline gabbro to syenite and peralkaline granite (N. Simpson Island and Blachford Lake) and even carbonatites on the W. margin of the Slave Craton (Big Spruce Lake).

(3). A major Mid-Aphebian dyke swarm (MADM) of mantle-derived transitional basalt was intruded into the Slave craton and preceeded a period of uplift and erosion in the East Arm.

A subsequent period of extensive crustal separation in the orogen produced a back arc basin and concomitant MORB-type magmatism (Akaitcho Group, Stanbridge and Vaillant Formations). In the East Arm, a period of erosion limited crustal extension, and block faulting was accompanied by extrusion and high-level intrusion of mantle-derived within-plate transitional basalts of the Union Island Group, each unit of which represented a separate phase of shallow-level partial melting of the mantle (UIG1M, UIGDM). Mapping revealed two distinct pillowed units in this group; the later, thicker mafic unit (UIG2M) showed a distinct chemistry and represented partial melting of a mantle segment of different composition from that which produced the earlier flows (UIG1M) and the diabase (UIGDM).

(4). During the deposition of the Sosan group, renewed fault movement, caused by E-W compression and flexure of the Slave craton (associated with the preliminary stages of crustal subduction in the orogen), produced several potassic alkali basalt magmas (SOGSI1M, SOGSI2M, SOGTNM) by localized pressure release along transcurrent faults. These were derived from separate partial melts of the mantle. In the Seton Island area, these magmas underwent low-pressure

fractional crystallization to produce two separate differentiated series. The first produced a bimodal sequence with trachy-rhyolite plugs (SOGSIF), and the second a trachybasalt, tristanite and undersaturated trachyte series (SOGSI3I). The third alkali basalt flow package (SOGTNM) in the Taltheilei Narrows area is associated with alkali-rhyolite (SOGTNF), to which it shows no clear genetic connection. Mapping showed that these two centres produced shallow water, phreatomagmatic eruptions and subaqueous ash flows. The reworked epiclastic deposits of Seton Island and sporadic welding of the tuffs in Taltheilei Narrows indicate possible subaerial emergence.

(5). During Kahochella Group times, the commencement of easterly crustal subduction, which caused the growth of the Hepburn massif, temporarily relieved E-W stress in the graben. As a result there was a deepening of the graben and continued pressure-release melting, sometimes along the same fault channelways which fed the volcanics of the Sosan Group, i.e. KAGTNM of Taltheilei Narrows.

Potassic alkali basalts to trachybasalts in the Pekanatui Point area (KAGPPM) were produced by melting of a heterogeneous mantle segment which may have had variable contents of amphibole and clinopyroxene. Other flows were produced by partial melting of a distinctly different mantle segment (KAGTNM). Subsequent intrusions of transitional to alkaline gabbro (to syenite) retained the characteristic

HFSE pattern of each mantle segment (JAGPPM, JAGTNM). Rhyolite domes (KAGPPF) are associated with the mafic flows but were not consanguinous. They yield alkaline HFSE ratios but contain remnant muscovite phenocrysts. The alkali basalt suites of the Kahochella Group yield lower Y values than the transitional basalt suites and indicate a relative depletion of the mantle source in garnet.

Field mapping indicated deeper water conditions of eruption for the volcanic centres of the Kahochella Group than for those of the Sosan Group. This is consistent with sedimentological evidence. However, Taltheilei Narrows was possibly an emergent centre showing reworked ash beds and pillowing of the distal parts of massive lava flows.

(6). As subduction and Hepburn plutonism continued, closure of the back-arc basin in the orogen restricted further dilation of the transcurrent faults in the East Arm. Magmatism of the Pearson Formation (PEM) was similar to an arc tholeiite but with high Ni and Fe. Residence time in the upper crustal magma chambers produced extremely high initial $^{87}Sr/^{86}Sr$ (0.7096). Unlike all of the other mafic suites, except WIGM, this flow-package shows no evidence of olivine fractionation. The dominant rock type is tholeiitic andesite produced by low pressure fractionation of mainly plagioclase and clinopyroxene.

(7). After closure of the back arc basin, renewed

compression produced gravity slides in the East Arm. A possible change in the angle of subduction triggered the development of a new calc-alkaline continental arc (Great Bear massif), with contemporaneous, back arc, hornblende quartz diorite in the East Arm (Compston quartz diorite laccoliths).

(8). After a period of continental collision, low grade regional metamorphism at 1810 Ma and shear melting in the orogen, a Helikian stage of E-W compression caused a 70 km dextral strike-slip movement on the Macdonald-Wilson Island fault in the East Arm. This caused contemporaneous, localized continental tholeiite extrusion in the Et-Then Group (ETGM). The HFSE concentrations in this final stage are similar to those for a primitive WPT or even an arc tholeiite.

Magmatism in the East Arm graben can therefore be related to local tectonic events which, in turn, were controlled by successive stages of rifting, compression, crustal subduction, closure of a marginal basin and continental collision within the Wopmay orogen.

Fig. 2-1. Major tectonic elements at the margins of the Slave structural province (from Hoffman, 1980a).

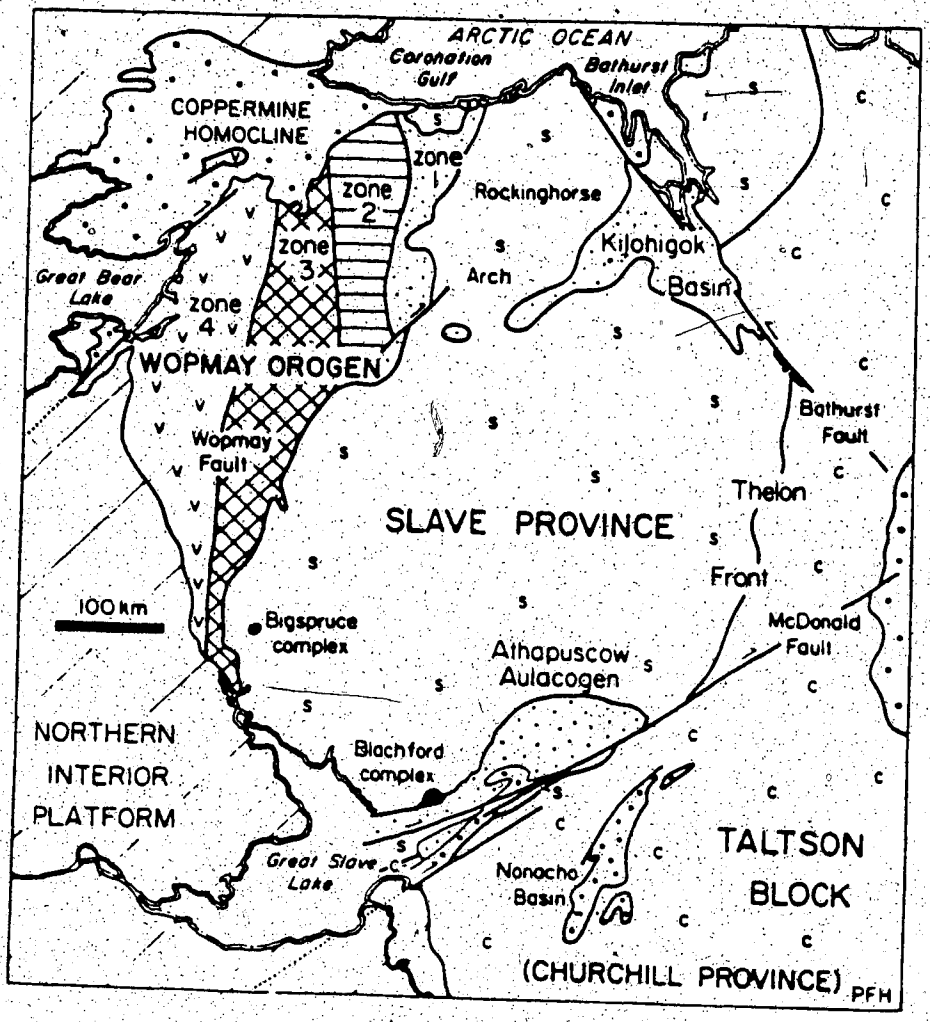

Fig. 2-2. Geological and tectonic (inset) maps of the East Arm of Great Slave Lake (from Hoffman, 1973).

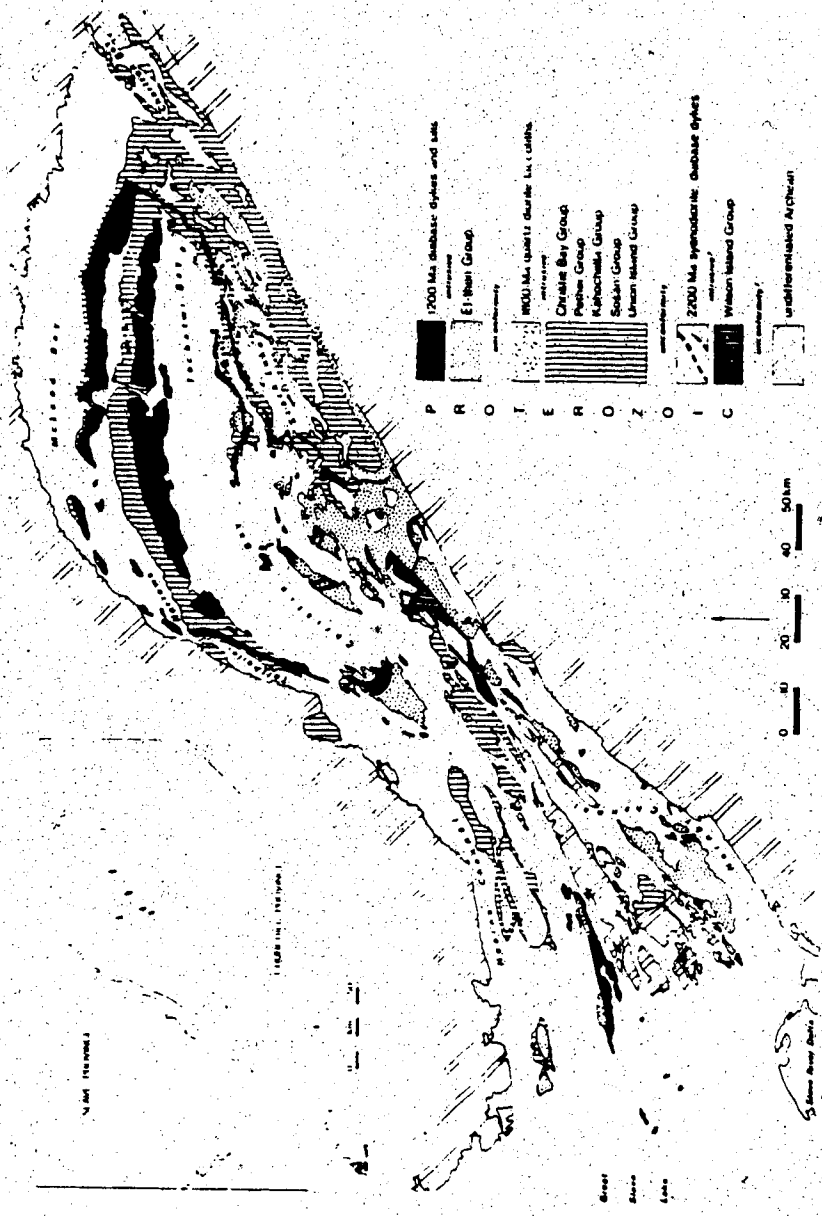

Fig. 2-3. Stratigraphic column, East Arm of Great Slave Lake (from Blackadar, 1981).

STRATIGRAPHIC COLUMN[1]
EAST ARM OF GREAT SLAVE LAKE

Age	Group	Description
Helikian	Et-Then Group	A nearly flat-lying sequence of coarse-grained terrigenous sedimentary rocks comprises fanglomerate overlain by sandstone.
	Unconformity	
Late Aphebian	Christie Bay Group	A complex assemblage of red beds - includes red mudstone with stromatolitic mega-breccia, red laminated and cross-bedded sandstone with carbonate-pebble conglomerate, red mudcracked mudstone with buff siltstone beds, and columnar basalt flows.
	Pethei Group	Stromatolitic and oolitic limestone and dolomite, thin bedded argillaceous limestone and mudstone, stromatolite mounds and graded greywacke beds.
	Kahochella Group	Red and green fissile mudstone, granular hematitic ironstone and spherulitic limestone, flat pebble intraformational conglomerate and red concretionary mudstone.
	Sosan Group	Pebbly crossbedded subarkose, stromatolitic limestone and basalt ash and lapilli-fall tuff fine cross bedded quartzite and red platy siltstone.
	Unconformity	
Great Slave Supergroup	Union Island Group	Arkose and granite rubble, non-stromatolitic dolomite, black mudstone, pillow basalt and gabbro sills, and cherty dolomite.
?		
	Unconformity	
Early Aphebian	Wilson Island Group	Basalt and rhyolite flows, conglomerate containing basement clasts, cross bedded quartzite, feldspathic quartzite, dolomitic quartzite, impure dolomite, argillaceous quartzite and argillite, porphyritic basalt flows.
	Unconformity	
Archean		Basement Rocks.

[1]Column adapted from Hoffman, 1969, 1973 and 1977 and Badham 1978b.

Summary of the depositional and volcanic history of the Epworth basin (Wopmay orogen), East Arm graben (Athapuscow aulacogen) and Goulburn basin (Kilohigok aulacogen)

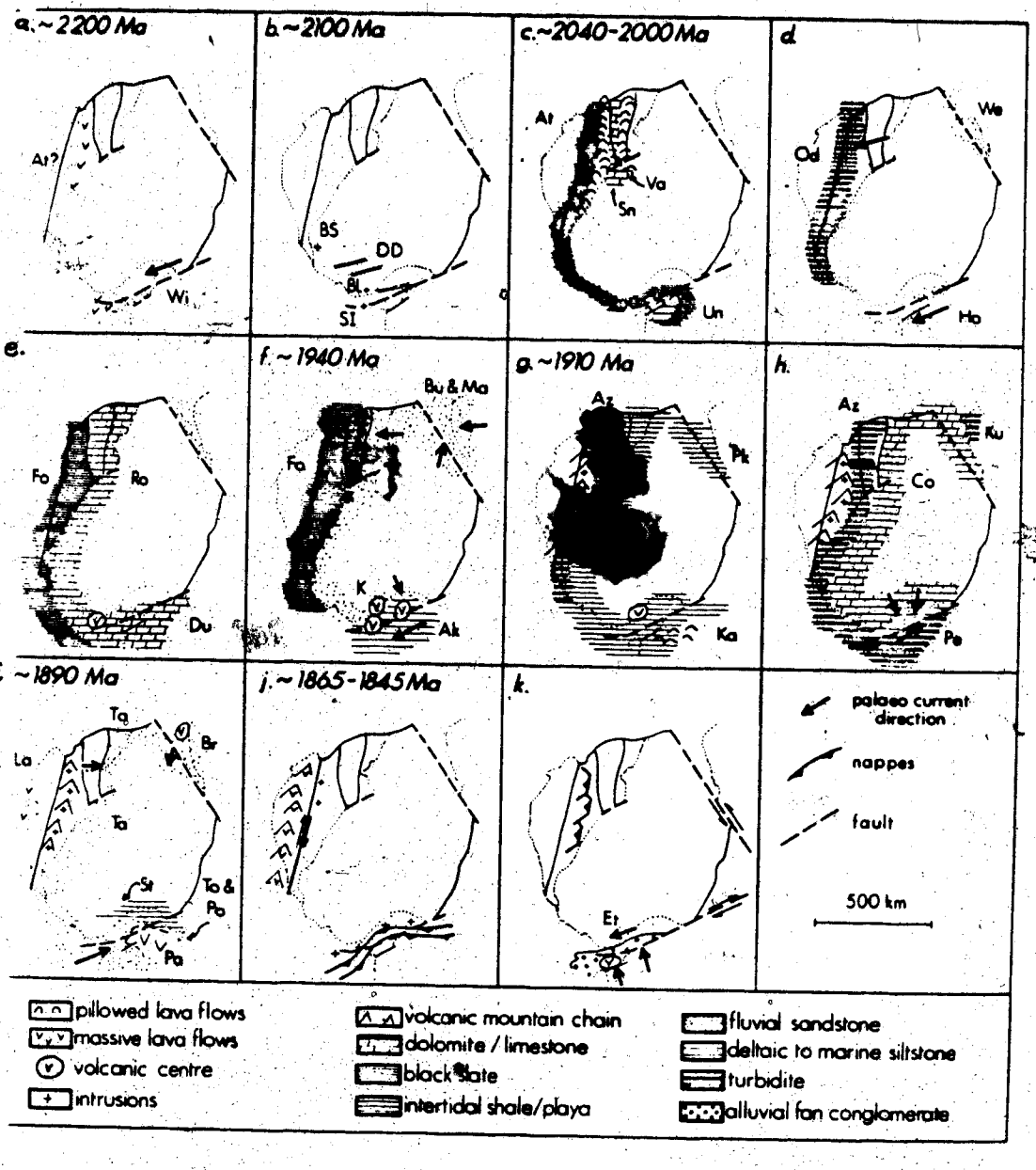

Fig. 2-5. The Wopmay Orogen I. First collision in the orogen, resulting in accretion of the Great Bear arc-bearing microcontinent (after Hoffman, 1980a).

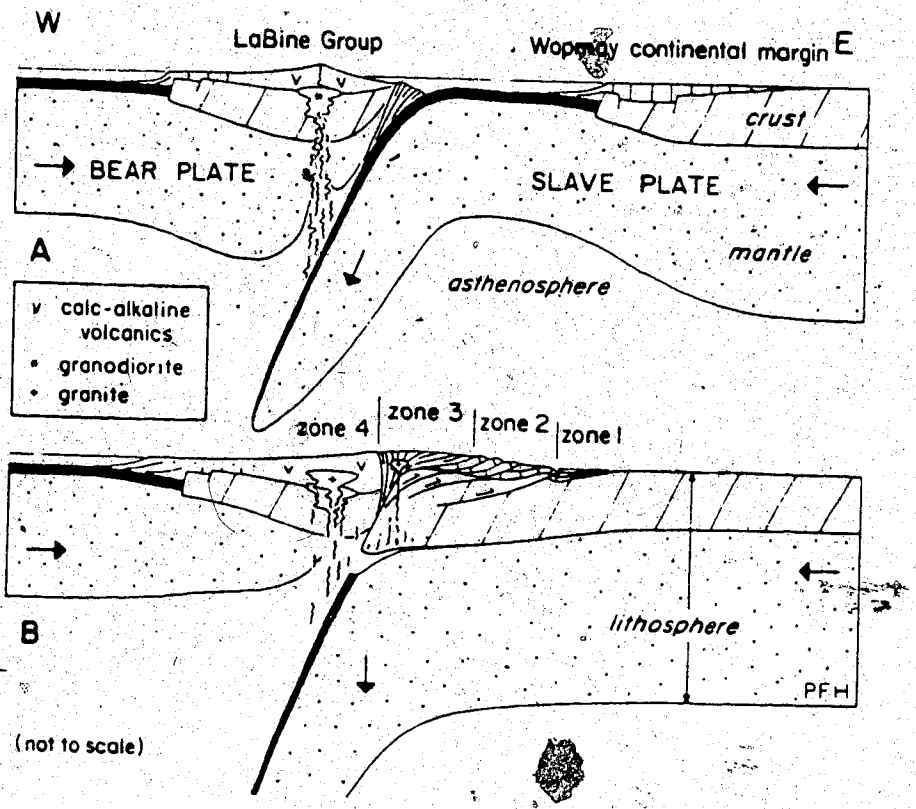

Fig. 2-6. The Wopmay Orogen II. Renewed subduction west of the accreted microcontinent, leading to continental collision. (after Hoffman, 1980a).

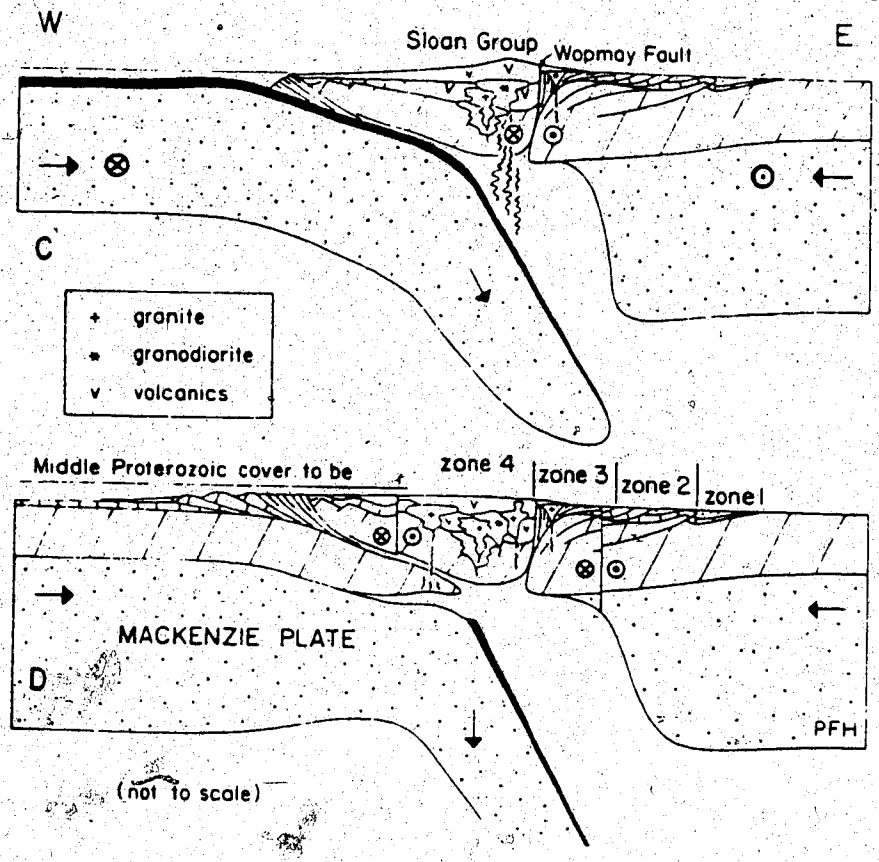

Fig. 2-7. Model for the development of the Wopmay Orogen. Zones are those used in Fig. 2-1.

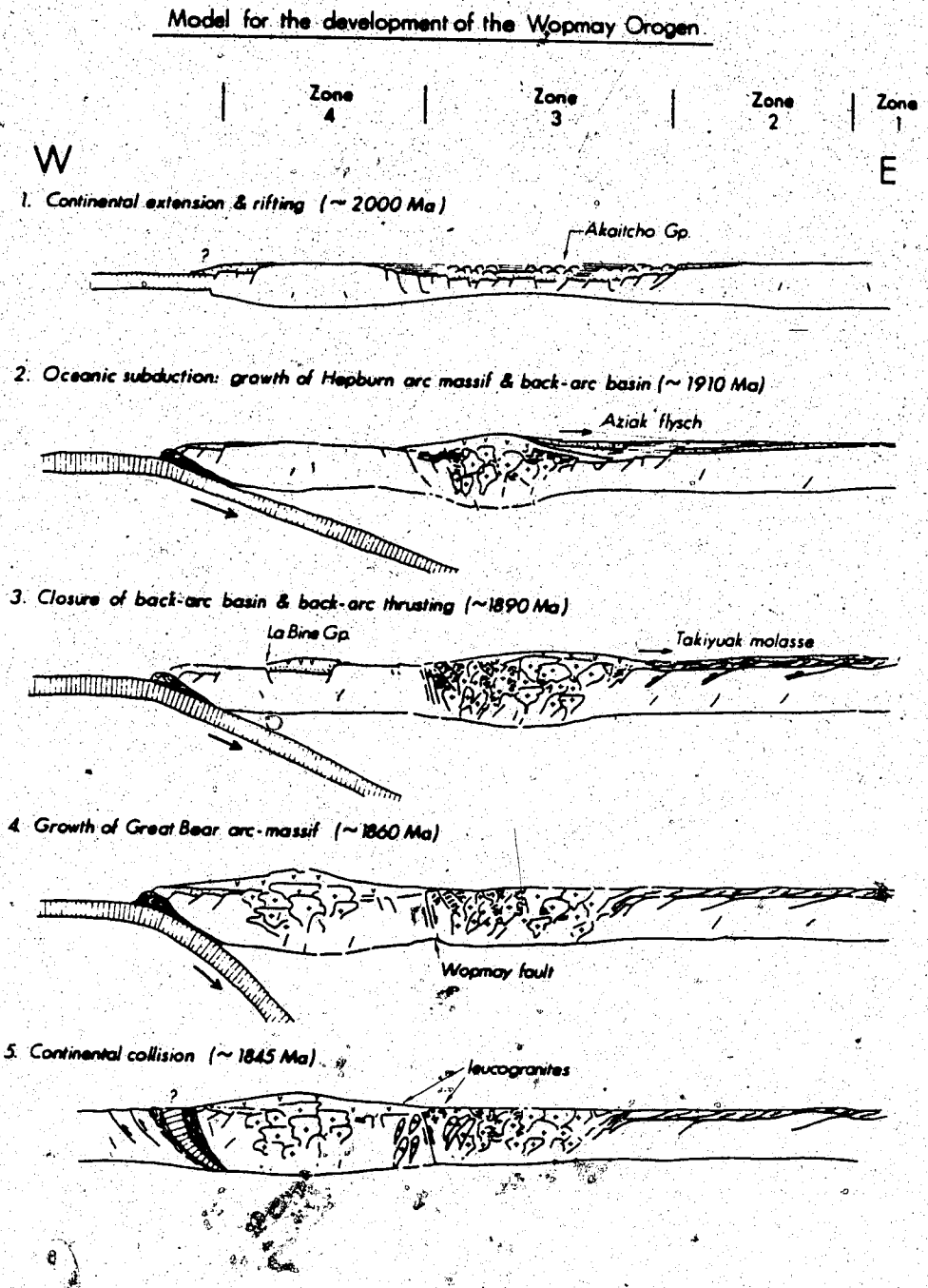

Fig. 3-1. Location Map for the East Arm of the Great Slave Lake.

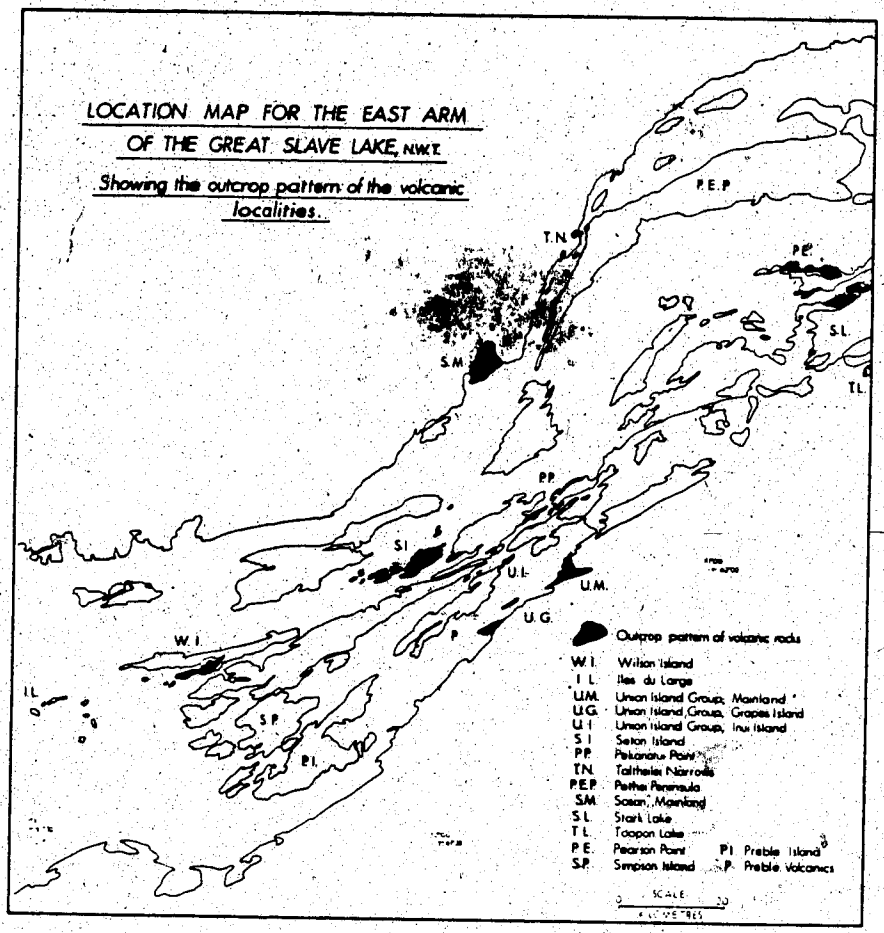

Fig. 3-2. Stratigraphical position of the volcanic suites of the East Arm, Great Slave Lake.

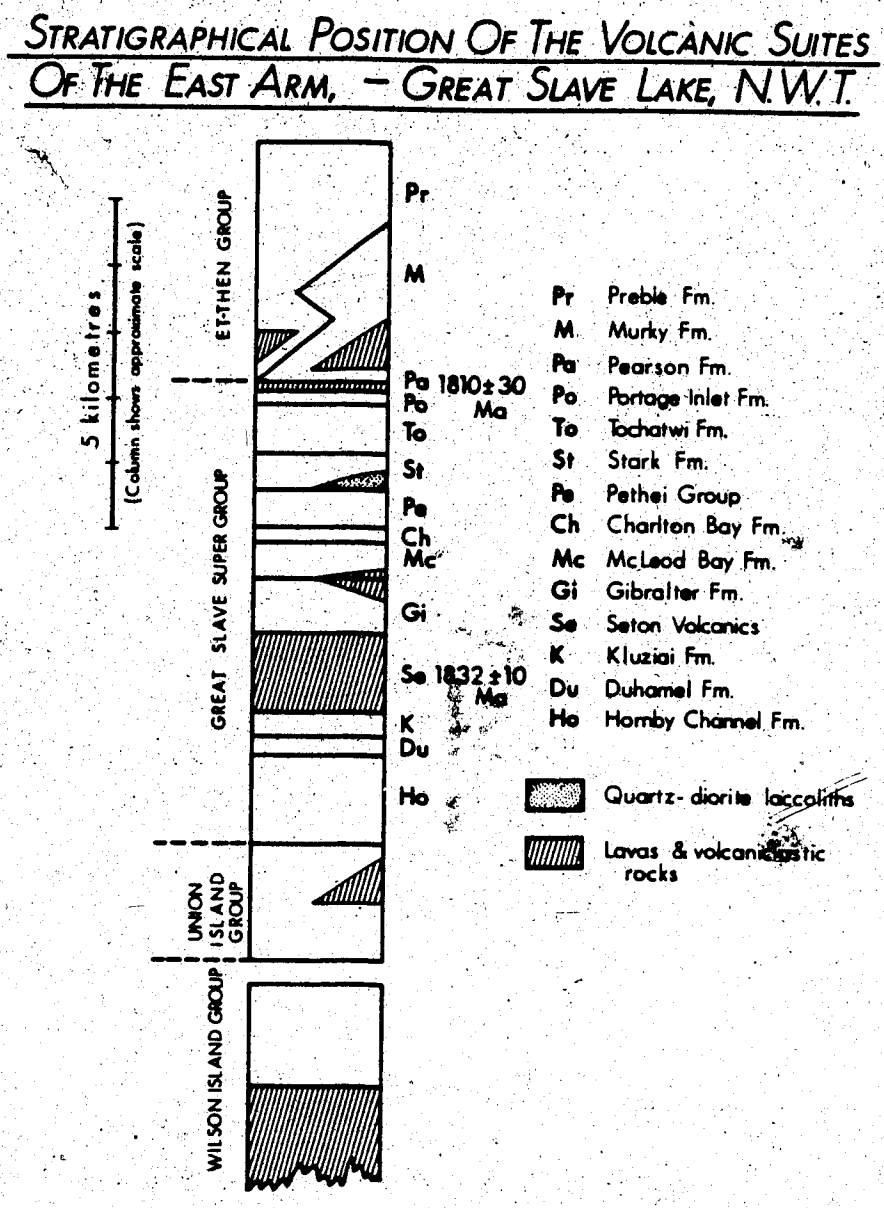

Fig. 3-3. Map of the volcanic bearing strata of the Wilson Island Group.

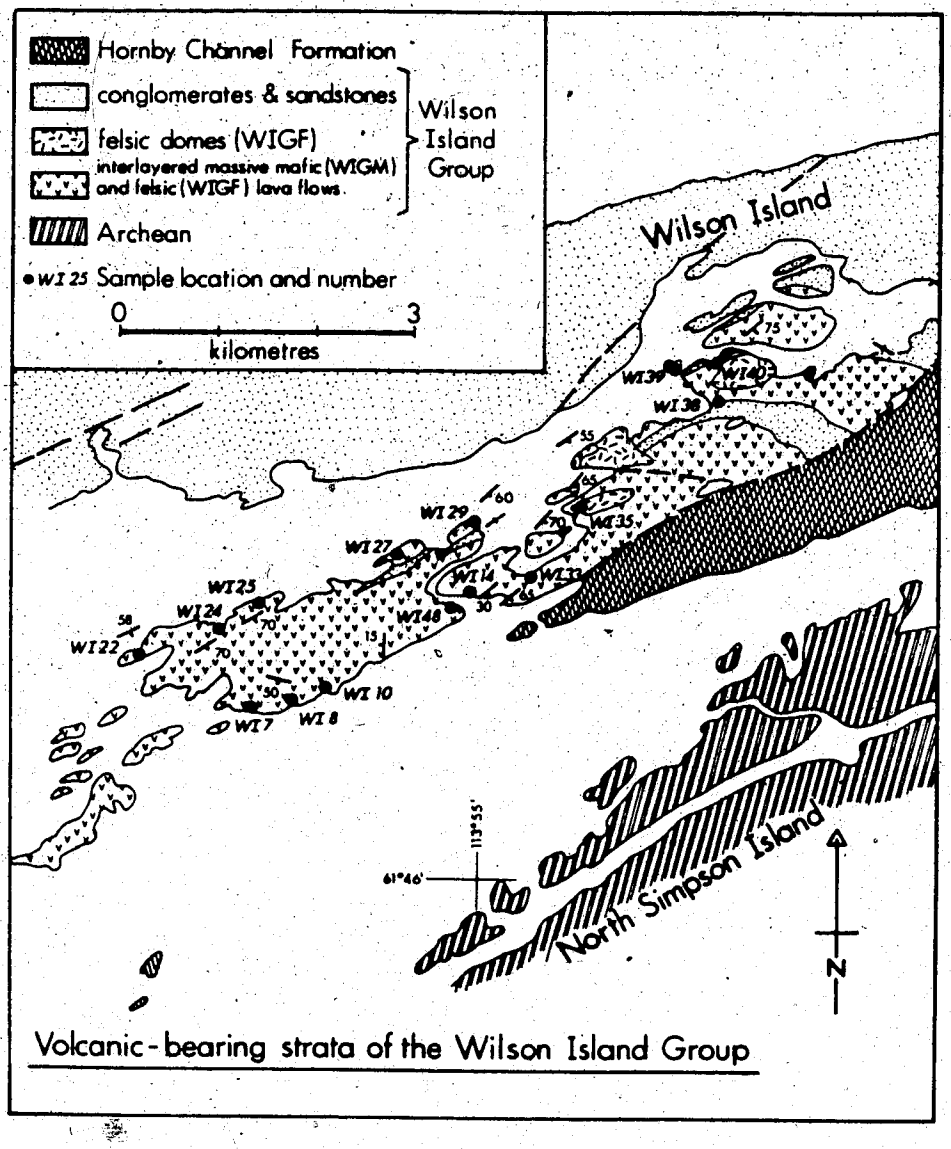

Fig. 3-4. Location and setting of the Mid Aphebian (Dogrib) diabase dykes.
Field sketch based on Badham (1979b), Burwash and Cavell (1978) and Reinhardt (1972).

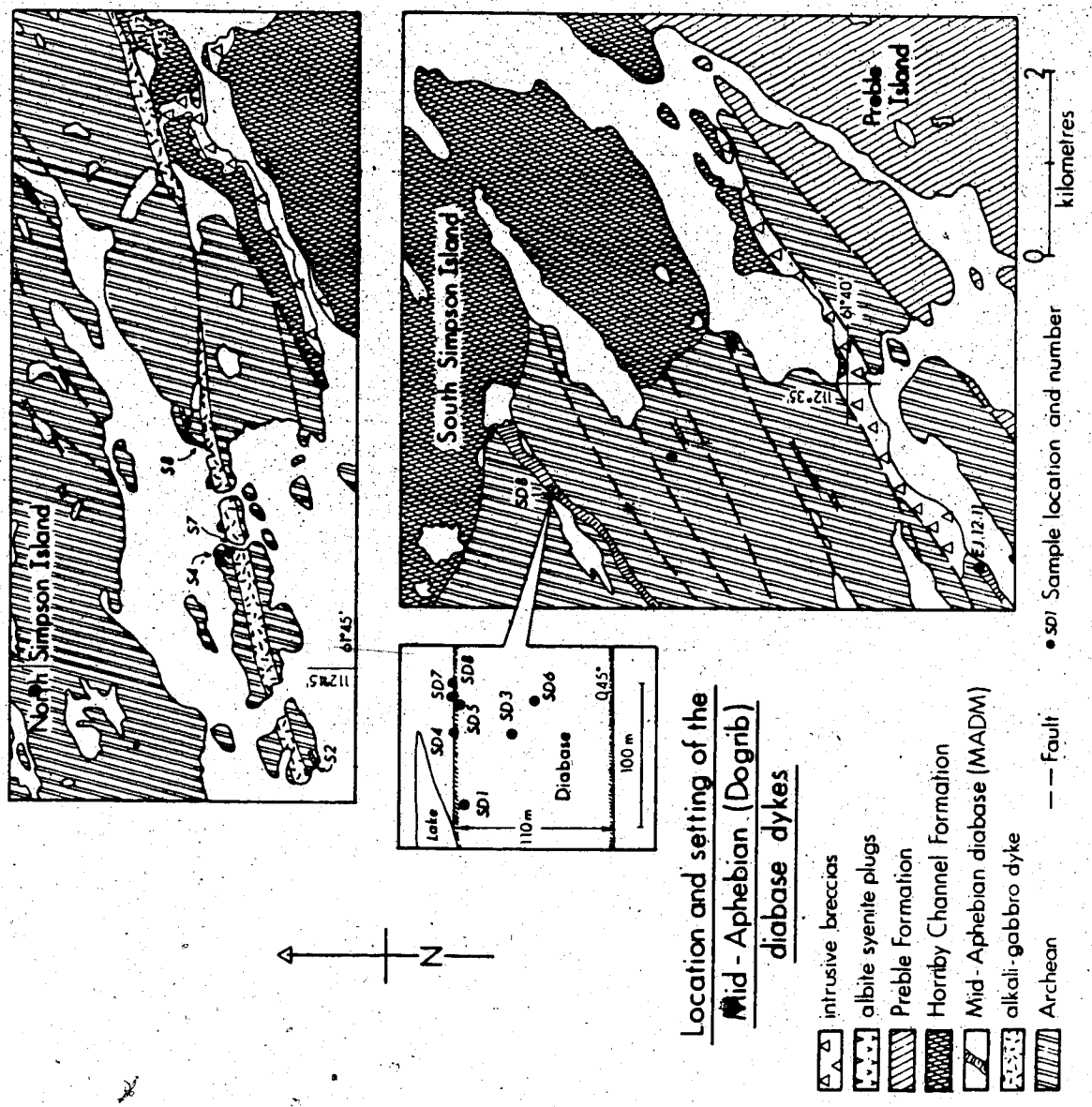

Fig. 3-5. Map of the volcanic-bearing strata of the Union Island Group.
General geological setting based on Hoffman (1977).

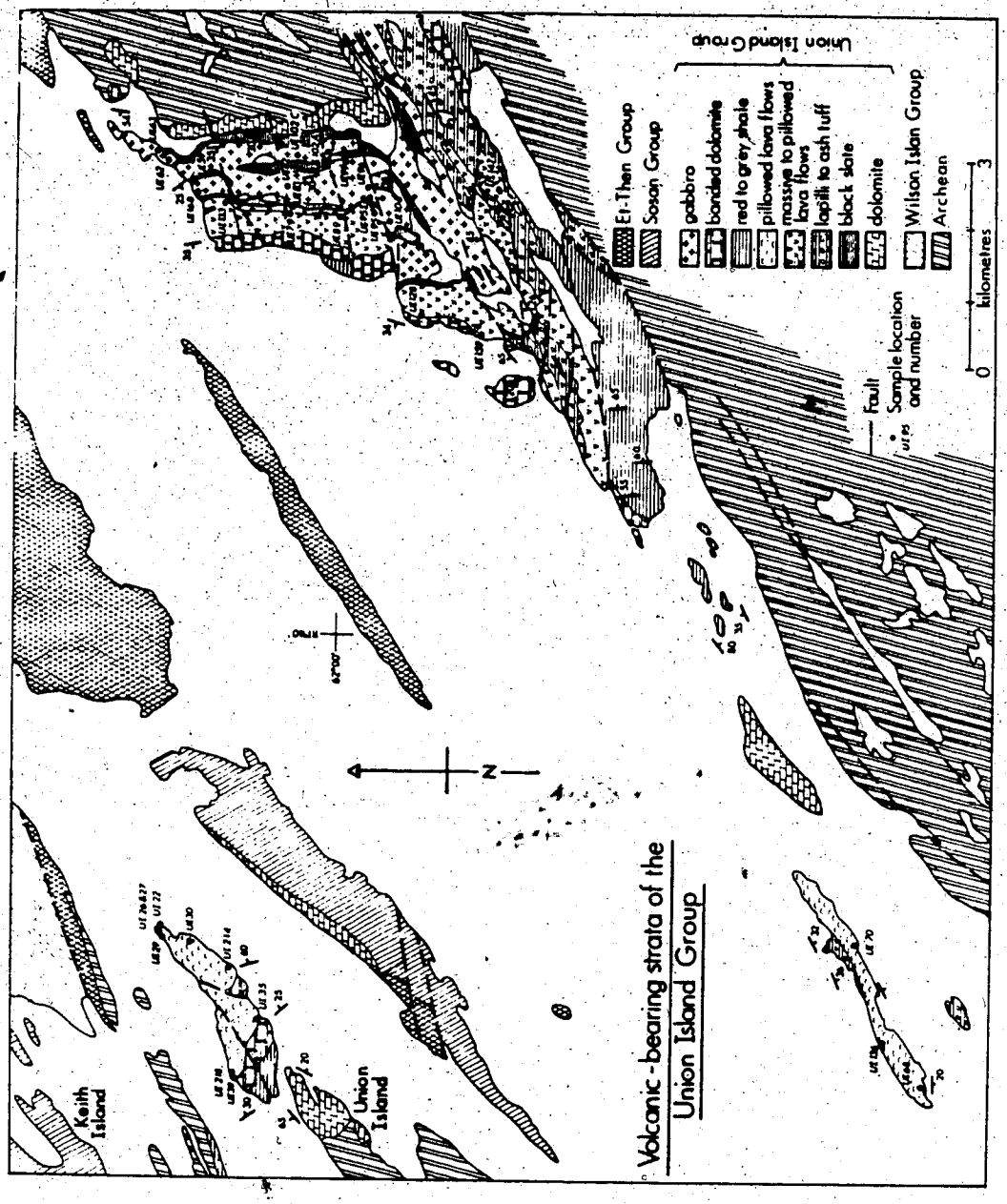

Fig. 3-6. Stratigraphy and facies relations in the Union Island Group (from Hoffman *et al.*, 1977).

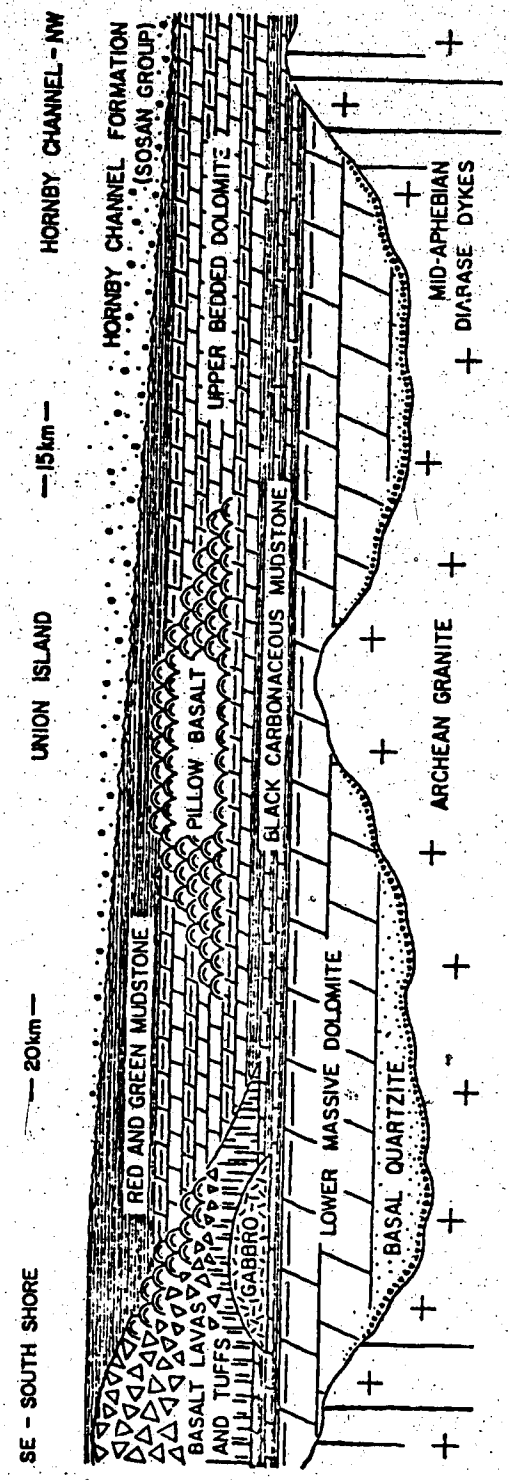

Fig. 3-7. Correlation of the volcanic-bearing strata of the Union Island Group.

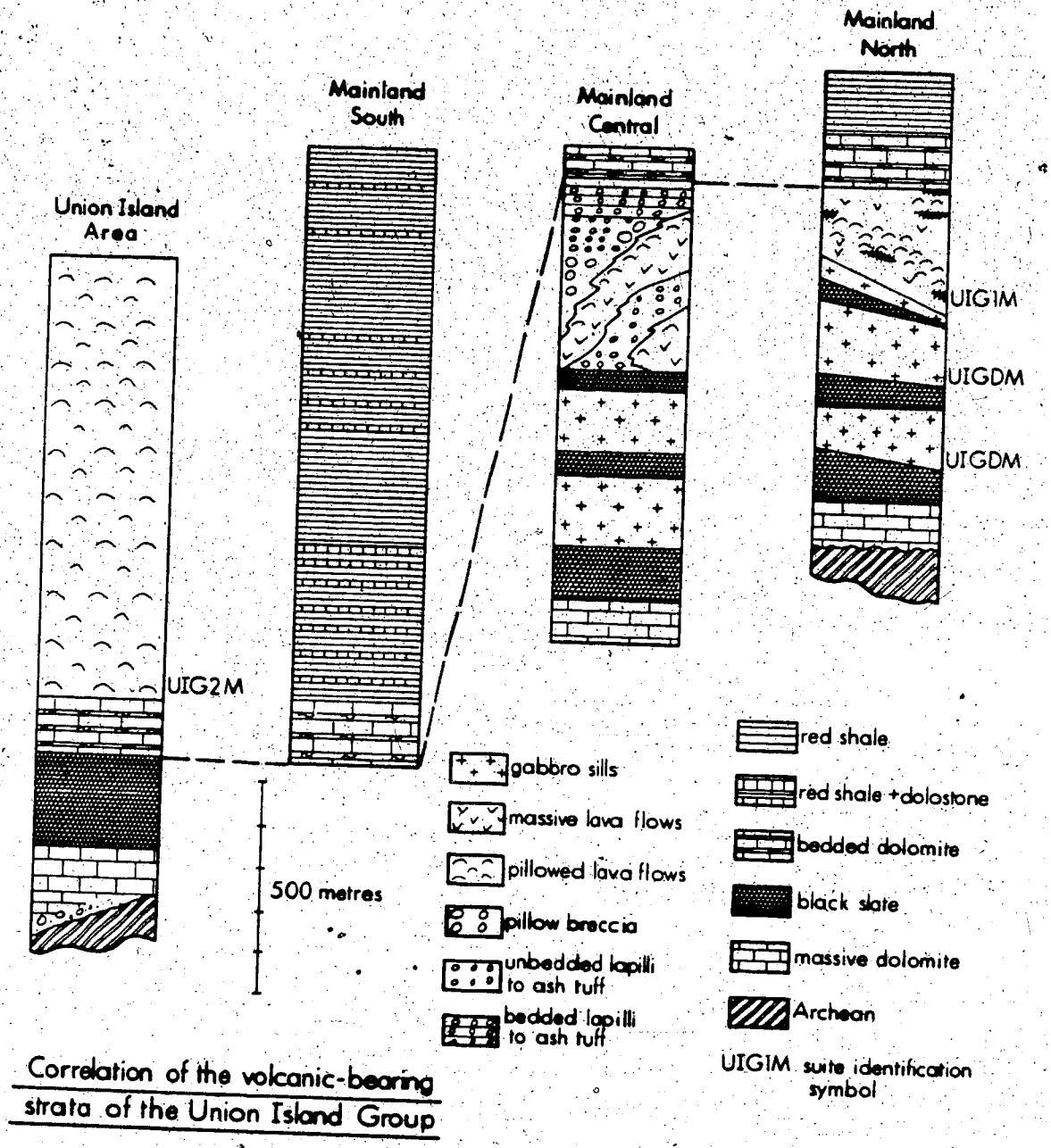

Correlation of the volcanic-bearing strata of the Union Island Group

Fig. 3-8. Correlation of the volcanic-bearing strata of the Sosan and Kahochella Groups.

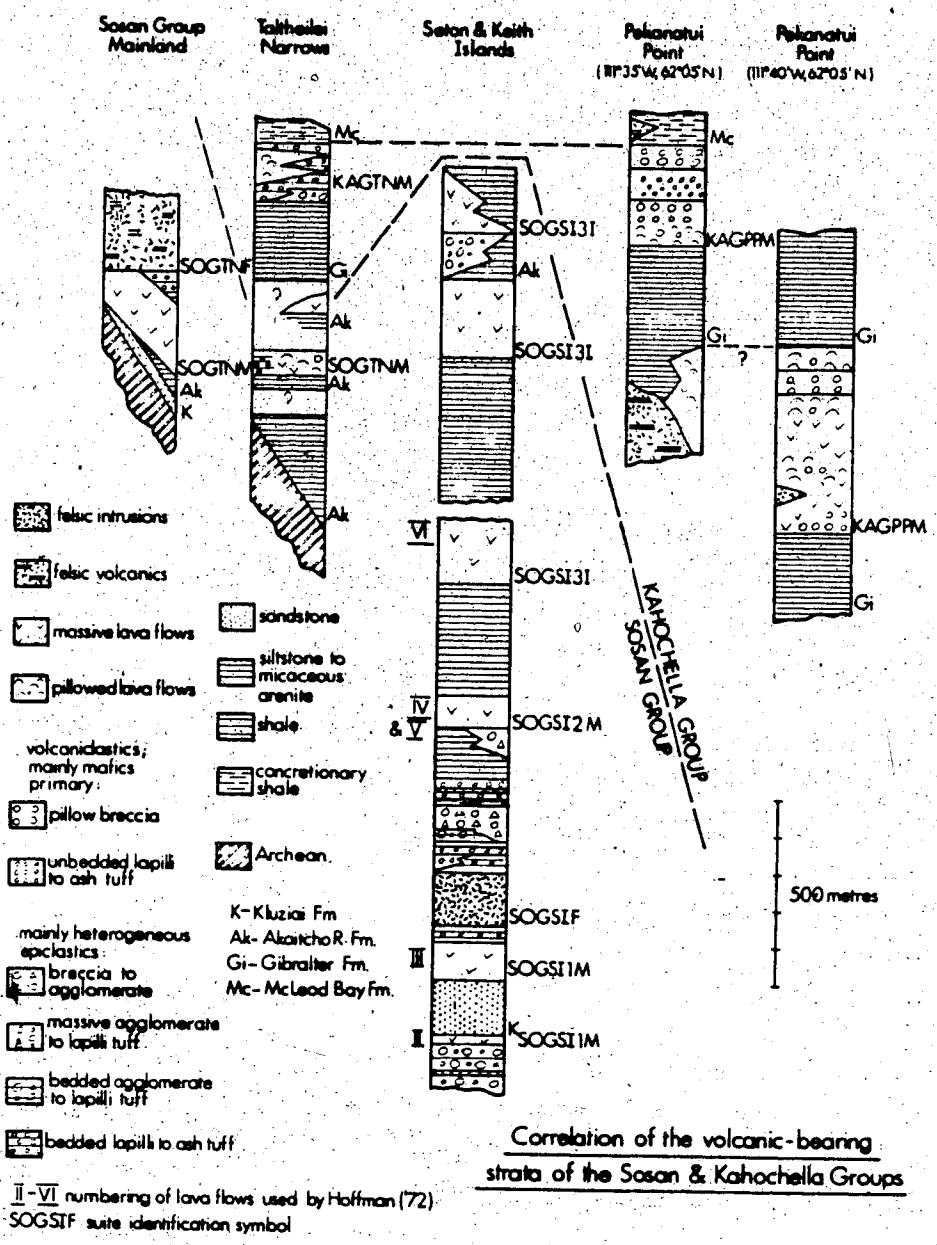

Correlation of the volcanic-bearing strata of the Sosan & Kahochella Groups

Fig. 3-9. Map of the volcanic-bearing strata of the Sosan and Kahochella Groups: Taltheilei Narrows area. Based in part on Hoffman (1977).

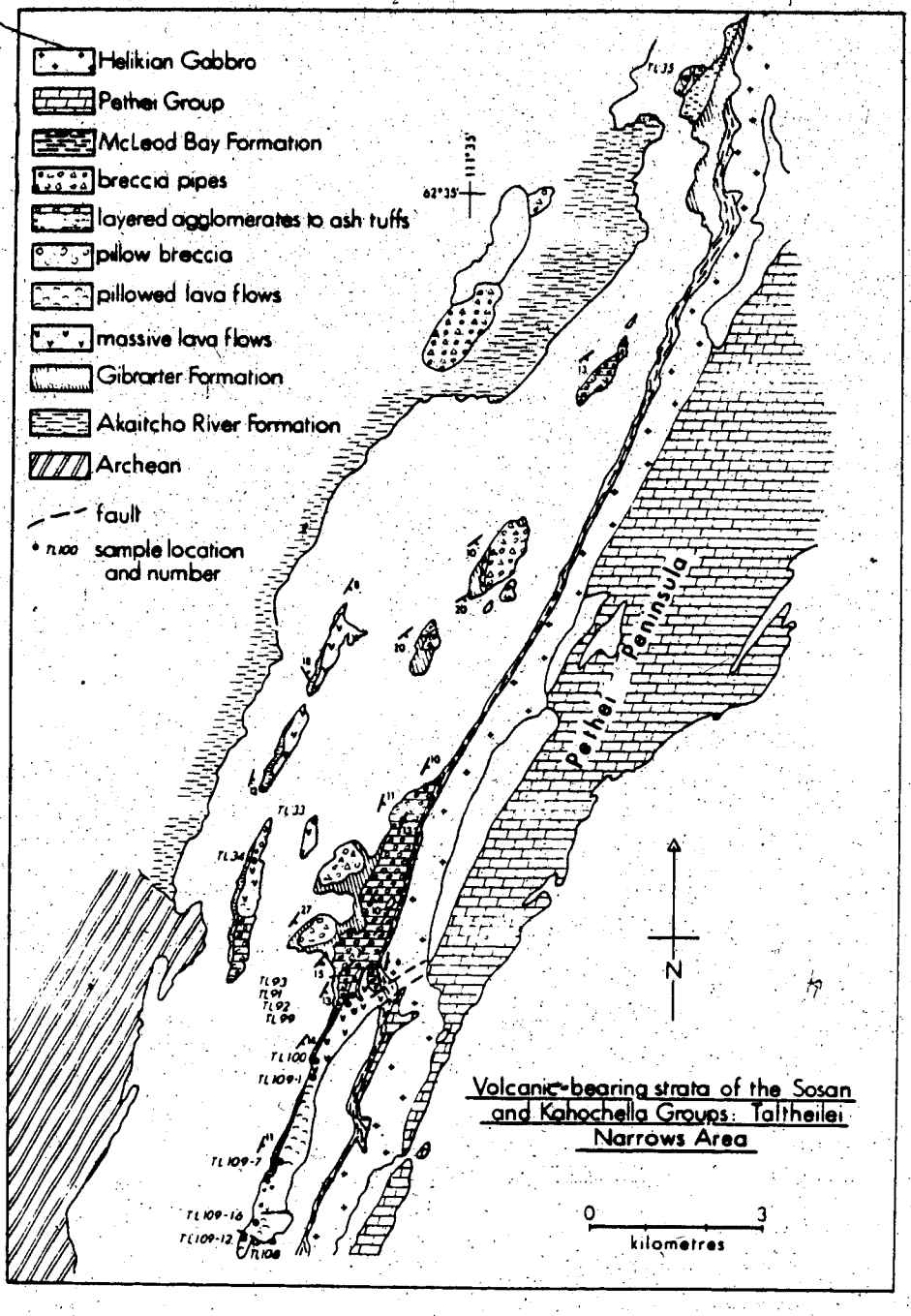

Fig. 3-10. Location and setting of Sosan Group volcanics: Mainland area.
Based in part on Hoffman (1977).

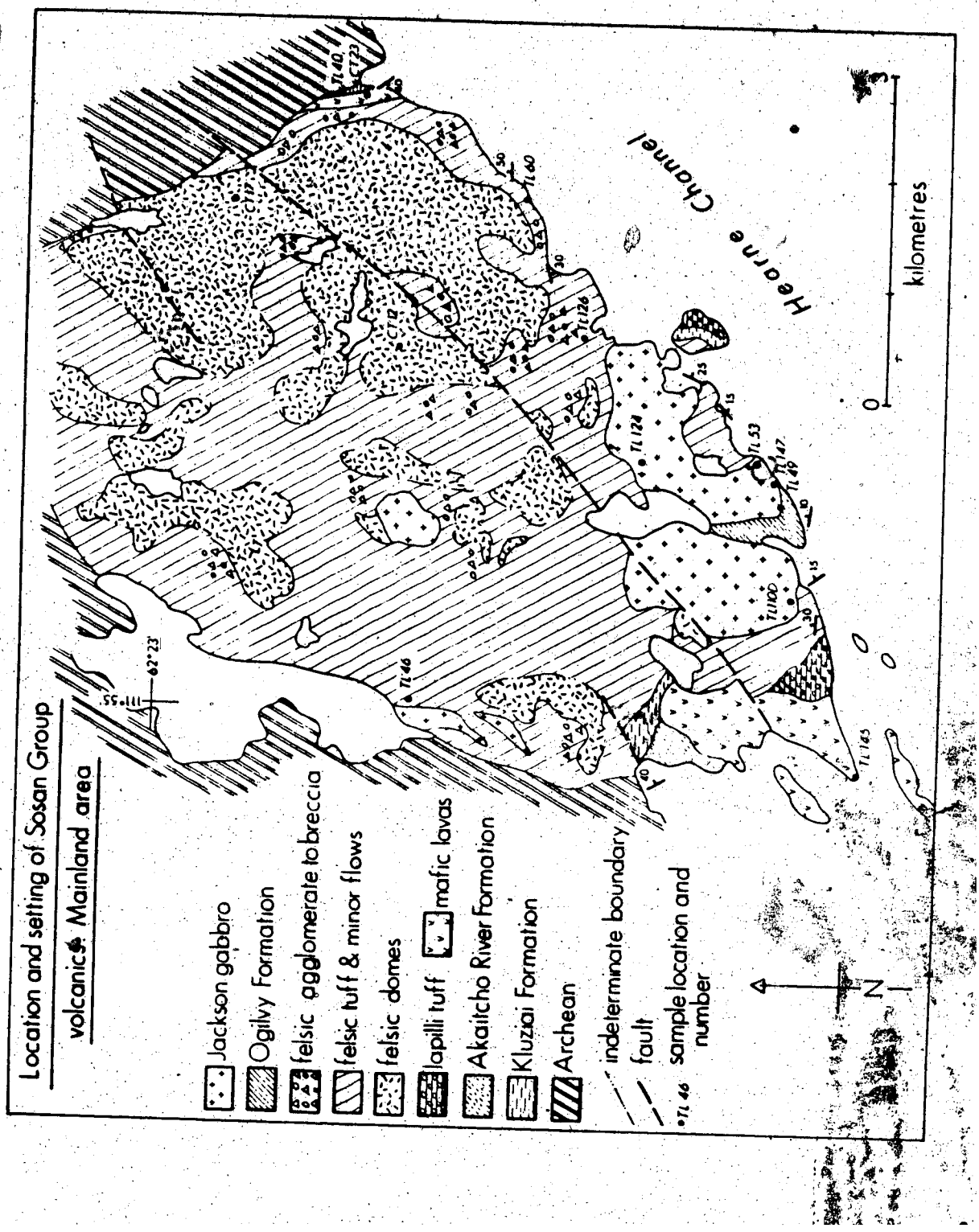

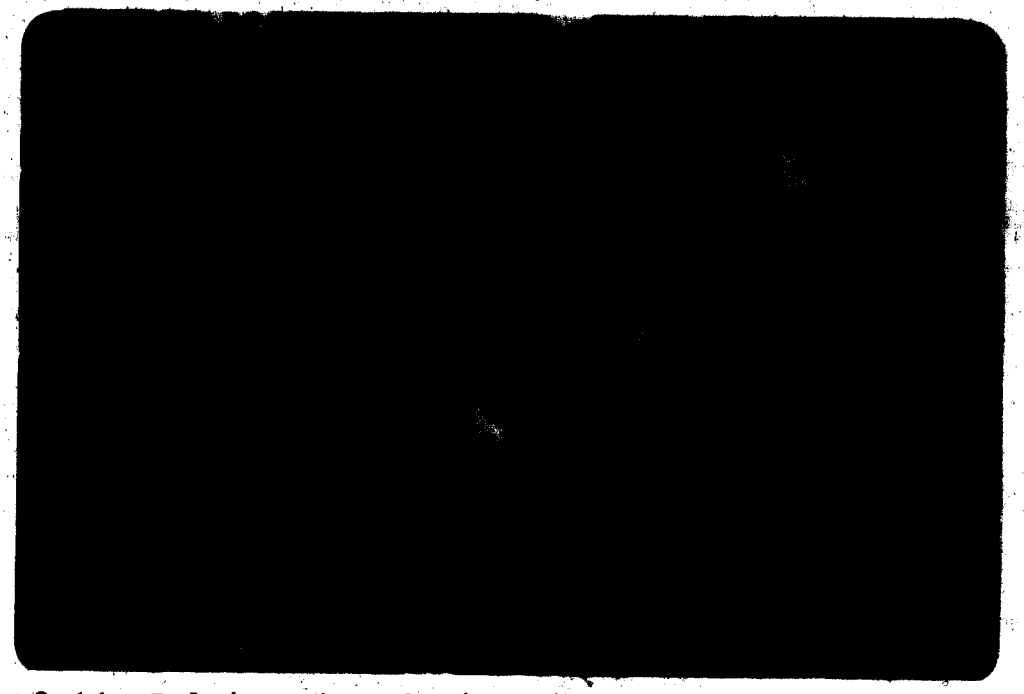

Fig. 3-11. Felsic ash tuff (CT22). Note rounded to subangular pumice and fragmental quartz and feldspar matrix. Field width 0.9 mm. Plane polarized light.

Fig. 3-12. Felsic welded ash tuff (TL118). Discontinuous shards moulded around megacrysts of sericitized K-feldspar. Field width 0.2 mm. Plane polarized light.

Fig. 3-13. Map of the volcanic-bearing strata of the Sosan Group: Seton Island area.
General geological setting based on Hoffman (1977).

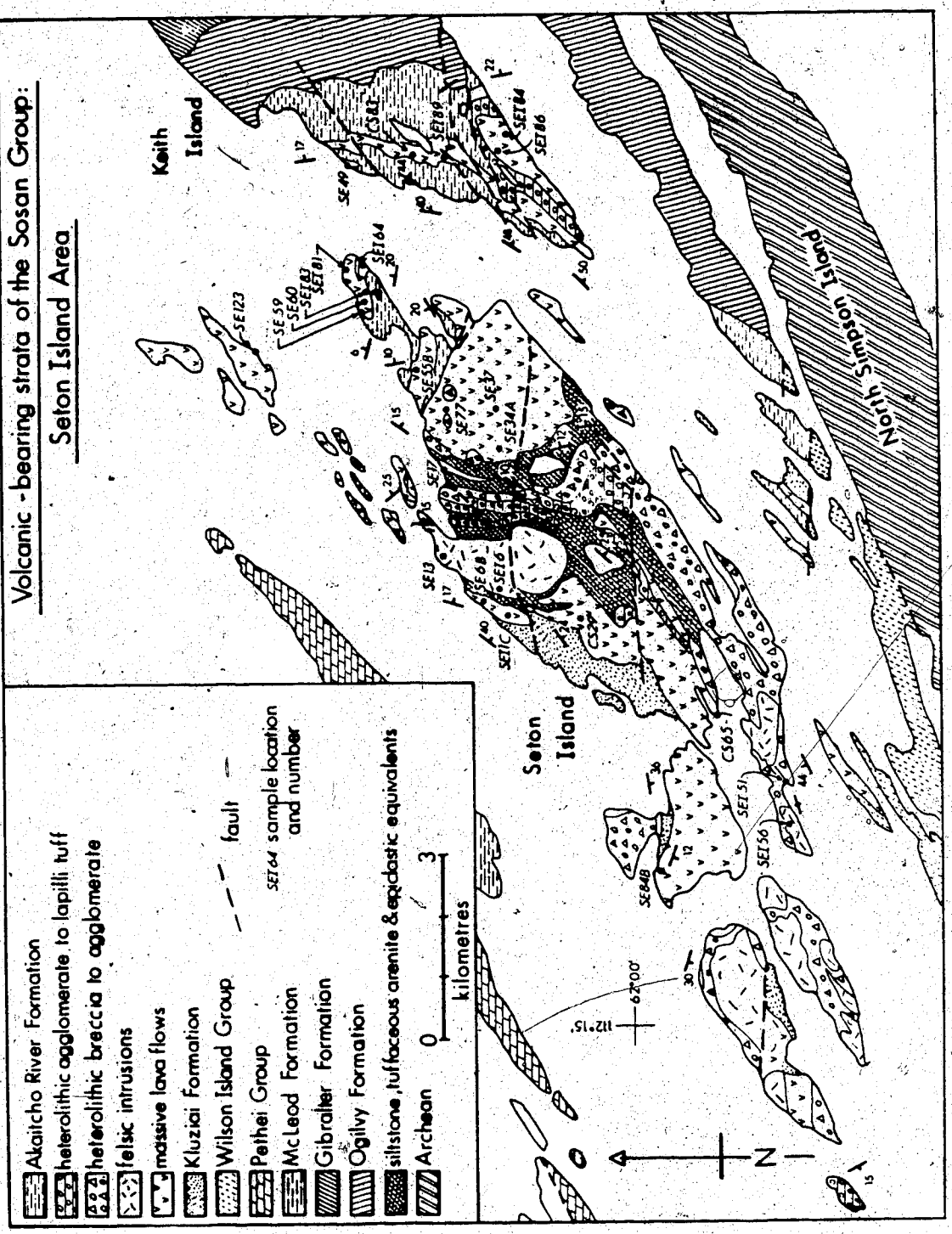

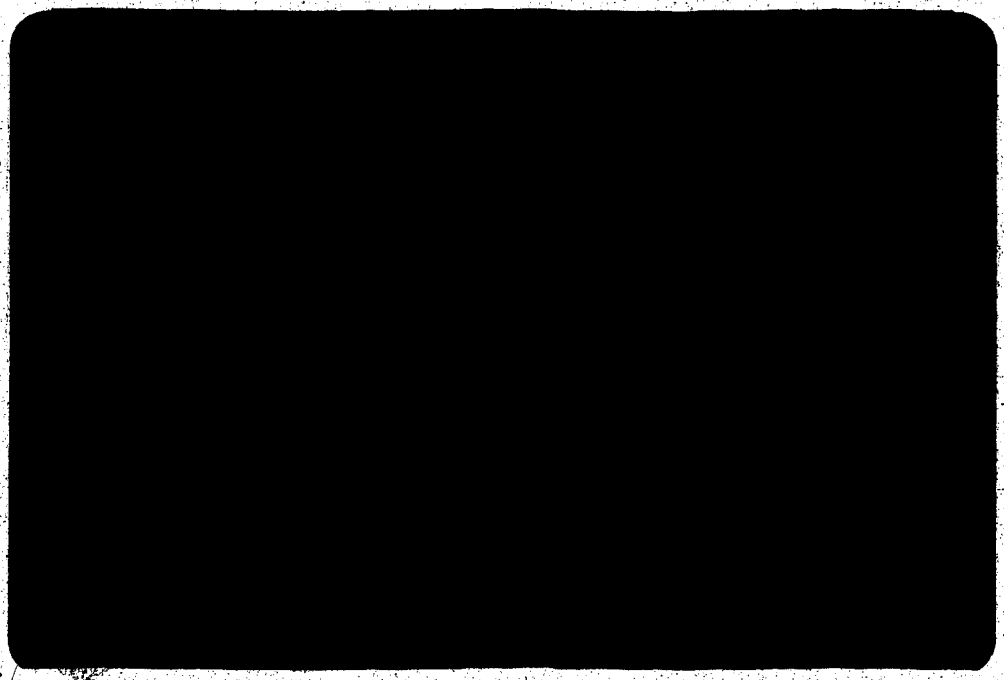

Fig. 3-14. Heterogeneous breccia to agglomerate (SEI40) showing angular to rounded rhyolite blocks.

Fig. 3-15. Heterogeneous ash to lapilli tuff (SE16D). Rounded trachyte to rhyolite ash and plagioclase crystals in matrix of quartz, chlorite and minor carbonate. Field width 0.9mm. Plane polarized light.

COLOURED PICTURES
Images en couleur

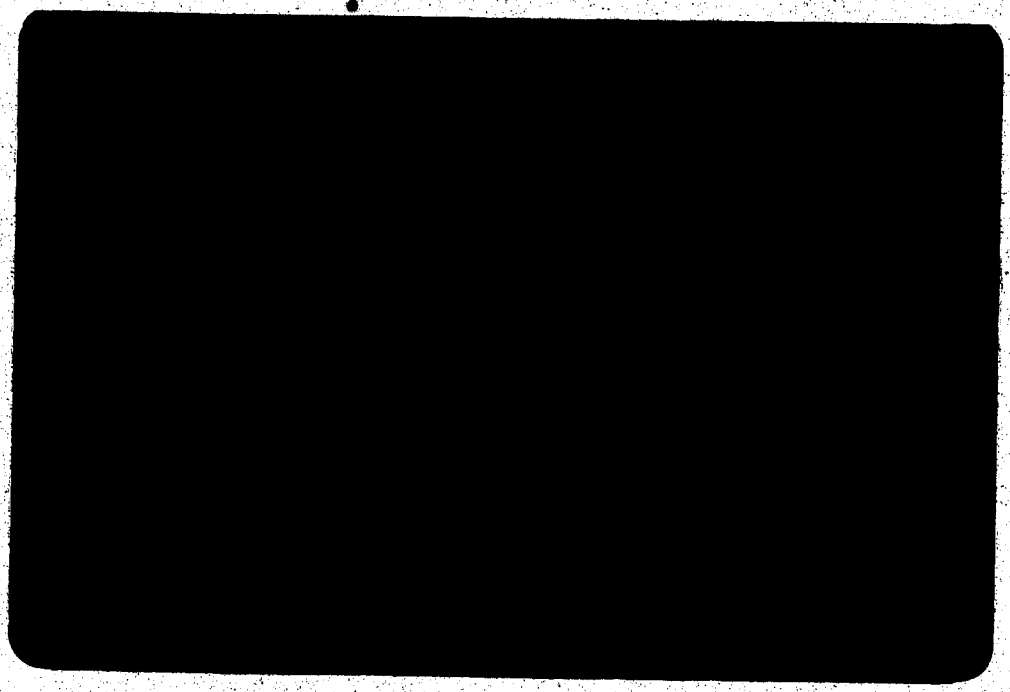

Fig. 3-16. Groundmass of vent breccia (TL39A). Vitreoclastic, amygdaloidal plagioclase porphyritic scoria (now replaced by chlorite and actinolite) and quartz feldspar matrix. Field width 0.9 mm. Plane polarized light.

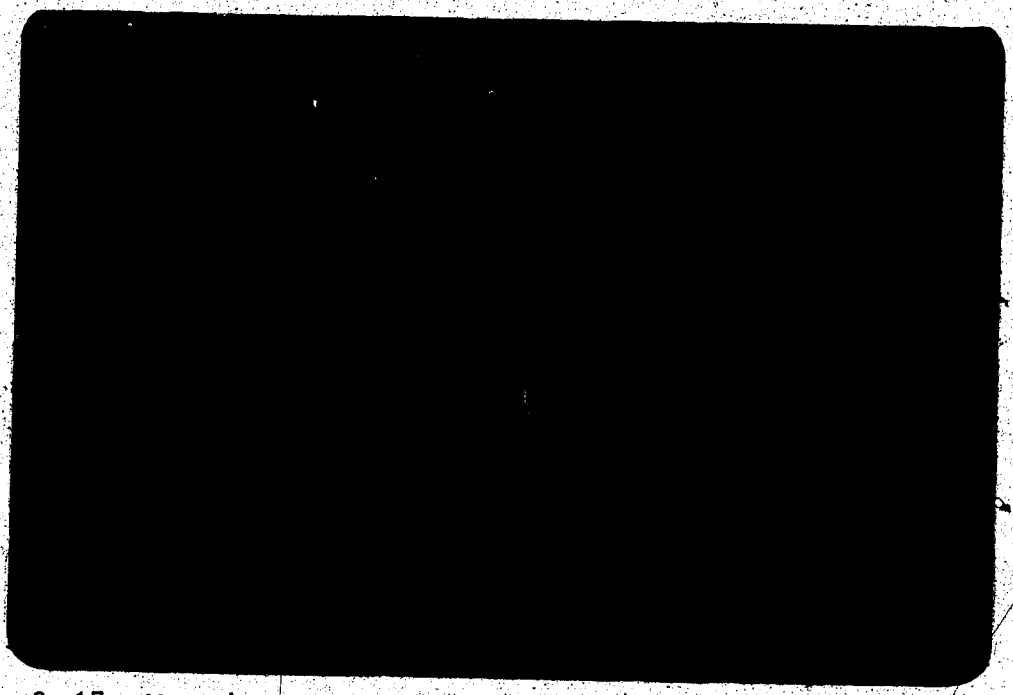

Fig. 3-17. Massive agglomerate (TL10) showing prominent, rounded rhyolite blocks and heterogeneous matrix.

COLOURED PICTURES
Images en couleur

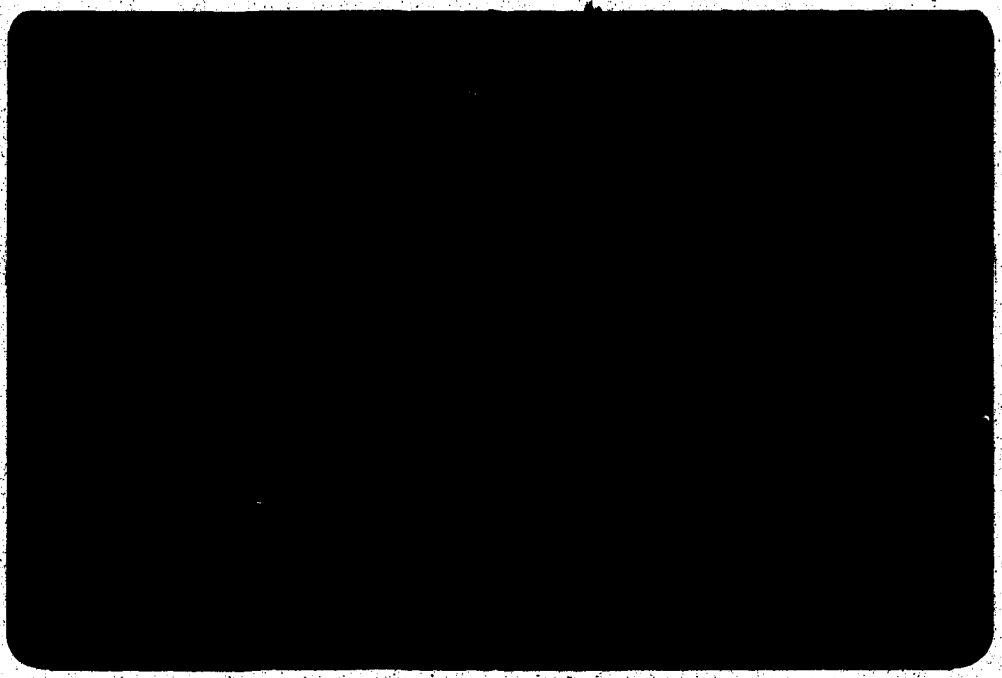

Fig. 3-18. Tabular-bedded ash tuff to agglomerate (TL65) containing rhyolite and mudstone blocks.

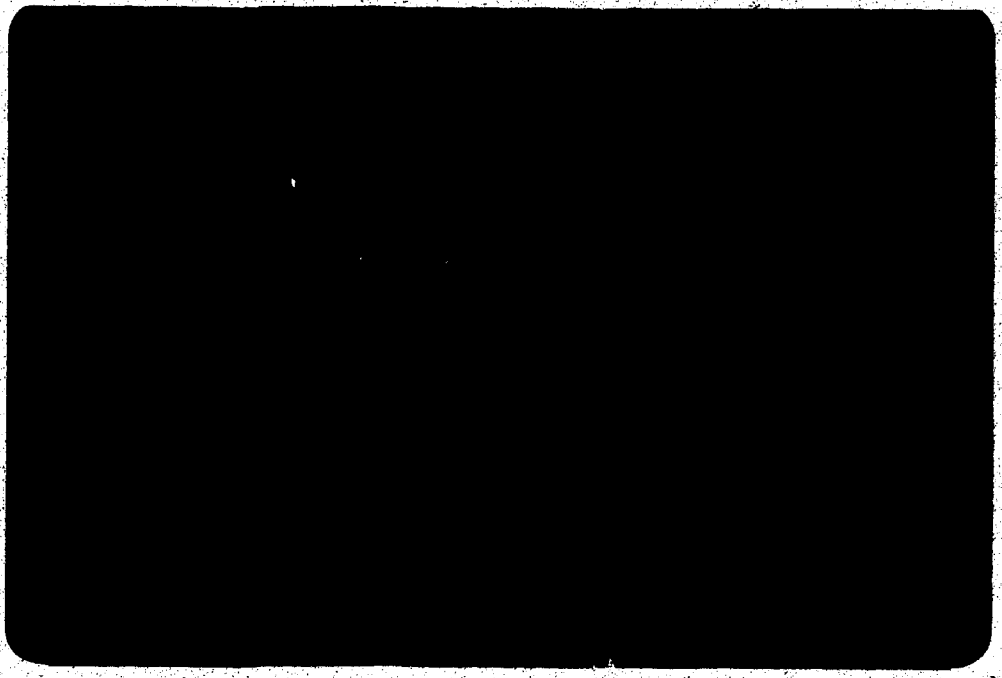

Fig. 3-19. Thin-bedded ash to lapilli tuff (TL29) with 1 to 5 cm thick bed

COLOURED PICTURES
Images en couleur

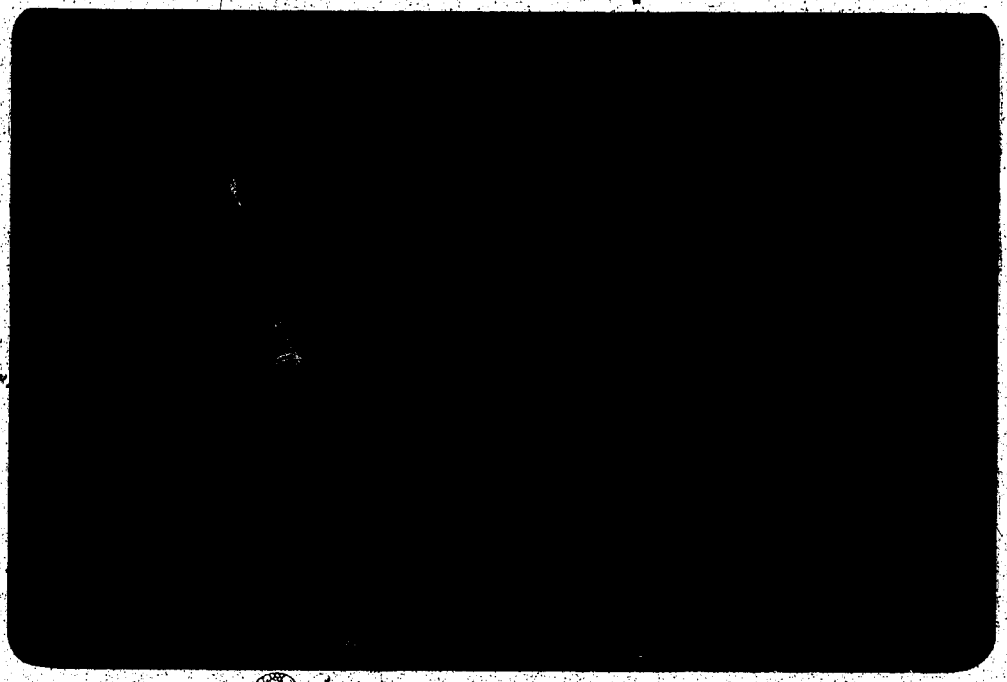

Fig. 3-20. Cross-bedded ash to lapilli tuff (TL75).

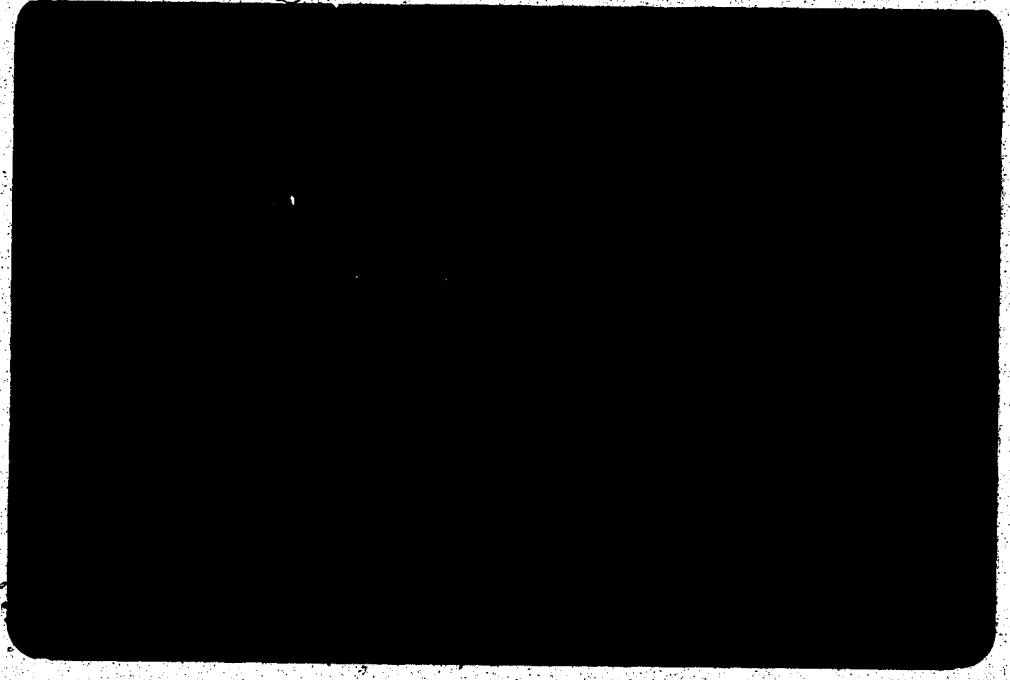

Fig. 3-21 Thin-bedded ash tuff (TL76). Disrupted scoria and felsic (?) matrix was reworked and rounded and cemented with carbonate. Field width 0.9 mm. Plane polarized light.

COLOURED PICTURES
Images en couleur

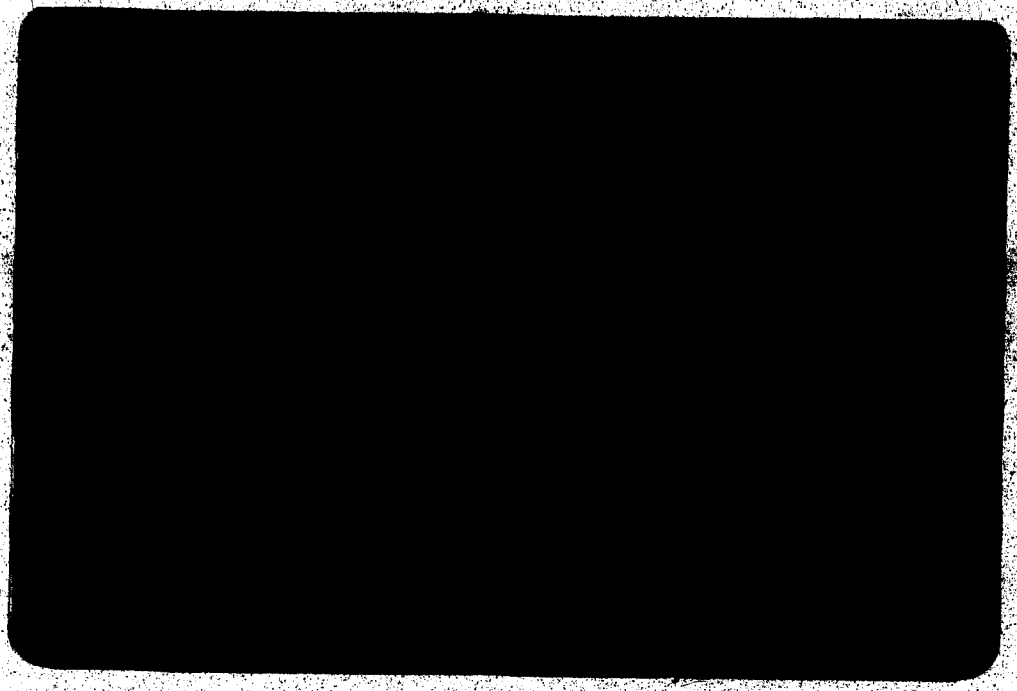

Fig. 3-22. Thin-bedded lapilli tuff (TL77). Reworked amygdaloidal mafic and minor felsic lithic ash and quartz crystal ash. Matrix is silt plus carbonate. Field width 0.9 mm. Plane polarized light.

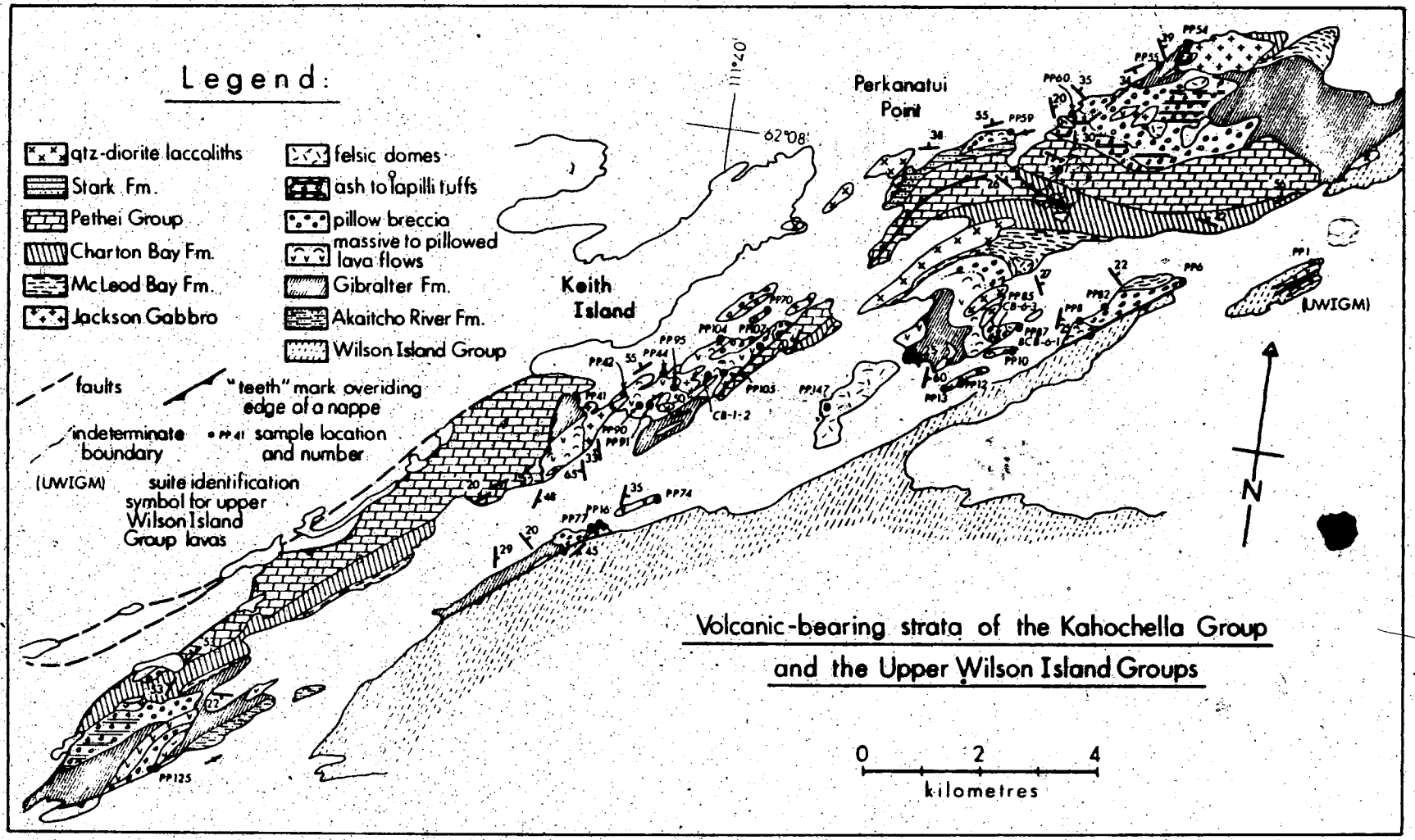

Volcanic-bearing strata of the Kahochella Group and the Upper Wilson Island Groups

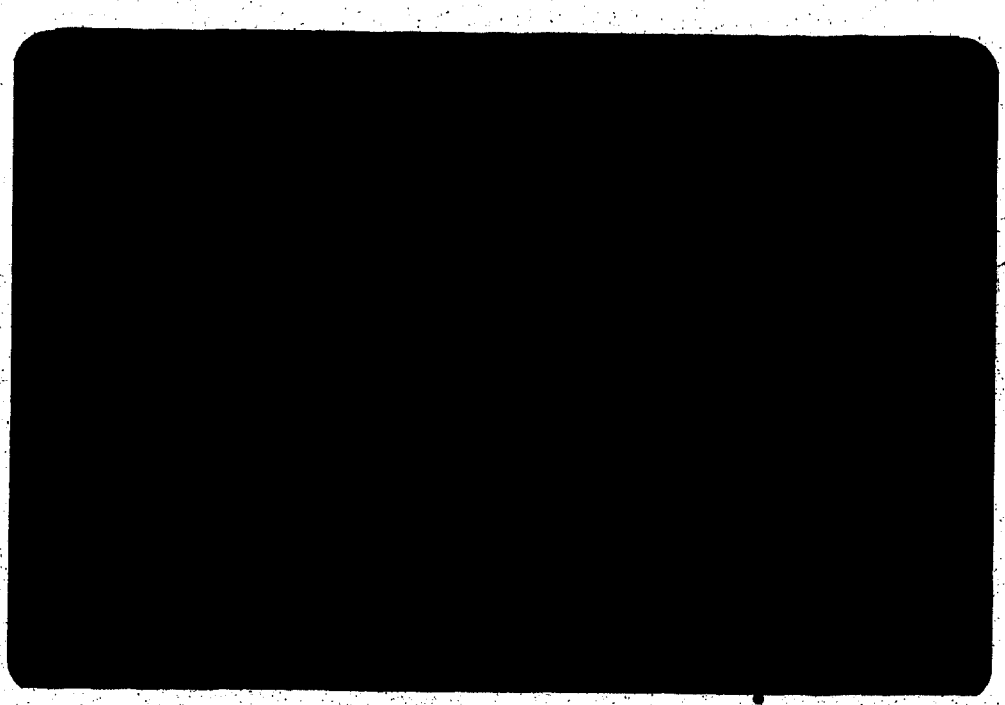

Fig. 3-24. Undeformed vitric ash (PP60C). Shards are chloritized. Matrix is dolomite. Field width 0.9mm. Plane polarized light.

Fig. 3-25. Pillow breccia (P17).

COLOURED PICTURES
Images en couleur

Fig. 3-26. Palinspastic reconstruction of the volcanic-bearing strata of the Sosan and Kahochella Groups.

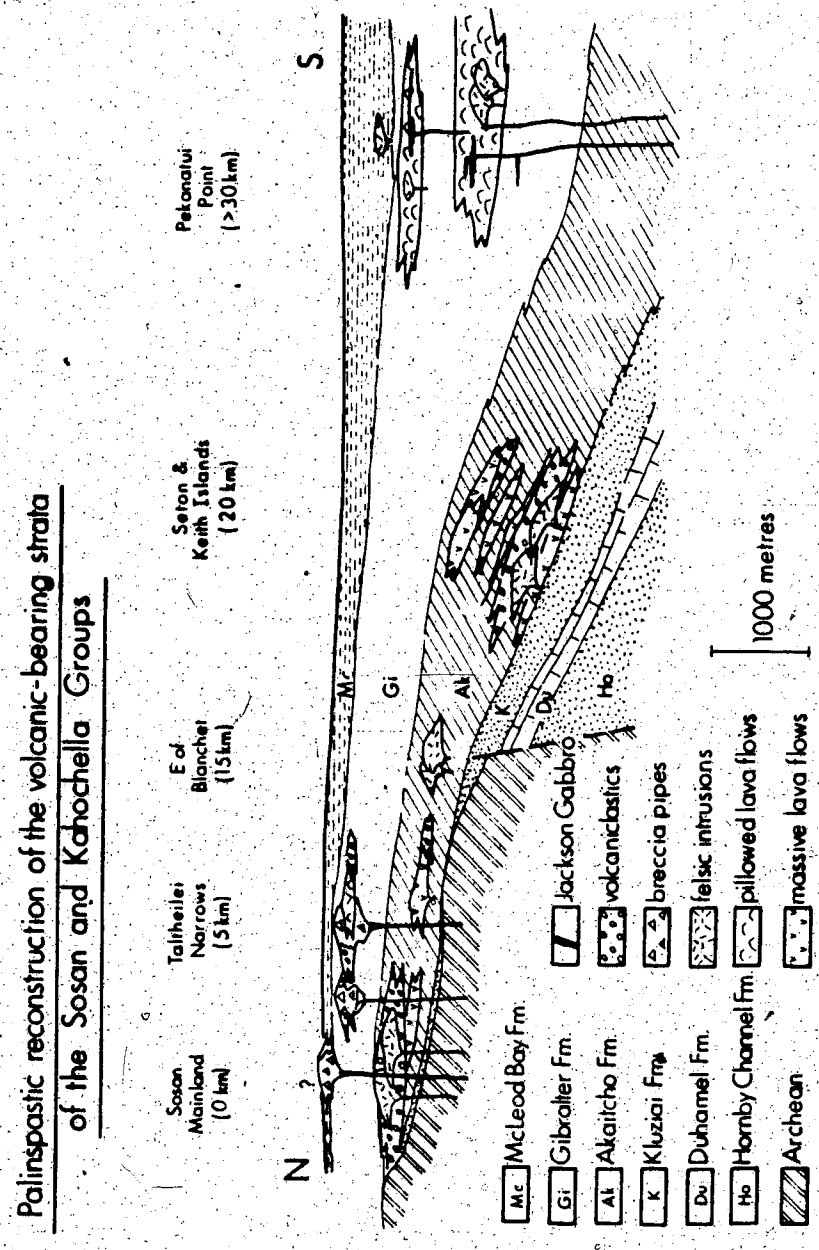

Fig. 3-27. Location and setting of the Pearson Formation. Based on Barnes (1951), Hoffman (1977) and Stockwell *et al.* (1968).

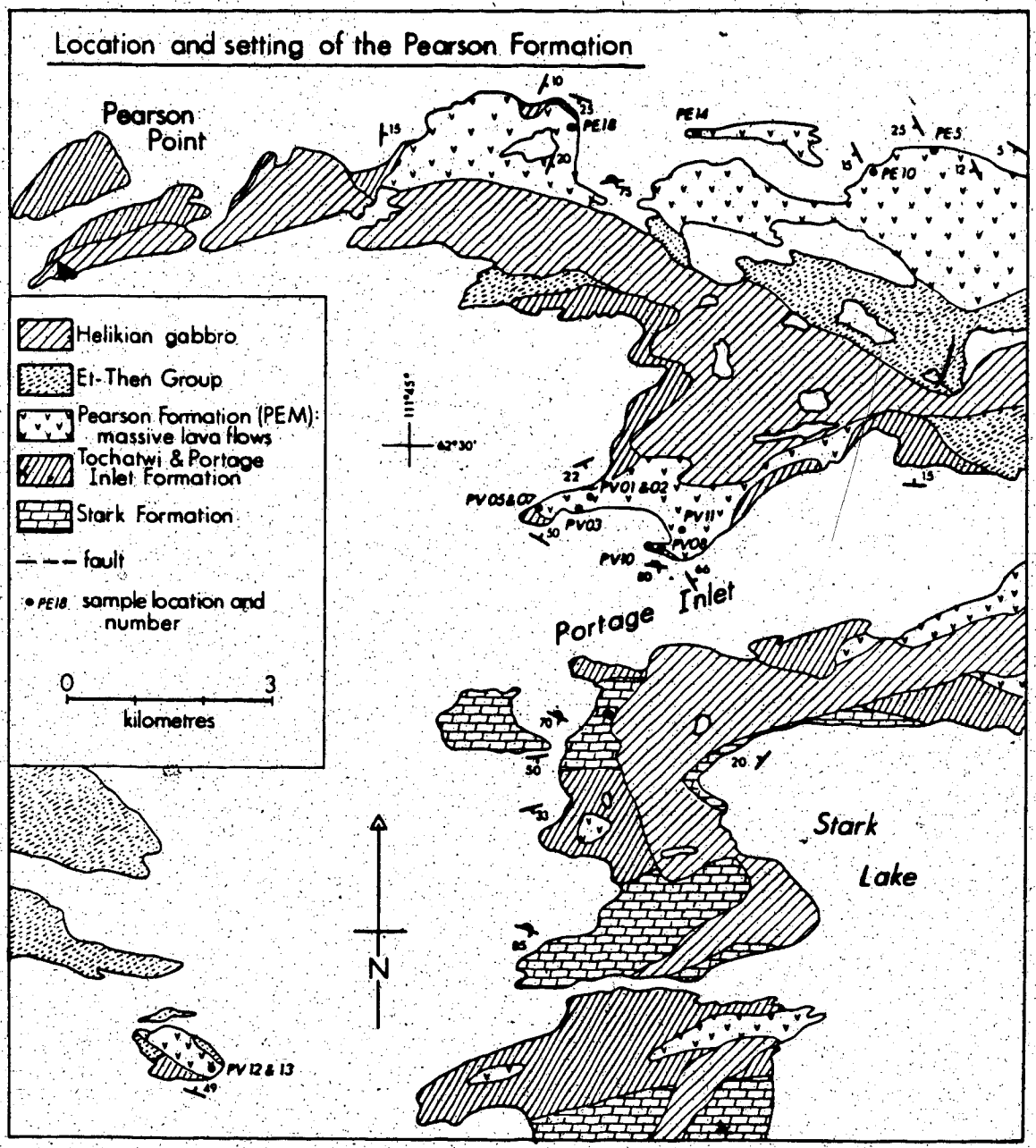

Fig. 3-28. Map of the volcanic-bearing strata of the Et-Then Group.

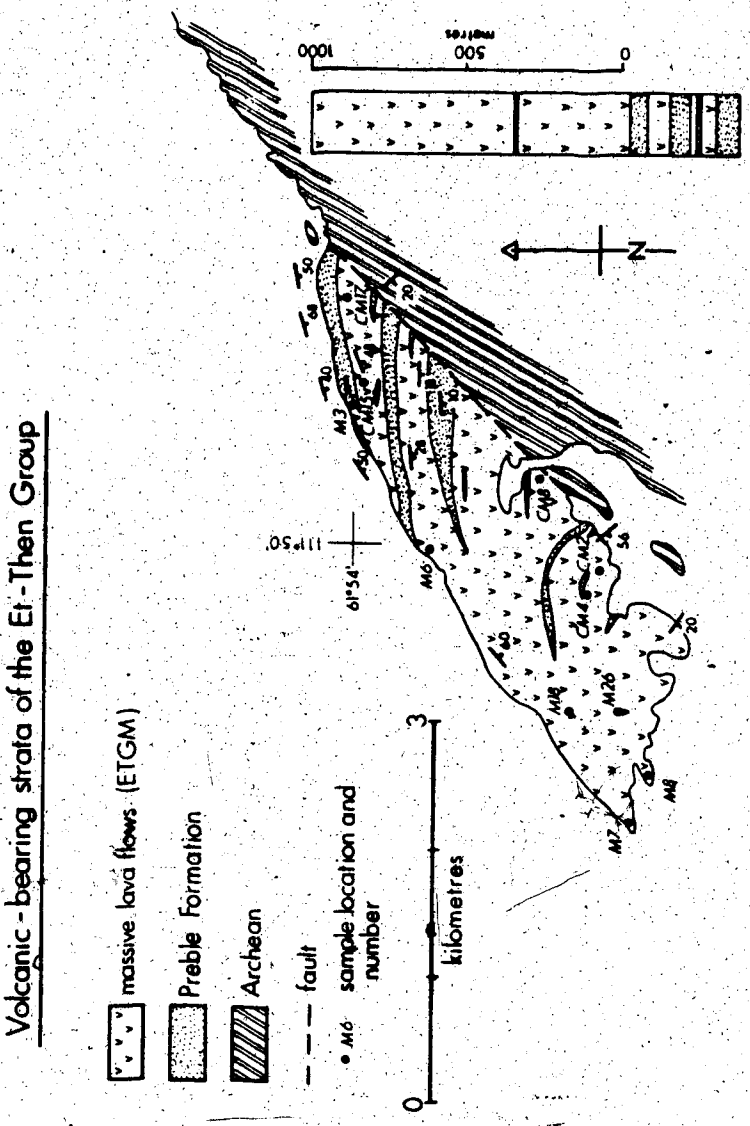

Mafic Unit	Wilson Island Gp. (WIGM)	Mid Apheb. Diabase (MADM)	Union Island Gp. (UIG1M & UIG2M)	Union Island Gp. Diabase (UIGDM)
Olivine		(tr) eu.ps. 6-8 side pre pl; 0.5	(0-10) eu. sub., pre pl; 0.2	(0-5) eu. sub. 6-side, pre pl; 0.5-1
Plag.	(>20-55) recryst. to sub. An_{48}; 0.2-2 Glastophene (tr); 1-2	(40-65) eu. zoned An_{53-57}→An_{47}; 0.5-3 phen. (tr); 5	(35-50) acic. & variol zoned; An_{70-49}; 0.1-0.5 phen. (0-10) eu; 0.5-1	(25-55) eu. zoned An_{68-34}; 0.5-10 phen (tr-5) eu.zoned; 2-10
Cpx.	(80?-40?) recryst.; now hb., bt. & ep.	(25-45) intgr.-oph., lilac-brn.-2.°g, $2V_\gamma 45°$; 0.5-2	(0-45*) sub-oph., intgr. & sk. α yell.-pink γ brn -yell. 2°.r, $2V_\gamma 35°$; 0.5	(25-45) sk., intgr. & oph. α, β pink-brn γ clr-yell. 2° . b-r, $2V_\gamma 30-45°$, $\gamma Az 45-53°$.; 0.5-10
Matrix	(?-10) glass? ps. by cbt.	(<5) q & (0-1) ap.	(0-45) glass? ps. by ch, q, cb	(0-45) glass?, (0-5) q, (tr) granophyre, (0-1) ap.
Opaque	(3-5) Ti-mgt; (<0.1)	(1-5) Ti-mgt-ilm_{ss} & ilm, eu. & sk.	(3-5) Ti-mgt. eu. & sk.; 0.2	(2-5) Ti-mgt-ilm_{ss} & ilm, eu.; 0.2
Texture	blstp./inequ. to intsrt. & oph.	oph.-intgr.	variol.-intsrt.-intgr.	intsrt.-intgr.-oph
Mafic Unit	Sosan Gp. (SOGTNM)	Sosan Gp. (SOGSIIM & SOGSI2M)	Kahochella Gp. (KAGTNM)	Kahochella (Gp. (KAGPPM))
Olivine	(0-10) eu.ps 6-side; 0.2-1.5	(5-10)? eu.ps. & fr. 6-side; 0.2	(0-5) eu.ps. 6-side pre & pos. pl.; 0.5-1	(0-5)? eu. & sub. ps. 6-side, pre pl.; 0.1
Plag.	(10-55) bladed & sk An_{72-60}→An_{34}; 0.2-1 (40-0) acic. phen(tr-10) zoned; resorb; 1-5	(40-55) eu., bladed & sk.; 0.2-0.4 phen(tr-10) eu. & resorb.; 0.5-5	(50-55) eu. zoned An_{71-60}→An_{50}; 0.5-1 phen(tr) sub. resorb.; 2-8	(5-40) bladed & sk. bent; 0.2-1 (40-15) acic. in matrix; <0.2
Cpx.	(tr-25*) intgr. 2.°b, $\gamma Az 43°$. & anh.ps., pre & post pl. ?; 0.2	(0-40*) intgr. pink phen (0-5) sub. pale brn. 2° .yell, $2V_\gamma 40°$, $\gamma Az 50°$; 2		(0-30*) intgr. brn., 2.°b $\gamma Az 45°$ (0-5) sub oph., 6-8 side; 0.2
Matrix	(25-50) glass? ps. by ch, (tr) q & ap.	(30-45) glass, minor q, (0-5) kf.; 0.2	(25-35) glass/cpx? ps. by ch.	(45-15) glass? ps. by ch., plag, q, kf
Opaque	(5-10) Ti-mgt.; 0.1-0.2	(5-10) Ti-mgt.; 0.2, py	(10) Ti-mgt.; 0.1	(5) Ti-mgt & ilm, sk.; pl py; 0.1
Texture	intsrt.-intgr.	intsrt.-pilotax.	intsrt.-pilotax.	variol.-intsrt.-intgr.

Mafic Unit	Jackson Gabbro (JAGTNM)	Pearson Fm? (PEM)	Et-then Gp. (ETGM)
Olivine	(0-5) eu. ps. 6 side; 0.2		(tr)? sub. ps.; 0.1
Plag.	(20-70) eu. zoned An 70-56 → An_{40}; 1-4 (30-0) bladed & ski.; 0.2-1	(25-55) eu. to sk., bimodal An_{61-56}→An_{47-32}; 0.2-1 (20-0) acic.; <0.2	(45-60) eu. to bladed & sk. zoned. An_{71-56}; 0.1-1 phen (<5) eu.; 2-5
Cpx.	(25-40*) intgr. non-pleo. 2.°g, $2V_{\gamma}50°$, $\gamma \wedge z39°$	(50-30*) sub oph. to intgr. non-pleo. 2.°g, $\gamma \wedge z39°$.; 2-0.05	(45-20*) intgr. pale brn. to non-pleo. 2.°bl-or., $\gamma \wedge z47-40°$.; 0.05-0.2
Matrix	(20-50) glass? ps. by ch. or myrmekite & (1) ap.	(40-10) glass? ps. by ch.	(<5-20) glass? ps. by ch., q, minor plag.
Opague	(5) Ti-mgt & ilm. eu. & sk.; <0.2	(5-10) Ti-mgt-ilm ss eu. & anh.; <0.2. py	(5-10) Ti-mgt-ilm. eu. & sk.; 0.01-0.5
Texture	oph.-intgr.-intsrt.	hyalopil.-intsrt.-intgr.	intgr-intsrt.
Intermediate Unit	Wilson Island Gp. (WIGM)	Sosan Gp. (SOGSI3I)	Sosan Gp. trachyte (SOGSI3I)
Olivine	-	-	-
Plag.	(>55) recryst. ; 0.2-0.5 blastophens. (tr-5); recryst. & granul.; 0.5-1.5	(45-80) bladed & sk.; 0.2 phen (10-0) eu.; 1-4	(40-75) eu. bladed; 0.2-0.5
Cpx.	(<30)? recryst. now bi ± hb.	(20-0)? ps., post pl.; 0.2-2	(0-5) anh. ps., post pl.
Matrix	(5) q & (tr) kf.	(35-20) fels + q + ap. to glass? (ch + q). (5-20) may be kf.	(10-50) fels + q + ap. (10-15) may be kf.
Opaque	(tr-5) now sph.	(tr-5) mgt.	(2-5) ti-mgt.
Texture	sparcely blastoporph.	intgr.-pilotax.	inequ.

Felsic Unit	Wilson Island Gp. (WIGF)	Sosan Gp. (SOGSIF)	Sosan Gp. (SOGTNF)	Kahochella Gp. (KAGPPF)
Phens.	ab (2-7) eu. & resorb., granul.; 0.5-5 or (2-5) eu & rounded, granul.; 0.5-2 q (tr) sub embayed; 0.5 hb (1-7)? now hbl, bi & ep clusters	ab (tr-10) eu.; 0.2-3 q (5-10) anh & corroded; 1	or (tr-10) eu. Carlsbad twin; 1 q (tr) anh. & corroded; 0.2-2 pl? (tr) q & cbt repl.; 0.5	ab (tr-5) eu.; 0.5-1 or (0-5) eu. sub., $2V_{\alpha}70^{\circ}$; <1 q (2-5) eu. & frac., embayed; 2-3 musc (tr) eu.; 1
Matrix	(50-70) ab, kf. (or seric.), (20-30) q.	(55-75) ab, kf, (15-25)q, (tr) granophyre	(70-80) kf, (or seric.), minor ab., (10-20) q	(55-80) kf. (or seric), minor ab, (20-30) q
Opaque	(1-5) fine mgt., now sph. & py.	(2-5) fine mgt., (hm & lc.)	(2-10) fine to eu. mgt.	(tr) hm.
Texture	blstp., amyg, spherul.	porph., inequ.	porph. flowbanded, amyg., spherul.	porph.
Unit				
Olivine				
Plag.				
Cpx.				
Matrix				
Opaque				
Texture				

	Et-then Gp.	Pearson Fm.	Jackson Gabb.	Kaho Taltheilei	Sosan Taltheilei	Kaho Pekan.	Sosan Seton I.	UIGp. Dtab	UIGp. Flows	Mid Apheb.
Ol.	ch		ch±q cb±ch	±ch±q±dl ch+ac ch+ep dl+ct	dl s+ch	ch±q±dl	ch±mt q+hm±ch	ch±ac±ep ch±dl	ch+ac+ep ch±ep ch±q ac±q ch+cb	ch+ac+ep ch+ac+mt ch+ac±hb+bi ct+dl±ch±mt
Cpx.	ch+ep ct	ch+sph±hb ch+sph±ac ch±q±cb ch+ep+pu ch+ct+mt	ch+ac+ep ch+ac+cz ch±cb hb+bi	ch+ep ch+cz	ch±bi ch±cz±cb±q	ch±q±ep dl±hm	ep±ch dl±ep ch±dl±q	ac±bi hb+ac	ch±cb±sph	ch+ac+ep ch+ep±hb ch+ac+ep±cb
Pl.	ab±ch±s±ep	ab+ch±cz ab+s±cz±pu ab+ch±s±ep ±sph	ab+s±ch ab+s±ch kf	ab±cz±ch±cb s±cz s+ch±ep	[illegible] cz	ab+s±ch±q ab+s±ch±dl ab+ep+ch	ab+s±dl s+q±ch s+ep±ch ep+ch±dl s+kf	ab s+ct s+ch+ep s+ch±cz±q	ab±s±ch±ct ab+ac+ch±ep ab+s+cz kf	ab±s±ch±cz
Matrix	ch±q±ep ch+q+bi	ch±pu±sp±q ch+sph+ct	ch±dl ch±ac±bi hb±bi	ch±ep±dl ch±dl±bi	ch±ep/cz ±cb±q ch±bi	ch+q±ep ch+q+dl dl±ct±fdl	ac+ch±ep±q ch±dl±fdl	ch+ac+ep ±q±s ch±hb±bi	ch±ep ch±q±ct+dl py	ch+ac ch+ep hb+bi
Amyg.	±ch±q±ct ab+ch+q±ep	ch±pu±sph±q ch+ct		ch±ac dl±ch ct±ch±q	ch±dl dl±ep	ch+q±dl ch±s+hm q+s+hm dl+ct	ch±dl±ep ch±q±dl dl	q+ch±cb	py+q+ch+cb ch+ep	ch+ac
Fe-Ti oxides	hm	lc	lc hm	sph	lc	sph/lc	sph	sph/lc		sph

Table 4-3. Summary of metamorphic mineralogy. Mineral abbreviations are the same as for Table 4-2. See also Table 4-4 for optical data for amphiboles (1, 2 and 3), chlorites (A, B, C and D) and pumpellyite. Dashed lines indicate minor amounts of each mineral.

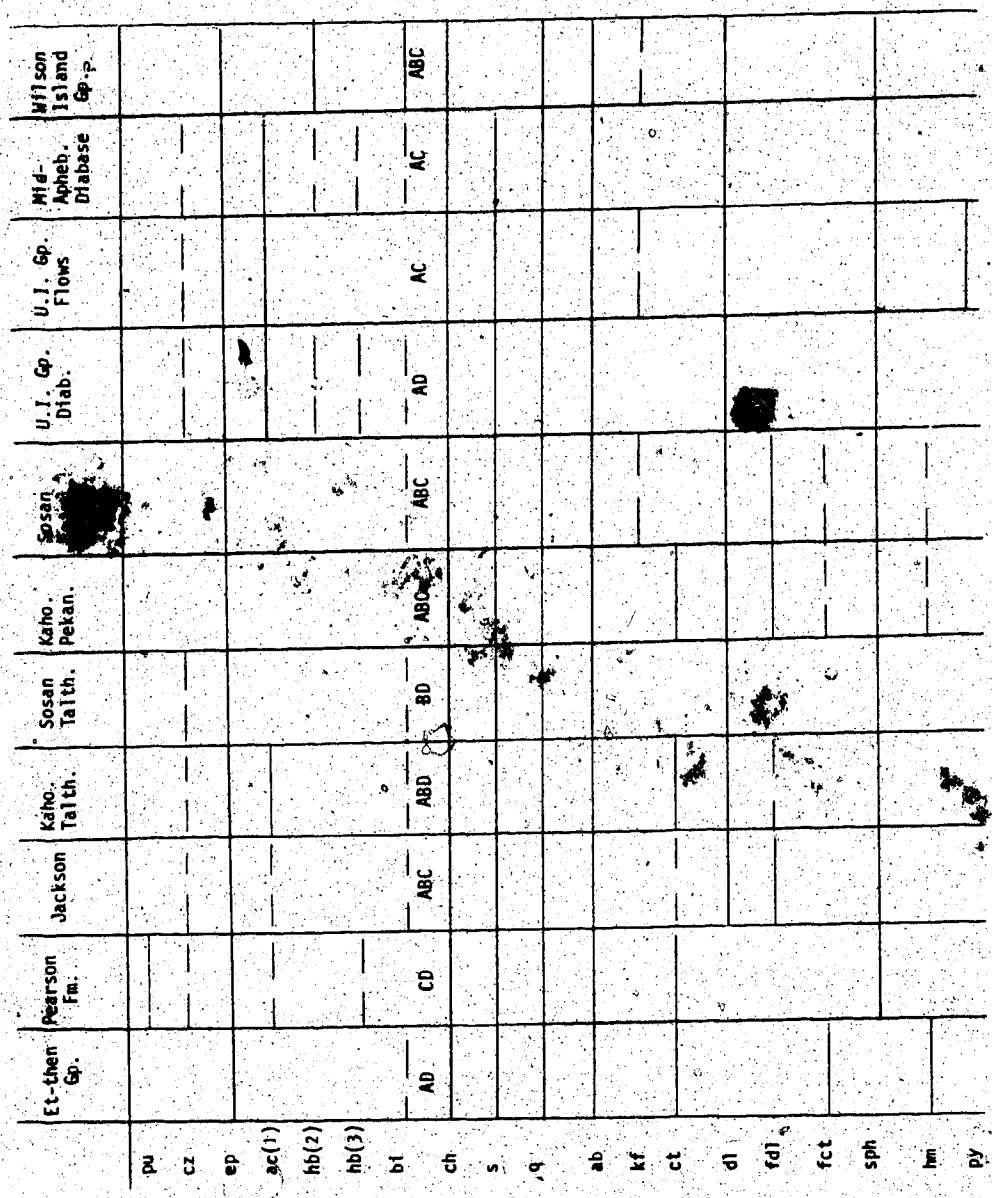

Table 4-4. Optical data for the metamorphic minerals of Table 4-3.

Amphiboles

	1	2	3
α	white	Straw yellow	cream yellow
β	yellow green	olive green	olive brown
γ	pale blue green	blue green	olive brown
δ	0.015-0.023	0.023-0.035	0.[illegible]-0.087
$\gamma \wedge Z°$	15-22	18	

Chlorites

	A	B	C	D
α	white	white	green	white
γ	green	blue green	white	pale green
sign	-	-	+	-
δ	∿.002	∿.002	∿.002	0.004-0.010
anomalous colour	blue	purple	brown	none

Pumpellyite

α	yellow
β	white
γ	blue green
δ	0.023
anomalous colour	blue in 1°

Table 4-5. Petrographic variation within the lava sequence of Seton Island.

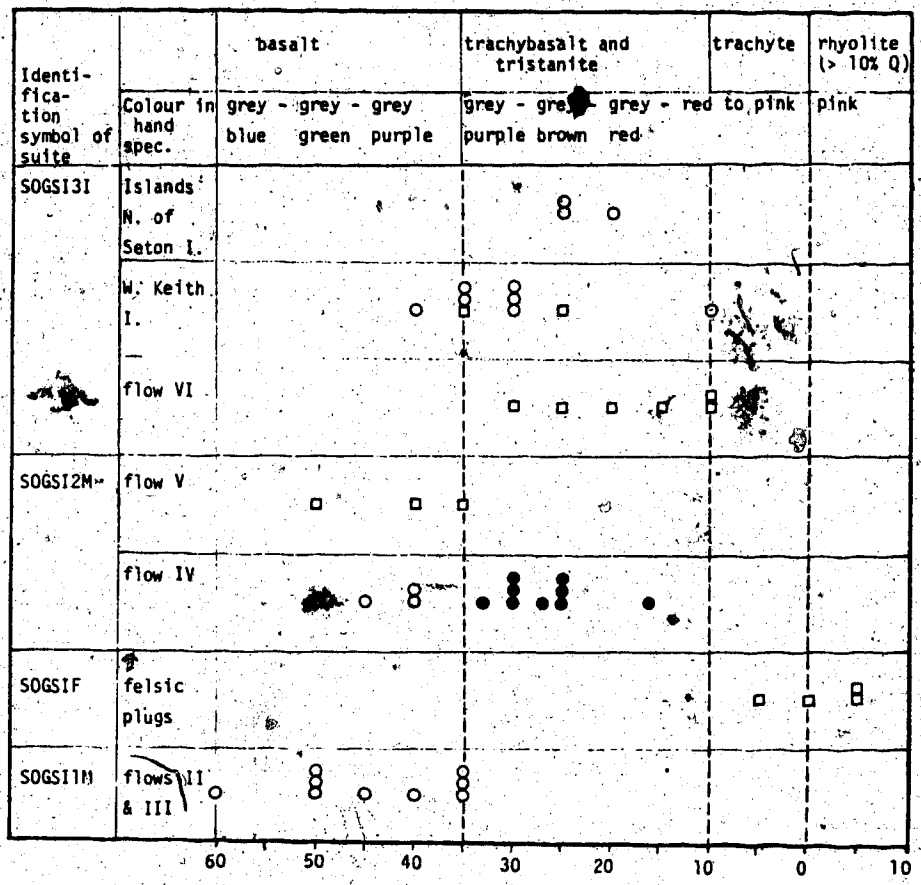

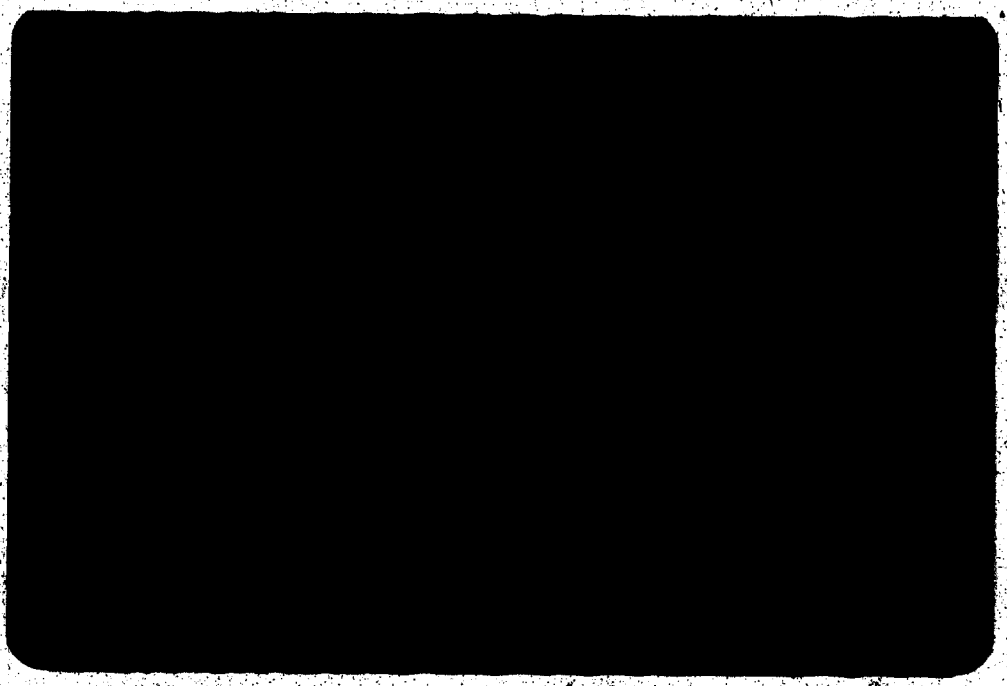

Fig. 4-1. Wilson Island Group basalt (WI10). Albitized blasto-phenocryst with zoned inclusion trails of hornblende and biotite. Note the granular epidote cluster. Field width 0.9 mm. X-polars.

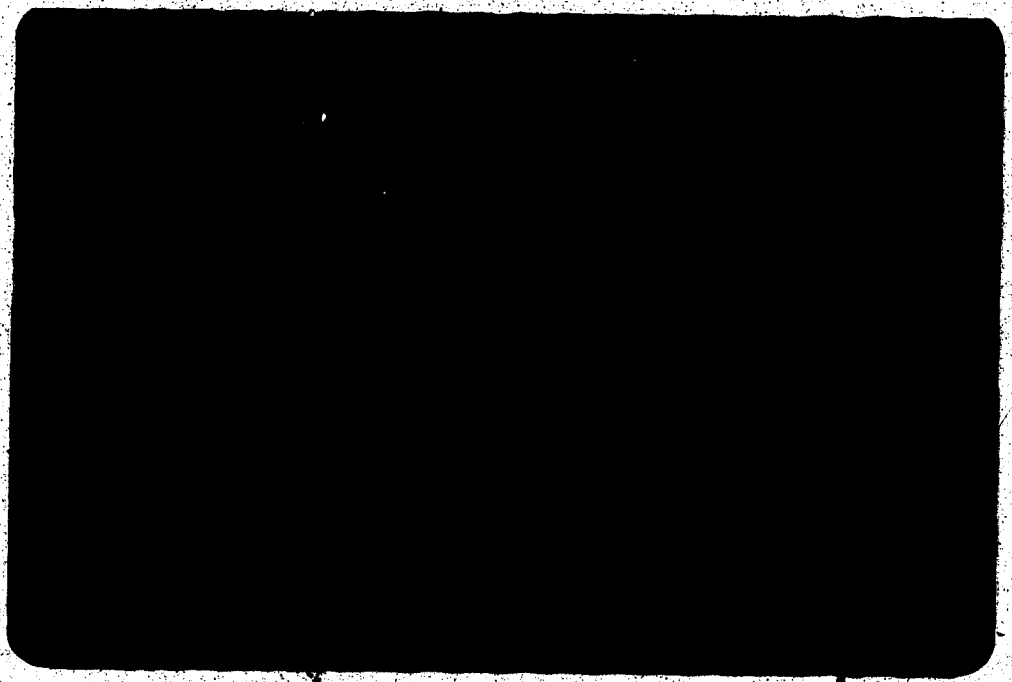

Fig. 4-2. Wilson Island Group intermediate lava (WI22E). Plagioclase blastophenocryst altered to albite with granular clinozoisite plus minor biotite and hornblende. Field-width 0.2 mm. X-polars.

COLOURED PICTURES
Images en couleur

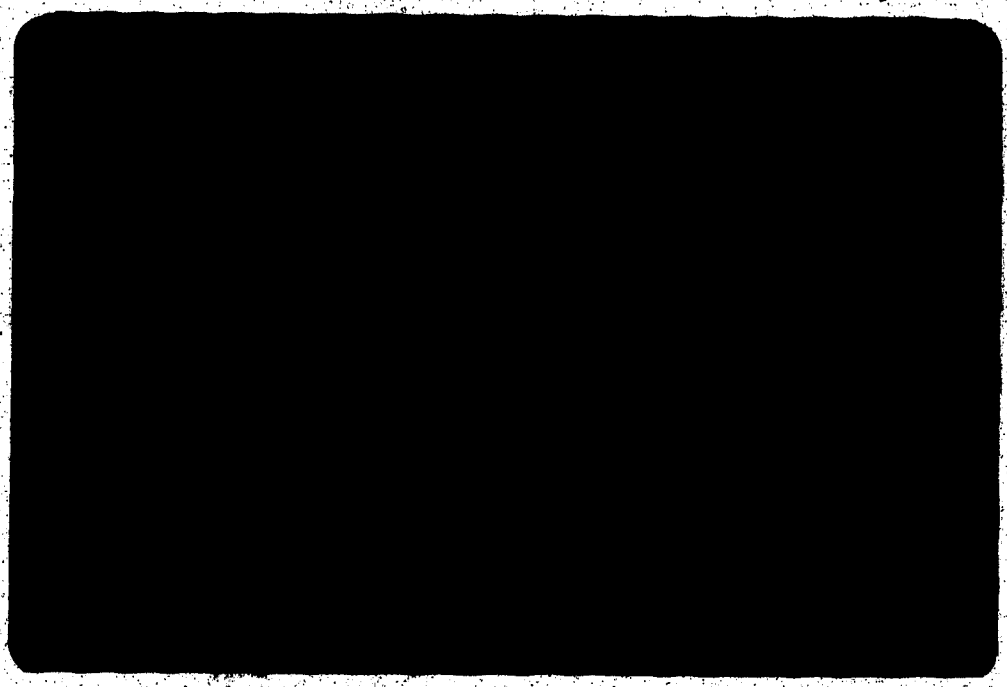

Fig. 4-3. Wilson Island Group basalt (WI10). Albite with hornblende and biotite inclusions. Weakly aligned intergranular hornblende and biotite intergrowths. Field width 0.16 mm. Plane polarized light.

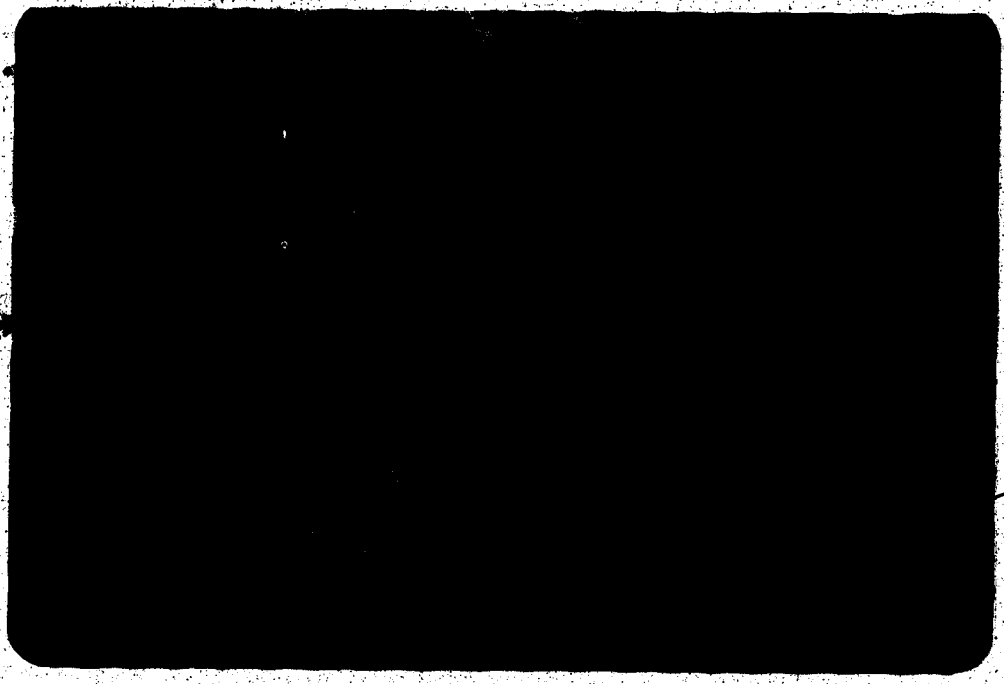

Fig. 4-4. Wilson Island Group intermediate lava (WI22E). Groundmass plagioclase is altered to K-feldspar (stained yellow). The weakly schistose groundmass is biotite rich. Field width 0.2 mm. Plane polarized light.

COLOURED PICTURES
Images en couleur.

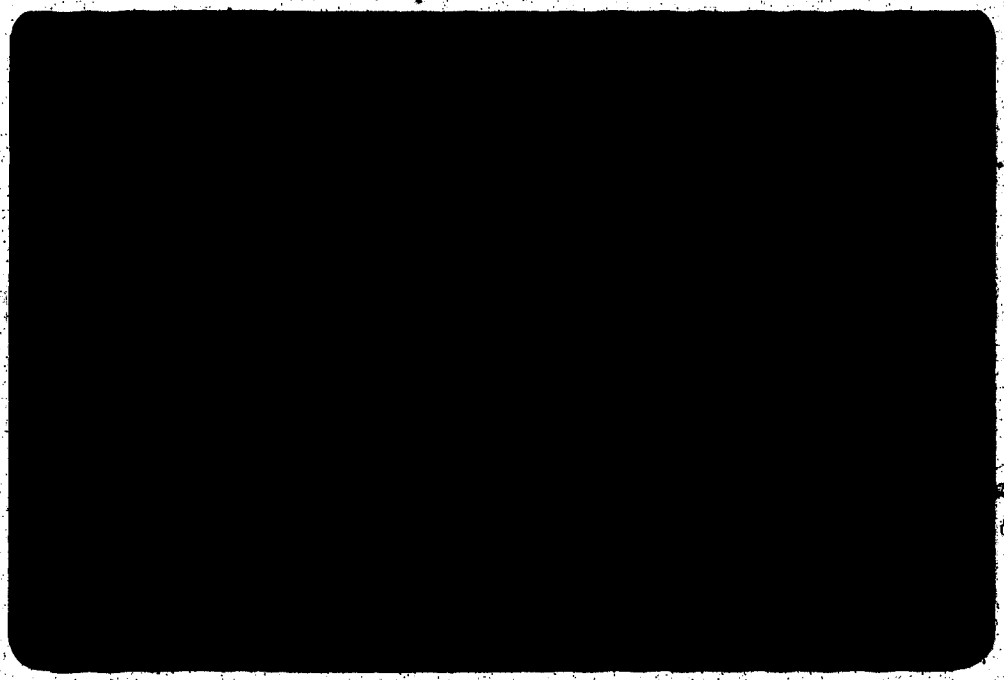

Fig. 4-5. Sheared Wilson Island Group rhyolite (WI22F). Plagioclase blastophenocryst disturbs schistocity of the groundmass and shows quartz and carbonate in pressure shadows. Field width 0.9 mm. X-polars.

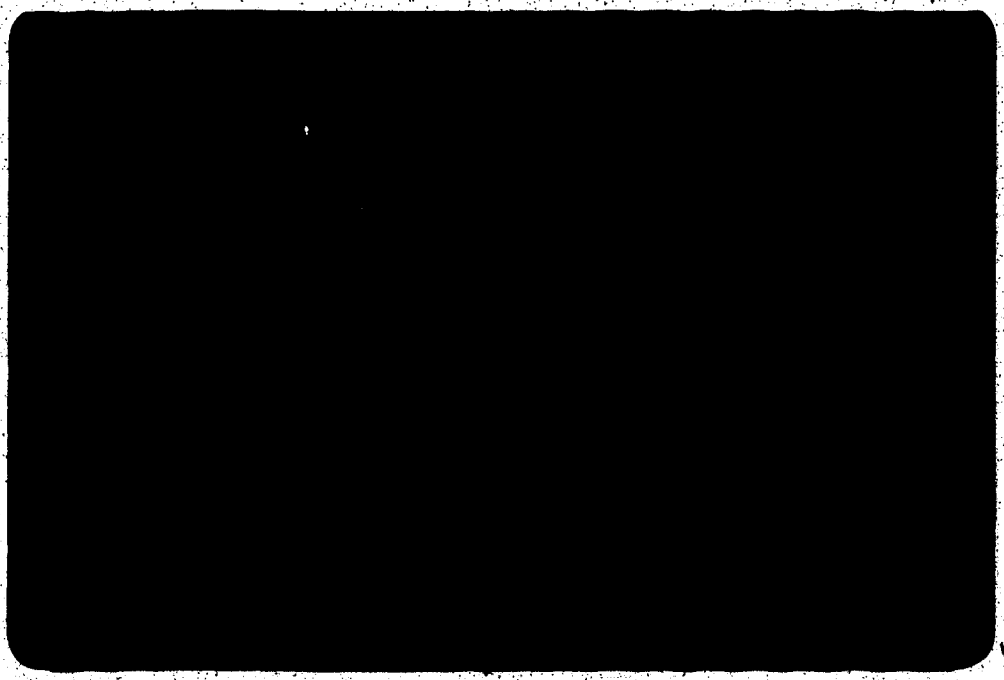

Fig. 4-6. Mid Aphebian diabase (SD3). Olivine pseudomorphs of felted chlorite, acicular actinolite and coarse, granular, birefringent yellow epidote. Field width 0.2 mm. X-polars.

COLOURED PICTURES
Images en couleur

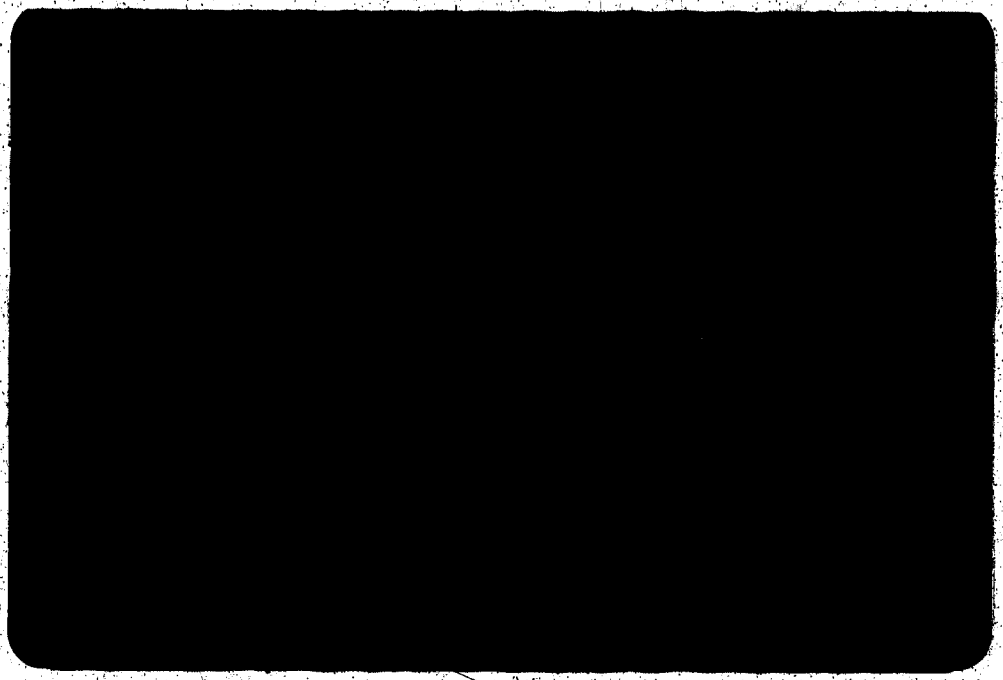

Fig. 4-7. Mid Aphebian diabase (SD3). Pink clinopyroxene is marginally altered to blue-green hornblende plus minor biotite. Matrix patches are green chlorite and pale actinolite. Titanomagnetite shows marginal alteration to sphene. Field width 0.9 mm. Plane polarized li[illegible]

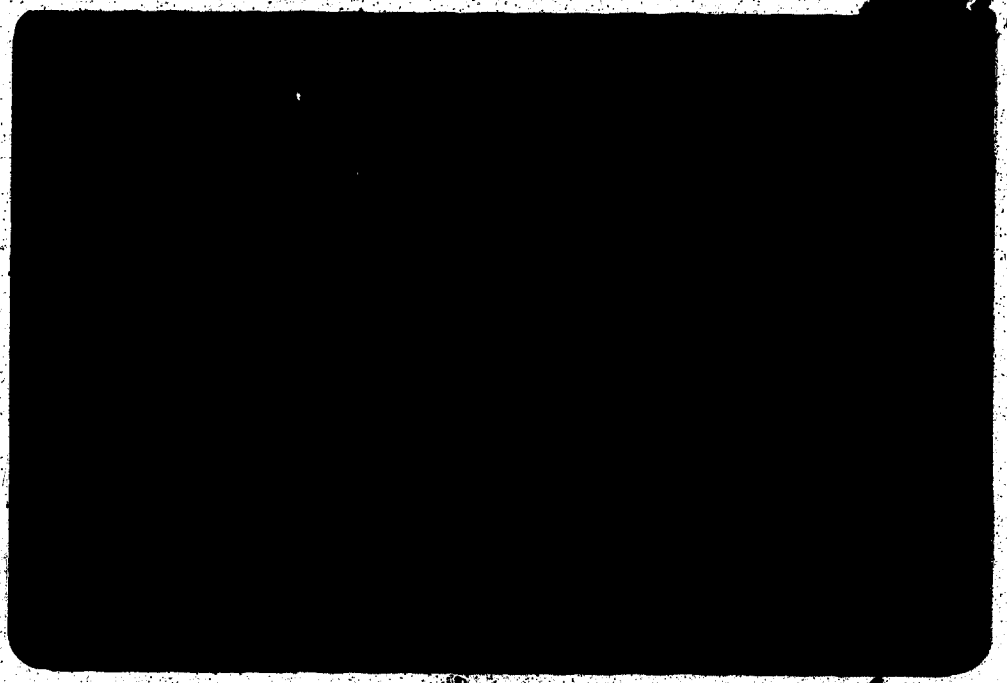

Fig. 4-8. Union Island Group basalt (UI27). Olivine pseudomorphs (now chlorite) have crystallized before plagioclase (now albite and sericite). Field width 0.9 mm. Plane polarized light.

COLOURED PICTURES
Images en couleur

Fig. 4-9. Union Island Group pillow basalt (UI35A). Plagioclase entirely altered to sericite and quartz. Field width 0.9 mm. X-polars.

Fig. 4-10. Sosan Group basalt, Seton Island (CS29). Olivine pseudomorphed by chlorite, quartz and fine magnetite. Field width 0.9 mm. Plane polarized light.

COLOURED PICTURES
Images en couleur

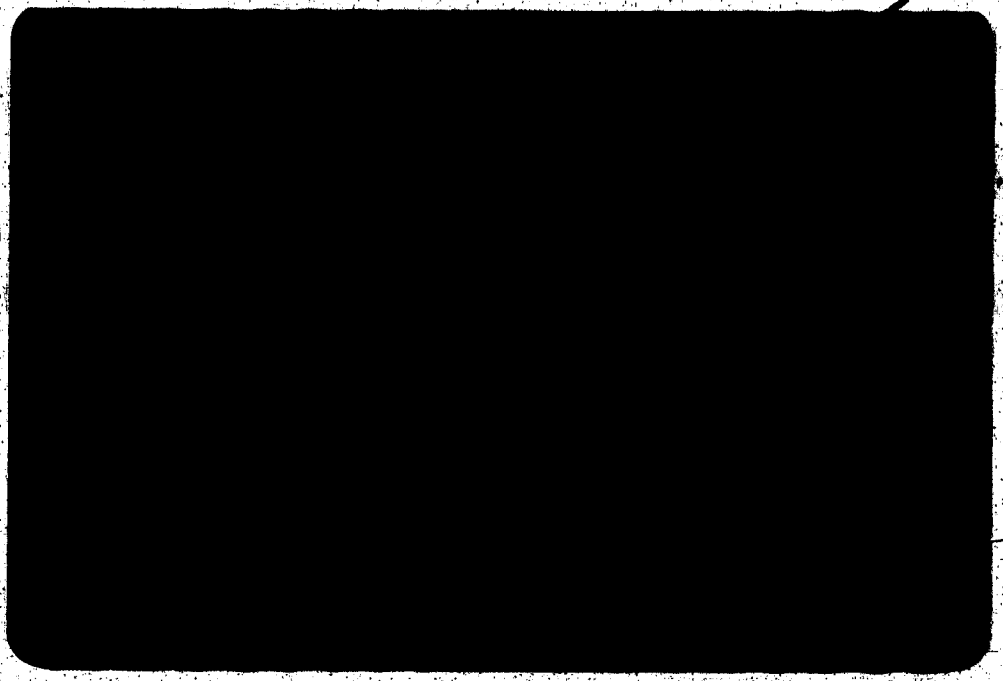

Fig. 4-11. Sosan Group trachyte, Seton Island (SE64B). Albite (stained pink) shows peripheral alteration to K-feldspar (stained yellow). Field width 0.9 mm. Plane polarized light.

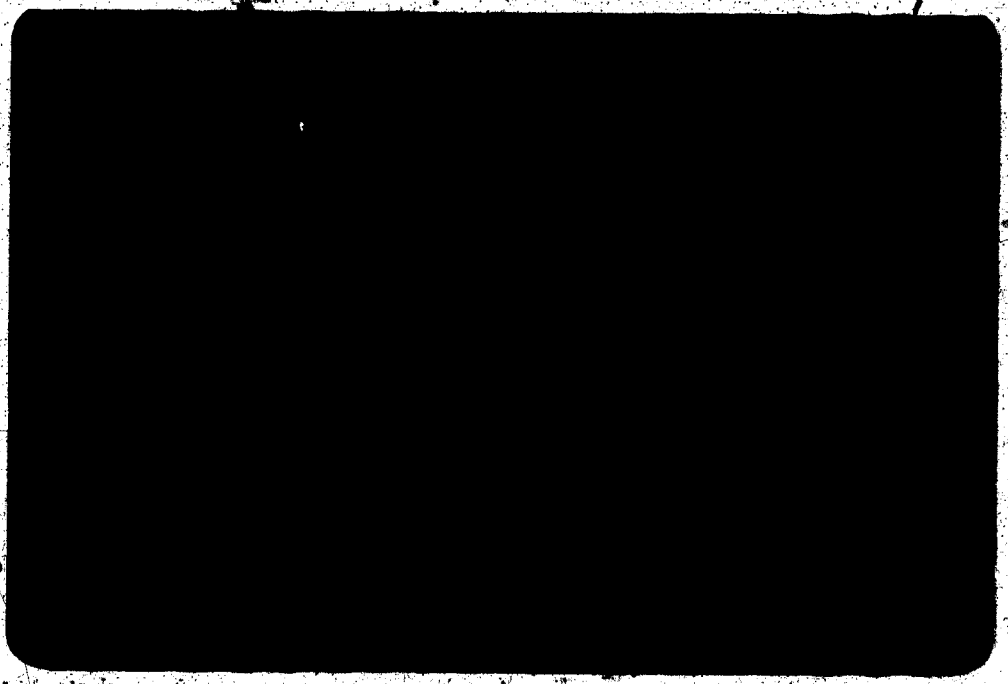

Fig. 4-12. Sosan Group trachy-rhyolite porphyry (SE117). Phenocrysts are composed of albite (stained pink and minor K-feldspar (stained yellow). Field width 0.9 mm. Plane polarized light.

COLOURED PICTURES
Images en couleur

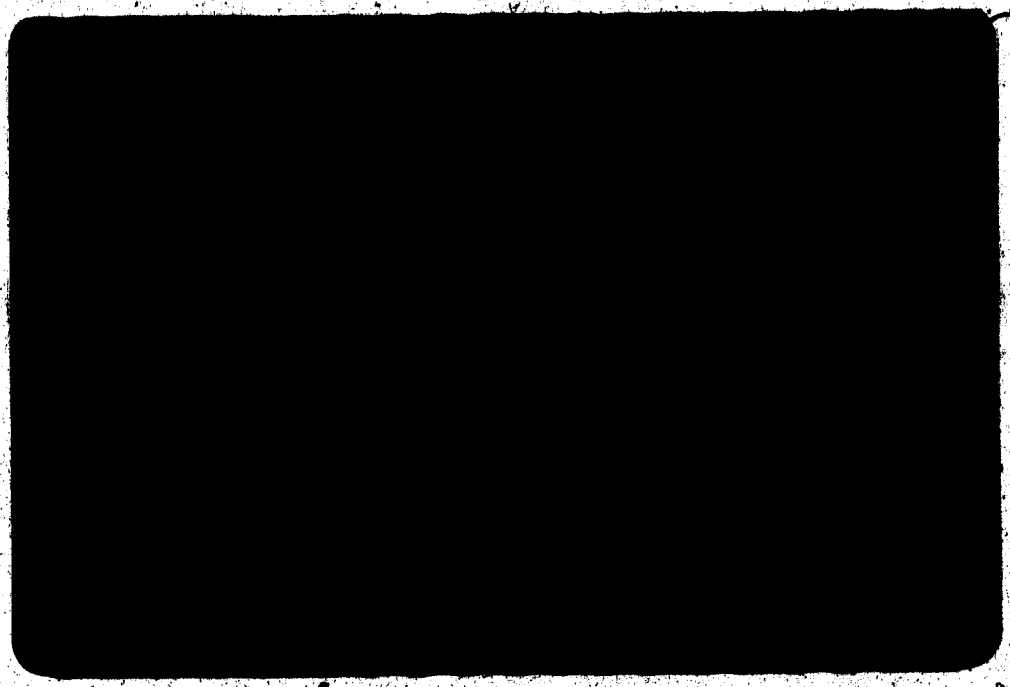

Fig. 4-13. Kahochella Group, Pekanatui Point basalt, (PP77B). Plastically deformed plagioclase (now albite) in 1.5 m pillow. Field width 0.9 mm. Plane polarized light.

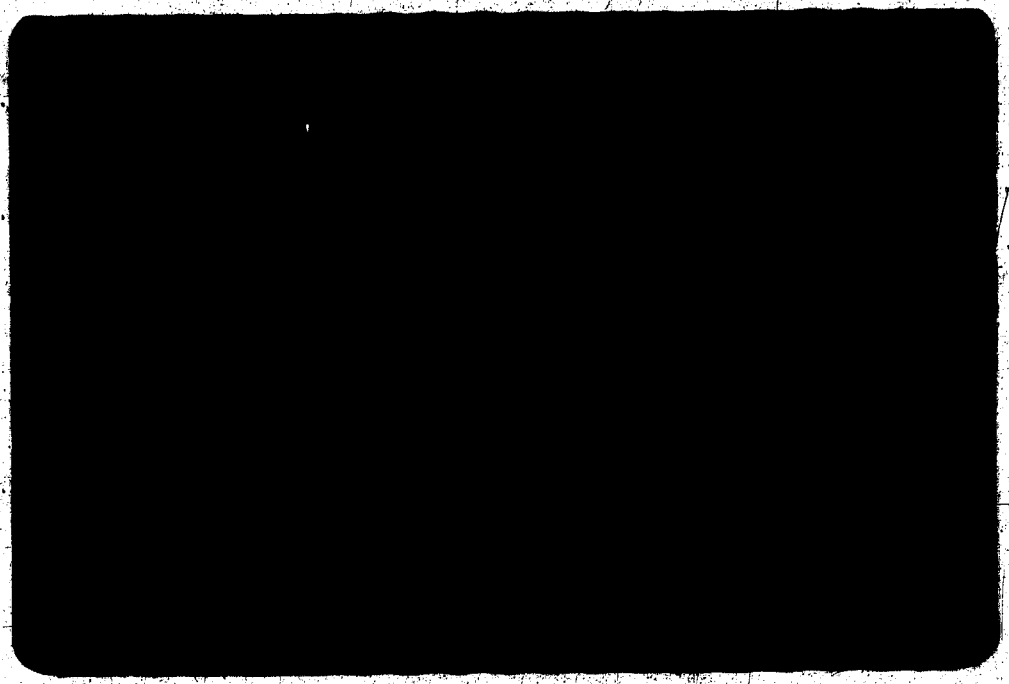

Fig. 4-14. Kahochella Group hyalopilitic basalt, Pekanatui Point (PP74B). Sub-ophitic clinopyroxene pseudomorphs (now chlorite) and chlorite to quartz zoned amygdales. Field width 0.9 mm. Plane polarized light.

COLOURED PICTURES
Images en couleur

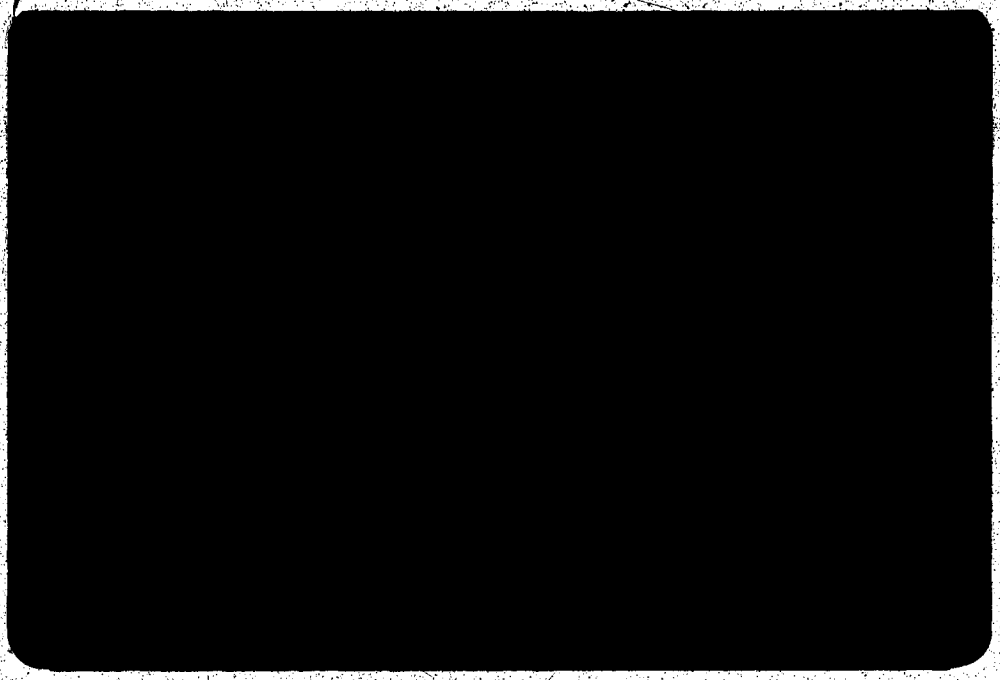

Fig. 4-15. Kahochella Group rhyolite, Pekanatui Point (PP87). Phenocrysts of muscovite and resorbed-quartz in a recrystallized groundmass. Field width 0.9 mm. X-polars.

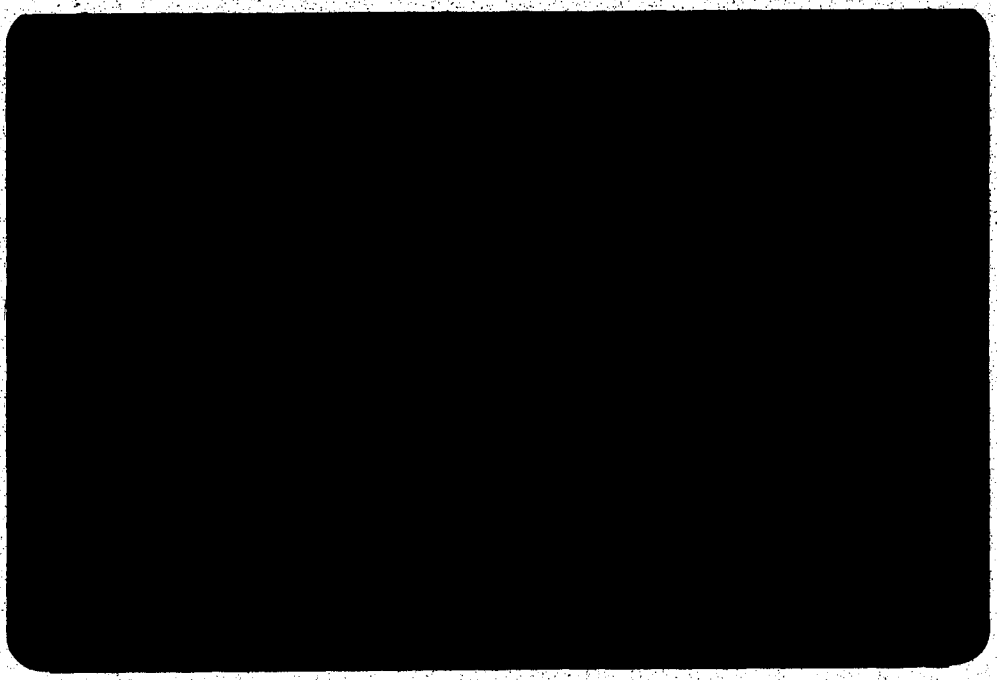

Fig. 4-16. Jackson gabbrodioritic margin, Taltheilei Narrows (TL110D). Phenocrysts of resorbed clinopyroxene and zoned plagioclase phenocrysts. Field width 0.9 mm. X-polars.

COLOURED PICTURES
Images en couleur

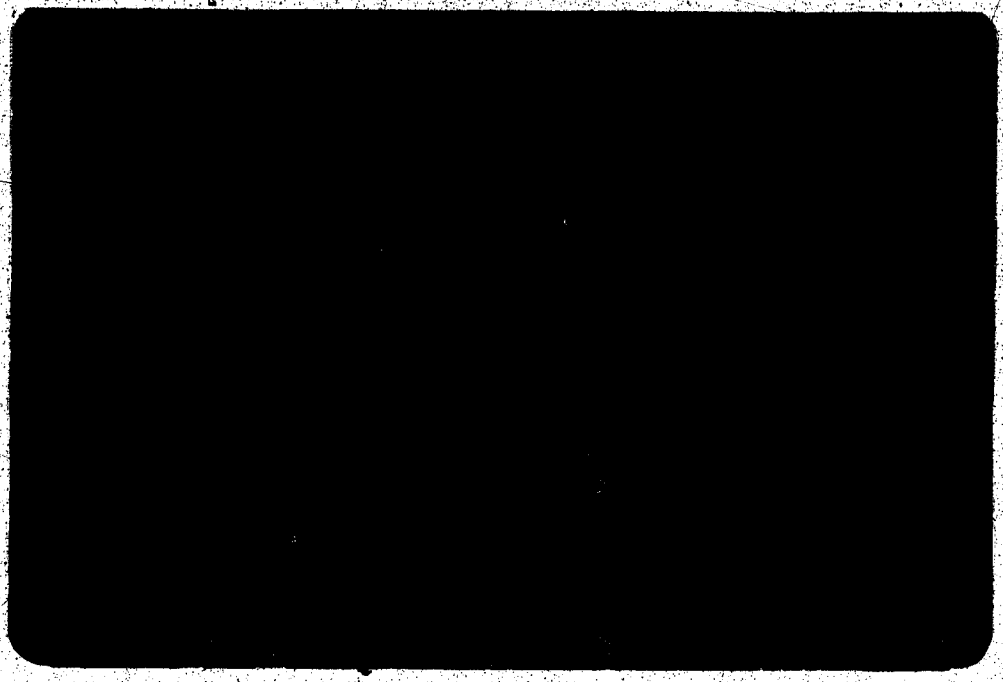

Fig. 4-17. Pearson Formation basalt (PE10). Sub-ophitic fresh clinopyroxene, sericitized plagioclase. Groundmass patches of felted, pale green radial chlorite containing deep-green granular pumpellyite. Field width 0.7 mm. Plane polarized light.

COLOURED PICTURES
Images en couleur

Table 5-1. Coefficients for the reactions displayed in Fig. 5-5 and 5-6.

Pu, Ac and Ep are assumed to be Fe-free; Ac is assumed to be Al-free. Negative symbols refer to the reactants. Products are on the high entropy side of the reaction.

Reaction Phases	Pu	Ep	Ac	Ch	Cr	Dl	Q	H_2O	CO_2
(Dl,Ac)	-15	23		3	14		12	29	-14
(Dl,Ep)	10		23	-25	-86		-169	42	86
(Dl,Ct)	-50	86	14	-4			-58	134	
(Dl,Ch)	-15	25	3		4		-9	37	-4
(Dl,Pu)		2	3	-3	-10		-21	8	10
(Pu,Ch,Ep)			1		3	-5	-8	-1	7
(Pu,Ct)		6	19	-9		-50	-143	14	100
(Pu,Ac)		-2		3	19	-15	-3	-11	11
(Ac,Ch)	-3	5			-1	3	3	8	-5
(Ac,Ct)	-19	31		1		14	18	47	-28
(Ac,Ep)	-2			5	31	-23	-3	-13	15

Pumpellyite, Pu - $Ca_4MgAl_5Si_6O_{21}(OH)_7$

Epidote, Ep - $Ca_2Al_3Si_3O_{11}(OH)$

Actinolite, Ac - $CaMg_5Si_8O_{22}(OH)_2$

Chlorite, Ch - $Mg_5Al_2Si_3(OH)_8$

Calcite, Ct - $CaCO_3$

Dolomite, Dl - $(Ca,Mg)(CO_3)_2$

Quartz, Q - SiO_2

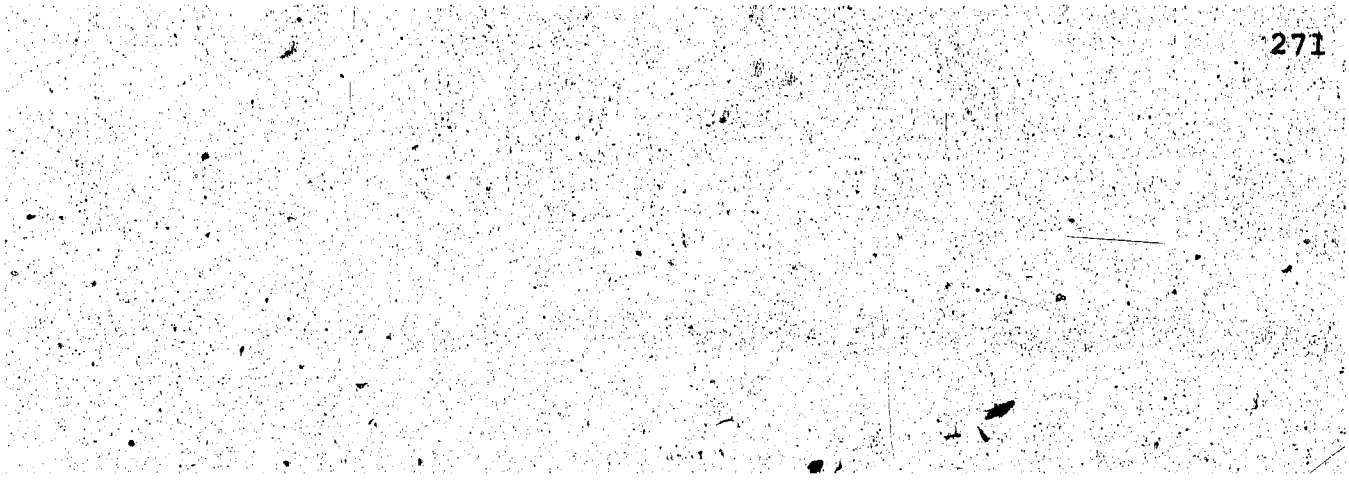

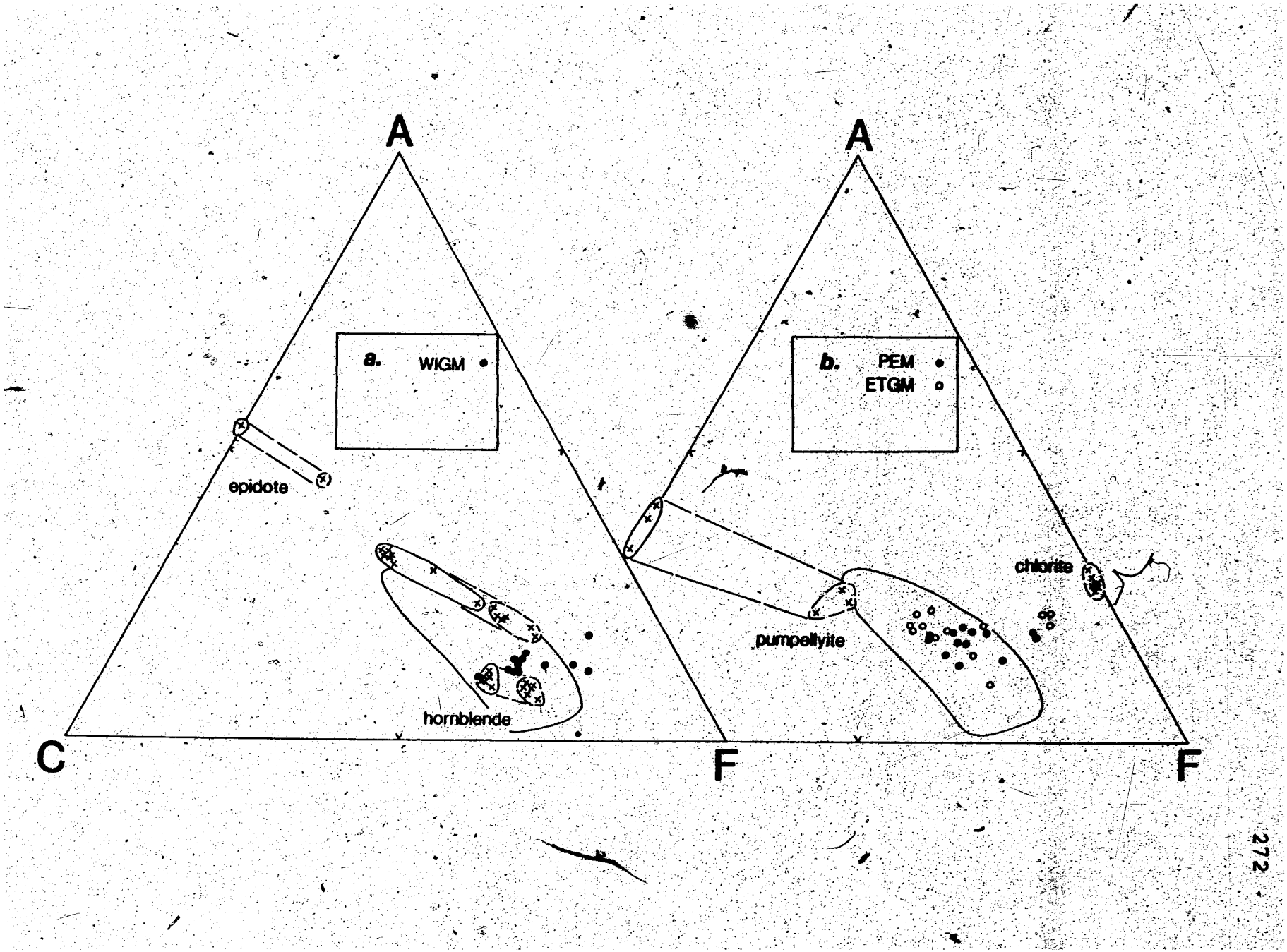
A
a.
WIGM
epidote
hornblende
C
F
A
b.
PEM
ETGM
chlorite
pumpellyite
F

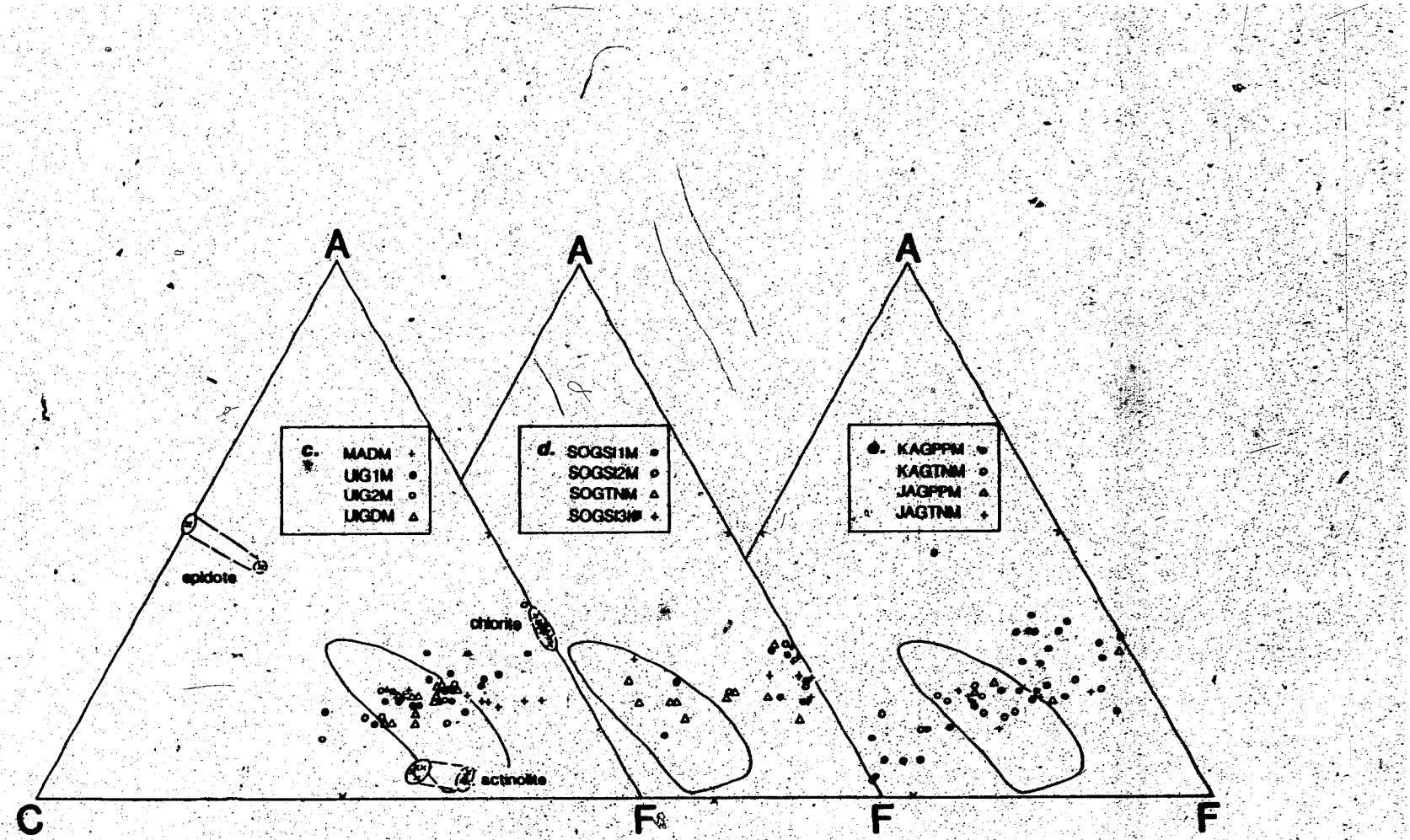
A
A
A
c.
MADM
UIG1M
UIG2M
UIGDM
d.
SOGSI1M
SOGSI2M
SOGTNM
SOGSI3M
e.
KAGPPM
KAGTNM
JAGPPM
JAGTNM
epidote
chlorite
actinolite
C
F
F
F

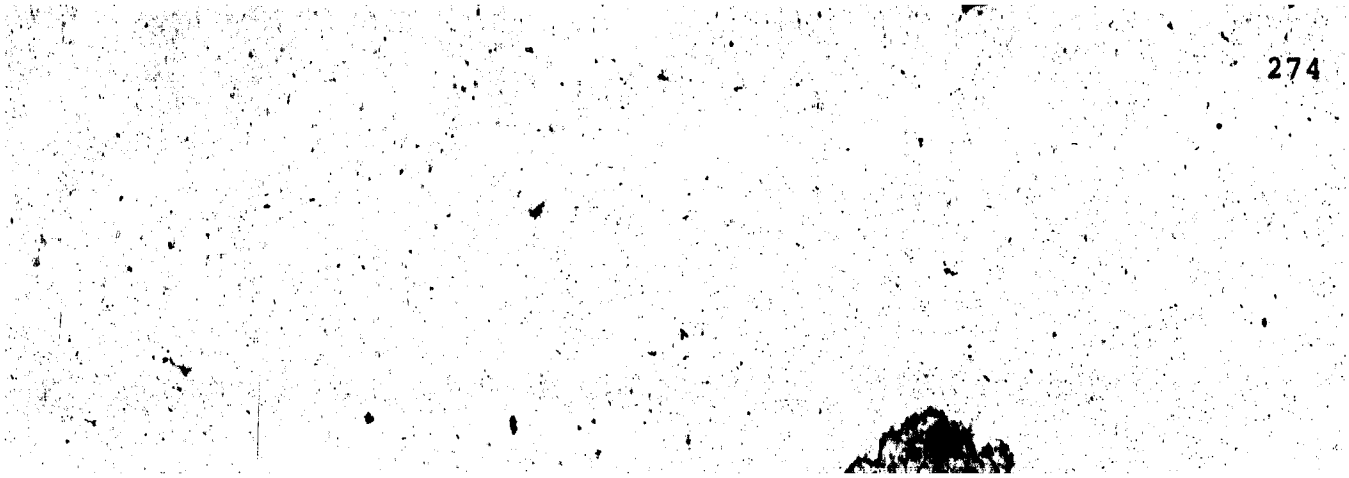

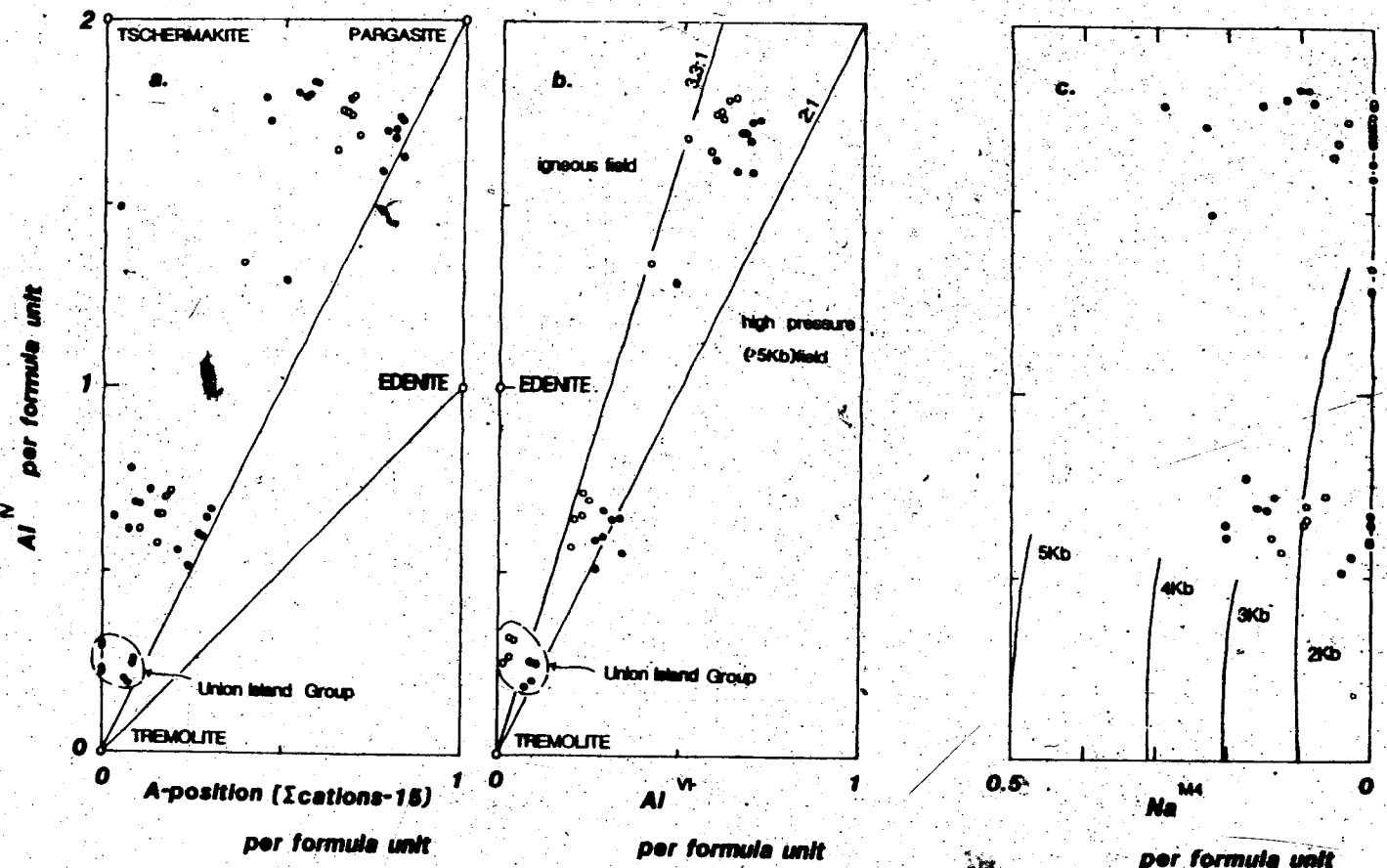
a.
TSCHERMAKITE
PARGASITE
EDENITE
Union Island Group
TREMOLITE
2
1
0
0
1
Al^{IV} per formula unit
A-position (Σcations-15)
per formula unit
b.
3:1
2:1
igneous field
high pressure
(>5Kb)field
EDENITE
Union Island Group
TREMOLITE
0
1
Al^{VI}
per formula unit
c.
5Kb
4Kb
3Kb
2Kb
0.5
0
Na^{M4}
per formula unit

Fig. 5-3. The probable limits of the temperature and pressure conditions within which the Wilson Island Group reached metamorphic equilibrium.
The shaded area represents the P-T limits of the Wilson Island Group. Phase relations for the low to medium-grade metamorphic transition in mafic rocks are from Jamieson (1981). Experimental work is from Liou *et al.*, (1974). 1. chlorite decreasing; 2. chlorite out; 3a. epidote out (QFM buffer, $Ps_{2.5}$); 3b. epidote out (NNO buffer); 3c. epidote out (HM buffer, $Ps_{3.3}$).

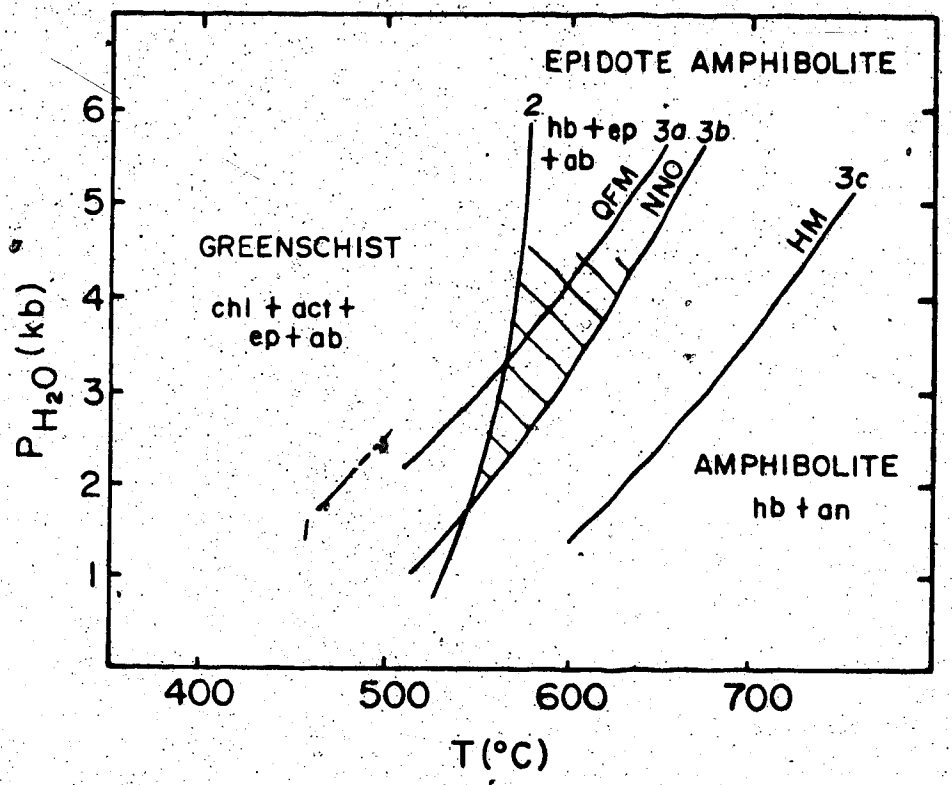

Fig. 5-4. Chlorite compositions, using the classification scheme of Hey (1954).

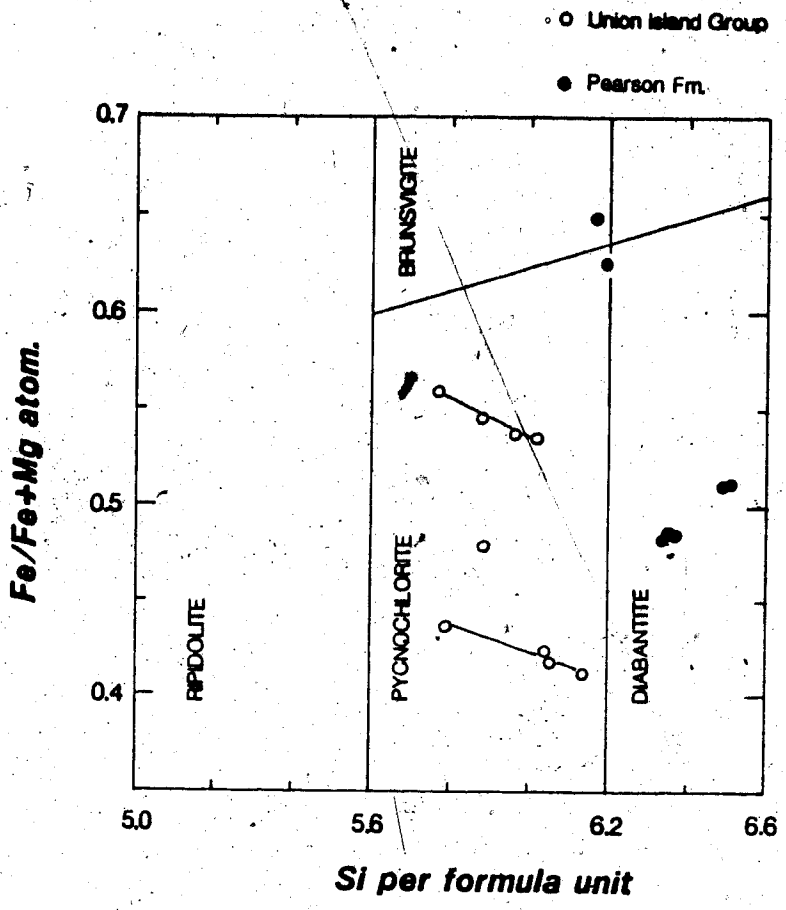

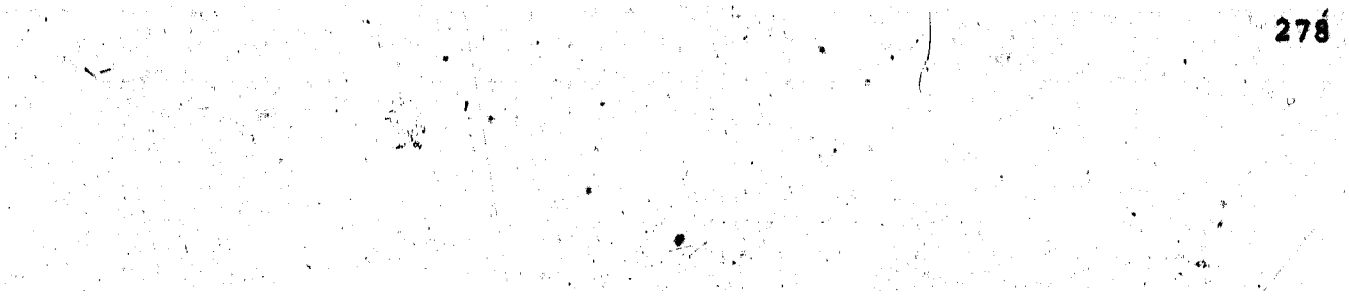

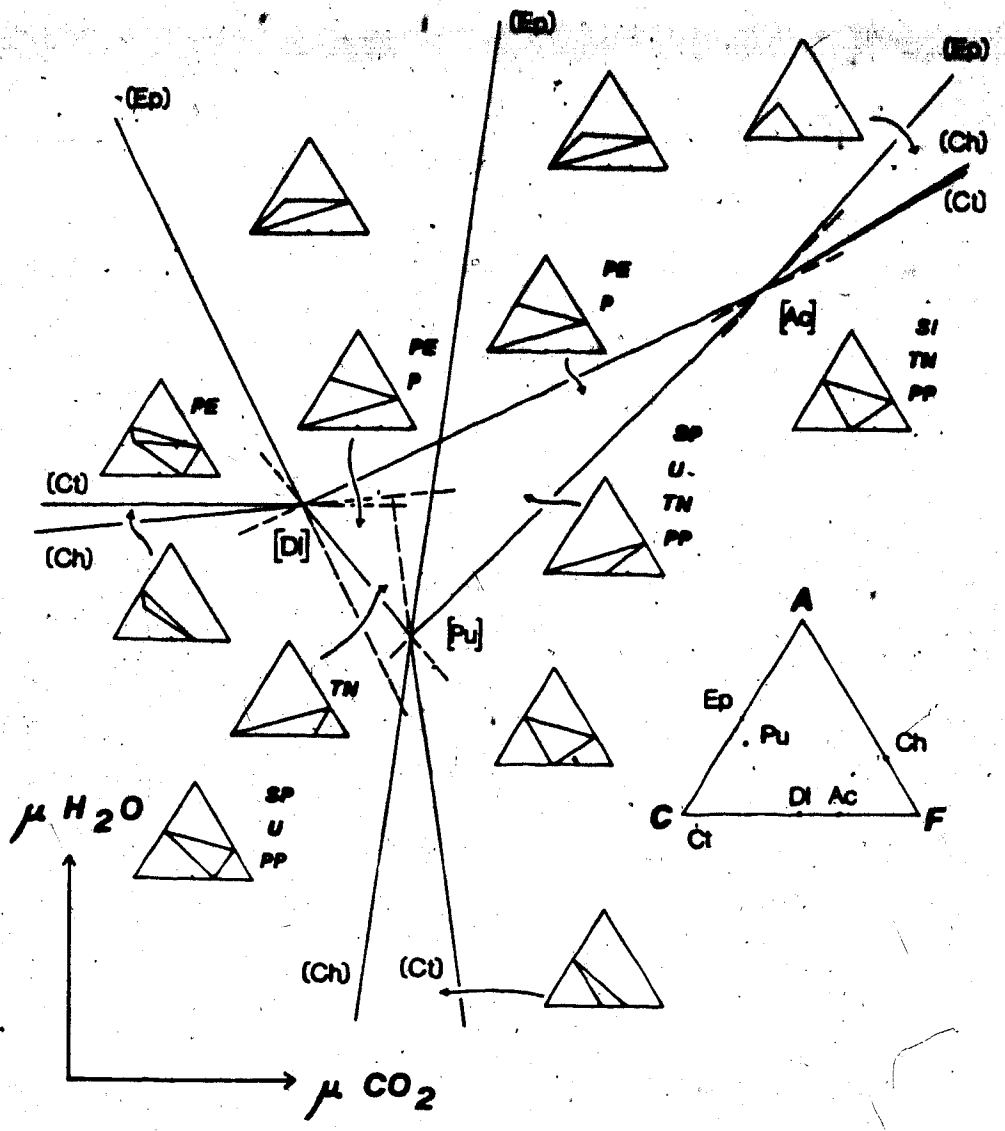
(Ep)
(Ep)
(Ep)
(Ch)
(Cl)
PE
P
PE
P
PE
[Ac]
SI
TN
PP
SP
U
TN
PP
(Cl)
(Ch)
[Di]
[Pu]
TN
A
Ep
Pu
Ch
Di Ac
C
Cl
F
μ H2O
SP
U
PP
(Ch)
(Cl)
μ CO2

Fig. 5-6. Isobaric temperature vs. fluid composition plot. The key is the same as for Fig. 5-5. Arrows show possible alteration trends for Pu-Ac and Ep-Ac facies.

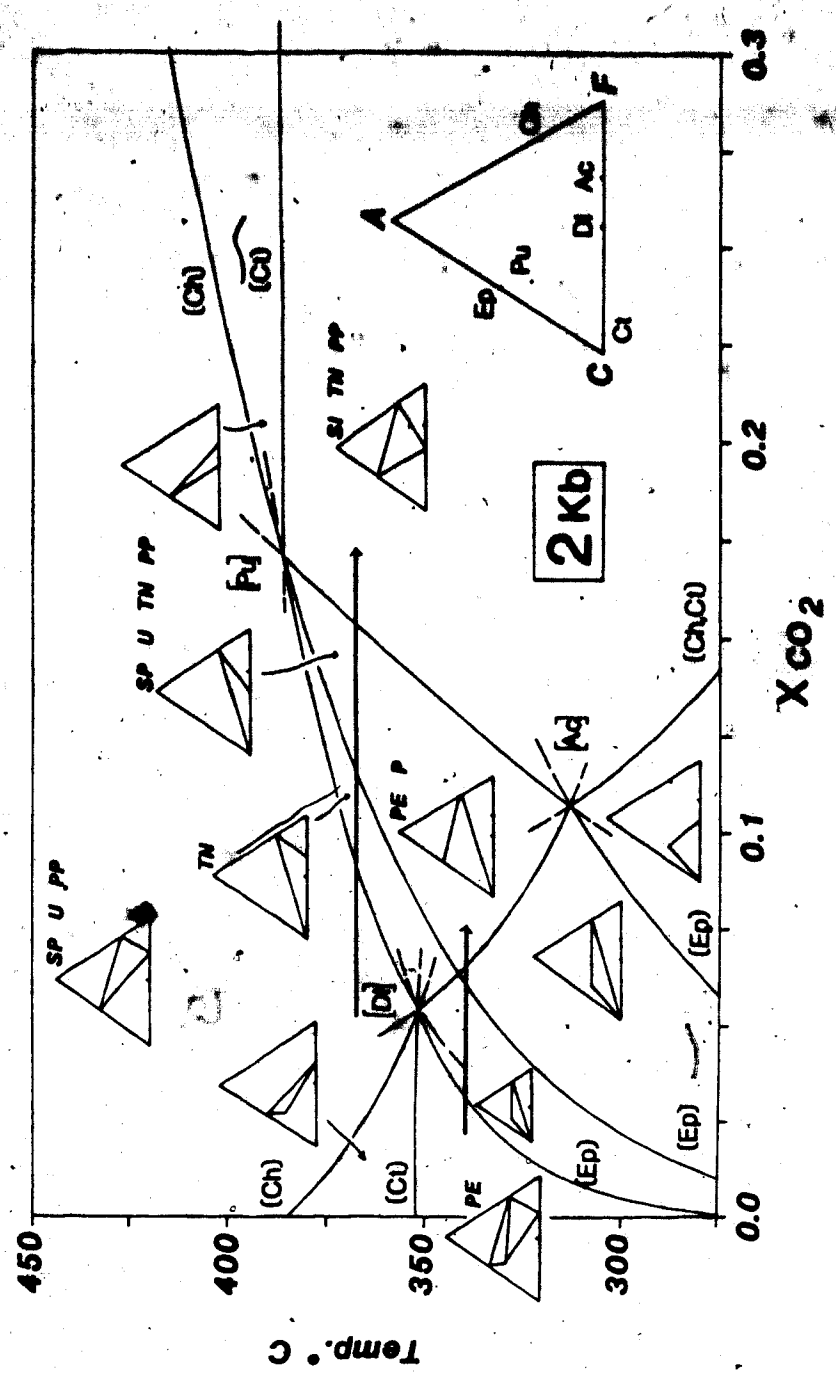

Fig. 5-7. ACF diagrams showing very-low-grade (and possibly low-grade) metamorphic assemblages observed with increasing X_{CO_2}.
Localities are the same as for Fig. 5-5. Observed assemblages are indicated for each locality.

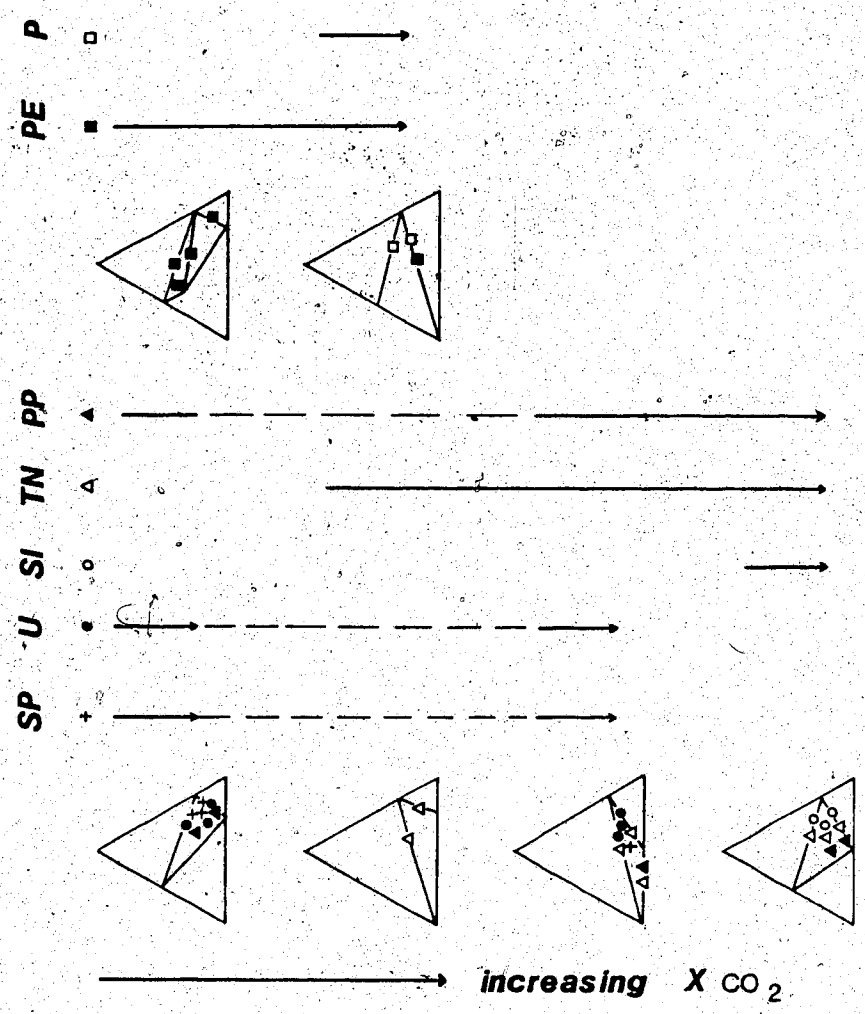

Stratigraphic Group	Tectonics	Magmatism	Sed. rate Age (Ma)	Isotopic Age (Ma)		ref.
		Mackenzie IV diabase		1315	K/Ar, W.R. bi	1
Et-Then	T.F. uncf.	Gabbro cone sheet basalt (P.)• -T.** trachyte plugs (S.P.)-A				
	folding	qtz. diorite laccoliths		1811±81	Rb/Sr W.R.	2
				1785	K/Ar. bi.	3
				1795		
	nappes			1845		
Christie Bay Pethei		Pearson Formation basalt (P.E.) -T.	1810	1809±30	Rb/Sr W.R.	14
Kahochella		"Jackson" gabbro dykes & plutons basalt, & rhyolite (P.P. & T.N.)-A	1850			
Sosan	B.F.	basalt, to trachyte & rhyolite (S.I. & S.M.)-A	1880	1805±16	Rb/Sr W.R.	4
				1832±10	Rb/Sr W.R.	5
				1804±23	Pb/Pb W.R.	6
	uncf.?		1910			
Union Island	B.F.	diabase sills - Tr basalt (U.M., U.G., U.I.)	1930			
	uncf.		1970			
		"Mid Aphebian" diabase dykes (S.P.) - T plutons		2100	Rb/Sr	text
		gabbro & granite (Blachford Lake)-A		2057±56	K/Ar am.	7
	myl.	gabbro 29 km. dyke (S.P.)-A		2170	K/Ar bi	8
				2200	K/Ar bi	9
	local?	Butte qtz. monzonite		2050	Pb/Pb Zr	10
Wilson Island		basalt - intermediates & rhyolite (W.I.) - T.		1810±19	Rb/Sr W.R.	14
	uncf.			1846±24	Rb/Sr W.R.	11
	myl.					
Slave Province basement				2370	K/Ar bi	12
				2460-2575	K/Ar bi	13

Table 6-2.Rb-Sr analytical results for the Wilson Island Group. All samples are from Wilson Island.

Sample Number	Rb/Sr (weight ratio)	Rb p.p.m.	Sr p.p.m.	$^{87}Rb/^{86}Sr$ atomic ratio*	$^{87}Sr/^{86}Sr$ atomic ratio**	$^{86}Sr/^{88}Sr$ atomic ratio
WI14D	0.386	79.8	206.5	1.1207	0.7346	0.11961
WI29G	0.484	62.7	129.5	1.4047	0.7411	0.11958
WI8C	0.617	87.0	141.0	1.7935	0.7513	0.11981
WI8B	0.631	96.8	153.5	1.8307	0.7527	0.11978
WI22E	1.236	95.5	77.2	3.6090	0.8009	0.11973
WI35D	1.715	121.5	70.9	5.0239	0.8348	0.11961

* $^{87}Rb/^{86}Sr$ error = ± 0.5%

** $^{87}Sr/^{86}Sr$ error = ± 0.0004

Table 6-3. Rb-Sr analytical results for the Pearson Formation.
All samples are from the Pearson Point peninsula.

Sample Number	Rb/Sr (weight ratio)	Rb p.p.m.	Sr p.p.m.	$^{87}Rb/^{86}Sr$ atomic ratio*	$^{87}Sr/^{86}Sr$ atomic ratio**	$^{86}Sr/^{88}Sr$ atomic ratio
PV01	0.051	17.9	349.6	0.1482	0.7130	0.11912
PE10	0.200	31.2	156.2	0.5775	0.7238	0.11895
PE5B	0.249	59.3	238.3	0.7205	0.7272	0.11910
PV07	0.317	59.2	186.5	0.9195	0.7325	0.11999
PV08	0.437	89.3	204.2	1.2664	0.7427	0.11921
PE5C	0.501	103.6	206.8	0.4509	0.7463	0.11942

* $^{87}Rb/^{86}Sr$ error = ± 0.5%

** $^{87}Sr/^{86}Sr$ error = ± 0.0004

Table 6-4. Published Rb-Sr isochron ages, initial ratios, regional trends and petrography for diabase dykes from the Slave Province and other Archean cratons. All dykes have ages > 2000 Ma.

Ol/Q - olivine to quartz tholeiite, Q/Ol - quartz tholeiite with minor olivine. Hy - modal hypersthene, Pi - pigeonite.

References: 1, Gates and Hurley (1973); 2, Stueber, *et al.* (1976); 3, Van Schmus (1965); 4, Leech (1966); 5, McGlynn and Irving (1975); 6, Heimlich, *et al.* (1973); 7, Hriskevich (1968).

Slave	Superior	Wyoming
Mackenzie I	Matachewan	Bighorn
2635 ± 78 (1)	2633 ± 91 (1)	2766 ± 114 (2)
0.7028 ± 0.0005	0.7000 ± 0.0010	0.7019 ± 0.0003
070°	000°	
OL/Q, Pi(4); OL(5)	Q	Q/OL, Pi(6)
Mackenzie IV	Nipissing	Bighorn
2128 ± 176 (1)	2109 ± 78 (3)	2154 ± 69 (2)
0.7019 ± 0.0010	0.7060	0.7034 ± 0.0003
120-150°	sill	
OL/Q, Pi(4)	Q, H, Pi(7)	Q/OL, Pi(6)
Mackenzie II & IV	Abitibi	
2049 ± 84 (1)	2102 ± 67 (1)	
0.7030 ± 0.0006	0.7045 ± 0.0004	
000-030°	020-070°	
120-150°		
OL/Q, Pi(4)	OL/Q	

Unit	Sample No.	cpx $^{87}Sr/^{86}Sr$ measured	cpx $^{87}Sr/^{86}Sr$ corrected*	$(^{87}Sr/^{86}Sr)$ from isochron	cpx δO^{18} ‰ SMOW	whole rock δO^{18} ‰ SMOW	Provenance
Pearson	PE5B-1			0.7089(4)	6.48		strong cc
Formation	PE5B-2	0.71023(26)	0.7096		6.08		
Jackson	PP12-1	0.70561(04)	0.7050				cc
Gabbro	PP12-2	0.70605(05)	0.7054		6.37		
	TL49B					8.75	
Sosan				0.7018(5)'			mantle
Gp. lavas				0.7025(8)'			
Union	UI102C	0.70335(05)	0.7027		6.17	7.05	mantle
Island Gp.	UI102A	0.70273(08)	0.7021		5.85	8.30	(*minor cc?)
diabase	UI63	0.70363(07)	0.7030		5.43	7.45	
Mid-Aphebian	SD3	0.70240(02)	0.7017		6.12	7.13	mantle
Diabase	SD6	0.70224(04)	0.7016		5.97	7.27	
Wilson Island Gp. basalt	WI40B			0.7051(8)		6.89	cc?

Fig. 6-1. Rb-Sr whole-rock isochron for the lava-flows of the Wilson Island Group.
The vertical bars indicate the $^{87}Sr/^{86}Sr$ error.

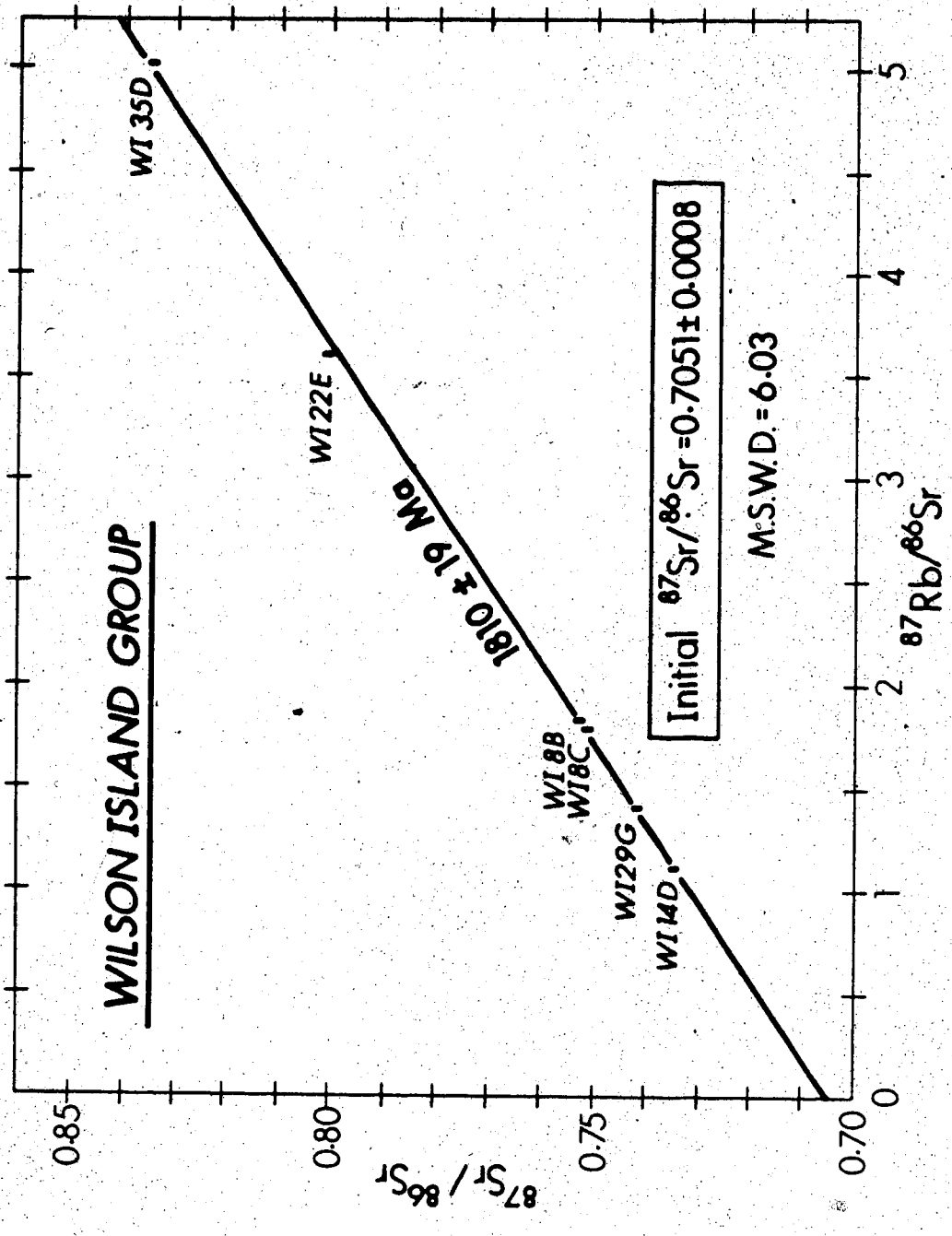

Fig. 6-2. Rb-Sr whole-rock isochron for the lava-flows of the Pearson Formation.
The vertical bars indicate the $^{87}Sr/^{86}Sr$ error.

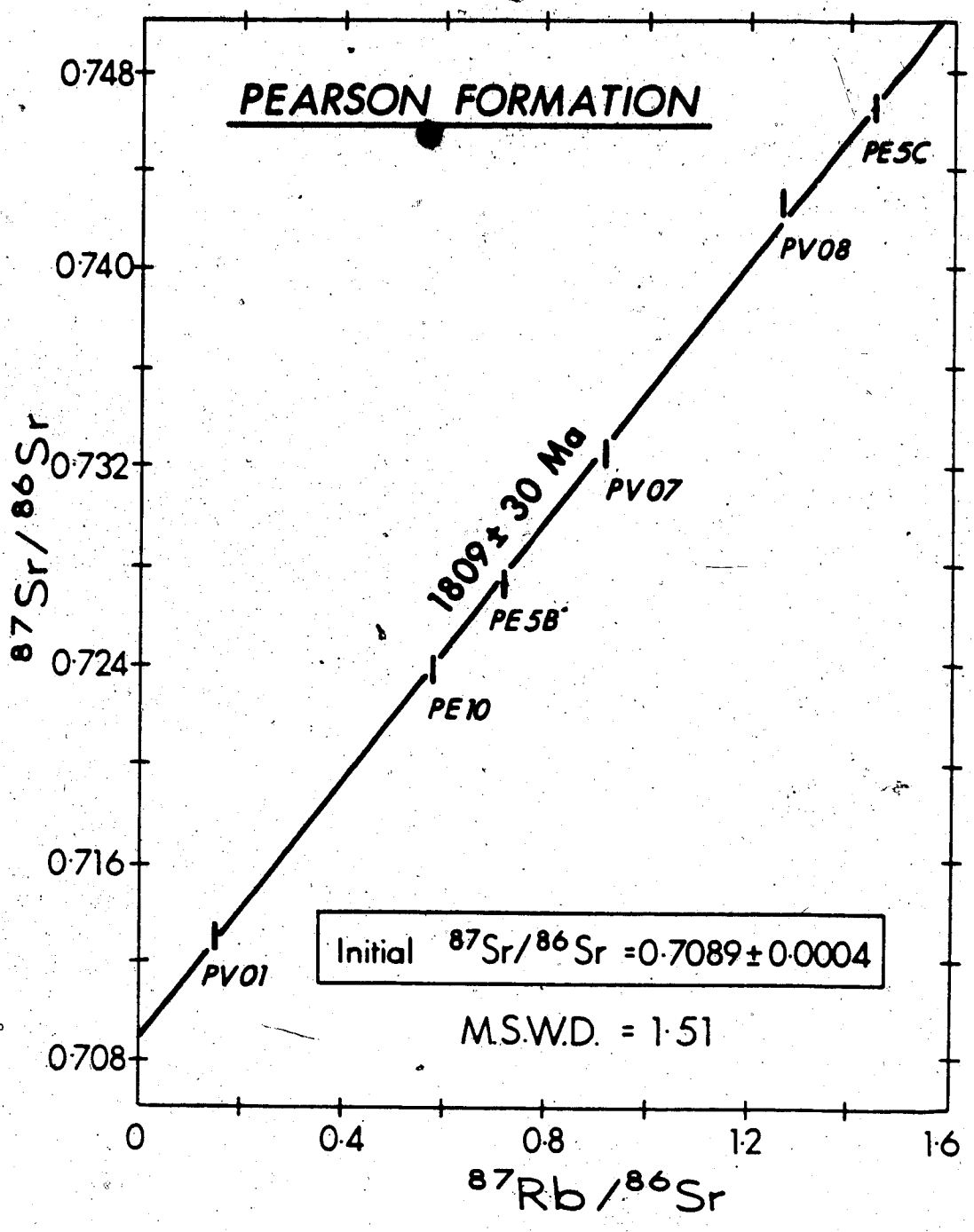

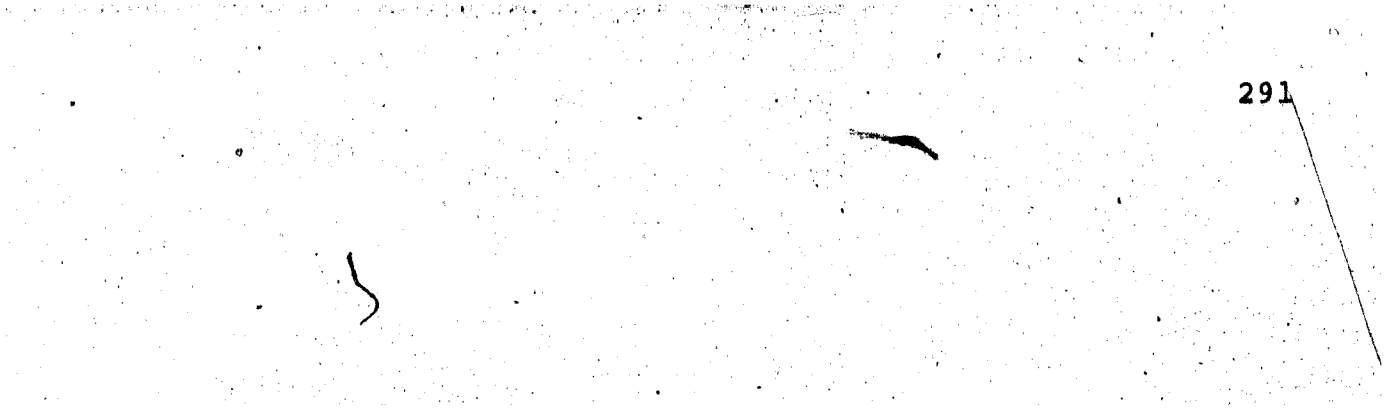

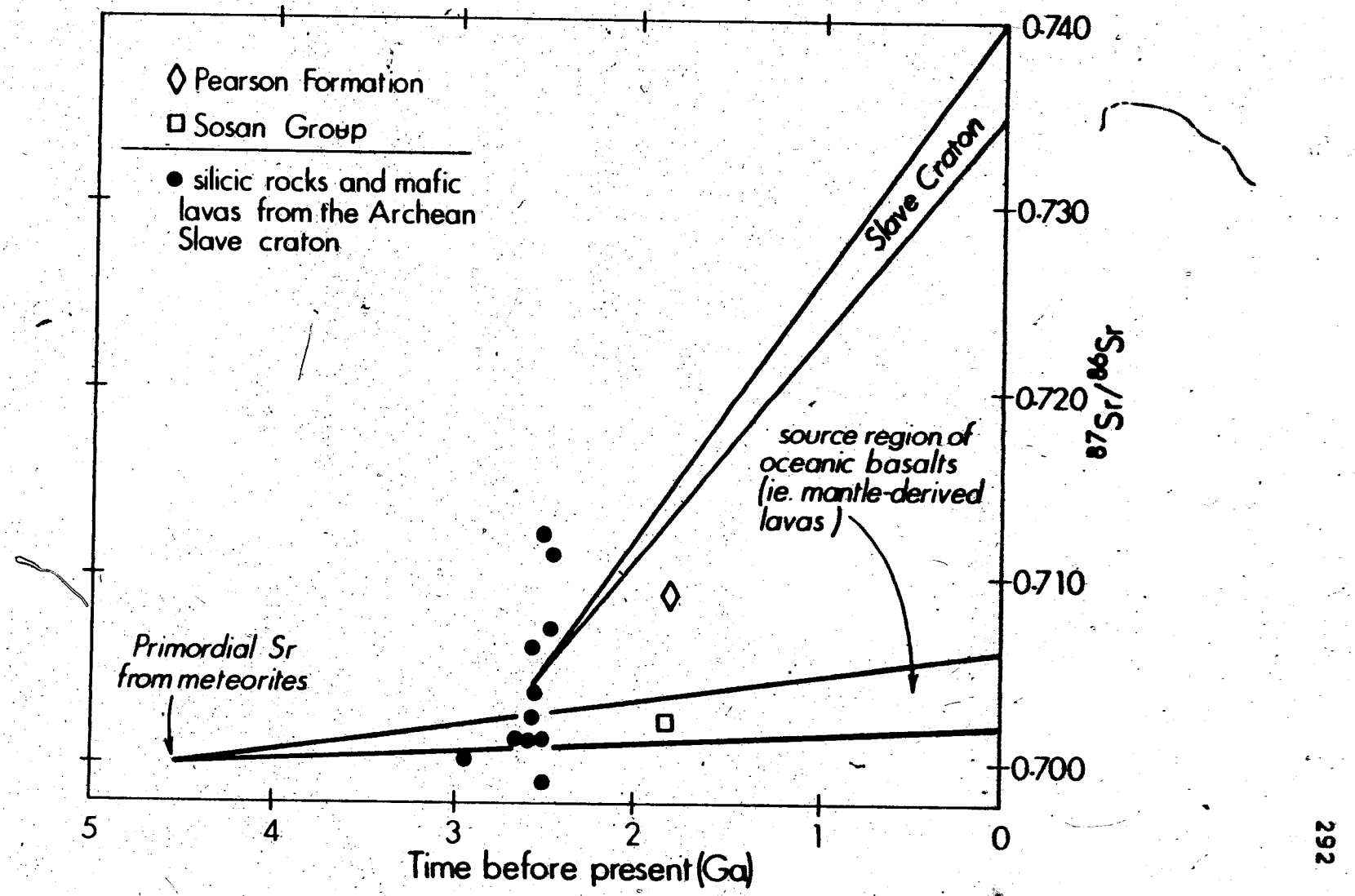
◊ Pearson Formation
□ Sosan Group
● silicic rocks and mafic lavas from the Archean Slave craton
Slave Craton
source region of oceanic basalts (ie. mantle-derived lavas)
Primordial Sr from meteorites
0.740
0.730
0.720
0.710
0.700
$^{87}Sr/^{86}Sr$
5
4
3
2
1
0
Time before present (Ga)

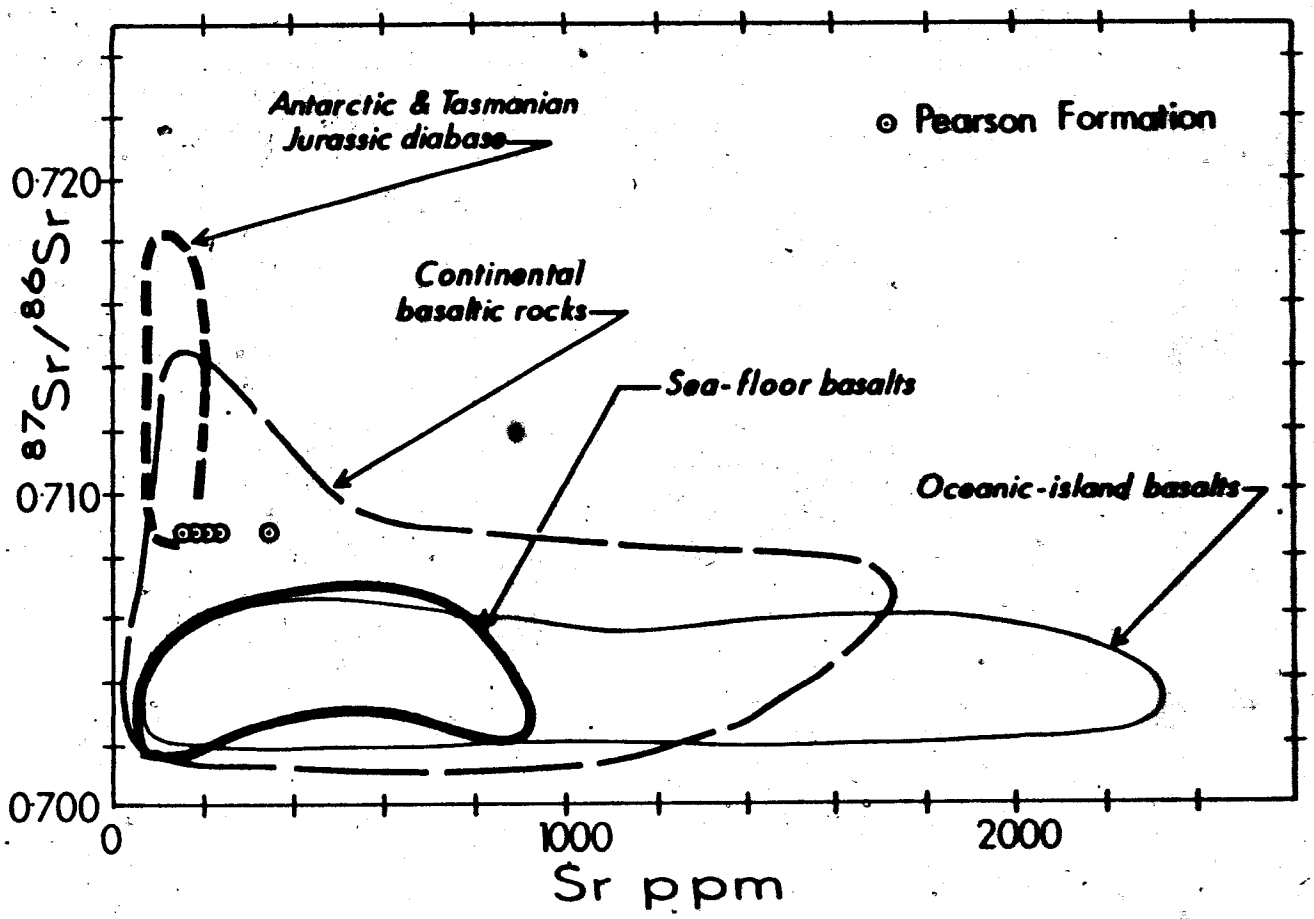
Antarctic & Tasmanian Jurassic diabase
Pearson Formation
Continental basaltic rocks
Sea-floor basalts
Oceanic-island basalts
0·720
0·710
0·700
$^{87}Sr/^{86}Sr$
0
1000
2000
Sr ppm

b

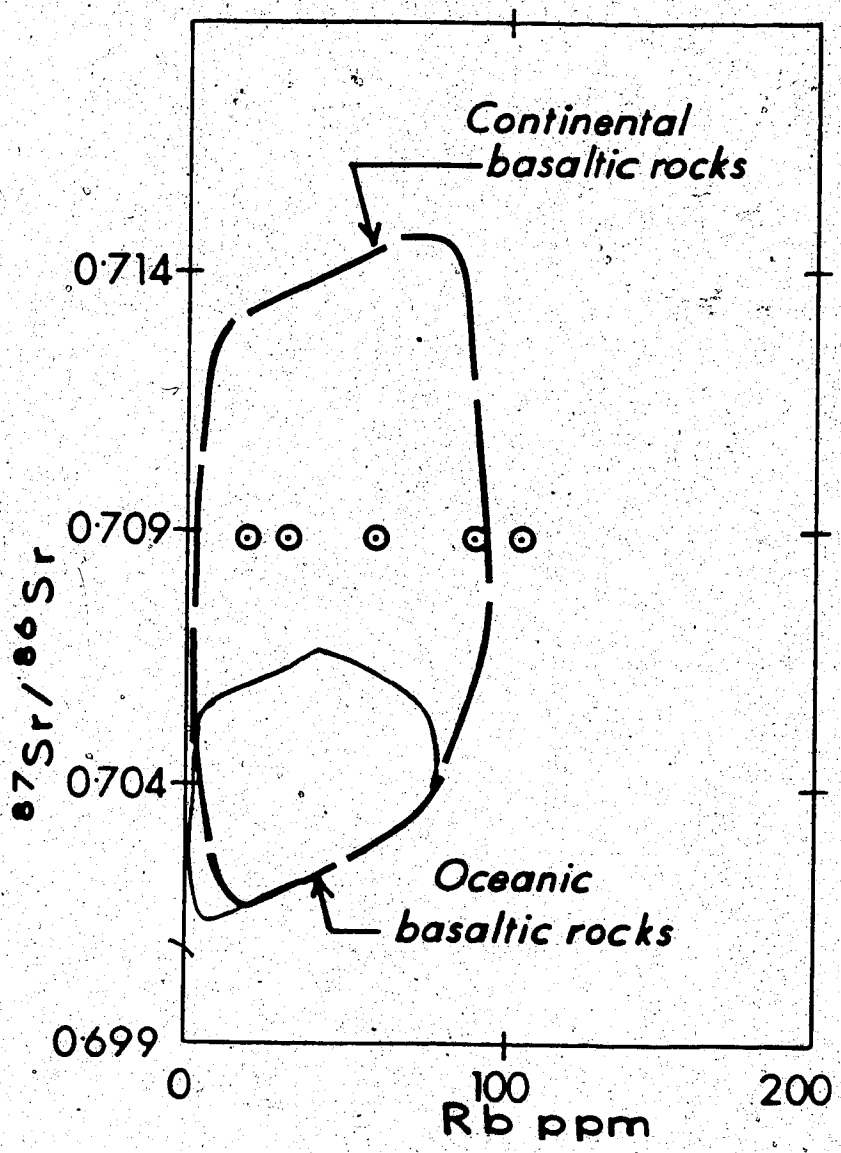

⊙ Pearson Formation

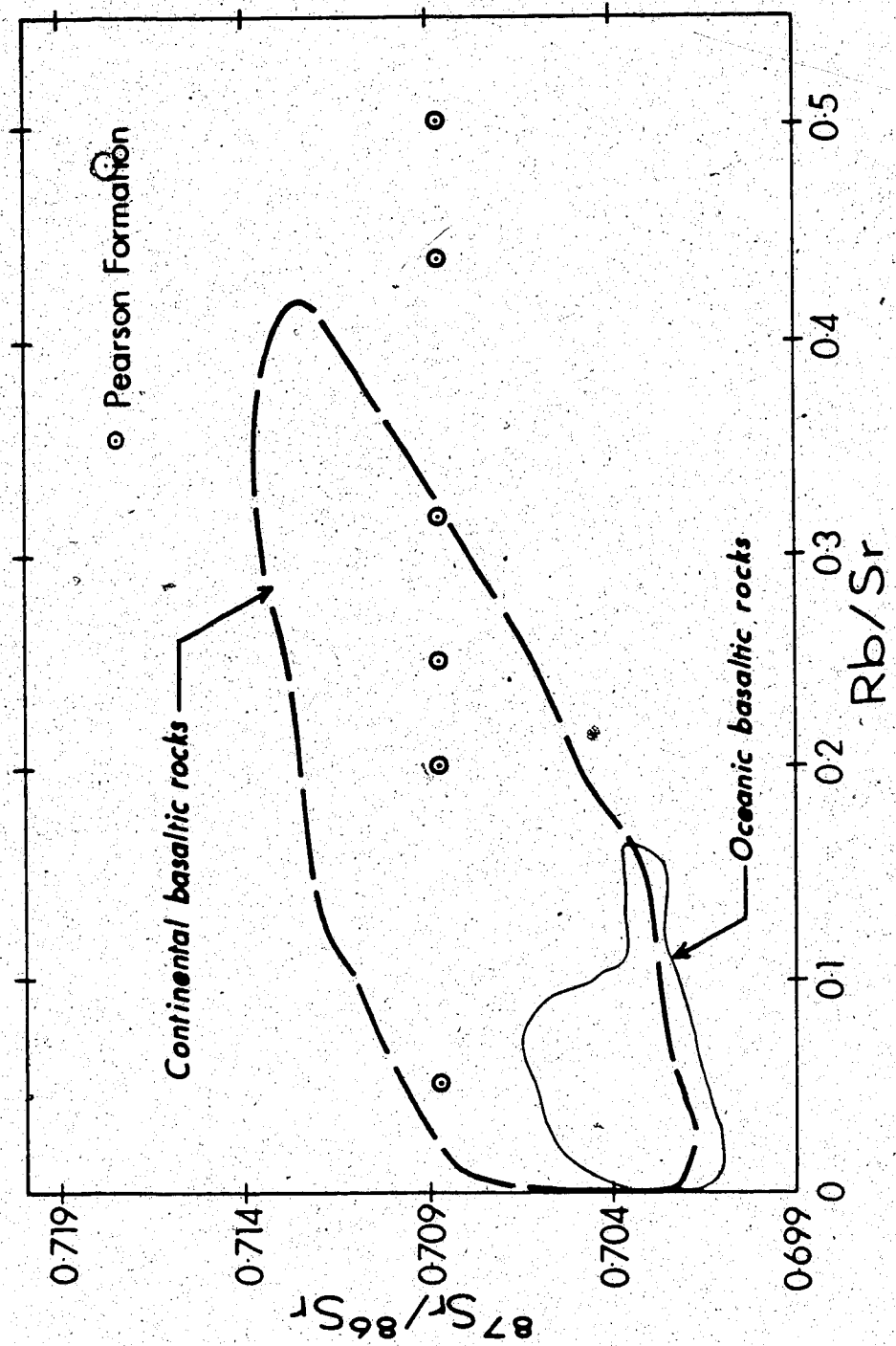
C
Pearson Formation
Continental basaltic rocks
Oceanic basaltic rocks
87Sr/86Sr
0·719
0·714
0·709
0·704
0·699
0
0·1
0·2
0·3
0·4
0·5
Rb/Sr

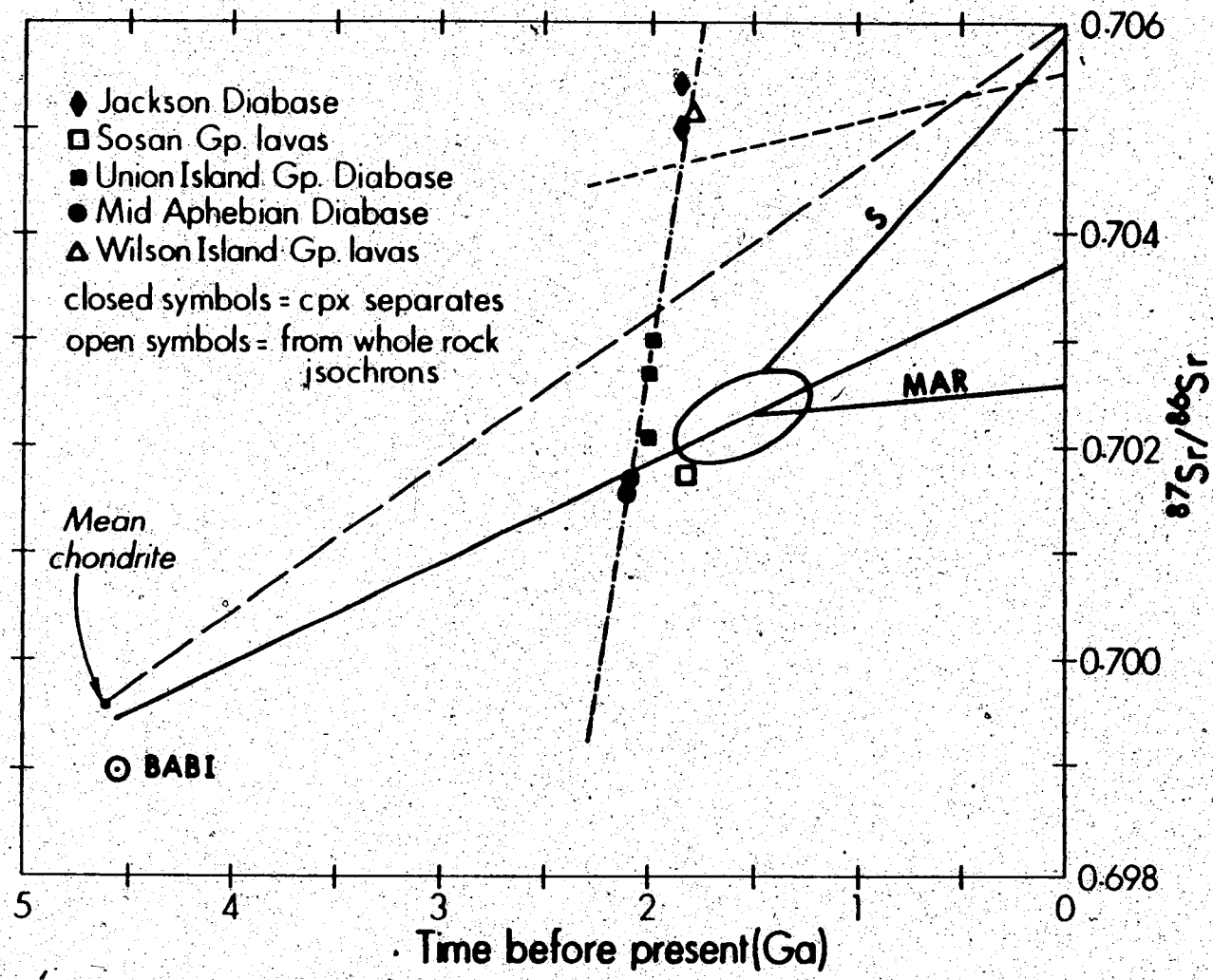
♦ Jackson Diabase
□ Sosan Gp. lavas
■ Union Island Gp. Diabase
● Mid Aphebian Diabase
△ Wilson Island Gp. lavas
closed symbols = cpx separates
open symbols = from whole rock isochrons
S
MAR
Mean chondrite
⊙ BABI
0.706
0.704
0.702
0.700
0.698
$^{87}Sr/^{86}Sr$
5
4
3
2
1
0
Time before present(Ga)

Table 1

Ref	Si	Ti	Al	$\frac{Fe^{3+}}{Fe^{2+}}$	Fe	Mn	Mg	Ca	Na	K	P	S	Li	B	Sc	V	Cr	Co	Ni	Cu	Zn	Ga	Rb	Sr	Y	Zr	Nb	Cs	Ba	La-Sm	Gd-Lu	Hf	Pb	U	H_2O
Sea-Floor Weathering of Ocean-Floor Basalts																																			
1. HFe;D		+			+		−	−	−	+																									+
2. P;C,D		S								+													+	−	S	S	S									
3. P;C	−	~S		+	+	−	−	−	−	+			+	+	S	S	(-)	S	(-)	+			+	+	S	S		+	+	−	(-)	S	+	+	+
4. NO;Al	−	+ S +		+	+	+ + −	−	−	+ S +	+ S +	+																								+
5. P;D																+	−	−	−				+	+		+		+							
6. P;D										+													+					+							
7. P;D	−	(-)	−	+	+	+	±	−	±		~S	−		+		(-)	S	S	±	±	S	−	+	(-)	S	(-)	S	+	±						+
8. P;D					+			−		+													+					+							+
9. P;D	−	(-)	−	+	+	+	±		−	+	S																									+
10. P;C																														+	S					
11. P;Vol	−	(+)	+	+	−	(-)	−	−	(-)	+	(+)																									+
12. P;D					+	−		−	−	+																									
13. FeCaMg;D																(-)	(-)	(-)	−	−		(-)						±	+	+					
14. P;D										+													+	S				−							
15. P;D	−			(+)	−		−		(+)	+	(+)	−					−						#	(+)											+
16. DW.<50°C							+	−	+	+																									
17. P;D	±	+	+	+	+	+	+	−	±	+	+																									+
18. NO;D	−	+			+		+	+ ±		+																									
19. P;D	−	~S	+	+	±	(S)	−	−	±	+			+	+	S	(-)	(-)		(-)	+			+	±	S	S			+	+		S	+	S	+
20. P;Vol.	−	−	−		−	−	−	−	−	+	+		+	+		S	S	S	S	+	+	S	+	S	S	S			+						+
21. P;D	−	±	±	+	±	±	−	−	±	+	(+)		+	+																						+

Table 1 (contin'd)

Ref	Si	Ti	Al	Fe^{3+}/Fe^{2+}	Fe	Mn	Mg	Ca	Na	K	P	S	Li	B	Sc	V	Cr	Co	Ni	Cu	Zn	Ga	Rb	Sr	Y	Zr	Nb	Cs	Ba	La-Sm	Gd-Lu	Hf	Pb	U	H_2O
Hydrothermal Alteration of Ocean-Floor Basalts																																		
Experimental Work																																		
0.5 kb/																																		
22. 200°	-				+/-	+/-	+	-	+	-		+							-	-														
.5-.8 kb/																																		
23. 200-500°	-		≈S		-	-	+	-	+/-	+/-										-													+
0.5 kb/																																		
24. 150-350°																														S	S			
-5-1 kb/																																		
25. 200-500°	-						+	-	+	-		+		-															-					
0.5-1 kb/																																		
26. >300°					-	-														-													
0.5 kb/																																		
27. 260°	-	+	S			-	+	-	-	-										-	-								-				
Zeolite																																		
28. D.W.							+	-		+																								
29. H;Av.	+/-			+					+																									
30. P;D	-	+	-		+		-	-	-	+																								+
Greenschist																																		
31. P;Av.	+	S	-		+			(-)	(+)		≈S													-										+
2. P;C,D		S								-													-	-	S	S	S							
32. P;D																														S	S			+
33. P;D																							+							≈S	S			
34. P;Al,D	-	S	≈S	+/-	+/-	+/-	+	-	+/-	+/-	+/-		+/-	+/-		S	S	≈S	≈S	-	-			-	S	S			≈S					+
29. P;D	+/-				+/-			-																										+
35. P;Av	+/-	S	S	+			+/-	-	-	-	S		+			(-)	-	(-)	≈S	+	+/-	S		+		(-)			≈S					+

Table 1 (contin'd)

Ref	Si	Ti	Al	Fe^{3+} / Fe^{2+}	Fe	Mn	Mg	Ca	Na	K	P	S	Li	B	Sc	V	Cr	Co	Ni	Cu	Zn	Ga	Rb	Sr	Y	Zr	Nb	Cs	Ba	La-Sm	Gd-Lu	Hf	Pb	U	H_2O
36. P;Av	±	≈S	≈S	+	±	≈S	±	-	+	-	≈S																								+
37. P;D								-	+																										+
Amphibolite																																			
2. P;C,D		S								-													-		S	S	S							
Alteration of Terrestrial Basalts																																			
Weathering																																			
38. P;OFB																														+	S				
Zeolite																																			
33. P;D																														S	S				
39. P;OFB																														+	S				
40. P;D																														S	S				
41. P;C	±	S					±			±													±	±	S	S	S			±		S			
Pumpellyite-Prehnite and Greenschist																																			
42. P;C	±	S			±		±	±	±	±	S						S		S					±	S				±						
40. H;D	-	S	-	+		+		-	-	S	S						S		S				≈S	S	S				S						
43. cbt;D		+	-		-		-	-							-		-	S	S	-	+	+		-	+	S	+	-	-	+	S	S		-	+
43. ep;D		-	+			-	+	-	-	-	-				S		S	-	-	+	-	+	○	-	+	±	+	-	-	-	S	S	S		+	
44. H;D							-	±	±			S					S	S	S	-				±	-											
45. H;D		S	±				-	-	±		S													±												

Table 1 (contin'd)

Ref	Si	Ti	Al	Fe^{3+}/Fe^{2+}	Fe	Mn	Mg	Ca	Na	K	P	S	Li	B	Sc	V	Cr	Co	Ni	Cu	Zn	Ga	Rb	Sr	Y	Zr	Nb	Cs	Ba	La-Sm	Gd-Lu	Hf	Pb	U	H_2O
46. P;D																														+	S				
47. P;C		S						S			S													±	S	S				±	≈S				
48. P;Al	-								-																										+
49. P;Ar	≈S	S	S		S	S	(-)	(+)	≈S	-	≈S																								+
50. Si;Al		≈S		-	-	S	-	-	+	-	≈S					-	(-)		-	-	-	≈S	≈S	+	≈S	(+)	≈S		(-)						-
51. P;Vol.	-		±	+			+	-	±	±																									+
Amphibolite																																			
52. P;C	-			+	-			-		+	+	-			S	(+)	+	(-)	S	±	-	S	+	±	S	(+)	S		±	S	S				+
53. P;D		S								-													-		S	S			-	S	S				
54. P;OFB																														±	S				

Fig. 7-1. Probable mineral hosts for elements of petrogenetic importance in altered basalts. Elements are listed in the order of relative concentration within each mineral. The number refers to the percentage of the whole-rock concentration of that element which is stored in that particular mineral phase.

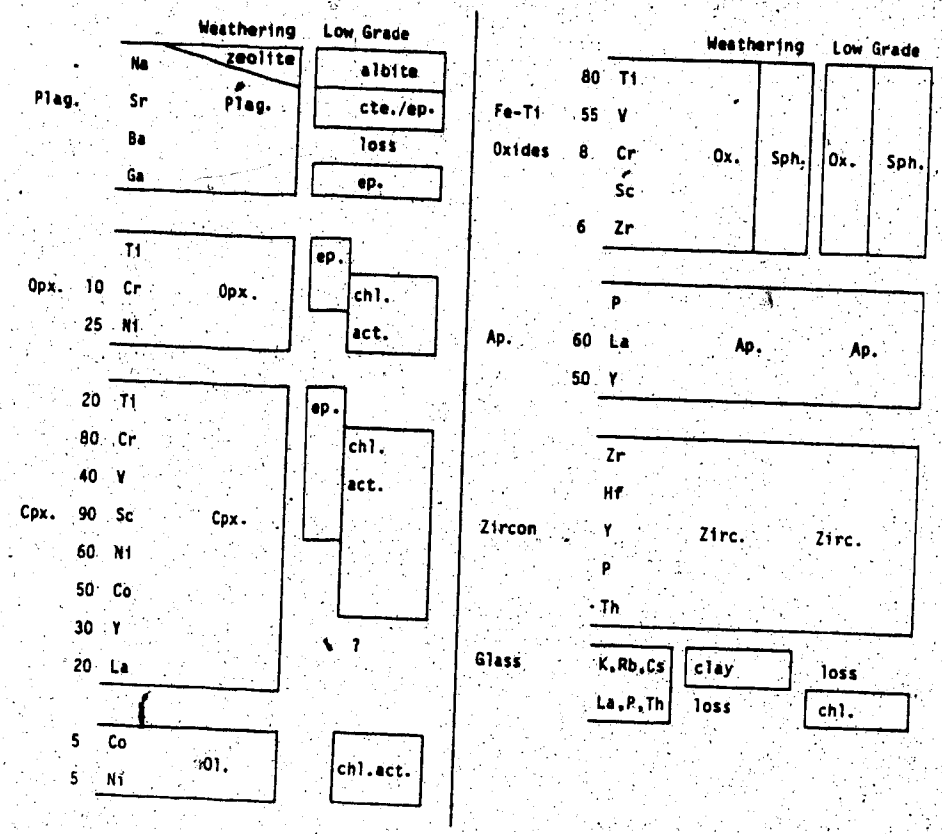

Fig. 8-1. Normative Ol - Ne - Q projection of Hawaiian alkaline volcanics, after Irvine and Baragar (1971). The heavy solid line is the alkaline/subalkaline divide suggested by Irvine and Baragar. Plots are in cation equivalents based on the cation norm.

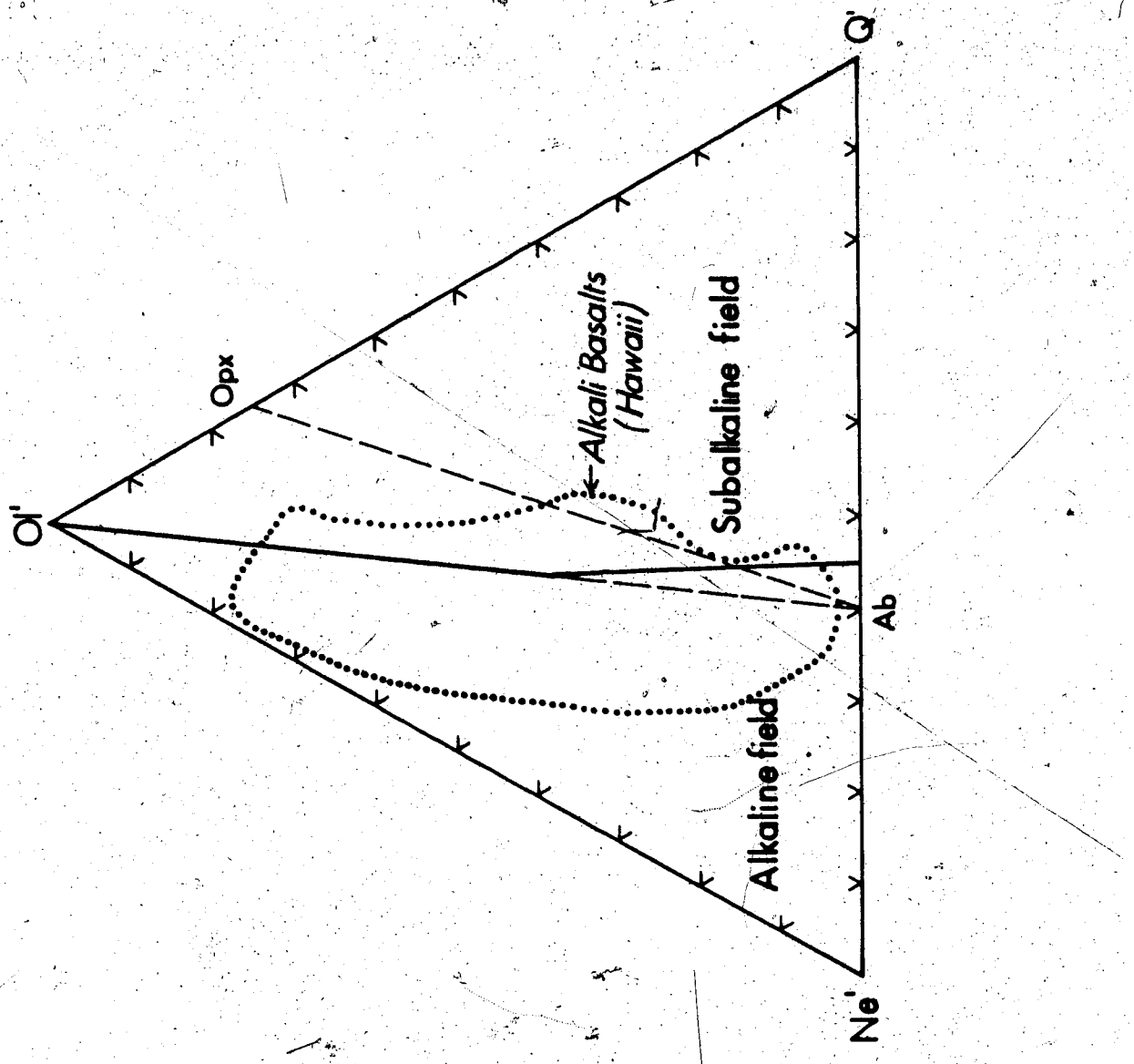

Fig. 8-2. Nb/Y - Zr/P_2O_5 diagram showing the field for transitional basalt suites, after de Albuquerque (1979).

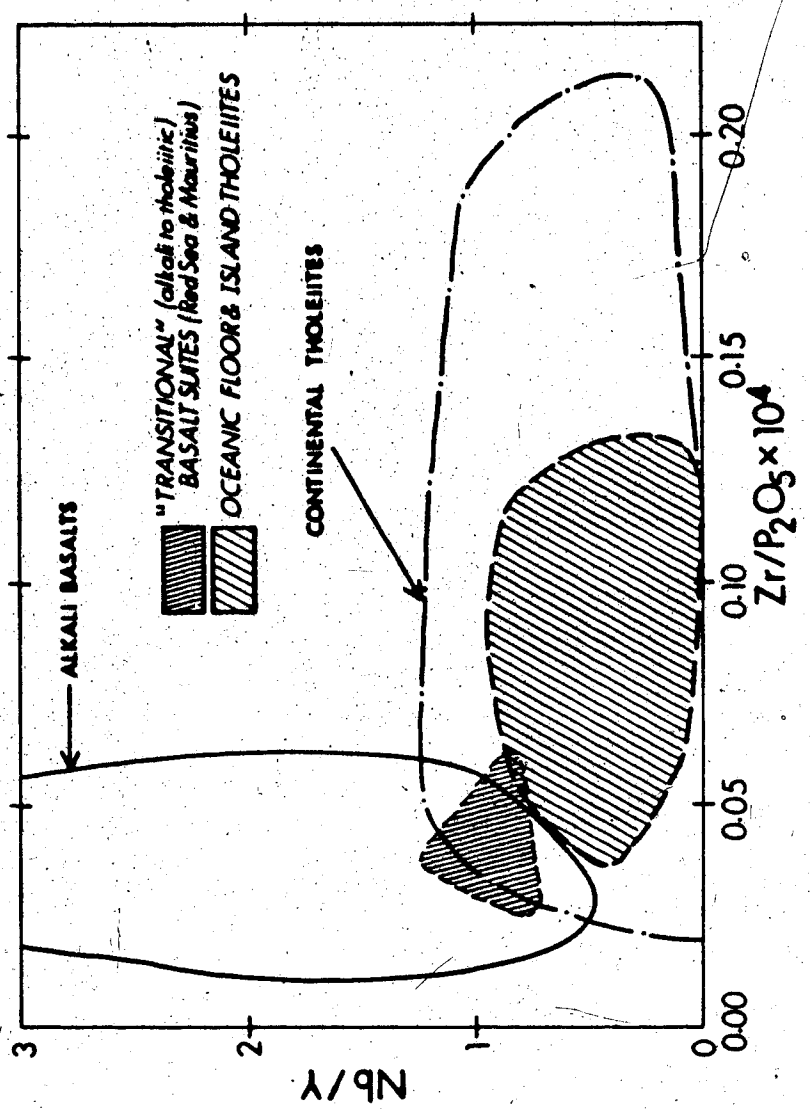

Fig. 8-3. TiO_2 - Zr/P_2O_5 diagram after Morrison (1978) showing data points for transitional, continental Hebridean basalts.

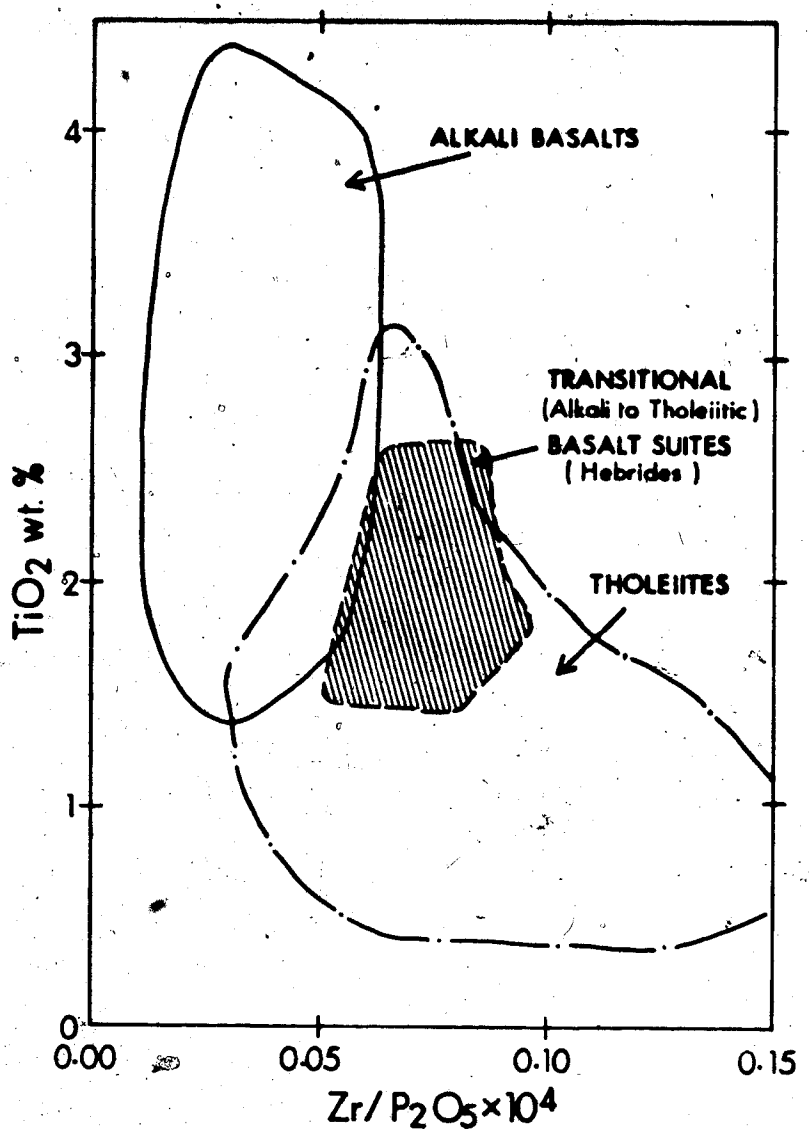

Fig. 8-4. Zr/TiO_2 - Nb/Y diagram showing the delimited fields for common volcanic rocks, from Winchester and Floyd (1977).

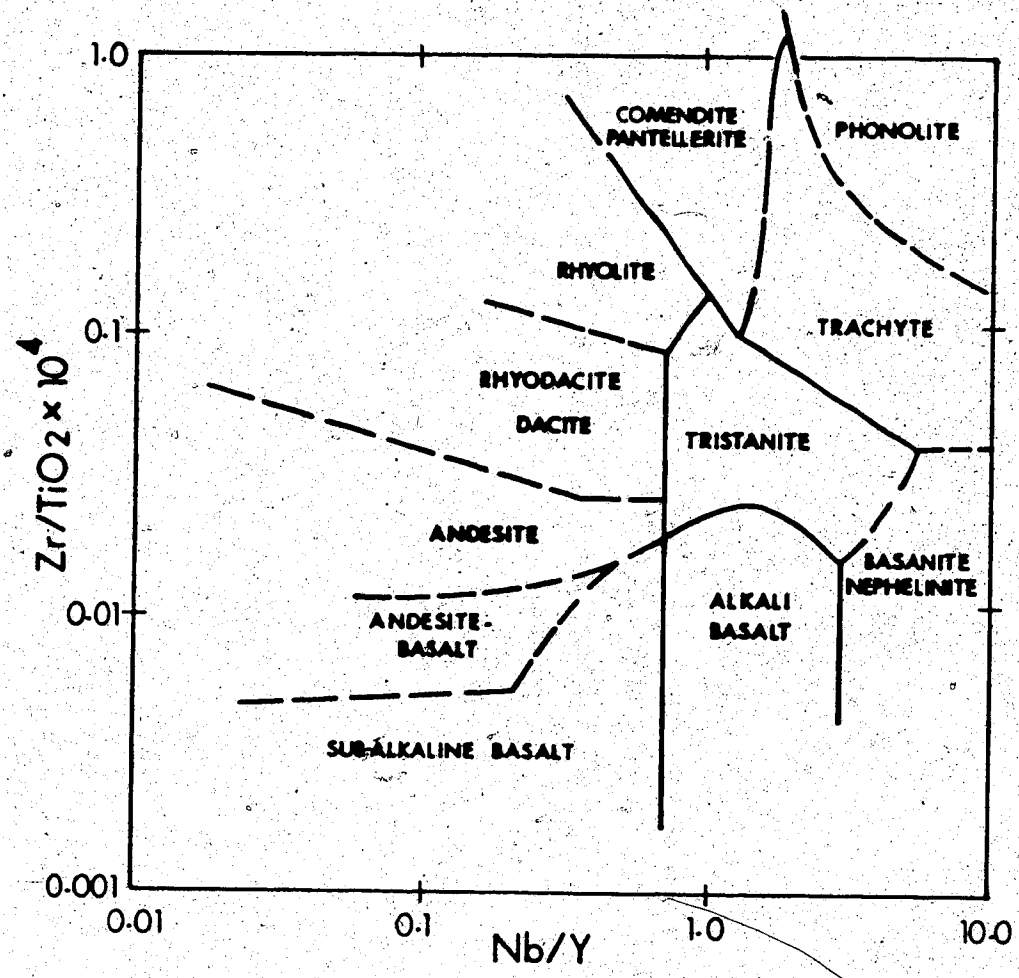

Fig. 8-5. Major element variation in average basalts from different tectonic environments.

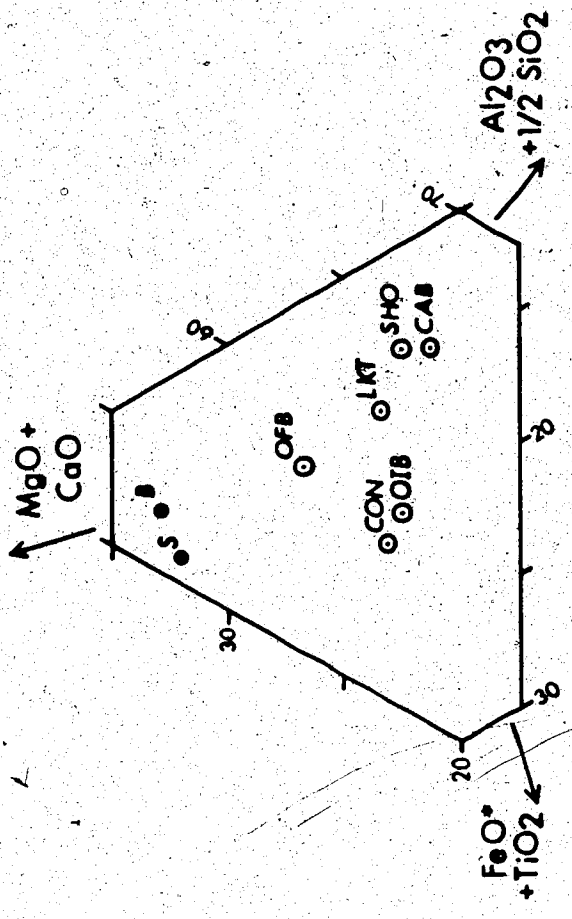

Fig. 8-6. MgO - FeO - Al_2O_3 diagram for basaltic andesites from different tectonic environments, from Pearce, Gorman and Birkett (1977).

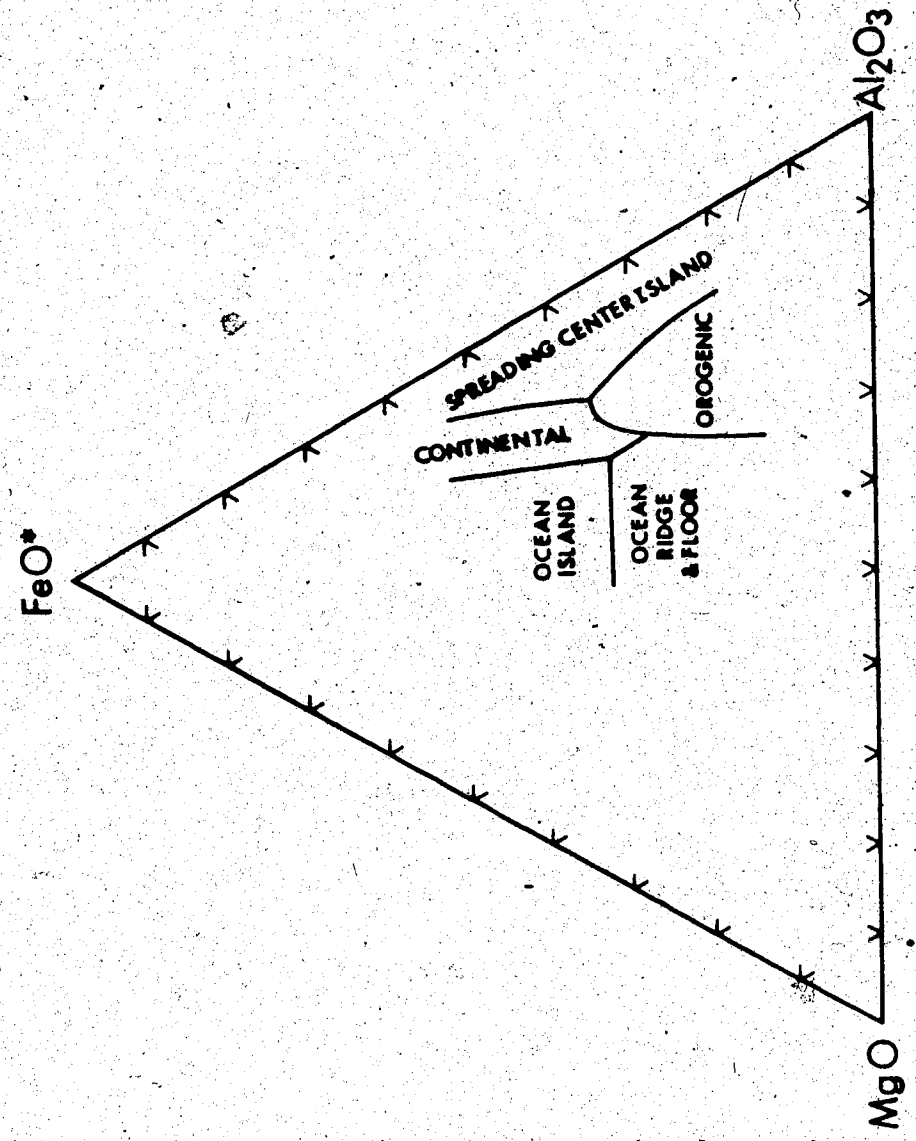

Fig. 8-7. Ti/100 - Zr - Y*3 diagram, after Pearce and Cann (1973).
This shows the similarity of some continental basalts (solid circle = Lesotho Karroo) to ocean floor basalts. Data from Cox and Hornung (1966). Fields: LKT = Low potassium tholeiite, CAB = calc-alkali basalt.

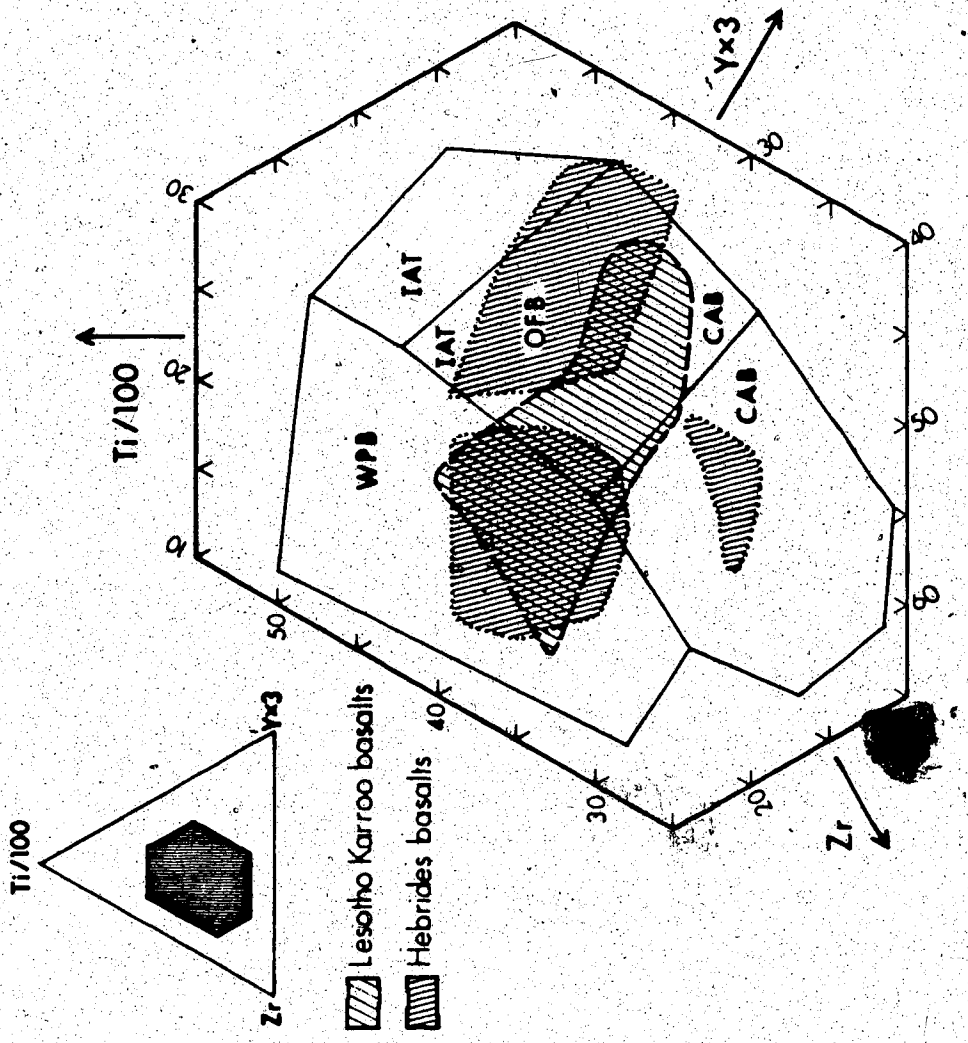

Fig. 8-8. Ti - Zr diagram, after Garcia (1979). Continental tholeiite suites are plotted showing how an incorrect tectonic environment can be suggested. Data are from Baffin Bay (Clarke, 1970), Lesotho Karroo (Cox and Hornung, 1966), Ferrar (Gunn, 1966), and Deccan (Vallance, 1974a).

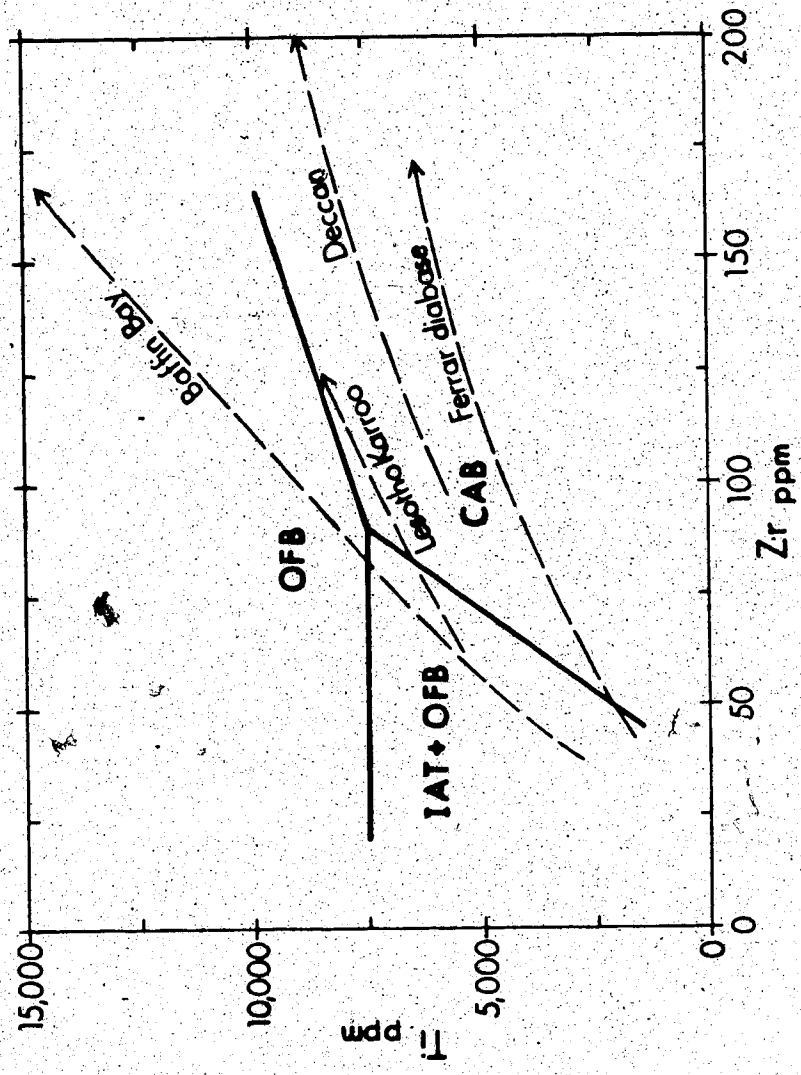

Fig. 8-9. Y + Zr - TiO_2*100 - Cr diagram for tholeiitic and calc-alkaline (CA) suites.

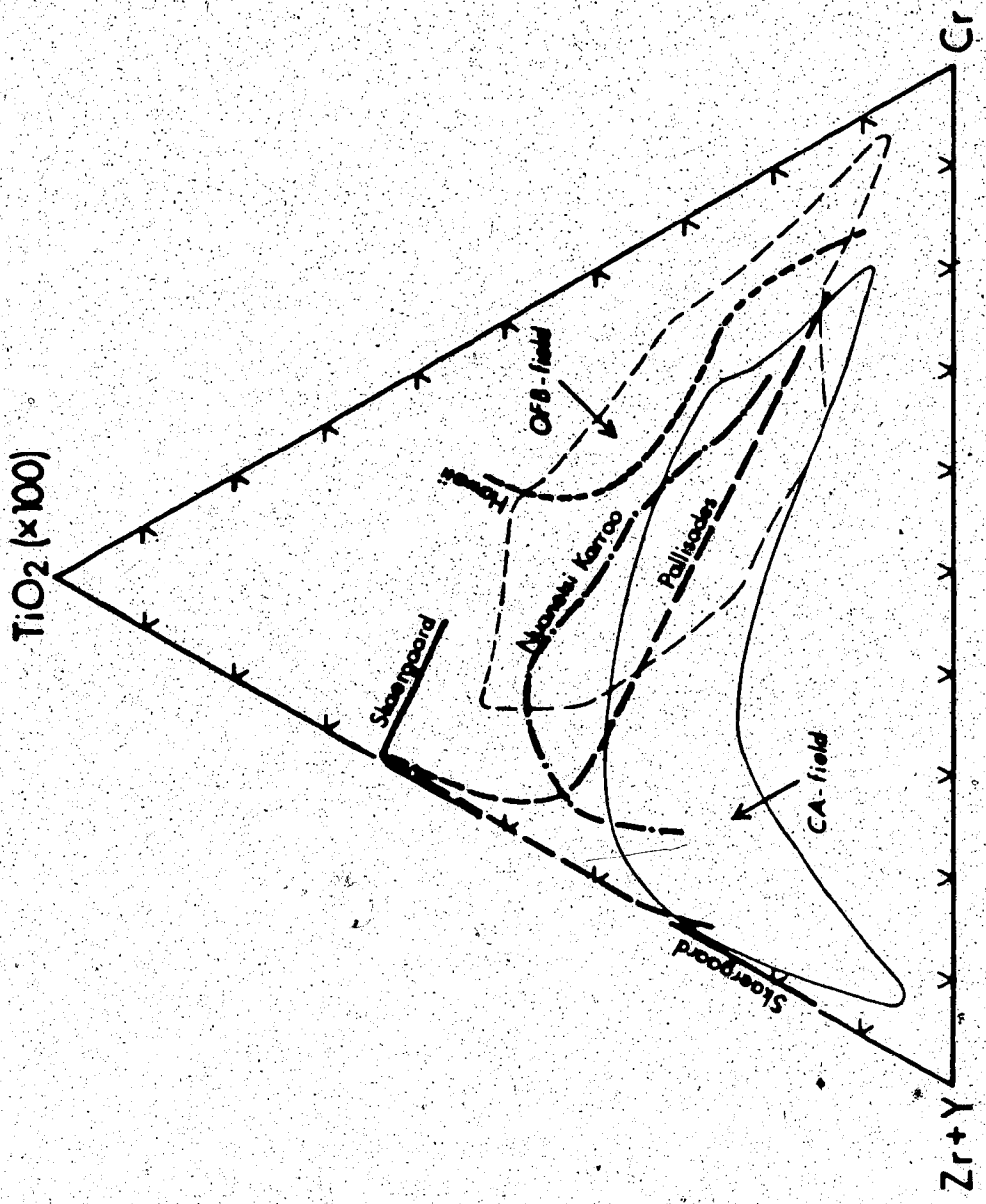

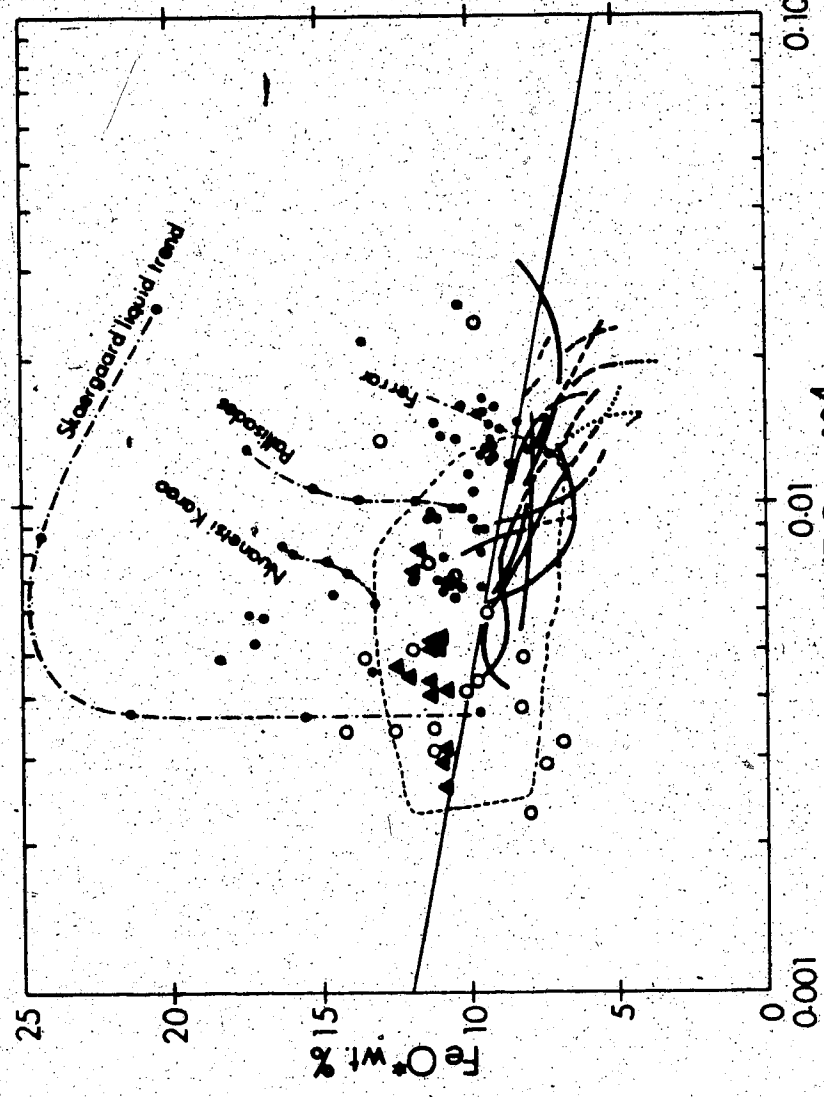
Skaergaard liquid trend
Fayalite
Ferrosilite
Nuanetsi Kamb
25
20
15
10
5
0
FeO* wt %
0.10
0.01
0.001
Zr/TiO2 × 10^4

Fig. 8-11. FeO(total) - Zr/TiO_2 diagram for tholeiitic and calc-alkaline suites showing usable discrimination fields.
CA = field of calc-alkaline differentiation trends; TH = field of continental tholeiites including the normal range of differentiation trends; IAT = field of island arc tholeiites; OFB = field of ocean floor tholeiites. Formula for TH/CA boundary curve: FeO* = $12.1-3.267\log(10^3.Zr/TiO_2.10^4)$.

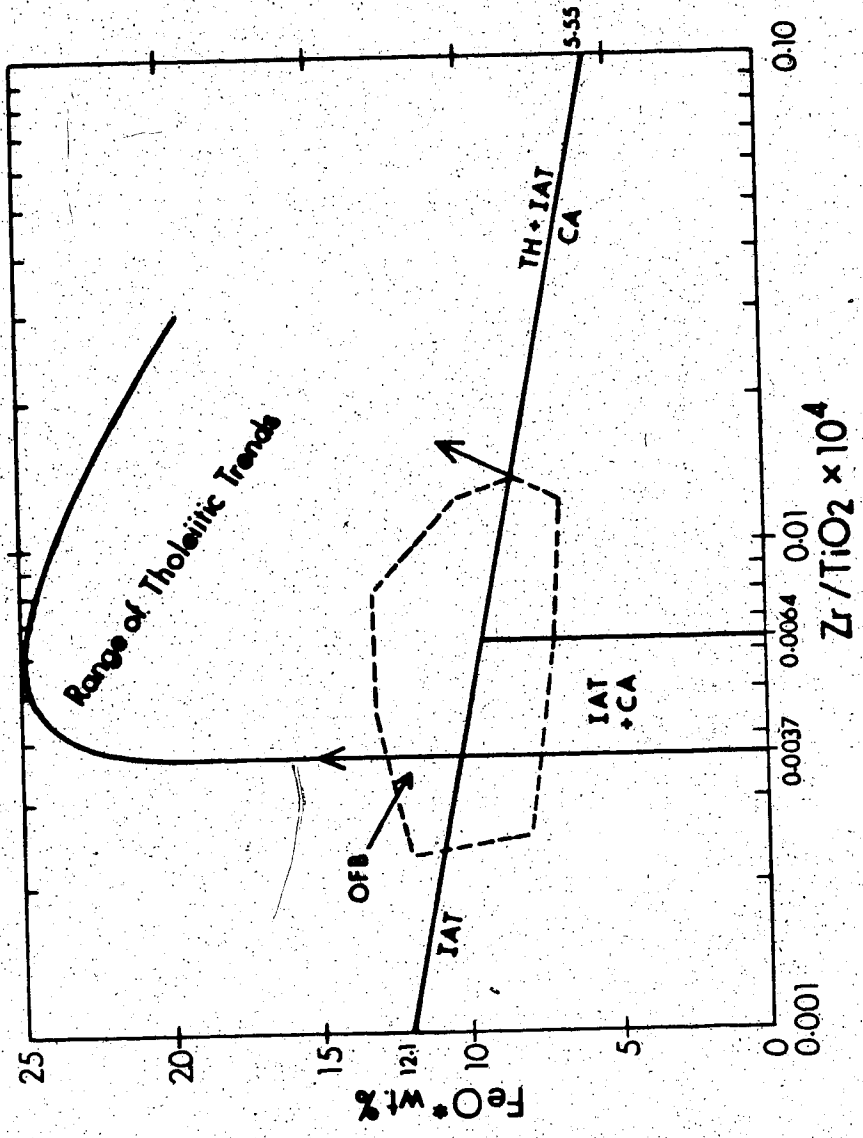

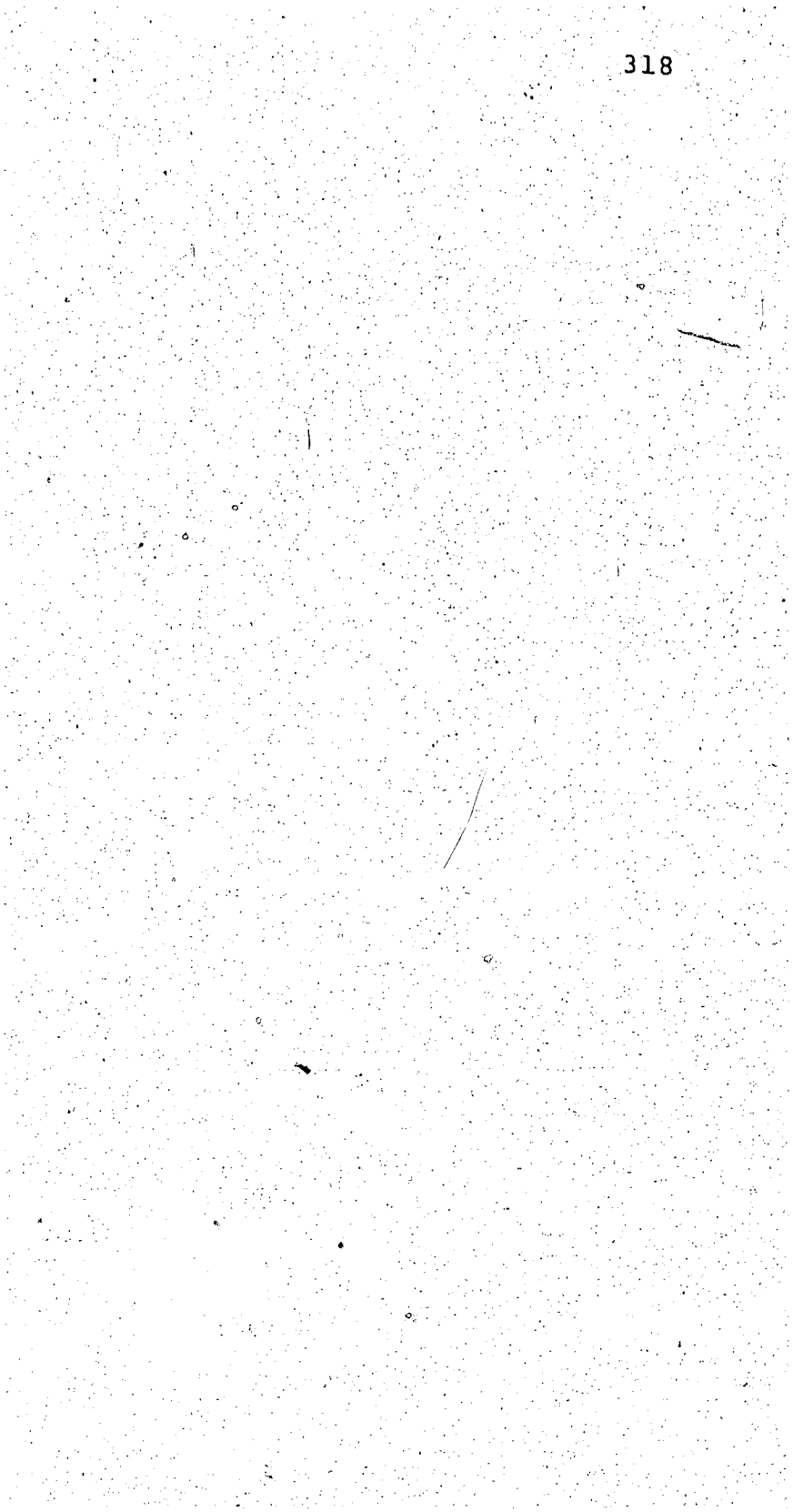

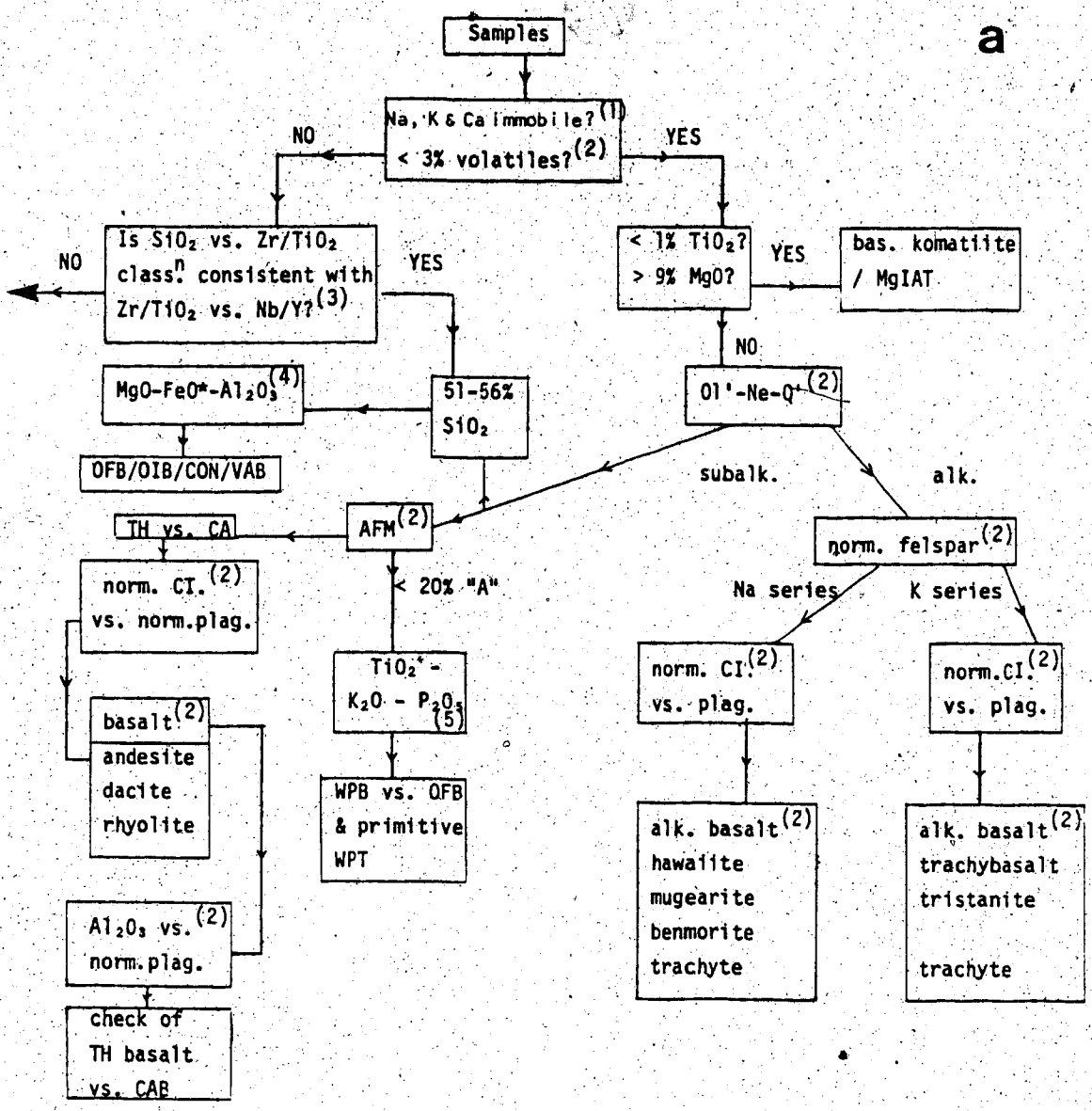
a
Samples
Na, K & Ca immobile? (1)
< 3% volatiles? (2)
NO
YES
Is SiO2 vs. Zr/TiO2 class.n consistent with Zr/TiO2 vs. Nb/Y? (3)
NO
YES
< 1% TiO2? > 9% MgO?
YES
bas. komatiite / MgIAT
NO
MgO-FeO*-Al2O3 (4)
51-56% SiO2
Ol'-Ne-Q' (2)
OFB/OIB/CON/VAB
subalk.
alk.
TH vs. CA
AFM (2)
norm. felspar (2)
norm. CI. (2) vs. norm.plag.
< 20% "A"
Na series
K series
TiO2* - K2O - P2O5 (5)
norm. CI. (2) vs. plag.
norm.CI. (2) vs. plag.
basalt (2)
andesite
dacite
rhyolite
WPB vs. OFB & primitive WPT
alk. basalt (2)
hawaiite
mugearite
benmorite
trachyte
alk. basalt (2)
trachybasalt
tristanite
trachyte
Al2O3 vs. (2) norm.plag.
check of TH basalt vs. CAB

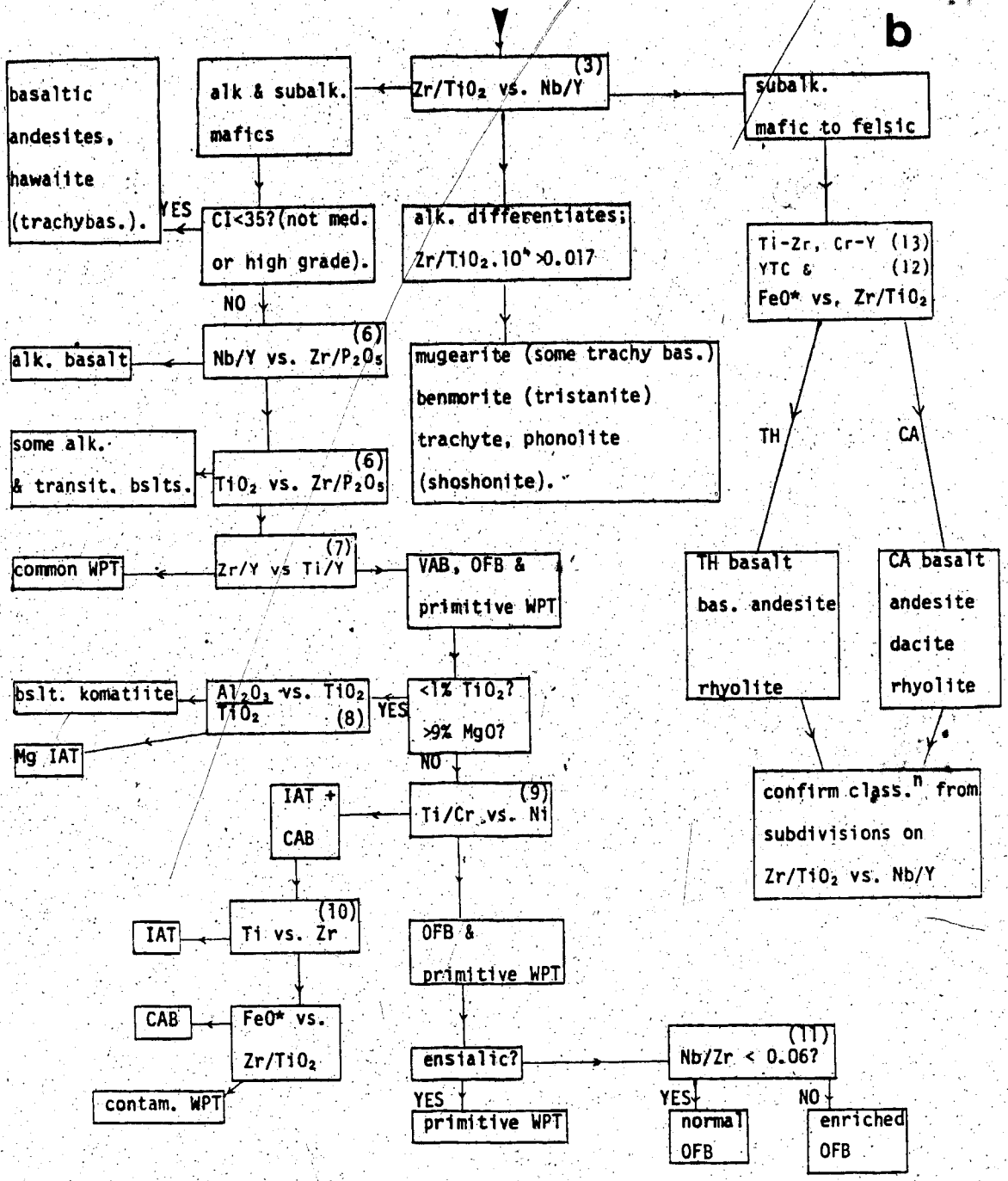
b
Zr/TiO2 vs. Nb/Y (3)
basaltic andesites, hawaiite (trachybas.).
alk & subalk. mafics
subalk. mafic to felsic
YES
Cl<35?(not med. or high grade).
alk. differentiates; Zr/TiO2.10^4 >0.017
Ti-Zr, Cr-Y (13) YTC & (12) FeO* vs. Zr/TiO2
NO
alk. basalt
Nb/Y vs. Zr/P2O5 (6)
mugearite (some trachy bas.) benmorite (tristanite) trachyte, phonolite (shoshonite).
TH
CA
some alk. & transit. bslts.
TiO2 vs. Zr/P2O5 (6)
common WPT
Zr/Y vs Ti/Y (7)
VAB, OFB & primitive WPT
TH basalt bas. andesite rhyolite
CA basalt andesite dacite rhyolite
bslt. komatiite
Al2O3 vs. TiO2 / TiO2 (8)
<1% TiO2? >9% MgO?
YES
Mg IAT
NO
confirm class.n from subdivisions on Zr/TiO2 vs. Nb/Y
IAT + CAB
Ti/Cr vs. Ni (9)
IAT
Ti vs. Zr (10)
OFB & primitive WPT
CAB
FeO* vs. Zr/TiO2
contam. WPT
ensialic?
Nb/Zr < 0.06? (11)
YES
NO
primitive WPT
normal OFB
enriched OFB

Fig. 9-1. Variation in the $CaSiO_3$-$MgSiO_3$-$FeSiO_3$ components in clinopyroxenes from Mid Aphebian diabase (MADM), Union Island Group basalts (UIG1M and UIG2M), Union Island Group diabase (UIGDM) and from the Pearson Formation (PEM).
Enclosed field indicates pyroxenes with a quench texture. The dashed line indicates the crystallization trend of the Skaergaard intrusion.

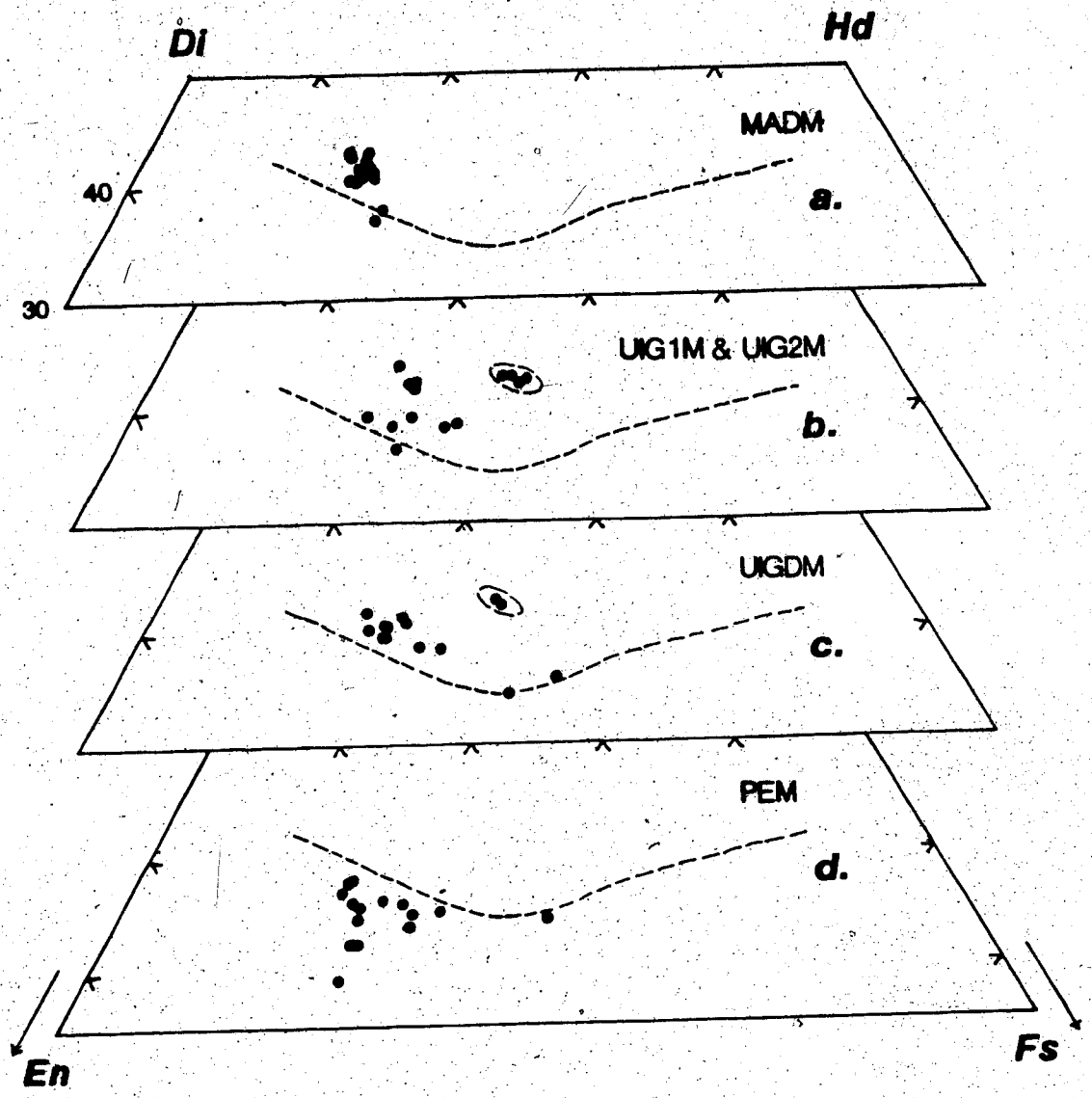

Fig. 9-2. Titanium variation in clinopyroxenes. See Fig. 9-1 for key to rock units. Enclosed fields indicate pyroxenes with a quench texture.

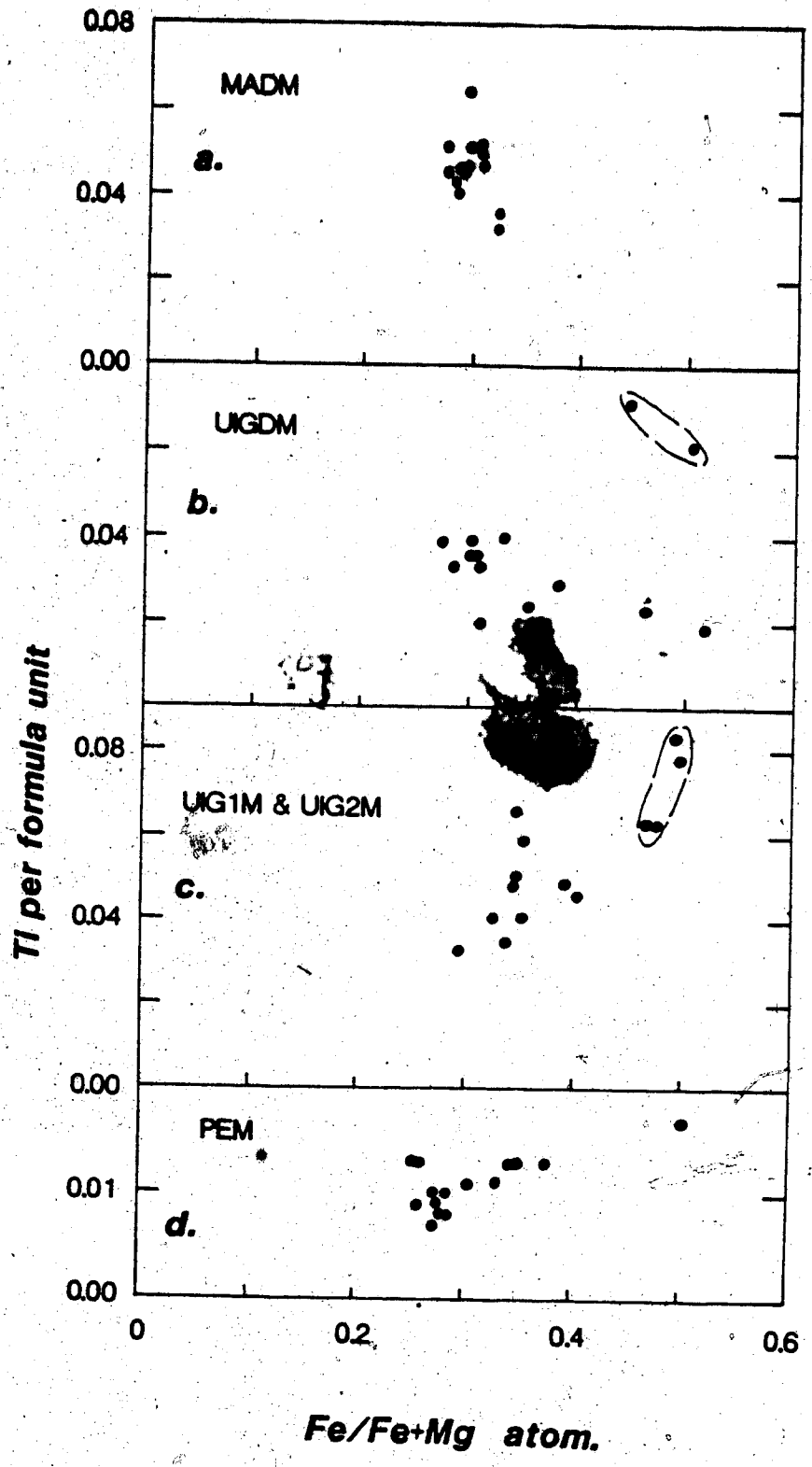

Fig. 9-3. Tectonic classification of clinopyroxenes using the discriminant-function routine of Nisbet and Pearce (1977).

The discriminant functions, F1 and F2 were described in Ch. 8 as was the magmatic classification. WPA is the field of within-plate alkali basalts. The field for ocean floor basalts (OFB) overlaps the fields for tholeiites from both volcanic arcs (VAB) and within-plate settings (WPT). Enclosed fields indicate pyroxenes with a quench texture. See Fig. 9-1 for key to rock units.

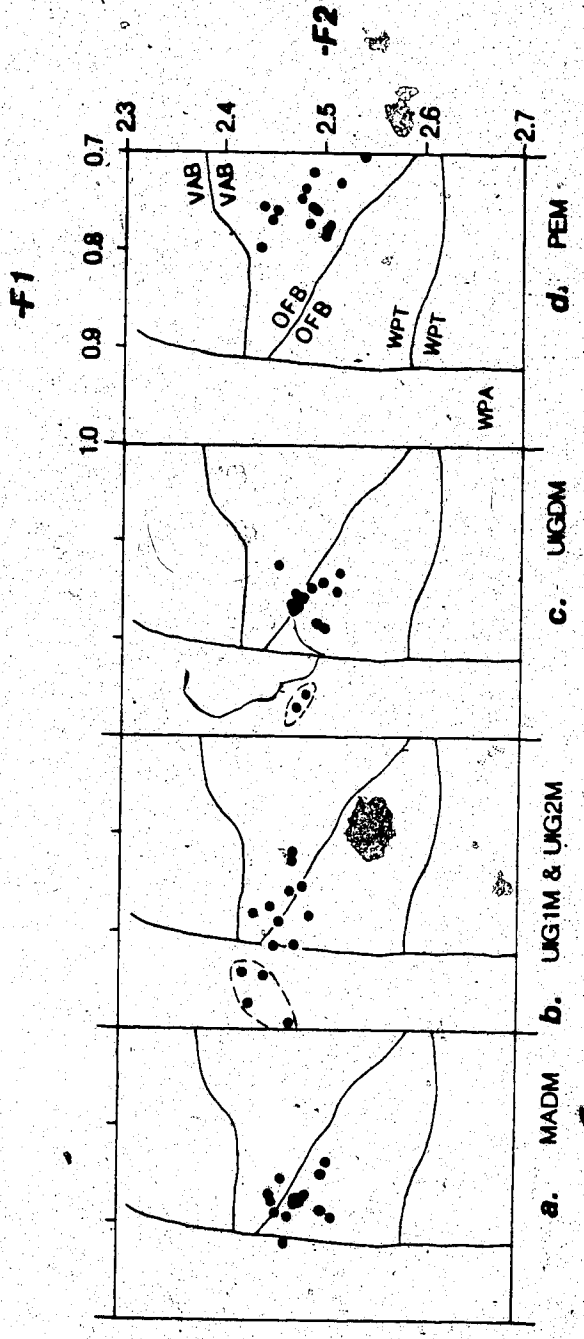

	WIGM	S.D.	WIGF	S.D.	UWIGM	S.D.
SiO_2	52.17	3.30	73.59	1.78	48.63	0.81
TiO_2	2.01	0.62	0.47	0.13	2.55	0.23
Al_2O_3	12.63	1.56	12.72	0.44	19.31	2.95
Fe_2O_3	3.53	0.34	0.90	0.27	2.49	0.26
FeO	11.18	1.07	2.84	0.85	7.89	0.82
MnO	0.35	0.06	0.03	0.02	0.13	0.07
MgO	6.57	1.89	0.61	0.31	7.00	1.17
CaO	6.18	2.07	0.50	0.42	5.06	3.61
Na_2O	2.81	1.03	4.48	1.79	4.54	0.50
K_2O	2.08	0.66	5.70	0.98	1.71	0.64
S	0.02	0.01	0.02	0.01	0.21	0.12
P_2O_5	0.48	0.26	0.07	0.05	0.59	0.13
H_2O^+	-	-	-	-	-	-
CO_2	-	-	-	-	-	-
Ba	583	307	1333	211	618	247
Nb	17	6	41	9	98	20
Zr	246	93	583	120	276	36
Y	43	11	75	21	25	1
Sr	107	45	57	31	140	32
Rb	67	26	138	29	59	34
Ga	-	-	-	-	-	-
Zn	284	104	25	27	121	8
Cu	56	18	7	21	89	11
Ni	28	9	7	4	79	31
Cr	58	59	11	9	208	60
V	278	45	-	-	-	-
Sc	46	6	-		-	-
M.I.	69		-		59	

	N. Simpson Island	S.D.	MADM	S.D.	UIGIM	S.D.
SiO_2	49.38	4.91	46.71	1.55	48.34	6.54
TiO_2	4.12	2.63	3.50	0.96	3.22	0.56
Al_2O_3	14.20	3.45	15.72	0.94	14.80	1.57
Fe_2O_3	3.47	4.21	3.65	0.33	3.85	0.97
FeO	10.98	4.21	11.57	1.06	12.19	3.07
MnO	0.20	0.11	0.21	0.06	0.19	0.05
MgO	5.99	3.88	7.93	2.01	6.53	1.67
CaO	4.89	1.90	5.88	2.21	6.97	2.85
Na_2O	3.74	1.44	[illegible]	0.51	2.28	1.24
K_2O	2.31	0.85	[illegible]	1.01	1.16	0.66
S	0.17	0.12	-	-	0.41	0.21
P_2O_5	0.55	0.19	0.34	0.12	0.34	0.09
H_2O^+	3.06	1.14	-	-	5.03	1.19
CO_2	3.81	3.07	-	-	3.94	1.86
Ba	831	772	236	342	296	189
[illegible]	140	41	18	6	52	17
[illegible]	476	203	169	45	330	93
[illegible]	98	23	28	4	38	9
Sr	345	141	254	90	151	88
Rb	56	34	28	12	30	23
Ga	36	6	27	3	22	-
Zn	93	81	-	-	120	80
Cu	76	139	-	-	132	25
Ni	103	228	-	-	51	21
Cr	119	183	-	-	50	29
V	331	341	-	-	315	42
Sc	-	-	-	-	42	5
M.I.	71		66	-	71	

	UIGDM	S.D.	UIG2M	S.D.	SDGSI1M	S.D.
SiO_2	48.50	1.23	50.70	5.58	46.36	1.53
TiO_2	2.78	0.84	2.00	0.32	3.27	0.90
Al_2O_3	14.50	1.46	16.07	2.70	17.04	2.52
Fe_2O_3	3.55	0.34	2.99	0.99	3.74	0.42
FeO	11.26	1.08	9.48	3.15	11.84	1.34
MnO	0.22	0.05	0.17	0.04	0.11	0.07
MgO	7.06	1.44	6.49	2.69	6.47	2.92
CaO	8.12	1.50	7.47	3.21	4.29	3.93
Na_2O	2.54	0.81	3.24	1.65	4.18	1.53
K_2O	1.05	0.57	0.98	0.48	1.81	1.55
S	0.31	0.14	0.56	0.50	-	-
P_2O_5	0.35	0.12	0.17	0.08	0.89	0.54
H_2O^+	4.09	1.07	4.01	2.03	-	-
CO_2	2.64	3.04	1.95	1.70	-	-
Ba	274	148	331	287	314	301
Nb	25	5	5	3	65	18
Zr	178	36	110	5	205	64
Y	27	4	18	3	32	17
Sr	353	101	320	192	190	210
Rb	32	20	36	21	47	40
Ga	23	3	19	1	22	5
Zn	108	16	110	54	-	-
Cu	101	25	66	40	-	-
Ni	-	-	96	12	78	56
Cr	-	-	334	30	358	294
V	-	-	298	15	233	105
Sc	-	-	34	6	37	1
M.I.	68		66		71	

	SOGSI2M	S.D.	SOGSI3I	S.D.	SOGSIF	S.D.
SiO_2	46.16	2.94	56.65	3.11	67.41	3.54
TiO_2	4.09	0.82	1.77	0.60	0.44	0.13
Al_2O_3	17.27	0.78	16.66	1.06	15.71	1.63
Fe_2O_3	4.16	0.46	2.69	0.80	1.17	0.85
FeO	13.19	1.44	8.51	2.54	3.72	2.05
MnO	0.13	0.05	0.14	0.23	0.09	0.07
MgO	5.75	1.56	3.65	1.69	1.35	1.65
CaO	1.87	1.39	1.50	1.63	0.94	0.92
Na_2O	4.03	1.84	3.86	2.06	5.51	3.22
K_2O	2.80	2.37	3.95	2.14	3.61	2.36
S	-	-	0.04	0.02	0.02	0.01
P_2O_5	0.54	0.20	0.61	0.32	0.06	0.04
H_2O^+	-	-	-	-	-	-
CO_2	-	-	-	-	-	-
Ba	504	338	604	525	288	201
Nb	35	7	72	17	162	101
Zr	223	87	481	111	857	466
Y	24	9	40	11	67	32
Sr	126	125	49	53	30	10
Rb	44	36	85	50	63	50
Ga	29	3	27	4	-	-
Zn	-	-	88	12	21	26
Cu	-	-	68	31	81	33
Ni	59	13	21	10	8	4
Cr	173	28	105	60	33	57
V	310	46	37	56	-	-
Sc	-	-	25	5	-	-
M.I.	75		75		-	

	SOGTNM	S.D.	SOGTNF	S.D.	KAGPPM	S.D.
SiO_2	49.12	3.41	72.36	4.49	53.38	6.45
TiO_2	2.76	0.65	0.68	0.98	1.91	0.36
Al_2O_3	15.84	1.15	13.33	1.54	17.05	3.30
Fe_2O_3	3.32	0.43	1.21	0.54	2.30	0.91
FeO	10.53	1.37	3.82	1.70	7.28	2.88
MnO	0.18	0.07	0.04	0.05	0.35	1.03
MgO	7.09	2.62	0.61	0.47	6.48	2.88
CaO	5.23	2.99	0.52	0.74	5.32	4.73
Na_2O	2.67	1.33	1.10	2.47	4.46	1.51
K_2O	2.87	2.39	6.24	2.39	1.33	1.17
S	-	-	0.02	0.01	0.10	0.06
P_2O_5	0.40	0.12	0.08	0.15	0.26	0.14
H_2O^+	3.46	1.03	-	-	3.24	1.62
CO_2	3.70	2.65	-	-	5.19	3.73
Ba	377	275	129	96	143	130
Nb	35	6	115	28	40	22
Zr	170	50	916	308	117	47
Y	21	4	81	22	18	5
Sr	276	200	13	14	59	45
Rb	39	21	143	52	39	40
Ga	23	4	-	-	-	-
Zn	-	-	9	6	94	122
Cu	-	-	105	27	67	51
Ni	107	85	9	3	145	81
Cr	264	237	46	91	306	94
V	241	53	-	-	184	55
Sc	32	7	-	-	29	7
M.I.	66		-	-	60	

	KAGPPF	S.D.	KAGTNM	S.D.	JAGPPM	S.D.
SiO_2	73.84	1.28	48.28	2.91	54.38	3.38
TiO_2	0.01	0.00	1.88	0.91	1.44	0.51
Al_2O_3	14.03	1.22	15.95	0.43	17.08	2.45
Fe_2O_3	0.27	0.01	3.26	0.70	2.35	0.11
FeO	0.84	0.04	10.34	2.20	7.46	0.35
MnO	0.02	0.01	0.29	0.18	0.12	0.07
MgO	0.79	0.07	6.11	1.64	7.29	2.25
CaO	1.96	0.28	8.58	3.62	4.51	2.42
Na_2O	0.64	0.71	3.31	1.04	3.93	1.02
K_2O	7.58	0.89	1.65	1.38	1.20	0.96
S	0.04	0.02	-	-	0.06	0.05
P_2O_5	0.01	0.00	0.33	0.05	0.20	0.35
H_2O^+	-	-	3.25	0.68	3.60	1.00
CO_2	-	-	6.89	2.92	0.40	0.21
Ba	415	256	111	106	100	36
Nb	130	10	30	6	38	53
Zr	64	17	113	20	119	133
Y	49	32	23	3	19	7
Sr	13	2	121	127	193	89
Rb	528	205	42	43	43	44
Ga	-	-	-	-	10	12
Zn	22	13	-	-	23	31
Cu	61	18	-	-	101	109
Ni	26	17	182	53	-	-
Cr	104	148	441	108	-	-
V	-	-	189	17	-	-
Sc	-	-	39	7	-	-
M.I.	-		69		57	

	JAGINM	S.D.	PEM	S.D.	Quartz Diorite	S.D.
SiO_2	47.08	4.77	55.34	1.30	63.80	4.16
TiO_2	3.39	1.04	0.95	0.06	0.66	0.11
Al_2O_3	15.64	1.63	15.19	0.57	18.25	0.85
Fe_2O_3	3.74	0.85	2.50	0.19	1.06	2.14
FeO	11.85	2.70	7.92	0.59	3.36	2.14
MnO	0.22	0.07	0.18	0.04	0.06	0.03
MgO	6.27	1.67	6.78	1.47	2.87	1.01
CaO	6.69	2.54	5.78	1.19	3.18	1.41
Na_2O	3.17	0.99	3.18	0.96	3.79	1.71
K_2O	1.58	0.81	2.04	0.73	2.98	1.65
S	-	-	0.26	0.05	-	-
P_2O_5	0.42	0.08	0.11	0.02	-	-
H_2O^+	3.27	1.14	2.86	0.80	1.78	1.95
CO_2	3.14	2.67	0.40	0.46	-	-
Ba	252	234	519	190	608	470
Nb	35	9	8	4	15	4
Zr	200	70	147	12	206	50
Y	24	5	25	3	37	20
Sr	372	274	238	67	137	72
Rb	29	15	59	30	97	67
Ga	19	13	18	1	17	5
Zn	18	48	123	46	44	36
Cu	-	-	155	107	8	7
Ni	-	-	92	18	32	35
Cr	-	-	9	8	33	19
V	-	-	214	14	-	-
Sc	-	-	32	5	-	-
M.I.	71		61		-	

	ETGM	S.D.
SiO_2	53.00	1.99
TiO_2	1.54	0.21
Al_2O_3	15.50	1.25
Fe_2O_3	2.96	0.32
FeO	9.39	1.02
MnO	0.23	0.05
MgO	6.38	0.76
CaO	6.31	2.34
Na_2O	3.06	1.00
K_2O	1.50	0.72
S	-	-
P_2O_5	0.14	0.11
H_2O^+	-	-
CO_2	-	-
Ba	570	352
Nb	4	5
Zr	99	31
Y	23	3
Sr	338	105
Rb	38	20
Ga	21	2
Zn	-	-
Cu	-	-
Ni	62	10
Cr	159	14
V	185	20
Sc	36	1
M.I.	.66	

Class[n] Type	Discrimination Technique	Valid Magma Types	WIG M	WIG F	UWIG M	MAD M	UIG1 M	UIG2 M	UIGD M	SOGSI1 SOGSI2 & SOGTN M	SOGSI3 I	SOGSI F	SOGTN F
MAGMATIC	Zr/Nb	MIF	SA	SA	A	TRN	TRN	SA-TRN	TRN	A	A	A	A
	Zr/TiO_2-Nb/Y	MIF	SAB-BA	SAR	BN	TRNB	AB	SAB-TRNB	TRNB	AB	TRAB-TRI	(TRA)	AR
	SiO_2-Nb/Y	MIF	SAB-BA	SAR	BN	TRNB	AB	SAB-TRNB	TRNB	AB	TRAB-TRI	TRA-R	AR
	Nb/Y-Zr/P_2O_5	M	SA	-	A	SA-TRN	SA-TRN	SA	SA-TRN	A	-	-	-
	TiO_2-Zr/P_2O_5	M	SA-TRN	-	A	TRN-A	TRN	TRN	TRN-A	A	-	-	-
TECTONIC	Ti/Y-Zr/Y	M	WP-(VAB)	-	WP	WP	WP	WP	WP	WP	-	-	-
	TiO_2-Zr	MIF	WP	WP	WP	WP	WP	WP	WP	WP	WP	WP	WP
	Cr-Y	MIF	WP	-	WP	-	WP	WP-(VAB)	-	WP	-	-	-
	TiO_2-Cr	M	-	-	-	-	-	-	-	-	-	-	-
	Ti/Cr-Ni	MI	-	-	-	-	-	-	-	-	-	-	-
	Y + Zr-TiO_2-Cr	MI	-	-	-	-	-	-	-	-	-	-	-
	FeO*-Zr/TiO_2	MI	-	-	-	-	-	-	-	-	-	-	-
	K_2O-TiO_2-P_2O_5	M	CON	-	-	-	-	CON-(MORB)	--	-	-	-	-
	MgO-FeO*-Al_2O_3	BA	CON/OI	-	-	-	-	CON	-	-	-	-	-

Class[n] Type	Discrimination Technique	Valid Magma Types	KAGPP M	KAGPP F	JAGPP M	KAGTN M	JAGTN M	PEM	ETGM
MAGMATIC	Zr/Nb	MIF	A	A	TRN	A	A	SA	SA
	Zr/TiO_2-Nb/Y	MIF	BN-TRAB	(PH)	AB	AB-TRAB	AB-TRAB	SAB-BA	SAB-BA
	SiO_2-Nb/Y	MIF	BN-(TRA)	AR	(BN-TRI)	AB-TRAB	AB	SAB-BA	SAB-BA
	Nb/Y-Zr/P_2O_5	M	A	-	A-TRN	A	A-TRN	SA	SA
	TiO -Zr/P_2O_5	M	A-TRN	-	TRN	A-TRN	A-TRN	SA	SA
TECTONIC	Ti/Y-Zr/Y	M	WP	-	WP	WP	WP	VAB	WP
	TiO_2-Zr	MIF	WP	?	WP-(VAB)	WP	WP	VAB	WP-(MORB)
	Cr-Y	MIF	WP-(VAB)	-		WP	-	VAB	WP
	TiO_2-Cr	M	-	-	-	-	-	VAB	WP-(MORB)
	Ti/Cr-Ni	MI	-	-	-	-	-	WP-(MORB)	WP-(MORB)
	Y + Zr-TiO_2-Cr	MI	-	-	-	-	-	(CAB)	?
	FeO*-Zr/Ti	MI	-	-	-	-	-	TH	TH
	K_2O-TiO_2-P_2O_5	H	-	-	-	-	-	CON	-
	MgO-FeO*-Al_2O_3	BA	-	-	-	-	-	CON-VAB	CON

Igneous Unit	Mean Mafic Index	OL. (Ni)	PLAG. (Al/Ti)	CPX. (Cr/Sc)	ILM./ MGT. (V)	Total. Fractn. (Y, Zr)
WIGM	69	-	30	25-30	3	65
WIGF	-		30			30
MADM	66					30
UIGIM	71	10-15	35	10-15	2-3	60
UIG2M	66	5	10	2	1-2	15
UIGDM	68					60
SOGSI1M	71	10	35	10	3	50
SOGSIF	-		>40			70
SOGSI2M	75	5	25	5	2-3	40
SOGSI3I	-	-	30	25	-	55
SOGTNM	66	10	25	20	3	50
SOGTNF	-		25			25
KAGPPM	60	20	50	15-20	10-15	>85
KAGTNM	69	5-10	15	5	2	30
PEM	61	-	10	15-20	1-2	20
ETGM	66	5-10	10	5	2-3	20

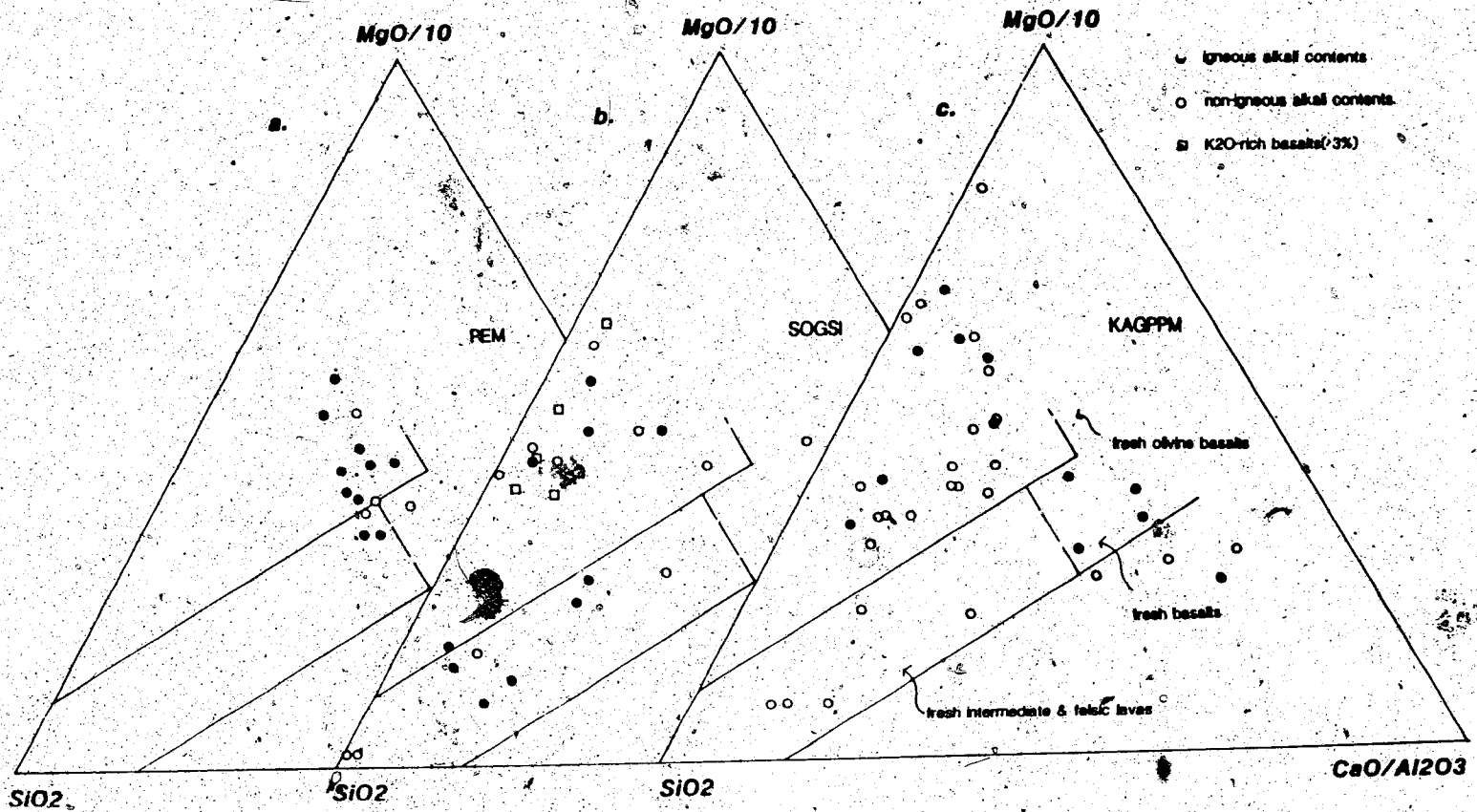
MgO/10
a.
REM
SiO2
MgO/10
b.
SOGSI
SiO2
MgO/10
c.
KAGPPM
igneous alkali contents
non-igneous alkali contents
K2O-rich basalts(>3%)
fresh olivine basalts
fresh basalts
fresh intermediate & felsic lavas
SiO2
CaO/Al2O3

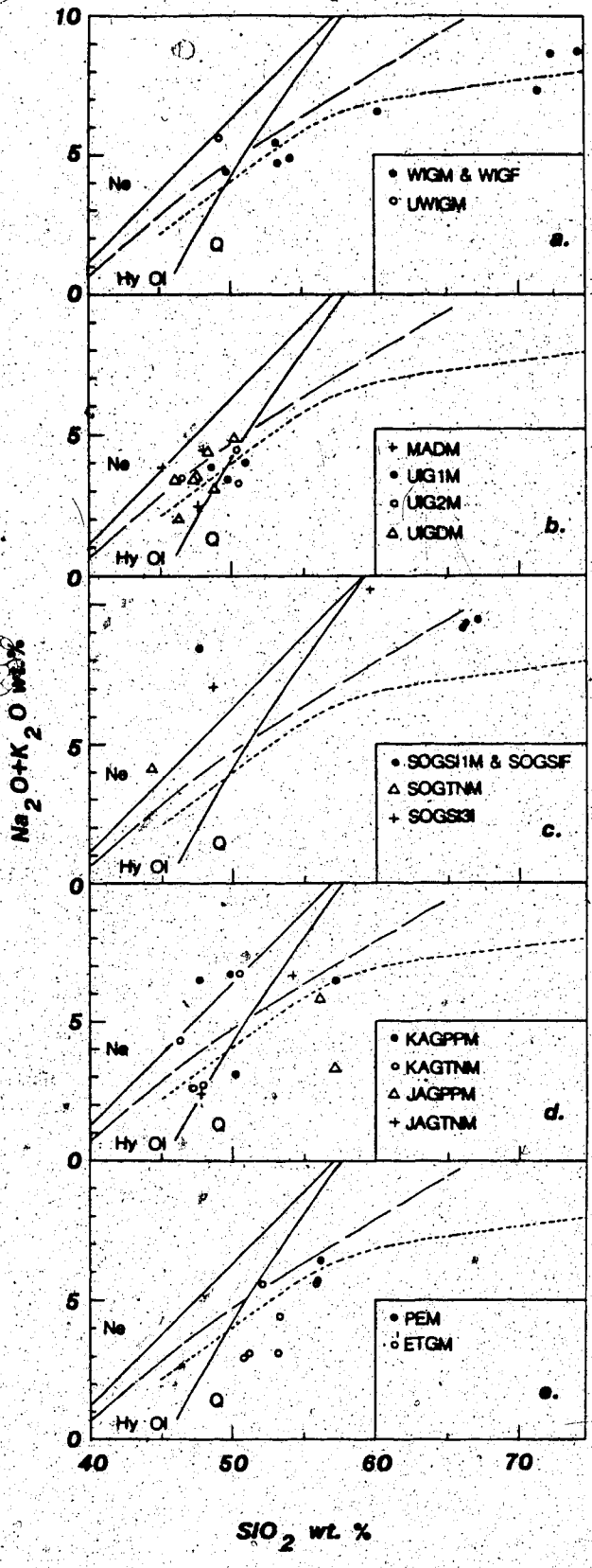
10
5
0
Ne
Q
Hy Ol
• WIGM & WIGF
○ UWIGM
a.
+ MADM
• UIG1M
○ UIG2M
△ UIGDM
b.
• SOGSI1M & SOGSIF
△ SOGTNM
+ SOGSI3I
c.
• KAGPPM
○ KAGTNM
△ JAGPPM
+ JAGTNM
d.
• PEM
○ ETGM
e.
40
50
60
70
Na_2O+K_2O wt.%
SiO_2 wt. %

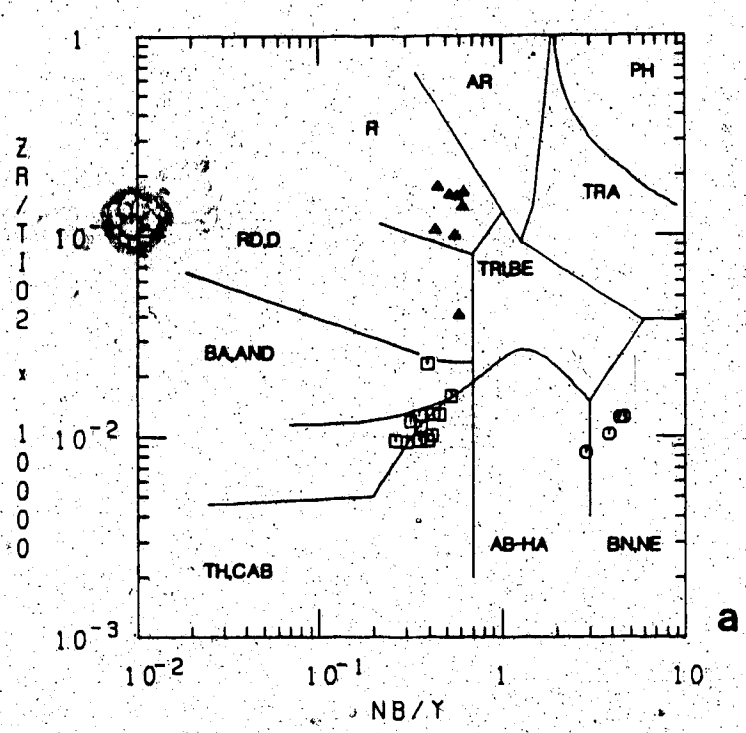
1
10^{-2}
10^{-3}
ZR/TIO2 x 10000
10^{-2}
10^{-1}
1
10
NB/Y
R
AR
PH
TRA
RD,D
TR,BE
BA,AND
AB-HA
BN,NE
TH,CAB
a

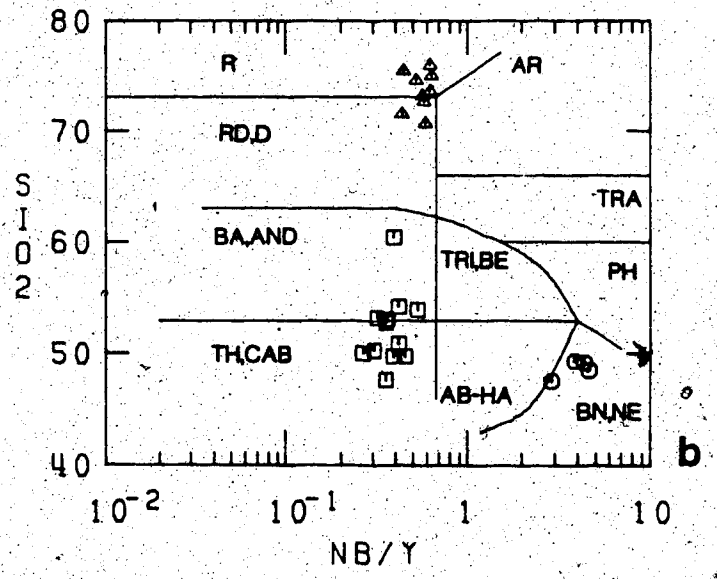
80
70
60
50
40
SIO2
10^{-2}
10^{-1}
1
10
NB/Y
R
AR
RD,D
TRA
BA,AND
TR,BE
PH
TH,CAB
AB-HA
BN,NE
b

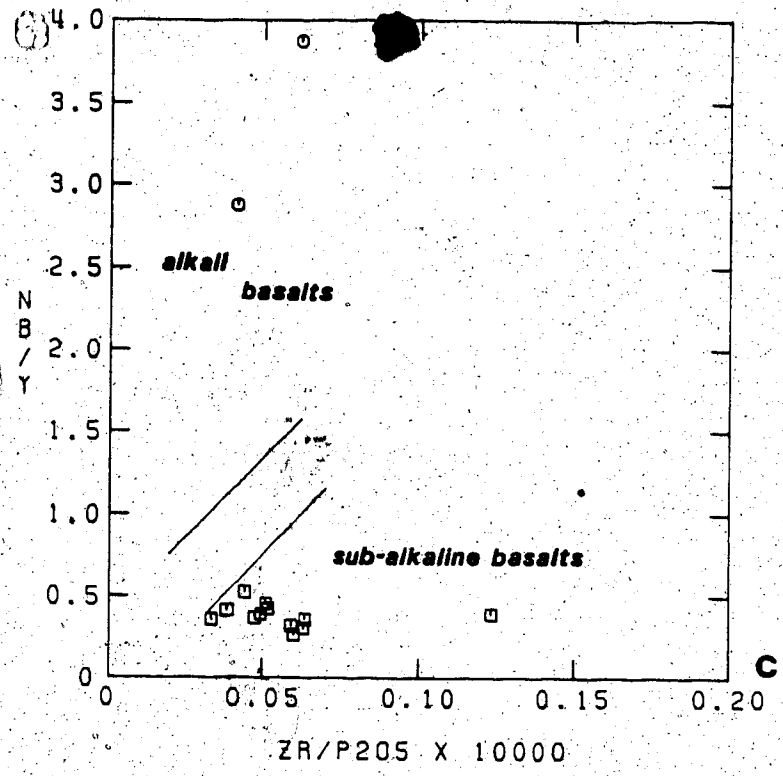
4.0
3.5
3.0
2.5
2.0
1.5
1.0
0.5
0
N
B
/
Y
alkali
basalts
sub-alkaline basalts
0
0.05
0.10
0.15
0.20
ZR/P2O5 X 10000

c

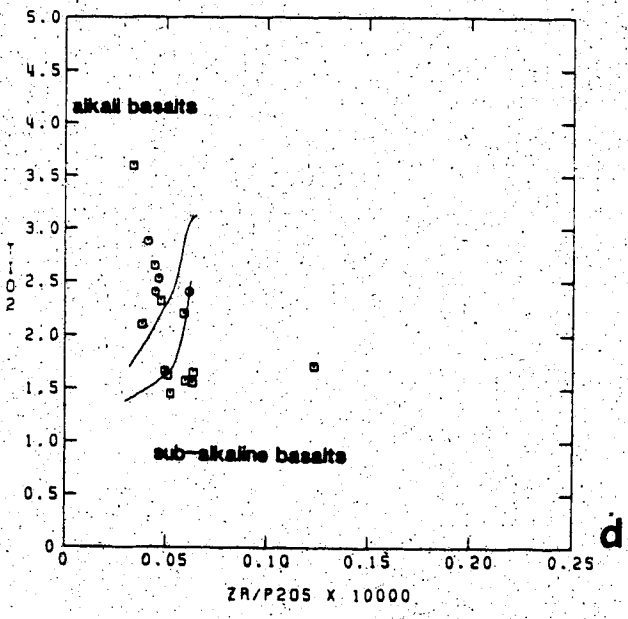
5.0
4.5
4.0
3.5
3.0
2.5
2.0
1.5
1.0
0.5
0
TiO2
alkali basalts
sub-alkaline basalts
0
0.05
0.10
0.15
0.20
0.25
ZR/P2O5 X 10000

d

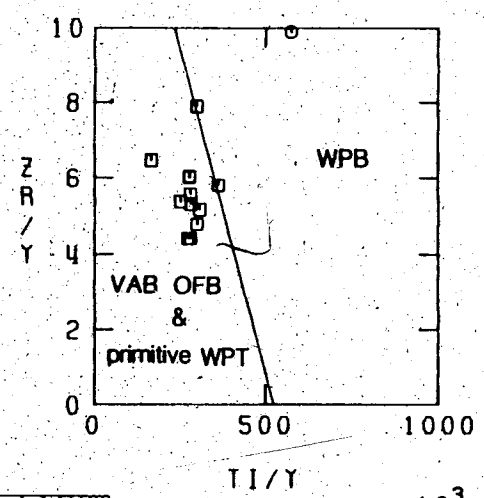
10
8
6
4
2
0
ZR/Y
WPB
VAB OFB
&
primitive WPT
0
500
1000
TI/Y

e

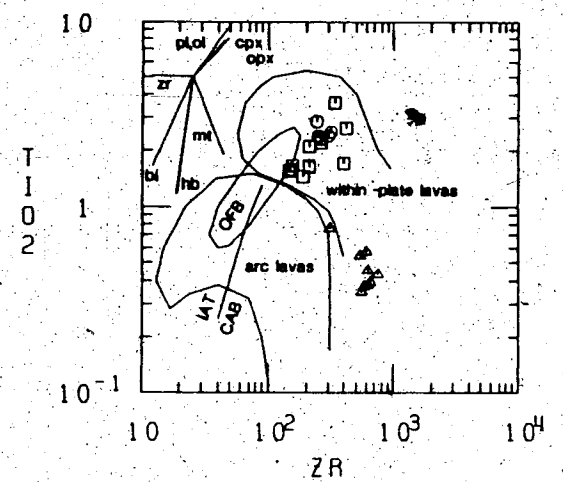
10
1
10^{-1}
TiO2
pl,ol
cpx
opx
zr
mt
bi
hb
OFB
within-plate lavas
arc lavas
IAT
CAB
10
10^2
10^3
10^4
ZR

f

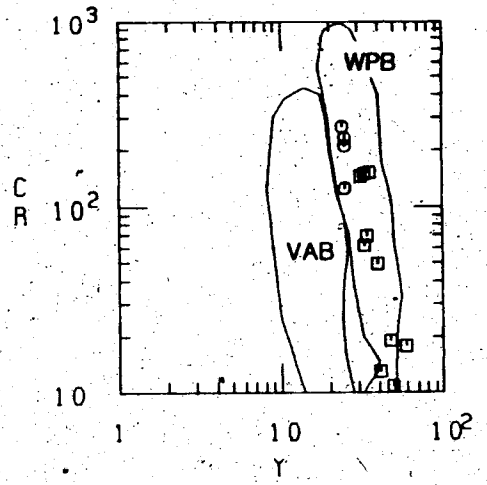
10^3
10^2
10
CR
WPB
OFB
VAB
1
10
10^2
Y

g

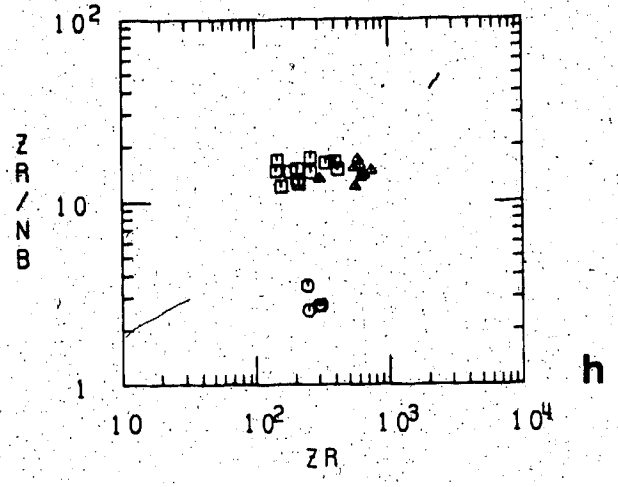
ZR/NB
ZR
h

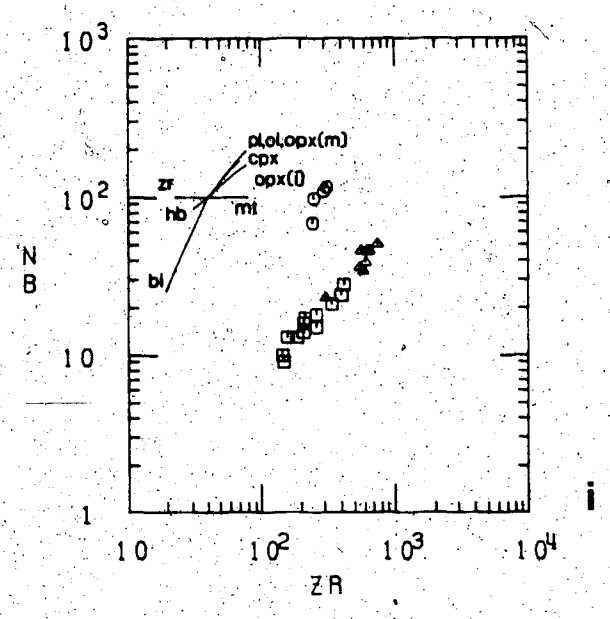
NB
ZR
pl,ol,opx(m)
cpx
opx(l)
zr
hb
mt
bi
i

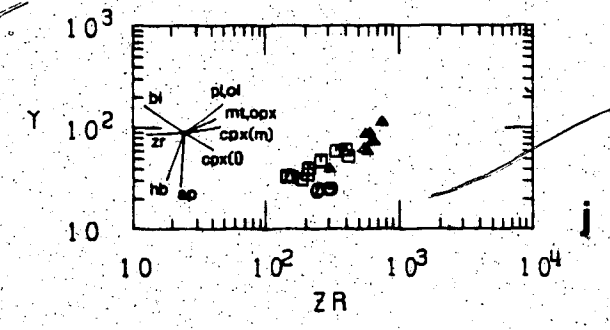
Y
ZR
bi
pl,ol
mt,opx
cpx(m)
zr
cpx(l)
hb
ap
j

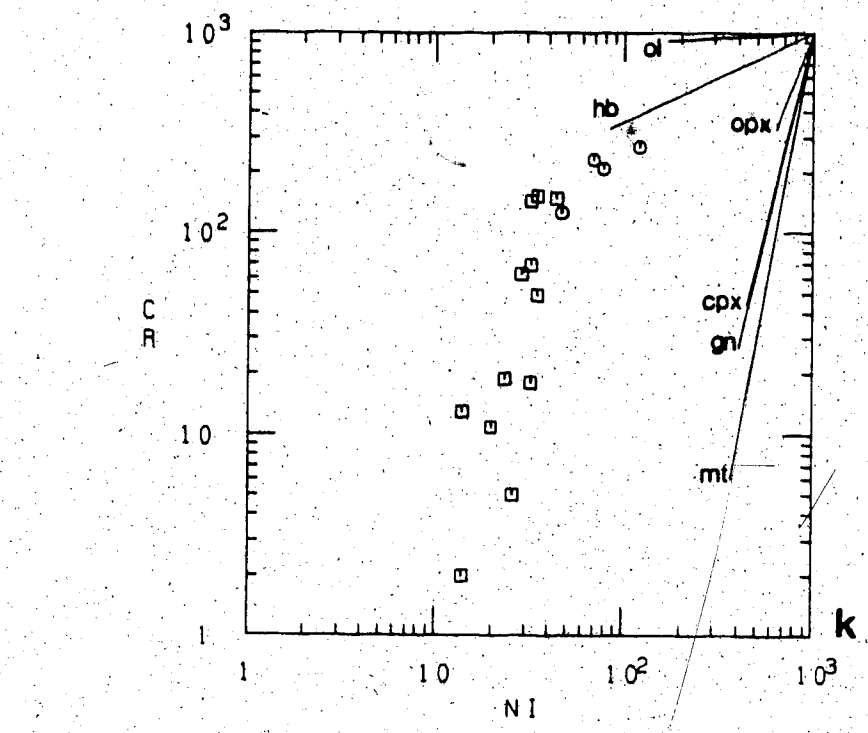
ol
hb
opx
cpx
gn
mt
C
R
NI
k

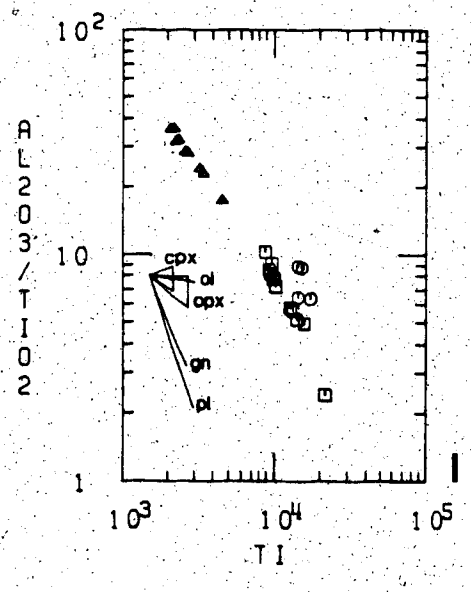
cpx
ol
opx
gn
pl
TI
l

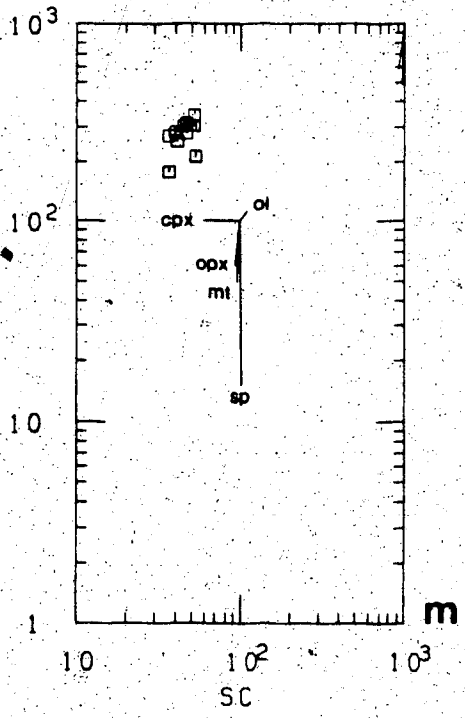
cpx
ol
opx
mt
sp
V
SC
m

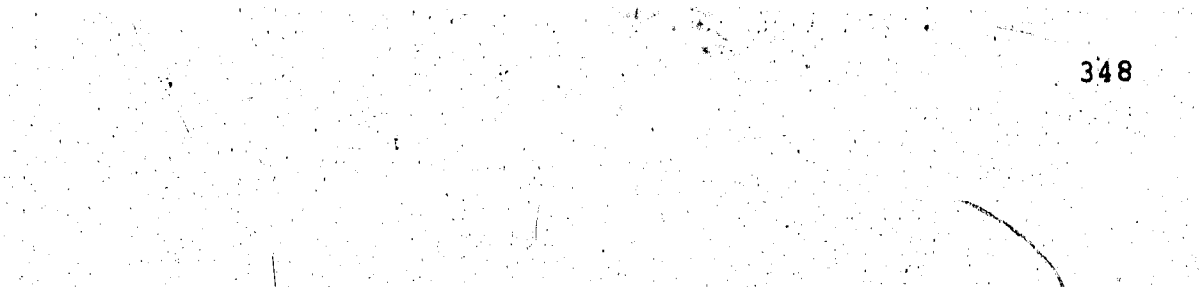

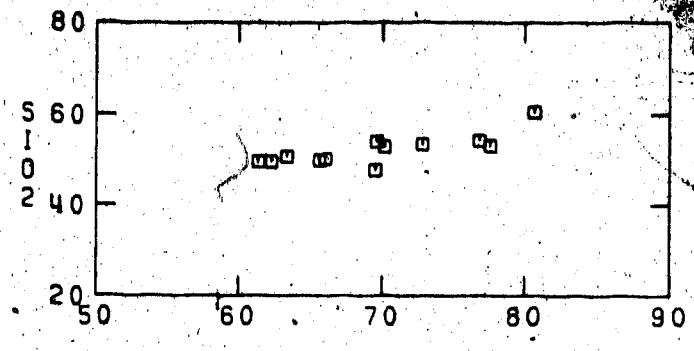
SiO2
80
60
40
20
50
60
70
80
90

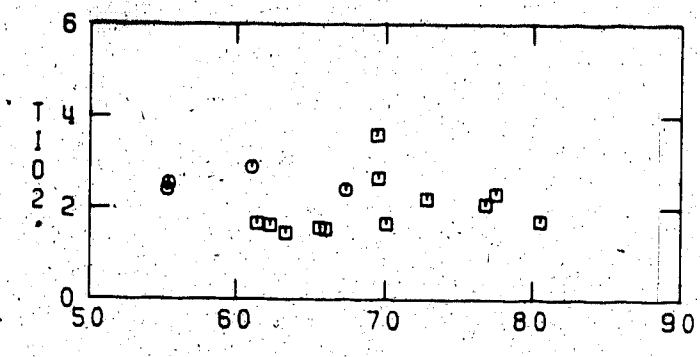
TiO2
6
4
2
0
50
60
70
80
90

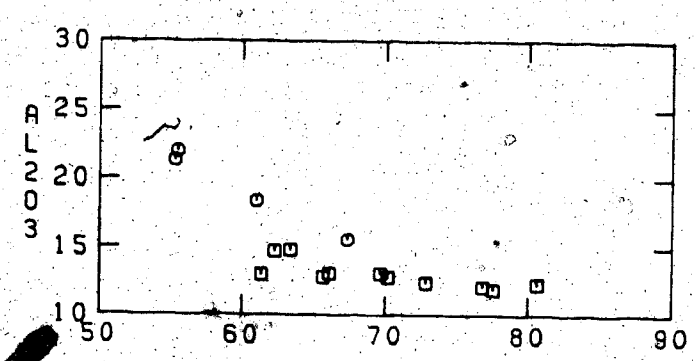
Al2O3
30
25
20
15
10
50
60
70
80
90

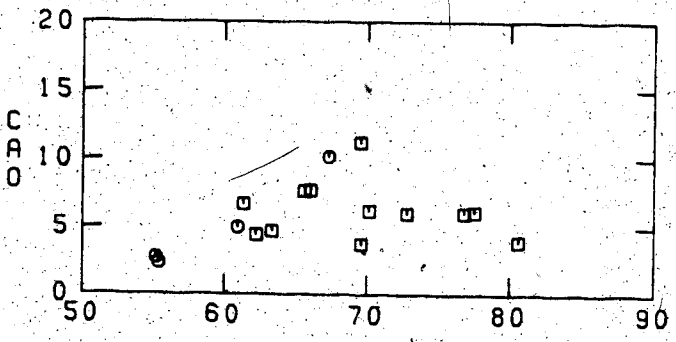
CaO
20
15
10
5
0
50
60
70
80
90

M.I.

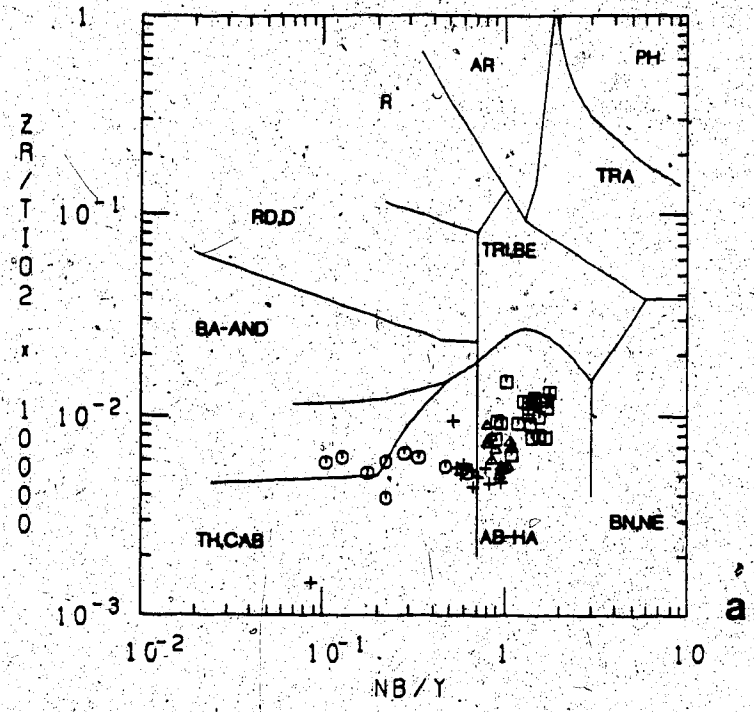
1
10^{-1}
10^{-2}
10^{-3}
ZR/TIO2 x 10000
AR
PH
R
TRA
RD,D
TRI,BE
BA-AND
TH,CAB
AB-HA
BN,NE
10^{-2}
10^{-1}
1
10
NB/Y
a

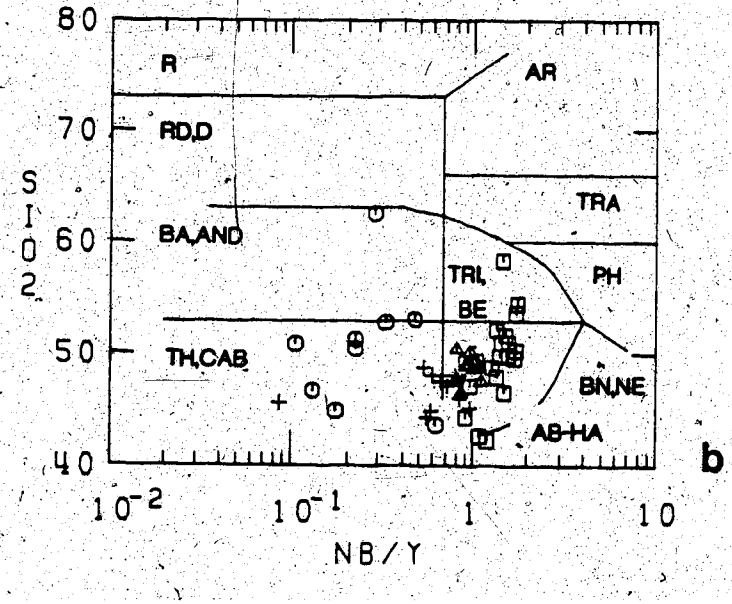
80
70
60
50
40
SIO2
R
AR
RD,D
TRA
BA,AND
TRI,
PH
BE
TH,CAB
BN,NE
AB-HA
10^{-2}
10^{-1}
1
10
NB/Y
b

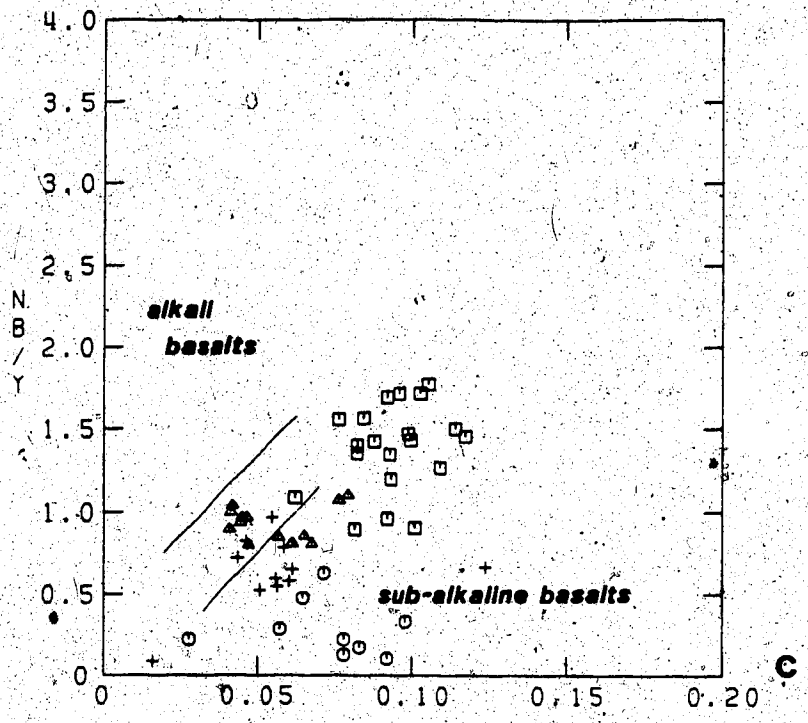
4.0
3.5
3.0
2.5
2.0
1.5
1.0
0.5
0
N.
B
/
Y
alkali
basalts
sub-alkaline basalts
0
0.05
0.10
0.15
0.20
ZR/P205 X 10000

c

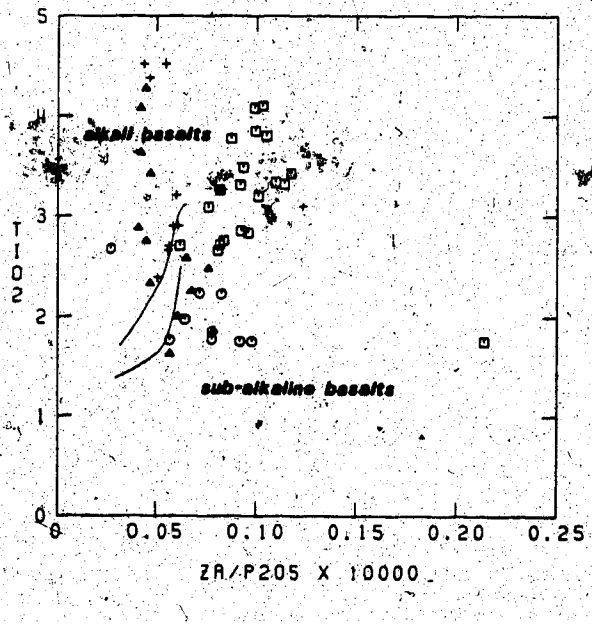
5
4
3
2
1
0
TIO2
alkali basalts
sub-alkaline basalts
0
0.05
0.10
0.15
0.20
0.25
ZR/P205 X 10000

d

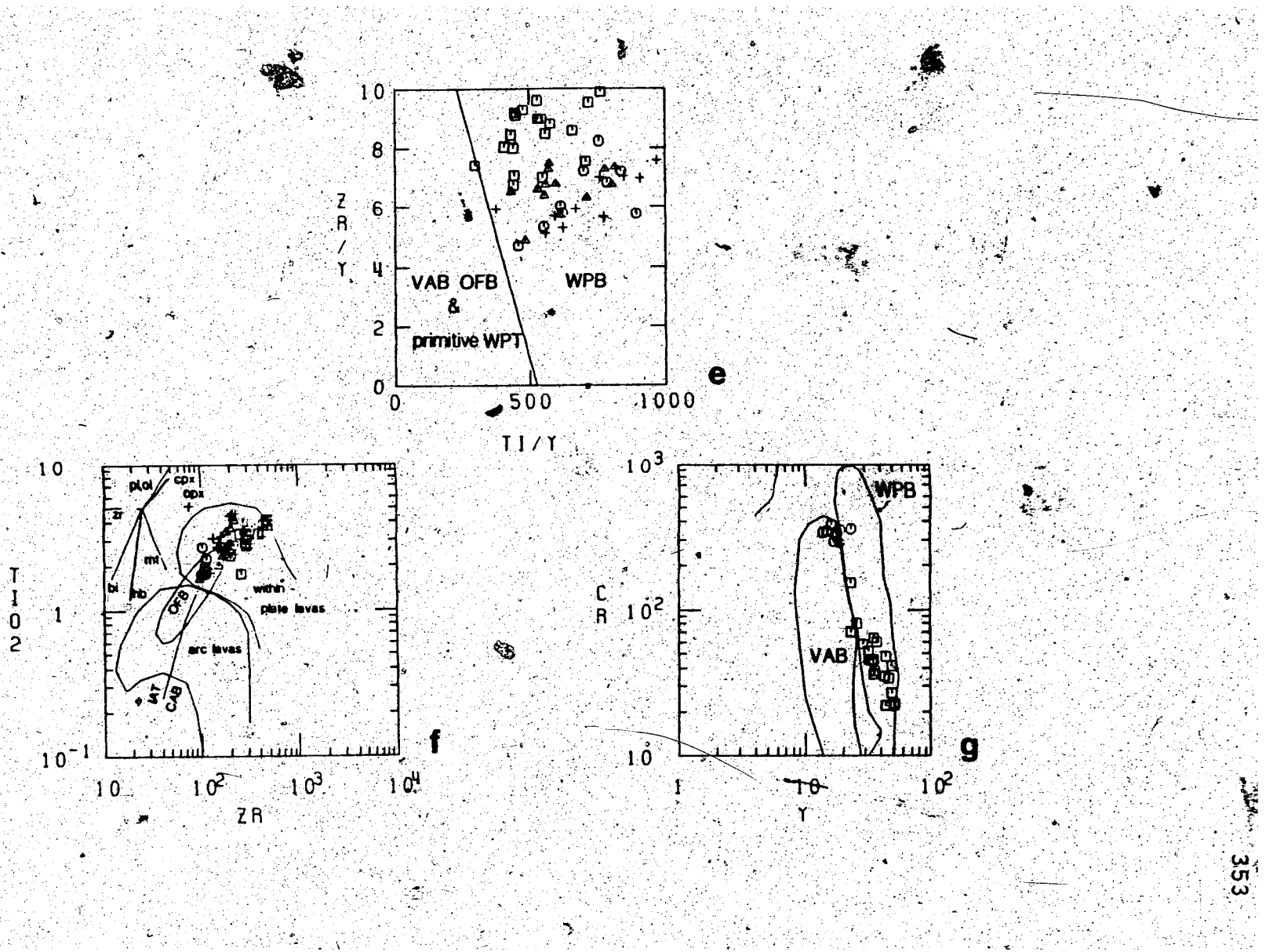
10
8
6
4
2
0
Z
R
/
Y
VAB OFB
&
primitive WPT
WPB
0
500
1000
TI/Y
e
10
1
10^{-1}
T
I
O
2
pl,ol
cpx
opx
zr
sm
bi
pb
OFB
within -
plate lavas
arc lavas
IAT
CAB
10
10^2
10^3
10^4
ZR
f
10^3
10^2
C
R
WPB
VAB
1.0
1
10
10^2
Y
g

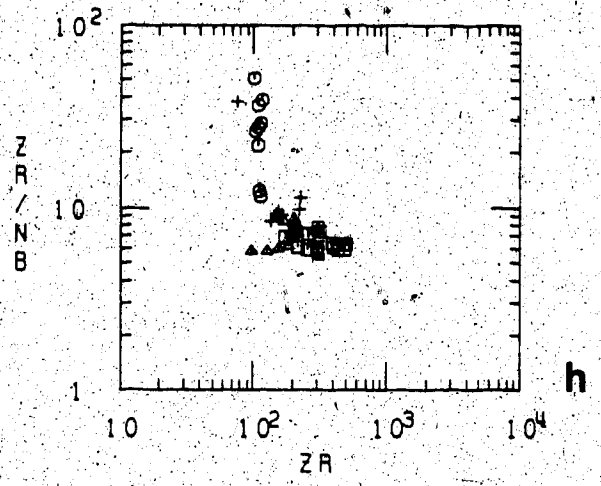
ZR/NB
ZR
h

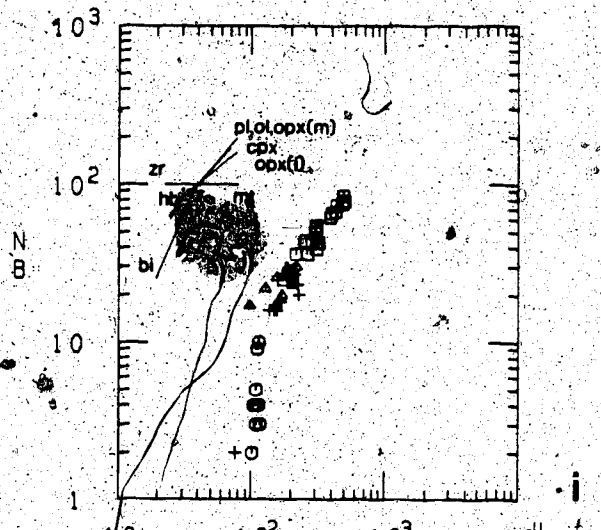
NB
ZR
pl,ol,opx(m)
cpx
opx(i)
zr
hb
bi
i

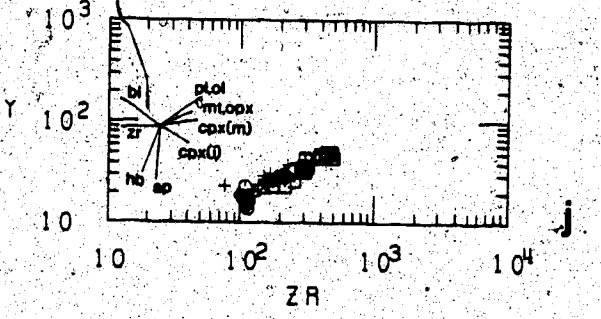
Y
ZR
bi
pl,ol
opx(m)
cpx(m)
cpx(i)
zr
hb
ap
j

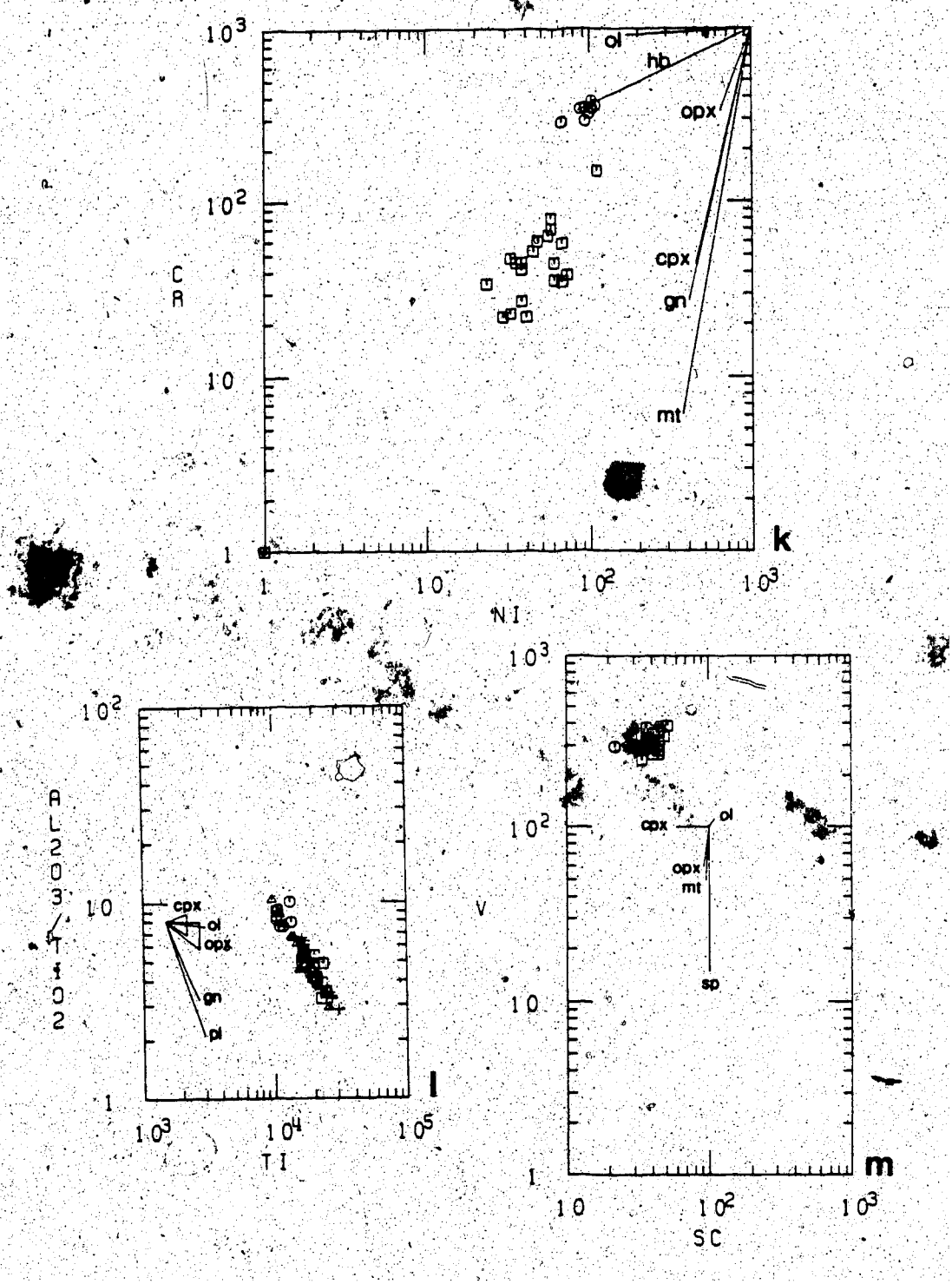
k
C
R
NI
ol
hb
opx
cpx
gn
mt
l
AL2O3/TiO2
TI
cpx
ol
opx
gn
pl
m
V
SC
cpx
ol
opx
mt
sp

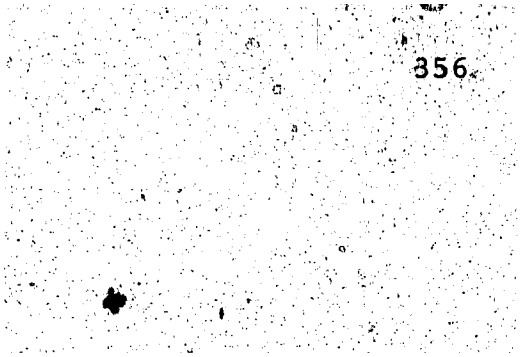
356.

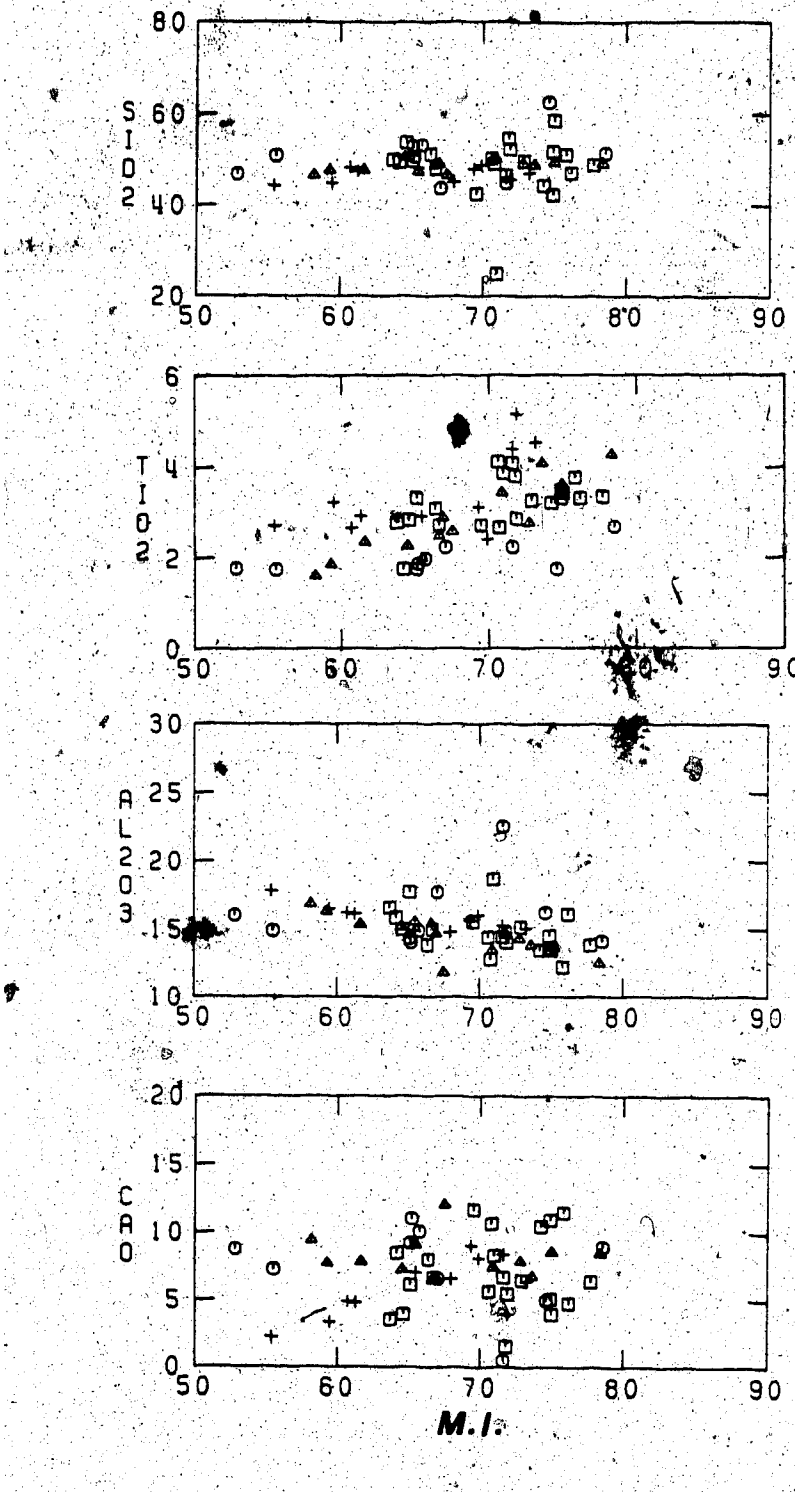
SiO2
80
60
40
20
50
60
70
80
90
TiO2
6
4
2
0
Al2O3
30
25
20
15
10
CaO
20
15
10
5
0
M.I.

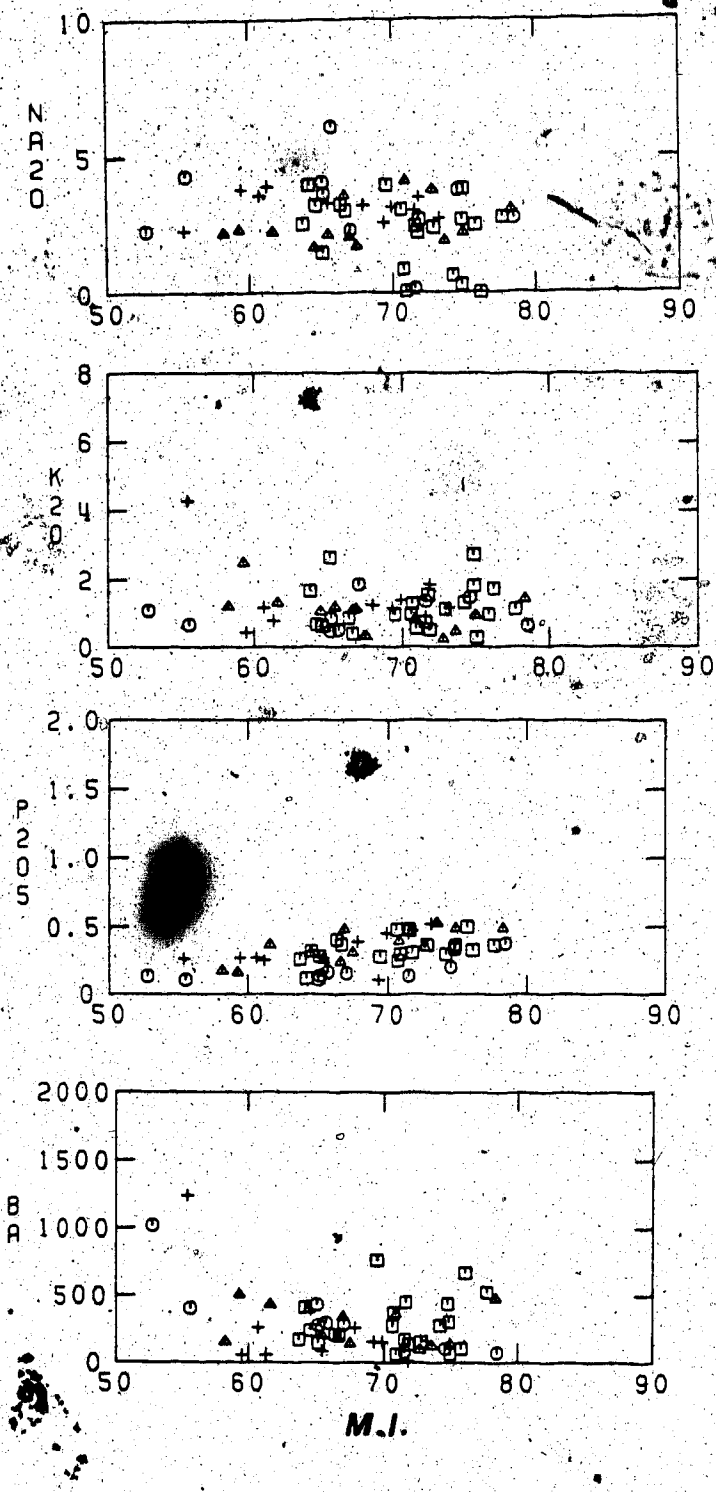
NA2O
K2O
P2O5
BA
M.I.

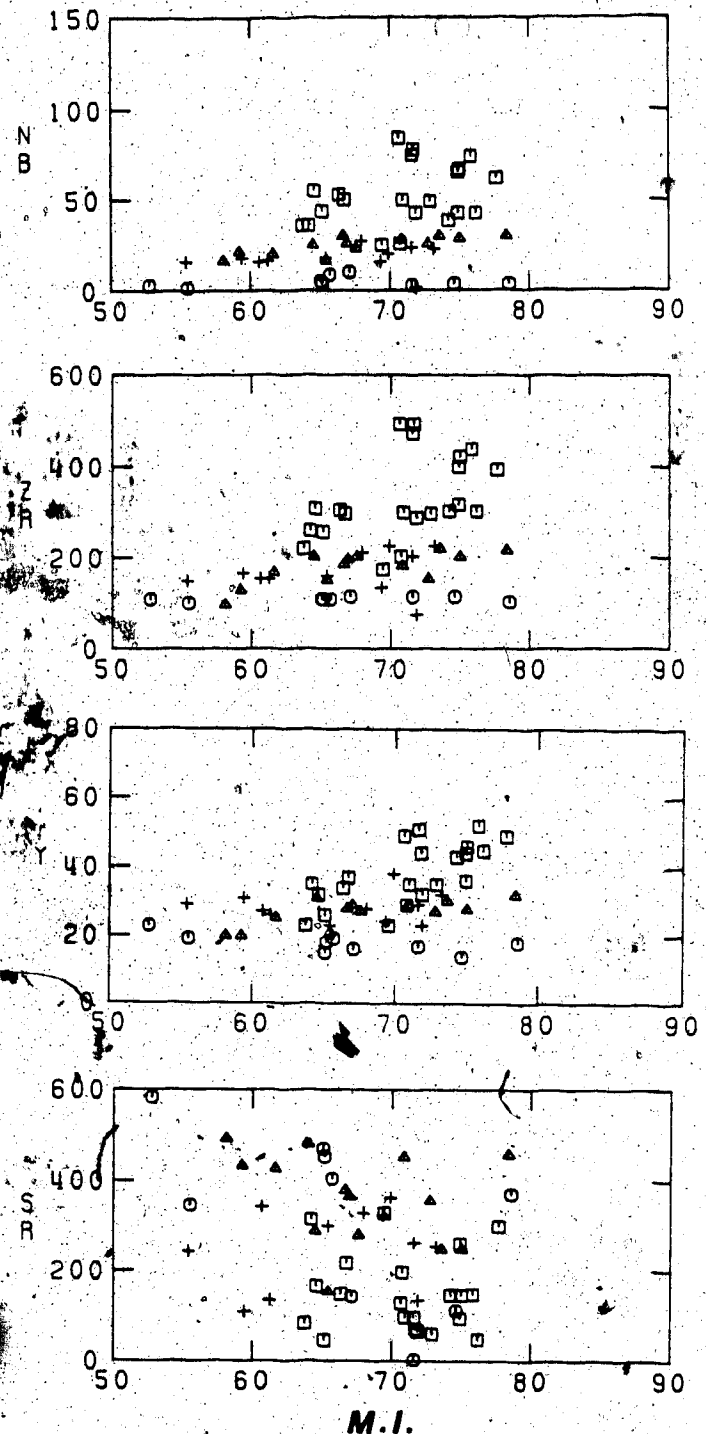
NB
ZR
Y
SR
M.I.

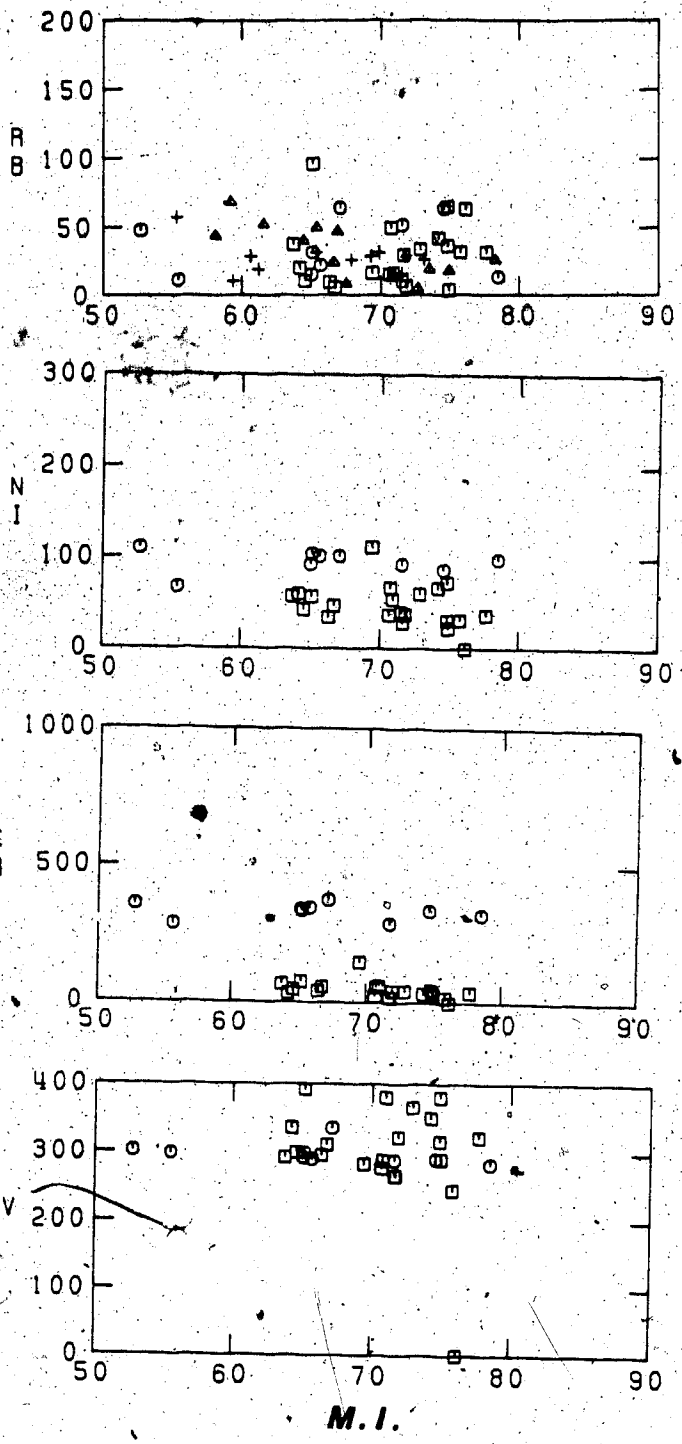

M. I.

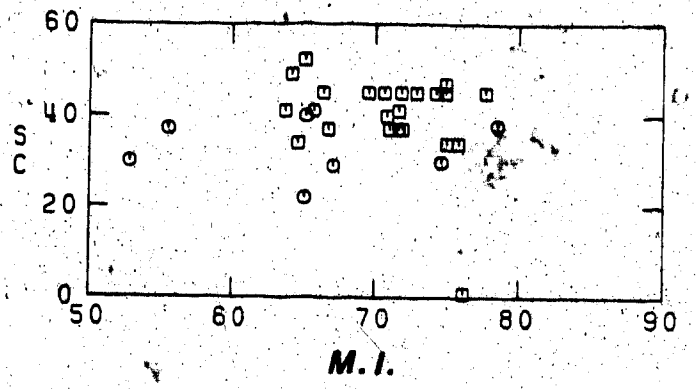
60
40
20
0
S
C
50
60
70
80
90
M. I.

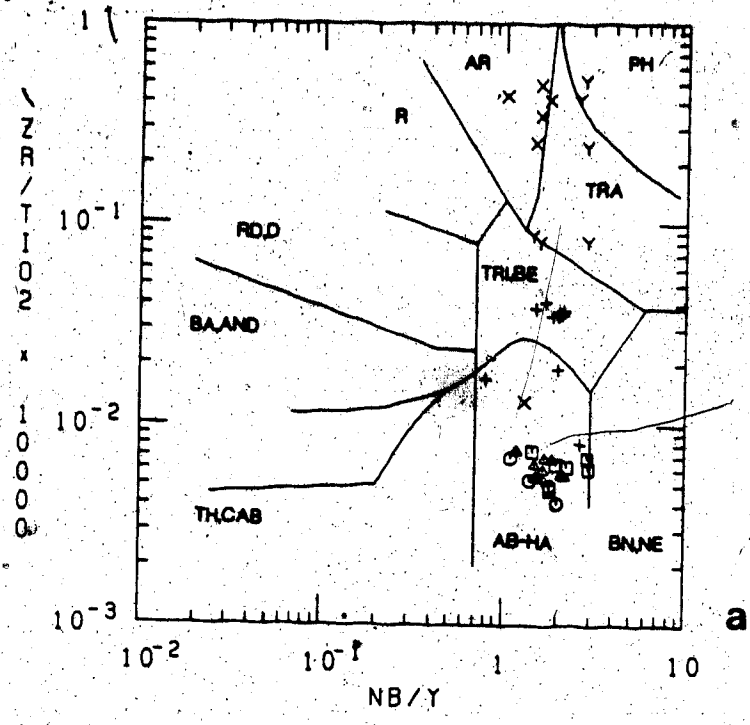
1
10^{-1}
10^{-2}
10^{-3}
ZR/TIO2 x 10000
AR
PH
R
TRA
RD,D
TRI,BE
BA,AND
TH,CAB
AB-HA
BN,NE
10^{-2}
10^{-1}
1
10
NB/Y

a

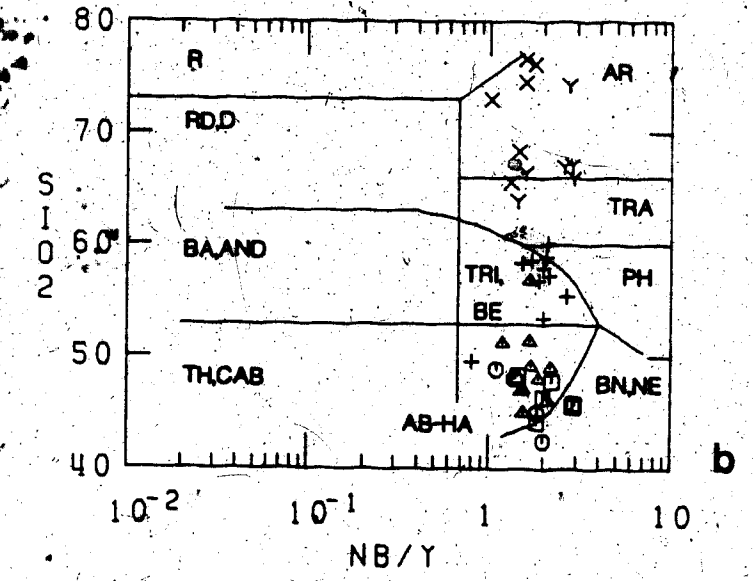
80
70
60
50
40
SIO2
R
AR
RD,D
TRA
BA,AND
TRI,
BE
PH
TH,CAB
BN,NE
AB-HA
10^{-2}
10^{-1}
1
10
NB/Y

b

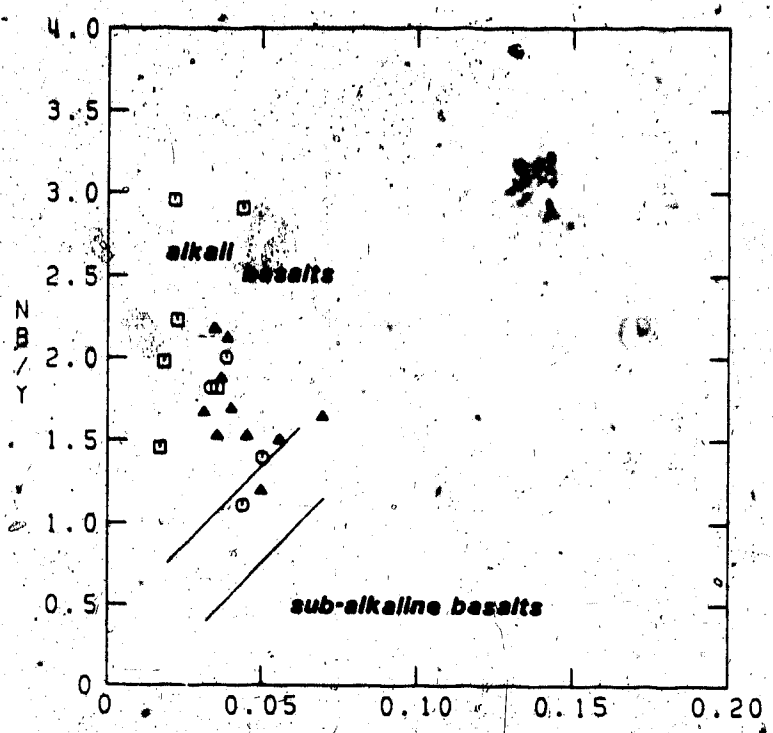
alkali basalts
sub-alkaline basalts
NB/Y
ZR/P205 X 10000
c

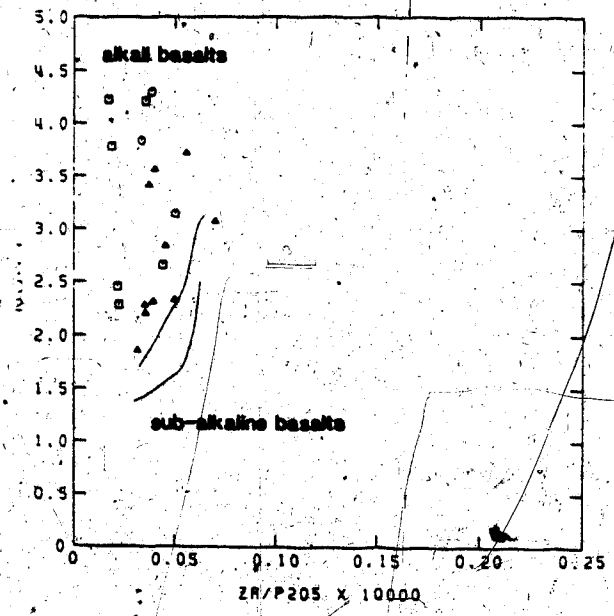
alkali basalts
sub-alkaline basalts
ZR/P205 X 10000
d

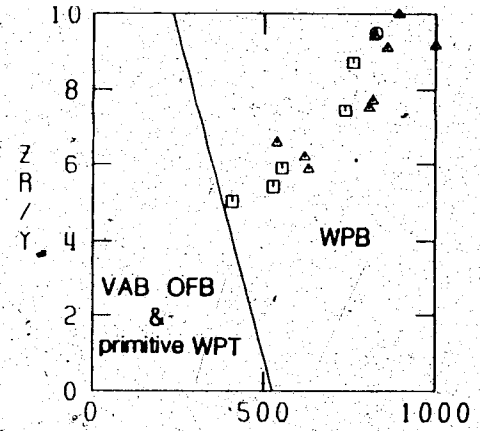
10
8
6
4
2
0
ZR/Y
WPB
VAB OFB
&
primitive WPT
0
500
1000
TI/Y

e

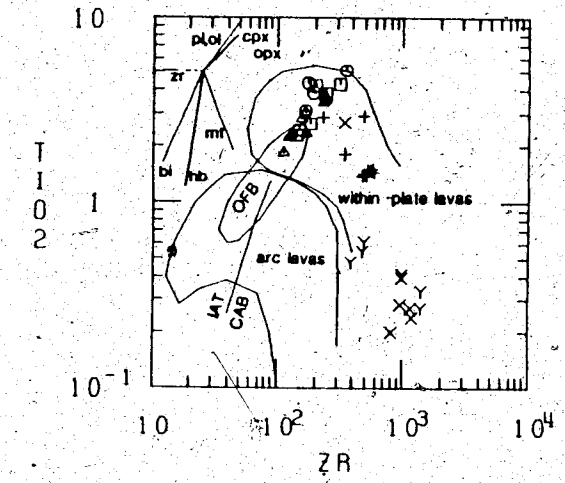
10
1
10^{-1}
TiO2
pl,ol
cpx
opx
zr
mt
bi
hb
OFB
within-plate lavas
arc lavas
CAB
10
10^2
10^3
10^4
ZR

f

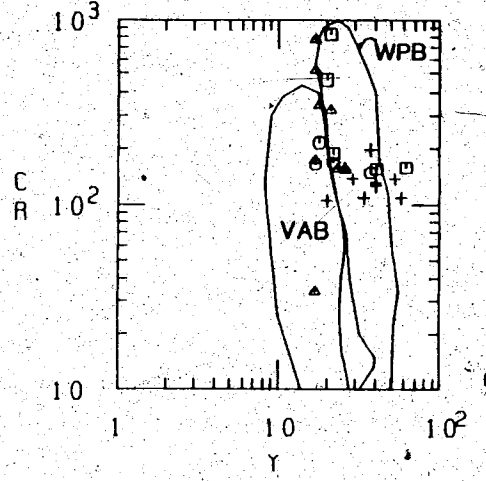
10^3
10^2
10
CR
WPB
VAB
1
10
10^2
Y

g

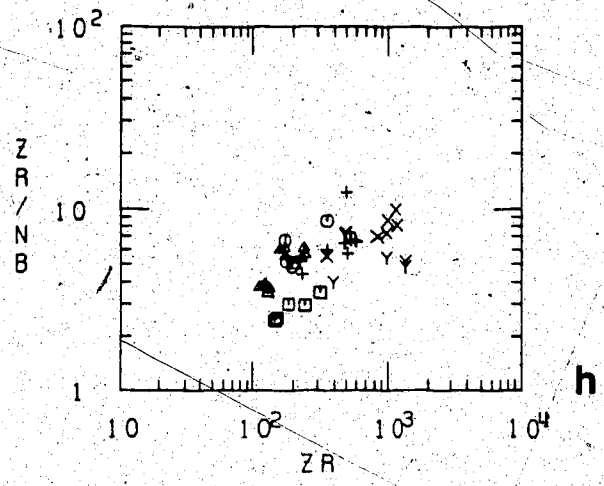
ZR/NB
ZR
h

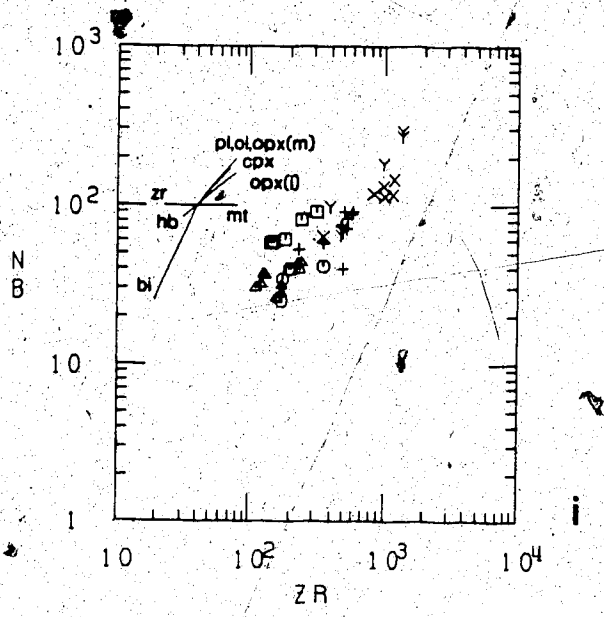
pl,ol,opx(m)
cpx
opx(l)
zr
hb
mt
bi
NB
ZR
i

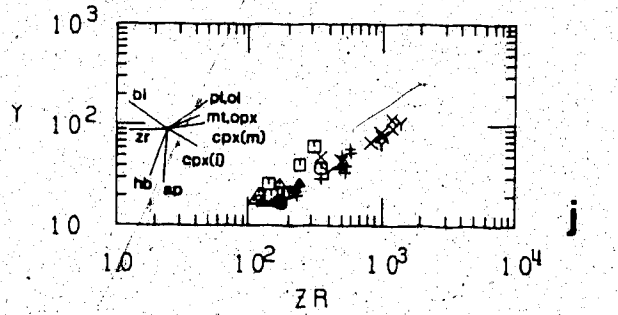
bi
pl,ol
mt,opx
cpx(m)
zr
cpx(l)
hb
ap
Y
ZR
j

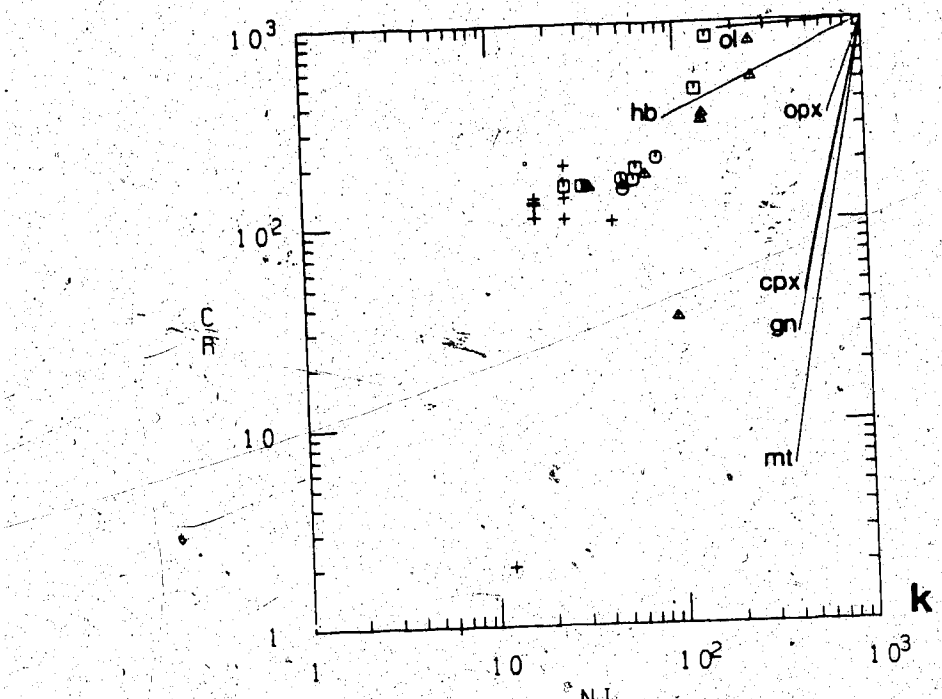
10^3
10^2
10
1
C
R
ol
hb
opx
cpx
gn
mt
k
1
10
10^2
10^3
NI

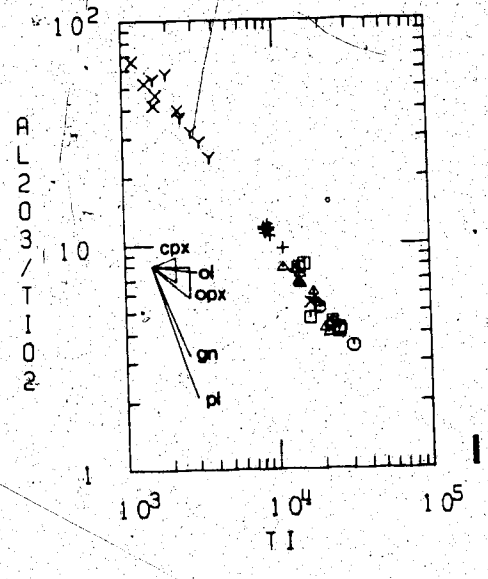
10^2
10
1
AL2O3/TIO2
cpx
ol
opx
gn
pl
l
10^3
10^4
10^5
TI

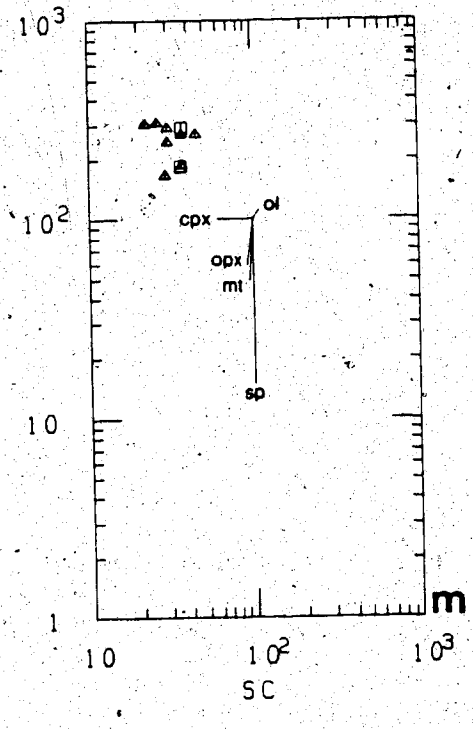
10^3
10^2
10
1
V
cpx
ol
opx
mt
sp
m
10
10^2
10^3
SC

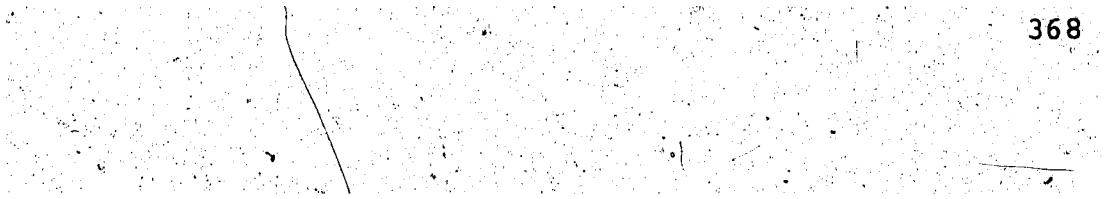

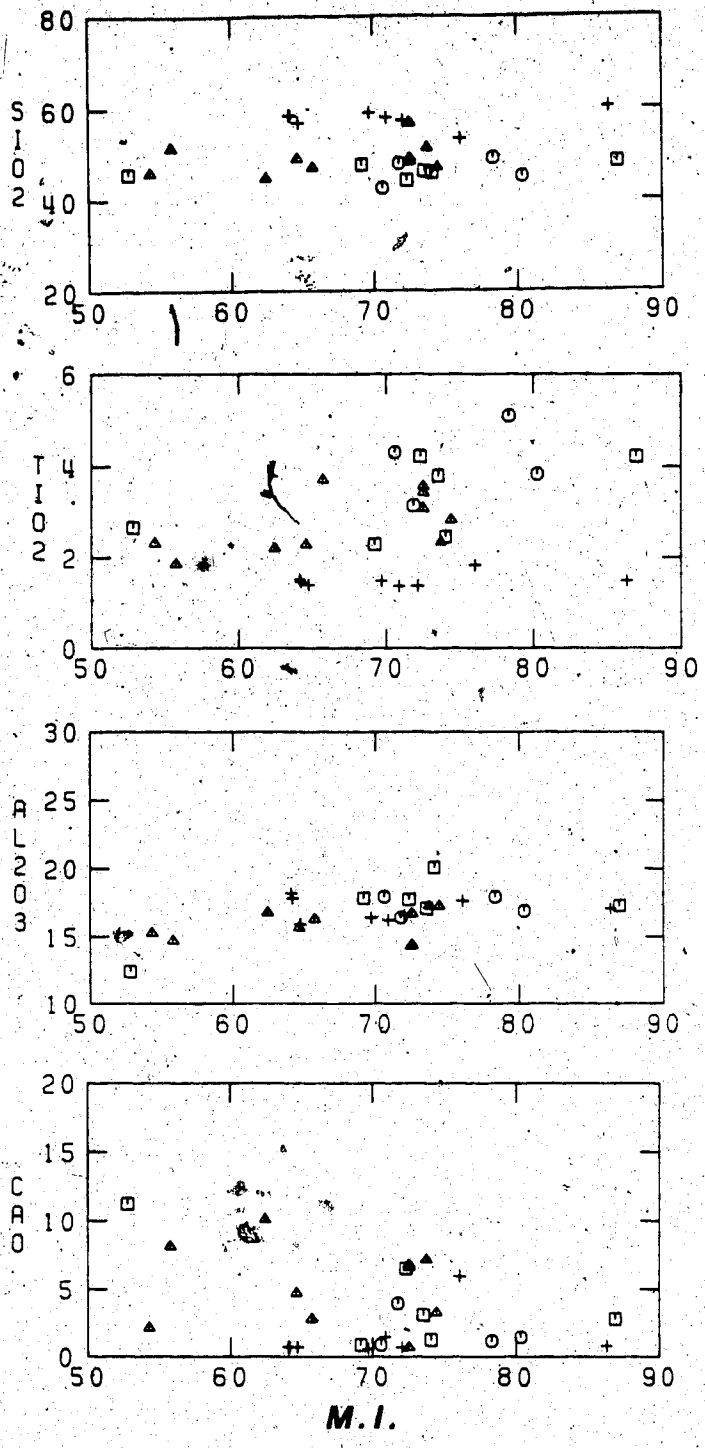
SIO2
80
60
40
20
50
60
70
80
90
TIO2
6
4
2
0
AL2O3
30
25
20
15
10
CAO
M.I.

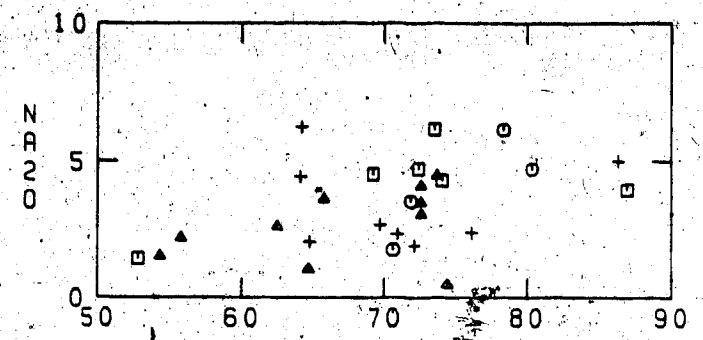
10
5
0
NA2O
50
60
70
80
90

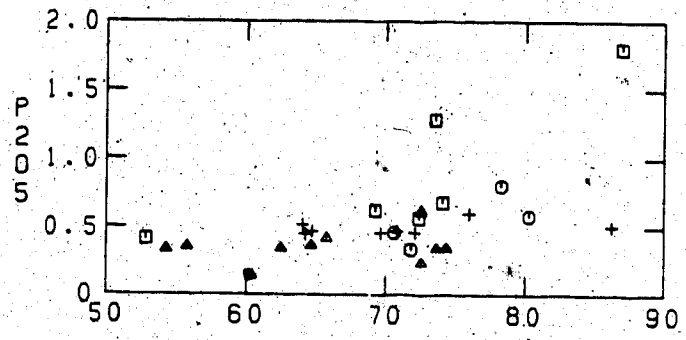
2.0
1.5
1.0
0.5
0
P2O5
50
60
70
80
90

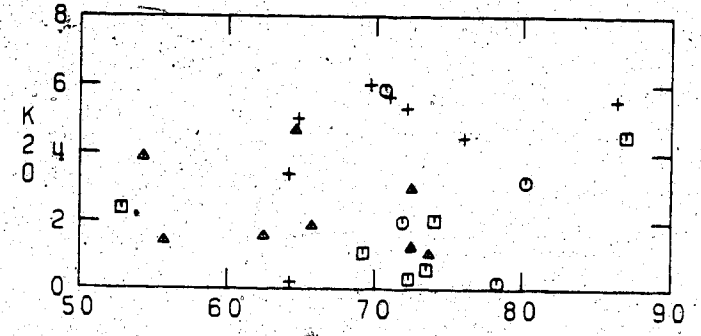
8
6
4
2
0
K2O
50
60
70
80
90

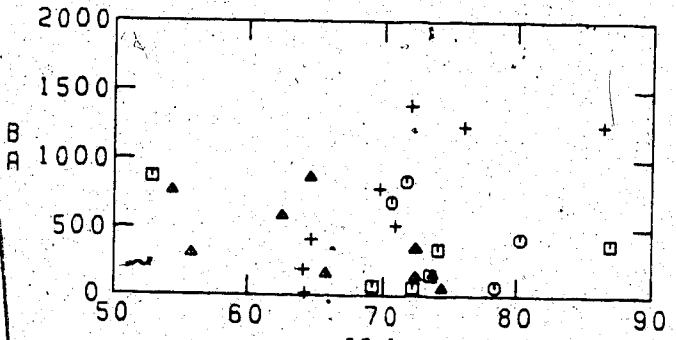
2000
1500
1000
500
0
BA
50
60
70
80
90
M.I.

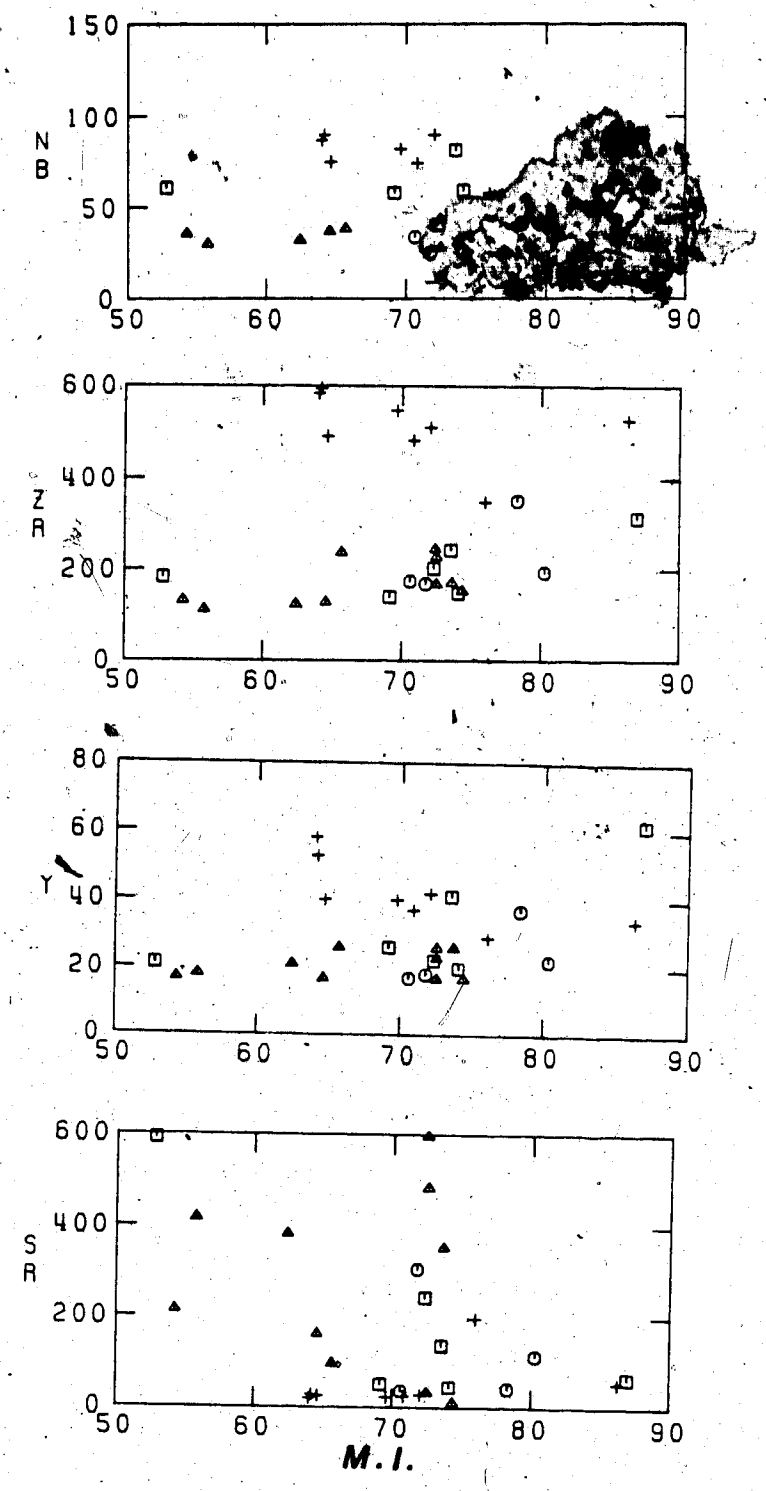
NB
150
100
50
0
50
60
70
80
90
ZR
600
400
200
0
50
60
70
80
90
Y
80
60
40
20
0
50
60
70
80
90
SR
600
400
200
0
50
60
70
80
90
M.I.

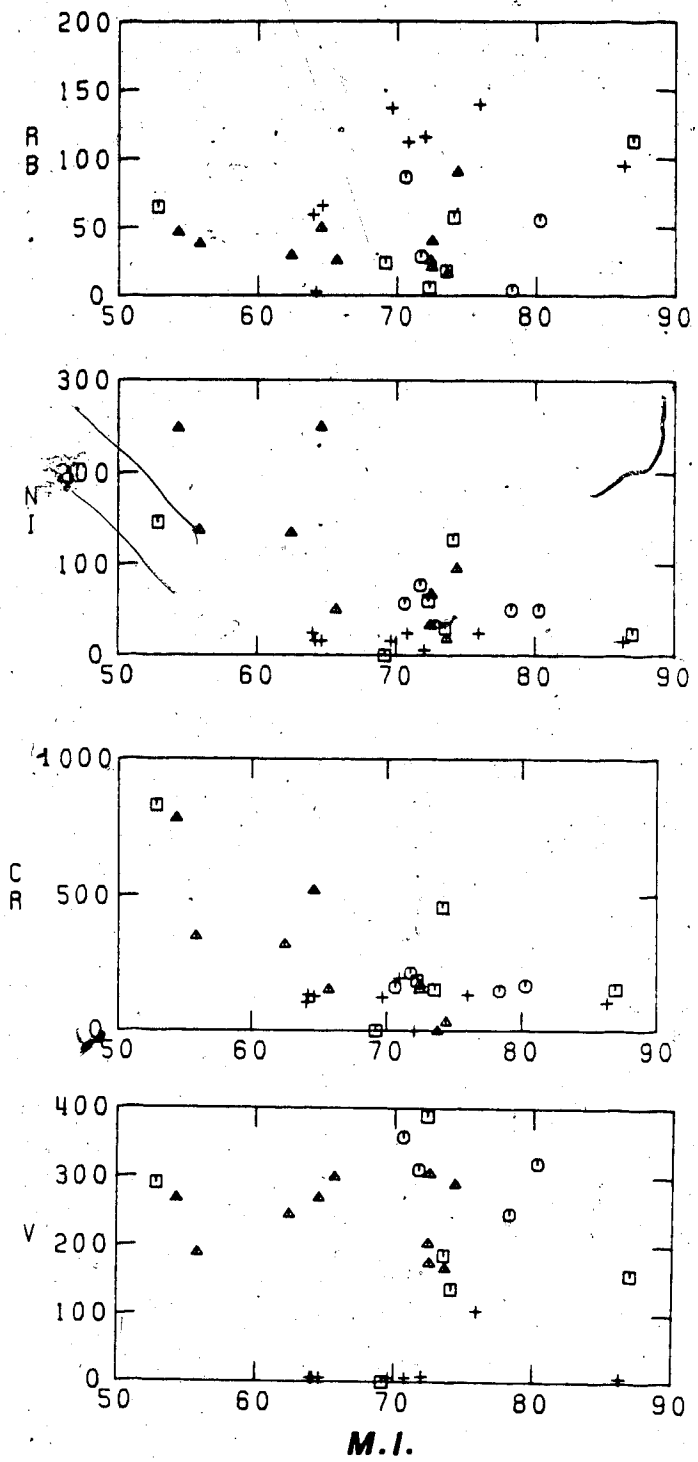
RB
NI
CR
V
200
150
100
50
0
300
1000
500
400
50
60
70
80
90
M.I.

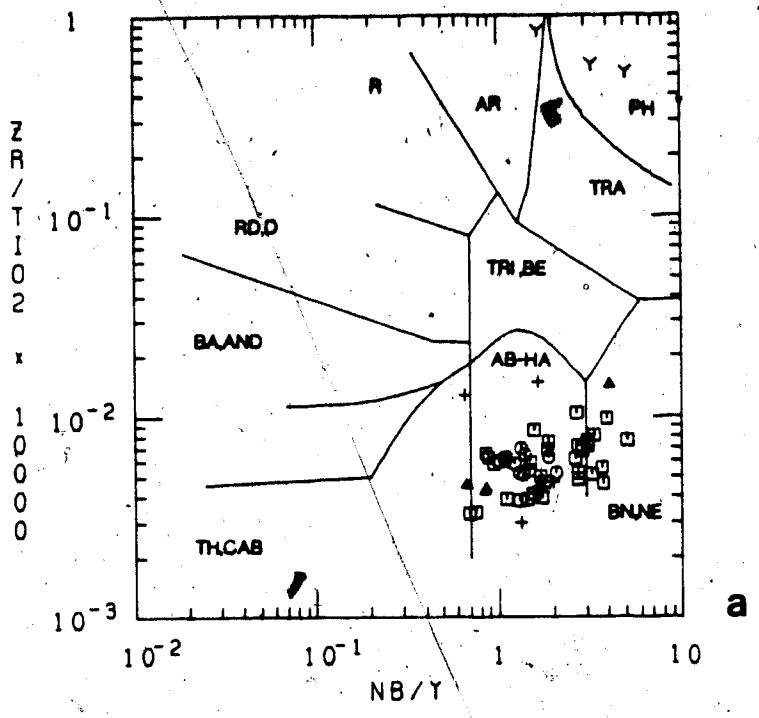
1
10^{-1}
10^{-2}
10^{-3}
ZR/TIO2 x 10000
R
AR
PH
TRA
RD,D
TRI,BE
BA,AND
AB-HA
BN,NE
TH,CAB
10^{-2}
10^{-1}
1
10
NB/Y
a

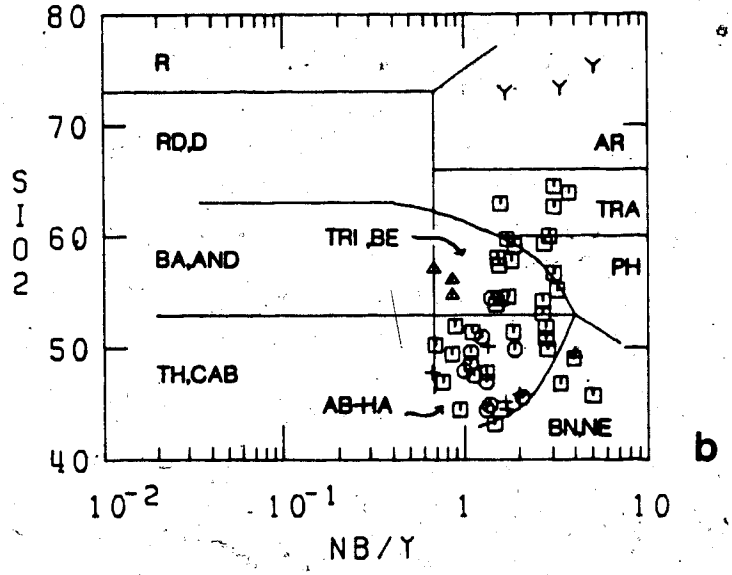
80
70
60
50
40
SIO2
R
RD,D
AR
TRA
TRI,BE
BA,AND
PH
TH,CAB
AB-HA
BN,NE
10^{-2}
10^{-1}
1
10
NB/Y
b

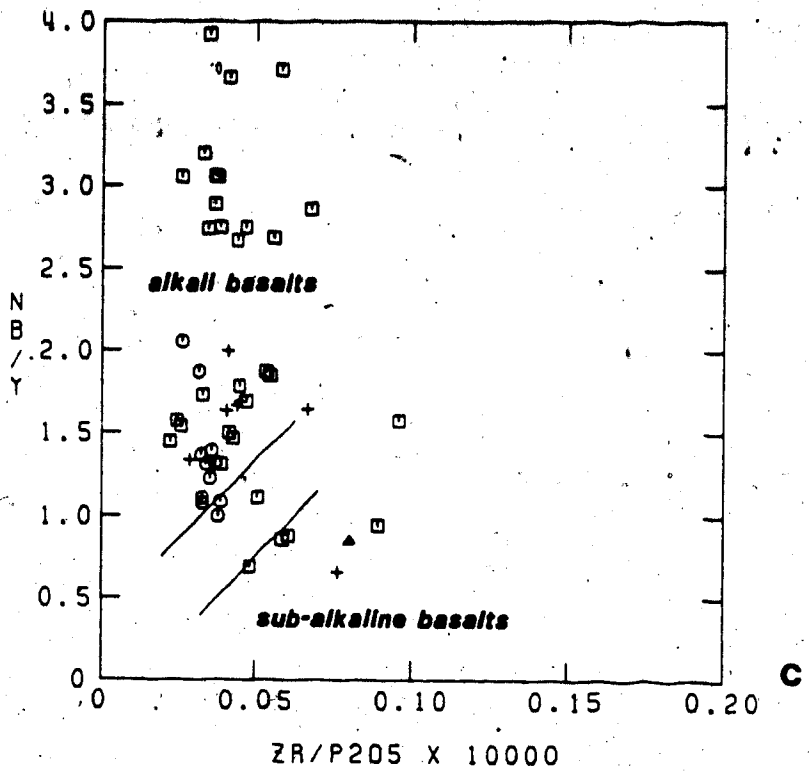
4.0
3.5
3.0
2.5
2.0
1.5
1.0
0.5
0
NB/Y
alkali basalts
sub-alkaline basalts
0.0
0.05
0.10
0.15
0.20
ZR/P2O5 X 10000

c

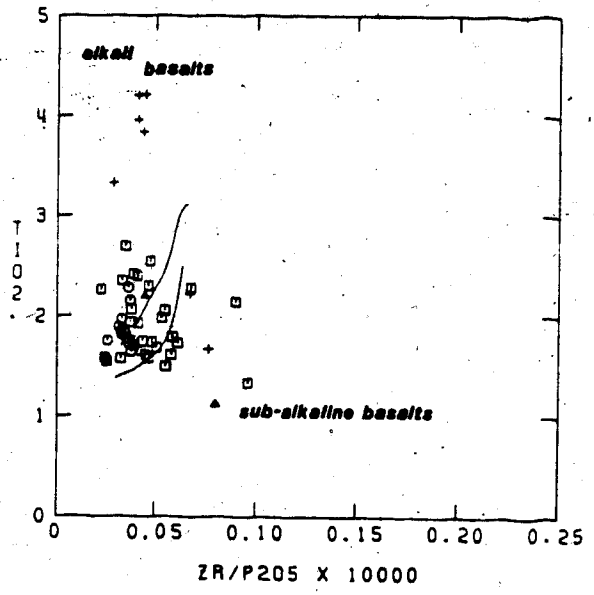
5
4
3
2
1
0
TiO2
alkali basalts
sub-alkaline basalts
0
0.05
0.10
0.15
0.20
0.25
ZR/P2O5 X 10000

d

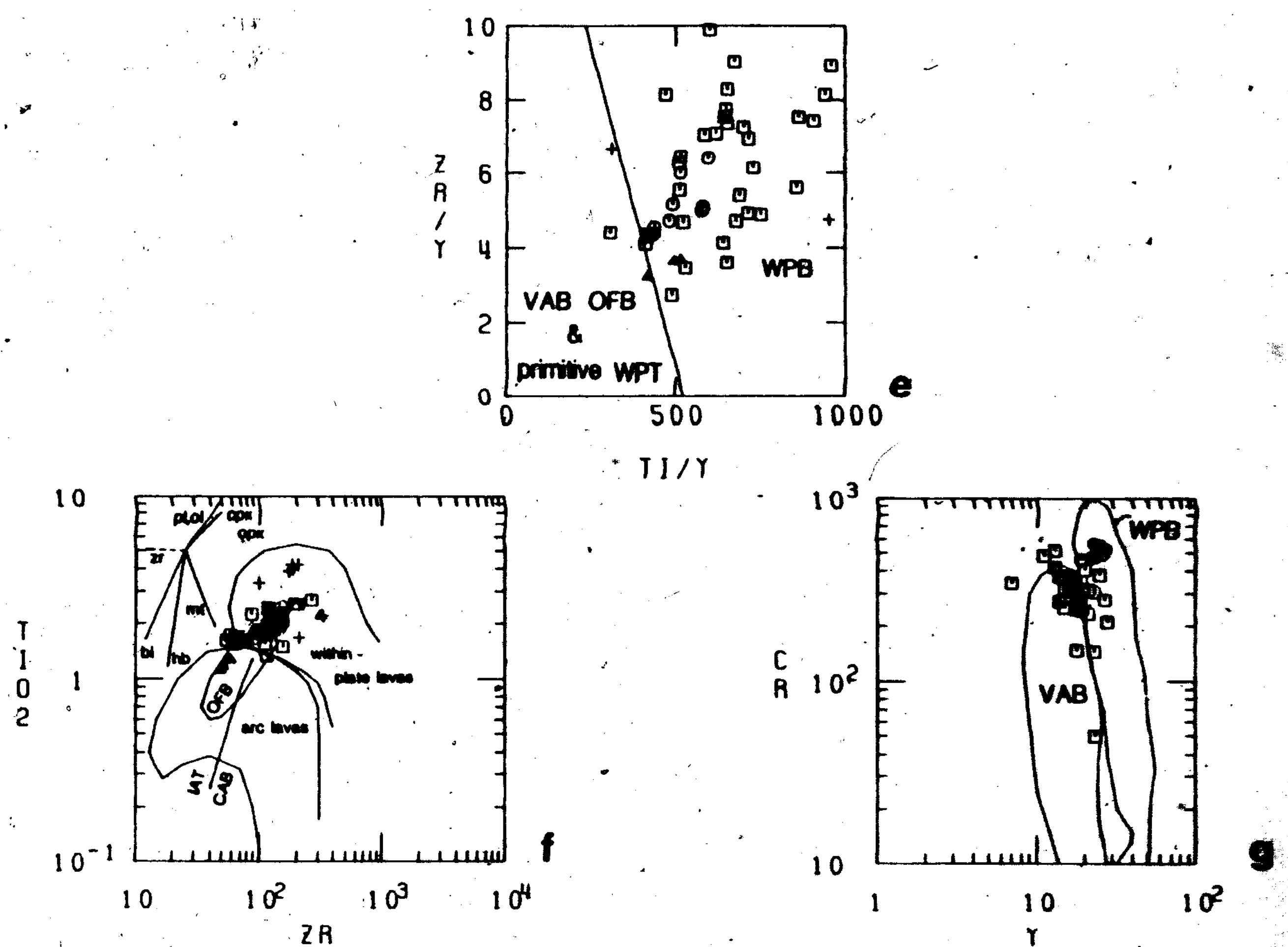
ZR/Y
TI/Y
VAB OFB
&
primitive WPT
WPB
e
TIO2
ZR
plol
cpx
opx
zr
mt
bl
hb
OFB
within-
plate lavas
arc lavas
IAT
CAB
f
CR
Y
VAB
WPB
g

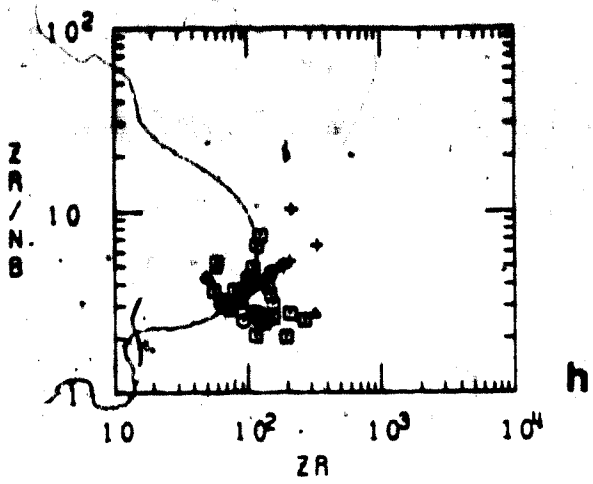
ZR/NB
ZR
h

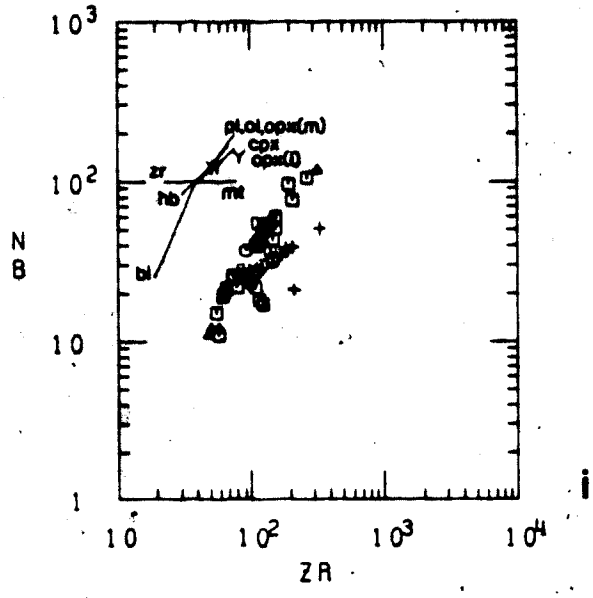
NB
ZR
i

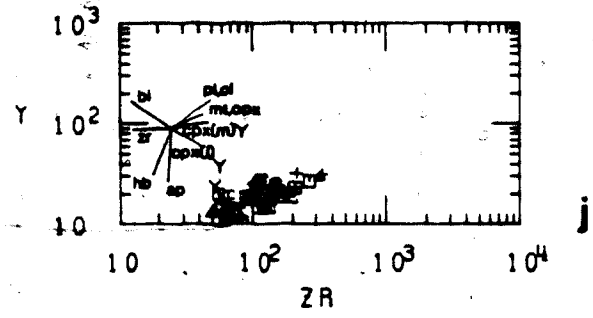
Y
ZR
j

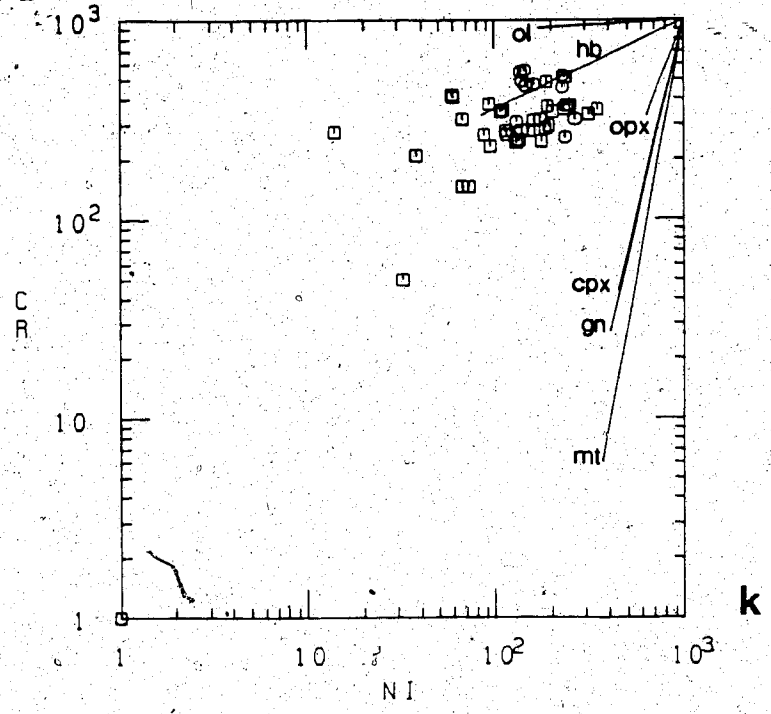
ol
hb
opx
cpx
gn
mt
C
R
NI
k

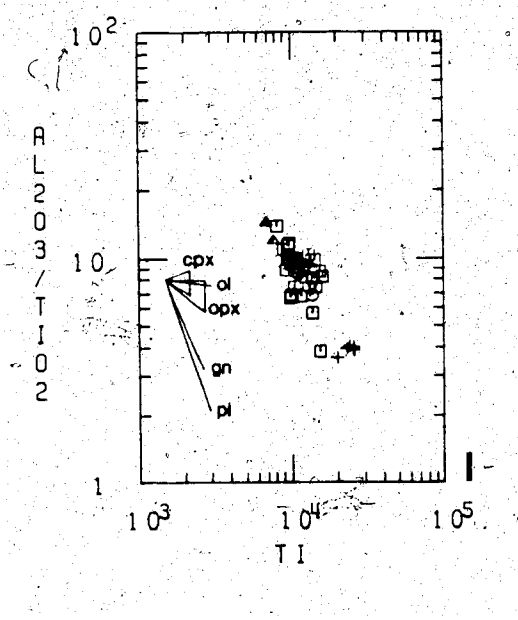
cpx
ol
opx
gn
pl
AL2O3/TIO2
TI
l

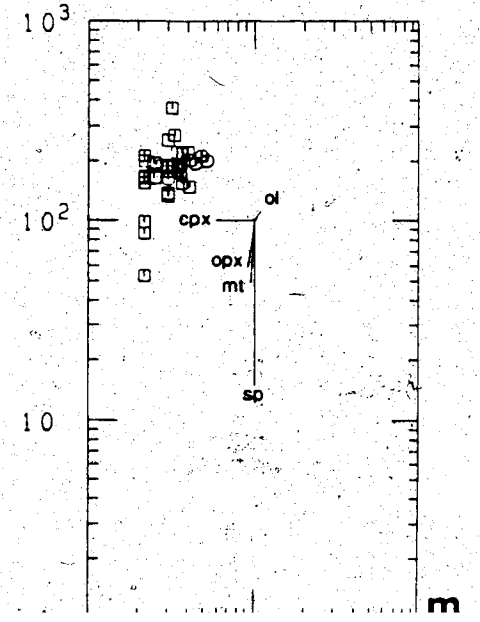
cpx
ol
opx
mt
sp
V
m

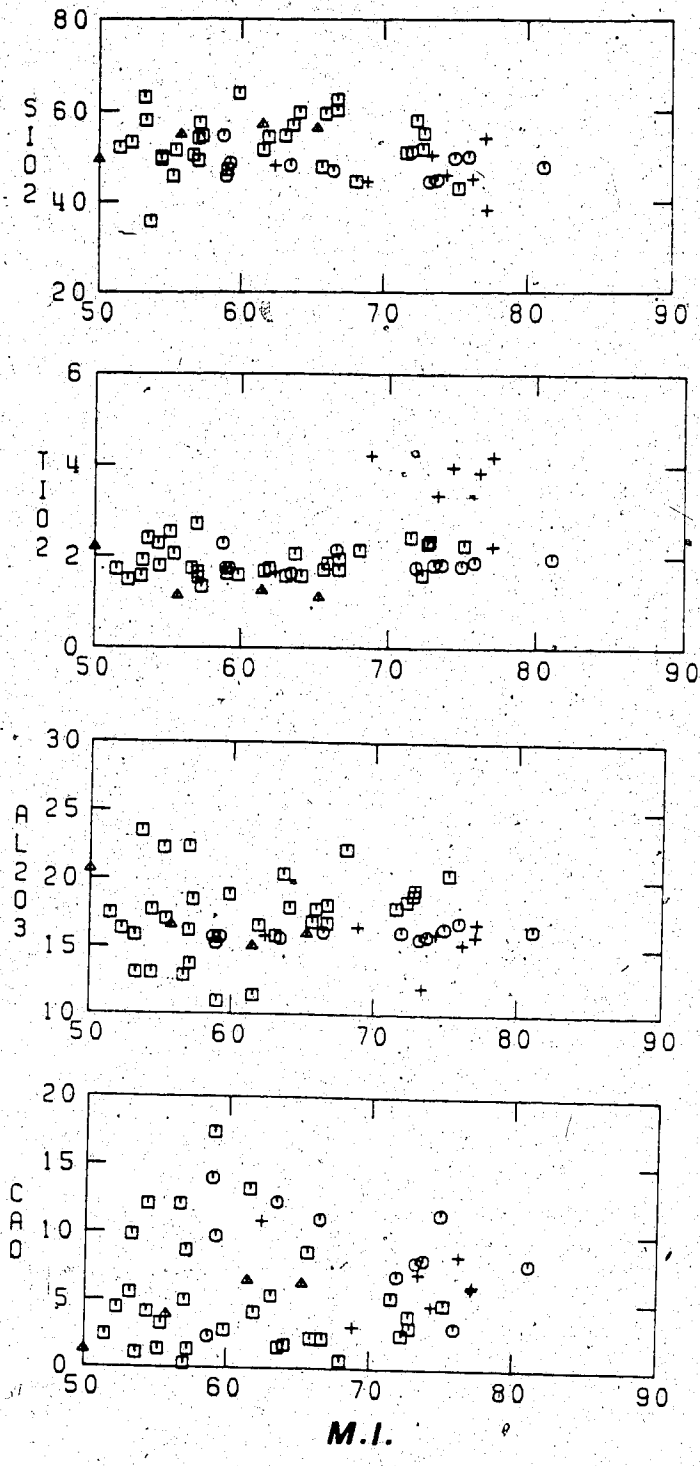
SiO2
80
60
40
20
50
60
70
80
90
TiO2
6
4
2
0
Al2O3
30
25
20
15
10
CaO
20
15
10
5
0
M.I.

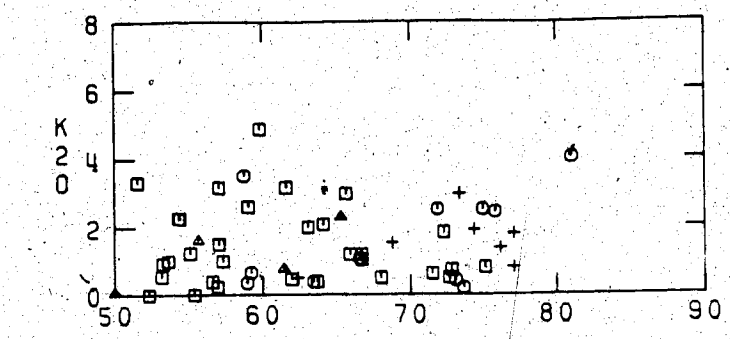
K2O
8
6
4
2
0
50
60
70
80
90

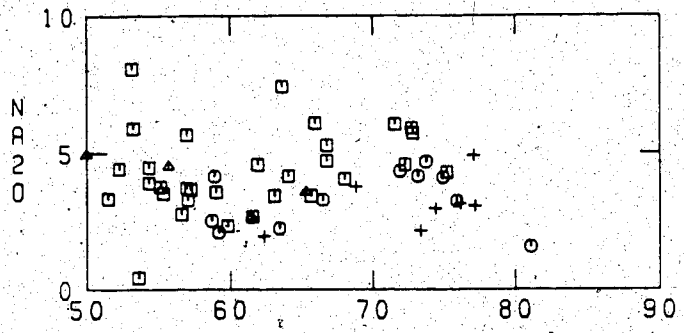
NA2O
10
5
0
50
60
70
80
90

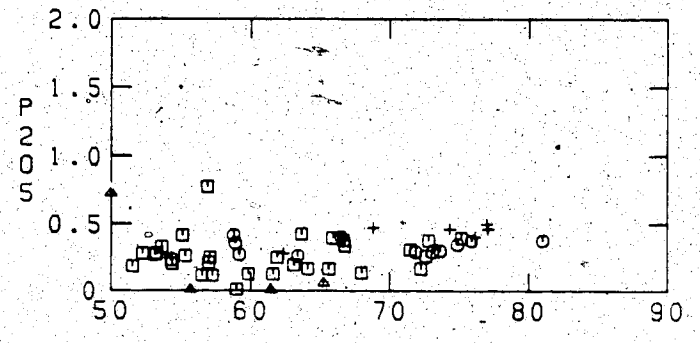
P2O5
2.0
1.5
1.0
0.5
0
50
60
70
80
90

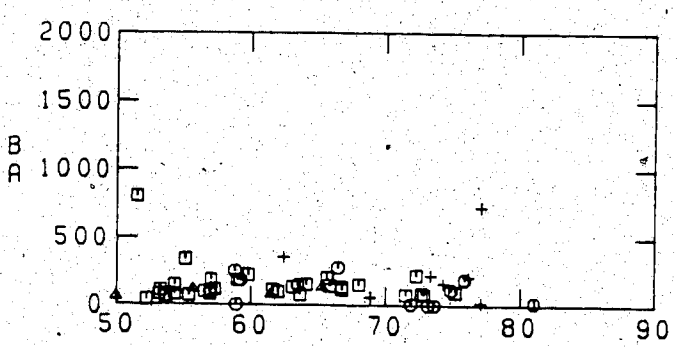
BA
2000
1500
1000
500
0
50
60
70
80
90

M. I.

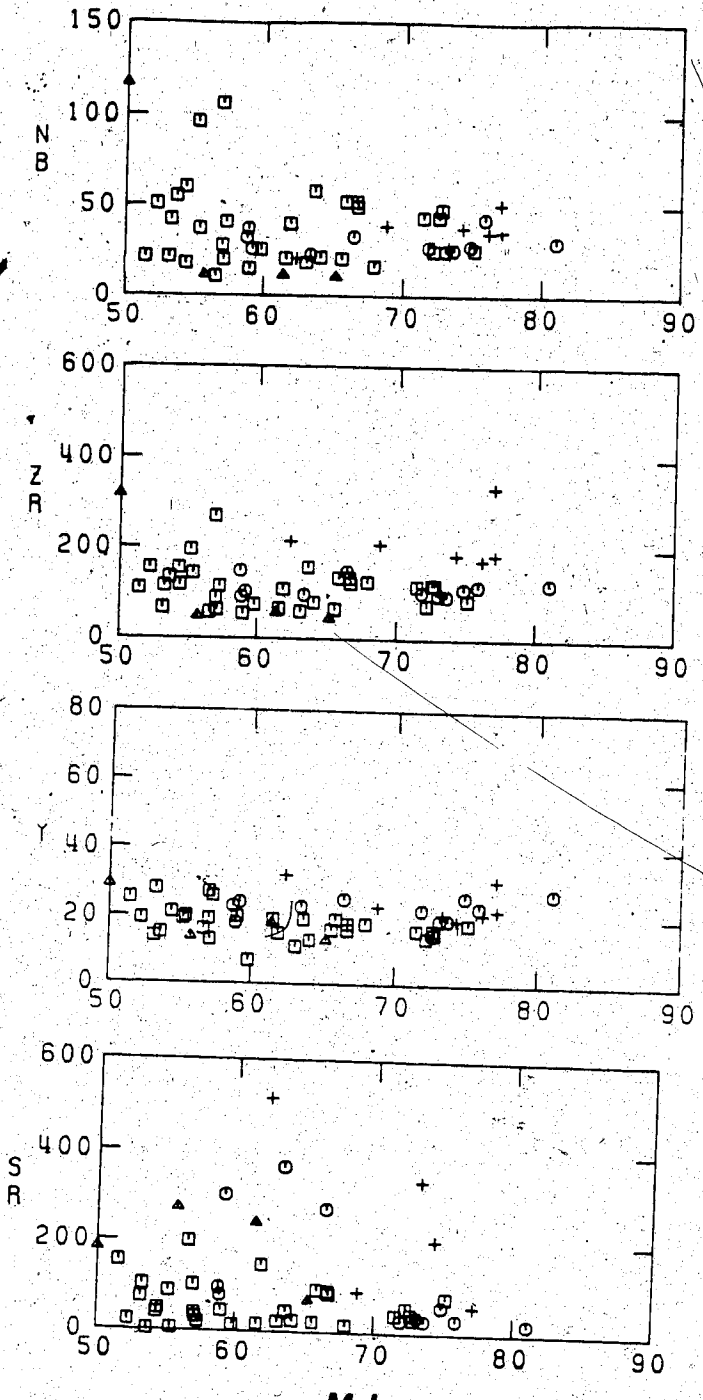
NB
150
100
50
0
ZR
600
400
200
0
Y
80
60
40
20
0
SR
600
400
200
0
50
60
70
80
90
M.I.

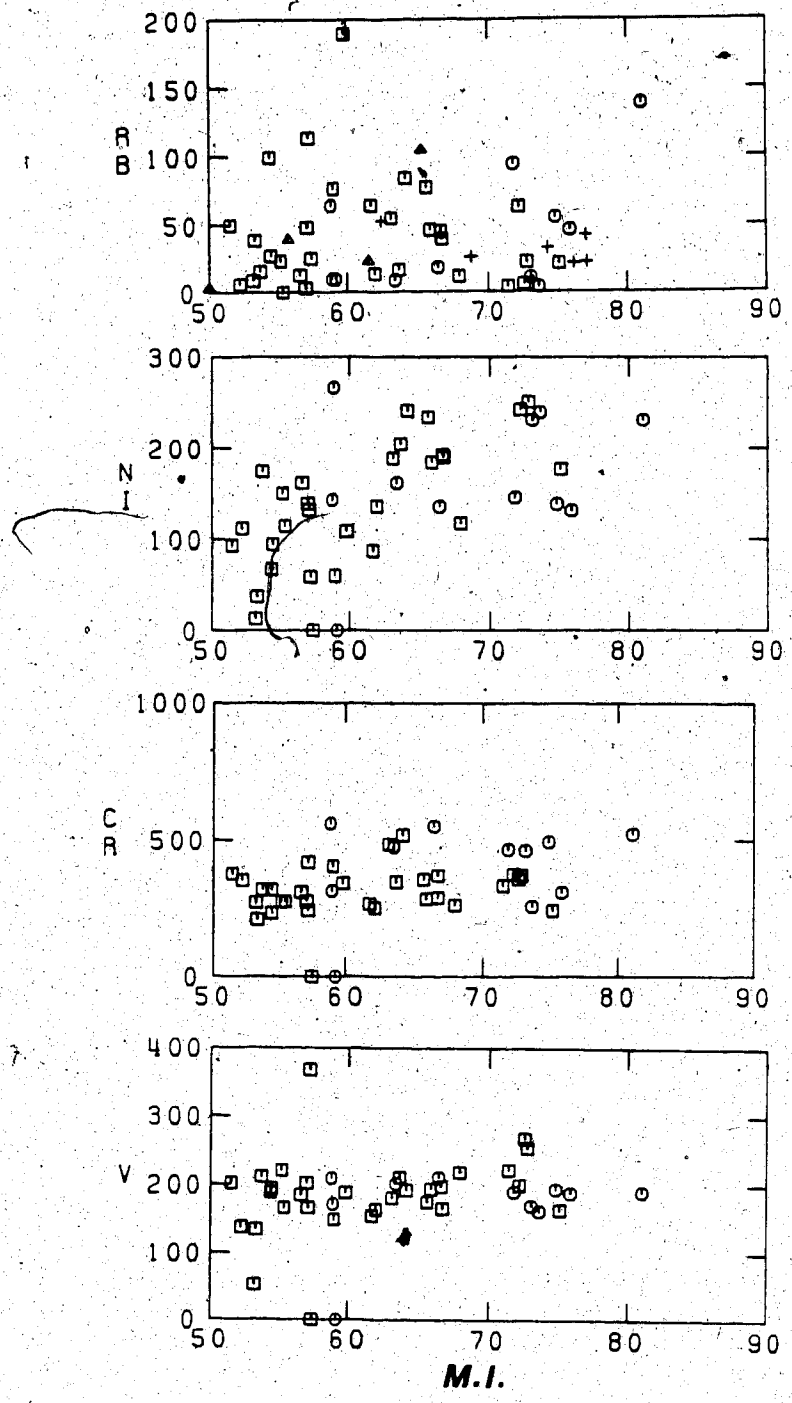
200
150
R
B 100
50
0
50
60
70
80
90
300
200
N
I
100
0
50
60
70
80
90
1000
C
R 500
0
50
60
70
80
90
400
300
V
200
100
0
50
60
70
80
90
M.I.

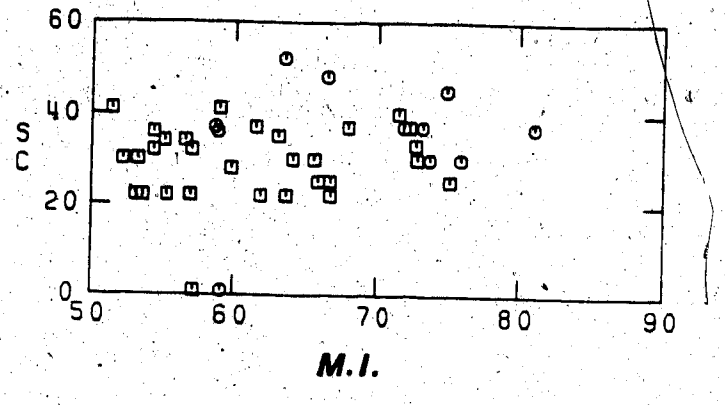
60
40
20
0
S
C
50
60
70
80
90
M.I.

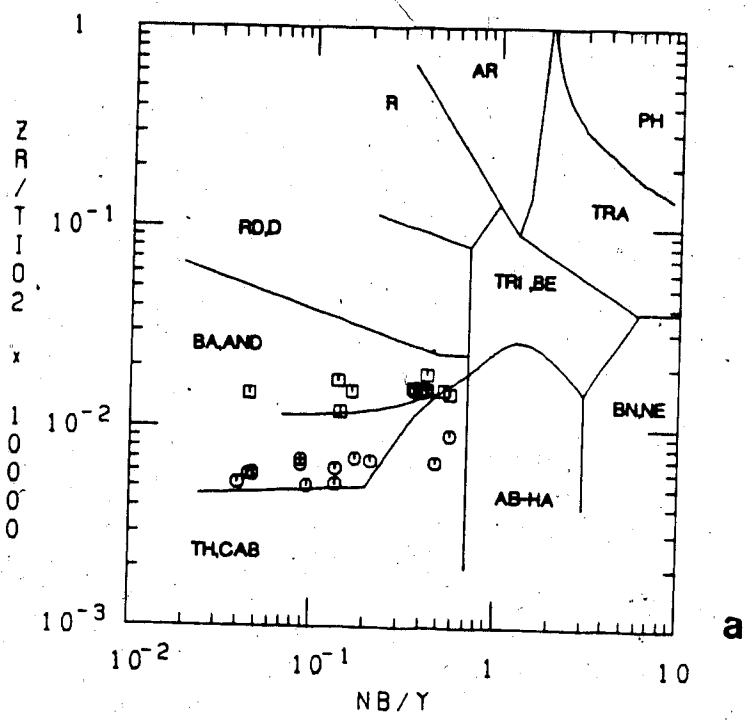
1
10^{-1}
10^{-2}
10^{-3}
ZR/TIO2 x 10000
AR
R
PH
TRA
RD,D
TRI ,BE
BA,AND
BN,NE
AB-HA
TH,CAB
10^{-2}
10^{-1}
1
10
NB/Y
a

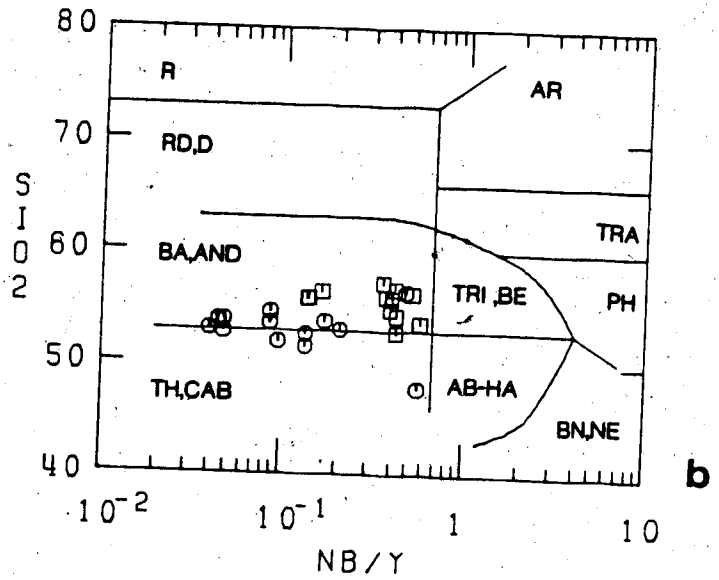
80
70
60
50
40
SIO2
R
AR
RD,D
TRA
BA,AND
TRI ,BE
PH
TH,CAB
AB-HA
BN,NE
10^{-2}
10^{-1}
1
10
NB/Y
b

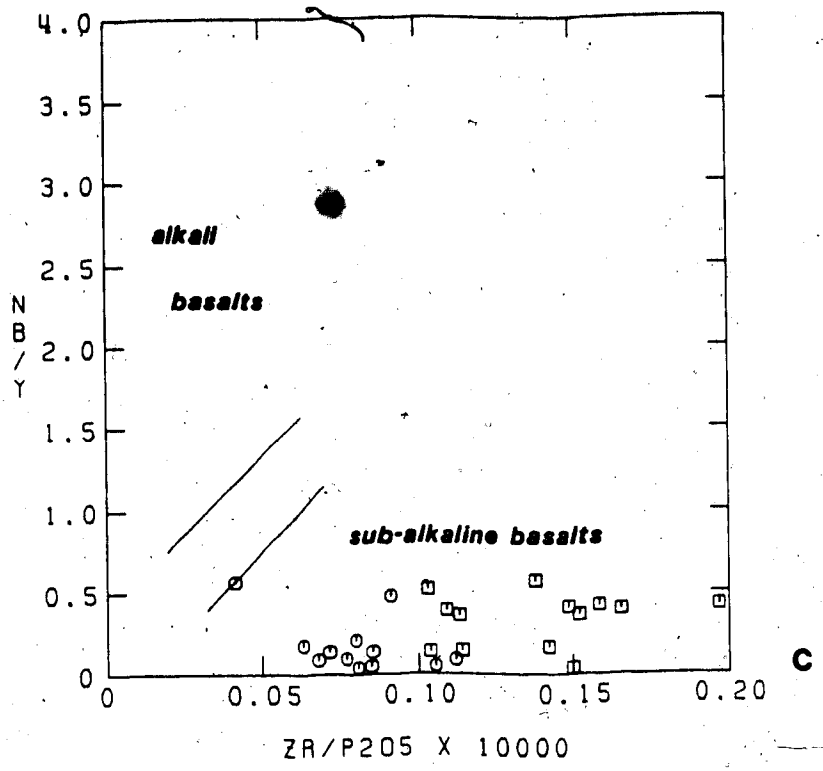
4.0
3.5
3.0
2.5
2.0
1.5
1.0
0.5
0
N
B
/
Y
alkali
basalts
sub-alkaline basalts
0
0.05
0.10
0.15
0.20
ZR/P2O5 X 10000

c

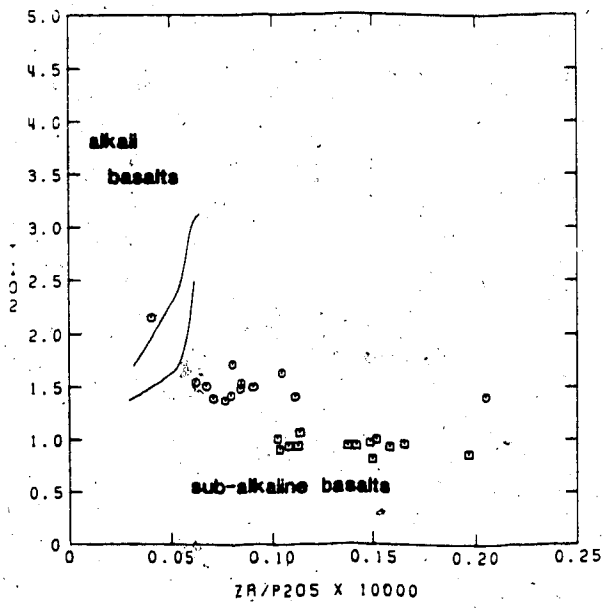
5.0
4.5
4.0
3.5
3.0
2.5
2.0
1.5
1.0
0.5
0
alkali
basalts
sub-alkaline basalts
0
0.05
0.10
0.15
0.20
0.25
ZR/P2O5 X 10000

d

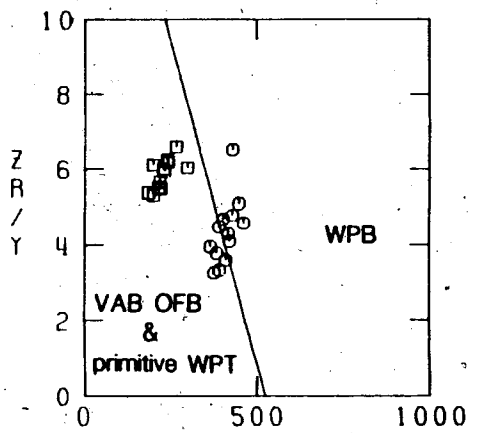
10
8
6
4
2
0
Zr/Y
WPB
VAB OFB
&
primitive WPT
0
500
1000
Ti/Y

e

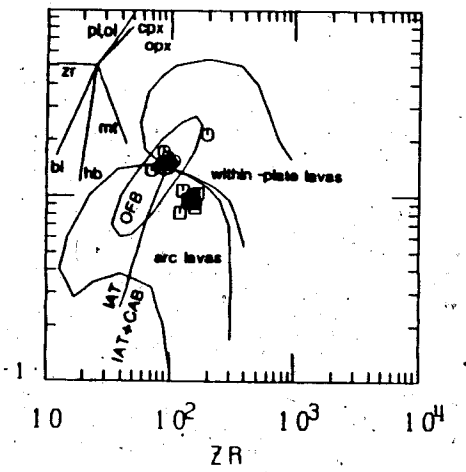
pl,ol
cpx
opx
zr
mt
bi
hb
within -plate lavas
OFB
arc lavas
MT
IAT+CAB
10
10²
10³
10⁴
ZR

f

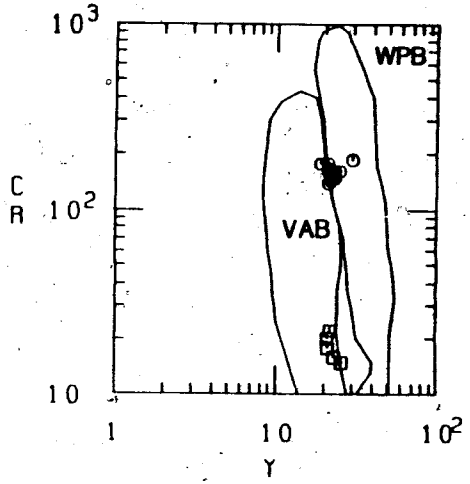
10³
10²
10
CR
WPB
VAB
1
10
10²
Y

g

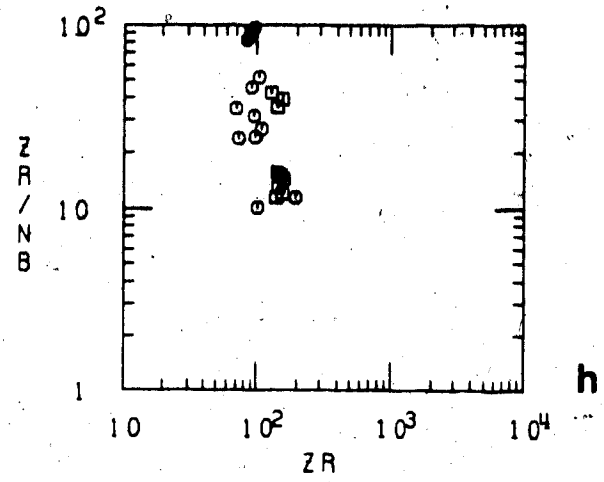
ZR/NB
ZR
h

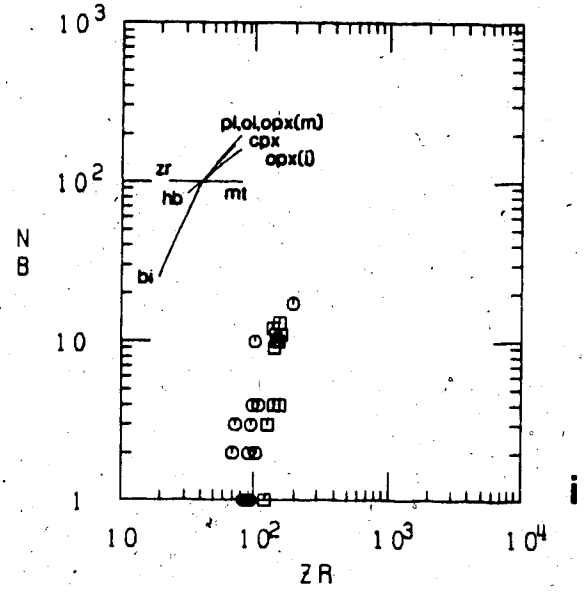
NB
ZR
pl,ol,opx(m)
cpx
opx(i)
zr
hb
mt
bi
i

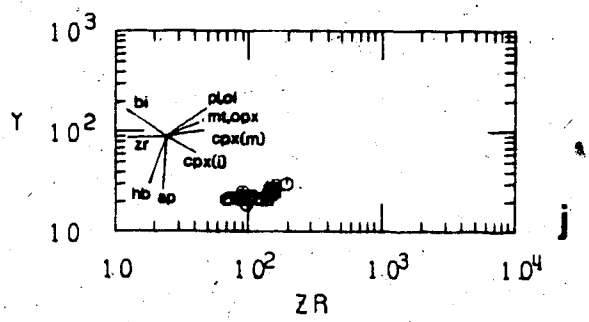
Y
ZR
bi
pl,ol
mt,opx
cpx(m)
zr
cpx(i)
hb
ap
j

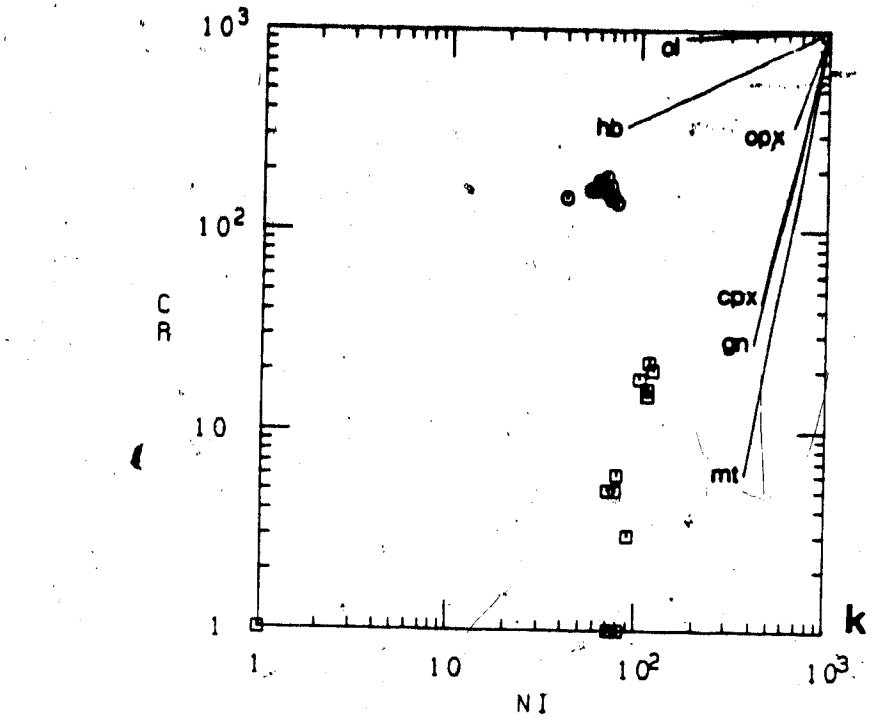
ol
hb
opx
cpx
gn
mt
k
CR
NI

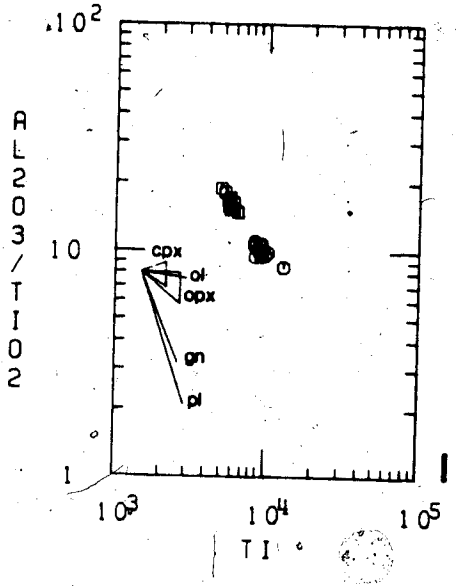
cpx
ol
opx
gn
pl
l
TI

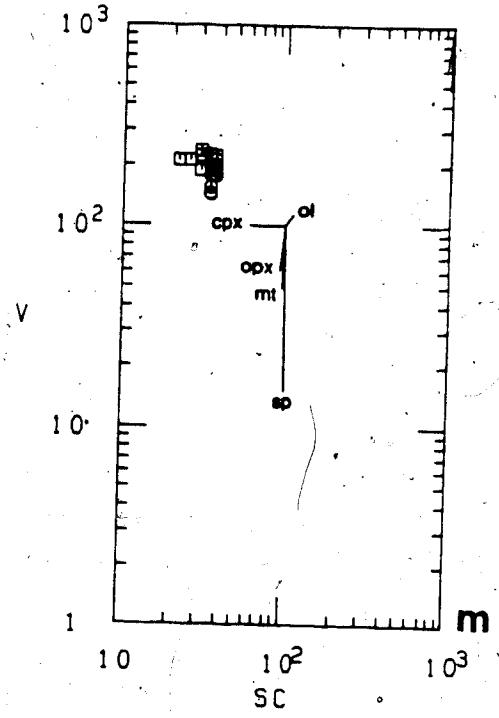
cpx
ol
opx
mt
sp
m
V
SC

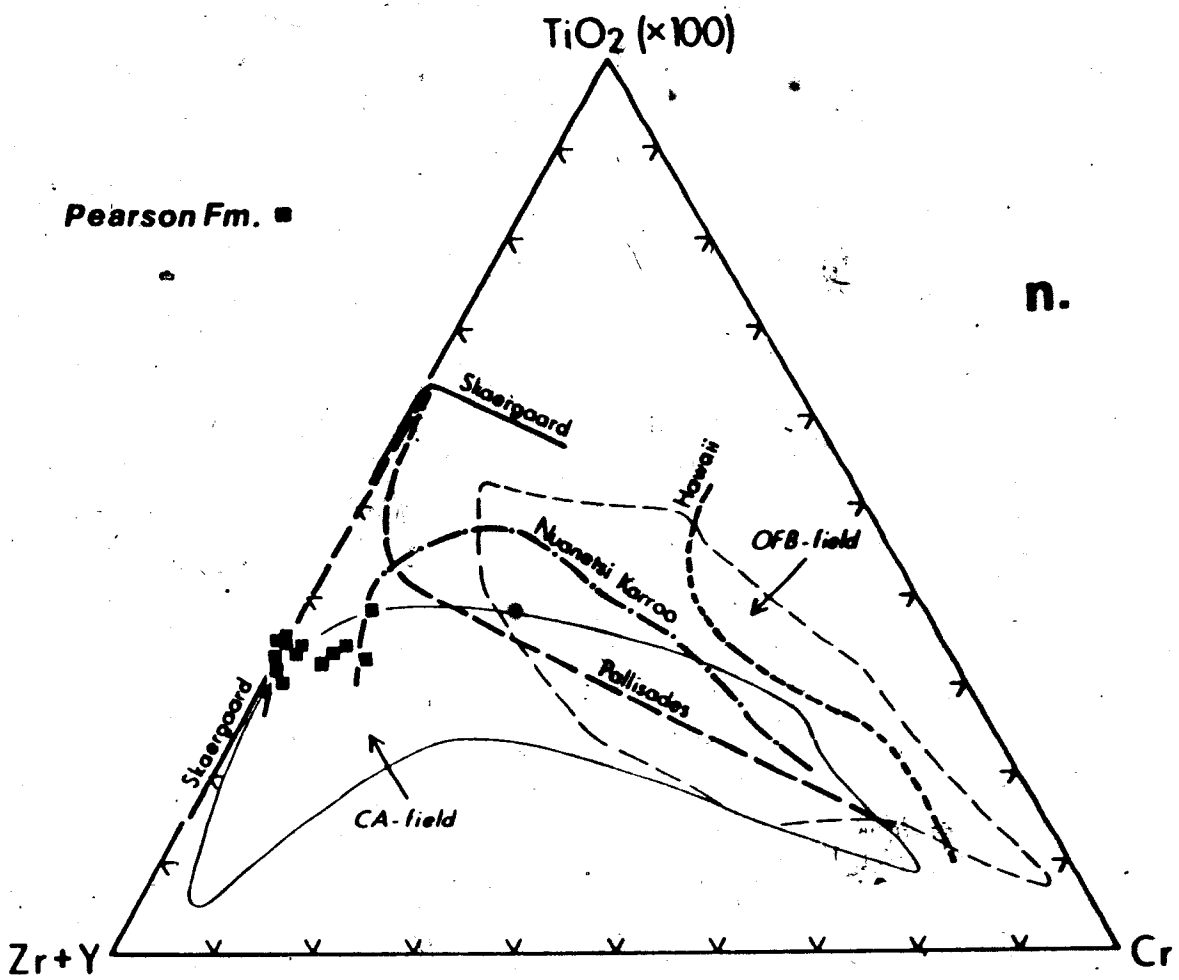
TiO2 (×100)
Pearson Fm.
n.
Skaergaard
Hawaii
Nuanetsi Karroo
OFB-field
Pallisades
Skaergaard
CA-field
Zr+Y
Cr

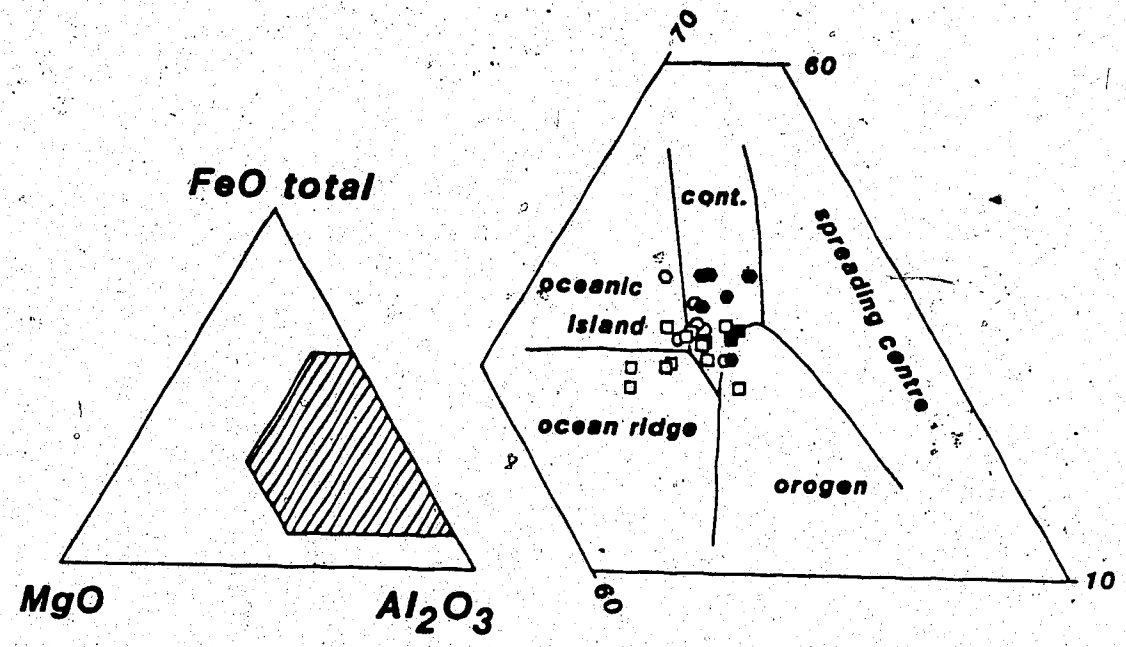

■ Pearson Fm.
● Et-Thon Gp.

(open symbols indicate mobile Ca &alk.)

O

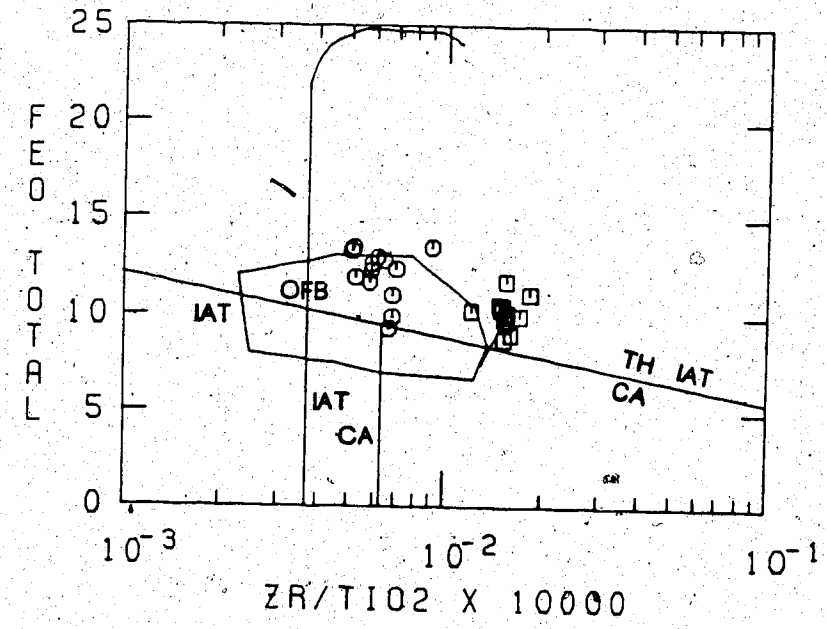

p

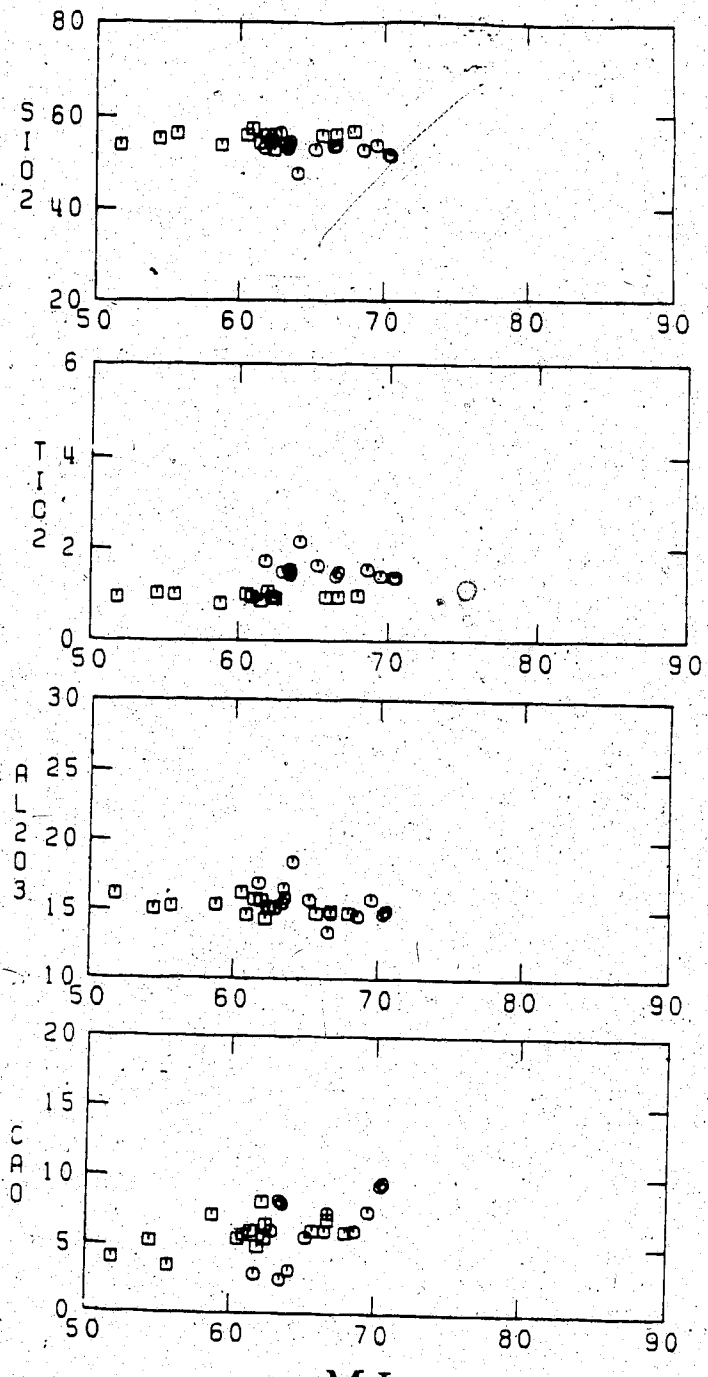
SiO2
80
60
40
20
TiO2
6
4
2
0
Al2O3
30
25
20
15
10
CaO
20
15
10
5
0
50
60
70
80
90
M.I.

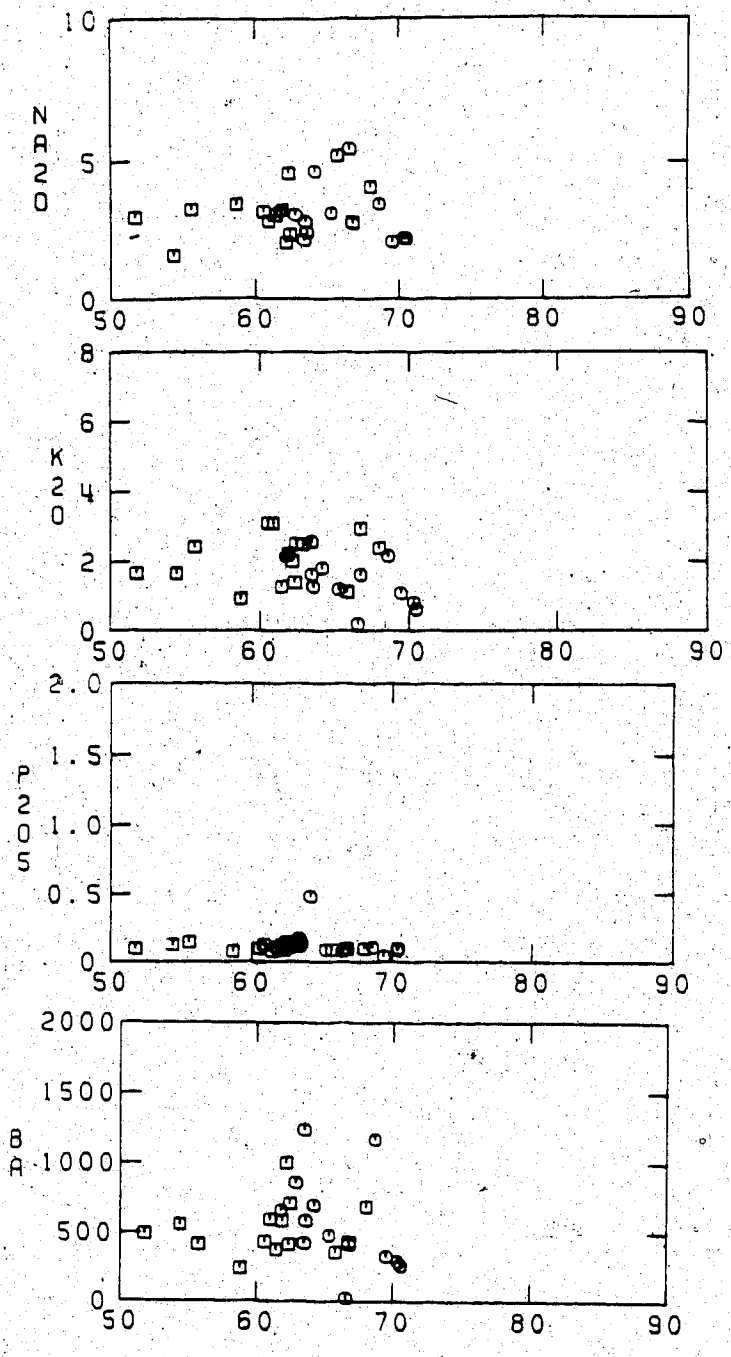
Na2O
10
5
0
50
60
70
80
90
K2O
8
6
4
2
0
P2O5
2.0
1.5
1.0
0.5
Ba
2000
1500
1000
500
M.I.

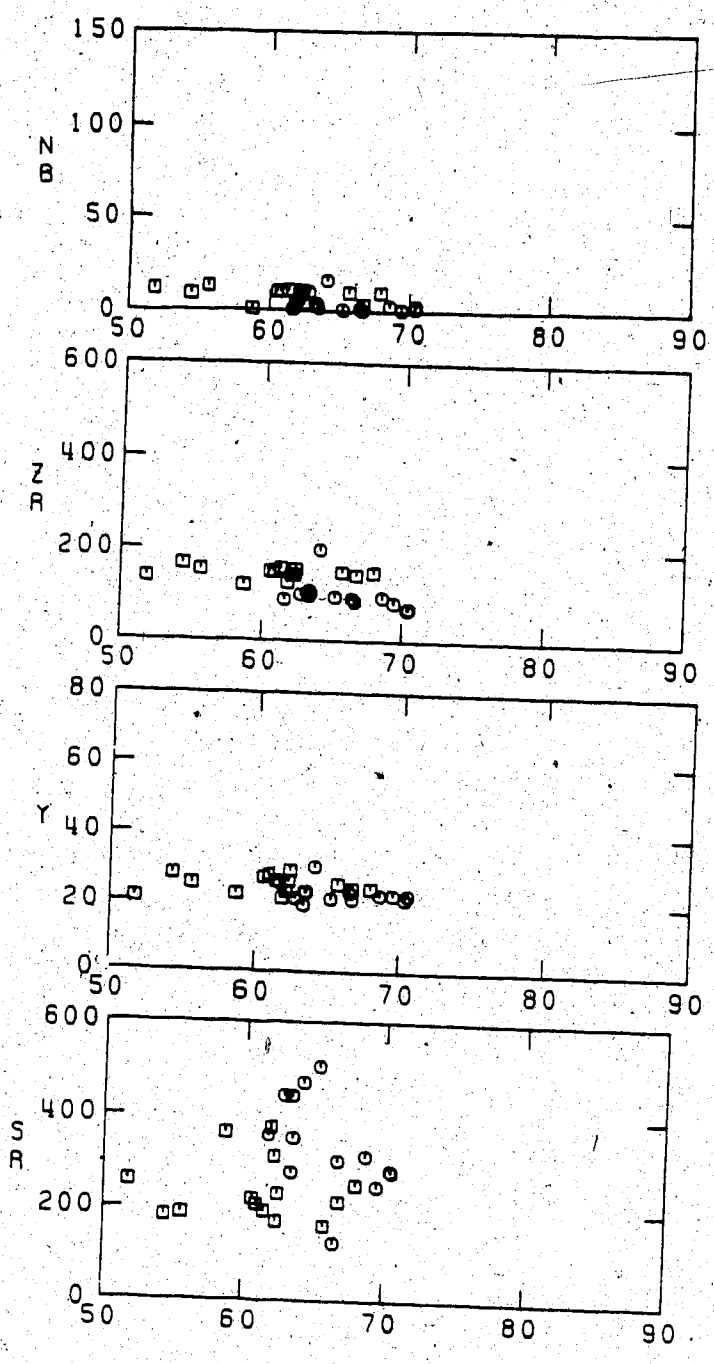

M.I.

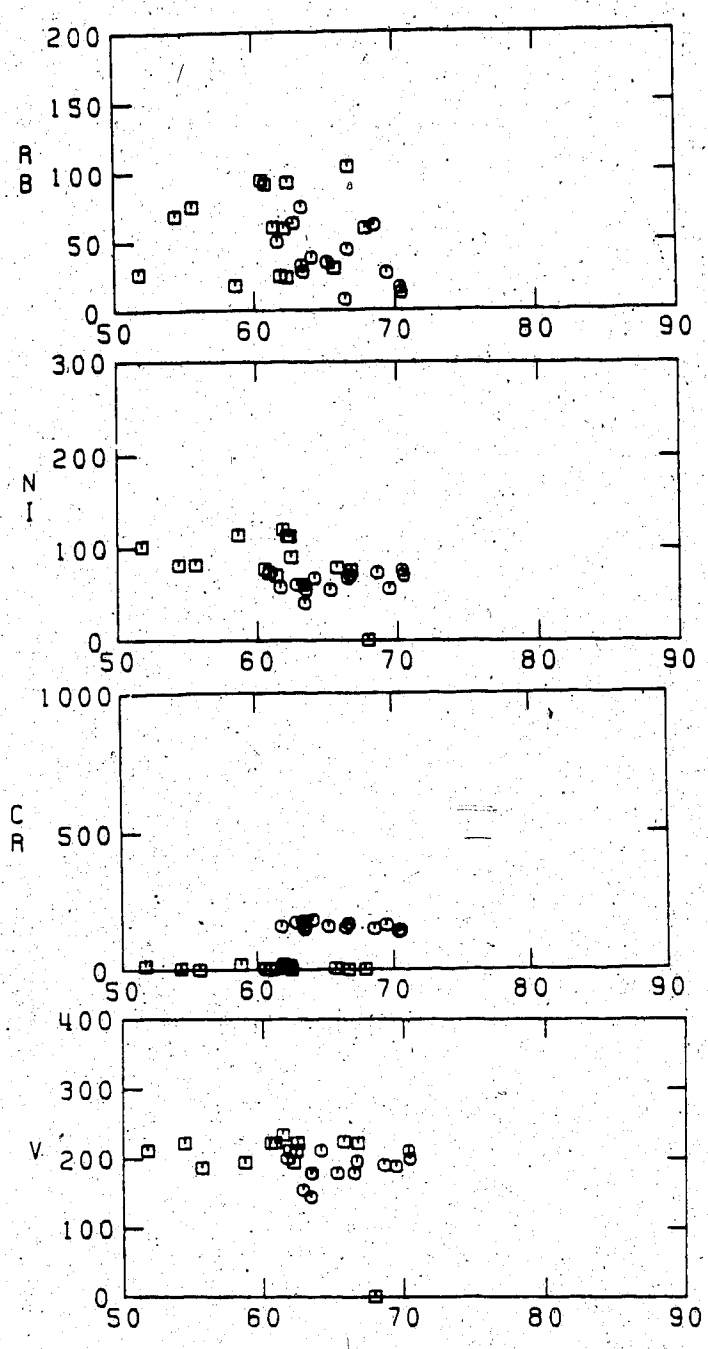

M.I.

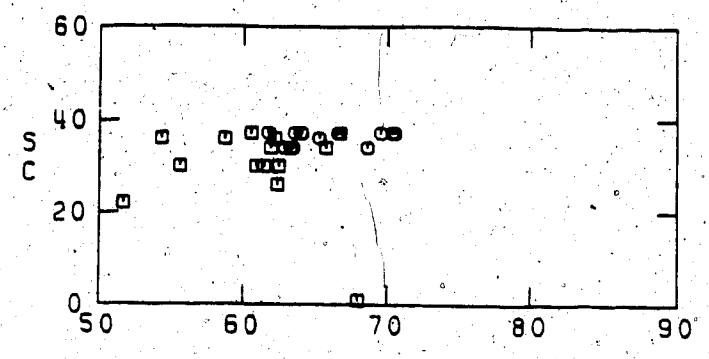
60
40
20
0
S
C
50
60
70
80
90
M.I.

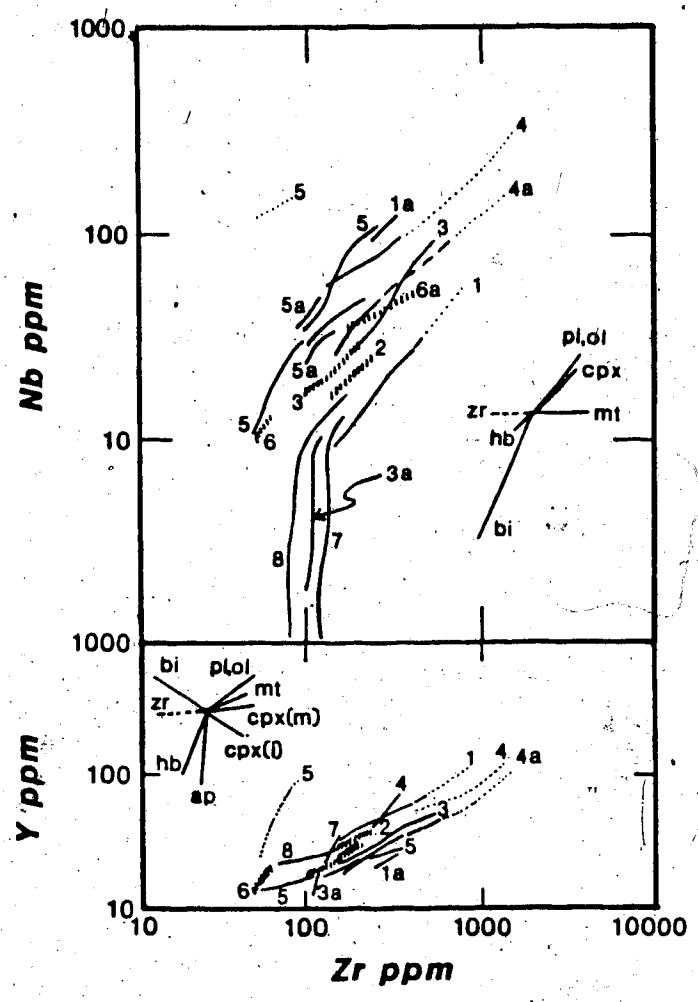
Nb ppm
1000
100
10
pl,ol
cpx
zr
mt
hb
bi
Y ppm
1000
100
10
bi
pl,ol
mt
zr
cpx(m)
cpx(l)
hb
ap
10
100
1000
10000
Zr ppm

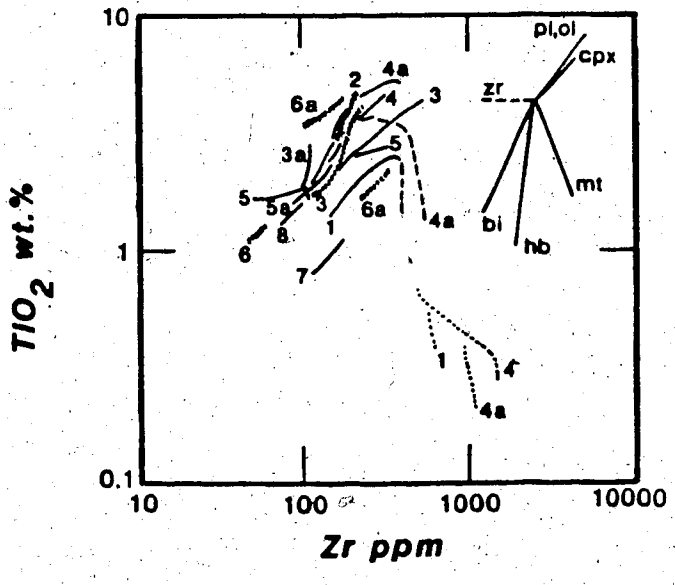
TiO2 wt.%
10
1
0.1
pl,ol
cpx
zr
mt
bi
hb
10
100
1000
10000
Zr ppm

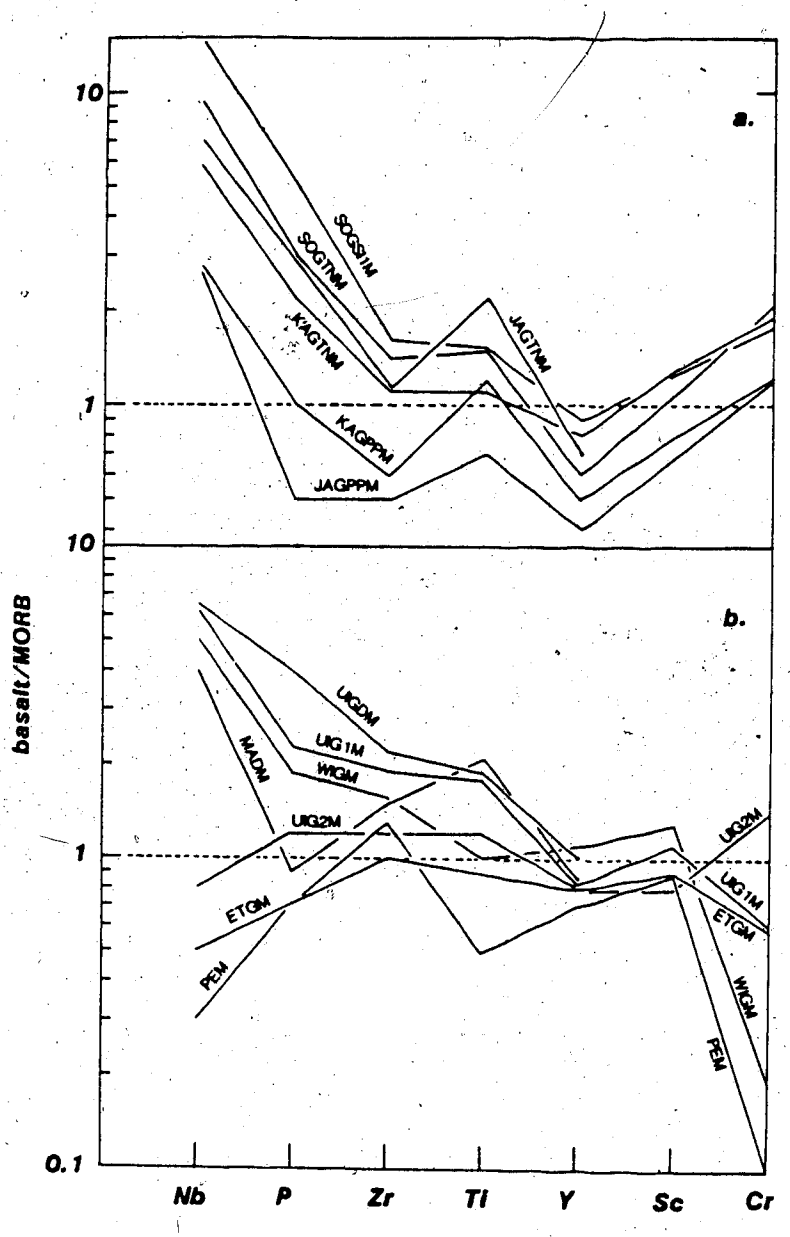
a.
b.
basalt/MORB
10
1
0.1
SOGSIM
SOGTNM
KIAGTNM
JAGTNM
KAGPPM
JAGPPM
UIGDM
UIG1M
WIGM
MADM
UIG2M
ETGM
PEM
Nb
P
Zr
Ti
Y
Sc
Cr

BIBLIOGRAPHY

Abbey, S. (1977). Studies in "standard samples" for use in the general analysis of silicate rocks and minerals. Part 5: 1977 edition of "useable" values. Geol. Surv. Can. Paper 77-34, 31pp.

Aleinikoff, J.M. (1977). Petrochemistry and tectonic origin of the Ammonoosuc volcanics, New Hampshire - Vermont. Geol. Soc. Amer. Bull., 88, pp. 1546-1552.

Allegre, C.J., Treuil, M., Minster, J.F. and Albarede, F. (1977). Systematic use of trace elements in igneous processes. Contrib. Mineral. and Petrol., 60, pp. 57-75.

Appleyard, E.C. and Bowles, E.G. (1978). The geology of the West Mine, Pilleys Island, Newfoundland. Geol. Surv. Can. Paper 78-1A, pp. 199-203.

Arculus, R.J. and Johnson, R.W. (1978). Criticism of generalised models for the magmatic evolution of arc-trench systems. Earth Planet. Sci. Letters, 39, pp. 118-126.

Arndt, N.T., Naldrett, A.J. and Pyke, D.R. (1977). Komatiitic and iron-rich tholeiitic lavas of Munro township, northeast Ontario. J. Petrol., 18, pp. 319-369.

Aumento, F., Loncarevic, B.D. and Ross, D.I. (1971). Hudson geotraverse: geology of the Mid-Atlantic Ridge at 45°.N. Phil Trans. Roy. Soc. London, A268, pp. 493-519.

Ayres, L.D. (1977). A transition from subaqueous to subaerial eruptive environments in the middle Precambrian Amisk Group at Amisk Lake, Saskatchewan - a progress report. Centre for Precambrian Studies, Univ. Manitoba, Annual Report - 1977, pp. 36-51.

Baadsgaard, H., Lambert, R.St.J. and Krupicka, J. (1976). Mineral isotopic age relationships in the polymetamorphic Amitsoq gneisses, Godthaab district, West Greenland. Geochim. Cosmochim. Acta, 40, pp. 513-527.

Baadsgaard, H., Morton, R.D. and Olade, M.A.D. (1973). Rb-Sr isotopic ace for the Precambrian lavas of the Seton Formation, East Arm of Great Slave Lake, Northwest Territories. Can. J. Earth Sci., 10, pp. 1579-1582.

Badham, J.P.N. (1978a). The early history and tectonic significance of the East Arm graben, Great Slave Lake, Canada. Tectonophys., 45, pp. 201-215.

Badham, J.P.N. (1978b). Has there been an oceanic margin to western North America since Archean time? Geology, 6, pp. 621-625.

Badham, J.P.N. (1978c). Magnetite - apatite - amphibole - uranium and silver - arsenide mineralizations in Lower Proterozoic igneous rocks, East Arm, Great Slave Lake, Canada. Econ. Geol., 73, pp. 1474-1491.

Badham, J.P.N. (1979a). Comment and reply on "Has there been an oceanic margin to western North America since Archean time?"; reply. Geology, 7, pp. 226-228.

Badham, J.P.N. (1979b). Geology and petrochemistry of lower Aphebian (2.4-2.0 Ga) alkaline plutonic and hypabyssal rocks in the East Arm of Great Slave Lake, Northwest Territories, Can. J. Earth Sci., 16, pp. 60-72.

Badham, J.P.N. (1981). Petrochemistry of late Aphebian (1.8 Ga) calc-alkaline diorites from the East Arm of Great Slave Lake, N.W.T., Canada. Can. J. Earth Sci., 18, pp. 1018-1028.

Badham, J.P.N., and Stanworth, C.W. (1977). Evaporites from the lower Proterozoic of the East Arm, Great Slave Lake. Nature, 268, pp. 516-518.

Bailey, E.B., Clough, C.T., Wright, W.B., Richey, J.E. and Wilson, G.V. (1924). Tertiary and Post-Tertiary geology of Mull. Mem. Geol. Surv. Scotland.

Baker, P.E., Gass, I.G., Harris, P.G. and LeMaitre, R.W. (1964). The volcanological report of the Royal Society expedition to Tristan da Cunha, 1962. Phil. Trans. Roy. Soc. London, A256, pp. 439-575.

Baker, B.H., Goles, G.G., Leeman, W.P., and Lindstrom, M.M. (1977). Geochemistry and petrogenesis of a basalt - benmoreite - trachyte suite from the southern part of the Gregory Rift, Kenya. Contrib. Mineral. and Petrol., 64, pp. 303-332.

Baker, B.H., Crossley, R. and Goles, G.G. (1978). Tectonic and magmatic evolution of the Southern part of the Kenya rift valley. In: Petrology and Geochemistry of Continental Rifts, Neumann, E.-R. and Ramberg, I.B. (Eds.), Reidel, Dordrecht, pp. 29-50.

Baragar, W.R.A. (1974). Volcanic studies in the Cape Smith - Wakeham Bay belt, New Quebec. Geol. Soc. Can. Paper 74-1A, pp. 155-7.

Baragar, W.R.A., Plant, A.G., Pringle, G.J. and Schau, M. (1977). Petrology and alteration of selected units of

Mid-Atlantic Ridge Basalts sampled from sites 332 and 335, DSDP. Can. J. Earth. Sci., 14, pp. 837-874.

Barker, D.S. (1977). Northern Trans-Pecos magmatic province: introduction and comparison with the Kenya rift. Geol. Soc. Amer. Bull., 88, pp. 1421-1427.

Barr, K.G. (1971). Crustal refraction experiment: Yellowknife 1966. J. Geophys. Res., 76, pp. 1929-1947.

Barron, B.J. (1976). Recognition of the original volcanic suite in altered mafic volcanic rocks at Sofala, New South Wales. Amer. J. Sci., 276, pp. 604-636.

Beccaluva, L., Ohnenstetter, D. and Ohnenstetter, M. (1979). Geochemical discrimination between ocean-floor and island-arc tholeiites - application to some ophiolites. Can J. Earth Sci., 16, pp. 1874-1882.

Beckinsale, R.D., Pankhurst, R.J., Skelhorn, R.R. and Walsh, J.N. (1978). Geochemistry and petrogenesis of the Early Tertiary lava pile of the Isle of Mull, Scotland. Contrib. Mineral. and Petrol., 66, pp. 415-427.

Bell, K. and Blenkinsop, J. (1978). Reset Rb/Sr whole-rock systems and chemical control. Nature, 273, pp. 532-534.

Beswick, A.E. and Soucie, G. (1978). A correction procedure for metasomatism in an Archean greenstone belt. Precamb. Research, 6, pp. 235-248.

Bischoff, J.L. and Dickson, F.W. (1975). Seawater - basalt interaction at 200°C and 500 bars: implications for origin of sea-floor heavy-metal deposits and regulation of seawater chemistry. Earth Planet. Sci. Letters, 25, pp. 385-347.

Bizouard, M., Barberi, F. and Varet, J. (1980). Mineralogy and petrology of Erta Ale and Boina volcanic series, Afar rift, Ethiopia. J. Petrol., 21, pp. 401-436.

Blackadar, D.W. (1981). The Aristifats diatreme; a Proterozoic copper-lead-cobalt-nickel deposit, Northwest Territories. Unpub. M.Sc. thesis, University of Alberta. 372 pp.

Blake, D.H. and Ewart, A. (1974). Petrography and geochemistry of the Cape Hoskins volcanoes, New Britain, Papua, New Guinea. J. Geol. Soc. Australia, 21, pp. 319-331.

Bloxham, J.W. and Lewis, A.D. (1972). Ti, Zr and Cr in some British pillow lavas and their petrogenetic affinities. Nature Phys. Sci., 237, pp. 134-136.

Bonatti, E., Honnorez, J. and Ferrara, G. (1971). Peridotite-gabbro-basalt complex from the equatorial Mid-Atlantic Ridge. Phil. Trans. Roy. Soc. London, A268, pp. 385-402.

Bose, M.K. (1972). Deccan basalts. Lithos, 5, pp. 131-145.

Brooks, C.K. (1973). Tertiary of Greenland - a volcanic and plutonic record of continental break-up. In: Arctic Geology, Proc. 2nd. Int. Symp. on Arctic Geol., 1971, Pitcher, M.G. (Ed)., Mem. Amer. Assoc. Petroleum Geol., 19, pp. 150-160.

Brooks, C.K. and Hart, S.R. (1974). On the significance of komatiite. Geology, 2, pp. 107-110.

Brooks, C. and Hart, S.R. (1978). Rb-Sr mantle isochrons and variations in the chemistry of Gondwanaland's lithosphere. Nature, 271, pp. 220-223.

Brooks, C.K. and Nielsen, T.F.D. (1978). Early stages in the differentiation of the Skaergaard magma as revealed by a closely related suite of dike rocks. Lithos, 11, pp. 1-14.

Brown, E.H. (1977). The crossite content of a Ca-amphibole as a guide to pressure of metamorphism. J. Petrol., 18, pp. 53-72.

Brown, G.M., Holland, J.G., Sigurdson, H., Tomblin, J.F. and Arculus, R.J. (1977). Geochemistry of the Lesser Antilles volcanic island arc. Geochim. Cosmochim. Acta, 41, pp. 785-801.

Bruhn, R.L., Stern, C.R. and DeWit, M. (1978). Field and geochemical data bearing on the development of a Mesozoic volcano-tectonic rift zone and back-arc basin in southernmost South America. Earth Planet. Sci. Letters, 41, pp. 32-46.

Bryan, W.B., Stice, G.D. and Ewart, A. (1972). Geology, petrography and geochemistry of the volcanic islands of Tonga. J. Geophys. Res., 77, pp. 1566-1585.

Bryan, W.B. and Thompson, G. (1977). Basalts from DSDP Leg 37 and the FAMOUS area: compositional and petrogenetic comparisons. Can. J. Earth Sci., 14, pp. 875-885.

Burke, K. (1977). Aulacogens and continental breakup. In: Annual Review of Earth and Planetary Sciences, Donath, F.A., Stehli, F.G. and Wetherill, G.W. (Eds.). Ann Reviews Inc., Calif., 5, pp. 371-396.

Burke, K. and Dewey, J.F. (1973). Plume generated triple

junctions: key indicators in applying plate tectonics to old rocks. J. Geol., 81, pp. 406-443.

Burwash, R.A. and Baadsgaard, H. (1962). Yellowknife-Nonacho age and structural relations. Roy. Soc. Can., Spec. Publ. no 4, pp. 22-29.

Burwash, R.A. and Cavell, P.A. (1978). Uranium-thorium enrichment in alkali olivine basalt magma - Simpson Islands dyke, Northwest territories Canada. Contrib. Mineral. and Petrol., 66, pp. 243-250.

Burwash, R.A. and Krupicka, J. (1970). Cratonic reactivation in the Precambrian basement of western Canada. Part II. Metasomatism and isostacy. Can. J. Earth Sci., 7, pp. 1275-1294.

Burwash, R.A., Krupicka, J. and Culbert, R.R. (1973). Cratonic reactivation in the Precambrian basement of western Canada. III. Crustal evolution. Can. J. Earth Sci., 10, pp. 283-291.

Burwash, R.A., Baadsgaard, H., Campbell, F.A., Cumming, G.L. and Folinsbee, R.E. (1963). Potassium-argon dates of diabase dyke systems, District of Mackenzie, N.W.T. Trans. Can. Inst. Mining Met., 66, pp. 303-307.

Campbell, F.H.A. (1980). Evolution of the Early Proterozoic Kilohigok Basin, N.W.T., Geol. Assoc. Can. Prog. with Abstr., 5, p. 44.

Campbell, F.H.A. and Cecile, M.P. (1981). Evolution of the early Proterozoic Kilohigok Basin, Bathurst Inlet - Victoria Island. Northwest Territories. In: Proterozoic Basins of Canada, Campbell, F.H.A. (Ed.). Geol. Surv. Can. Paper 81-10, pp. 103-131.

Cann, J.R. (1969). Spilites from the Carlsberg Ridge, Indian Ocean. J. Petrol., 10, pp. 1-19.

Cann, J.R. (1970). Rb, Sr, Y; Zr and Nb in some ocean floor basaltic rocks. Earth Planet. Sci. Letters, 10, pp. 7-11.

Carlisle, D. (1963). Pillow breccias and their aquagene tuffs, Quadra Island, British Columbia. J. Geol., 71, pp. 48-71.

Carmichael, I.S.E. (1964). The petrology of Thingmuli, a Tertiary volcano in eastern Iceland. J. Petrol., 5, pp. 435-460.

Carter, S.R., Evensen, N.M., Hamilton, P.J. and O'Nions, R.K. (1978). Neodymium and strontium isotope evidence

for crustal contamination of continental volcanics. Science, 202, pp. 743-747.

Cawthorn, R.G. and O'Hara, M.J. (1976). Amphibole fractionation in calc-alkaline magma genesis. Amer. J. Sci., 276, pp. 309-329.

Chayes, F. (1966). Alkaline and subalkaline basalts. Amer. J. Sci., 264, pp. 128-145.

Chayes, F. (1971). Ratio Correlation:a Manual for Students of Petrology and Geochemistry. Univ. of Chicago Press, 99 pp.

Christie, K.W., Davidson, A. and Fahrig, W.F. (1975). The palaeomag-netism of Kaminak dykes - no evidence of significant Hudsonian plate motion. Can. J. Earth Sci., 12, pp. 2048-2064.

Church, B.N. (1975). Quantitative classification and chemical comparison of common volcanic rocks. Geol. Soc. Amer. Bull., 86, pp. 257-263.

Civetta, L., de Fino, M., Gasparini, P., Ghiara, M.R., LaVolpe, L. and Lirer, L. (1975). Structural meaning of east-central Afar volcanism (Ethiopia, T.F.A.I.) J. Geol., 83, pp. 363-373.

Clarke, D.B. (1970). Tertiary basalts of Baffin Bay: possible primary magma from the mantle. Contrib. Mineral. and Petrol, 25, pp. 203-224.

Clarke, D.B. (1977). The tertiary volcanic procince of Baffin Bay. In: Volcanic Regimes in Canada, Baragar, W.R.A., Coleman, L.C. and Hall, J.M. (Eds.). Geol. Ass. Can. Spec. Pap., 16, pp. 445-460.

Clayton, R.N. and Mayeda, T.K. (1963). The use of bromine pentafluoride in the extraction of oxygen from oxides and silicates for isotopic analysis. Geochim. Cosmochim. Acta, 27, pp. 43-52.

Coats, R.R. (1963). Basaltic andesites. In: Basalts, Vol. 2, Hess, H.H. and Poldervaart, A. (Eds.), J. Wiley and Sons, N.Y., pp. 689-736.

Coish, R.A. (1977). Ocean floor metamorphism in the Betts Cove ophiolite, Newfoundland. Contrib. Mineral. and Petrol., 60, pp. 255-270.

Coish, R.A. and Taylor, L.A. (1978). The effects of cooling rate on the chemistry of pyroxenes from DSDP leg 34 basalt. Geol. Soc. Amer. Abs. with Prog., 10, p.382.

Colley, H. and Warden, A.J. (1974). Petrology of the New Hebrides. Geol. Soc. Amer. Bull., 85, pp. 1635-1646.

Compston, W., McDougall, I. and Heier, K.S. (1968). Geochemical comparison of the Mesozoic basaltic rocks of Antarctica, South Africa, South America and Tasmania. Geochim. Cosmochim. Acta, 32, pp. 129-149.

Condie, K.C. (1976). Trace-element geochemistry of Archean greenstone belts. Earth Sci. Rev., 12, pp. 393-417.

Condie, K.C., Viljoen, M.J. and Kable, E.J.D. (1977). Effects of alteration on element distributions in Archean tholeiites from the Barberton greenstone belt, South Africa. Contrib. Mineral. and Petrol., 64, pp. 75-89.

Coombs, D.S. (1963). Trends and affinities of basaltic magmas and pyroxones as illustrated on the diopside, olivine, silica diagram. Mineral. Soc. Amer. Spec. Pap., 1, pp. 227-250.

Coombs, D.S., Nakamura, Y. and Vuagnat, M. (1976). Pumpellyite-actinolite facies schists of the Taveyanne Formation near Loeche, Valais, Switzerland. J. Petrology, 17, pp. 440-471.

Copeland, R.A., Frey, F.A. and Wones, D.R. (1971). Origin of clay minerals in a Mid Atlantic Ridge sediment [redacted]rth Planet. Sci. Letters, 10, pp. 186-192.

Cox, K.G. and Bell, J.D. (1972). A crystal fractionation model for basaltic rocks of the New Georgia Group, British Solomon Islands. Contrib. Mineral. and Petrol, 37, pp. 1-13.

Cox, K.G. and Hornung, G. (1966). The petrology of the Karroo basalts of Basutoland. Amer. Mineral., 51, pp. 1414-1432.

Cox, K.G., Macdonald, R. and Hornung, G. (1967). Geochemical and petrographic provinces in the Karroo basalts of southern Africa. Amer. Mineral., 52, pp. 1451-1474.

Cox, K.G., Bell, J.D. and Pankhurst, R.J. (1979). The Interpretation of Igneous Rocks, G. Allen and Unwin Ltd., London. 450 pp.

Craig, H. (1961). Standard for reporting concentrations of deuterium and oxygen-18 in natural waters. Science, 133, pp. 1833-1834.

Crawford, M.L. (1981). Fluid inclusions in metamorphic rocks - low and medium grade. In: Short Course in Fluid

Inclusions: Applications to Petrology, Hollister, L.S. and Crawford, M.L. (Eds.). Mineral. Assoc. Can., pp. 157-181.

Cumming, G.L. (1980). Lead isochron of the Seton Formation, East Arm of Great Slave Lake, Northwest Territories. Can. J. Earth Sci., 17, pp. 1591-1593.

Dalziell, I.W.D. and Elliot, D.H. (1973). The Scotia arc and Antarctic margin. In: The Ocean Basins and Margins, V.1, Nairn, A.E.M. and Stelhi, F.G. (Eds.). Plenum Press, N.Y., pp. 171-246.

Davidson, A. (1972). Brislane Lake pluton, District of Mackenzie. In: Rubidium Strontium Isochron Age Studies, Rept. no 1, Wanless, R.K. and Loveridge, W.D. (Eds.). Geol. Surv. Can. Paper 72-23, p. 7.

Davidson, A. (1978). The Blachford Lake intrusive suite: and Aphebian alkaline plutonic complex in the Slave province, Northwest Territories. Geol. Surv. Can. Paper 78-1A, pp. 119-127.

Davies, G.A. (1980). Problems of intraplate extensional tectonics, western United States. In: Continental Tectonics, National Acad. Sci., Washington, D.C. pp. 84-95.

Davies, J.F., Grant, R.W.E. and Whitehead, R.E.S. (1979). Immobile trace elements and Archean volcanic stratigraphy in the Timmins mining area, Ontario. Can. J. Earth Sci., 16, pp. 305-311.

Davies, R.D. and Allsopp, H.L. (1976). Strontium isotopic evidence relating to the evolution of the lower Precambrian granitic crust in Swaziland. Geology, 4, pp. 553-556.

Davis, D.W., Gray, G., Cumming, G.L. and Baadsgaard, H. (1977). Determination of the ^{87}Rb decay constant. Geochim. Cosmochim. Acta, 41, pp. 1745-1749.

Dawson, J.B. and Smith, J.V. (1982). Upper mantle amphiboles: a review. Mineral. Mag., 45, pp. 35-46.

de Albuquerque, C.A.R. (1979). Origin of the plutonic mafic rocks of southern Nova Scotia. Geol. Soc. Amer. Bull., 90, pp. 719-731.

de Boer, J. and Snider, F.G. (1979). Magnetic and chemical variation of Mesozoic diabase dikes from eastern North America: evidence for a hotspot in the Carolinas. Geol. Soc. Amer. Bull., 90, pp. 185-198.

Deer, W.A., Howie, R.A. and Zussman, J. (1963). Rock Forming Minerals, V.2., Longmans.

Dewey, J.F. and Burke, K. (1974). Hot spots and continental break-up. Geology, 2, pp. 57-60.

Donaldson, C.H., Usselman, T.M., Williams, R.J. and Lofgren, G.E. (1975). Experimental modelling of the cooling history of Apollo 12 olivine basalts. proc. Lunar Sci. Conf. 6th, pp. 843-869.

Donaldson, J.A., Irving, E., Tanner, J. and McGlynn, J. (1976). Stockwell symposium on the Hudsonian orogeny and plate tectonics, Geoscience Can., 3, pp. 285-291.

Donnelly, T.W. (1966). Geology of St. Thomas and St. John, U.S. Virgin Islands. Mem. Geol. Soc. Amer., 260, pp. 481-500.

Duncan, R.A. and Compston, W. (1976). Sr-isotopic evidence for an old mantle source region for French Polynesian volcanism. Geology, 4, pp. 728-732.

Easton, R.M. (1980). Stratigraphy and geochemistry of the Akaitcho Group, Hepburn Lake map area, District of Mackenzie: an initial rift succession in Wopmay orogen (early Proterozoic). Geol. Surv. Can. Paper 80-1B, pp. 47-57.

Easton, R.M. (1981). Stratigraphy of the Akaitcho Group and the development of an early Proterozoic continental margin, Wopmay orogen, Northwest Territories. In: Proterozoic basins of Canada, Campbell, F.H.A. (Ed.). Geol. Surv. Can. Paper 81-10, pp. 79-95.

Elston, W.E. and Bornhorst, T.J. (1979). The Rio Grande rift in context of regional post-40 M.Y. volcanic and tectonic events. In: Rio Grande Rift: Tectonics and Magmatism, Riecker, R.E. (Ed.). Amer. Geophys. Union, pp. 416-438.

Elthon, D. and Ridley, W.I. (1979). Comment on: "the partitioning of nickel between olivine and silicate melt" by S.R. Hart and K.E. Davis. Earth Planet. Sci. Letters, 44, pp. 162-164.

Engel, C.G. and Fisher, R.L. (1975). Granitic to ultramafic rock complexes of the Indian Ocean ridge system, western Indian Ocean. Geol. Soc. Amer. Bull., 86, pp. 1553-1578.

Erlank, A.J. and Kable, E.J.D. (1976). The significance of incompatible elements in Mid-Atlantic Ridge basalts from 45°N with particular reference to Zr/Nb. Contrib. Mineral. and Petrol., 54, pp. 281-291.

Erlank, A.J. and Reid, D.L. (1974). Geochemistry, mineralogy and petrology of basalts, leg 25, D.S.D.P. Init. Rept. Deep Sea Drilling Proj., Nat. Sci. Fndn., 25, pp. 543-551.

Ernst, W.G. (1976). Petrologic phase equilibria. W.H. Freeman and co., San Francisco. 333 pp.

Ewart, A. and Bryan, W.B. (1972). Petrography and geochemistry of the igneous rocks from Eua, Tongan Islands. Bull. Geol. Soc. Amer., 83, pp. 3281-3298.

Fahrig, W.F. and Wanless, R.K. (1963). Age and significance of diabase dyke swarms of the Canadian shield. Nature, 200, pp. 934-937.

Faure, G. and Powell, J.L. (1972). Strontium isotope geology. Springer, Berlin. 188 pp.

Fawcett, J.J., Brooks, C.K. and Rucklidge, J.C. (1973). Chemical petrology of Tertiary flood basalts from Scoresby Sund area. Meddelelser om Gronland, 195, no. 6. pp. 54.

Fernandez, L.A. (1980). Geology and petrology of the Nordeste volcanic complex, Sao Miguel, Azores: summary. Geol. Soc. Amer. Bull., 91, pp. 675-680.

Field, D. and Elliott, R.B. (1974). The chemistry of gabbro/amphibolite transitions in South Norway. Contrib. Mineral. and Petrol., 47, pp. 63-76.

Fisher, R.V. (1966). Rocks composed of volcanic fragments and their classification. Earth Sci. Reviews, 1, pp. 287-298.

Fleet, A.J., Henderson, P. and Kempe, D.R.C. (1976). Rare earth element and related chemistry of some drilled southern Indian Ocean basalts and volcanogenic sediments. J. Geophys. Res., 81, pp. 4257-4268.

Fleet, M.E. and Barnet, R.L. (1978). Al(IV)/Al(VI)partitioning in calciferous amphiboles from the Frood mine, Sudbury, Ontario. Can. Mineral., 16, pp. 527-532.

Flower, M.F.J., Schmincke, H.-U. and Bowman, H. (1976). Rare earth and other trace elements in historic Azorean lavas. J. Volcanol. and Geotherm. Research, 1, pp. 127-147.

Floyd, P.A. (1976). Geochemical variation in the greenstones of S.W. England. J. Petrol., 17, pp. 522-545.

Floyd, P.A. (1977). Rare earth element mobility and geochemical characterisation of spilitic rocks. Nature, 269, pp. 134-137.

Floyd, P.A., Lees, G.J. and Roach, R.A. (1976). Basic intrusions in the Ordovician of north Wales - geochemical data and tectonic setting. Proc. Geol. Assoc., 87, pp. 389-400.

Floyd, P.A. and Winchester, J.A. (1975). Magma type and tectonic setting discrimination using immobile elements. Earth Planet. Sci. Letters, 27, pp. 211-218.

Floyd, P.A. and Winchester, J.A. (1978). Identification and discrimination of altered and metamorphased volcanic rocks using immobile elements. Chem. Geol., 21, pp. 291-306.

Folinsbee, R.E., Baadsgaard, H. and Cumming, G.L. (1970). Geochronology of the Cretaceous - Tertiary boundary of the western plains of North America. Ecologae Geol. Helv., 63, p. 91.

Franklin, J.M. (1975). (Ed.). Archean metallogeny and stratigraphy, Mattabi field trip, Institute on Lake Superior Geol., 23rd ann. mtg., Lakehead Univ.

Frey, F.A., Bryan, W.B., and Thompson, G. (1974). Atlantic ocean floor: geochemistry and petrology of basalts from Legs 2 and 3 of the Deep Sea Drilling Project. J. Geophys. Res., 79, pp. 5507-5527.

Friedrichsen, H. and Hoernes, S. (1978). Stable isotope exchange between oceanic crust and ocean water. Short papers 4th Internat. Conf. Geochron. Cosmochron., Isotope Geol., U.S. Geol. Surv. Open File Rept. 78-701, pp. 123-6.

Frith, R., Frith, R.A. and Doig, R. (1977). The geochronology of the granitic rocks along the Bear-Slave structural province boundary, northwest Canadian shield. Can. J. Earth Sci., 14, pp. 1356-1373.

Furnes, H., Faerseth, R.B. and Tysseland, M. (1978). Petrogenesis of continental metabasalts from the S.W. Norwegian Caledonides. Neues Jahrb. Mineral. Abhandlung, 132, pp.34-51.

Gale, G.H. (1973). Paleozoic basaltic komatiite and ocean floor type basalts from northeastern Newfoundland. Earth Planet. Sci. Letters, 18, pp. 22-28.

Garcia, M. (1975). Clinopyroxene composition, an indicator of magma type in altered volcanic rocks. Geol. Soc.

Amer., Prog. with Abstr., 7, pp. 1082-1083.

Garcia, M.O. (1978). Criteria for the identification of ancient volcanic arcs. Earth Sci. Reviews, 14, pp. 147-165.

Garcia, M.O. (1979). Petrology of the Rogue and Galice formations, Klamath mountains, Oregon: identification of a Jurassic island arc sequence. J. Geol., 86, pp. 24-41.

Garrels, R.M. and Christ, C.L. (1965). Solutions, minerals and equilibria. Harper and Row, N.Y., 450 pp.

Gass, I.G., Mallick, D.I.J. and Cox, K.G. (1973). Volcanic islands of the Red Sea. J. Geol. Soc. London, 129, pp. 275-310.

Gates, T.M. and Hurley, P.M. (1973). Evaluation of Rb-Sr dating methods applied to Matachewan, Abitibi, Mackenzie and Sudbury dike swarms in Canada. Can. J. Earth Sci., 10, pp. 900-919.

Gibson, H.L. and Watkinson, D.H. (1979). Silicification in the Amulet "rhyolite" formation, Turcotte lake Section, Noranda area, Quebec. Geol. Soc. Can. Paper 79-1B pp. 111-120.

Gibson, I.L. (1966). Crustal flexures and flood basalts. Tectonophys., 3, pp. 447-456.

Glassley, W. (1974). A model for phase equilibria in the prehnite-pumpellyite facies. Contrib. Mineral. and Petrol., 413, pp. 317-332.

Goff, S.P. and Scarfe, C.M. (1978). Preliminary report on the volcanic suites of the East Arm, Great Slave Lake, N.W.T. Mineral Industry Report 1975, Northwest Territories, EGS 1978-5, Dept. Indian and Northern Affairs, Ottawa, pp. 129-134.

Goff, S.P., Baadsgaard, H., Muehlenbachs, K. and Scarfe, C.M. (1982). Rb-Sr isochron ages, magmatic $^{87}Sr/^{86}Sr$ initial ratios, and oxygen isotope geochemistry of the Proterozoic lava flows and intrusions of the East Arm of Great Slave Lake, Northwest Territories, Canada. Can. J. Earth Sci., 19, pp. 343-356.

Graham, C. (1976a). Petrochemistry and tectonic significance of Dalradian metabasaltic rocks of the S.W. Scottish Highlands. J. Geol. Soc. London, 132, pp. 61-84.

Graham, C.M. (1976b). Petrochemical affinities of Dalradian metabasaltic rocks: discussion of paper by J.A. Winchester and P.A. Floyd. Earth Planet. Sci. Letters,

32, pp. 210-212.

Grapes, R.H. and Graham C.M. (1978). The actinolite-hornblende series in metabasites and the so-called miscibility gap: a review. Lithos, 11, pp. 85-97.

Grapes, R.H., Hashimoto, S. and Miyashita, S. (1977). Amphiboles of a metagabbro-amphibolite sequence, Hidaka metamorphic belt, Hokkaido. J. Petrology, 18, pp. 285-318.

Green, D.C. and Baadsgaard, H. (1968). Geochronology of the Yellowknife area, N.W.T., Canada. Can. J. Earth Sci., 5, pp. 725-735.

Green, D.C. and Baadsgaard, H. (1971). Temporal evolution and petrogenesis of an Archean crustal segment at Yellowknife, N.W.T., Canada. J. Petrol., 12, pp. 177-217.

Green, D.H. and Ringwood, A.E. (1967). The genesis of basaltic magmas. Contrib. Mineral. and Petrol., 15, pp. 103-190.

Green, J.C. (1977). Keweenawan plateau volcanism in the Lake Superior region. In: Volcanic Regimes in Canada, Baragar, W.R.A., Coleman. L.C. and Hall, J.M. (Eds.). Geol. Assoc. Can. Spec. Paper, 16, pp. 407-422.

Greenwood, H.J. (1967). Mineral equilibria in the system $MgO-SiO_2-H_2O-CO_2$. In: Researches in Geochemistry, Abelson, K. (Ed.). J. Wiley, N.Y., pp. 542-567.

Griffin, W.L. and Murthy, V.R. (1969). Distribution of K, Rb, Sr and Ba in some minerals relevant to basalt genesis. Geochim. Cosmochim. Acta, 33, pp. 1389-1414.

Gunn, B.M. (1966). Modal and element variation in Antarctic tholeiites. Geochim. Cosmochim. Acta, 30, pp. 881-920.

Hajash, A. (1975). Hydrothermal processes along mid-ocean ridges: and experimental investigation. Contrib. Mineral. and Petrol., 53, pp. 205-226 pp.

Ham, W.E. (1962). Classification of carbonate rocks: a symposium. Amer. Assoc. Petroleum Geol., Mem. 1, 279 pp.

Hamet, J. and Allegre, C.J. (1976). Rb-Sr systematics in granite from central Nepal (Manaslu): significance of the Oligocene age and high $^{87}Sr/^{86}Sr$ ratio in Himalayan orogeny. Geology, 4, pp. 470-472.

Hart, R.A. (1970). Chemical exchange between seawater and

deep ocean basalts. Earth Planet. Sci. Letters, 9, pp. 269-279.

Hart, R.A. (1973). A model for chemical exchange in the basalt - seawater system of oceanic layer II. Can. J. Earth Sci., 10, pp. 799-816.

Hart, S.R. (1969). K,Rb, Cs contents and K/Rb and K/Cs ratios of fresh and altered submarine basalts. Earth Planet Sci. Letters, 6, pp. 295-303.

Hart, S.R. and Brooks, C. (1974). Clinopyroxene-matrix partitioning of K, Rb, Cs, Sr and Ba. Geochim. Cosmochim. Acta, 38, pp. 1799-1806.

Hart, S.R. and Brooks, C. (1977). The geochemistry and evolution of Early Precambrian mantle. Contrib. Mineral. and Petrol., 61, pp. 109-128.

Hart, S.R. and Nalwark, A.J. (1970). K, Rb, Cs and Sr relationships in submarine basalts from the Puerto Rico Trench. Geochim. Cosmochim. Acta, 34, pp. 145-155.

Hart, S.R., Erlank, A.J. and Kable, E.J.D. (1974). Sea Floor basalt alteration: some chemical and Sr isotopic effects. Contrib. Mineral. and Petrol., 44, pp. 219-230.

Harte, B. and Graham, C.M. (1975). The graphical analysis of greenschist to amphibolite facies mineral assemblages in metabasites. J. Petrol., 16, pp. 347-370.

Hattori, H., Sugisaki, R. and Tanaka, T. (1972). Nature of hydration in Japanese Palaeozoic geosynclinal basalt. Earth Planet. Sci. Letters, 15, pp. 271-285.

Haynes, S.J. and McQuillan, H. (1974). Evolution of the Zagros suture zone, southern Iran. Geol. Soc. Amer. Bull., 85, pp. 739-744.

Hedge, C.E., Peterman, Z.E. and Dickinson, W.R. (1972). Petrogenesis of lava from western Samoa. Geol. Soc. Amer. Bull., 83, pp. 2709-2714.

Heimlich, R.A., Nelson, G.C. and Gallagher, G.L. (1973). Metamorphosed basic dykes from the Southern Bighorn mountains, Wyoming. Geol. Soc. Amer. Bull., 84, pp. 1439-1450.

Hekinian, R. (1971). Chemical and mineralogical differences between Abyssal hill basalts and ridge tholeiites in the Eastern Pacific Ocean. Marine Geology, 11, pp. 77-91.

Hellman, P.L. and Henderson, P. (1977). Are rare earth elements mobile during spilitisation? Nature, 267, pp.

38-40.

Hellman, P.L., Smith, R.E. and Henderson, P. (1979). The mobility of the rare earth elements: evidence and implications from selected terrains affected by burial metamorphism. Contrib. Mineral. and Petrol., 71, pp. 23-44.

Heming, R.F. (1974). Geology and petrology of Rabaul caldera, Papua New Guinea. Geol. Soc. Amer. Bull., 85, pp. 1253-1264.

Herrmann, A.G., Potts, M.J. and Knake, D. (1974). Geochemistry of the rare earth elements in spilites from the oceanic and continental crust. Contrib. Mineral. and Petrol., 44, pp. 1-16.

Hey, M.H. (1954). A new review of the chlorites. Mineral. Mag., 30, pp. 277-292.

Hildebrand, R.S. (1981). Early Proterozoic Labine Group of Wopmay orogen: remnant of a continental volcanic are developed during oblique convergence. In: Proterozoic Basins of Canada, Campbell, F.M.A. (Ed.). Geol. Surv. Can. Paper 81-10, pp. 133-156.

Hoffman, P.F. (1968). Stratigraphy of the Great Slave Supergroup (Aphebian), East Arm of Great Slave Lake, District of Mackenzie. Geol. Surv. Can. Paper 68-42; 92 pp.

Hoffman, P. (1969). Proterozoic palaeocurrents and depositional history of the East Arm fold belt, Great Slave Lake, Northwest Territories. Can. J. Earth Sci., 6, pp. 441-462.

Hoffman, P. (1972). Aphebian supracrustal rocks of the Athapuscow aulacogen, East Arm of the Great Slave Lake, District of Mackenzie. Geol. Surv. Can. Paper 73-1A, pp. 151-156.

Hoffman, P. (1973). Evolution of an early Proterozoic continental margin: the Coronation geosyncline and associated aulacogens, northwest Canadian Shield. In: Evolution of the Precambrian Crust, Sutton, J. and Windley, B.F. (Eds.)., Phil. Trans. Roy. Soc., London, Ser. A, 273, pp. 547-581.

Hoffman, P. (1977). Preliminary geology of Proterozoic formations in the East Arm of Great Slave Lake, District of Mackenzie. Geol. Surv. Can., Open File 475C.

Hoffman, P. (1978). Age of exotic blocks in diatreme dykes of the Athapuscow aulacogen, Simpson Islands area, East

Arm of Great Slave Lake, District of Mackenzie. Geol. Surv. Can. Paper 78-1A, pp. 145-146.

Hoffman, P. (1979). Comment and reply on "Has there been an oceanic margin to western North America since Archean time?"; comment. Geology, 7, pp. 226-228.

Hoffman, P.F. (1980a). Wopmay orogen: a Wilson cycle of early Proterozoic age in the northwest of the Canadian shield. In: The Continental Crust and its Mineral Deposits, Strangway, D.W. (Ed.). Geol. Assoc. Can. Spec. Paper, 20, pp. 523-549.

Hoffman, P.F. (1980b). Paired plutonic belts of Wopmay orogen, N.W.T. Signature of Proterozoic continental collisions? Geol. Soc. Amer. Prog. with Abstr., 12, p. 448.

Hoffman, P.F. (1980c). Autopsy of the East Arm fold belt (2.1-1.8 Ga) Great Slave Lake, N.W.T. Geol. Assoc. Can. Prog. with Abstr., 5, p. 61.

Hoffman, P.F. (1981). Revision of stratigraphic nomenclature, foreland thrust-fold belt of Wopmay orogen, district of Mackenzie. Geol. Surv. Can. Paper 81-1A, pp. 247-250.

Hoffman, P.F. and McGlynn, J.C. (1977). Great Bear Batholith: a volcano-plutonic depression. In: Volcanic Regimes in Canada, Baragar, W.R.A., Coleman, L.C. and Hall, J.M. (Eds.). Geol. Assoc. Can. Spec. Paper, 16, pp. 169-192.

Hoffman, P., Fraser, J.A. and McGlynn, J.C. (1970). The Coronation geosyncline of Aphebian age, District of Mackenzie. In: Symposium on Basins and geosynclines of the Canadian Shield, Baer, A.J. (Ed.). Geol. Surv. Can. Paper 70-40, pp. 200-212.

Hoffman, P., Dewey, J.F. and Burke, K. (1974). Aulacogens and their genetic relation to geosynclines, with a Proterozoic example from Great Slave Lake, Canada. In: Modern and Ancient Geosynclinal Sedimentation, Dott, R.H. and Shaver, R.H. (Eds.). Soc. Econ. Paleont. Mineral. Spec. Publ. no. 19, pp. 38-55.

Hoffman, P., Bell, I.R., Hildebrand, R.S. and Thorstad, C. (1977). Geology of the Athapuscow aulacogen, East Arm of the Great Slave Lake, District of Mackenzie. Geol. Surv. Can. Paper 77-1A, pp. 117-129.

Hoffman, P., St.-Onge, M. Carmichael, D.M. and de Bie, I. (1978). Geology of the Coronation geosyncline (Aphebian), Hepburn Lake sheet (86J), Bear Province,

District of Mackenzie. Geol. Surv. Can. Paper 78-1A, pp. 147-151.

Hoffman, P., St.-Onge, M.R. Easton, R.M., Grotzinger, J. and Schulze, D.E. (1980). Syntectonic plutonism in north-central Wopmay orogen (early Proterozoic), Hepburn Lake Map area, District of Mackenzie. Geol. Surv. Can., Paper 80-1A, pp. 171-177.

Hoschek, G. (1969). The stability of staurolite and chloritoid and their significance in metamorphism of pelitic rocks. Contrib. Mineral. and Petrol., 22, pp. 208-232.

Hriskevich, M.E. (1968). Petrology of the Nipissing diabase sill of the Cobalt area, Ontario, Canada. Geol. Soc. Amer. Bull., 79, pp. 1387-1404.

Hsu, K.J. (1979). Thin-skinned plate tectonics during Neo-Alpine orogenesis. Amer. J. Sci., 279, pp. 353-366.

Hubbard, N.J. (1969). A chemical comparison of oceanic ridge, Hawaiian tholeiitic and Hawaiian alkalic basalts. Earth Plan. Sci. Letters, 5, pp. 346-352.

Hughes, C.J. (1970). The late Precambrian Avalonian orogeny in Avalon, southeast Newfoundland. Amer. J. Sci., 269, pp. 183-190.

Hughes, C.J. (1973). Spilites, keratophyres and the igneous spectrum. Geol. Mag., 109, pp. 513-527.

Hughes, C.J. and Bruckner, W.D. (1971). Late Precambrian rocks of eastern Avalon Peninsula, Newfoundland - a volcanic island complex. Can. J. Earth Sci., 8, pp. 899-915.

Humphris, S.E. (1978). Geochemistry of long-term seawater-basalt reactions at low temperatures, DSDP Holes 417A and 418A. Geol. Soc. Amer. Prog. with Abstr., 10, p. 426.

Humphris, S.E. and Thompson, G. (1978a). Hydrothermal alteration of oceanic basalts by seawater. Geochim. Cosmochim. Acta, 42, pp. 107-125.

Humphris, S.E. and Thompson, G. (1978b). Trace element mobility during hydrothermal alteration of oceanic basalts. Geochim. Cosmochim. Actra, 42, pp. 127-136.

Humphris, S.E., Morrison, M.A. and Thompson, R.N. (1978). Influence of rock crystallisation history upon subsequent lanthanide mobility during hydrothermal alteration of basalts. Chem. Geol., 23, pp. 125-137.

Innes, D.G. and Bennett, G. (1980). Huronian volcanics in Ontario - evidence for early Proterozoic rifting. Geol. Assoc. Can., Prog. with Abstr., 5, p. 62.

Irvine, T.N. (1976). Metastable liquid immiscibility and MgO - FeO - SiO_2 fractionation patterns in the system Mg_2SiO_4 - Fe_2SiO_4 - $CaAl_2Si_2O_8$ - $KAlSi_3O_8$ - SiO_2. Carnegie Inst. Wash. Yb., 75, pp. 597-611.

Irvine, T.N. and Baragar, W.R.A. (1971). A guide to the chemical classification of the common volcanic rocks. Can. J. Earth Sci., 8, pp. 523-548.

Irving, A.J. (1978). A review of experimental studies of crystal/liquid trace-element partitioning. Geochim. Cosmochim. Acta., 42, pp. 743-770.

Jakes, P. and Gill, J. (1970). Rare-earth elements and the island arc tholeiitic series. Earth Planet. Sci. Letters, 9, pp. 17-28.

Jamieson, R.A. (1981). Metamorphism during ophiolite emplacement - the petrology of the St. Anthony Complex. J. Petrol., 22, pp. 397-449.

Jensen, L.S. (1976). A new cation plot for classifying subalkalic volcanic rocks. Ontario Div. Mines, Misc. Pap. 66, 22 pp.

Johnson, J.R. (1979). Transitional basalts and tholeiites from the East Pacific Rise, 0°. N. J. Geophys. Res., 84, pp. 1635-1651.

Johnson, R.W., Mackenzie, D.E. and Smith, I.E.M. (1978). Volcanic rock associations at convergent plate boundaries: reappraisal of the concept using case histories from Papua New Guinea. Geol. Soc. Amer. Bull., 89, pp. 96-106.

Jolly, W.T. and Smith, R.E. (1972). Degradation and metamorphic differentiation of the Keweenawan tholeiitic lavas of Northern Michigan, U.S.A., J. Petrol, 13, pp. 273-309.

Joplin, G.A. (1965). The problem of the potash-rich basaltic rocks. Mineral. Mag., 34, pp. 266-275.

Joplin, G.A. (1968). The shoshonite association. J. Geol. Soc. Australia, 15, pp. 275-294.

Kay, R.W. and Gast, P.W. (1973). The rare earth content and origin of alkali-rich basalts. J. Geol., 81, pp. 653-682.

Kay, R.W. and Senechal, R.G. (1976). The rare earth geochemistry of the Troodos ophiolite complex. J. Geophys. Res., 81, pp. 964-970.

Kempe, D.R.C. (1974). The petrology of the basalts, leg 26. Init. Rept. Deep Sea Drilling Proj., Nat. Sci. Fndn., 26, pp. 465-503.

Kennedy, W.Q. (1933). Trends of differentiation in basaltic magmas. Amer. J. Sci., 25, pp. 239-256.

Keppie, J.D., Dostal, J. and Zentilli, M. (1979). Early Silurian volcanic rocks at Arisaig, Nova Scotia. Can. J. Earth Sci., 16, pp. 1533-1644.

Kerrich, R., Fyfe, W.S., Gorman, B.E. and Allison, I. (1977). Local modification of rock chemistry by deformation. Contrib. Mineral. and Petrol., 65, pp. 183-190.

Kerrick, D.M. (1974). Review of metamorphic mixed-volatile (H_2O-CO_2) equilibria. Amer. Mineral., 59, pp. 729-762.

Kidd, W.S.F. (1977). The Baie Verte lineament, Newfoundland: ophiolite complex floor and mafic volcanic fill of a small Ordovician marginal basin. In: Island Arcs, Deep Sea Trenches and Back-Arc Basins, Talwani, M. and Pitman, W.C. (Eds.), pp. 407-418, Amer. Geophys. Union, Washington, D.C.

Korzhinsky, D.S. (1959). Physico-chemical basis of the analysis of the paragenesis of minerals. Consultants Bureau Inc., N.Y. 142 pp.

Kushiro, I. (1969). Discussion of paper "The origin of basaltic and nephelinitic Magmas in the earth's mantle." Tectonophys., 7, pp. 427-436.

Kyser, T.K. and O'Neil, J.R. (1978). Oxygen isotope relations among oceanic tholeiites, alkali basalts and ultramafic nodules. Short papers of the Fourth International Conference, Geochron., Cosmochron. and Isotope geol., Zartman, R.E. (Ed.). U.S. Geol. Surv. Open File Rept. 78-701, pp. 237-240.

Lajoie, J. (1979). Facies models 15, volcaniclastic rocks. Geoscience Canada, 6, pp. 129-139.

Langmuir, C.H. Bender, J.F., Bence, A.E., Hanson, G.N. and Taylor, S.R. (1977). Petrogenesis of basalts from the FAMOUS area: Mid-Atlantic ridge. Earth Planet. Sci. Letters, 36, pp. 133-156.

Lawrence, J.R. et.al. (1979). Importance of alteration of

volcanic material in the sediments of Deep Sea Drilling Site 323: chemistry, O^{18}/O^{16} and Sr^{87}/Sr^{86}. Geochim. Cosmochim. Acta, 43, pp. 573-588.

Leake, B. (1978). Nomenclature of amphiboles. Can. Mineral., 16, pp. 501-520.

LeBas, M.J. (1962). The role of aluminium in igneous clinopyroxenes with relation to their parentage. Amer. J. Sci., 260, pp. 267-288.

Leech, A.P. (1966). Potassium-argon dates of basic intrusive rocks of the District of Mackenzie, N.W.T. Can. J. Earth Sci., 3, pp. 389-412.

Leech, G.B., Lowdon, J.A., Stockwell, C.H. and Wanless, R.K. (1963). Age determinations and geologic studies (Including isotopic ages report 4). Geol. Surv. Can. Paper 63-17. 140 pp.

Le Maitre, R.W. (1976). The chemical variability of some common igneous rocks. J. Petrol., 17, pp. 589-637.

Leterrier, J., Maury, R.C., Thonon, P., Girard, D. and Marchal, M. (1982). Clinopyroxene composition as a method of identification of the magmatic affinities of palaeo-volcanic series. Earth Planet. Sci. Letters, 59, pp. 139-154.

B. Levi (1969). Burial metamorphic episodes in the Andean geosyncline, central Chile. Geologische Rundschau, 59, pp. 994-1012.

Lidiak, E.G. (1965). Petrology of andesitic, spilitic and keratophyric flow rock, north-central Puerto Rico. Geol. Soc. Amer. Bull., 76, pp. 57-88.

Liou, J.G. (1973). Synthesis and stability relations of epidote $Ca_2Al_2FeSi_3O_{12}(OH)$. J. Petrol., 14, pp. 381-413.

Liou, J.G. (1979). Zeolite facies metamorphism of basaltic rocks from the East Taiwan ophiolite. Amer. Mineral., 64, pp. 1-14.

Liou, J.G. and Dickson, F.W. (1978). The interaction of NaCl solution and seawater with andesite, 200-400°C, 500-1000 bars. EOS, Trans. Amer. Geophys. Union, 59, p. 1221.

Liou, J.G., Kuniyoshi, S. and Ito, K. (1974). Experimental studies of the phase relations between greenschist and amphibolite in a basaltic system. Amer. J. Sci., 274, pp. 613-632.

Lowdon, J.A. (1961). Age determinations by the Geological

Survey of Canada, Rept. 2. Geol. Surv. Can. Paper 61-17, 127 pp.

Lowman, R.D.W. and Bloxam, T.W. (1981). The petrology of the Lower Palaeozoic Fishguard Volcanic Group and associated rocks E. of Fishguard, N. Pembrokeshire (Dyfed), S. Wales. J. Geol. Soc. London, 138, pp. 47-68.

Ludden, J.N. and Thompson, G. (1979). An evaluation of the behaviour of the rare earth elements during the weathering of sea-floor basalt. Earth Planet. Sci. Letters, 43, pp. 85-92.

MacDonald, G.A. (1968). Composition and origin of Hawaiian lavas. Geol. Soc. Amer. [illegible] 116, pp. 477-522.

Macdonald, R. (1980). Trace element evidence for mantle heterogeneity beneath the Scottish Midland Valley in the Carboniferous and Permian. Phil. Trans. Roy. Soc. London, A297, pp. 245-257.

MacGeehan, P.J. (1978). The geochemistry of altered volcanic rocks at Mattagami, Quebec: a geothermal model for massive sulphide genesis. Can. J. Earth Sci., 15, pp. 551-570.

[illegible]enzie, D.E. and Chappell, B.W. (1972). Shoshonitic and calc-alkaline lavas from the highlands of Papua New Guinea. Contrib. Mineral. and Petrol., 35, pp. 50-62.

Manson, V. (1967). Geochemistry of basaltic rocks: major elements. In: Basalts V.1, Hess, H.H. and Poldervaart, A. (Eds.). J. Wiley & Sons, N.Y., pp. 215-269.

Mariner, R.H. and Surdam, R.C. (1970). Alkalinity and formation of zeolites in saline alkaline lakes: Science, 170, pp. 977-980.

Marshall, M. (1975). Petrology and chemical composition of basaltic rocks recovered on Leg 32, D.S.D.P. Init. Rept. Deep Sea Drilling Proj., Nat. Sci. Fndn., 26, pp. 563-570.

Martineau, M.P. and Lambert, R.St.J. (1974). The Big Spruce Lake nepheline-syenite/carbonatite complex, N.W.T. (abstract) Proc. Geol. Assoc. Can., 1, p. 59.

Mason, R. (1978). Petrology of the metamorphic rocks. Allen and Unwin, London. 254 pp.

Mattey, D.P., Gibson, I.L. Marriner, G.F. and Thompson, R.N. (1977). The diagnostic geochemistry, relative abundance and special distribution of high-calcium, low-alkali olivine tholeiite dykes in the Lower Tertiary regional

swarm of the Isle of Skye, N.W. Scotland. Mineral Mag., 41, pp. 273-85.

Matthews, D.H. (1971). Altered basalts from Swallow Bank, and abyssal hill in the N.E. Atlantic, and from a nearby seamount. Phil. Trans. Roy. Soc. London, 268A, pp. 551-571.

Maury, R. and Szeky-Fux, V. (1975). Temperature data for tuff flows and lavas of the Tokaj Mountains from the I.R. spectras of organic matter in fossil woods. Acta Geol. Acad. Sci. Hungaricae, 19, pp. 233-241.

McBirney, A.R. and Williams, H. (1969). Geology and petrology of the Galapagos islands. Geol. Soc. Amer. Memoir, 118, 197 pp.

McGlynn, J.C. (1972). Basler Lake granite, District of Mackenzie. In: Rubidium Strontium Isochron Age Studies, Rept. no. 1, Wanless, R.K. and Loveridge, W.D. (Eds.). Geol. Surv. Can. Paper 72-23, p. 7.

McGlynn, J.C. and Henderson, J.B. (1972). The Slave Province. In: Variations in Tectonic Styles in Canada, Price, R.A. and Douglas, R.J.W. (Eds.). Geol. Assoc. Can., Spec. Paper 11, pp. 505-526.

McGlynn, J.C. and Irving, E. (1975). Paleomagnetism of early Aphebian dykes from the Slave structural province, Canada. Tectonophys., 26, pp. 23-28.

McGlynn, J.C. and Irving, E. (1978). Multicomponent magnetization of the Pearson Formation (Great Slave Supergroup, N.W.T.) and the Coronation loop. Can. J. Earth Sci., 15, pp. 642-654.

McIntyre, G.A., Brooks, C., Compston, W. and Turek, A. (1966). The statistical assessment of Rb-Sr isochrons. J. Geophys. Res., 71, pp. 5459-5468.

McIver, J.R. and Lenthall, D.H. (1974). Mafic and ultramafic extrusives of the Barberton Mountain land in terms of the CMAS system. Precam. Res., 1, pp. 327-343.

Melson, W.G. and Van Andel, T.H. (1966). Metamorphism in the Mid-Atlantic Ridge, 22°N latitude. Marine Geol., 4, pp. 165-186.

Melson, W.G., Thompson, G. and Van Andel, T.H. (1968). Volcanism and metamorphism in the Mid-Atlantic Ridge near 24° and 30° north latitude. J. Geophys. Res., 73, pp. 5925-5941.

Menzies, M., Blanchard, D. and Jacobs, J. (1977). Rare earth

and trace element geochemistry of metabasalts from the Point Sal ophiolite, California. Earth Planet. Sci. Letters, 37, pp. 203-215.

Menzies, M., Seyfried, W. and Blanchard, D. (1979). Experimental evidence of rare earth element immobility in greenstones. Nature, 282, pp. 398-399.

Meyer, W., Pilger, A., Rosler, A. and Stets, J. (1975). Tectonic evolution of the northern part of the main Ethiopian rift in southern Ethiopia. In: Afar Depression of Ethiopia, V.2, Pilger, A. and Rosler, A. (Eds.). Schweizbart'sche Stultgart, pp. 352-362.

Mitchell, A.H.G. (1981). Phanerozoic plate boundaries in mainland S.E. Asia, the Himalayas and Tibet. J. Geol. Soc. London, 138, pp. 109-122.

Miyashiro, A. (1973). The Troodos ophiolitic complex was probably formed in an island arc. Earth Planet Sci. Letters, 19, pp. 218-224.

Miyashiro, A. (1975). Classification, characteristics and origin of ophiolites. J. Geol., 83, pp. 249-281.

Miyashiro, A. (1978). Nature of alkalic rock series. Contrib. Mineral. and Petrol., 66, pp. 91-104.

Miyashiro, A. and Shido, F. (1975). Tholeiitic and calc-alkalic series in relation to the behaviours of titanium, vanadium, chromium and nickel. Amer. J. Sci., 275, pp. 265-277.

Miyashiro, A., Shido, F. and Ewing, M. (1971). Metamorphism in the Mid-Atlantic Ridge near 24° and 30°N. Phil. Trans. Roy. Soc. London, 268A, pp. 589-603.

Mohr, P.A. (1978). Afar. Annual Review of Earth and Planetary Sciences, 6, pp. 145-172.

Moore, J.G. (1966). Rate of palagonitization of submarine basalt adjacent to Hawaii, U.S. Geol. Survey Prof. Paper 550-D, D163-D171.

Moore, J.G., Phillips, R.L., Griggs, R.W., Peterson, D.W. and Swanson, D.O. (1973). Flow of lava into the sea, 1969-1971, Kilauea Volcano, Hawaii. Geol. Soc. Amer. Bull., 84, pp. 537-546.

Moore, J.M. (1977). Orogenic volcanism in the Proterozoic of Canada. In: Volcanic Regimes in Canada, Baragar, W.R.A., Coleman, L.C. and Hall, J.M. (Eds.). Geol. Ass. Can. Spec. Pap., 16, pp. 445-460.

Morrison, M.A. (1978). The use of "immobile" trace elements to distinguish the palaeotectonic affinities of metabasalts: applications to the Palaeocene basalts of Mull and Skye, northwest Scotland. Earth Planet. Sci. Letters, 39, pp. 407-416.

Morrison, M.A., Thompson, R.N., Gibson, I.L. and Marriner, G.F. (1980). Phil. Trans. Roy. Soc. London, A297, pp. 229-244.

Mottl, M.J. and Holland, H.D. (1978). Chemical exchange during hydrothermal alteration of basalt by seawater - I. Expermental results for major and minor components of seawater. Geochim. Cosmochim. Acta, 42, pp. 1103-1115.

Mottl, J.J., Holland, H.D. and Corr, R.F. (1979). Chemical exchange during hydrothermal alteration of basalt by seawater - II. Experimental results for Fe, Mn and sulfur species. Geochim. Cosmochim. Acta, 43, pp. 869-884.

Muelenbachs, K. (1977). Oxygen isotope geochemistry of rocks from DSDP Leg 37. Can. J. Earth Sci., 14, pp. 771-776.

Naldrett, A.J. and Goodwin, A.M. (1977). Volcanic rocks of the Blake River Group, Abitibi greenstone belt, Ontario, and their sulphur content. Can. J. Earth Sci., 14, pp. 539-550.

Nesbitt, R.W., Sun, S.-S. and Purvis, A.C. (1979). Komatiites: geochemistry and genesis. Can. Mineral., 17, pp. 165-186.

Nicholls, G.D. and Islam, M.R. (1971). Geochemical investigations of basalts and associated rocks from the ocean floor and their implications. Phil. Trans. Roy. Soc. London, 268, pp. 469-486.

Nielsen, T.F.D. (1978). The Tertiary dike swarms of the Kangerdlugssuaq area, East Greenland. Contrib. Mineral. and Petrol., 67, pp. 63-78.

Nisbet, E.G. and Pearce, J.A. (1977). Clinopyroxene composition in mafic lavas from different tectonic settings. Contrib. Mineral. and Petrol., 63, pp. 149-160.

Nitsch, K.H. (1971). Stabilitatsbeziekiungen von prehnit und pumpellyithaltigen paragenesen. Contrib. Mineral. and Petrol., 30, pp. 240-260.

Nockolds, S.R. and Allen, R. (1953, 1956). The geochemistry of some igneous rock series, I, III. Geochim. Cosmoschim. Acta; 4, pp. 105-142; 9, pp. 34-77.

Nockolds, S.R., Knox, R.W.O'B. and Chinner, G.A. (1978). Petrology for students. Cambridge Univ. Press, 435 pp.

Norry, M.J., Truckle, P.H., Lippard, S.J., Hawkesworth, C.J., Weaver, S.D. and Marriner, G.F. (1980). Isotopic and trace element evidence from lavas, bearing on mantle heterogeneity beneath Kenya. Phil. Trans. Roy. Soc. London, A297, pp. 259-271.

Oba, T. (1980). Phase relations in the tremolite-pargasite join. Contrib. Mineral. and Petrol., 63, pp. 149-160.

Offler, R., Baker, C.K. and Gamble, J. (1981). Pumpellyites in two low grade metamorphic terranes north of Newcastle, NSW Australia. Contrib. Mineral. and Petrol., 76, pp. 171-176.

O'Hara, M.J. (1968). The bearing of phase equilibria studies on the origin and evolution of basic and ultrabasic rocks. Earth Sci. Rev., 4, pp. 69-133.

Olade, M.A.D. (1975). Trace element and isotopic data and their bearing on the genesis of Precambrian spilites from the Athapuscow aulacogen, Great Slave Lake, Canada. Geol. Mag., 112, pp. 283-793.

Olade, M.A.D. and Morton, R.D. (1972). Observations on the Proterozoic Seton Formation, East Arm of the Great Slave Lake, Northwest Territories. Can. J. Earth Sci., 9, pp. 1110-1123.

Osborn, E.F. (1959). Role of oxygen pressure in the crystallization and differentiation of basaltic magma. Amer. J. Sci., 257, pp. 609-647.

Ovenshine, A.T., Winkler, G.R., Andrews, P.B. and Gostin, V.A. (1975). Chemical analyses and minor element composition of Leg 29 basalts. In: Init. Rept. Deep Sea Drilling Proj., Nat. Sci. Fndn., Kennett, J.P. et al. (Eds.), 29, pp. 1097-1102.

Papezik, V.S. (1970). Petrochemistry of volcanic rocks of the Harbow Main Group, Avalon peninsula, Newfoundland. Can. J. Earth Sci., 7, pp. 1485-1498.

Papezik, V.S. and Hodych, J.P. (1980). Early Mesozoic diabase dikes of the Avalon Peninsula, Newfoundland: Petrochemistry, mineralogy, and origin. Can. J. Earth Sci., 10, pp. 1417-1430.

Papike, J.J. (1980). Pyroxene mineralogy of the moon and meteorites. Reviews in Mineralogy, V.7, Pyroxenes, Prewitt, C.T. (Ed.)., Mineral. Soc. Amer., pp. 495-525.

Pearce, J.A. (1975). Basalt geochemistry used to investigate past tectonic environments on Cyprus. Tectonophys., 25, pp. 41-67.

Pearce, J.A. (1976). Statistical analysis of major element patterns in basalts. J. Petrol., 17, pp. 15-43.

Pearce, J.A. (1980). Geochemical evidence for the genesis and eruptive setting of lavas from Tethyan Ophiolites. In: Ophidites, Panayiotou, A. (Ed.). Geol. Survey Dept., Cyprus, pp. 261-272.

Pearce, J.A. and Cann, J.R. (1973). Tectonic setting of basic volcanic rocks determined using trace element analyses. Earth Planet. Sci. Letters, 19, pp. 290-300.

Pearce, J.A. and Flower, M.F.J. (1977). The relative importance of petrogenetic variables in magma genesis at accreting plate margins: a preliminary investigation. J. Geol. Soc. London, 134, pp. 1-25.

Pearce, J.A. and Gale, G.H. (1977). Identification of ore-deposition environment from trace-element geochemistry of associated igneous host rocks. In: Volcanic Processes in Ore Genesis. Geol. Soc. London Publ., 7, pp. 14-24.

Pearce, J.A. and Norry, M.J. (1979). Petrogenetic implications of Ti, Zr, Y, and Nb variations in volcanic rocks. Cotnrib. Mineral. and Petrol., 69, pp. 33-47.

Pearce, T.H., Gorman, B.E. and Birkett, T.C. (1975). The TiO_2-K_2O-P_2O_5 diagram: a method of discriminating between oceanic and non-oceanic basalts. Earth Planet. Sci. Letters, 24, pp. 419-426.

Pearce, T.H., Gorman, B.E. and Birkett, T.C. (1977). The relationship between major element chemistry and tectonic environment of basic intermediate volcanic rocks. Earth Planet. Sci. Letters, 36, pp. 121-132.

Philpotts, J.A., Schnetzler, C.C. and Hart, S.R. (1970). Sub marine basalts: some K, Rb, Sr, Ba and rare-earth data bearing on their alteration, modification by plagioclase and possible source materials. Earth and Planet. Sci. Letters, 7, pp. 293-299.

Pichler, H. (1965). Acid hyaloclastites. Bull. Volcanol., 28, pp. 293-311.

Pluysnina, L.P. and Ivanova, I.P. (1981). Thermodynamic regime of greenstone metamorphism of basic volcanic rocks after experimental data. Can. J. Earth Sci., 18, pp. 1303-1309.

Poldervaart, A. (1964). Chemical definition of alkali basalts and tholeiites. Bull. Geol. Soc. Amer., 75, pp. 229-232.

Rea, W.J. (1974). The volcanic geology and petrology of Montserrat, West Indies. J. Geol. Soc. London, 130, pp. 341-366.

Reed, J.C. and Morgan, B.A. (1971). Chemical alteration and spilitization of the Catoctin greenstones, Shenandoah National Park, Virginia. J. Geol., 79, pp. 526-548.

Reid, W.P. (1969). Mineral staining tests. Mineral Indust. Bull. Colorado School of Mines, 12.

Reinhardt, E.W. (1969a). Wilson Island - Petitot Islands area, East Arm Great Slave Lake (85 h/10, 11, 15 (south half)). Geol. Surv. Can. Paper 69-1A, pp. 177-181.

Reinhardt, E.W. (1969b). Geology of the Precambrian rocks of Thubun Lakes map-area in relationship to the McDonald fault system, District of Mackenzie (75 E/12 and parts of 75 E/13 and 85 H/9). Geol. Surv. Can. Paper 69-21, 29 pp.

Reinhardt, E.W. (1972). Occurrences of exotic breccias in the Petitot Islands (85 H/10) and Wilson Island (85H/15) Map-areas, East Arm of Great Slave Lake, District of Mackenzie. Geol. Surv. Can. Paper 72-25, 43 pp.

Richardson, S.W. and Powell, R. (1976). Thermal causes of the Dalradian metamorphism in the central highlands of Scotland. Scottish J. Geol., 12, pp. 237-268.

Richter, D.A. and Roy, D.C. (1974). Sub-greenschist metamorphic assemblages in northern Maine. Can. Mineral., 12, pp. 469-474.

Ridley, W.I., Rhodes, J.M., Reid, A.M., Bass, M.N. (1974). Basalts from leg 6 of the Deep Sea Drilling Project. J. Petrol., 15, pp. 140-159.

Roberts, R.G. and Reardon, E.J. (1978). Alteration ad ore-forming processes at Mattagami Lake Mine, Quebec. Can. J. Earth Sci., 15, pp. 1-21.

Robertson, A.H.F. and Fleet, A.J. (1976). The origins of rare earths in metalliferous sediments of the Troodos Massif. Earth Planet. Sci. Letters, 28, pp. 385-394.

Robinson, P.T. (1979). Low temperature alteration of oceanic basalts. Geol. Assoc. Can. / Mineral. Assoc. Can., 4, Prog. with Abstr., p. 74.

Rowbotham, G. and Bevins, R.E. (1978). Textures and compositions of pyroxenes in basic igneous rocks of Ordovician age from north Pembrokeshire. J. Geol. Soc. London, 135 p. 589.

Saunders, A.D. and Tarney, J. (1977). Seawater ocean-crust interaction: contrasting geochemical effects at low and high temperatures. In: Solid-Fluid Interactions, Triennial mtg. of Mineral. Soc. of Gt. Britain and Ireland, Synopses of Contribs., p. 30.

Saunders, A.D. and Tarney, J. (1979). The geochemistry of basalts from a back-arc spreading centre in the East Scotia Sea. Geochim. Cosmochim. Acta, 43, pp. 555-572.

Saunders, A.D., Tarney, J., Marsh, N.G. and Wood, D.A. (1980). Ophiolites as ocean crust or marginal basin crust: a geochemical approach. In: Ophiolites, Panayiotou, A. (Ed.)., Geol. Surv. Dept., Cyprus, pp. 193-204.

Scarfe, C.M. and Smith, D.G.W. (1977). Secondary minerals in some basaltic rocks from DSDP Leg 37. Can. J. Earth Sci., 14, pp. 903-910.

Schau, M. (1977). "Komatiites" and quartzites in the Archean Prince Albert Group. In: Volcanic Regimes in Canada, Baragar, W.R.A., Coleman, L.C. and Hall, J.M. (Eds.). Geol. Ass. Can., Sp. Pap., 16, pp. 341-354.

Scheidegger, K.F. and Stakes, D.S. (1977). Mineralogy, chemistry and crystallization sequence of clay minerals in altered tholeiitic basalts from the Peru trench. Earth Planet. Sci. Letters, 36, pp. 413-422.

Schimann, K. and Smith, D.G.W. (1980). The optical fusion of whole rock powders and their analysis by an electron microprobe technique. Can. Mineral., 18, pp. 131-142.

Schwarz, E.J. and Fujiwara, Y. (1977). Komatiitic basalts from the Proterozoic Cape Smith Range in northern Quebec, Canada. In: Volcanic Regimes in Canada, Baragar, W.R.A., Coleman, L.C. and Hall, J.M. (Eds.). Geol. Assoc. Can., Sp. Pap., 16, pp. 193-201.

Schwarzer, R.R. and Rogers, J.J.W. (1974). A world-wide comparison of alkali olivine basalts and their differentiation trends. Earth Planet. Sci. Letters, 23, pp. 286.

Schweitzer, E.L., Papike, J.J., and Bence, A.E. (1978). Clinopyroxenes from deep sea basalts: a statistical analysis. J. Geophys. Res., 5, pp. 573-576.

Scott, R.B. and Hajash, A. (1976). Initial submarine alteration of basaltic pillow lavas: a microprobe study. Amer. J. Sci., 276, pp. 480-501.

Segalstad, T.V. (1978). Petrology of the Skien basaltic rocks and the early basaltic (B_1) volcanism of the Permian Oslo rift. In: Petrology and Geochemistry of Continental Rifts, Neumann, E.-R. and Ramberg, I.B. (Eds.). Reidel, Dordrecht, pp. 209-216.

Seki, Y. (1978). Chemical characters of sea water-meteoric water mixtures interacted with volcanogenic sediments at low temperatures. EOS, Trans. Amer. Geophys. Union, 59, p. 1220.

Seki, Y., Onuki, M., Oba, T. and Mori, R. (1970). Sanbagawa metamorphism in the central Kii Peninsula, Japan. Japanese J. Geol. Geog., 41, pp. 65-78.

Sengor, A.M.C. and Kidd, W.S.F. (1979). Post-collisional tectonics of the Turkish-Iranian Plateau and a comparison with Tibet. Tectonophys., 55, pp. 361-376.

Seyfried, W. and Bischoff, J.L. (1977). Hydrothermal transport of heavy metals by seawater: the role of seawater/basalt ratio. Earth Planet. Sci. Letters, 34, pp. 71-77.

Seyfried, W.E., Shanks, W.C. and Dibble, W.E. (1978). Clay mineral formation in DSDP Leg 34 Basalt, Earth Planet. Sci. Letters, 41, pp. 265-276.

Shapiro, L. and Brannock, W.W (1962). Rapid analysis of silicate, carbonate and phosphate rocks. U. S. Geol. Surv. Bull. 1144-A. 56 pp.

Shervais, J.W. (1982). Ti-V plots and the petrogenesis of modern and ophiolitic lavas. Earth Planet. Sci. Letters, 59, pp. 101-118.

Shido, F., Miyashiro, A. and Ewing, M. (1974). Compositional variation in pillow lavas from the Mid-Atlantic Ridge. Marine Geol., 16, pp. 177-190.

Simonian, K.O. and Gass, I.G. (1978). Arakapas fault belt, Cyprus: a fossil transform fault. Geol. Soc. Amer. Bull., 89, pp. 1220-1230.

Smewing, J.D. and Potts, P.J. (1976). Rare-earth abundances in basalts and metabasalts from the Troodos Massif, Cyprus. Contrib. Mineral. and Petrol., 57, pp. 245-258.

Smewing, J.D., Simonian, K.O. and Gass, I.G. (1975). Metabasalts from the Troodos Massif, Cyprus: genetic

implication deduced from petrography and trace element geochemistry. Contrib. Mineral. and Petrol., 51, pp. 49-64.

Smith, D.G.W. and Gold, C.M. (1976). A scheme for fully quantitative energy dispersive microprobe analysis. Advances in X-Ray Analysis, 19, Proc. 24th. Ann. Conf. on Applications of X-Ray Analysis. pp. 191-201.

Smith, R.C., Rose, A.W. and Lanning, R.M. (1975). Geology and geochemistry of Triassic diabase in Pennyslvania. Geol. Soc. Amer. Bull., 86, pp. 943-955.

Smith, R.E. (1968). Redistribution of major elements in the alteration of some basic lavas during burial metamorphism. J. Petrol, 9, pp. 191-219.

Smith, R.E. (1974). The production of spilitic lithologies by burial metamorphism of flood basalts from the Canadian Keweenawan, Lake Superior. In: Spilites and Spilitic Rocks, Amstutz, G.C. (Ed.), pp. 403-416.

Smith, R.E. and Smith, S.E. (1976). Comments on the use of Ti, Zr, Y, Sr, K, P and Nb in classification of basaltic magmas. Earth Planet. Sci. Letters, 32, pp. 114-120.

Stakes, D.S. and Scheidegger, K.F. (1978). Temporal variations in secondary minerals from Nazca plate basalts and aging of the oceanic crust. Geol. Soc. America, Prog. with Abstr., 10, p. 496.

Stark, J.T. (1963). Petrology of the volcanic rocks of Guam. U.S. Geol. Surv. Prof. Pap., 403-C.

Stauffer, M.R., Mukherjee, A.C. and Koo, J. (1975). The Amisk Group: an Aphebian (?) island arc deposit. Can. J. Earth Sci., 12, pp. 2021-2035.

Steiger, R.H. and Jäger, E. (1977). Subcommission on geochronology: convention on the use of decay constants in geo- and cosmochronology. Earth Planet. Sci. Letters, 36, pp. 359-362.

Stockwell, C.H. (1936). Eastern portion of the Great Slave Lake. Geol. Surv. Can. Maps 377A and 378A.

Stockwell, C.H., Brown, I.C., Barnes, F.Q. and Wright, G.M. (1968). Christie Bay, District of Mackenzie. Geol. Surv. Can. Map 1122A.

Stoeser, D.B. (1975). Igneous rocks from Leg 30 of the D.S.D.P. In: Init. Rept. Deep Sea Drilling Proj., Nat. Sci. Fndn., Andrews, J.E. et. al. (Eds.), 30, pp. 401-414.

Stonecipher, S.A. (1977). Chemical and mineralogical chracteristics of deep sea zeolite host sediments - genetic implications. EDS, Trans. Amer. Geophys. Union, 58, p. 1151.

Strong, D.F. (1973). Lush's Bight and Roberts Arm Groups of central Newfoundland: possible juxtaposed oceanic and island-arc volcanic suites. Geol. Soc. Amer. Bull., 84, pp. 3917-3928.

Strong, D.F. and Minatidis, D.G. (1975). Geochemistry and tectonic setting of the late Precambrian Holyrood plutonic series of eastern Newfoundland. Lithos, 8, pp. 283-295.

Strong, D.F., O'Brien, S.J., Taylor, S.W., Strong, P.G., Wilton, D.H. (1978). Aborted Proterozoic rifting in eastern Newfoundland. Can. J. Earth Sci., 15, pp. 117-131.

Strong, D.F., Dickson, W.L. and Pickerill, R.K. (1979). Chemistry and prehnite-pumpellyite facies metamorphism of calc-alkaline Carboniferous volcanic rocks of southeastern New Brunswick. Can. J. Earth Sci., 16, pp. 1071-1085.

Stueber, A.M., Heimlich, R.A. and Ikramuddin, M. (1976). Rb-Sr ages of Precambrian mafic dykes, Bighorn Mountains, Wyoming. Geol. Soc. Amer. Bull., 87, pp. 909-914.

Sullivan, K.D. and Keen, C.E. (1977). Newfoundland seamounts: petrology and geochemistry. In: Volcanic Regimes in Canada, Baragar, W.R.A., Coleman, L.C. and Hall, J.M. (Eds.). Geol. Assoc. Can., Sp. Pap., 16, pp. 461-476.

Sun, S.S. and Hanson, G.N. (1975). Origin of Ross Island basanitoids and limitations upon the heterogeneiity of mantle sources for alkali basalts and nephelinites. Contrib. Mineral. and Petrol., 52, pp. 77-106.

Sun, S.-S. and Nesbitt, R.W. (1978a). Petrogenesis of Archean ultrabasic and basic volcanics: evidence from rare earth elements. Contrib. Mineral. and Petrol., 65, pp. 301-325.

Sun, S.-S. and Nesbitt, R.W. (1978b). Geochemical regularities and genetic significance of ophiolitic basalts. Geology, 6, pp. 689-693.

Sun, S.-S., Nesbitt, R.W. and Sharaskin, A.Ya. (1979). Geochemical characteristics of mid-ocean ridge basalts. Earth Planet. Sci. Letters, 44, pp. 119-138.

Surdam, R.C. (1973). Low grade metamorphism of tuffaceous rocks in the Karmutsen Group, Vancouver Island, B.C. Geol. Soc. Amer. Bull., 84, pp. 1911-1922.

Taylor, S.R. and White, J.R. (1966). Trace element abundances in andesites. Bull. Volcanol., 29, pp. 177-194.

Taylor, S.R., Capp, A.C., Graham, A.L. and Blake, S.M. (1969). Trace element abundances in andesites, II. Saipan, Bougainville and Fiji. Contrib. Mineral. and Petrol., 23, pp. 1-26.

Thompson, G. (1973). A geochemical study of the low-temperature interaction of seawater and oceanic igneous rocks. EOS, Trans. Amer. Geophys. Union, 54, pp. 1015-1019.

Thompson, G. and Humphris, S.E. (1977). Seawater-rock interactions in the oceanic basement. In: Proc. 2nd. Internat. Symp. on Water-Rock Interaction. Eds. H. Paquet and Y. Tardy, III 13-18, Science Geologique, Univ. Louis Pasteur, Strasbourg, France.

Thompson, G. and Melson, W.G. (1970). Boron contents of serpentinites and metabasalts in the oceanic crust: implications for the baron cycle in the oceans. Earth Planet. Sci. Letters, 8, pp. 61-65.

Thompson, G. and Melson, W.G. (1972). The petrology of oceanic crust across fracture zones in the Atlantic Ocean: evidence of a new kind of sea floor spreading. J. Geol., 80, pp. 526-538.

Thompson, R.N. (1974). Primary basalts and magma genesis I. Skye, North-West Scotland. Contrib. Mineral. and Petrol., 45, pp. 317-341.

Thompson, R.N., Esson, J. and Dunham, A.C. (1972). Major element chemical variation in the Eocene lavas of the Isle of Skye, Scotland. J. Petrol, 13, pp. 219-253.

Thorpe, R.S. (1972). Ocean floor basalt affinity of Precambrian glaucophane schist from Anglesey. Nature Phys. Sci., 240, pp. 164-166.

Tilley, C.E. (1950). Some aspects of magmatic evolution. Quart. J. Geol. Soc. Land., 106, pp. 37-61.

Tilley, C.E. and Muir, I.D. (1964). Intermediate members of the oceanic basalt-trachyte association. Geol. Foren. Stockholm Forh., 85, pp. 434-443.

Trzcienski, W.E. and Birkett, T.C. (1982). Compositional

variations of pumpellyite along the western margin of the Quebec Appalachians. Can. Mineral., 20, pp. 203-209.

Tull, J.F. and Stow, S.H. (1980). The Hillabee Greenstone: a mafic volcanic complex in the Appalachian Piedmont of Alabama. Geol. Soc. Amer. Bull., 91, pp. 1-36.

Vallance, T.G. (1969). Spilites again: some consequences of the degradation of basalts. Proc. Linnean Soc. N.S.W., 94, pp. 8-51.

Vallance, T.G. (1974a). Spilitic degradation of a tholeiitic basalt. J. Petrol., 15, pp. 79-96.

Vallance, T.G. (1974b). Pyroxenes and the basalt, spilite relation. In: Spilites and Spilitic Rocks, Amstutz, G.C. (Ed.). Springer-Verlag, pp. 59-68.

Van Schmus, R. (1965). The geochronology of the Blind River Bruce Mines area near Ontario. J. Geol., 73, pp. 755-780.

Van Schmus, W.R. and Bowring, S.A. (1980). Chronology of igneous events in the Wopmay orogen, Northwest Territories, Canada. Geol. Soc. Amer. Prog. with Abstr., 12, p. 540.

Viljoen, M.J. and Viljoen, R.P. (1969). The geology and geochemistry of the lower ultramafic unit of the Onverwacht Group and a proposed new class of igneous rocks. Geol. Soc. S. Africa Spec. Pub. 2, pp. 55-86.

Vogel, D.E. (1975). Precambrian weathering in acid metavolcanic rocks from the Superior province, Villebon Township, south-central Quebec. Can. J. Earth Sci., 12, pp. 2080-2085.

Vuagnat, M. (1974). A new appraisal of Alpine spilites. In: Spilites and Spilitic Rocks, Amstutz, G.C. (Ed.). Springer-Verlag, pp. 417-426.

Wager, L.R. and Mitchell, R.L. (1951). The distribution of trace elements during strong fractionation of basic magma - A further study of the Skaergaard intrusion, East Greenland. Geochim. Cosmochim. Acta., 1, pp. 129-208.

Walker, G.P.L. and Croasdale, R. (1971). Characteristics of some basaltic pyroclasts. Bull. Volcanol., 35, pp. 303-317.

Walker, K.R. (1969). The Palisades sill, New Jersey: a reinvestigation, Geol. Soc. Amer. Spec. Pap., 111, 178 pp.

Walker, R.R. (1977). The geology and uranium deposits of Proterozoic rocks on Simpson Island, Northwest Territories. Unpub. M.Sc. thesis, University of Alberta, Edmonton, Alta. 193 pp.

Wallace, H. (1981). Keweenawan geology of the Lake Superior Basin. Geol. Surv. Can. Paper 81-10, pp. 399-417.

Wendlandt, R.F. and Harrison, W.J. (1979). Rare earth partitioning between immiscible carbonate and silicate liquids and CO_2 vapour: results and implications for the formation of light-rare-earth-enriched rocks. Contrib. Mineral. and Petrol, 69, pp. 409-419.

White, W.M., Tapia, M.D.M. and Schilling, J.-G. (1979). The petrology and geochemistry of the Azores islands. Contrib. Mineral. and Petrol., 69, pp. 201-213.

Wilkinson, J.F.G. (1968). The petrography of basaltic rocks. In: Basalts, Vol. 1, Hess, H.H. and Poldervaart, A. (Eds.), J. Wiley & Sons, N.Y., pp. 163-214.

Wilkinson, J.M. and Cann, J.R. (1974). Trace elements and tectonic relationships of basaltic rocks in the Ballantrae igneous complex, Ayrshire. Geol. Mag., 111, pp. 35-41.

Williams, M. and McBirney, R. (1979). Volcanology, Freeman, Cooper & Co., San Francisco, 397 pp.

Winchester, J.A. and Floyd, P.A. (1976). Goechemical magma type discrimination: application to altered and metamorphosed basic igneous rocks. Earth Planet. Sci. Letters, 28, pp. 459-469.

Winchester, J.A. and Floyd, P.A. (1977). Geochemical discrimination of different magma series and their differentiation products using immobile elements. Chem. geol., 20, pp. 325-343.

Winkler, H.G.F. (1979). Petrogenesis of metamorphic rocks, 5th Edn. Springer-Verlag, New York Inc. 348 pp.

Wood, D.A. (1978). Major and trace element variations in the Tertiary lavas of eastern Iceland with respect the Iceland geochemical anomaly. J. Petrol., 19, pp. 393-436.

Wood, D.A. (1979). Dynamic partial melting: its application to the petrogeneses of basalts erupted in Iceland, the Faeroe Islands, the Isle of Skye (Scotland) and the Troodos Massif (Cyprus). Geochim. Cosmochim. Acta, 43, pp. 1031-1046.

Wood, D.A., Gibson, I.L. and Thompson, R.N. (1976). Elemental mobility during zeolite facies metamorphism of the Tertiary basalts of eastern Iceland. Contrib. Mineral. and Petrol., 55, pp. 241-254.

Wood, D.A., Joron, J.-L. and Treuil, M. (1979). A re-appraisal of the use of trace elements to classify and discriminate between magma series erupted in different tectonic settings. Earth Planet. Sci. Letters, 45, pp. 326-336.

Wright, G.M. (1951). Second Preliminary Map. Christie Bay, District of Mackenzie, Northwest Territories. Geol. Surv. Can. Paper 51-25.

Wright, J.V., Smith, A.L. and Self, S. (1980). A working terminology of pyroclastic deposits. J. Volcanology and Geothermal Research, 8, pp. 315-336.

Yeo, G.M. (1976). Sedimentology and geochemistry of the Wilson Island Group, Northwest Territories. Geol. Assoc. Can. Prog. with Abstr., 1, p. 83.

Yoder, H.S. and Tilley, C.E. (1962). Origin of basalt magmas: an experimental study of natural and synthetic rock systems. J. Petrol., 3, pp. 342-532.

York, D. (1969). Least-squares fitting of a straight line with correlated errors. Earth Planet. Sci. Letters, 5, pp. 320-324.

Zen, E. (1972). Gibbs free energy, enthalpy and entropy of ten rock forming minerals: calculations, discrepancies, implications. Amer. Mineral., 57, pp. 524-553.

Zen, E-an and Thompson, A.B. (1974). Low grade metamorphism: mineral equilibrium relations. In: Annual Review of Earth and Planetary Sciences, Borath, F.A. (Ed.). Ann. Reviews Inc., Calif., 2, pp. 179-212.

APPENDIX I. DETERMINATIVE METHODS

For detailed petrographic work, thin sections were stained for K-feldspar, using K cobaltinitrite and for plagioclase using K rhodizonate. A multipurpose stain was used for distinguishing calcite and dolomite of both iron-free and ferrous types (Reid, 1969).

Analyses of both major elements, and HFSE and LIL trace elements, were carried out by X-ray fluorescence. The mafic lavas from the Wilson Island Group, Union Island Group and the Pekanatui Point Kahochella Group as well as all rhyolites were analyzed by J.G. Holland of Durham University using a Phillips 1212 automatic XRF spectrometer coupled to a Torrens 108 automatic sample holder. Samples and standards were pressed into powder briquettes using a polyvinyl alcohol binder. A W tube was used for trace element analysis and a Cr tube used for major elements. The procedure is described in Brown *et al.* (1977). The precision was checked by inserting duplicate samples. The coefficient of variation, based on replicate analysis was less than 2% for the major elements and less than 10% for the trace elements. The accuracy of Rb and Sr was checked by plotting XRF vs. isotope dilution analyses on 12 samples. This produced correlations with an r^2 of 0.95 and 0.98 respectively. The accuracy of other elements was checked by analyzing samples of BCR-1. XRF analyses for La and Ce were also carried out, at Durham, on some of the samples from the Wilson Island Group.

An attempt was made to produce the remaining major and trace elements analyses at the University of Alberta. A Phillips PW 1410 manual XRF unit was used to analyze for Rb, Sr, Y, Zr and Nb. Optimum machine settings used were 60 KV and 40 ma for the W tube, a detector voltage of 1060 V, amplifier attenuation of 1 and pulse-height-analyzer lower-level and window settings of 220 and 460 V respectively. An LiF 220 diffracting crystal was used. Corrections for absorption and fluorescence effects were minimized by using standards which were similar in composition and mineralogy to the unknowns. Standards (SPG1 to 6) were developed by multiple XRF analysis of of six previously analyzed mafic samples (U126, U168B, U179E, PP8A, PP82A, PP10X) which covered the range in observed concentrations of Rb to Nb. Four separate discs of each sample were each analyzed four times for each element by J.G. Holland at the University of Durham. In addition, a greenstone standard (KUM-3) was obtained from P.A. Floyd and twelve samples analyzed for Rb and Sr by isotope dilution were used. Both samples and standards were prepared as cellulose-backed pressed-powder discs. Absorption effects were further reduced by normalizing peak count-rates to background rates, the intensity of which varies to some extent with the mass absorption coefficient of the matrix. Extensive tests on greenstone material gave similar results to those yielded by normalizing peak count rates to the intensity of the Compton-scattered radiation from the

principal line of the X-ray tube (P.A. Floyd and G.J. Lees, Pers. comm., 1978). A correction for curved background below the peaks of interest was obtained by comparing the intensities at true background and measured background positions on a silica-gel disc and using this as a correction. Total counting times used were 200 secs. each on peak and background and overlap corrections were made for the effect of SrKβ on ZrKα and RbKβ on YKα. The resulting precision (coefficient of variation) due to counting statistics and machine drift was 2 to 4% for most elements but rose to 10% for low concentrations (10 ppm) of Rb and Nb. Lower limits of detection were 1 to 2 ppm based on counting statistics. Good linear response of count rate vs. ppm was obtained for Sr, Nb, Zr and Rb (r^2 of 0.99, 0.99, 0.97 and 0.96 respectively) but not for Y (r^2 of 0.51). Using samples analyzed by J.G. Holland as a test, these curves were found to be accurate only within 99% confidence limits for Rb concentrations above 20 ppm and for Zr. Predicted concentrations were consistently high, especially at low concentration levels, and indicate a difficulty in accurate estimation of background intensity. This especially affects Y and Nb analyses. In addition, pulse height analysis displayed an additional high-energy peak for all five elements. Each peak had twice the energy of the characteristic peak and occurred at count-rates far too low to cause pulse pile-up in the scintillation counter. This effect was probably caused by a cracked crystal.

Interference from the spurious peak may have also affected the results. Because of the discouraging overall results, data from this instrument was not used.

Major element analysis of the mafic samples was originally attempted by electron microprobe analysis of homogeneous glasses produced from 0.5 gm aliquots of rock powder. These glasses were produced under vacuum in an image furnace which used first-surface gold reflectors to concentrate the thermal output from a lamp with a high infra-red output (Schimann and Smith, 1980). Repeated experiment showed that it was not possible to reach sufficiently high temperatures with this technique to produce a homogeneous glass with no crystals: after rapid quenching, most glass charges contained discrete Fe-Ti oxides. This could have been caused by poor infra-red reflection caused by deterioration of the gold-plated reflection surfaces. Regilding of these surfaces did not improve the performance of the reflectors possibly because the gold plate was now too thick. The ten homogeneous glasses which were produced gave very similar major element analyses to those subsequently produced by XRF by R.H. McNutt.

Because of the problems outlined above, the remaining 95 major and trace element analyses were produced by R.H. McNutt on the Philips 1450 AHP XRF spectrometer at McMaster University. Trace element analyses were produced on pressed-powder pellets whereas major elements were

determined on 2:1 diluted ($Li_2B_4O_7$) fused discs. Raw counts were corrected for background and matrix effects. When compared to analyses from Durham, using t-tests, McMaster analyses of SPG1 to 6 showed similar Sr, Y and P at the 95% confidence level and similar Nb at the 99% level. Rb, Zr and Fe were slightly lower whereas Ti and Al were slightly higher at the 99% confidence level.

The transition elements Sc, V, Cr and Ni were analyzed by atomic absorption using a Perkin Elmer 503 spectrophotometer. An air-acetylene gas mixture was used for Cr and Ni but N_2O-acetylene was used for V and Sc to provide greater sensitivity. To reduce matrix effects, the mafic and intermediate USGS standards AGV-1, BCR-1 and BHVO-1 and GSC standard MRG-1 were used as standard samples. MRG-1 was omitted from the calibration curve for Cr and Ni because, on plots of absorption response vs. concentration in solution, MRG samples of different dilutions formed a line which did not pass through the origin and which was distinct from, but parallel to, the curves formed by USGS standards. The University of Alberta aliquot is therefore lower in Cr and Ni than the mean values from Abbey (1977), more realistic values being 359 and 177 ppm respectively. This variation is likely because the sample is a gabbro. For similar reasons, AGV-1 was omitted from the Sc calibration curve.

For the Pekanatui Point and Union Island Group lavas, H_2O was determined by Penfield tube and CO_2 by a volumetric technique whereby the sample was decomposed in 3:1 boiled,

distilled H_2O and HCl and then the evolved CO_2 was absorbed in KOH solution (Shapiro and Brannock, 1962). For the remaining samples, H_2O and CO_2 analyses were produced by C. Brooks at the University of Montreal using a gas chromatograph with an attatched furnace. Calcium oxalate and calcium carbonate were used as standards. The accuracy was checked by analyzing MRG-1.

The variation in oxidation ratio in the Union Island Group was determined by analyzing a small sample suite for FeO by titration with K-dichromate.

Major element analyses of minerals were carried out by energy - dispersive electron microprobe analysis using an Applied Research Laboratories EMX electron microprobe fitted with an ORTEC energy dispersive spectrometer. The latter uses an Li-drifted silicon solid state detector. The operating voltage and aperture current were 15 kV and 0.225 mA, respectively. Total live-time counts of 400 secs were accumulated for each analyzed sample; this being the aggregate of 2 to 7 individual analysis points per grain. For the analysis of plagioclase, a rastered beam was used and 16 points were probed on each grain. Where possible, the sample was continuously moved across the beam to minimize Na loss from volatilization. Where zoning was noted, the entire analysis time was restricted to one optically continuous zone and both core and margin were probed in some cases. A willemite standard was run before and after each analysis session to calibrate the location and distortion of each

characteristic energy pulse with reference to its correct energy location in the multichannel analyzer. Displacement in the position of the characteristic Zn and Si peaks was used as the basis of the correction. The standards used were as shown in Table I-1. The raw count data were processed using the computer program EDATA (Smith and Gold, 1976) which calculates the atomic number of the standard. absorption and fluorescence corrections as well as corrections for peak overlap and background intensity and adjustments for peak shift and probe current drift. Detection limits under these conditions tend to decrase with elements of increasing atomic number from ~0.2% for Na to ~0.03% for Cl. The detection limit then tends to increase with increasing atomic number to ~0.2% for Zn. The data was stored on magnetic tape by the electron microprobe laboratory at the University of Alberta under the title GOFF EAST ARM.

For Rb-Sr isotopic analysis, initially sixteen Pearson Formation samples and twenty-one Wilson Island Group samples were analysed semiquantitatively for Rb/Sr by XRF. A sample set with a wide range in Rb/Sr was then chosen for isotopic analysis. With the exception of WI35D which was a rhyolite, all Wilson Island Group samples were fine to medium grained epidote-albite-amphibolites with varying amounts of biotite. The Pearson Formation samples were pumpellyite, Fe-rich epidote, actinolite - albite mafic rocks. All carbonate-bearing samples were excluded.

Rb and Sr isotope dilution determinations were made on six samples from each suite which showed favourable ranges in Rb/Sr ratios. Each homogeneous sample was chosen to contain approximately 20 micrograms of Rb or Sr and was spiked with ^{87}Rb or ^{84}Sr. Rb was separated with K as the sulphate and converted to the perchlorate, whereas Sr was separated by $Ba(NO_3)_2$ coprecipitation and purified in a cation exchange column. Both sample sets were loaded on triple-Re filaments for isotopic analysis, using a single-focussing mass spectrometer with a 30 cm. radius of curvature.

For the Pearson Formation samples, replicate analysis of the standard NBS•SRM 987 gave a best value of $^{87}Sr/^{86}Sr$ = 0.71067 and $^{87}Sr/^{86}Sr$ ratios were normalized to the accepted value of 0.71017. During analysis of the Wilson Island Group samples, repeated analysis of the same standard was within the error of the accepted value.

A decay constant for ^{87}Rb of 1.42×10^{-11} yr^{-1} was used as suggested by the Geochronology Subcommission of 1976 (Steiger and Jäger, 1977) and also as measured by Davis *et al.* (1977). All other Rb-Sr dates quoted have been recalculated to this value. Other constants employed were $^{85}Rb/^{87}Rb$ = 2.601 and $^{84}Sr/^{86}Sr$ = 0.1194. All Sr isotopic data were normalized to this latter value. A whole rock Rb-Sr isochron was fitted using an APL computer program (RBSR-ISOCHRON) written by Baadsgaard and using the method of McIntyre *et al.* (1966) and York (1969). Quoted errors

were at the 95% (2-sigma) confidence level.

Clinopyroxene fractions were separated from crushed rock samples using tetrabromoethane. The more magnetic fraction was removed by a Franz 130 isodynamic separator, and the sample purified by coarse-picking under a binocular microscope. Surface contamination was removed from the grain surfaces by washing in acetone, treating for 10 minutes in warm 2.5N HCl, boiling in concentrated Na_2CO_3 solution, and then immersing for 20 minutes in 5% HF. The samples were then checked again under a binocular microscope and discoloured or cloudy grains were removed. Final concentrates of > 100 mg per samples were used for Sr isotopic analysis (unspiked) and > 20 mg for oxygen isotopic analysis.

Oxygen isotopic analyses of the rocks and minerals were carried out using the BrF_5 method (Clayton and Mayeda, 1963). The isotopic composition of sample x is given as:

$$x = \left[\frac{(O^{18}/O^{16})}{(O^{18}/O^{16})_{std.}} - 1 \right] \times 1000$$

The analyses are reported relative to Standard Mean Ocean Water (SMOW, Craig 1961, $1000 \ln\alpha CO_2\text{-}H_2O = 1.0407$).

Table I-1. Standards used in electron microprobe analysis of minerals.

	Cpx.				Plag.			Ch.			Pu. PE10 Sph. PV10 Ep.	Ep.	Ac.	Hbl.
	54C	U127	U150A	PE5B	W140B	SD6		PE10			W140B	U165	U163	W18 W140B
	SD4	U1118	U163	U165	U1128A	U163	PE10	PV10	PE5B	PV07				
	SD6	U1128A	U165	PE10	PV30	PP44	PV07							
Si	029	163	029	279	106	029	279	279	029	106	279	029	163	163
Ti	163	163	152	152	152	152	163	152	152	152	152	152	152	163
Al	163	163	163	279	163	029	112	279	163	163	279	029	112	163
Fe	163	163	137	137	163	137	163	137	137	137	137	152	152	152
Mn	-	112	112	-	112	112	-	-	112	112	-	112	112	112
Mg	163	163	106	106	163	106	163	106	106	106	106	106	106	163
Ca	112	112	112	112	112	112	163	112	112	112	112	112	112	163
Na	163	163	163	029	163	029	029	029	163	163	029	029	029	163
K	-	-	163	279	163	279	163	279	163	163	279	-	163	163

029 albite 639-178
106 forsterite smm 4-18
112 garnet 639-1
137 hematite 639-15
152 ilmenite 639-16
163 kaersutite 639-3
279 sanidine 639-9
- default standards

APPENDIX II. ENERGY DISPERSIVE ELECTRON MICROPROBE ANALYSES OF IGNEOUS AND METAMORPHIC MINERALS.

	S4C-1 (MADM)	S4C-2 (MADM)	S4C-3 (MADM)	S4C-4 (MADM)	SD4-1 (MADM)	SD4-2 (MADM)
SiO_2	48.29	49.85	49.18	49.47	50.13	50.22
TiO_2	2.27	1.65	1.85	1.78	1.74	1.66
Al_2O_3	4.37	3.14	3.66	3.45	3.57	3.27
Cr_2O_3	-	-	-	-	-	-
V_2O_5	-	-	-	-	-	-
FeO tot.	10.35	10.75	10.79	10.30	11.25	11.08
MnO	0.14	0.14	0.17	0.07	0.25	0.19
MgO	13.82	14.48	13.88	13.61	14.16	14.02
CaO	20.17	19.55	19.80	20.18	19.50	19.53
Na_2O	0.27	0.15	0.21	0.10	0.24	0.18
Total	99.67	99.72	99.54	98.95	100.80	100.15
-F1	0.922	0.875	0.895	0.889	0.895	0.889
-F2	2.470	2.477	2.473	2.458	2.515	2.505
Si	1.819	1.873	1.854	1.874	1.866	1.882
Al iv	0.181	0.127	0.146	0.126	0.134	0.118
Al vi	0.013	0.012	0.017	0.028	0.023	0.026
Ti	0.064	0.047	0.052	0.051	0.049	0.047
Cr	-	-	-	-	-	-
V	-	-	-	-	-	-
Fe	0.326	0.338	0.340	0.326	0.350	0.347
Mn	0.004	0.005	0.005	0.002	0.006	0.006
Mg	0.776	0.811	0.780	0.768	0.786	0.783
Ca	0.814	0.787	0.800	0.819	0.778	0.784
Na	0.020	0.011	0.015	0.008	0.018	0.013
$CaSiO_3$	42.4	40.6	41.5	42.8	40.5	40.8
$MgSiO_3$	40.4	41.8	40.5	40.1	40.9	40.8
$(Fe,Mn)SiO_3$	17.2	17.6	18.0	17.1	18.6	18.4

Table II-1. Pyroxene Analyses.

Oxygen was determined by stoichiometry assuming total Fe as FeO. Structural formulae were calculated on a basis of 6 oxygen anions. F1 & F2 tectonic discriminant functions were calculated using eigenvalues from Nisbet and Pearce (1977). The index for the host rock suite is given in brackets. The dash indicates that the element was not detected. Reported values of Na, Ni and Cl are at the limits of detection. Ba and Zn values are not significant.

	SD4-3 (MADM)	SD4-4 (MADM)	SD4-5 (MADM)	SD4-6 (MADM)	SD6-1 (MADM)	SD6-2 (MADM)
SiO_2	50.20	48.74	49.31	49.82	50.66	51.19
TiO_2	1.42	1.81	1.60	1.61	1.28	1.13
Al_2O_3	3.24	4.73	4.39	3.92	2.50	1.93
Cr_2O_3	-	-	-	-	-	-
V_2O_5	-	-	-	-	-	-
FeO tot.	10.30	9.45	9.74	10.40	12.41	12.46
MnO	0.07	0.10	0.06	0.14	0.25	0.26
MgO	14.54	13.92	14.18	14.27	14.49	15.14
CaO	19.46	20.07	20.03	19.84	18.39	18.25
Na_2O	0.19	0.17	0.28	0.24	0.17	0.10
Total	99.41	98.99	99.58	100.23	100.07	100.45
-F1	0.856	0.879	0.870	0.879	0.851	0.838
-F2	2.465	2.454	2.452	2.483	2.504	2.510
Si	1.883	1.829	1.844	1.857	1.903	1.914
Al iv	0.117	0.171	0.156	0.143	0.097	0.085
Al vi	0.027	0.038	0.037	0.029	0.014	-
Ti	0.040	0.051	0.045	0.045	0.036	0.032
Cr	-	-	-	-	-	-
V	-	-	-	-	-	-
Fe	0.323	0.297	0.304	0.324	0.390	0.390
Mn	0.002	0.003	0.002	0.004	0.008	0.008
Mg	0.813	0.779	0.790	0.793	0.812	0.844
Ca	0.782	0.807	0.802	0.793	0.737	0.731
Na	0.014	0.012	0.020	0.018	0.012	0.007
$CaSiO_3$	40.7	42.8	42.3	41.4	37.9	37.0
$MgSiO_3$	42.3	41.3	41.6	41.4	41.7	42.8
$(Fe,Mn)SiO_3$	17.0	15.9	16.1	17.2	20.4	20.2

	SD6-3 (MADM)	SD6-4 (MADM)	UI118-1 (UIG1M)	UI118-2 (UIG1M)	UI118-3 (UIG1M)	UI118-4 (UIG1M)
SiO_2	50.24	49.93	46.81	46.50	47.68	47.33
TiO_2	1.51	1.64	2.86	2.66	2.18	2.14
Al_2O_3	3.14	3.26	3.82	3.52	3.56	3.45
Cr_2O_3	-	-	0.90	0.07	0.05	-
V_2O_5	-	-	0.20	0.18	0.14	0.15
FeO tot.	10.27	10.56	16.79	16.76	15.78	16.11
MnO	0.19	0.13	0.23	0.21	0.21	0.24
MgO	14.58	14.55	9.77	9.45	10.04	9.87
CaO	19.58	19.80	19.58	19.48	19.90	19.90
Na_2O	0.16	0.18	0.29	0.22	0.18	0.16
Total	99.65	100.05	100.42	99.06	99.71	99.37
-F1	0.871	0.878	0.995	0.973	0.946	0.942
-F2	2.489	2.478	2.469	2.430	2.442	2.425
Si	1.881	1.866	1.810	1.824	1.845	1.843
Al iv	0.119	0.134	0.174	0.163	0.155	0.157
Al vi	0.019	0.009	-	-	0.007	0.001
Ti	0.043	0.0	0.083	0.078	0.063	0.063
Cr	-	-	0.003	0.002	0.001	-
V	-	-	0.005	0.005	0.004	0.004
Fe	0.322	0.330	0.543	0.550	0.511	0.525
Mn	0.006	0.004	0.008	0.007	0.007	0.008
Mg	0.814	0.810	0.563	0.552	0.579	0.573
Ca	0.785	0.793	0.811	0.819	0.825	0.830
Na	0.011	0.013	0.022	0.017	0.013	0.012
$CaSiO_3$	40.8	40.9	42.1	42.4	43.0	42.9
$MgSiO_3$	42.2	41.8	29.3	28.7	30.1	29.6
$(Fe,Mn)SiO_3$	17.0	17.3	28.6	28.9	26.9	27.5

	UI128A -1 (UIG1M)	UI128A -2 (UIG1M)	UI128A -3 (UIG1M)	UI128A -4 (UIG1M)	UI128A -5 (UIG1m)	UI128A -6 (UIG1M)
SiO_2	48.32	50.10	49.65	49.21	48.71	49.26
TiO_2	1.59	1.16	1.21	1.44	1.71	1.45
Al_2O_3	3.55	3.59	2.91	3.68	3.69	3.85
Cr_2O_3	-	0.09	-	-	0.08	0.06
V_2O_5	0.08	0.07	0.08	0.08	0.14	0.16
FeO tot.	14.87	11.00	13.10	12.88	14.58	12.31
MnO	0.30	0.19	0.26	0.26	0.34	0.29
MgO	12.20	14.72	14.43	13.37	12.63	14.13
CaO	18.27	18.97	17.38	18.76	18.15	18.59
Na_2O	0.27	0.10	0.11	0.17	0.24	0.16
Total	99.44	99.98	99.13	99.83	100.34*	100.32*
-F1	0.875	0.830	0.819	0.8[illegible]	0.884	0.853
-F2	2.451	2.473	2.473	2.470	2.490	2.483
Si	1.857	1.876	1.888	1.864	1.851	1.852
Al iv	0.143	0.124	0.112	0.136	0.149	0.148
Al vi	0.018	0.034	0.018	0.028	0.016	0.023
Ti	0.046	0.033	0.035	0.041	0.049	0.041
Cr	-	0.003	-	-	0.003	0.002
V	0.002	0.002	0.002	0.002	0.004	0.004
Fe	0.478	0.344	0.417	0.408	0.463	0.387
Mn	0.010	0.006	0.008	0.008	0.011	0.009
Mg	0.699	0.821	0.818	0.755	0.715	0.792
Ca	0.752	0.761	0.708	0.761	0.739	0.749
Na	0.020	0.007	0.008	0.013	0.018	0.012
$CaSiO_3$	38.8	39.4	36.3	39.4	38.3	38.7
$MgSiO_3$	36.0	42.5	41.9	39.1	37.1	40.9
$(Fe,Mn)SiO_3$	25.2	18.1	21.8	21.5	24.6	20.4

*Both include 0.07% NiO.

	UI27-1 (UIG2M)	UI27-2 (UIG2M)	UI27-3 (UIG2M)	UI27-4 (UIG2M)	UI59A-1 (UIGDM)	UI59A-2 (UIGDM)
SiO_2	48.63	48.33	47.35	48.26	47.87	48.76
TiO_2	1.80	1.68	2.32	2.09	2.49	2.14
Al_2O_3	4.28	4.91	5.19	4.52	3.66	3.05
Cr_2O_3	0.11	0.14	0.21	0.23	-	-
V_2O_5	0.13	0.21	0.09	0.17	-	0.11
FeO tot.	12.15	11.22	12.03	12.41	15.22	15.73
MnO	0.18	0.15	0.13	0.20	0.20	0.25
MgO	12.98	12.82	12.57	12.82	10.53	10.54
CaO	20.30	20.95	19.90	19.86	20.04	19.93
Na_2O	-	-	0.10	0.12	0.22	0.23
Total	100.56	100.41	99.88	100.68	100.22	100.74
-F1	0.890	0.882	0.914	0.911	[illegible]	[illegible]957
-F2	2.459	2.435	2.454	2.476	[illegible]	[illegible]84
Si	1.832	1.819	1.797	1.818	[illegible]	1.864
Al iv	0.168	0.181	0.203	0.182	[illegible]	0.136
Al vi	0.022	0.037	[illegible]	0.019	0.004	0.001
Ti	0.051	0.048	[illegible]	0.059	0.072	0.062
Cr	0.003	0.004	[illegible]	0.007	-	-
V	0.003	0.005	[illegible]	0.004	-	0.003
Fe	0.383	0.353	[illegible]	0.391	0.489	0.503
Mn	0.006	0.005	[illegible]	0.006	0.007	0.008
Mg	0.729	0.719	0.711	0.720	0.602	0.601
Ca	0.819	0.845	0.809	0.802	0.824	0.816
Na	-	-	0.007	0.009	0.016	0.017
$CaSiO_3$	42.3	44.0	42.5	41.8	42.9	42.3
$MgSiO_3$	37.6	37.4	37.3	37.5	31.3	31.2
$(Fe,Mn)SiO_3$	20.1	18.6	20.2	20.[illegible]	25.8	26.5

	UI63-1 (UIGDM)	UI63-2 (UIGDM)	UI63-3 (UIGDM)	UI65-1 (UIGDM)	UI65-2 (UIGDM)	UI65-3 (UIGDM)
SiO_2	50.34	51.52	50.27	51.05	50.67	50.44
TiO_2	1.28	0.69	1.39	1.18	1.16	1.31
Al_2O_3	2.42	1.39	2.99	2.11	2.49	2.49
Cr_2O_3	0.08	-	0.22	-	-	-
V_2O_5	0.12	0.06	0.16	-	-	-
FeO tot.	11.24	11.66	9.83	10.70	11.53	11.22
MnO	0.28	0.21	0.17	0.21	0.20	0.20
MgO	14.17	14.57	14.48	14.99	14.49	14.34
CaO	19.47	19.37	20.08	19.74	19.25	19.76
Na_2O	0.23	0.16	0.19	0.23	0.29	0.27
Total	99.69*	99.61	99.78	100.23	100.08	100.04
-F1	0.868	0.825	0.869	0.860	0.854	0.870
-F2	2.475	2.455	2.468	2.482	2.474	2.470
Si	1.899	1.942	1.884	1.909	1.903	1.896
Al iv	0.101	0.058	0.116	0.091	0.097	0.104
Al vi	0.006	0.004	0.016	0.002	0.013	0.006
Ti	0.036	0.020	0.039	0.039	0.033	0.037
Cr	0.002	-	0.007	-	-	-
V	0.003	0.002	0.004	-	-	-
Fe	0.355	0.368	0.308	0.335	0.362	0.353
Mn	0.009	0.007	0.005	0.007	0.006	0.007
Mg	0.797	0.818	0.809	0.836	0.811	0.803
Ca	0.787	0.782	0.806	0.791	0.774	0.796
Na	0.017	0.012	0.014	0.017	0.021	0.020
$CaSiO_3$	40.4	39.6	41.8	40.2	39.6	40.6
$MgSiO_3$	40.9	41.4	41.9	42.5	41.5	41.0
$(Fe,Mn)SiO_3$	18.7	19.0	16.3	17.3	18.9	18.4

*includes 0.06% K_2O

	UI 101A -1 (UIGDM)	UI 102A -2 (UIGDM)	UI 102A -3 (UIGDM)	UI 102C -1 (UIGDM)	UI 102C -2 (UIGDM)	UI 102C -3 (UIGDM)
SiO_2	50.98	50.91	52.01	50.93	51.04	50.71
TiO_2	1.41	1.38	0.87	1.01	0.81	0.67
Al_2O_3	2.34	2.36	1.39	1.65	1.24	1.27
Cr_2O_3	-	-	-	-	-	-
V_2O_5	0.11	-	-	-	-	-
FeO tot.	12.11	12.00	13.46	14.61	18.55	20.31
MnO	0.19	0.18	0.28	0.24	0.42	0.49
MgO	13.75	13.69	13.84	13.18	12.08	10.58
CaO	19.93	19.93	19.92	18.75	16.69	17.18
Na_2O	0.20	0.14	0.15	0.10	-	-
Total	101.01	100.59	100.92	100.46	100.84	101.20
-F1	0.890	0.884	0.852	0.850	0.832	0.842
-F2	2.500	2.494	2.512	2.478	2.516	2.498
Si	1.903	1.907	1.946	1.928	1.947	1.947
Al iv	0.097	0.093	0.054	0.072	0.053	0.053
Al vi	0.006	0.011	0.007	0.001	0.003	0.005
Ti	0.040	0.039	0.024	0.029	0.023	0.019
Cr	-	-	-	-	-	-
V	0.003	-	-	-	-	-
Fe	0.378	0.376	0.421	0.462	0.592	0.652
Mn	0.006	0.006	0.009	0.008	0.014	0.016
Mg	0.765	0.764	0.772	0.743	0.687	0.606
Ca	0.797	0.800	0.759	0.760	0.682	0.707
Na	0.014	0.010	0.011	0.008	-	-
$CaSiO_3$	41.0	41.1	38.7	38.5	34.5	35.7
$MgSiO_3$	39.3	39.3	39.4	37.7	34.8	30.6
$(Fe,Mn)SiO_3$	19.7	19.6	21.9	23.8	30.7	33.7

	PE5B-1 (PEM)	PE5B-2 (PEM)	PE5B-3 (PEM)	PE5B-4 (PEM)	PE5B-5 (PEM)	PE10-1 (PEM)
SiO_2	51.54	51.98	52.36	51.87	52.23	52.76
TiO_2	1.46	0.34	0.29	0.32	0.36	0.25
Al_2O_3	1.86	1.83	1.71	1.69	1.94	1.52
Cr_2O_3	-	-	-	0.05	-	-
V_2O_5	0.10	0.11	0.10	0.06	0.12	-
FeO tot.	13.94	11.36	12.04	11.50	10.83	12.04
MnO	0.23	0.17	0.24	0.20	0.16	0.22
MgO	14.93	16.06	16.85	16.77	16.09	17.90
CaO	16.24	17.02	15.68	15.40	17.36	14.23
Na_2O	-	-	-	-	-	-
Total	99.29	99.92*	99.28	97.86	99.09	98.92
-F1	0.760	0.749	0.731	0.721	0.756	0.704
-F2	2.490	2.477	2.515	2.488	2.487	2.539
Si	1.958	1.952	1.957	1.962	1.954	1.969
Al iv	0.052	0.048	0.043	0.038	0.046	0.031
Al vi	0.031	0.033	0.032	0.062	0.039	0.036
Ti	0.013	0.010	0.008	0.009	0.010	0.007
Cr	-	-	-	0.002	-	-
V	0.002	0.003	0.003	0.002	0.003	-
Fe	0.441	0.357	0.376	0.364	0.339	0.376
Mn	0.007	0.005	0.008	0.006	0.005	0.007
Mg	0.841	0.899	0.939	0.945	0.897	0.996
Ca	0.658	0.685	0.628	0.624	0.696	0.569
Na	-	-	-	-	-	-
$CaSiO_3$	33.8	35.2	32.2	32.2	35.9	29.2
$MgSiO_3$	43.2	56.2	48.1	48.7	46.3	51.1
$(Fe,Mn)SiO_3$	23.0	18.6	19.7	19.1	17.8	19.7

*includes 0.05% ZnO.

	PE10-2 (PEM)	PE10-3 (PEM)	PE10-4 (PEM)	PE10-5 (PEM)	PV10-1 (PEM)	PV10-2 (PEM)
SiO_2	52.53	53.10	52.61	51.90	51.54	50.91
TiO_2	0.45	0.34	0.46	0.30	0.37	0.37
Al_2O_3	1.89	1.85	1.83	2.08	1.60	1.80
Cr_2O_3	0.07	-	-	-	-	-
V_2O_5	-	-	-	-	-	0.14
FeO tot.	9.95	10.12	10.03	11.37	12.28	13.17
MnO	0.18	0.12	0.17	0.17	0.17	0.21
MgO	16.48	16.15	15.98	16.36	15.50	14.88
CaO	18.06	18.43	18.37	16.62	17.58	17.23
Na_2O	0.17	-	0.06	0.04	-	-
Total	99.88*[1]	100.27*[2]	99.51	98.83	99.03	98.71
-F1	0.780	0.775	0.785	0.738	0.760	0.756
-F2	2.499	2.506	2.499	2.480	2.452	2.437
Si	1.949	1.962	1.958	1.949	1.947	1.938
Al iv	0.051	0.038	0.042	0.051	0.053	0.062
Al vi	0.032	0.042	0.038	0.041	0.018	0.019
Ti	0.013	0.009	0.013	0.008	0.011	0.011
Cr	0.002	-	-	-	-	-
V	-	-	-	-	-	0.003
Fe	0.309	0.313	0.312	0.357	0.388	0.419
Mn	0.006	0.004	0.005	0.006	0.005	0.007
Mg	0.911	0.889	0.886	0.916	0.873	0.844
Ca	0.718	0.729	0.733	0.669	0.712	0.703
Na	0.012	-	0.005	0.003	-	-
$CaSiO_3$	36.9	37.7	37.8	34.4	36.0	35.6
$MgSiO_3$	46.9	45.9	45.8	47.0	44.1	42.8
$(Fe,Mn)SiO_3$	16.2	16.4	16.4	18.6	19.9	21.6

*[1] includes 0.04% Cl and 0.06% BaO

*[2] includes 0.16% BaO

	PV10-3 (PEM)	PV10-4 (PEM)	PV10-5 (PEM)
SiO_2	49.83	50.65	51.60
TiO_2	0.58	0.46	0.45
Al_2O_3	1.47	1.99	1.71
Cr_2O_3	-	-	-
V_2O_5	-	0.09	0.07
FeO tot.	20.01	15.14	14.07
MnO	0.31	0.24	0.25
MgO	11.07	13.96	14.99
CaO	16.25	16.94	17.19
Na_2O	0.08	0.06	-
Total	99.59	99.55*	100.34
-F1	0.799	0.771	0.773
-F2	2.435	2.447	2.484
Si	1.940	1.929	1.938
Al iv	0.060	0.071	0.062
Al vi	0.007	0.018	0.013
Ti	0.017	0.013	0.013
Cr	-	-	-
V	-	0.002	0.002
Fe	0.652	0.482	0.442
Mn	0.010	0.008	0.008
Mg	0.643	0.792	0.839
Ca	0.678	0.691	0.692
Na	0.006	0.005	-
$CaSiO_3$	34.2	35.0	34.9
$MgSiO_3$	32.4	40.2	42.4
$(Fe,Mn)SiO_3$	33.4	24.8	22.7

*includes 0.04% K_2O

	WI40B-1 (WIGM)	WI40B-2 (WIGM)	WI40B-3 (WIGM)	SD6-1 (MADM)	SD6-2 (MADM)	SD6-3 (MADM)
SiO_2	66.97	66.58	67.10	56.02	55.84	54.12
TiO_2	0.09	0.10	0.00	0.11	0.09	0.25
Al_2O_3	19.89	19.23	19.79	25.92	26.52	27.08
Fe_2O_3	0.74	1.42	0.76	1.22	0.98	1.23
MgO	0.14	0.39	0.16	0.15	-	0.13
CaO	0.83	0.70	0.54	9.52	10.12	10.97
Na_2O	10.83	10.77	10.97	5.83	5.56	5.04
K_2O	0.54	0.42	0.78	0.44	0.39	0.42
Total	99.96	99.49	100.03	99.21	99.50	99.24
Si	2.948	2.952	2.954	2.543	2.532	2.473
Al iv	1.032	1.005	1.027	1.386	1.418	1.459
Ti	0.003	0.003	0.000	0.004	0.003	0.009
Fe	0.025	0.048	0.026	0.042	0.034	0.042
Mg	0.009	0.026	0.011	0.010	-	0.009
Ca	0.039	0.033	0.025	0.463	0.494	0.537
Na	0.924	0.926	0.936	0.513	0.490	0.446
K	0.030	0.024	0.044	0.025	0.023	0.024
Or	3.0	2.4	4.4	2.5	2.3	2.4
Ab	93.0	94.2	93.1	51.5	48.7	44.3
An	4.0	3.4	2.5	46.0	49.0	53.3

Table II-2. Plagioclase analyses

Oxygen was calculated by stoichiometry. Structural formulae calculated on a basis of 8 oxygen anions. The index for the host rock suite is given in brackets. Dash indicates that element was not detected. Values for V, Mn and Cr are at the limits of detection. Values for Zn are not significant.

	UI 128A -1 (UIG1M)	UI 128A -2 (UIG1M)	UI 128A -4 (UIG1M)	UI 128A -5 (UIG1M)	UI 128A -6 (UIG1M)	UI 128A -7 (UIG1M)
SiO_2	54.26	56.32	53.06	53.56	52.40	52.77
TiO_2	0.10	0.18	-	0.08	0.09	0.06
Al_2O_3	26.99	25.86	28.18	27.69	27.76	28.20
Fe_2O_3	1.50	1.37	1.10	1.17	1.18	1.28
MgO	0.11	0.17	0.13	0.15	0.13	0.13
CaO	10.61	9.75	12.59	11.97	12.76	12.71
Na_2O	4.76	5.56	4.15	4.50	4.13	4.15
K_2O	0.83	0.62	0.32	0.37	0.34	0.28
Total	99.15	99.88*'	99.53	99.47	98.79	99.56
Si	2.492	2.557	2.430	2.453	2.423	2.420
Al iv	1.461	1.384	1.521	1.494	1.513	1.524
Ti	0.003	0.006	-	0.003	0.003	0.002
Fe	0.052	0.047	0.038	0.040	0.041	0.044
Mg	0.008	0.011	0.009	0.010	0.009	0.009
Ca	0.522	0.474	0.618	0.587	0.632	0.624
Na	0.423	0.490	0.368	0.399	0.370	0.369
K	0.048	0.036	0.019	0.021	0.020	0.016
Or	4.8	3.6	1.9	2.1	2.0	1.6
Ab	42.6	49.0	36.6	39.6	36.2	36.6
An	52.6	47.4	61.5	58.3	61.8	61.8

*' includes 0.06% Cr_2O_3

	UI63-1 (UIGDM)	UI102A -1 (UIGDM)	UI102C -1 (UIGDM)	UI102C -2 (UIGDM)	UI102C -3 (UIGDM)	PP44-1 (KAPGGM)
SiO_2	58.90	67.53	59.75	60.45	60.53	68.75
TiO_2	0.09	-	0.10	-	0.09	-
Al_2O_3	24.38	20.21	24.77	24.36	24.29	19.34
Fe_2O_3	1.00	0.36	0.73	0.86	0.81	0.21
MgO	0.17	0.21	0.11	-	-	0.07
CaO	7.06	1.57	7.71	6.93	6.81	0.05
Na_2O	7.07	10.60	6.64	6.98	7.16	11.39
K_2O	0.81	0.19	0.64	0.65	0.66	0.39
Total	99.47	100.78*'	100.44	100.22	100.36	100.20
Si	2.663	2.944	2.667	2.699	2.699	3.000
Al iv	1.299	1.039	1.303	1.281	1.276	0.995
Ti	0.003	-	0.003	-	0.003	-
Fe	0.034	0.012	0.024	0.029	0.027	0.007
Mg	0.011	0.013	0.007	-	-	0.005
Ca	0.342	0.073	0.369	0.331	0.325	0.002
Na	0.619	0.896	0.575	0.604	0.618	0.964
K	0.047	0.011	0.036	0.037	0.038	0.022
Or	4.7	1.1	3.7	3.8	3.9	2.2
Ab	61.4	91.4	58.6	62.1	63.0	97.6
An	33.9	7.5	37.7	34.1	33.1	0.2

*' includes 0.11% ZnO

	PP44-2 (KAGPPM)	PP44-3 (KAGPPM)	PE10-1 (PEM)	PE10-2 (PEM)	PE10-3 (PEM)	PV07-1 (PEM)
SiO_2	68.78	68.09	68.75	67.99	67.63	59.58
TiO_2	-	0.07	-	0.06	-	0.12
Al_2O_3	19.19	19.51	19.74	19.51	19.58	25.73
Fe_2O_3	0.21	0.43	0.28	0.36	0.30	0.80
MgO	-	0.07	-	0.12	-	0.07
CaO	0.05	0.07	0.43	0.34	0.51	8.20
Na_2O	11.30	10.97	11.47	11.38	11.36	6.50
K_2O	0.38	0.59	0.22	0.29	0.22	0.67
Cl			0.13	0.16	0.14	
Total	99.91	99.79	100.99	100.43*	99.70	101.67
Si	3.009	2.988	2.986	2.978	2.978	2.632
Al iv	0.989	1.009	1.010	1.007	1.016	1.340
Ti	-	0.002	-	0.002	-	0.004
Fe	0.007	0.014	0.009	0.012	0.010	0.027
Mg	-	0.004	-	0.008	-	0.005
Ca	0.003	0.003	0.020	0.016	0.024	0.388
Na	0.958	0.933	0.965	0.967	0.970	0.557
K	0.021	0.033	0.012	0.016	0.013	0.038
Cl			0.009	0.012	0.010	
Or	2.1	3.4	1.2	1.6	1.3	3.9
Ab	97.6	96.3	96.8	96.8	96.3	56.6
An	0.3	0.3	2.0	1.6	2.4	39.5

*includes 0.11% ZnO, 0.06% Cr_2O_3 and 0.05% MnO.

	PV07-2 (PEM)	PV07-3 (PEM)	PV07-4 (PEM)	PV07-5 (PEM)
SiO_2	57.91	63.79	55.83	58.27
TiO_2	0.10	0.16	0.08	0.07
Al_2O_3	26.45	22.62	26.20	25.39
Fe_2O_3	0.89	0.79	1.50	1.20
MgO	-	0.09	0.26	0.19
CaO	9.19	6.51	7.62	5.58
Na_2O	5.68	5.70	5.61	6.61
K_2O	0.67	1.54	2.27	2.28
Total	100.88	101.31*'	99.36	99.58
Si	2.586	2.801	2.557	2.640
Al iv	1.392	1.170	1.414	1.356
Ti	0.003	0.005	0.003	0.002
Fe	0.030	0.026	0.052	0.041
Mg	-	0.006	0.018	0.013
Ca	0.440	0.306	0.374	0.271
Na	0.492	0.485	0.498	0.581
K	0.038	0.086	0.133	0.132
Or	3.9	9.8	13.2	13.4
Ab	50.7	55.3	49.6	59.1
An	45.4	34.9	37.2	27.5

*' includes 0.06% Cr_2O_3 and 0.05% V_2O_5

	WI8B-1 (WIGM)	WI8B-2 (WIGM)	WI8B-3 (WIGM)	WI8B-4 (WIGM)	WI8B-5 (WIGM)	WI8B-6 (WIDM)
SiO_2	40.46	40.84	40.50	39.99	40.36	39.86
TiO_2	0.34	0.37	0.55	0.29	0.45	0.34
Al_2O_3	12.89	12.16	11.97	13.31	12.92	13.11
Fe_2O_3	8.16	8.19	8.19	8.04	8.04	8.05
FeO	18.81	18.86	18.88	18.59	18.59	18.61
MnO	0.53	0.47	0.48	0.51	0.54	0.52
MgO	4.40	4.58	5.68	4.25	4.48	4.27
CaO	11.69	10.74	9.38	11.57	11.43	11.45
Na_2O	1.36	1.53	0.99	1.44	1.32	1.44
K_2O	1.25	1.20	2.29	1.27	1.35	1.26
Cl	0.13	0.12	0.11	0.15	0.13	0.15
Si	6.246	6.351	6.315	6.208	6.247	6.213
Al iv	1.754	1.649	1.685	1.792	1.753	1.787
Al vi	0.591	0.580	0.516	0.644	0.603	0.623
Ti	0.040	0.044	0.063	0.034	0.053	0.040
Fe^{3+}	1.318	1.332	1.337	1.304	1.300	1.312
Fe^{2+}	2.059	2.079	2.086	2.048	2.042	2.059
Mn	0.069	0.061	0.063	0.067	0.071	0.068
Mg	1.011	1.062	1.320	0.983	1.033	0.993
Ca	1.933	1.790	1.567	1.924	1.895	1.913
Na	0.409	0.460	0.295	0.433	0.397	0.434
K	0.245	0.238	0.455	0.252	0.266	0.250
Cl	0.035	0.031	0.029	0.039	0.034	0.040
Σcations	15.675	15.646	15.702	15.689	15.660	15.692
Fe^{2+},Mn[M4]	0.088	0.158	0.385	0.080	0.102	0.095
Na[M4]	0.000	0.052	0.048	0.000	0.003	0.000

Table II-3. Amphibole analyses

Oxygen was calculated using stoichiometry. Fe_2O_3 for actinolites was calcualted using Fe^{3+}/Fe^{2+} = 0.35, an average value for actinolites from low-grade terrains from the data of Deer et al. (1963). Fe_2O_3 for hornblendes was calculated using FeO total = 0.365 Fe_2O_3 + 3.8 based on hornblendes from an epidote amphibolite terrain (Grapes et al., 1977). Structural formulae are calculated on a basis of 23 oxygen anions anhydrous using the procedure of Leake (1978). The index for the host rock suite is given in brackets for each analysis. Dash indicates that element was not detected. Fluorine was sought but not detected. Values for Cl are real but are close to the detection limit in WI40B.

	WI8B-7 (WIGM)	WI40B -1 (WIGM)	WI40B -2 (WIGM)	WI40B -2A (WIGM)	WI40B -3 (WIGM)	WI40B -4 (WIGM)
SiO_2	40.12	44.52	50.78	50.23	49.58	49.79
TiO_2	0.40	0.23	-	0.10	0.08	0.06
Al_2O_3	12.80	9.95	4.48	5.00	5.52	5.50
Fe_2O_3	8.05	5.83	4.67	4.68	4.75	4.67
FeO	18.61	14.53	12.40	12.42	12.53	12.83
MnO	0.54	0.87	0.77	0.83	0.79	0.66
MgO	4.30	11.05	12.56	12.39	12.29	12.19
CaO	11.15	10.18	11.53	11.80	11.69	11.92
Na_2O	1.49	0.79	0.89	0.75	0.75	0.80
K_2O	1.34	0.23	0.15	0.20	0.23	0.23
Cl	0.15	-	-	0.04	0.04	-
Si	6.261	6.661	7.430	7.351	7.281	7.302
Al iv	1.739	1.339	0.570	0.649	0.719	0.698
Al vi	0.614	0.416	0.202	0.212	0.236	0.253
Ti	0.045	0.026	-	0.011	0.009	0.007
Fe^{3+}	1.313	1.893	0.689	0.691	0.703	0.689
Fe^{2+}	2.061	1.580	1.342	1.344	1.360	1.344
Mn	0.070	0.110	0.095	0.102	0.098	0.082
Mg	1.000	2.464	2.740	2.704	2.691	2.664
Ca	1.863	1.631	1.807	1.850	1.839	1.872
Na	0.450	0.229	0.252	0.213	0.214	0.227
K	0.268	0.044	0.027	0.038	0.043	0.042
Cl	0.040	-	-	0.010	0.011	-
Σcations	15.684	15.393	15.154	15.165	15.193	15.180
Fe^{2+},Mn[M4]	0.103	0.489	0.068	0.064	0.097	0.039
Na[M4]	0.034	0.000	0.125	0.086	0.064	0.089

	WI40B -4A (WIGM)	WI40B -5 (WIGM)	UI63-1 (UIGDM)	UI63-2 (UIGDM)	UI63-3 (UIGDM)	UI63-4 (UIGDM)
SiO_2	49.99	49.53	52.60	52.39	52.30	52.79
TiO_2	0.06	0.13	-	-	-	-
Al_2O_3	5.09	5.06	2.06	2.07	1.72	1.55
Fe_2O_3	4.63	4.71	5.34	5.36	5.57	5.38
FeO	12.32	12.46	13.64	13.67	14.06	13.69
MnO	0.72	0.69	0.15	0.16	0.15	0.19
MgO	12.32	11.71	12.70	12.49	11.78	12.27
CaO	11.83	11.24	12.09	12.00	12.11	12.33
Na_2O	0.78	0.79	-	0.07	-	0.07
K_2O	0.17	0.18	0.11	0.07	0.13	0.04
Cl	-	-	-	-	-	-
Si	7.347	7.390	7.679	7.684	7.734	7.746
Al iv	0.653	0.610	0.321	0.316	0.266	0.254
Al vi	0.614	0.416	0.034	0.042	0.034	0.013
Ti	0.006	0.015	-	-	-	-
Fe^{3+}	0.685	0.707	0.794	0.801	0.841	0.803
Fe^{2+}	1.340	1.374	1.458	1.468	1.516	1.470
Mn	0.089	0.086	0.019	0.020	0.019	0.023
Mg	2.699	2.604	2.763	2.730	2.596	2.683
Ca	1.862	1.797	1.891	1.886	1.919	1.939
Na	0.220	0.205	-	0.020	-	0.020
K	0.032	0.034	0.020	0.012	0.024	0.008
Cl	-	-				
Σcations	15.162	15.102	14.979	14.979	14.949	14.959
Fe^{2+},Mn[M4]	0.048	0.066	0.068	0.061	0.006	0.000
Na[M4]	0.090	0.137				

	UI118-1 (UIG1M)	UI118-2 (UIG1M)	UI118-3 (UIG1M)	UI118-4 (UIG1M)	UI39A-1 (UIG2M)	UI39A-2 (UIG2M)
SiO_2	28.77	27.20	27.94	28.24	28.05	29.92
TiO_2	-	-	-	-	-	-
Al_2O_3	17.52	18.97	18.29	17.54	18.72	16.62
FeO tot.	28.68	29.28	29.04	28.54	24.03	23.03
MnO	0.18	0.10	0.16	0.12	0.26	0.22
MgO	13.97	12.98	13.59	13.88	17.39	18.56
CaO	0.21	0.11	0.15	0.12	0.12	0.21
Na_2O	-	-	-	-	-	-
K_2O	0.19	0.05	0.08	0.17	-	-
(H_2O)	9.91	10.73	10.18	10.82	10.97	11.00
Si	6.019	5.769	5.877	5.973	5.793	6.134
Al iv	1.981	2.231	2.123	2.027	2.207	1.866
Al vi	2.341	2.513	2.413	2.347	2.352	2.152
Ti	-	-	-	-	-	-
Fe	5.019	5.195	5.110	5.049	4.152	3.950
Mn	0.032	0.019	0.028	0.021	0.045	0.038
Mg	4.356	4.103	4.260	4.375	5.353	5.671
Ca	0.047	0.024	0.034	0.027	0.027	0.046
Na	-	-	-	-	-	-
K	0.051	0.042	0.022	0.045	-	-
Fe/(Fe+Mg)	0.535	0.559	0.545	0.536	0.437	0.411

Table II-4. Chlorite analyses.

Oxygen was calculated by stoichiometry and H_2O by difference from 100%. Structural formulae were calculated on a basis of 28 oxygen anions, anhydrous. The index for the host rock suite is given in brackets. Dash indicates element not detected. Values for Cl and Ni are close to the limits of detection. Values for Zn are not significant.

	UI39A -3A*¹ (UIG2M)	UI39A -3B (UIG2M)	UI653 -1*² (UIGDM)	PE5B-1 (PEM)	PE10-1 (PEM)	PV07-1 (PEM)
SiO_2	29.50	29.41	28.22	28.60	28.78	30.75
TiO_2	-	-	-	-	-	-
Al_2O_3	18.01	17.12	17.18	15	15.25	15.09
FeO tot.	23.19	23.32	26.95	3	33.68	26.93
MnO	0.26	0.27	0.23		0.19	0.14
MgO	17.68	18.22	16		11.36	16.03
CaO	0.14	0.09	0		0.22	0.37
Na_2O	-	-			0.10	0.05
K_2O	-	-	-	-	-	-
(H_2O)	10.61	11.10	10.60	10.33	10.41	10.65
Si	6.042	6.051	5.881	6.172	6.194	6.371
Al iv	1.958	1.949	2.119	1.828	1.806	1.629
Al vi	2.390	2.204	2.101	2.148	2.062	2.056
Ti	-	-	-	-	-	
Fe	3.972	4.014	4.697	6.228	6.061	4.666
Mn	0.045	0.047	0.040	0.050	0.035	0.024
Mg	5.397	5.586	5.103	3.370	3.642	4.950
Ca	0.030	0.020	0.027	0.043	0.052	0.082
Na	-	-	-	-	0.041	0.020
K	-	-	-	-	-	-
Fe/(Fe+Mg)	0.424	0.418	0.479	0.649	0.625	0.485

*¹ includes 0.12% S and 0.03% Cl

*² includes 0.09% NiO and 0.06% ZnO

	PV07-2 (PEM)	PV07-3 (PEM)	PV10-2 (PEM)	PV10-2 (PEM)
SiO_2	30.62	30.73	31.29	31.07
TiO_2	-	-	-	-
Al_2O_3	15.21	15.17	14.51	14.91
FeO tot.	26.84	27.10	28.19	28.19
MnO	0.20	0.19	0.22	0.21
MgO	16.14	16.08	15.14	15.15
CaO	0.39	0.25	0.47	0.51
Na_2O	-	0.05	-	-
K_2O	0.06	0.04	-	-
(H_2O)	10.56	10.39	10.18	10.68
Si	6.339	6.355	6.488	6.488
Al iv	1.661	1.645	1.512	1.512
Al vi	2.050	2.051	2.033	1.979
Ti	-	-	-	-
Fe	4.646	4.687	4.887	4.922
Mn	0.035	0.033	0.038	0.038
Mg	4.980	4.957	4.679	4.714
Ca	0.087	0.054	0.104	0.114
Na	-	0.021	-	-
K	0.015	0.010	-	-
Fe/(Fe+Mg)	0.483	0.486	0.511	0.511

	Ep WI40B-1 (WIGM)	Ep UI65-1 (UIGDM)	Pu PE10-1 (PEM)	Pu PE10-2 (PEM)	Pu PE10-3 (PEM)	Sp PV10-1 (PEM)
SiO_2	39.48	37.67	36.06	35.32	35.33	32.10
TiO_2	-	1.73	-	0.05	-	31.63
Al_2O_3	23.52	21.73	12.70	11.07	11.46	3.35
Cr_2O_3	-	-	0.08	0.05	-	-
Fe_2O_3 tot.	13.69	14.20				
FeO tot.			21.87	20.02	22.33	4.09
MnO	0.28	-	-	-	-	-
MgO	-	-	1.25	1.97	1.79	1.11
CaO	22.63	23.17	21.21	24.75	20.99	26.03
(H_2O)	0.41	1.50	6.83	6.77	8.10	
Total	100.00	100.00	100.00	100.00	100.00	98.30
Si	3.075	2.995	6.139	5.972	6.100	1.065
Al	2.159	2.036	2.548	2.205	2.332	0.131
Ti	-	0.103	-	0.007	-	0.790
Cr	-	-	0.011	0.007	-	-
Fe	0.802	0.850	3.114	2.830	3.224	0.113
Mn	0.019	-	-	-	-	-
Mg	-	-	0.317	0.496	0.461	0.055
Ca	1.889	1.974	3.869	4.484	3.883	0.926
Ps%	27.1	29.5				
Fe/(Fe+Mg)			0.908	0.851	0.875	

Table II-5. Analyses of epidote (Ep) pumpellyite (Pu) and sphene (Sp).

Oxygen was calculated by stoichiometry and H_2O by difference from 100%. Sphene was not analysed for REE. Structural formulae were calculated on a basis of 12.5 and 5 oxygen anions for epidote and sphene, respectively, and Σcations=16 for pumpellyite (Coombs et al., 1976). Pistacite contents, ie. $100Fe^{3+}/(Fe^{3+}+Al)$ are given for epidotes. The index for the host rock suite is given in brackets.

APPENDIX III. WHOLE-ROCK MAJOR AND TRACE ELEMENT ANALYSES.

Ol-Hy and Q-Hy refer to the normative compositions of mafic and intermediate samples which show alkali and CaO contents characteristic of fresh igneous rocks, according to the discrimination routines of Ch. 8.

* marks mafic and intermediate compositions which classify as unaltered, according to the same techniques, but which show no normative diopside.

marks felsic compositions which can be similarly classified as unaltered.

Major element and trace HFSE analyses, by XRF, were carried out at the Universities of Durham (D), and McMaster (H). H_2O and CO_2 analyses were determined at the Universities of Montreal (M) and Alberta (A). (see Appendix I.).

N.B. The major elements are recalculated to 100%, excluding volatiles. The second decimal place has little significance for any of the elements listed.

WIGM

	1	2	3	4	5	6	7	8	9
SIO2	50.26	50.09	49.77	50.83	49.71	52.74	54.13	53.26	53.12
TIO2	1.55	1.57	1.66	1.45	1.62	1.65	2.10	2.20	2.32
AL2O	13.11	12.77	13.01	14.74	14.67	12.82	12.16	12.46	11.93
FE2O	3.48	3.58	3.56	3.34	3.46	3.63	3.72	3.66	3.83
FEO	10.79	11.13	11.06	10.39	10.77	11.31	11.56	11.35	11.90
MNO	0.32	0.33	0.46	0.45	0.31	0.34	0.35	0.33	0.27
MGO	7.31	7.69	9.18	7.94	8.61	6.36	4.61	5.60	4.56
CAO	7.70	7.62	6.63	4.67	4.39	6.24	5.97	6.00	6.12
NA2O	2.49	2.36	2.94	4.59	4.50	2.24	2.63	2.78	3.00
K2O	2.75	2.60	1.39	1.22	1.55	2.31	2.23	1.91	2.39
S	0.01	0.01	0.01	0.04	0.01	0.01	0.01	0.01	0.03
P2O5	0.23	0.25	0.32	0.36	0.41	0.33	0.55	0.44	0.55
H2O	0.0	0.0	0.0	0.0	0.0	0.0	0.0	0.0	0.0
CO2	0.0	0.0	0.0	0.0	0.0	0.0	0.0	0.0	0.0
BA	948.00	894.00	420.00	480.00	591.00	569.00	958.00	322.00	808.00
NB	10.00	9.00	13.00	13.00	16.00	14.00	17.00	15.00	18.00
ZR	146.00	150.00	158.00	188.00	210.00	210.00	212.00	261.00	261.00
Y	33.00	34.00	33.00	31.00	35.00	39.00	41.00	47.00	49.00
SR	134.00	119.00	83.00	78.00	42.00	127.00	188.00	151.00	137.00
RB	102.00	88.00	42.00	29.00	35.00	83.00	73.00	82.00	87.00
GA	0.0	0.0	0.0	0.0	0.0	0.0	0.0	0.0	0.0
ZN	197.00	206.00	267.00	541.00	380.00	301.00	248.00	340.00	247.00
CU	88.00	48.00	53.00	73.00	32.00	52.00	38.00	52.00	68.00
NI	29.00	32.00	44.00	32.00	35.00	35.00	14.00	24.00	20.00
CR	62.00	69.00	149.00	144.00	153.00	49.00	13.00	19.00	11.00
V	303.00	313.00	341.00	255.00	280.00	305.00	302.00	303.00	279.00
SC	52.00	47.00	52.00	41.00	40.00	49.00	47.00	45.00	47.00

1. WI48A D
2. WI7 D
3. WI38 D 01Hy
4. WI40B D
5. WI40C D
6. WI8C D
7. WI14D D QHy
8. WI10 D QHzy
9. WI8B D QHy

WIGM

	10	11	12
SIO2	47.75	53.91	60.48
TIO2	3.59	2.65	1.71
AL2O	8.56	13.09	12.28
FE2O	4.35	3.52	2.83
FEO	13.49	10.94	8.86
MNO	0.38	0.32	0.28
MGO	7.81	6.31	2.82
CAO	11.25	3.72	3.89
NA2O	0.66	2.33	3.24
K2O	1.14	2.24	3.28
S	0.03	0.02	0.02
P2O5	1.01	0.95	0.32
H2O	0.0	0.0	0.0
CO2	0.0	0.0	0.0
BA	218.00	782.00	0.0
NB	21.00	28.00	24.00
ZR	342.00	419.00	395.00
Y	59.00	53.00	61.00
SR	39.00	117.00	70.00
RB	29.00	59.00	90.00
GA	0.0	0.0	0.0
ZN	206.00	322.00	154.00
CU	82.00	53.00	38.00
NI	32.00	26.00	14.00
CR	18.00	5.00	2.00
V	212.00	268.00	178.00
SC	53.00	37.00	37.00

10. WI33B D
11. WI29G D
12. WI22E D QHy

WIGR

	1	2	3	4	5	6	7	8	9
SIO2	70.63	73.10	74.59	72.57	71.57	75.92	73.65	74.95	75.34
TIO2	0.76	0.54	0.35	0.37	0.57	0.38	0.45	0.39	0.43
AL2O	13.18	12.88	12.68	13.43	12.90	12.01	12.68	12.46	12.27
FE2O	1.38	0.79	0.70	0.99	1.30	0.64	0.83	0.77	0.70
FEO	4.35	2.48	2.20	3.12	4.10	2.00	2.60	2.43	2.22
MNO	0.03	0.04	0.03	0.03	0.07	0.01	0.05	0.01	0.01
MGO	1.17	0.88	0.34	0.39	0.55	0.35	0.99	0.43	0.42
CAO	0.54	0.40	0.40	0.37	1.55	0.20	0.55	0.23	0.22
NA2O	2.68	1.55	3.19	4.03	4.20	6.13	5.62	6.20	6.68
K2O	5.08	7.25	5.49	4.64	4.20	6.13	5.62	6.20	5.68
S	0.01	0.01	0.01	0.04	0.01	0.04	0.02	0.03	0.01
P2O5	0.19	0.08	0.03	0.04	0.10	0.05	0.05	0.03	0.06
H2O	0.0	0.0	0.0	0.0	0.0	0.0	0.0	0.0	0.0
CO2	0.0	0.0	0.0	0.0	0.0	0.0	0.0	0.0	0.0
BA	1337.00	1486.00	1071.00	956.00	1573.00	1223.00	1409.00	1530.00	1414.00
NB	23.00	36.00	46.00	34.00	39.00	46.00	45.00	46.00	51.00
ZR	306.00	544.00	556.00	580.00	609.00	626.00	628.00	646.00	748.00
Y	39.00	64.00	88.00	59.00	90.00	74.00	73.00	73.00	114.00
SR	37.00	86.00	48.00	40.00	120.00	32.00	78.00	37.00	33.00
RB	143.00	170.00	125.00	89.00	104.00	173.00	140.00	134.00	167.00
GA	0.0	0.0	0.0	0.0	0.0	0.0	0.0	0.0	0.0
ZN	21.00	23.00	13.00	18.00	90.00	2.00	37.00	16.00	3.00
CU	61.00	51.00	108.00	67.00	62.00	82.00	105.00	75.00	49.00
NI	5.00	11.00	6.00	2.00	6.00	10.00	10.00	1.00	11.00
CR	6.00	24.00	23.00	4.00	2.00	19.00	15.00	0.0	10.00
V	0.0	0.0	0.0	0.0	0.0	0.0	0.0	0.0	0.0
SC	0.0	0.0	0.0	0.0	0.0	0.0	0.0	0.0	0.0

1.	WI39	D	
2.	WI48D	D	
3.	WI24F	D	"
4.	WI24H	D	"
5.	WI8A	D	"
6.	WI25C	D	
7.	WI35D	D	
8.	WI27B	D	
9.	WI27A	D	

UWIGM

	1	2	3	4
SIO2	49.21	48.48	47.55	49.29
TIO2	2.40	2.53	2.88	2.40
AL2O	21.33	21.96	18.42	15.53
FE2O	2.19	2.43	2.79	2.65
FEO	6.86	7.57	8.72	8.31
MNO	0.07	0.08	0.16	0.22
MGO	7.30	8.03	7.35	5.31
CAO	2.71	2.35	4.98	10.18
NA2O	5.11	4.75	3.95	4.34
K2O	1.98	1.11	2.48	1.27
S	0.33	0.06	0.26	0.19
P2O5	0.67	0.68	0.59	0.40
H2O	0.0	0.0	0.0	0.0
CO2	0.0	0.0	0.0	0.0
BA	955.00	649.00	457.00	412.00
NB	109.00	115.00	69.00	97.00
ZR	299.00	314.00	242.00	247.00
Y	25.00	25.00	24.00	25.00
SR	178.00	154.00	116.00	111.00
RB	58.00	28.00	106.00	45.00
GA	0.0	0.0	0.0	0.0
ZN	125.00	112.00	129.00	117.00
CU	88.00	73.00	96.00	97.00
NI	79.00	69.00	120.00	47.00
CR	209.00	232.00	267.00	125.00
V	0.0	0.0	0.0	0.0
SC	0.0	0.0	0.0	0.0

1. PP1A D
2. PP1A1 D
3. PP1B D
4. PP1D D *

MADM

	1	2	3	4	5	6	7	8	9	
SIO2	44.94	0.0	48.03	43.82	47.58	46.97	47.56	44.28	45.39	
TIO2	5.09	0.0	3.10	2.67	2.63	2.87	2.87	3.17	4.33	
AL2O	14.47	0.0	15.66	17.61	16.06	15.90	14.71	16.26	15.03	
FE2O	18.89	0.0	3.63	15.43	14.79	15.46	15.53	17.44	16.48	
FEO	0.0	0.0	10.36	0.0	0.0	0.0	0.0	0.0	0.0	
MNO	0.26	0.0	0.16	0.13	0.30	0.19	0.20	0.14	0.23	
MGO	6.81	0.0	6.17	11.41	8.82	9.00	7.55	10.96	6.02	
CAO	3.86	0.0	9.02	2.19	4.85	4.70	6.98	3.32	8.23	
NA2O	3.43	0.0	2.57	2.28	3.55	3.88	3.26	3.74	2.99	
K2O	1.81	0.0	1.17	4.20	1.14	0.78	1.07	0.43	0.87	
S	0.0	0.0	0.0	0.0	0.0	0.0	0.0	0.0	0.0	
P2O5	0.46	0.0	0.11	0.26	0.27	0.25	0.27	0.27	0.43	
H2O	0.0	0.0	0.0	0.0	0.0	0.0	0.0	0.0	0.0	
CO2	0.0	0.0	0.0	0.0	0.0	0.0	0.0	0.0	0.0	
BA	10.00	156.00	152.00	1239.00	260.00	63.00	94.00	57.00	139.00	
NB	2.00	16.00	16.00	16.00	16.00	17.00	18.00	18.00	24.00	
ZR	76.00	133.00	136.00	149.00	154.00	155.00	161.00	165.00	202.00	
Y	23.00	24.00	24.00	29.00	27.00	26.00	23.00	31.00	29.00	
SR	136.00	402.00	323.00	244.00	341.00	134.00	299.00	109.00	264.00	
RB	29.00	22.00	29.00	57.00	29.00	19.00	32.00	11.00	17.00	
GA	20.00	26.00	27.00	25.00	24.00	27.00	28.00	25.00	28.00	
ZN	0.0	0.0	0.0	0.0	0.0	0.0	0.0	0.0	0.0	
CU	0.0	0.0	0.0	0.0	0.0	0.0	0.0	0.0	0.0	
NI	0.0	0.0	0.0	0.0	0.0	0.0	0.0	0.0	0.0	
CR	0.0	0.0	500.00	0.0	0.0	0.0	0.0	0.0	0.0	
V	0.0	0.0	0.0	0.0	0.0	0.0	0.0	0.0	0.0	
SC	0.0	0.0	0.0	0.0	0.0	0.0	0.0	0.0	0.0	0.0

1. S7B H
2. SD6 H 01Hy
3. SD1 H
4. SD4 H
5. SD8 H
6. EJ.12.11 H
7. SD7 H
8. S8A H 01Hy
9. S4C H

MADM

	10	11	12	13	14
SIO2	44.54	48.25	46.53	45.40	47.68
TIO2	4.46	2.36	4.46	6.00	2.80
AL2O	14.56	15.81	14.84	13.80	15.31
FE2O	17.39	14.66	17.13	4.71	3.53
FEO	0.0	0.0	1.00	13.42	10.05
MNO	0.29	0.20	0.21	0.17	0.0
MGO	7.54	5.81	6.15	7.58	8.35
CAO	6.52	7.99	6.34	5.09	9.74
NA2O	3.13	3.11	2.69	2.28	2.05
K2O	1.20	1.37	1.14	1.29	0.49
S	0.0	0.0	0.0	0.0	0.0
P2O5	0.38	0.44	0.51	0.27	0.0
H2O	0.0	0.0	0.0	0.0	0.0
CO2	0.0	0.0	0.0	0.0	0.0
BA	257.00	160.00	167.00	0.0	0.0
NB	27.00	20.00	23.00	0.0	0.0
ZR	212.00	226.00	225.00	0.0	0.0
Y	28.00	38.00	32.00	0.0	0.0
SR	327.00	362.00	254.00	0.0	0.0
RB	26.00	32.00	26.00	0.0	0.0
GA	27.00	29.00	32.00	0.0	0.0
ZN	0.0	0.0	0.0	0.0	0.0
CU	0.0	0.0	0.0	0.0	0.0
NI	0.0	0.0	0.0	0.0	0.0
CR	0.0	0.0	0.0	0.0	0.0
V	0.0	0.0	0.0	0.0	0.0
SC	0.0	0.0	0.0	0.0	0.0

10. SD3 H 01Hy
11. S4A H

UIG1M

	1	2	3	4	5	6	7	8	9
SIO2	42.70	49.17	44.40	47.13	42.29	49.84	48.89	49.75	49.58
TIO2	2.71	2.66	3.20	3.31	3.48	2.76	1.73	3.26	3.31
AL2O	15.54	12.80	13.43	16.07	14.54	16.60	15.65	15.14	17.71
FE2O	3.71	3.78	4.69	4.88	4.77	3.54	13.52	3.83	2.98
FEO	11.31	11.75	14.51	15.11	14.72	10.77	0.0	11.66	9.10
MNO	0.22	0.15	0.23	0.26	0.22	0.18	0.21	0.14	0.08
MGO	6.58	6.41	6.65	6.25	6.53	8.13	6.95	5.75	6.46
CAO	11.70	10.68	10.47	4.81	10.91	3.59	8.36	6.52	6.14
NA2O	3.97	0.88	0.66	0.01	0.33	2.52	3.93	2.37	4.51
K2O	0.98	1.25	1.29	1.72	1.80	1.65	0.64	1.10	2.65
S	0.59	0.40	0.34	0.26	0.16	0.29	0.0	0.22	0.36
P2O5	0.28	0.25	0.30	0.33	0.34	0.26	0.12	0.36	0.28
H2O	4.97	5.14	5.57	5.78	5.63	5.32	0.0	4.76	4.97
CO2	6.42	3.07	6.48	5.21	6.41	3.68	0.0	5.25	4.23
BA	758.00	374.00	283.00	668.00	307.00	177.00	416.00	152.00	143.00
NB	25.00	26.00	39.00	43.00	43.00	36.00	36.00	49.00	44.00
ZR	174.00	203.00	303.00	303.00	317.00	219.00	259.00	296.00	257.00
Y	23.00	29.00	43.00	45.00	36.00	23.00	35.00	35.00	26.00
SR	327.00	196.00	147.00	50.00	95.00	83.00	313.00	62.00	46.00
RB	17.00	50.00	42.00	63.00	65.00	37.00	20.00	34.00	96.00
GA	0.0	0.0	0.0	0.0	0.0	0.0	22.00	0.0	0.0
ZN	91.00	129.00	160.00	143.00	131.00	65.00	0.0	86.00	37.00
CU	102.00	134.00	170.00	140.00	146.00	112.00	0.0	132.00	116.00
NI	112.00	68.00	68.00	1.00	73.00	58.00	61.00	61.00	58.00
CR	151.00	58.00	35.00	1.00	38.00	70.00	36.00	45.00	80.00
V	283.00	289.00	352.00	1.00	382.00	293.00	336.00	367.00	393.00
SC	45.00	40.00	45.00	0.0	47.00	41.00	49.00	45.00	52.00

1. UI136B D A
2. UI68D D A
3. UI68A D A
4. UI68B D A
5. UI68C D A
6. UI133A D A
7. UI128A H
8. UI128B D A QHy
9. UI79A D A

UIG1M

	10	11	12	13	14	15	16	17	18
SIO2	46.57	50.31	54.46	24.90	47.94	53.59	50.96	51.03	48.75
TIO2	4.08	4.10	3.80	3.85	2.72	2.83	3.77	3.09	3.34
AL2O	14.43	14.36	14.80	18.70	14.99	14.93	12.18	13.81	13.82
FE2O	4.25	3.58	3.71	7.60	3.91	3.20	3.24	3.14	4.43
FEO	12.93	10.90	11.30	22.72	11.91	9.76	9.88	9.59	13.46
MNO	0.18	0.15	0.10	0.24	0.20	0.16	0.17	0.19	0.25
MGO	6.81	6.01	5.90	12.38	7.88	7.09	4.18	6.44	5.14
CAO	6.64	5.66	1.58	8.31	6.65	3.94	11.52	8.00	6.42
NA2O	2.46	3.07	2.20	0.08	3.01	3.19	2.49	3.23	2.77
K2O	0.73	0.98	1.54	0.56	0.38	0.61	0.96	0.86	1.10
S	0.85	0.77	0.24	0.67	0.11	0.72	0.31	0.42	0.31
P2O5	0.48	0.48	0.47	0.30	0.36	0.32	0.50	0.40	0.36
H2O	5.36	4.58	4.71	9.37	4.85	4.26	3.69	4.02	5.05
CO2	3.44	3.06	0.59	4.89	3.69	2.06	6.59	4.52	1.69
BA	179.00	278.00	445.00	70.00	209.00	240.00	113.00	216.00	529.00
NB	75.00	84.00	78.00	50.00	50.00	55.00	74.00	53.00	62.00
ZR	474.00	493.00	494.00	299.00	296.00	307.00	438.00	305.00	393.00
Y	51.00	49.00	44.00	35.00	37.00	32.00	52.00	34.00	49.00
SR	99.00	128.00	71.00	98.00	217.00	166.00	148.00	150.00	299.00
RB	11.00	16.00	30.00	17.00	6.00	11.00	32.00	10.00	32.00
GA	0.0	0.0	0.0	0.0	0.0	0.0	0.0	0.0	0.0
ZN	257.00	352.00	62.00	103.00	78.00	65.00	42.00	65.00	101.00
CU	160.00	155.00	111.00	96.00	144.00	142.00	138.00	112.00	165.00
NI	40.00	38.00	29.00	55.00	47.00	44.00	32.00	35.00	38.00
CR	22.00	27.00	22.00	64.00	60.00	52.00	23.00	45.00	41.00
V	266.00	278.00	266.00	381.00	312.00	300.00	245.00	296.00	322.00
SC	41.00	45.00	45.00	37.00	37.00	34.00	34.00	45.00	45.00

10. UI79E D A
11. UI79B D A
12. UI79F D A
13. UI83 D A
14. UI89E D A
15. UI89D D A
16. UI89B D A
17. UI95D D M QHy
18. UI95A D A QHy

UIG1M

	19	20	21
SIO2	51.70	52.15	58.39
TIO2	3.32	2.85	3.43
AL2O	13.59	14.01	13.45
FE2O	4.00	3.84	2.97
FEO	12.18	11.72	9.08
MNO	0.25	0.19	0.14
MGO	5.43	6.08	4.01
CAO	5.03	5.46	3.92
NA2O	2.69	2.66	3.81
K2O	2.69	0.50	0.29
S	0.36	0.46	0.27
P2O5	0.35	0.31	0.36
H2O	4.24	4.60	3.64
CO2	0.78	5.11	2.12
BA	440.00	140.00	75.00
NB	66.00	43.00	67.00
ZR	399.00	287.00	423.00
Y	44.00	32.00	46.00
SR	261.00	67.00	145.00
RB	36.00	7.00	4.00
GA	0.0	0.0	0.0
ZN	76.00	104.00	242.00
CU	151.00	133.00	71.00
NI	32.00	38.00	23.00
CR	48.00	45.00	34.00
V	317,00	323.00	290.00
SC	45.00	37.00	37.00

19. UI95B D A
20. UI159A D A
21. UI147 D A

UIGDM

	1	2	3	4	5	6	7	8	9
SIO2	46.12	47.07	47.48	48.38	47.81	48.15	49.58	49.11	46.46
TIO2	1.60	1.84	2.00	2.72	2.33	2.45	3.39	2.89	2.58
AL2O	16.65	16.08	15.54	14.09	15.36	15.26	13.30	14.74	11.82
FE2O	13.59	13.61	3.47	16.69	3.36	15.51	15.08	2.09	4.02
FEO	0.0	0.0	10.78	0.0	10.48	0.0	0.0	13.01	12.46
MNO	0.19	0.22	0.16	0.29	0.17	0.22	0.32	0.19	0.22
MGO	9.00	8.61	7.53	5.75	8.62	7.15	5.70	7.52	7.90
CAO	9.29	7.66	9.15	7.78	7.80	6.44	7.39	6.57	12.06
NA2O	2.19	2.30	2.15	3.72	2.23	3.54	4.04	2.08	1.72
K2O	1.19	2.45	1.21	0.24	1.30	1.05	0.82	1.10	0.34
S	0.0	0.0	0.53	0.0	0.33	0.0	0.0	0.31	0.20
P2O5	0.17	0.16	0.25	0.34	0.36	0.24	0.39	0.48	0.31
H2O	0.0	0.0	5.01	0.0	2.56	0.0	0.0	3.46	5.53
CO2	0.0	0.0	5.89	0.0	0.13	0.0	0.0	0.80	7.14
BA	155.00	507.00	204.00	95.00	428.00	181.00	369.00	341.00	142.00
NB	17.00	22.00	17.00	26.00	20.00	30.00	28.00	26.00	23.00
ZR	98.00	128.00	153.00	155.00	169.00	185.00	184.00	197.00	202.00
Y	20.00	20.00	21.00	27.00	25.00	28.00	29.00	29.00	27.00
SR	493.00	433.00	156.00	355.00	427.00	379.00	452.00	364.00	280.00
RB	44.00	69.00	50.00	5.00	53.00	24.00	14.00	47.00	9.00
GA	19.00	20.00	0.0	23.00	0.0	23.00	21.00	0.0	0.0
ZN	0.0	0.0	87.00	0.0	15.00	0.0	0.0	116.00	129.00
CU	0.0	0.0	71.00	0.0	90.00	0.0	0.0	119.00	91.00
NI	0.0	0.0	177.00	0.0	140.00	0.0	0.0	91.00	60.00
CR	0.0	0.0	147.00	0.0	76.00	0.0	0.0	88.00	171.00
V	0.0	0.0	0.0	0.0	0.0	0.0	0.0	0.0	0.0
SC	0.0	0.0	0.0	0.0	0.0	0.0	0.0	0.0	0.0

1. UI99 H 01Hy
2. UI63 H
3. UI62 D A 01Hy
4. UI82 H
5. UI59B D A 01Hy
6. UI95I H
7. UI102A H 01Hy
8. UI59A D A
9. UI70 D A 01Hy

UIGDM

	10	11	12	13
SIO2	50.40	48.74	48.44	48.02
TIO2	2.25	3.58	4.22	4.02
AL2O	15.15	13.20	12.33	13.63
FE2O	3.40	17.05	17.16	18.51
FEO	10.57	0.0	0.0	0.0
MNO	0.19	0.21	0.25	0.20
MGO	7.68	5.24	4.37	6.11
CAO	7.22	8.41	8.33	6.65
NA2O	1.66	2.16	3.03	1.88
K2O	1.06	0.91	1.39	0.46
S	0.19	0.0	0.0	0.0
P2O5	0.30	0.48	0.48	0.52
H2O	3.81	4.18	0.0	0.0
CO2	0.94	0.94	0.0	0.0
BA	394.00	145.00	476.00	127.00
NB	25.00	29.00	30.00	30.00
ZR	203.00	204.00	216.00	220.00
Y	31.00	28.00	32.00	30.00
SR	288.00	249.00	460.00	249.00
RB	40.00	18.00	26.00	19.00
GA	0.0	26.00	27.00	28.00
ZN	104.00	0.0	0.0	0.0
CU	132.00	0.0	0.0	0.0
NI	61.00	0.0	0.0	0.0
CR	205.00	0.0	0.0	0.0
V	0.0	0.0	0.0	0.0
SC	0.0	0.0	0.0	0.0

10. UI16B D A
11. UI06 H QHy
12. UI02C H QHy
13. [illegible] H

UIG2M

	1	2	3	4	5	6	7	8	9
SIO2	46.70	50.52	43.66	53.08	50.63	52.78	44.88	62.52	50.37
TIO2	1.77	1.85	2.23	1.97	2.64	1.75	2.22	1.76	1.73
AL2O	16.04	14.03	17.75	14.83	13.92	14.30	22.50	16.20	14.76
FE2O	2.94	2.77	4.10	1.99	16.09	2.69	4.91	1.62	11.98
FEO	9.18	8.63	12.50	6.13	0.0	8.39	15.12	5.10	0.0
MNO	0.17	0.19	0.26	0.16	0.18	0.18	0.14	0.10	0.19
MGO	10.80	6.08	8.12	4.23	4.06	5.94	7.94	2.29	8.82
CAO	8.71	11.07	6.59	10.10	8.81	9.20	0.49	4.93	7.18
NA2O	2.29	3.64	2.28	6.08	2.68	4.03	0.15	3.74	4.23
K2O	1.09	0.84	1.82	0.52	0.61	0.47	1.35	1.47	0.64
S	0.34	0.48	1.06	1.45	0.0	0.32	0.17	0.09	0.0
P2O5	0.14	0.14	0.16	0.17	0.37	0.11	0.14	0.20	0.11
H2O	4.08	2.75	6.10	3.14	0.0	1.99	7.48	2.60	0.0
CO2	0.77	1.74	3.67	4.70	0.0	0.33	0.33	2.14	0.0
BA	1014.00	277.00	286.00	298.00	85.00	430.00	83.00	109.00	400.00
NB	3.00	4.00	10.00	9.00	4.00	5.00	3.00	4.00	2.00
ZR	109.00	109.00	115.00	110.00	104.00	108.00	116.00	115.00	102.00
Y	23.00	18.00	16.00	19.00	18.00	15.00	17.00	14.00	19.00
SR	584.00	453.00	142.00	405.00	371.00	470.00	3.00	112.00	344.00
RB	48.00	32.00	64.00	22.00	14.00	16.00	52.00	64.00	12.00
GA	0.0	0.0	0.0	0.0	19.00	0.0	0.0	0.0	18.00
ZN	111.00	99.00	203.00	126.00	0.0	58.00	134.00	38.00	0.0
CU	70.00	121.00	98.00	79.00	0.0	61.00	15.00	16.00	0.0
NI	110.00	105.00	102.00	102.00	99.00	93.00	93.00	88.00	68.00
CR	358.00	340.00	378.00	348.00	323.00	345.00	291.00	340.00	286.00
V	302.00	301.00	336.00	291.00	283.00	293.00	289.00	291.00	299.00
SC	30.00	40.00	29.00	41.00	38.00	22.00	37.00	30.00	37.00

1.	UI27	D A OlHy
2.	UI39	D A OlNe
3.	UI26	D A
4.	UI30	D A
5.	UI214	H QHy
6.	UI29	D A
7.	UI35A	D A
8.	UI22	D A
9.	UI218	H

SOGSI1M

	1	2	3	4	5	6
SIO2	47.09	45.20	45.13	43.59	45.78	47.76
TIO2	2.25	2.42	2.63	4.15	3.73	4.17
AL2O	17.59	19.77	12.27	17.47	16.78	16.99
FE2O	18.43	18.48	13.46	16.73	16.98	15.94
FEO	0.0	0.0	0.0	0.0	0.0	0.0
MNO	0.05	0.09	0.16	0.21	0.15	0.02
MGO	7.56	5.95	11.06	5.90	5.63	2.21
CAO	0.93	1.22	11.11	6.41	3.01	2.76
NA2O	4.44	4.22	1.44	4.67	6.07	3.92
K2O	1.05	1.98	2.35	0.30	0.59	4.46
S	0.0	0.0	0.0	0.0	0.0	0.0
P2O5	0.61	0.67	0.41	0.56	1.27	1.78
H2O	0.0	0.0	0.0	0.0	0.0	0.0
CO2	0.0	0.0	0.0	0.0	0.0	0.0
BA	73.00	345.00	862.00	64.00	154.00	386.00
NB	58.00	59.00	61.00	40.00	81.00	90.00
ZR	141.00	149.00	183.00	202.00	242.00	313.00
Y	26.00	20.00	21.00	22.00	41.00	62.00
SR	53.00	47.00	591.00	243.00	139.00	67.00
RB	24.00	57.00	65.00	6.00	18.00	113.00
GA	22.00	19.00	17.00	28.00	28.00	20.00
ZN	0.0	0.0	0.0	0.0	0.0	0.0
CU	0.0	0.0	0.0	0.0	0.0	0.0
NI	1.00	127.00	146.00	60.00	31.00	25.00
CR	1.00	459.00	832.00	187.00	154.00	156.00
V	1.00	138.00	291.00	389.00	186.00	159.00
SC	1.00	1.00	37.00	1.00	36.00	1.00

1. SE6B H
2. CS29 H
3. SE84B H
4. SEI51 H
5. CS65-1 H
6. SEI1C H *

SOGSI2M

	1	2	3	4
SIO2	47.39	41.88	44.35	48.37
TIO2	3.10	4.23	3.77	5.02
AL2O	16.16	17.62	16.57	17.72
FE2O	17.30	19.76	20.68	16.44
FEO	0.0	0.0	0.0	0.0
MNO	0.17	0.13	0.15	0.06
MGO	6.25	7.56	4.68	4.19
CAO	3.87	0.86	1.48	1.18
NA2O	3.48	1.75	4.63	6.03
K2O	1.95	5.76	3.11	0.20
S	0.0	0.0	0.0	0.0
P2O5	0.33	0.45	0.57	0.79
H2O	0.0	0.0	0.0	0.0
CO2	0.0	0.0	0.0	0.0
BA	838.00	686.00	423.00	67.00
NB	25.00	34.00	40.00	41.00
ZR	169.00	176.00	194.00	352.00
Y	18.00	17.00	22.00	37.00
SR	306.00	37.00	115.00	44.00
RB	29.00	87.00	55.00	4.00
GA	25.00	29.00	27.00	33.00
ZN	0.0	0.0	0.0	0.0
CU	0.0	0.0	0.0	0.0
NI	77.00	58.00	50.00	51.00
CR	213.00	165.00	167.00	148.00
V	312.00	358.00	320.00	248.00
SC	0.0	0.0	0.0	0.0

1. SE37 H
2. SE55B H
3. SE34A H
4. SE77 H

SOGSI3I

	1	2	3	4	5	6	7	8	9
SIO2	54.77	53.48	57.40	56.29	48.82	57.24	58.49	59.70	57.95
TIO2	2.83	1.83	1.37	1.40	2.86	1.38	1.49	1.48	1.52
AL2O	16.22	17.59	16.03	15.76	14.30	16.54	16.29	16.92	18.03
FE2O	14.85	2.46	11.00	12.24	20.65	2.87	10.03	8.84	8.91
FEO	0.0	7.74	0.0	0.0	0.0	8.95	0.0	0.0	0.0
MNO	0.04	0.29	0.13	0.03	0.75	0.05	0.03	0.02	0.02
MGO	1.20	3.21	4.16	6.15	1.90	4.57	4.02	1.29	4.60
CAO	1.17	5.91	1.48	0.68	2.23	0.69	0.61	0.79	0.71
NA2O	7.99	2.39	2.34	2.04	3.46	1.90	2.63	4.95	4.39
K2O	0.23	4.46	5.63	4.97	3.57	5.33	5.96	5.51	3.36
S	0.0	0.05	0.0	0.0	0.0	0.0	0.0	0.0	0.0
P2O5	0.71	0.60	0.46	0.46	1.46	0.46	0.46	0.50	0.51
H2O	0.0	0.0	0.0	0.0	0.0	0.0	0.0	0.0	0.0
CO2	0.0	0.0	0.0	0.0	0.0	0.0	0.0	0.0	0.0
BA	23.00	1239.00	512.00	412.00	230.00	1383.00	784.00	1243.00	191.00
NB	53.00	58.00	74.00	75.00	40.00	90.00	82.00	71.00	87.00
ZR	231.00	348.00	482.00	490.00	495.00	511.00	547.00	528.00	583.00
Y	20.00	29.00	37.00	40.00	50.00	42.00	40.00	34.00	58.00
SR	32.00	198.00	26.00	27.00	43.00	31.00	25.00	54.00	21.00
RB	4.00	140.00	112.00	66.00	114.00	116.00	137.00	95.00	59.00
GA	19.00	0.0	28.00	31.00	28.00	0.0	29.00	27.00	29.00
ZN	0.0	96.00	0.0	0.0	0.0	79.00	0.0	0.0	0.0
CU	0.0	90.00	0.0	0.0	0.0	46.00	0.0	0.0	0.0
NI	44.00	25.00	25.00	17.00	12.00	6.00	17.00	17.00	25.00
CR	104.00	135.00	198.00	130.00	2.00	0.0	125.00	108.00	107.00
V	166.00	105.00	7.00	6.00	53.00	8.00	6.00	6.00	6.00
SC	22.00	0.0	0.0	0.0	30.00	22.00	0.0	0.0	0.0

1.	SEI86	H	
2.	SEI84C	D	
3.	SE60	H	
4.	SE49	H	
5.	SE123	H	*
6.	SE64A	D	
7.	SEI83	H	
8.	SE64B	H	*
9.	CS83	H	

SOGSI3I

	10^1
SIO2	58.13
TIO2	1.44
AL2O	17.70
FE2O	10.02
FEO	0.0
MNO	0.04
MGO	5.15
CAO	0.67
NA2O	6.19
K2O	0.20
S	0.0
P2O5	0.45
H2O	0.0
CO2	0.0
BA	23.00
NB	90.00
ZR	595.00
Y	53.00
SR	30.00
RB	3.00
GA	28.00
ZN	0.0
CU	0.0
NI	17.00
CR	135.00
V	6.00
SC	0.0

10. SEI89 H

SOGSIF

	1	2	3	4	5	6
SIO2	66.02	63.85	66.34	67.11	66.92	74.23
TIO2	0.48	0.54	0.61	0.41	0.33	0.27
AL2O	15.23	15.40	14.89	14.99	19.00	14.75
FE2O	1.53	2.05	1.57	1.08	0.44	0.43
FEO	4.78	6.43	4.91	3.37	1.43	1.36
MNO	0.79	4.59	1.22	1.14	0.16	0.18
MGO	1.77	0.16	0.98	2.30	0.33	0.07
CAO	4.08	1.93	3.95	4.27	10.52	8.31
NA2O	5.09	4.93	5.40	5.09	0.75	0.38
K2O	0.13	0.03	0.06	0.21	0.02	0.07
S	0.01	0.02	0.02	0.02	0.01	0.02
P2O5	0.09	0.08	0.06	0.02	0.09	0.0
H2O	0.0	0.0	0.0	0.0	0.0	0.0
CO2	0.0	0.0	0.0	0.0	0.0	0.0
BA	638.00	306.00	265.00	324.00	51.00	142.00
NB	98.00	65.00	67.00	183.00	270.00	289.00
ZR	392.00	475.00	497.00	986.00	1393.00	1397.00
Y	34.00	46.00	43.00	65.00	105.00	106.00
SR	29.00	15.00	35.00	30.00	44.00	28.00
RB	118.00	70.00	64.00	115.00	8.00	4.00
GA	0.0	0.0	0.0	0.0	0.0	0.0
ZN	24.00	70.00	22.00	8.00	1.00	2.00
CU	115.00	47.00	57.00	72.00	128.00	67.00
NI	6.00	14.00	8.00	5.00	2.00	10.00
CR	0.0	148.00	4.00	6.00	10.00	28.00
V	0.0	0.0	0.0	0.0	0.0	0.0
SC	0.0	0.0	0.0	0.0	0.0	0.0

1. CS60 D #
2. SE13C D
3. SEI6 D #
4. SE117 D #
5. SE17C D
6. SEI56 D

SOGTNM

	1	2	3	4	5	6	7	8	9
SIO2	48.43	45.51	44.49	46.40	50.96	46.61	56.27	50.78	47.52
TIO2	2.26	2.29	2.18	3.67	1.84	2.80	3.04	2.31	3.37
AL2O	15.40	15.06	16.59	16.08	14.52	17.06	16.50	17.04	14.20
FE2O	15.30	16.44	14.12	16.90	11.89	15.74	12.49	12.63	16.52
FEO	0.0	0.0	0.0	0.0	0.0	0.0	0.0	0.0	0.0
MNO	0.17	0.17	0.30	0.24	0.12	0.15	0.04	0.18	0.22
MGO	7.73	12.72	7.82	8.12	8.68	4.99	4.36	4.15	5.77
CAO	4.66	2.13	9.99	2.73	8.06	3.24	0.68	7.08	6.50
NA2O	1.07	1.51	2.62	3.58	2.16	0.49	3.43	4.45	4.03
K2O	4.61	3.84	1.56	1.86	1.42	8.58	2.95	1.04	1.25
S	0.0	0.0	0.0	0.0	0.0	0.0	0.0	0.0	0.0
P2O5	0.36	0.33	0.34	0.42	0.35	0.34	0.24	0.34	0.61
H2O	4.21	5.54	3.29	4.37	2.76	3.37	3.75	2.36	2.43
CO2	5.25	0.82	9.51	2.58	4.35	3.92	0.45	2.83	5.34
BA	870.00	762.00	584.00	164.00	306.00	62.00	147.00	170.00	356.00
NB	37.00	36.00	32.00	39.00	30.00	26.00	28.00	31.00	43.00
ZR	128.00	131.00	123.00	237.00	112.00	156.00	169.00	172.00	230.00
Y	17.00	17.00	21.00	26.00	18.00	17.00	17.00	26.00	23.00
SR	163.00	214.00	381.00	98.00	415.00	14.00	35.00	353.00	485.00
RB	50.00	47.00	30.00	26.00	38.00	90.00	40.00	17.00	21.00
GA	20.00	18.00	19.00	30.00	18.00	26.00	24.00	23.00	25.00
ZN	0.0	0.0	0.0	0.0	0.0	0.0	0.0	0.0	0.0
CU	0.0	0.0	0.0	0.0	0.0	0.0	0.0	0.0	0.0
NI	249.00	248.00	134.00	51.00	137.00	96.00	67.00	19.00	33.00
CR	516.00	781.00	320.00	156.00	346.00	34.00	174.00	1.00	155.00
V	269.00	268.00	246.00	301.00	188.00	290.00	306.00	168.00	175.00
SC	45.00	37.00	30.00	22.00	37.00	30.00	26.00	29.00	0.0

1. TL40A H M
2. TL40C H M
3. CT23-2 H M OlNe
4. TL40D H M
5. TL35A H M
6. TL74D H M
7. TL74A H M
8. TL145 H M
9. TL33-1 H M

SOGTNM

	10
SIO2	48.54
TIO2	3.52
AL2O	14.11
FE2O	16.42
FEO	0.0
MNO	0.17
MGO	5.74
CAO	6.66
NA2O	3.02
K2O	1.22
S	0.0
P2O5	0.60
H2O	2.49
CO2	1.92
BA	346.00
NB	44.00
ZR	245.00
Y	26.00
SR	599.00
RB	26.00
GA	27.00
ZN	0.0
CU	0.0
NI	34.00
CR	152.00
V	203.00
SC	0.0

10. TL33-2 H M

SOGTNF

	1	2	3	4	5	6
SIO2	65.50	76.18	74.53	68.36	73.02	76.58
TIO2	2.67	0.20	0.28	0.39	0.27	0.24
AL2O	14.75	12.98	12.92	15.52	11.32	12.46
FE2O	1.86	0.50	1.04	1.08	1.86	0.93
FEO	5.80	1.56	3.26	3.50	5.85	2.93
MNO	0.09	0.02	0.01	0.13	0.01	0.01
MGO	0.65	0.30	0.39	1.54	0.34	0.44
CAO	0.65	0.12	0.11	1.97	0.23	0.04
NA2O	6.13	0.17	0.05	0.08	0.07	0.07
K2O	1.50	7.94	7.39	7.40	6.99	6.23
S	0.02	0.02	0.01	0.01	0.02	0.01
P2O5	0.39	0.02	0.01	0.02	0.02	0.01
H2O	0.0	0.0	0.0	0.0	0.0	0.0
CO2	0.0	0.0	0.0	0.0	0.0	0.0
BA	24.00	293.00	132.00	157.00	122.00	46.00
NB	63.00	118.00	131.00	114.00	116.00	145.00
ZR	349.00	828.00	973.00	992.00	1161.00	1190.00
Y	48.00	67.00	84.00	78.00	114.00	92.00
SR	40.00	9.00	8.00	12.00	1.00	5.00
RB	40.00	157.00	181.00	173.00	151.00	156.00
GA	0.0	0.0	0.0	0.0	0.0	0.0
ZN	3.00	1.00	16.00	9.00	13.00	9.00
CU	67.00	138.00	133.00	101.00	100.00	90.00
NI	14.00	10.00	5.00	7.00	6.00	9.00
CR	232.00	1.00	4.00	18.00	22.00	1.00
V	0.0	0.0	0.0	0.0	0.0	0.0
SC	0.0	0.0	0.0	0.0	0.0	0.0

1. TL130 D
2. TL126 D
3. TL46 D
4. TL60 D
5. CT12-2 D
6. CT17 D

KAGPPM

	1	2	3	4	5	6	7	8	9
SIO2	50.37	62.90	51.42	53.92	51.91	54.24	64.40	51.79	50.90
TIO2	1.74	1.58	1.68	1.65	1.73	1.75	1.54	2.30	2.42
AL2O	12.88	15.79	11.51	16.21	17.39	16.56	13.56	18.88	17.93
FE2O	2.66	0.66	2.37	2.44	2.42	2.69	1.23	2.87	2.83
FEO	8.27	2.08	7.40	7.64	7.57	8.37	3.85	8.93	8.84
MNO	0.31	0.16	0.35	0.15	6.17	0.13	0.13	0.13	0.17
MGO	8.37	2.41	6.09	7.58	9.40	6.79	5.69	4.43	4.65
CAO	12.04	5.50	13.17	4.95	2.43	4.13	3.87	3.95	5.24
NA2O	2.78	8.08	2.67	3.70	3.36	4.57	5.06	5.90	6.04
K2O	0.41	0.55	3.16	1.49	3.33	0.47	0.19	0.51	0.61
S	0.10	0.03	0.11	0.11	0.18	0.07	0.09	0.09	0.13
P2O5	0.12	0.27	0.13	0.21	0.18	0.25	0.44	0.26	0.31
H2O	2.55	0.45	2.00	3.52	3.89	3.40	1.83	3.36	3.21
CO2	9.93	6.04	13.63	5.83	2.72	4.73	4.14	4.37	6.00
BA	104.00	78.00	119.00	111.00	797.00	98.00	63.00	90.00	80.00
NB	11.00	22.00	21.00	28.00	22.00	40.00	55.00	44.00	44.00
ZR	58.00	66.00	66.00	89.00	109.00	109.00	113.00	121.00	119.00
Y	16.00	14.00	19.00	19.00	25.00	15.00	18.00	16.00	16.00
SR	199.00	76.00	18.00	42.00	156.00	149.00	34.00	43.00	42.00
RB	13.00	9.00	64.00	48.00	50.00	14.00	10.00	6.00	4.00
GA	0.0	0.0	0.0	0.0	0.0	0.0	0.0	0.0	0.0
ZN	32.00	19.00	18.00	40.00	310.00	36.00	82.00	56.00	42.00
CU	159.00	110.00	50.00	90.00	0.0	40.00	241.00	120.00	27.00
NI	161.00	14.00	87.00	131.00	93.00	135.00	73.00	351.00	315.00
CR	310.00	274.00	266.00	242.00	377.00	251.00	147.00	356.00	335.00
V	184.00	53.00	154.00	166.00	202.00	164.00	99.00	268.00	222.00
SC	34.00	22.00	37.00	22.00	41.00	22.00	22.00	33.00	40.00

1. PP91 D A 01Hy
2. PP60B D M
3. PP59A D M
4. PP104 D M
5. PP54 D A
6. PP107 D M
7. PP90 D M
8. PP53Z D A
9. PP53Y D A

KAGPPM

	10	11	12	13	14	15	16	17	18
SIO2	55.10	49.53	44.55	35.76	51.39	59.16	53.10	45.78	46.88
TIO2	2.35	1.79	2.14	2.40	2.06	1.98	1.49	2.55	2.58
AL2O	19.24	17.76	22.13	23.53	17.05	17.91	16.34	22.27	9.99
FE2O	2.34	2.66	4.26	4.62	3.01	0.92	2.54	3.01	1.41
FEO	7.32	8.32	13.22	14.33	9.38	2.88	7.92	9.37	4:45
MNO	0.10	0.18	0.11	0.08	0.09	0.05	0.11	0.14	0.42
MGO	3.60	9.19	8.23	16.34	9.97	5.84	9.54	10.05	9.54
CAO	3.08	4.13	0.57	1.09	3.23	4.29	4.44	1.39	19.58
NA2O	5.70	3.92	4.07	0.43	3.51	6.65	4.41	3.76	4.88
K2O	0.75	2.26	0.53	1.00	0.02	0.02	0.03	1.24	0.22
S	0.08	0.09	0.10	0.17	0.03	0.03	0.08	0.04	0.08
P2O5	0.37	0.20	0.14	0.33	0.26	0.28	0.28	0.41	0.0
H2O	3.12	4.06	5.70	9.20	4.65	1.39	3.81	5.10	2.38
CO2	3.26	4.66	0.13	0.92	3.85	4.54	5.05	0.68	10.19
BA	81.00	143.00	157.00	58.00	67.00	46.00	46.00	335.00	99.00
NB	48.00	18.00	17.00	55.00	37.00	43.00	51.00	96.00	76.00
ZR	122.00	117.00	125.00	134.00	142.00	149.00	155.00	195.00	208.00
Y	15.00	21.00	18.00	15.00	20.00	23.00	19.00	19.00	23.00
SR	33.00	51.00	19.00	4.00	8.00	57.00	24.00	89.00	72.00
RB	22.00	27.00	12.00	16.00	0.0	4.00	6.00	23.00	9.00
GA	0.0	0.0	0.0	0.0	0.0	0.0	0.0	0.0	0.0
ZN	50.00	293.00	409.00	70.00	71.00	7.00	170.00	136.00	14.00
CU	42.00	93.00	26.00	26.00	26.00	49.00	32.00	19.00	131.00
NI	251.00	95.00	117.00	174.00	114.00	67.00	111.00	150.00	32.00
CR	371.00	233.00	264.00	319.00	275.00	145.00	351.00	275.00	50.00
V	254.00	195.00	218.00	211.00	166.00	155.00	137.00	221.00	87.00
SC	30.00	36.00	37.00	22.00	22.00	22.00	30.00	34.00	22.00

10. PP53X D A
11. PP55A D A
12. PP55A1 D A
13. PP70 D M
14. CB-1-2B D M
15. PP125C D M
16. PP44 D A
17. PP42 D A
18. PP105 D M

KAGPPM

	19	20	21	22	23	24	25	26	27
SIO2	49.00	47.02	57.42	54.62	47.76	63.94	59.74	57.78	43.26
TIO2	2.70	1.63	1.55	1.57	1.71	1.61	1.58	1.61	2.26
AL2O	22.36	10.98	13.73	15.85	16.86	18.84	17.93	18.41	20.35
FE2O	2.61	2.31	1.59	2.57	2.89	0.77	1.94	2.27	4.33
FEO	8.15	7.23	4.99	8.02	8.99	2.43	6.07	7.10	13.43
MNO	0.10	0.48	0.31	0.15	0.28	0.08	0.05	0.09	0.18
MGO	8.12	6.62	4.94	6.19	6.22	2.15	4.48	3.59	5.87
CAO	0.29	17.41	8.70	5.31	8.57	2.81	1.78	2.50	4.80
NA2O	5.64	3.59	3.29	3.45	3.43	2.34	4.12	4.59	4.29
K2O	0.24	2.61	3.18	1.97	2.97	4.85	2.08	1.82	0.82
S	0.03	0.23	0.08	0.24	0.31	0.12	0.11	0.12	0.02
P2O5	0.77	0.01	0.25	0.19	0.17	0.13	0.17	0.17	0.39
H2O	4.55	1.77	2.19	3.61	3.78	2.10	3.66	3.11	4.89
CO2	0.33	14.67	8.15	6.32	10.43	3.49	1.86	3.10	4.94
BA	82.00	184.00	181.00	140.00	202.00	219.00	160.00	222.00	100.00
NB	106.00	15.00	20.00	19.00	21.00	26.00	22.00	25.00	26.00
ZR	267.00	55.00	64.00	62.00	66.00	75.00	80.00	76.00	88.00
Y	27.00	20.00	13.00	11.00	16.00	7.00	13.00	14.00	18.00
SR	105.00	46.00	33.00	24.00	24.00	15.00	26.00	58.00	82.00
RB	3.00	76.00	113.00	54.00	77.00	190.00	84.00	63.00	21.00
GA	0.0	0.0	0.0	0.0	0.0	0.0	0.0	0.0	0.0
ZN	85.00	30.00	26.00	60.00	43.00	23.00	77.00	61.00	540.00
CU	56.00	130.00	41.00	30.00	36.00	70.00	103.00	40.00	127.00
NI	138.00	60.00	59.00	188.00	234.00	108.00	240.00	242.00	177.00
CR	278.00	407.00	419.00	486.00	355.00	344.00	519.00	375.00	246.00
V	201.00	148.00	368.00	181.00	176.00	189.00	192.00	200.00	164.00
SC	22.00	41.00	32.00	35.00	30.00	28.00	30.00	37.00	25.00

19. PP95 D M
20. PP10Y D A
21. PP10X D A QHy
22. PP10B D A
23. PP82A D A OlNe
24. PP82C D M
25. PP8A D A
26. PP85 D M
27. CB-6-5A D M

KAGPPM

	28	29	30	31	32	33	34
SIO2	54.53	58.04	62.59	59.35	60.06	56.74	49.93
TIO2	1.34	1.93	1.73	1.86	1.94	2.07	2.28
AL2O	18.44	13.03	16.77	17.81	18.08	20.33	13.06
FE2O	2.70	1.24	1.59	1.75	1.81	1.70	2.01
FEO	8.44	3.91	4.97	5.44	5.68	5.31	6.30
MNO	0.10	0.40	0.09	0.10	0.10	0.06	0.35
MGO	8.29	4.51	3.27	3.72	3.74	4.00	6.97
CAO	1.33	9.77	2.27	2.26	2.27	1.55	12.10
NA2O	3.67	5.91	5.28	6.09	4.71	7.40	4.46
K2O	0.99	0.93	1.05	1.18	1.19	0.38	2.27
S	0.08	0.07	0.08	0.10	0.10	0.06	0.04
P2O5	0.12	0.28	0.34	0.39	0.37	0.42	0.23
H2O	4.50	1.21	2.58	2.44	2.59	2.40	1.06
CO2	4.30	9.29	2.22	2.22	2.40	1.17	10.76
BA	117.00	109.00	123.00	145.00	133.00	78.00	81.00
NB	41.00	42.00	49.00	52.00	52.00	58.00	60.00
ZR	115.00	115.00	124.00	134.00	136.00	157.00	155.00
Y	26.00	28.00	16.00	19.00	18.00	19.00	21.00
SR	22.00	104.00	88.00	94.00	93.00	48.00	42.00
RB	25.00	38.00	39.00	46.00	45.00	17.00	99.00
GA	0.0	0.0	0.0	0.0	0.0	0.0	0.0
ZN	205.00	17.00	39.00	40.00	41.00	48.00	15.00
CU	39.00	120.00	82.00	48.00	35.00	27.00	28.00
NI	1.00	38.00	190.00	184.00	193.00	204.00	67.00
CR	1.00	209.00	370.00	287.00	292.00	347.00	318.00
V	1.00	133.00	165.00	195.00	198.00	211.00	188.00
SC	1.00	30.00	22.00	25.00	25.00	22.00	32.00

28. CB-6-3B D A
29. PP16C1 D A
30. PP16C2 D A
31. PP16C4 D M
32. PP16C3 D M
33. PP77B D A
34. PP6 D A' O1Ne

KAGPPF

	1	2	3
SIO2	75.29	73.37	72.87
TIO2	0.0	0.01	0.0
AL2O	12.66	14.42	15.01
FE2O	0.28	0.26	0.26
FEO	0.89	0.81	0.83
MNO	0.03	0.02	0.01
MGO	0.86	0.72	0.78
CAO	2.19	1.64	2.04
NA2O	0.25	0.22	1.46
K2O	7.53	8.50	6.72
S	0.02	0.06	0.03
P2O5	0.0	0.0	0.0
H2O	0.0	0.0	0.0
CO2	0.0	0.0	0.0
BA	507.00	612.00	126.00
NB	123.00	125.00	142.00
ZR	52.00	57.00	83.00
Y	24.00	38.00	85.00
SR	12.00	12.00	16.00
RB	400.00	419.00	764.00
GA	0.0	0.0	0.0
ZN	28.00	30.00	7.00
CU	48.00	81.00	54.00
NI	24.00	44.00	10.00
CR	24.00	13.00	275.00
V	1.00	1.00	1.00
SC	1.00	1.00	1.00

1. PP87 D
2. CB-6-1A D
3. PP147 D

KAGINM

	1	2	3	4	5	6	7	8	9
SIO2	45.26	47.41	43.83	44.27	50.45	48.15	49.24	49.17	46.96
TIO2	1.73	1.62	1.81	1.81	1.75	1.73	1.79	1.86	1.94
AL2O	15.11	15.49	15.42	15.55	15.93	15.61	16.23	16.58	16.06
FE2O	11.55	13.25	19.29	18.64	12.96	13.25	10.96	17.96	17.23
FEO	0.0	0.0	0.0	0.0	0.0	0.0	0.0	0.0	0.0
MNO	0.25	0.18	0.57	0.54	0.41	0.19	0.18	0.12	0.48
MGO	7.42	7.04	6.53	6.14	4.67	8.43	3.38	5.26	3.71
CAO	13.87	12.10	7.78	7.94	6.80	9.63	11.33	3.08	7.72
NA2O	4.10	2.24	4.07	4.61	4.27	2.08	4.05	3.21	1.58
K2O	0.36	0.41	0.42	0.21	2.49	0.67	2.50	2.39	3.96
S	0.0	0.0	0.0	0.0	0.0	0.0	0.0	0.0	0.0
P2O5	0.35	0.26	0.28	0.29	0.29	0.27	0.34	0.37	0.37
H2O	3.64	1.71	3.45	3.59	2.58	3.35	2.83	3.80	3.13
CO2	9.29	5.00	9.33	9.71	8.40	4.19	7.68	5.07	10.32
BA	2.00	155.00	6.00	0.0	13.00	184.00	115.00	196.00	26.00
NB	37.00	23.00	25.00	26.00	27.00	26.00	28.00	43.00	30.00
ZR	92.00	99.00	97.00	95.00	104.00	105.00	113.00	119.00	123.00
Y	18.00	23.00	19.00	19.00	22.00	24.00	26.00	23.00	27.00
SR	81.00	364.00	39.00	30.00	30.00	302.00	60.00	32.00	24.00
RB	10.00	9.00	11.00	4.00	94.00	10.00	55.00	46.00	139.00
GA	0.0	0.0	0.0	0.0	0.0	0.0	0.0	0.0	0.0
ZN	0.0	0.0	0.0	0.0	0.0	0.0	0.0	0.0	0.0
CU	0.0	0.0	0.0	0.0	0.0	0.0	0.0	0.0	0.0
NI	266.00	161.00	231.00	239.00	145.00	0.0	139.00	131.00	231.00
CR	317.00	474.00	0.46	0.00	0.00	0.00	0.00	0.00	0.00
V	172.00	201.00	170.00	161.00	191.00	195.00	188.00	191.00	210.00
SC	36.00	52.00	37.00	30.00	37.00	45.00	30.00	37.00	37.00

1. TL99 H M
2. TL100-11 H M QHy
3. TL109-1 H M
4. TL109-7 H M
5. TL109-7A H M OINe
6. TL100-10 H M QHy
7. TL91 H M
8. TL108 H M
9. TL109-12 H M

KAGTNM

	10	11
SIO2	53.93	46.45
TIO2	2.26	2.13
AL2O	15.54	15.93
FE2O	11.85	13.42
FEO	0.0	0.0
MNO	0.07	0.21
MGO	7.66	6.24
CAO	2.27	10.87
NA2O	2.52	3.27
K2O	3.48	1.08
S	0.0	0.0
P2O5	0.41	0.40
H2O	4.22	3.45
CO2	0.92	5.88
BA	248.00	279.00
NB	32.00	33.00
ZR	148.00	150.00
Y	23.00	25.00
SR	97.00	274.00
RB	64.00	18.00
GA	0.0	0.0
ZN	0.0	0.0
CU	0.0	0.0
NI	143.00	136.00
CR	0.00	0.0
V	212.00	0.0
SC	48.00	0.0

10. TL92 H M
11. TL93 H M OlNe

JAGPPM

	1	2	3	4
SIO2	56.18	54.69	57.10	49.53
TIO2	1.12	1.16	1.26	2.20
AL2O	16.03	16.60	15.06	20.63
FE2O	2.25	2.50	2.64	2.48
FEO	7.02	7.11	7.53	7.76
MNO	0.22	0.09	0.12	0.06
MGO	4.92	7.62	6.37	10.23
CAO	6.30	3.97	6.47	1.31
NA2O	3.57	4.52	2.68	4.96
K2O	2.30	1.61	0.78	0.10
S	0.05	0.12	0.0	0.05
P2O5	0.06	0.0	0.0	0.72
H2O	0.0	3.40	2.72	4.68
CO2	0.0	0.18	0.60	0.43
BA	141.00	115.00	83.00	59.00
NB	11.00	12.00	12.00	117.00
ZR	48.00	51.00	58.00	318.00
Y	13.00	14.00	18.00	29.00
SR	72.00	274.00	243.00	184.00
RB	105.00	39.00	23.00	3.00
GA	0.0	19.00	21.00	0.0
ZN	28.00	0.0	0.0	65.00
CU	178.00	0.0	0.0	24.00
NI	150.00	1.00	1.00	59.00
CR	292.00	580.00	1.00	97.00
V	1.00	1.00	1.00	1.00
SC	1.00	1.00	1.00	1.00

1. PP13 D QHy
2. PP74A H M
3. PP12 H M QHy
4. PP41 D M

JAGTNM

	1	2	3	4	5	6	7
SIO2	50.15	45.21	38.20	45.86	44.47	47.89	54.05
TIO2	3.33	3.84	4.20	3.96	4.21	1.67	2.22
AL2O	12.00	15.23	16.75	16.00	16.53	15.85	15.83
FE2O	15.97	16.90	23.42	17.81	17.74	12.97	2.70
FEO	0.0	0.0	0.0	0.0	0.0	0.0	8.44
MNO	0.19	0.21	0.37	0.22	0.17	0.19	0.18
MGO	5.80	5.28	6.95	6.15	8.04	7.83	3.31
CAO	7.09	8.40	6.16	4.69	3.07	10.81	6.05
NA2O	2.14	3.15	3.04	2.96	3.76	1.98	4.92
K2O	2.98	1.37	0.81	1.91	1.53	0.53	1.78
S	0.0	0.0	0.0	0.0	0.0	0.0	0.03
P2O5	0.35	0.40	0.46	0.46	0.47	0.28	0.50
H2O	2.69	2.29	5.10	3.91	3.50	2.10	0.0
CO2	4.06	2.20	7.01	4.89	0.40	0.27	0.0
BA	222.00	215.00	21.00	166.00	64.00	352.00	722.00
NB	28.00	35.00	36.00	38.00	39.00	21.00	51.00
ZR	100.00	174.00	186.00	187.00	209.00	214.00	333.00
Y	21.00	21.00	22.00	19.00	23.00	32.00	31.00
SR	336.00	785.00	62.00	205.00	92.00	515.00	606.00
RB	8.00	21.00	22.00	33.00	26.00	53.00	42.00
GA	0.0	25.00	25.00	25.00	27.00	28.00	0.0
ZN	0.0	0.0	0.0	0.0	0.0	0.0	128.00
CU	0.0	0.0	0.0	0.0	0.0	0.0	64.00
NI	0.0	0.0	0.0	0.0	0.0	0.0	7.00
CR	0.0	370.00	0.0	0.0	0.0	0.0	8.00
V	0.0	0.0	0.0	0.0	0.0	0.0	0.0
SC	0.0	0.0	0.0	0.0	0.0	0.0	0.0

1. TL109-1B H M
2. TL124 H M
3. TL49B H M
4. TL53C H M
5. TL147 H M
6. TL109-16 H M 01Hy
7. TL110 D D 01Hy

PEM

	1	2	3	4	5	6	7	8	9
SIO2	53.17	55.35	53.20	54.90	52.26	55.87	56.78	55.40	56.22
TIO2	0.81	1.05	0.93	0.94	0.92	0.93	0.93	0.95	0.96
AL2O	15.21	15.52	15.95	14.33	15.02	14.72	14.45	14.56	14.54
FE2O	11.60	11.24	11.36	2.60	12.97	10.79	9.99	11.19	10.96
FEO	0.0	0.0	0.0	8.11	0.0	0.0	0.0	0.0	0.0
MNO	0.18	0.15	0.12	0.18	0.23	0.19	0.24	0.16	0.17
MGO	7.50	6.38	9.75	6.51	7.22	4.96	5.91	5.37	4.76
CAO	7.12	4.82	4.02	8.09	5.38	6.77	5.71	5.98	5.87
NA2O	3.40	3.20	2.93	2.06	4.53	2.78	2.80	5.18	4.07
K2O	0.93	2.18	1.64	1.98	1.38	2.91	3.06	1.11	2.35
S	0.0	0.0	0.0	0.29	0.0	0.0	0.0	0.0	0.0
P2O5	0.08	0.11	0.10	0.13	0.09	0.10	0.13	0.09	0.10
H2O	3.49	0.0	4.94	3.06	2.84	2.30	1.99	2.25	1.97
CO2	0.55	0.0	0.19	0.27	0.30	0.20	0.15	0.14	0.23
BA	243.00	578.00	489.00	1285.00	415.00	432.00	591.00	352.00	689.00
NB	1.00	3.00	12.00	9.00	11.00	4.00	10.00	10.00	10.00
ZR	121.00	127.00	139.00	142.00	144.00	143.00	149.00	150.00	150.00
Y	22.00	21.00	21.00	23.00	26.00	24.00	28.00	25.00	24.00
SR	363.00	373.00	257.00	310.00	172.00	213.00	209.00	163.00	251.00
RB	18.00	25.00	27.00	59.00	24.00	104.00	91.00	31.00	59.00
GA	18.00	17.00	19.00	0.0	17.00	19.00	19.00	20.00	17.00
ZN	0.0	0.0	0.0	97.00	0.0	0.0	0.0	0.0	0.0
CU	0.0	0.0	0.0	96.00	0.0	0.0	0.0	0.0	0.0
NI	114.00	120.00	102.00	113.00	113.00	76.00	73.00	79.00	1.00
CR	22.00	20.00	18.00	16.00	15.00	0.0	0.0	6.00	0.0
V	195.00	212.00	212.00	194.00	211.00	222.00	223.00	224.00	0.0
SC	36.00	34.00	22.00	36.00	26.00	37.00	30.00	34.00	0.0

1. PV01 H M
2. PV03 H
3. PE14 H M
4. PV02 D A
5. PV11 H M
6. PE5C H M QHy
7. PV13 H M
8. PE10 H M
9. PE5B H M QHy

PEM

	10	11	12	13	14
SIO2	55.60	55.92	55.81	53.83	55.09
TIO2	0.99	0.91	1.00	0.86	1.03
AL2O	16.10	15.10	15.15	15.55	15.04
FE2O	9.66	2.47	10.73	12.14	2.63
FEO	0.0	7.75	0.0	0.0	8.22
MNO	0.19	0.17	0.21	0.24	0.09
MGO	5.80	6.14	7.87	7.02	9.09
CAO	5.37	6.46	3.47	5.98	5.28
NA2O	3.12	2.35	3.21	3.04	1.57
K2O	3.07	2.47	2.40	1.26	1.65
S	0.0	0.22	0.0	0.0	0.37
P2O5	0.10	0.15	0.15	0.08	0.13
H2O	2.90	2.68	0.0	3.00	2.98
CO2	1.80	0.13	0.0	0.29	0.60
BA	427.00	705.00	415.00	371.00	552.00
NB	10.00	4.00	13.00	11.00	9.00
ZR	153.00	156.00	156.00	159.00	167.00
Y	27.00	29.00	25.00	26.00	28.00
SR	219.00	232.00	190.00	195.00	183.00
RB	94.00	92.00	75.00	60.00	69.00
GA	20.00	0.0	19.00	19.00	0.0
ZN	0.0	95.00	0.0	0.0	176.00
CU	0.0	91.00	0.0	0.0	278.00
NI	77.00	90.00	81.00	70.00	82.00
CR	5.00	3.00	1.00	5.00	5.00
V	222.00	222.00	187.00	234.00	223.00
SC	37.00	30.00	30.00	30.00	36.00

10. PV08 H M
11. PV10 D A
12. PV12 H
13. PV07 H M
14. PV05 D A

	1	2	3	4	5	6	7	8	9
SIO2	47.24	52.52	53.16	52.19	52.99	52.60	52.09	53.37	54.18
TIO2	2.13	1.70	1.53	1.61	1.39	1.41	1.52	1.47	1.49
AL2O	18.13	16.68	16.35	15.43	13.19	15.32	14.36	14.54	15.72
FE2O	14.75	13.12	13.53	13.84	14.01	12.10	14.18	12.85	10.87
FEO	0.0	0.0	0.0	0.0	0.0	0.0	0.0	0.0	0.0
MNO	0.20	0.28	0.30	0.27	0.32	0.15	0.22	0.20	0.26
MGO	7.61	7.49	7.19	6.79	6.50	6.44	5.98	5.91	5.75
CAO	3.12	2.84	2.48	5.50	5.91	8.15	5.97	7.23	7.93
NA2O	4.59	3.16	2.77	3.11	5.40	2.13	3.45	2.75	2.40
K2O	1.78	2.12	2.53	1.18	0.22	1.58	2.13	1.59	1.24
S	0.0	0.0	0.0	0.0	0.0	0.0	0.0	0.0	0.0
P2O5	0.47	0.11	0.17	0.09	0.08	0.12	0.11	0.10	0.15
H2O	0.0	0.0	0.0	0.0	0.0	0.0	0.0	0.0	0.0
CO2	0.0	0.0	0.0	0.0	0.0	0.0	0.0	0.0	0.0
BA	694.00	662.00	1231.00	482.00	22.00	419.00	1170.00	415.00	584.00
NB	17.00	0.0	4.00	1.00	2.00	4.00	3.00	1.00	2.00
ZR	196.00	90.00	108.00	96.00	91.00	97.00	95.00	86.00	103.00
Y	30.00	25.00	23.00	21.00	23.00	19.00	22.00	21.00	23.00
SR	469.00	356.00	443.00	503.00	127.00	278.00	315.00	303.00	351.00
RB	38.00	50.00	74.00	35.00	8.00	33.00	61.00	44.00	28.00
GA	24.00	24.00	23.00	20.00	18.00	20.00	21.00	21.00	22.00
ZN	0.0	0.0	0.0	0.0	0.0	0.0	0.0	0.0	0.0
CU	0.0	0.0	0.0	0.0	0.0	0.0	0.0	0.0	0.0
NI	67.00	58.00	41.00	55.00	68.00	61.00	73.00	70.00	55.00
CR	184.00	160.00	147.00	160.00	153.00	176.00	148.00	166.00	160.00
V	212.00	200.00	144.00	178.00	178.00	178.00	190.00	196.00	178.00
SC	37.00	37.00	34.00	36.00	37.00	34.00	34.00	37.00	37.00

1.	M8A	H	
2.	M7	H	
3.	M18	H	
4.	M6A	H	
5.	M26	H	
6.	CM15	H	
7.	CM17-1	H	OIHy
8.	M3H	H	QHy
9.	CM8	H	

ETGM

	10	11	12	13
SIO2	50.93	51.32	55.94	53.31
TIO2	1.37	1.36	1.49	1.40
AL2O	14.69	14.52	14.94	15.56
FE2O	14.75	14.58	10.23	13.52
FEO	0.0	0.0	0.0	0.0
MNO	0.21	0.21	0.21	0.18
MGO	5.68	5.66	5.57	5.47
CAO	9.44	9.22	5.98	7.36
NA2O	2.21	2.23	3.05	2.09
K2O	0.62	0.82	2.47	1.07
S	0.0	0.0	0.0	0.0
P2O5	0.10	0.09	0.11	0.04
H2O	0.0	0.0	0.0	0.0
CO2	0.0	0.0	0.0	0.0
BA	260.00	289.00	852.00	328.00
NB	3.00	2.00	10.00	0.0
ZR	72.00	70.00	101.00	83.00
Y	22.00	21.00	21.00	22.00
SR	279.00	282.00	443.00	248.00
RB	13.00	17.00	63.00	27.00
GA	23.00	21.00	18.00	22.00
ZN	0.0	0.0	0.0	0.0
CU	0.0	0.0	0.0	0.0
NI	70.00	76.00	61.00	56.00
CR	143.00	138.00	175.00	161.00
V	200.00	211.00	155.00	189.00
SC	37.00	37.00	34.00	37.00

10. CM2-2 H QHy
11. CM4 H QHy
12. M3C
13. M6B H QHy